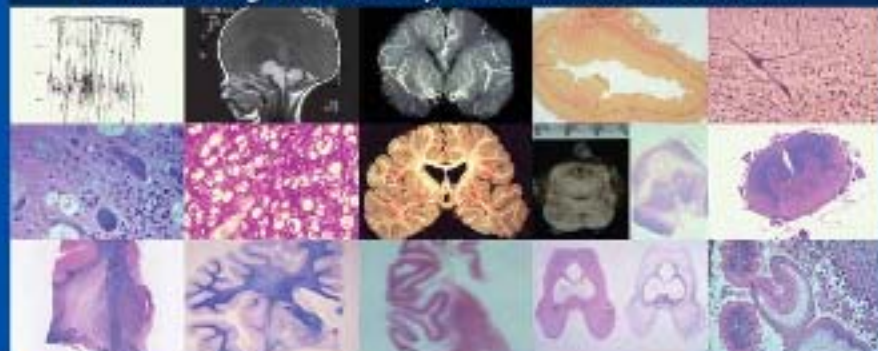
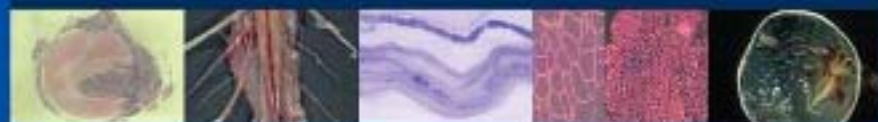


D. Armstrong · W. Halliday · C. Hawkins · S. Takashima



Pediatric Neuropathology

A Text–Atlas



 Springer

Dawna Armstrong, William Halliday, Cynthia Hawkins,
Sachio Takashima

Pediatric Neuropathology
A Text–Atlas

Dawna Armstrong, William Halliday,
Cynthia Hawkins, Sachio Takashima

Pediatric Neuropathology

A Text–Atlas

With 1,020 Figures, Including 917 in Color

 Springer

Dawna Armstrong, M.D.
Formerly Professor of Pathology, Baylor College of Medicine
Houston, Texas, USA

William Halliday, M.D.
Professor, University of Toronto;
Staff Neuropathologist, The Hospital for Sick Children, DPLM
555 University Ave., Toronto, M5G 1X8, Canada

Cynthia Hawkins, M.D., Ph.D.
Assistant Professor, University of Toronto;
Staff Neuropathologist, The Hospital for Sick Children, DPLM
555 University Ave., Toronto, M5G 1X8, Canada

Sachio Takashima, M.D.
Professor, International University of Health and Welfare;
Director, Yanagawa Institute for Developmental Disabilities
Yanagawa, Fukuoka, Japan

ISBN 978-4-431-70246-7 Springer Tokyo Berlin Heidelberg New York

Library of Congress Control Number: 2007927414

Printed on acid-free paper

© Springer 2007

Printed in Japan

This work is subject to copyright. All rights are reserved, whether the whole or part of the material is concerned, specifically the rights of translation, reprinting, reuse of illustrations, recitation, broadcasting, reproduction on microfilms or in other ways, and storage in data banks.

The use of registered names, trademarks, etc. in this publication does not imply, even in the absence of a specific statement, that such names are exempt from the relevant protective laws and regulations and therefore free for general use.

Product liability: The publisher can give no guarantee for information about drug dosage and application thereof contained in this book. In every individual case the respective user must check its accuracy by consulting other pharmaceutical literature.

Springer is a part of Springer Science+Business Media
springer.com

Typesetting: SNP Best-set Typesetter Ltd., Hong Kong
Printing and binding: Asia Printing Office Corporation, Japan

Pediatric Neuropathology: A Text-Atlas is dedicated to our friend
and colleague

Dr. Laurence E. Becker
Pediatric Neuropathologist
Hospital for Sick Children, Toronto
1974–2002

Preface

Dr. Takashima and Dr. Becker were planning this text-atlas when Dr. Becker was prematurely taken from us. We have, with enthusiasm, completed the book according to the original plan. The material is gathered from our combined experiences over 30 years at the Hospital for Sick Children, Toronto; the Texas Children's Hospital, Houston; the Health Sciences Centre (Winnipeg Children's Hospital), Winnipeg; and the National Institute of Neuroscience, Tokyo. We acknowledge with gratitude the families who have allowed us to study these cases. It is our hope that our involvement has contributed to a better understanding of pediatric neuropathology.

The discipline of neuropathology with its interpretation of morphology stands between the patient with his or her physician and the neurobiologist with his or her science. It requires a correlation of clinical, morphological, and biological information. When interpreting pediatric neuropathology, brain development must also be considered. Thus, each case at its unique age can potentially (1) disclose critical periods of brain development that may be interrupted by a particular disease process or (2) define cell populations of selective vulnerability.

The past three decades have provided amazing techniques that increase the neuropathologist's ability to define morphology. Histochemistry, immunocytochemistry, in situ hybridization, and fluorescence in situ hybridization (FISH) now allow us to define specific cell types, proteins, and chromosomes that are involved in pediatric neurological disease. Brain imaging reveals exquisite details of brain lesions, and neurobiologists offer tests that define tissue-specific genetic abnormalities. Our new technologies have required increased interaction between clinician, pathologist, and scientist; but they also rely heavily on the knowledge and techniques of classic neuropathology.

In the text-atlas we have attempted to summarize the categories of disease that affect the pediatric patient and have used examples of these diseases taken from our case records. In each case, when possible, there is a brief paragraph summarizing the current clinical, morphological, and biological information about the disease. This information is greatly abbreviated, but with illustrative images we have emphasized morphology—the hallmark of neuropathology and the starting place for further investigation.

The text-atlas is incomplete. There are many diseases we do not understand, especially those most debilitating disorders of childhood—the pervasive developmental disorders, which interrupt neural connectivity and function with no obvious morphological alteration. It is our hope that the text-atlas will be a useful guide for students of neuropathology, neurology, and neuroscience, and that these students will go on to make our understanding more complete.

D.A., S.T., W.H., C.H.

Acknowledgments

The authors are grateful to many colleagues, past and present, who have supported, stimulated, and educated them. Some have also provided important images for the production of this atlas.

Vernon Edwards, (Retired) Formerly of the Department of Pathology, The Hospital for Sick Children, Toronto, Canada

Yasuhiro Arai, M.D., Department of Pediatrics, Juntendo University, Tokyo, Japan

Masayuki Itoh, M.D., Ph.D., National Institute of Neuroscience, National Center of Neurology and Psychiatry, Tokyo, Japan

Masashi Mizuguchi, M.D., Department of Pediatrics, Tokyo University, Tokyo, Japan

Mitsuhiro Kato, M.D., Department of Pediatrics, Yamagata University, Yamagata, Japan

Akemi Kakita, M.D., Department of Pathological Neuroscience, Brain Research Institute, Niigata University, Niigata, Japan

Komyo Eto, M.D., National Institute for Minamata Disease, Minamata, Kumamoto, Japan

Meena Bhattacharjee, M.D., Department of Pathology, Baylor College of Medicine, Texas Children's Hospital, Houston, Texas, USA

Takeshi Kanaumi, M.D., Department of Pediatrics, Fukuoka University, Fukuoka, Japan

Barry Rewcastle, M.D., (Retired) Formerly of the Division of Neuropathology, University of Toronto, Toronto, Canada

Jan Goddard-Finegold, M.D., Department of Pediatrics, Baylor College of Medicine, Houston, Texas, USA

Marc Del Bigio, M.D., Ph.D., Department of Pathology, University of Manitoba, Manitoba, Canada

Contents

Preface	VII
Acknowledgments	IX
1. Normal Development	1
1.1. Developmental Characteristics of the Fetal Brain:	
Gross Brain	2
1.2. Developmental Characteristics of Neurons	4
1.3. Dendritic and Synapse Development	6
1.4. Glial Development and Myelination in the Cerebral	
White Matter	8
1.5. Vascular Architecture in Developing Brains	10
2. Malformations	13
2.1. Neural Tube Defects, Anencephaly	14
2.2. Meningoencephalocele, Encephalocele	16
2.3. Iniencephaly	18
2.4. Spinal Dysraphisms	20
2.5. Chiari (Arnold-Chiari) Malformations	22
2.6. Dandy-Walker Malformation	24
2.7. Holoprosencephaly (Synonyms: Holotelencephaly,	
Telencephalosynapsis, Arhinencephaly)	26
2.8. Semilobar and Lobar Holoprosencephaly	28
2.9. Callosal Agenesis (Synonym: Agenesis of Corpus	
Callosum)	30
2.10. Neuronal Heterotopia	32
2.11. Classic (Type 1) Lissencephaly (Agyria-Pachygyria)	34
2.12. Miller-Dieker Syndrome, Double Cortex Syndrome,	
X-Linked Lissencephaly with Abnormal Genitalia	36
2.13. Hemimegalencephaly and Focal Cortical Dysplasia	38
2.14. Cobblestone (Type 2) Lissencephaly: Fukuyama	
Congenital Muscular Dystrophy	42
2.15. Walker-Warburg Syndrome	44
2.16. Malformations of Cortical Organization	46
2.17. Thanatophoric Dysplasia Type 1	48
2.18. Hydrocephalus	50
2.19. Porencephaly	52
2.20. Schizencephaly	54
2.21. Hydranencephaly	56

2.22.	Cysts: Subependymal Cysts, Colloid Cysts, Gliependymal Cysts	58
2.23.	Arachnoid Cyst, Neuroenteric Cyst.....	60
2.24.	Malformation of the Cranium: Craniosynostosis, Meckel-Gruber Syndrome, Amniotic Band	62
2.25.	Malformation of the Brain Stem	64
2.26.	Agenesis of the Vermis of the Cerebellum and Joubert Syndrome.....	66
2.27.	Malformation of the Cerebellar Hemispheres and Spinal Cord	68
2.28.	Infantile Olivopontocerebellar Atrophy/Hypoplasia, Pontocerebellar Hypoplasia	70
3.	Chromosomal Abnormalities	73
3.1.	Down Syndrome.....	74
3.2.	Trisomy 13 and Trisomy 18.....	76
3.3.	Chromosome 1q-.....	78
3.4.	Chromosome 4p-.....	80
4.	Perinatal Brain Damage	83
4.1.	Birth Trauma in Term Infants	84
4.2.	Periventricular/Intraventricular Hemorrhage and Cerebellar Hemorrhage in Preterm Infants	86
4.3.	Sequelae of IVH and Other Hemorrhages in Preterm Infants.....	88
4.4.	Perinatal Hypoxic-Ischemic Encephalopathy.....	90
4.5.	Parasagittal Infarction, Ulegyria, Lobar Sclerosis	92
4.6.	Sequelae of Cerebral Necrosis in Fetal and Perinatal Hypoxia	94
4.7.	Periventricular Leukomalacia.....	96
4.8.	Sequelae of Periventricular Leukomalacia	98
4.9.	Subcortical Leukomalacia, Multicystic Encephalomalacia.....	100
4.10.	Hippocampal Necrosis and Pontosubicular Neuron Necrosis	102
4.11.	Perinatal Brain Stem Necrosis, Moebius Syndrome, Ondine's Curse	104
4.12.	Cerebellar Hemorrhage, Olivocerebellar Transneuronal Degeneration, Cerebellar Infarction, Cerebellar Cystic Leukomalacia.....	106
4.13.	Kernicterus	108
5.	Vascular Diseases	111
5.1.	Arteriovenous Malformation	112
5.2.	Aneurysm	114
5.3.	Moyamoya Disease.....	116
5.4.	Cavernous Hemangioma and Pediatric Strokes.....	118
5.5.	Venous Thrombosis (Septic/Other).....	120

6. Increased Intracranial Pressure	123
6.1. Cerebral Edema	124
6.2. Sequelae of Hypoxic Encephalopathy During Childhood	126
7. Neurocutaneous Syndromes	129
7.1. Tuberous Sclerosis Complex (Bourneville's Disease) . . .	130
7.2. Neurofibromatosis 1 (von Recklinghausen's Disease) . . .	132
7.3. Sturge-Weber Syndrome	134
7.4. Ataxia Telangiectasia.....	136
8. Lipidosis	139
8.1. GM ₁ Gangliosidoses.....	140
8.2. GM ₂ Gangliosidosis	142
8.3. Gaucher's Disease	144
8.4. Niemann-Pick Disease.....	146
8.5. Neuronal Ceroid Lipofuscinosis.....	148
8.6. Neuronal Ceroid Lipofuscinosis.....	150
8.7. Farber's Disease, Wolman's Disease, Fabry's Disease.....	152
9. Mucopolipidosis	155
9.1. Galactosialidosis	156
9.2. I Cell Disease, Mucopolipidosis Type 2	158
9.3. Multiple Sulfatase Deficiency.....	160
9.4. Mucopolysaccharidoses	162
9.5. Sialidosis Type 2.....	164
10. Glycogen Storage Disease	167
10.1. Pompe's Disease.....	168
11. Peroxisomal Disorders	171
11.1. Zellweger's Syndrome	172
11.2. Neonatal Adrenoleukodystrophy.....	174
11.3. Adrenoleukodystrophy	176
12. Urea Cycle Disorders	179
12.1. Argininosuccinic Aciduria	180
12.2. Glutaric Aciduria	182
12.3. Ornithine Transcarbamylase Deficiency.....	184

13. Amino Acid Metabolism Disorders	187
13.1. Homocystinuria	188
13.2. Phenylketonuria and Maple Syrup Urine Disease	190
14. Mitochondrial Cytopathy	193
14.1. Wernicke's Encephalopathy	194
14.2. Subacute Necrotizing Encephalopathy of Leigh (Leigh's Syndrome)	196
14.3. Mitochondrial Encephalomyopathy, Lactic Acidosis, and Stroke-like Episode (MELAS) Syndrome	198
14.4. Alpers-Huttenlocher Syndrome (Progressive Neuronal Degeneration in Childhood With Liver Disease)	200
15. Other Heredodegenerative Diseases	203
15.1. Dentato-Rubro-Pallido-Luysian Atrophy	204
15.2. Friedreich's Ataxia	206
15.3. Lafora Body Disease	208
15.4. Rett Syndrome	210
15.5. Autism	212
15.6. Congenital Myotonic Dystrophy	214
16. Basal Ganglia Diseases	217
16.1. Wilson's Disease	218
16.2. Menkes Syndrome	220
16.3. Juvenile Huntington Disease	222
17. Neuroaxonal Degeneration	225
17.1. Infantile Neuroaxonal Dystrophy (Seitelberger's Disease)	226
17.2. Hallervorden-Spatz Disease	228
18. Leukodystrophy	231
18.1. Vanishing Leukoencephalopathy (Childhood Ataxia with Central Hypomyelination Syndrome)	232
18.2. Metachromatic Leukodystrophy	234
18.3. Krabbe's Disease (Globoid Cell Leukodystrophy or Galactosylceramide Lipidosis)	236
18.4. Alexander's Disease	238
18.5. Canavan's Disease, Spongy Degeneration of the Neuraxis (Canavan-van Bogaert-Bertrand Disease)	240
18.6. Cockayne's Syndrome, Connatal Cockayne's Syndrome	242
18.7. Pelizaeus-Merzbacher Disease	244

19. Demyelination	247
19.1. Acute Disseminated Encephalomyelitis (Postinfectious/ Postvaccination Perivenous Encephalomyelitis)	248
19.2. Acute Necrotizing Encephalopathy	250
20. Infection	253
20.1. Congenital Cytomegalovirus Infection	254
20.2. Disseminated Varicella Zoster	256
20.3. Herpes Simplex Type 1 Encephalitis	258
20.4. Japanese Encephalitis	260
20.5. Pediatric Human Immunodeficiency Virus (HIV) and Opportunistic Infection	262
20.6. Progressive Multifocal Leukoencephalitis and Acute Hemorrhagic Leukoencephalitis (Hurst's Disease)	264
20.7. Rabies, Poliomyelitis, Parvovirus B19 Infection	266
20.8. Subacute Sclerosing Panencephalitis	268
20.9. Tuberculosis	270
20.10. Acute Bacterial Meningitis and Brain Abscess	272
20.11. Fungal Infections	274
20.12. Toxoplasmosis, Congenital Toxoplasmosis	276
20.13. Amebiasis	278
20.14. Echinococcus, Trichinella Spiralis, Cysticercus	280
21. Intoxication	283
21.1. Minamata Disease	284
21.2. Fetal Alcohol Syndrome, Other Drug Intoxication	286
21.3. Carbon Monoxide Intoxication; Other Chemical and Drug Intoxication	288
22. Tumors	291
22.1. Astrocytic Tumors	292
22.2. Pilocytic Astrocytoma	294
22.3. Miscellaneous Astrocytomas	296
22.4. Ependymomas and Oligodendrogliomas	298
22.5. Choroid Plexus Tumors	300
22.6. Neuroepithelial Tumors of Uncertain Origin	302
22.7. Neuronal and Mixed Neuronal-Glial Tumors	304
22.8. Desmoplastic Infantile Astrocytoma and Desmoplastic Infantile Ganglioglioma	306
22.9. Dysembryoplastic Neuroepithelial Tumor (Grade I)	308
22.10. Embryonal Tumors	310
22.11. Medulloblastoma (Grade IV)	312
22.12. Supratentorial Primitive Neuroectodermal Tumors	314
22.13. Atypical Teratoid/Rhabdoid Tumor (Grade IV)	316
22.14. Peripheral Neuroblastic Tumors	318
22.15. Pineal Parenchymal Tumors	320
22.16. Meningeal Tumors	322

22.17.	Tumors of the Sellar Region: Developmental Mass Lesions and Cysts	324
22.18.	Developmental Masses and Cysts	326
22.19.	Tumors of the Hematopoietic System.....	328
22.20.	Germ Cell Tumors	330
22.21.1.	Tumors of Cranial and Peripheral Nerves: Schwannoma and Neurofibroma	332
22.21.2.	Tumors of Cranial and Peripheral Nerves: Perineurinoma and Malignant Peripheral Nerve Sheath Tumor	334
22.22.	Familial Tumor Syndromes Involving the Nervous System	336
23.	Motor Neuron Disease	339
23.1.	Spinal Muscular Atrophy (Werdnig-Hoffmann Disease)	340
24.	Peripheral Neuropathy	343
24.1.	Peripheral Neuropathy Diseases	344
24.2.	Hereditary Motor and Sensory Neuropathies (Charcot-Marie-Tooth Disease)	346
24.3.	Hereditary Sensory and Autonomic Neuropathies	348
25.	Muscle Disease	351
25.1.	Muscle Development	352
25.2.	Classification of Muscle Disease: Normal Muscle Structure	354
25.3.	Progressive Muscular Dystrophy	356
25.4.	Congenital and Other Muscular Dystrophies (Merosin Deficiency, Fukuyama Congenital Muscular Dystrophy)	358
25.5.	Congenital Myotonic Dystrophy and Late-Onset Myotonic Dystrophy	360
25.6.	Congenital Myopathies; Myopathies With Abnormal Structure	362
25.7.	Inflammatory Myopathies	364
25.8.	Metabolic Myopathies	366
25.9.	Mitochondrial Cytopathies	368
25.10.	Miscellaneous Muscle Pathology	370
25.11.	Muscle in Neurogenic Disorders	372
26.	Epilepsy	375
26.1.	Ammon's Horn Sclerosis	376
26.2.	Microdysgenesis	378
26.3.	Epilepsy with Inflammatory Lesions	380

26.4.	Malformations and Epilepsy	382
26.5.	Tumors and Epilepsy	384
27. Accidents, Sudden Death		387
27.1.	Trauma During Infancy	388
27.2.	Sudden Infant Death Syndrome	390
27.3.	Child Abuse	392
References		395
Subject Index		407

1 Normal Development

1.1 Developmental Characteristics of the Fetal Brain: Gross Brain

Characteristics of Fetal Cerebral Hemispheres

The cerebral surface develops gradually from the fetal flat (lissencephalic) brain to the adult gyral pattern, increasing the cortical surface area until the second year of life. The sylvian fissure is apparent at approximately 14 weeks' gestation (GW). The primary sulci, such as rolandic, calcarine, superior temporal, and precentral sulci, appear after 20 GW, the secondary sulci appear from 28 GW, and the tertiary sulci from 36 GW. The gestational age of a brain can be estimated by counting the number of convolutions (gyri) crossed by a line drawn from the frontal to the occipital pole above the insula and adding 21 to the gyral count [1]. Gestational age can also be estimated by counting gyri and sulci in neuro-

images [ultrasonography and magnetic resonance imaging (MRI)].

The posterior horns of lateral ventricles are large (colpocephalic) during the second trimester of fetal life. The volume of the germinal matrix increases until 26 GW and begins to decrease at 30 GW. The germinal matrix, or neuroepithelium, persists as small islands in the wall of the ventricle until after birth. The largest island is the ganglionic eminence between the thalamus and the caudate. It is present at birth and disappears during the first year of life [2]. The periventricular germinal matrix produces neural stem cells in the innermost zone of the epithelium. These progenitor cells first produce neurons, which are translocated and migrate toward their final destination. The immature astrocytes and oligodendrocytes differentiate and migrate later.



Fig. 1.1-1. Fetal brain at 23 weeks' gestation, lateral view. The Sylvian fissure is widely open, and the first sulci are found in the central area.

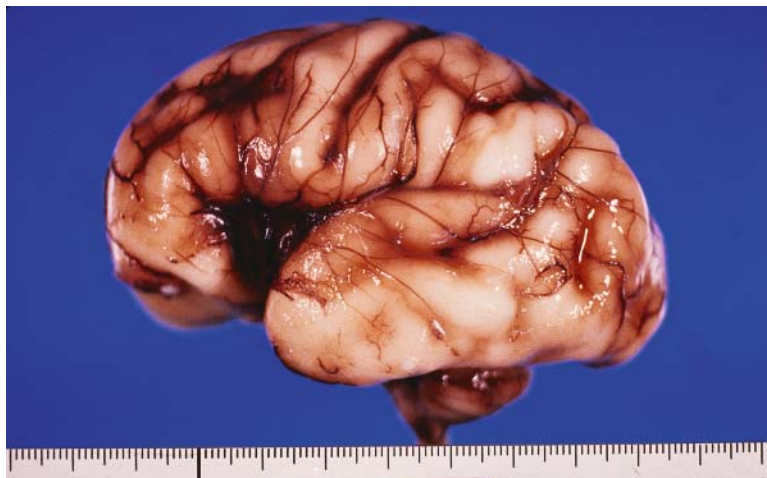


Fig. 1.1-2. Fetal brain at 31 weeks' gestation, lateral view. The sylvian fissure is slightly open, and secondary sulci are found in the whole hemisphere.



Fig. 1.1-3. *Left.* basal view of the fetal brain in **1.1-1**. The cerebellum is very small compared with the brain stem. *Right.* Horizontal section of the fetal brain in **1.1-1**. Posterior horns are large in the very immature brain.

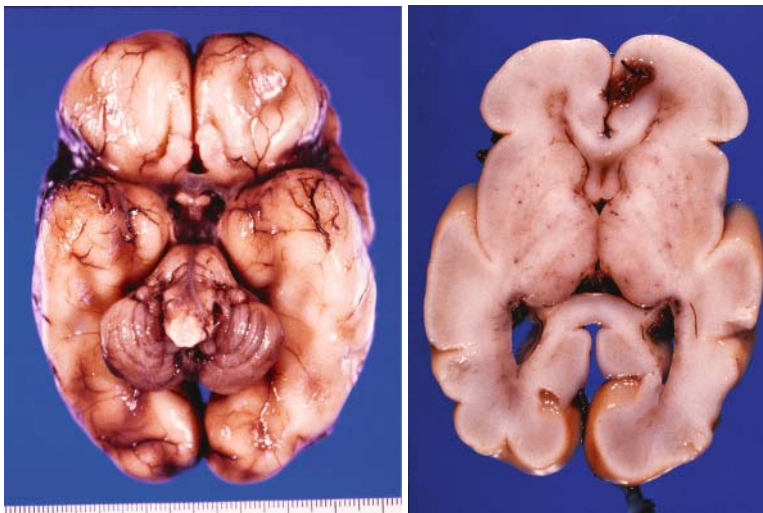


Fig. 1.1-4. *Left.* Basal view of the fetal brain seen in **1.1-2**. The cerebellum is still small. *Right.* Horizontal section of the fetal brain seen in **1.1-2**. Posterior horns are still large in the preterm fetus. The cavum septi pellucidi is normally present in all fetuses and newborns and disappears during the first 2 years.



Fig. 1.1-5. Preterm fetal brain. The coronal section shows no sulcus formation (except sylvian fissures) and a thick subependymal germinal layer. H&E.

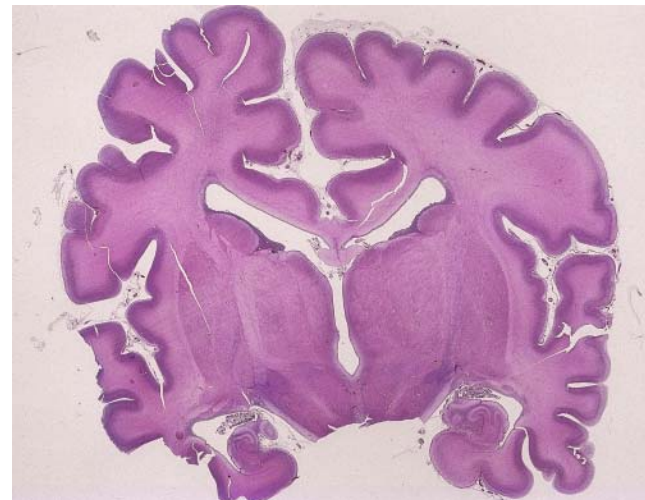


Fig. 1.1-6. Term neonatal brain. The coronal section shows various depths of sulci and little subependymal germinal layer. H&E.

1.2 Developmental Characteristics of Neurons

Neurons, astrocytes and oligodendrocytes are derived from neural stem cells in the neuroepithelium of the ventricular wall [3]. Neurons develop in a caudal-rostral order from spinal cord to cerebral cortex. Those in the spinal cord and brain stem develop during the early fetal period; most neurons in the cerebral and cerebellar cortex develop and mature during the late fetal and infantile periods.

In the telencephalon, at 6–8 GW, Cajal Retzius (CR) and subplate neurons migrate from the neuroepithelium to form the preplate [4]. Subsequently, maturing pyramidal cortical neurons migrate along the radial glia [5] separating the CR and subplate neurons to form the six-layered cerebral cortex. The neurons of layer VI migrate first in an “inside-out” sequence. Tangential migration of granular neurons follows, completing the population of the cortex. Proteins such as Lis-1 [6] and Reelin [7] regulate neuronal migration and cortical

organization. Reelin is produced by the CR neurons. A superficial granular layer, originating from the periventricular germinal epithelium, appears transiently underneath the leptomeninges of the cortex at 13–39 GW [8].

In the cerebellum Purkinje cells from the alar plate of the neural tube and the granule cells from the rhombic lip migrate toward the cortex of cerebellar folia, forming a complex circuitry with the brain stem, spinal cord, cerebellar nuclei, and basal ganglia. The external granular cell layer is under the control of *Math1*, which influences the normal development of the internal granular cell layer [9]. The maturation of the cerebellum lags behind the cerebral hemisphere, so mature numbers of folia and of internal granular neurons develop after birth. Involution of the external granular layer proceeds until 1 year of age. The maturation of the vermis occurs before that of the cerebellar hemispheres [10].

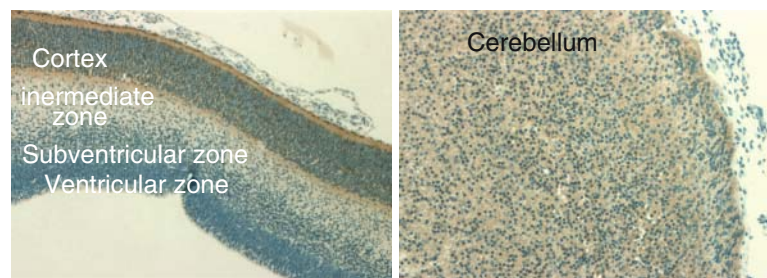


Fig. 1.2-1. The developing telencephalon and cerebellum at 14 weeks.

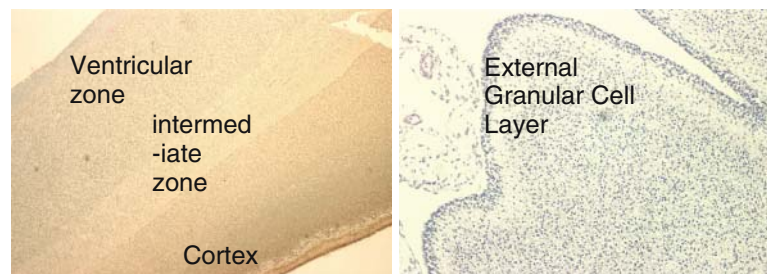


Fig. 1.2-2. The developing telencephalon and cerebellum at 17 weeks.

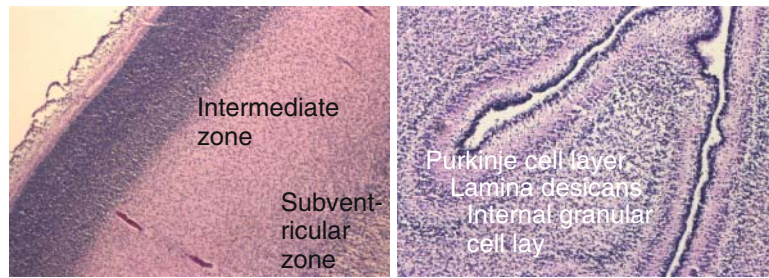


Fig. 1.2-3. The developing cerebral hemisphere and cerebellum at 19 weeks.

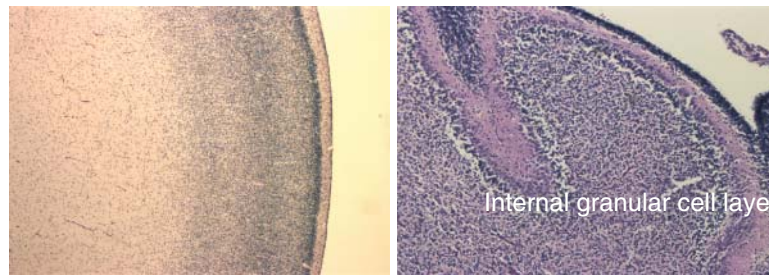


Fig. 1.2-4. The developing cerebral cortex and cerebellum at 28 weeks.

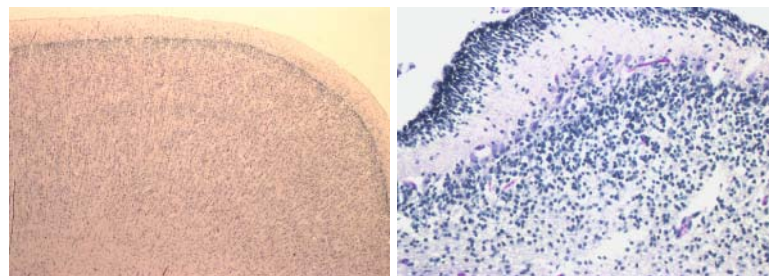


Fig. 1.2-5. The developing cerebral cortex and cerebellum at 33 weeks.

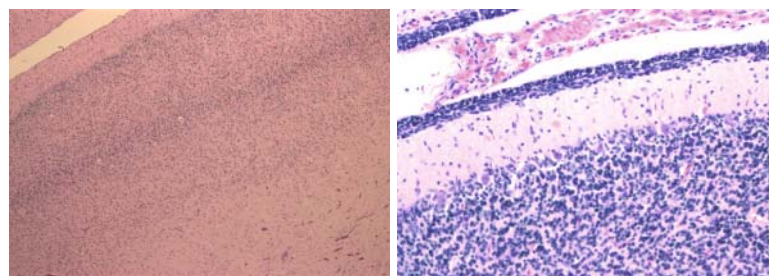


Fig. 1.2-6. The developing cerebral cortex and cerebellum at 40 weeks.

1.3 Dendritic and Synapse Development

Neurons are composed of soma, dendrites, and axons. The soma (nucleus and cytoplasm) has a variable shape and size depending on its location in the brain and its function. The soma of the developing neuron extends several neurites: one becomes the axon, developing pre-synaptic specializations; the others become dendrites, developing postsynaptic specializations. Many factors determine the destiny of the neurites. Axons produce growth cones that are guided to target neurons by extracellular matrix, the cell surface, and diffusion molecules. Some factors cause revulsion, inhibition, or cessation of movement. Neuronal survival is influenced by factors from the neurons they innervate, synaptic inputs, and neighboring neurons and glia. The point of communication between neurons is the synapse, formed when the growth cone contacts an appropriate “postsynaptic cell”; and there is expression of chemical transmitters required

for neural transmission. The synapse is about $1\mu\text{m}$ in size and is localized to dendritic protrusions, the spines [11,12]. In the immature brain, neuronal somas are closely packed. When the neurons mature, the packing density decreases as the individual neurons develop expanding dendritic branches and axonal arborizations.

Dendritic and spine development can be defined in camera lucida drawings of Golgi preparations. Dendritic and synaptic development of neurons varies in each area of the cerebral cortex. For example, the neurons in the motor cortex mature a month ahead of those in the visual cortex. Within the cortical layers there is also variation in the time of dendritic maturation. For example, at 20 GW basal dendrites are developed only in the deeper pyramidal cell layers [11,13].

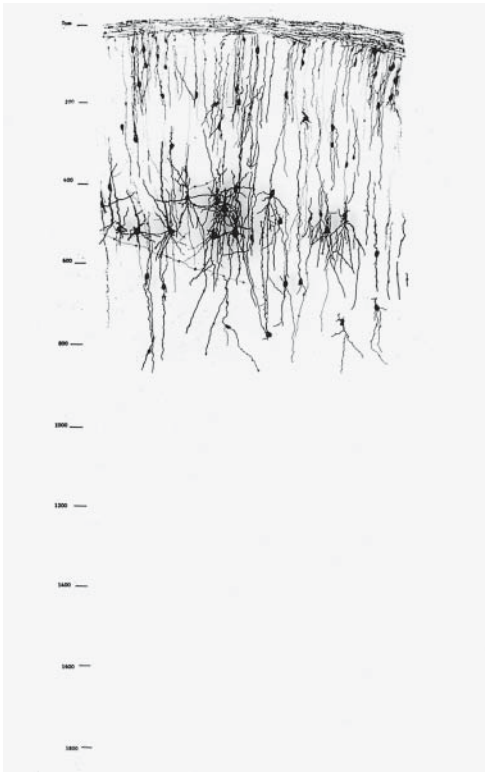


Fig. 1.3-1. The visual cortex at 24 weeks' gestation. The cell processes of superficial and poorly differentiated neurons remain attached to the pia. The deep pyramidal neurons are relatively developed, exhibiting short basal dendrites.

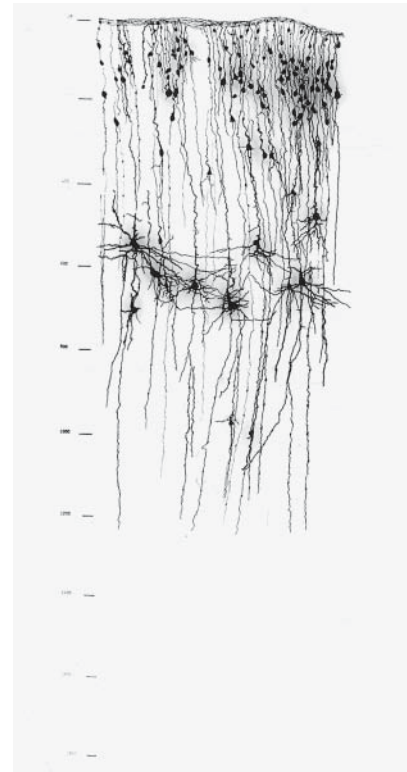


Fig. 1.3-2. At 28 weeks' gestation the superficial neurons are poorly differentiated. Layer 3 pyramidal neurons are more developed, with small branched basal dendrites and occasional spines on the apical dendrites. Layer 5 neurons have more basal dendrites and spines.



Fig. 1.3-3. At 40 weeks' gestation (term) there is a marked increase in the number of satellite and other association neurons. Fusiform cells are present in the deepest cortical layers. Spines are less on the proximal portions of pyramidal cell dendrites and are increased on the more distal portions of dendrites.



Fig. 1.3-4. At 6 months of age many more stellate neurons have appeared. The length and thickness of dendrites has increased, and apical dendrites have numerous branches.

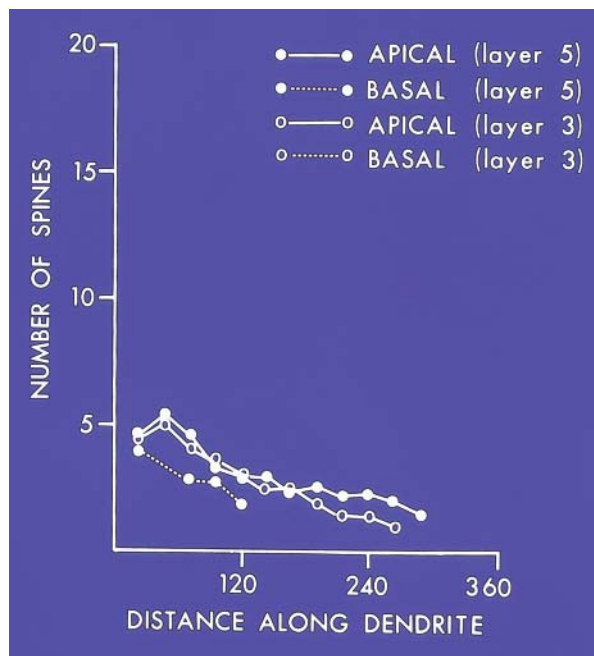


Fig. 1.3-5. At 28 weeks' gestation there are more spines on the proximal dendrites than on the distal dendrites.

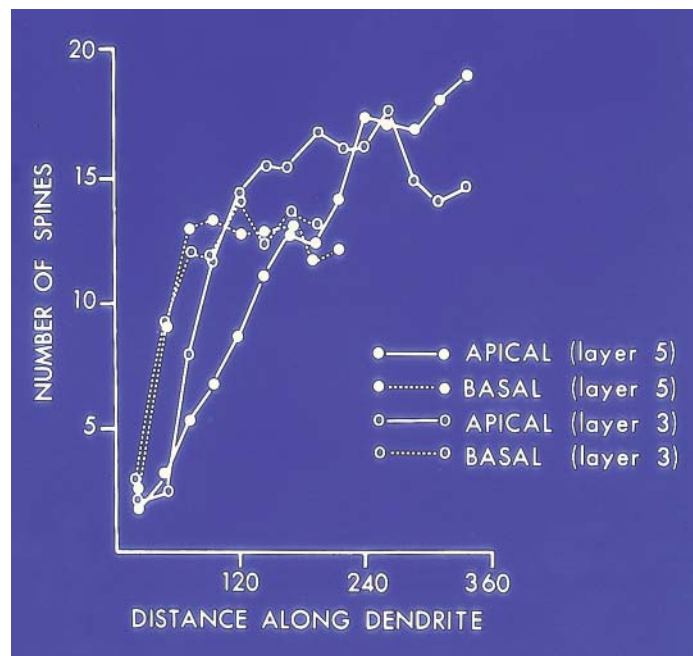


Fig. 1.3-6. At 6 months of age, there is a small number of spines on the proximal portions of the apical and basal dendrites. The numbers gradually increase with increasing distance from the neuronal soma.

1.4 Glial Development and Myelination in the Cerebral White Matter

The glial cells are the astrocyte, the oligodendroglial cell, and the microglial cell. The astrocyte and oligodendrocyte arise from specific neural precursor cells and migrate from the germinal matrix. There are several astrocytic types based on their morphology and position in the nervous system: The protoplasmic astrocyte has glutamate transporters and contributes to the blood–brain barrier; the reactive astrocyte shows marked glial fibrillary acidic protein (GFAP) immunoreactivity and contains nerve growth factors. There are Bergman astrocytes in the cerebellum, Müller cells in the retina, and radial glia in cerebral vesicles during development. The astrocyte, which has been identified to have voltage-gated ion channels and receptors for neurotransmitters, serves important functions in brain development, maintaining neurons, and the blood–brain barrier. The oligodendroglial cell is responsible for the production and

maintenance of myelin. Myelination glia are immature forms of oligodendroglia with pale vesicular nuclei, nucleoli, and wispy tails of eccentric cytoplasm [8]. The maturing oligodendroglial cells can be identified by markers: the late oligodendroglial progenitor (NG2 proteoglycan+, O1+), the immature oligodendrocyte (O4+O1+), and the mature oligodendrocyte (myelin basic protein +) [14,15]. They are increased during the premyelination period. Microglia are the resident macrophages of the brain and are derived from mononuclear phagocyte precursor cells, which enter the brain during the period of developmental cell death. They are small, elongated bipolar cells with several finger-like processes and are ubiquitous in the parenchyma; they react to brain injury by producing cytokines [16,17], proteases, and nitric oxide.

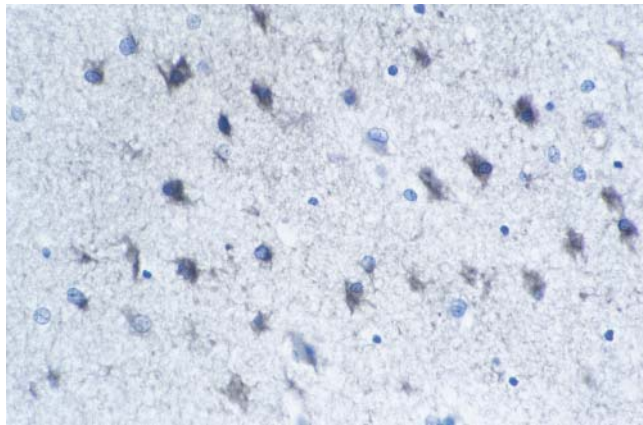


Fig. 1.4-1. Astrocytes in the cerebral white matter of a neonate identified by glial fibrillary acidic protein (GFAP) immunohistochemistry. The number of GFAP-positive astrocytes transiently increases from the perinatal period to the infantile period, and their location shifts from the deep white matter to the superficial white matter [18].

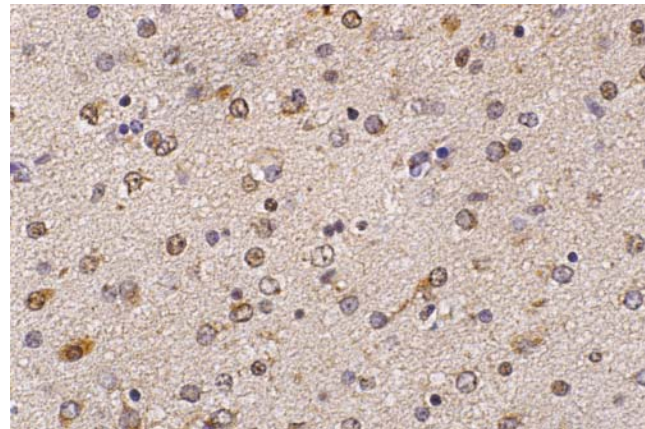


Fig. 1.4-2. Oligodendroglia identified with immunoreactivity to myelin basic protein (MBP) in the internal capsule. Myelination first occurs in the pallidothalamic fibers of the posterior internal capsule at 25 weeks' gestation [16].

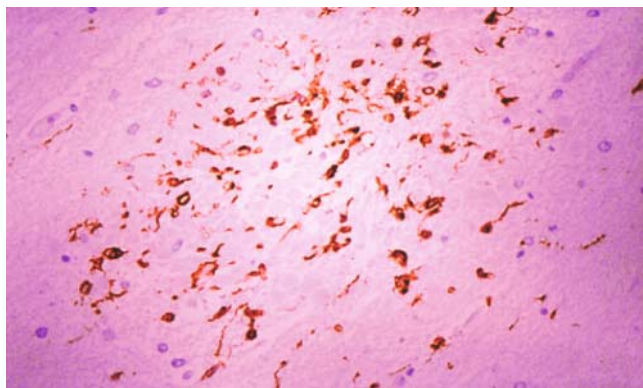


Fig. 1.4-3. Microglia in a region of necrosis identified by ionized calcium-binding adaptor molecule 1 (Iba1) immunohistochemical stains. Iba1 is used as a marker of activated microglia, and it transiently increases in the perinatal white matter of normal brains [17].

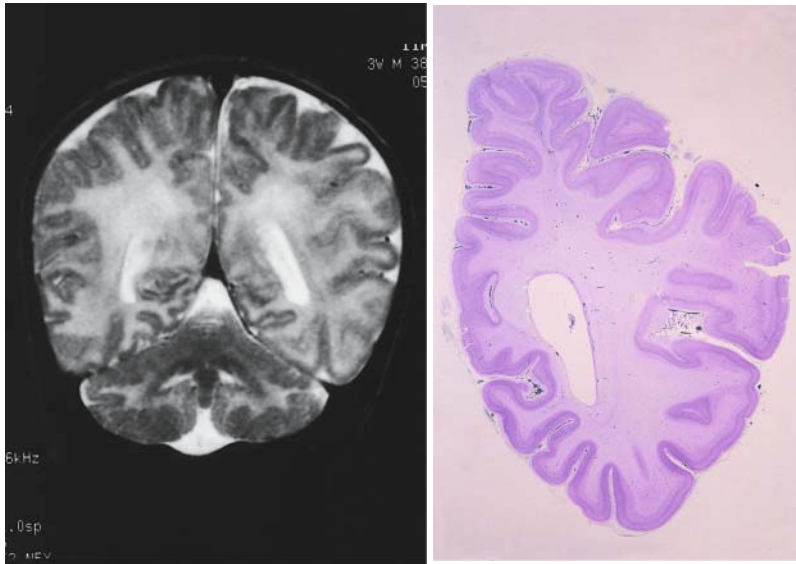


Fig. 1.4-4. Myelination of cerebral white matter at 40 weeks' gestation represented in a T2-weighted magnetic resonance (MR) image and a whole mount of brain stained with luxol fast blue (LFB).

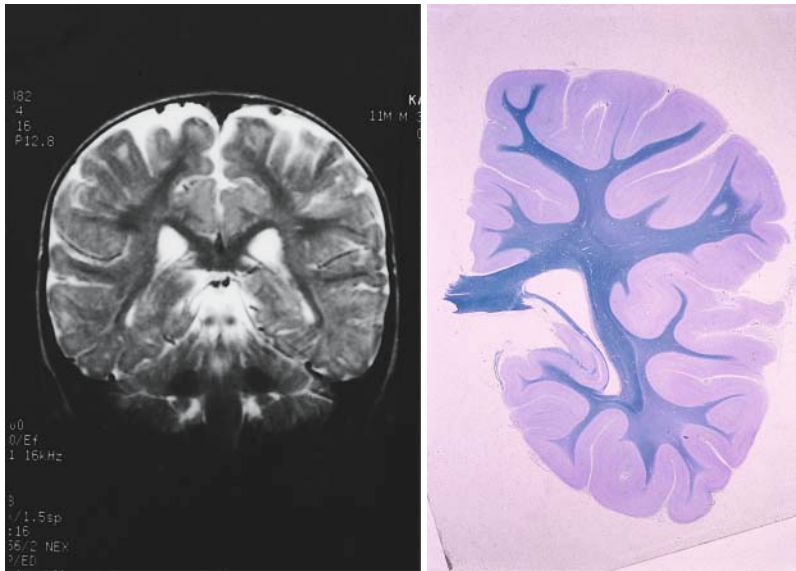


Fig. 1.4-5. Myelination of cerebral white matter at 8 months represented in a T2-weighted MR image and in a whole mount of brain stained with LFB.

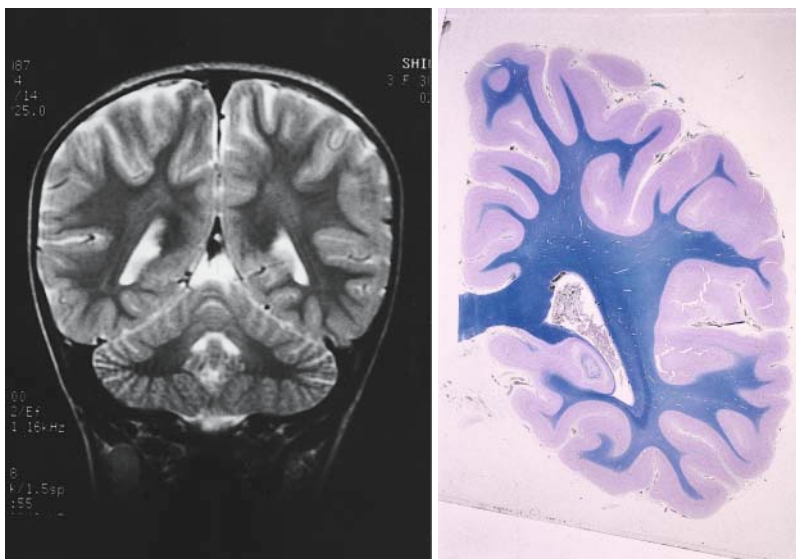


Fig. 1.4-6. Myelination of cerebral white matter at 3 years represented in a T2-weighted MR image and in a whole mount of brain stained with LFB.

1.5 Vascular Architecture in Developing Brains

The vascular pattern in the meningeal vessels varies with gestational age. The anterior, middle, and posterior cerebral arteries appear during the fourth month of gestation. The middle cerebral artery spreads out more rapidly with aging than the other cerebral arteries. In the venous system, the superior, inferior, anterior, and posterior cerebral veins are present. The superior, inferior, and posterior cerebral veins develop most rapidly.

In the cerebral hemispheres, the perforating arteries branching from the leptomeningeal arteries supply the cortex and underlying superficial and deep white matter as the cortical, subcortical, and medullary arterial branches, respectively. As the brain matures with the formation of gyri, the medullary arteries arising from the sulci appear shorter and their number of lateral branches increases.

The venous drainage of the cerebral mantle is divided, with cortical and subcortical veins draining into the meninges, and medullary veins from the deep white matter draining toward the ventricle. The deep white matter is drained by a fan-shaped array of medullary veins that flow vertically into the subependymal veins. The medullary veins in the deep cerebral white matter mature before the subcortical veins and before the arteries of the deep white matter [19]. This developmental discrepancy between deep white matter arteries and veins may be a predisposing factor for periventricular leukomalacia (PVL) and periventricular white matter hemorrhage [20].

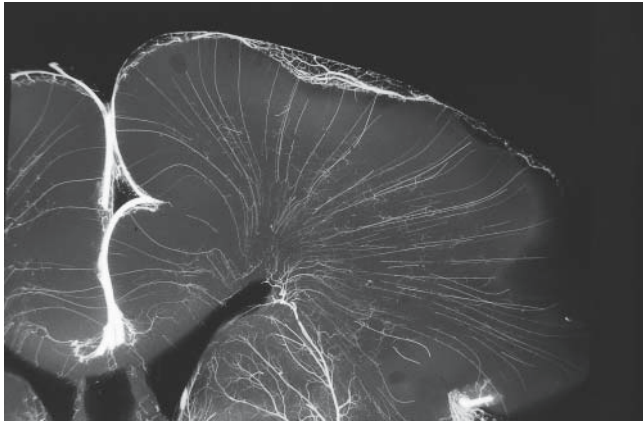


Fig. 1.5-1. Arterial architecture of the frontal lobe in a preterm neonate at 26 weeks' gestation.



Fig. 1.5-2. Arterial architecture of the cerebral hemisphere in a preterm neonate at 30 weeks' gestation.

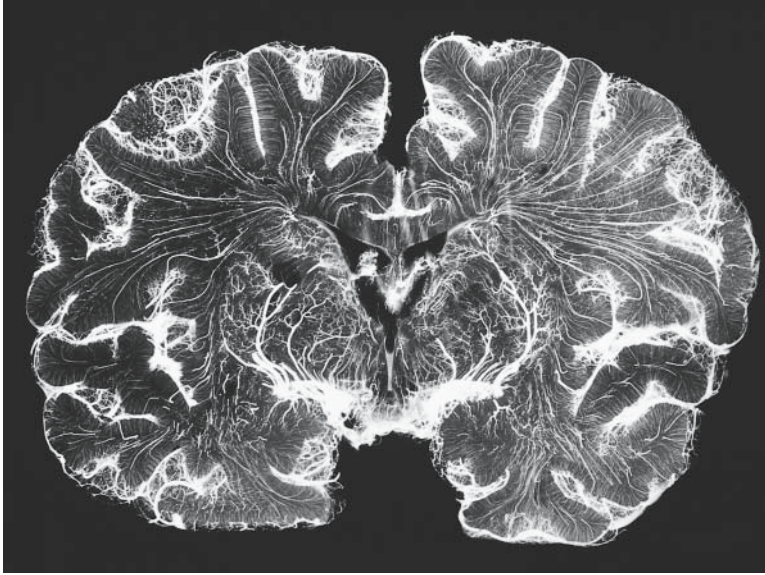


Fig. 1.5-3. Arterial architecture of the cerebral hemispheres at the level of the mammillary body in a 1-year-old child.

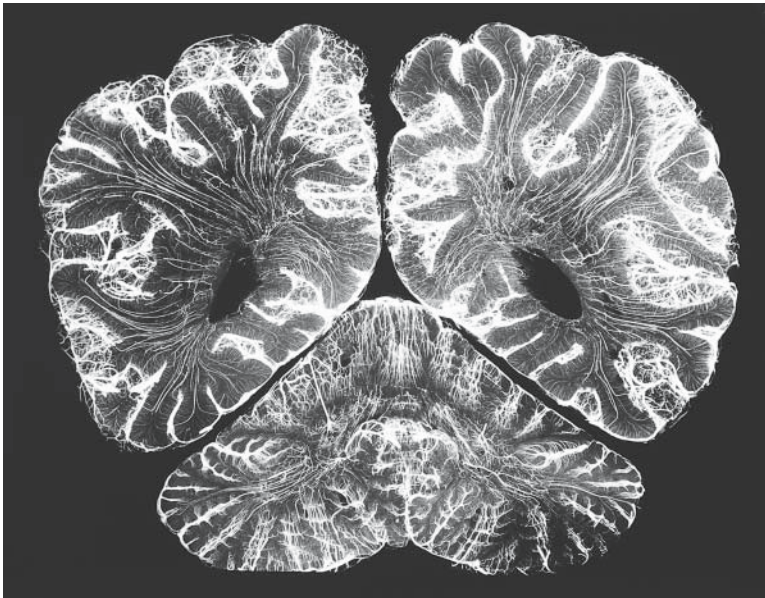


Fig. 1.5-4. Arterial architecture of the cerebral hemispheres and cerebellum at the level of the occipital horn in a 1-year-old child.



Fig. 1.5-5. Venous architecture of the cerebral hemisphere in a preterm neonate at 28 weeks' gestation. Note the brush-like veins in the subependymal matrix.

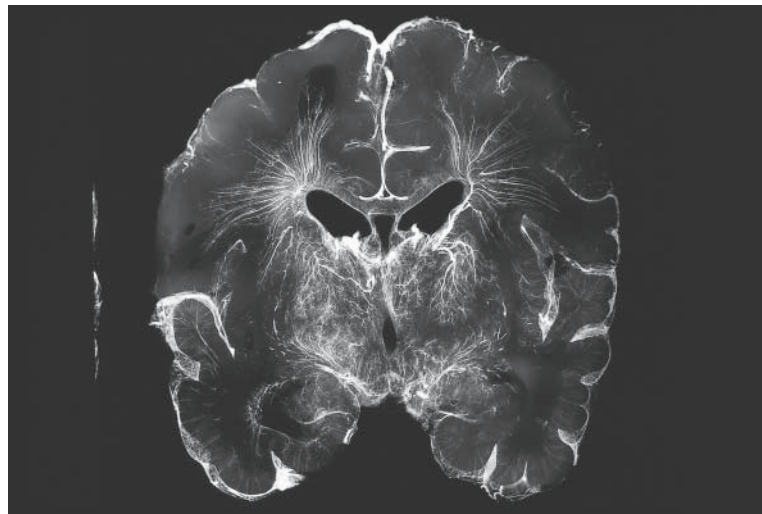


Fig. 1.5-6. Venous architecture of the cerebral hemisphere in a full-term neonate.

2 Malformations

2.1 Neural Tube Defects, Anencephaly

The brain and upper spinal cord form from the neural plate during primary neurulation beginning at 22 days' gestation; the sacral spinal cord forms from the tail bud during secondary neurulation [1]. The various classifications of neural tube defects (NTDs) is complex and somewhat contradictory [2]. Practically, they can be considered as "open" (e.g., anencephaly, craniorachischisis, myelomeningocele) or "closed" (e.g., encephaloceles, meningoceles, split spinal cord). There are several pathoetiologies [3]. Folic acid supplementation before and during early pregnancy prevents most NTDs [3,4]. A mutant mouse model for NTD, *Spotch*, is being used to define the mechanism of teratogenesis by folate insufficiency [5]. A second mutant, *curly tail*, has an NTD that responds to myoinositol [6].

Craniorachischisis is the most severe form of NTD in which the brain and spinal cord are exposed to the surrounding amniotic fluid, resulting in neural tissue degeneration and angioma-like formations. Anencephaly is characterized by the absence of the calvarium and abnormalities of the base of the skull and the sphenoid bone with shallow orbits causing protrusion of the eyes. The cerebral hemispheres are replaced by the area cerebrovasculosa, a mass of neuroglial tissue and vessels. Exencephaly is rarely described in human fetal brain because the brain tissues usually become necrotic when exposed to amniotic fluid; the exencephalic appearance is converted to anencephaly by mid to late gestation [7].



Fig. 2.1-1. Craniorachischisis. Anencephaly with cervical rachischisis in a fetal case at 19 gestational weeks (GW).



Fig. 2.1-2. Anencephaly with the area cerebrovasculosa in the head.



Fig. 2.1-3. Acalvaria (acrania). The head appears intact but lacks the calvarium (skull cap).

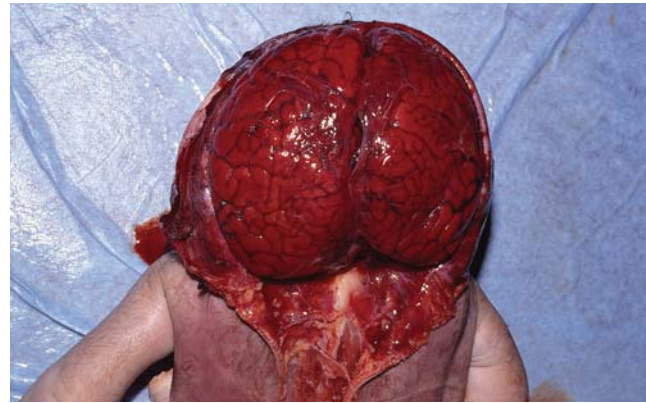


Fig. 2.1-4. Acrania (same case as in 2.1-3). The brain situated underneath the skin and scalp appears complete.

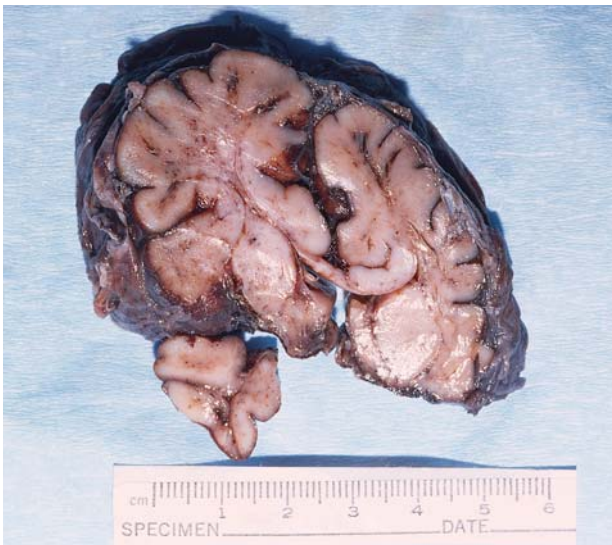


Fig. 2.1-5. Acrania (same case as in 2.1-3). Coronal section of both hemispheres shows relatively normal gyral formation.

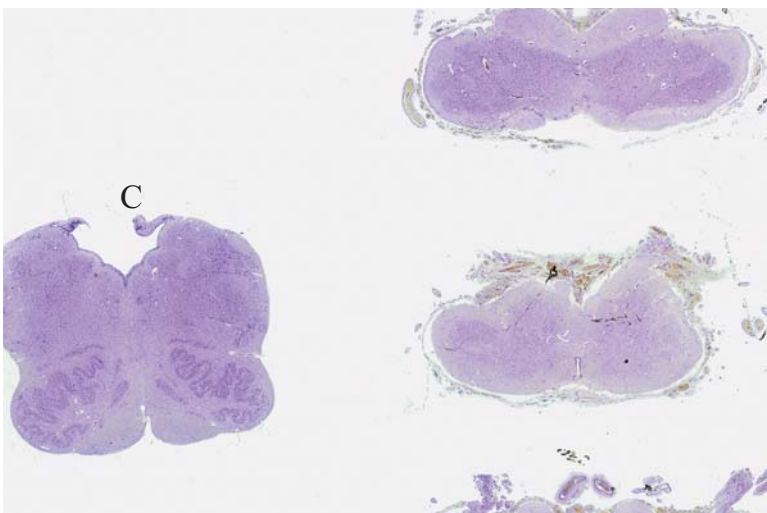


Fig. 2.1-6. Acrania (same case as in 2.1-3). The brain stem (right) is small compared with that of a normal age-matched control (*left*). H&E.

2.2 Meningoencephalocele, Encephalocele

A meningocele is the herniation of dura and arachnoid through a vertebral or calvarial defect, with the spinal cord or brain remaining in the spinal canal or cranium. A midline vertebral or cranial defect without any herniation is termed spina bifida or cranium bifidum respectively. Myelocele or encephalocele consists of a developmental vertebral or cranial defect through which there are herniations of the spinal cord or brain tissues.

Meningomyelocele or meningoencephalocele is herniation of part of the brain or spinal cord and meninges through a vertebral or calvarial defect associated with

skin and hair abnormalities. In 80% of meningoencephalocele cases, the defect occurs in the occipital region and is associated with skin abnormalities. Occipital encephalocele occurs through the occipital bone and contains fragments of disorganized cerebral hemispheres with ventricular cavities. Polymicrogyria may be associated with meningoencephaloceles. The occipital encephalocele is an important component of Meckel-Gruber syndrome, which is a lethal autosomal recessive disorder that maps to 17q21–14 and consists of polydactyly, polycystic kidney, hepatic fibrosis, and various brain malformations (see Section 2.24) [2].



Fig. 2.2-1. Occipital meningoencephalocele in a fetus of 20 weeks' gestation.



Fig. 2.2-2. Lateral views of the brain in 2.2-1 shows a meningoencephalocele at the level of the cerebellum.

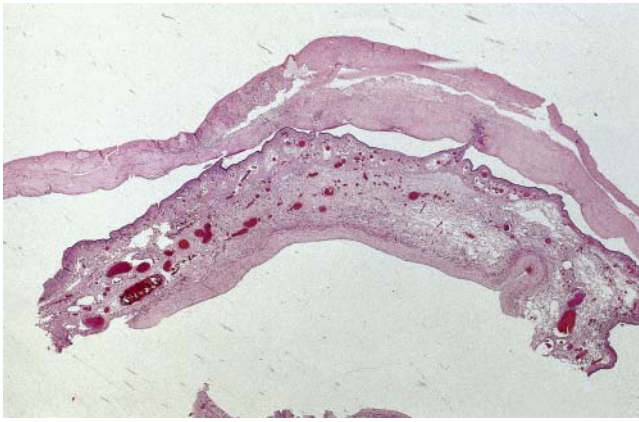


Fig. 2.2-3. Meningoencephalocele of a fetus. Histology shows spongy changes and increased vascularity in thin cerebral hemisphere under thick meninges and normal skin. H&E.



Fig. 2.2-4. Meningoencephalocele of a fetus. Note the marked astrogliosis in the molecular layer and part of the cellular layer of the cortex. GFAP immunohistochemical stain.

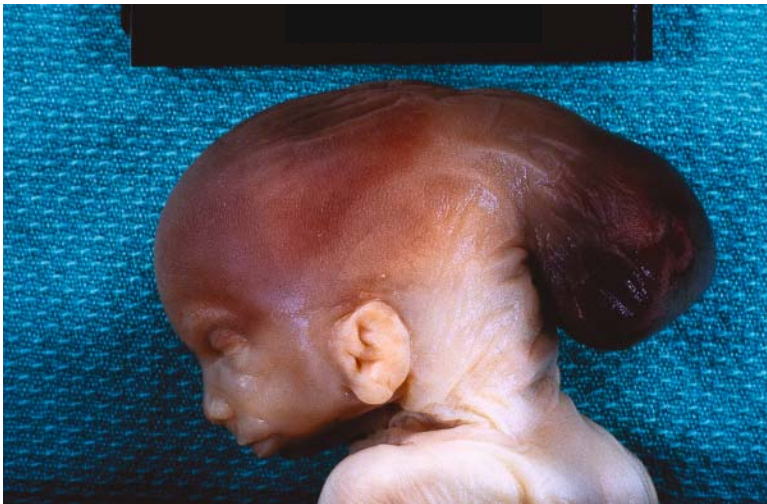


Fig. 2.2-5. Meckel-Gruber syndrome in a term neonate. This lethal autosomal recessive syndrome consists of occipital encephalocele, polydactyly, polycystic kidney, and hepatic fibrosis with bile duct proliferation.



Fig. 2.2-6. Meningoencephalocele in the nuchal region.

2.3 Iniencephaly

Iniencephaly is a rare axial dysraphic complex malformation characterized by (1) an occipital bone defect, (2) cervical dysraphic changes, and (3) retroflexion of the whole spine [8,9]. Iniencephaly differs from anencephaly in that the cranial cavity is present and skin covers the head and retroflexed region [9]. Severe retroflexion of the neck is found by fetal ultrasonography and magnetic resonancy imaging (MRI).

Anomalies of the central nervous system (CNS) may be numerous, ranging from lesions similar to those in anencephaly to less-advanced dysgenesis of the brain.

NTDs affecting the spinal cord consist of iniencephaly, meningocele, and meningomyelocele. Iniencephaly is characterized by spina bifida of the cervical vertebrae usually associated with anomalies of the brain stem.



Fig. 2.3-1. Iniencephaly: retroflexion of the neck.

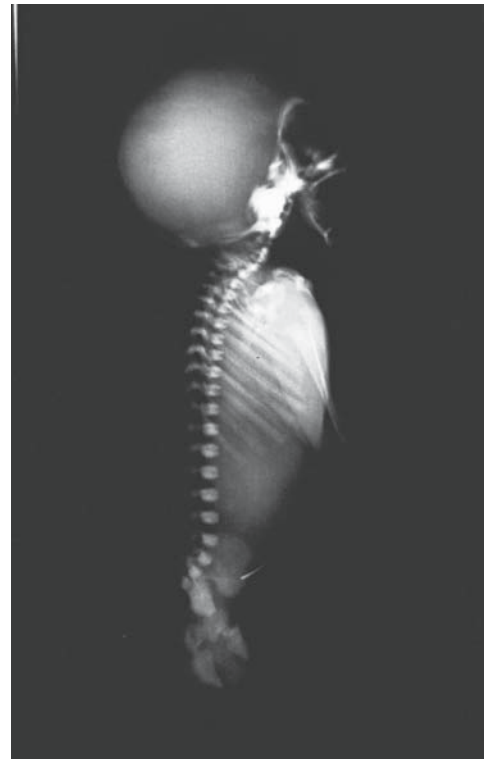


Fig. 2.3-2. Iniencephaly. Radiograph from lateral side of the whole body.



Fig. 2.3-3. Iniencephaly in a term neonate. Iniencephaly is characterized by spina bifida of the cervical vertebrae usually associated with abnormalities of the brain stem.



Fig. 2.3-4. Iniencephaly of the brain and spinal cord, viewed from below. Note the asymmetry of the cerebral hemispheres, small cerebellum, and cervical spinal cord.



Fig. 2.3-5. Iniencephaly viewed from above. Note the asymmetry of the cerebral hemispheres.

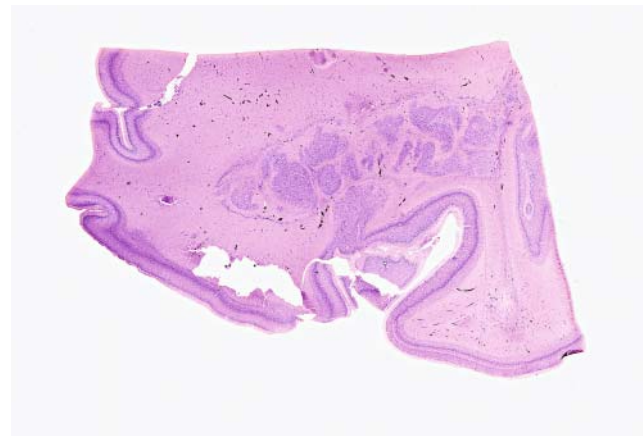


Fig. 2.3-6. Iniencephaly: section of cerebral hemisphere. Note the subcortical heterotopia. H&E.

2.4 Spinal Dysraphisms

Malformations related to defects of the neural tube are known as dysraphic disorders. Spina bifida is a less severe type of anomaly, consisting of a failure of fusion of the posterior lamina of the spinal canal. The defects of the neural tube that involve the spinal cord include a range of malformations, from mild to severe [2]. A meningocele results when there is herniation of dura and arachnoid meninges through the spinal defect; the spinal cord remains in the canal. In the meningocele, a more severe malformation, there is a herniated sack containing spinal cord elements with meninges. This may be covered by thin skin or may be open, exposing the dorsally placed spinal cord, which is surrounded by a vascular network, the so-called zona medullovasculosa [10]. Most patients with a meningocele

have an associated Chiari malformation. The spinal cord rostral to a meningocele can demonstrate various malformations. For example, hydromyelia, syringomyelia of the cervical spinal cord, or partial or complete diastematomyelia can occur in 20%–50% of meningocele patients [11]. Hydromyelia is a dilatation of the central canal of the cord, and syringomyelia is a slowly progressive cavity formation in the spinal cord that rarely occurs in infants. Hydromyelia is usually asymptomatic. In syringomyelia there is cavity formation involving the area of the anterior white matter commissure that interrupts crossing fibers of the lateral spinothalamic tracts, causing bilateral loss of temperature and pain sensation.



Fig. 2.4-1. Neural tube defect (NTD). This is an open NTD, a meningocele, with abnormal skin around an exposed abnormal “neural placode” and meninges exposed through a nonfused spine.

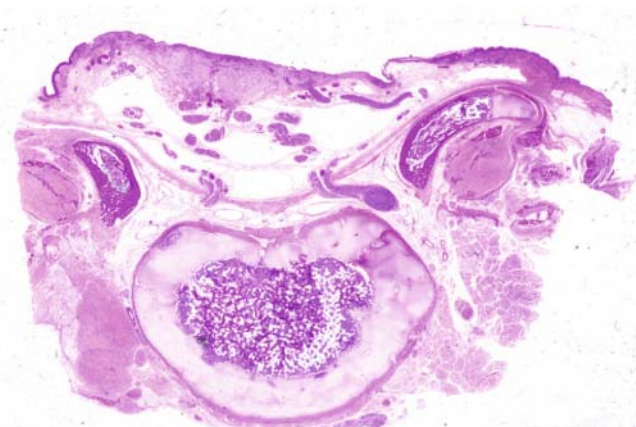


Fig. 2.4-2. Microscopy of the protrusion of the posterior part of the spinal cord due to myelocele. There is marked astrogliosis and loss of neurons and myelin sheaths. H&E.



Fig. 2.4-3. Arnold-Chiari malformation type 1. Protrusion of tonsils into the foramen magnum.

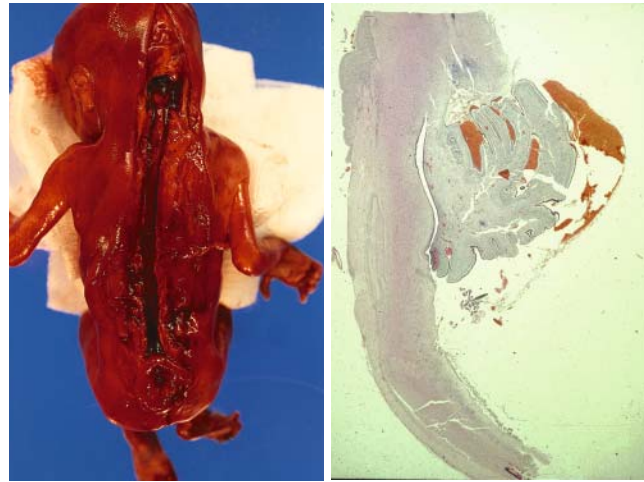


Fig. 2.4-4. Arnold-Chiari malformation type 2 in a 20-GW fetus. *Left.* Gross photograph with the spinal cord dissected to show the displaced cerebellar tonsils in the cervical subarachnoid space. *Right.* Whole mount of the hindbrain reveals the elongated brain stem, the displaced vermis, and narrowing of the fourth ventricle. H&E.

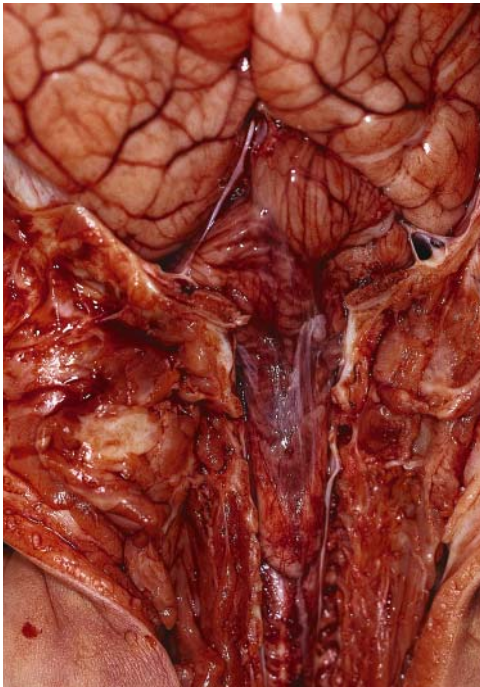


Fig. 2.4-5. Arnold-Chiari malformation type 2 demonstrating, in a posterior view, the protrusion of tonsil and vermis below the foramen magnum with buckling of the cord.

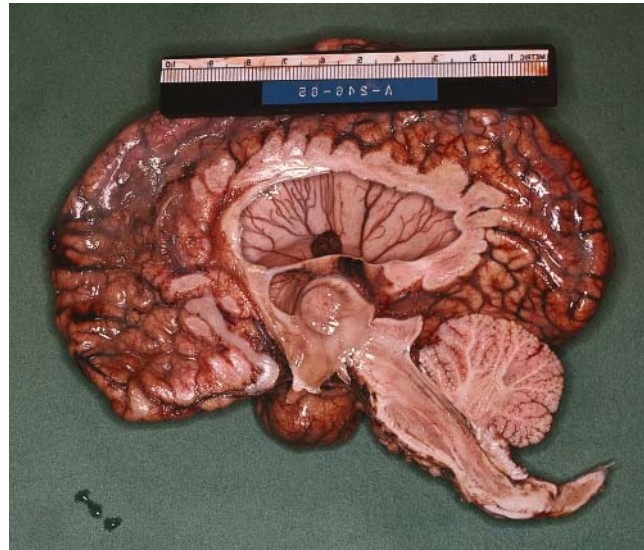


Fig. 2.4-6. Arnold-Chiari malformation type 2. Sagittal section of a child's brain demonstrates elongation of the brain stem and vermis with narrowing of the fourth ventricle, hydrocephalus, and buckling of the upper cervical spinal cord.

2.5 Chiari (Arnold-Chiari) Malformations

Four types of cerebellar malformation have been classified as Chiari malformations, but type 4 is considered by some to be a separate entity [2].

Type 1: Cerebellar tonsils in the foramen magnum.

Type 2: Cerebellar tonsils or vermis, medulla oblongata, and the fourth ventricle are displaced into the foramen magnum. This type is generally known as classic Arnold-Chiari malformation and is commonly associated with a small posterior fossa, lumbar meningo-myelocele, aqueduct stenosis, beaking of midbrain tectum, hydrocephalus, and other defects.

Type 3: Cerebellar suboccipital encephalocele. This type may be associated with an elongated brain stem, beaking of tectum, and lumbar spina bifida.

Type 4: Cerebellar hypoplasia.

The precise mechanism of type 2 and 3 Arnold-Chiari malformations is unknown. Several theories have been proposed: (1) tethering of brain at the brain stem–cervical cord junction; (2) cerebrospinal fluid (CSF) pressure causing excessive localized brain stem pressure and distortion; (3) hypoplasia of the posterior cranial fossa bony structures.

Recently, prenatal surgery at midgestation to stop the leakage of CSF is being attempted to allow more normal growth of the brain stem and cerebellum [12].



Fig. 2.5-1. Arnold-Chiari type 3. Postoperative state of occipital meningoencephalocele.



Fig. 2.5-2. Arnold-Chiari type 3. The base of the brain. Note the elongation of the cerebellar hemispheres and the defect of the vermis.



Fig. 2.5-3. Arnold-Chiari type 3. Coronal section of both cerebral hemispheres shows marked dilatation of the lateral ventricles and periventricular cysts.



Fig. 2.5-4. Arnold-Chiari type 3. There is elongation of the cerebellar hemispheres and fourth ventricle as well as a defective vermis.



Fig. 2.5-5. Arnold-Chiari type 3. Lateral view of the cerebellar hemispheres. The midbrain has beaking of the tectum and a small aqueduct. The pons is anterior to an elongated fourth ventricle.

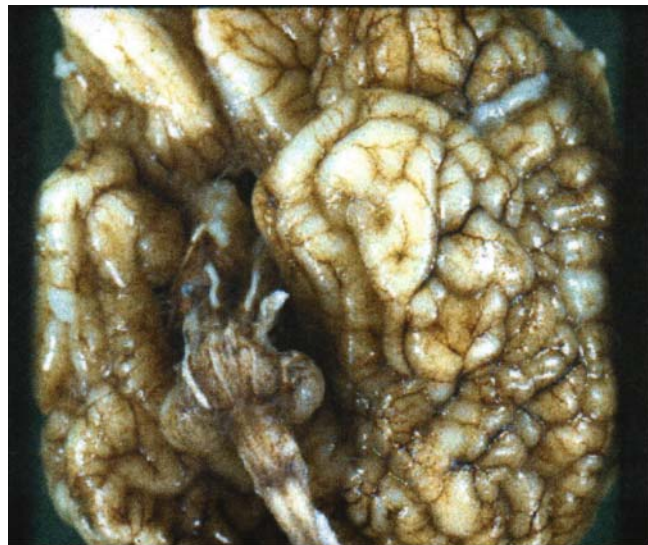


Fig. 2.5-6. Arnold-Chiari type 4. Hypoplastic cerebellum.

2.6 Dandy-Walker Malformation

The criteria for the Dandy-Walker malformation (DWM) are debated [13,14]. The syndrome was originally defined as (1) hydrocephalus, (2) partial or complete absence of the cerebellar vermis, and (3) a posterior fossa cyst continuous with the fourth ventricle. Harding and Copp [2] considered three criteria to be essential: agenesis (complete or partial) of the vermis, cystic dilatation of the fourth ventricle, and enlargement of the posterior fossa. Raybaud [15] classified the DWM into three categories: (1) true DWM; (2) Dandy-Walker variant; and (3) retrocerebellar arachnoid pouch. There are frequently many other associated CNS and systemic malformations.

The teratogenic timing and the pathomechanism of DWM are being investigated. Experimental studies in mice suggest that there is an arrest of development of rhombocephalic structures [11]. There are case reports noting that DWM is an important finding in partial

trisomy or tetrasomy 9 [16,17]. Through physical mapping of 3q2 in several individuals with DWM, interstitial deletions have been defined in ZIC1 and ZIC4 [18]. Mice with heterozygous deletion of these two linked genes have a phenotype that closely resembles DWM, providing a mouse model for this malformation.

Joubert syndrome is a familial disorder with abnormalities of respiration and eye movements, ataxia, and mental retardation. There is hypoplasia of the cerebellar vermis (molar tooth sign), ventricular dilatation, and malformations of the cerebellar and some brain stem nuclei [2]. It is genetically heterogeneous with known loci on 9q34 (JBTS1), 11p11-12 (CORS2), and 6q23 (JBTS3) [2,19]. AHI1, which encodes the Joubertin protein, is expressed strongly in embryonic hindbrain and forebrain [20,21].



Fig. 2.6-1. Dandy-Walker malformation (DWM). Sagittal view of the brain stem and cerebellum with partial agenesis of vermis and cystic dilatation of fourth ventricle.

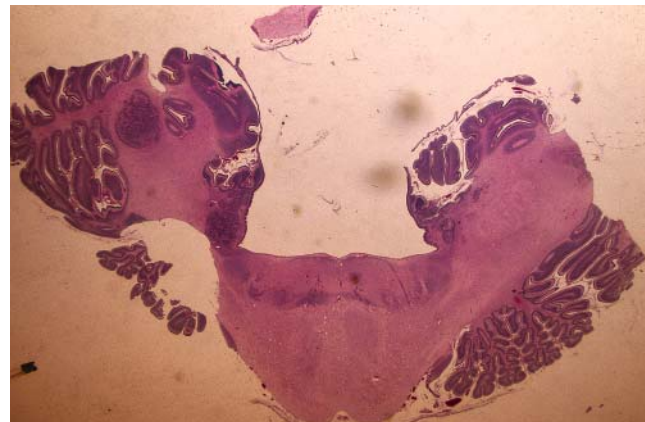


Fig. 2.6-2. Horizontal view of the pons and cerebellum with a defect of the vermis and dilatation of the fourth ventricle. H&E.

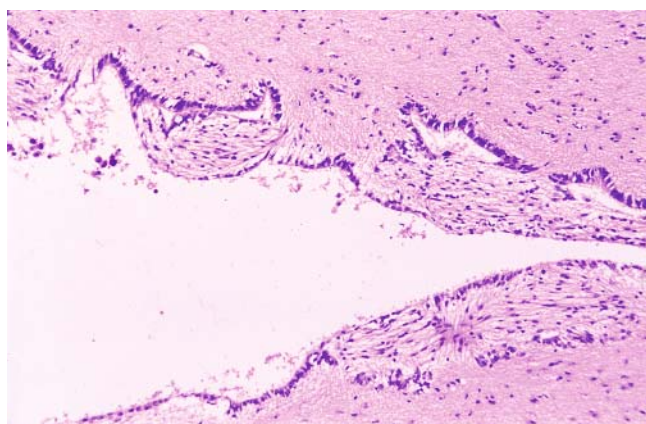


Fig. 2.6-3. Posterior dilatation of the fourth ventricle with ectopic proliferation of astroglial tissues. H&E.

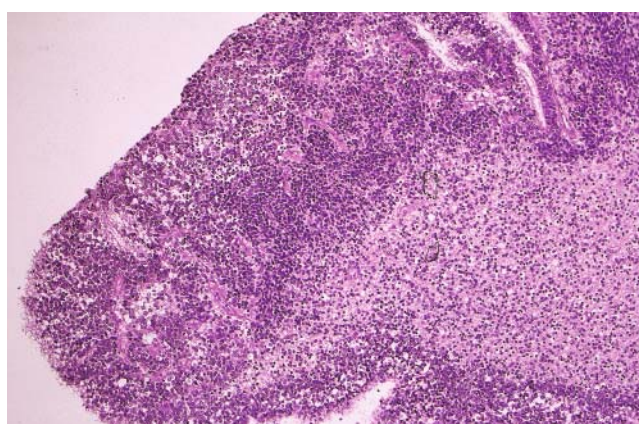


Fig. 2.6-4. Polymicrogyria in part of the cerebellar cortex. H&E.

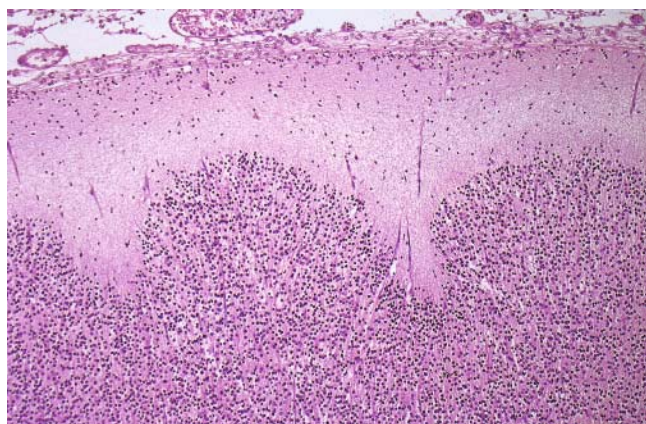


Fig. 2.6-5. Microgyria in the cerebral cortex, an associated lesion in Dandy-Walker syndrome. H&E.

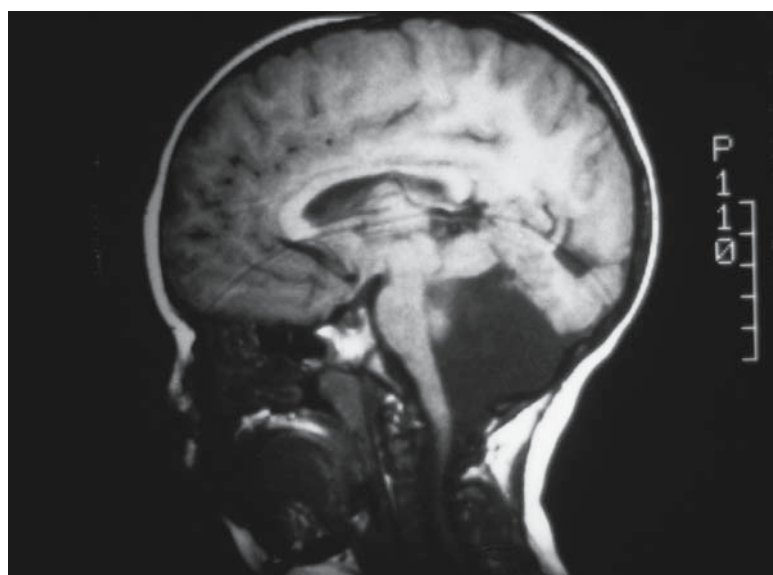


Fig. 2.6-6. MRI of the head demonstrating a defect of the vermis and cystic dilatation of the fourth ventricle.

2.7 Holoprosencephaly (Synonyms: Holotelencephaly, Telencephalosynapsis, Arhinencephaly)

Holoprosencephaly is usually a sporadic malformation resulting from a failure of cleavage of the cerebral hemispheres and absence of the interhemispheric fissure with a single anterior ventricle. This complex of hemispheric deformities is typically associated with olfactory aplasia and a dorsal supracerebellar meningeal cyst. There are frequently leptomeningeal glioneuronal heterotopias [22], and there is usually a facial deformity: a proboscis in the most severe form called cyclopia, or hypotelorism with a single nasal cavity [2]. It has been associated with maternal diabetes, maternal infection, fetal alcohol syndrome, and trisomy 13. Associated genes include sonic hedgehog (SHH) in HPE3, ZIC2 in HPE5, SIX3 in HPE2, and TG interacting factor (TGIF) in HPE4 [23–26].

Holoprosencephaly is classified morphologically as:

1. The complete, alobar type: no separation of the telencephalon single ventricle in a small brain
2. The incomplete, semilobar type: variable degrees of separation of the posterior cerebrum
3. The lobar, atypical, unclassified type: a small focal fusion of the midline with T-shaped or Y-shaped lateral and third ventricles

Another morphological form, the middle interhemispheric variant of holoprosencephaly, has been recognized [10].



Fig. 2.7-1. Alobar holoprosencephaly. Posterior view from a large dorsal cyst shows fusion of cerebral hemispheres and a single ventricle.

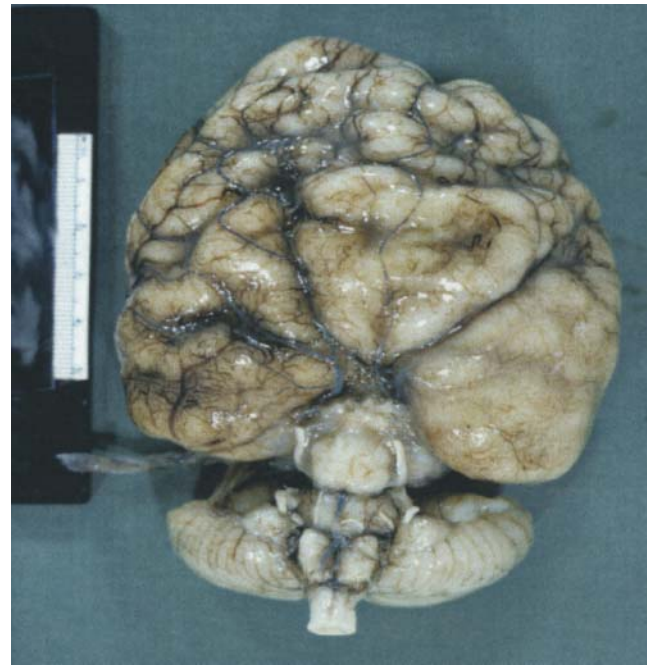


Fig. 2.7-2. Alobar holoprosencephaly. Anterior view shows fusion of cerebral hemispheres, absence of olfactory nerves, abnormal sulcus formation, and a single anterior cerebral artery.

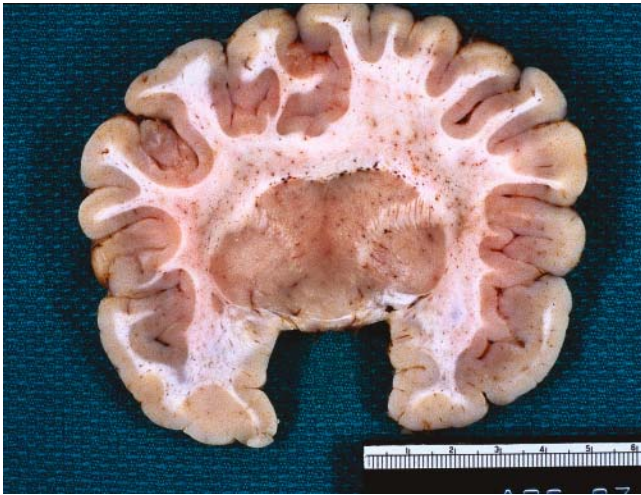


Fig. 2.7-3. Alobar holoprosencephaly. Coronal section of the cerebrum at the level of the head of the basal ganglia exhibits fusion of both hemispheres and thalami.

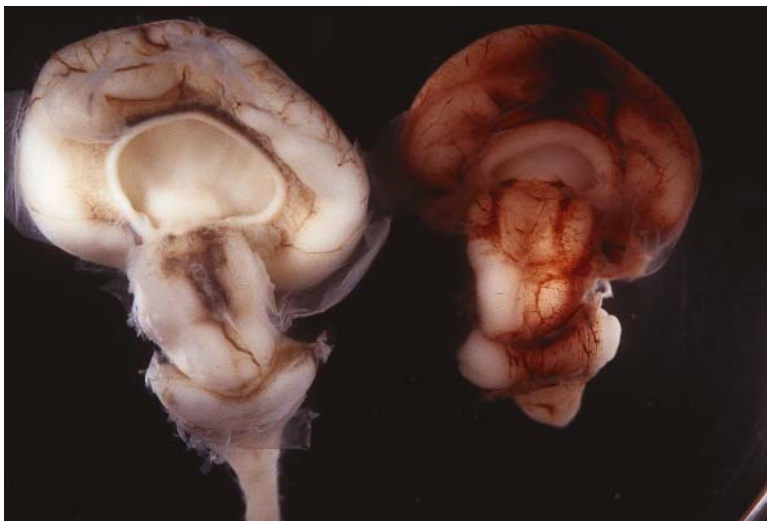


Fig. 2.7-4. Alobar holoprosencephaly of fetal brains. Note the relatively large brain stem, small cerebrum, and very small cerebellum compared with that in 2.7-1.



Fig. 2.7-5. Alobar holoprosencephaly in a whole mount of fetal brain (20 weeks' gestation). Note the fusion of the cerebral hemispheres and thalamus. H&E.

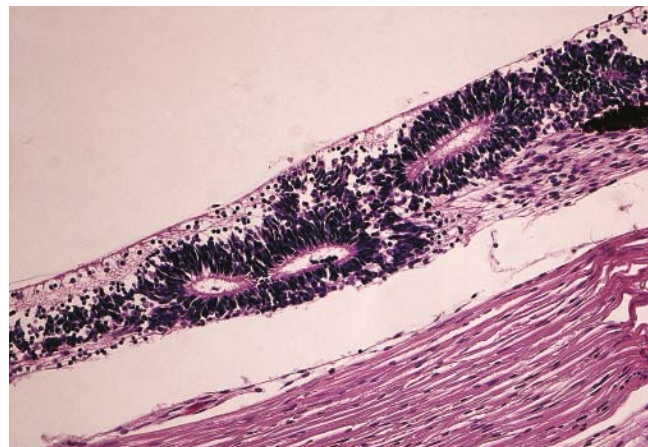


Fig. 2.7-6. Alobar holoprosencephaly: retina. It shows dysplasia with rosette formation. H&E.

2.8 Semilobar and Lobar Holoprosencephaly

With semilobar holoprosencephaly there is a partial lack of hemispheric division in the frontal lobes. The anterior single ventricle separates posteriorly, forming two temporal and two posterior horns. In the frontal lobes the subcortical structures form an undifferentiated mass in which the striatal structures are not identified. The third ventricle does not exist.

With lobar holoprosencephaly there is an almost normal division of hemispheres, with a midline continuity of the cerebral cortex of the frontal pole, or the orbital surface or above the corpus callosum. There is variable involvement of the olfactory system and the

corpus callosum. The frontal lobes may be hypoplastic [2].

With holoprosencephaly the meninges in the midline may show leptomeningeal glioneuronal heterotopias. These may extend from the basal prosencephalon to the pons, with the thickest distribution occurring in the basal prosencephalon [22].

The facial deformities associated with holoprosencephaly are of various types but do not correspond exactly to the severity of the brain malformations. They include cyclopia (usually synophthalmia), ethmocephaly, cebocephaly, or premaxillary agenesis [27].

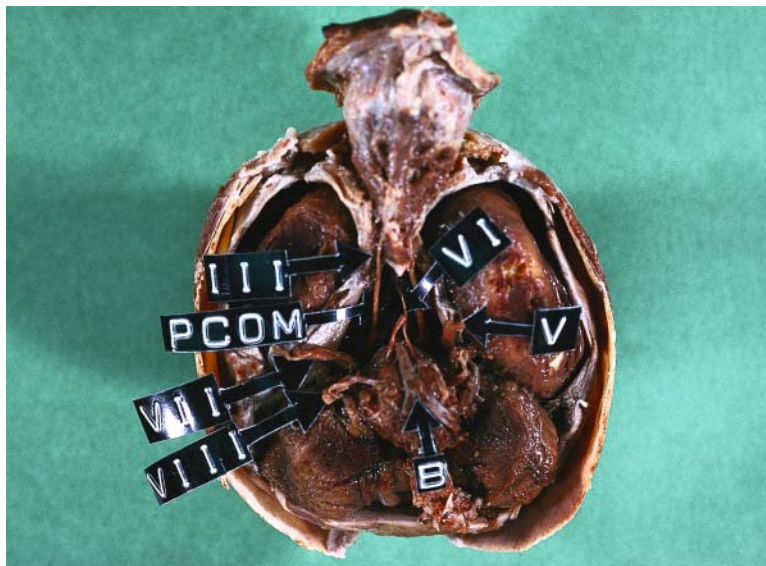


Fig. 2.8-1. Semilobar holoprosencephaly in a fetus with cyclopia.



Fig. 2.8-2. Semilobar holoprosencephaly (coronal section of the brain in 2.8-1).

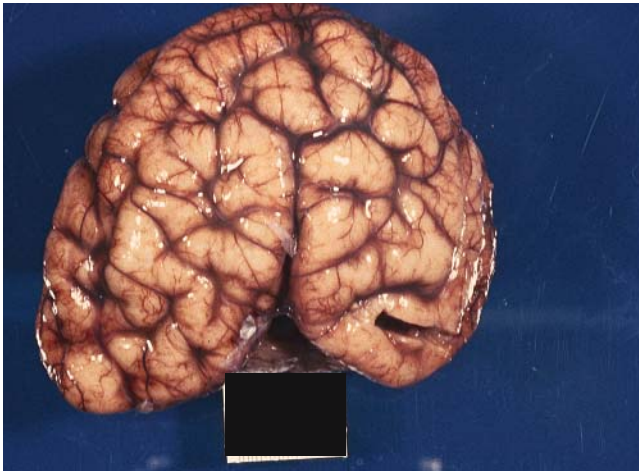


Fig. 2.8-3. Semilobar holoprosencephaly in a neonate, posterior view.

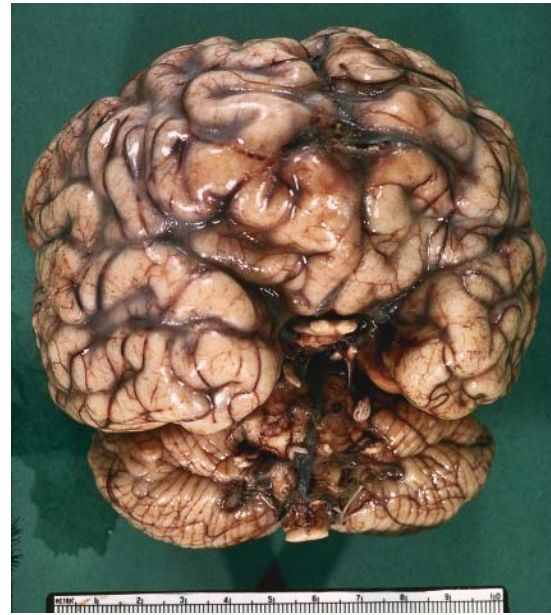


Fig. 2.8-4. Semilobar holoprosencephaly in a neonate, anterior view.



Fig. 2.8-5. Lobar holoprosencephaly in a child. Coronal section of the cerebrum at the thalamus. There is minimal fusion of the frontal lobes.

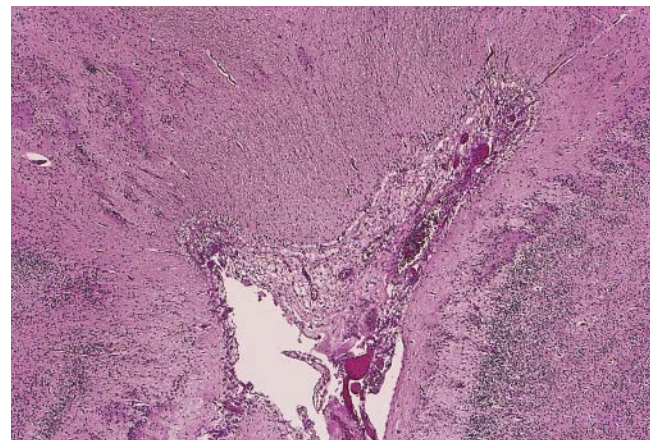


Fig. 2.8-6. Leptomeningeal glioneuronal heterotopia (LGH) at the midline base of the brain shown in 2.8-4. H&E.

2.9 Callosal Agenesis (Synonym: Agenesis of Corpus Callosum)

With agenesis of the corpus callosum (ACC) there are complete (total) and incomplete (partial) types.

Complete ACC: The entire corpus callosum is defective and its longitudinal fibers form the laterally situated Probst bundle, which contains the anteroposterior association axons.

Incomplete ACC: The splenium is defective, and the genu remains wholly or partially intact. The anterior parts (the genu and rostrum) usually are present [28].

The lesion may be an isolated malformation or part of a more complex malformation. Agenesis of the corpus callosum is apparent on inspection of the interhemispheric fissure.

The medial aspect of the hemispheres reveals the absence of the corpus callosum and the horizontal cingulate gyrus. There is an abnormal vertical orientation of all other medial gyri.

Septo-optic dysplasia (Morsier's syndrome) consists of agenesis of septum pellucidum, a primitive optic vesicle with hypoplasia of the optic nerves, chiasm, and infundibulum. It is associated with hypotonia, blindness, and endocrine dysfunction (e.g., deficient growth, hypoglycemia, and diabetes insipidus).

Aicardi syndrome is an X-linked dominant condition with infantile spasms, callosal agenesis, polymicrogyria, heterotopias, and retinal coloboma [29].

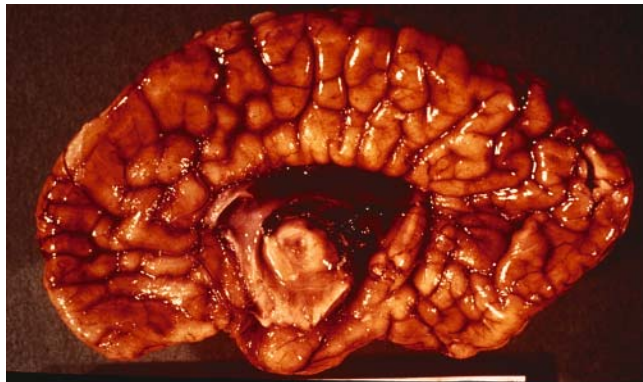


Fig. 2.9-1. Agenesis of corpus callosum. Medial surface of the brain shows complete callosal agenesis and an absence of the cingulate gyrus.



Fig. 2.9-2. Agenesis of corpus callosum. Coronal section of the brain shows callosal agenesis, Probst bundles, a butterfly-shaped ventricle, and polymicrogyria.

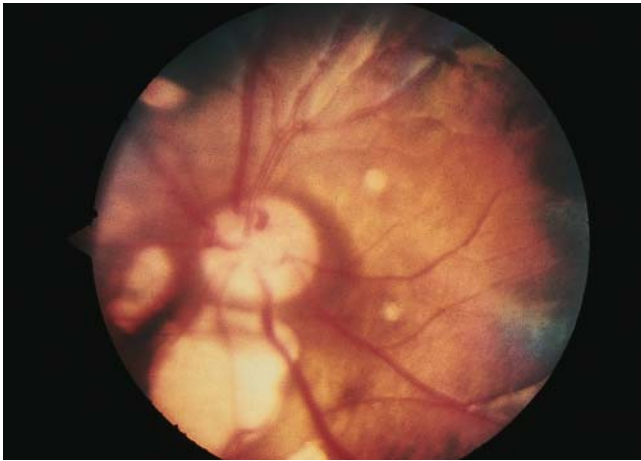


Fig. 2.9-3. Aicardi syndrome: an X-linked dominant condition with infantile spasms, callosal agenesis, polymicrogyria, heterotopias, and retinal coloboma, as illustrated here [29].

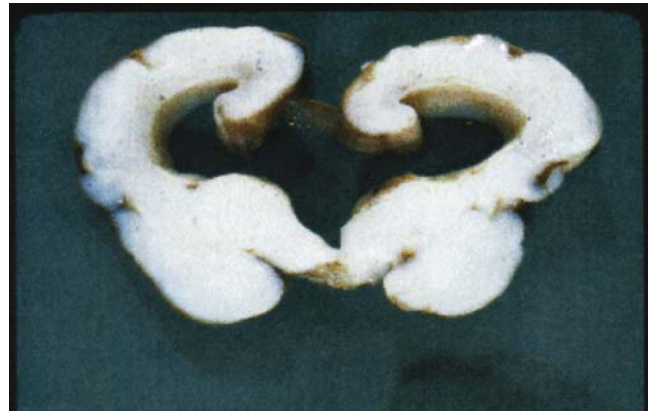


Fig. 2.9-4. Agenesis of corpus callosum. Coronal section of the cerebral hemispheres, which are connected by the meninges.

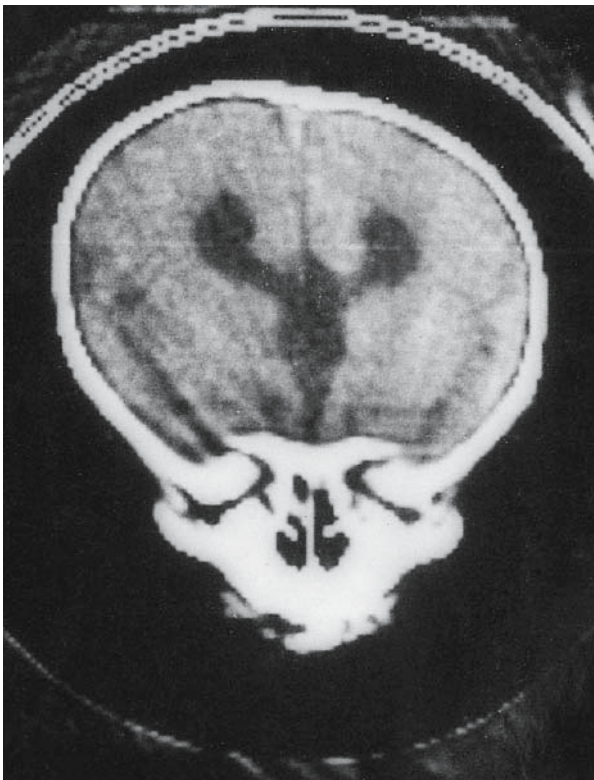


Fig. 2.9-5. Agenesis of corpus callosum. Computed tomography (CT) shows the “bat-wing” pattern of the ventricles.



Fig. 2.9-6. Septo-optic dysplasia. Note the absence of the septum pellucidum and the abnormal hypothalamus and optic nerves.

2.10 Neuronal Heterotopia

During embryogenesis the migration of postmitotic neurons from the ventricular zone to the cortical plate creates one of the most critical stages of brain development. An interruption of the process at an early stage of neuronal migration produces neuronal heterotopia, which may be diffuse, nodular, or laminar.

1. Diffuse neuronal heterotopias are discussed in the chapter on epilepsy (see Chapter 26, Section 26.4).

2. Nodular heterotopia is frequently found with other malformations and is defined as subependymal, subcortical, or marginal glioneuronal heterotopia. The heterotopia may be seen in peroxisomal, mitochondrial, and chromosomal disorders. Some specific disorders with heterotopias have been identified. Familial

bilateral periventricular nodular heterotopia is caused by mutations in the X-linked gene *filamin-1* [2,30,31]. The disorder affects girls, causing focal epilepsy and sometimes mild mental retardation. A rare recessive case of periventricular nodular heterotopia due to mutations in the *ARGEF2* gene has also been reported in children with microcephaly and early-onset seizures [32].

3. With laminar heterotopia, also referred to as “double cortex,” there is a heterotopic subcortical band of gray matter separated from the cortex by white matter [33]. Females with mutations in the X-linked gene *doublecortin* develop subcortical band heterotopia. Males with *doublecortin* mutations exhibit lissencephaly (XLIS) [32,33].

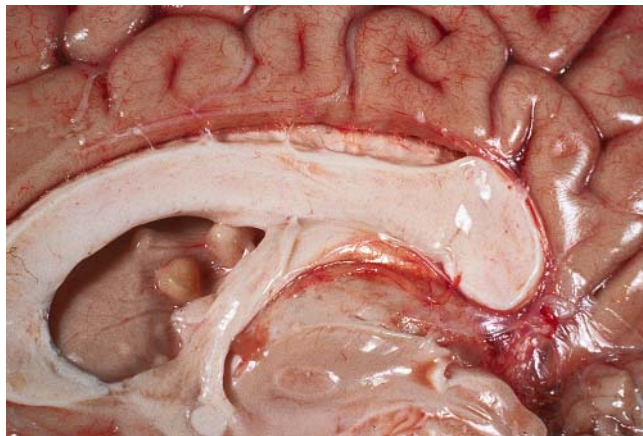


Fig. 2.10-1. Nodular heterotopia. Sagittal section of the hemisphere shows several nodular heterotopias on the lateral ventricular wall.

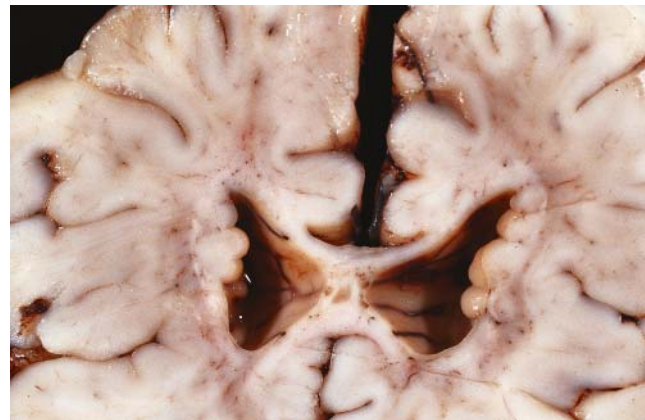


Fig. 2.10-2. Bilateral periventricular nodular heterotopia. Coronal section of brain reveals heterotopia in the anterior horns of the lateral ventricles.

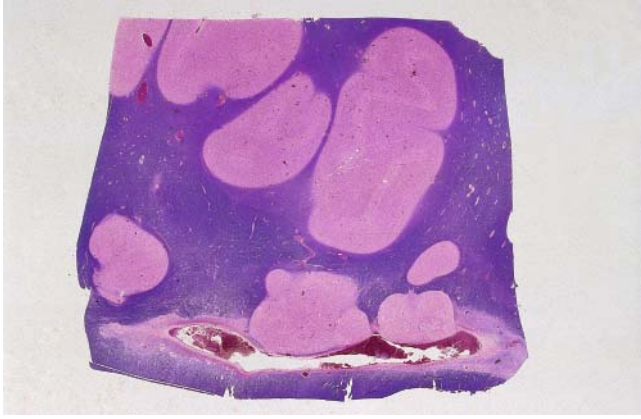


Fig. 2.10-3. Nodular heterotopia. Section of deep white matter reveals neuronal heterotopia (defined in pink). H&E/LFB.

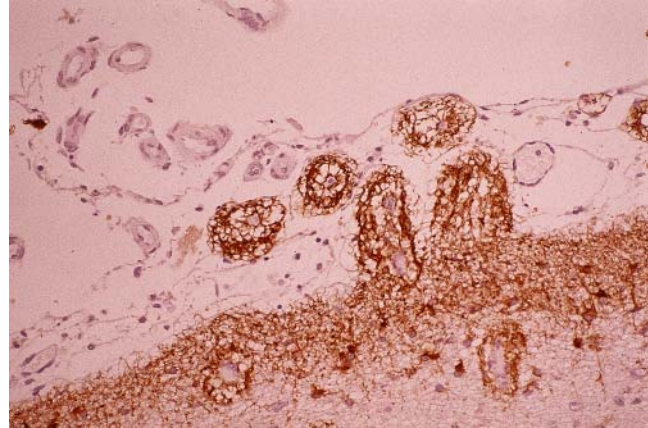


Fig. 2.10-4. Leptomeningeal or marginal glioneuronal heterotopia defined with antibodies to GFAP.

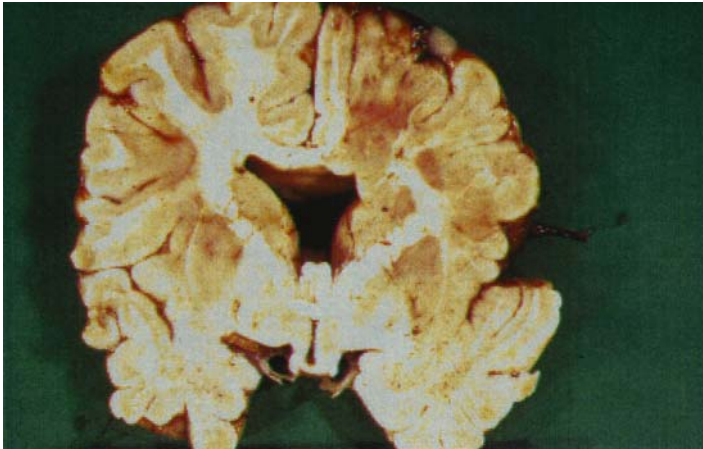


Fig. 2.10-5. Coronal section of cerebral hemisphere with gray matter heterotopia interrupting the corpus callosum.

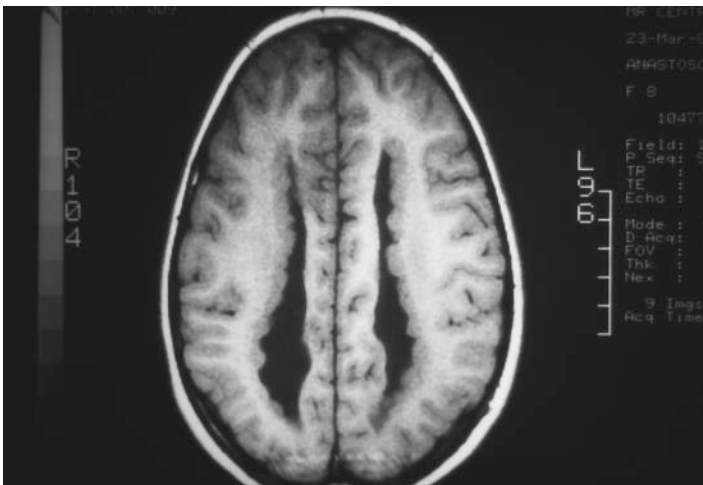


Fig. 2.10-6. Bilateral periventricular heterotopia. MRI defines the multiple nodular heterotopia. (Courtesy of Dr. A. Kakita.)

2.11 Classic (Type 1) Lissencephaly (Agyria-Pachygyria)

Lissencephaly (LIS) is characterized by a smooth or nearly smooth cerebral surface. It encompasses a spectrum of gyral malformations, from complete agyria to regional pachygyria [34].

1. Chromosome 17-related
 - a. Miller-Dieker syndrome, LIS1 [34,35]
 - b. Isolated lissencephaly sequence
2. X-linked
 - a. Lissencephaly, male: doublecortin [36]
 - b. Subcortical band heterotopias, female: doublecortin [36]
3. Other loci
 - a. Autosomal recessive lissencephaly with cerebellar hypoplasia, reelin [36]
 - b. Familial bilateral periventricular nodular heterotopia, females: FLN1 (filamin) [36]

- c. X-linked lissencephaly with abnormal genitalia [XLAG, ARX (aristaless-related homeobox)] [37,38])

There is a correlation between the clinical abnormality and the pathology so a pathology classification was devised [39] and genetic differences have now been detected. With lissencephaly type 1, which is observed in patients with *LIS1* mutations at 17p13.3, there is a characteristic thick cortex, a smooth cortical surface (more marked in the posterior than anterior regions of the brain), and microscopically a prominent sparse zone (layer 3) in the cortex [40]. LIS1 protein is expressed in fetal and adult brains [41]. A recent examination of 16 cases of lissencephaly type 1 has further correlated the microscopic features according to the numbers of cortical layers and the main location on the cortex: LIS-4LP, LIS-4LA, LIS-3L, and LIS-2L. The type of malformation correlates with the genotype [36].



Fig. 2.11-1. Lissencephaly type 1, exhibiting agyria and an open sylvian fissure.



Fig. 2.11-2. Lissencephaly type 1. Coronal section exhibits a thick cerebral cortex, small amount of white matter, hypoplasia of the operculum, enlarged lateral ventricles, and nodular heterotopia on the right.



Fig. 2.11-3. Lissencephaly type 1. Note the reactive astrocytes around vessels in the sparsely cellular layer of the cerebral cortex. GFAP immunohistochemistry. The cortex consists of four layers: molecular, superficial cellular, sparse cellular, and deep cellular.

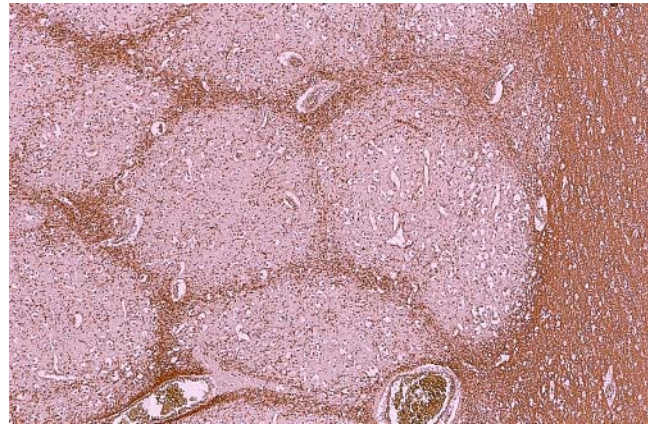


Fig. 2.11-4. Lissencephaly type 1. The deep cortical layer of the cerebral cortex shows a reticular cortical pattern separated by myelin sheaths. Myelin basic protein (MBP) immunohistochemistry.

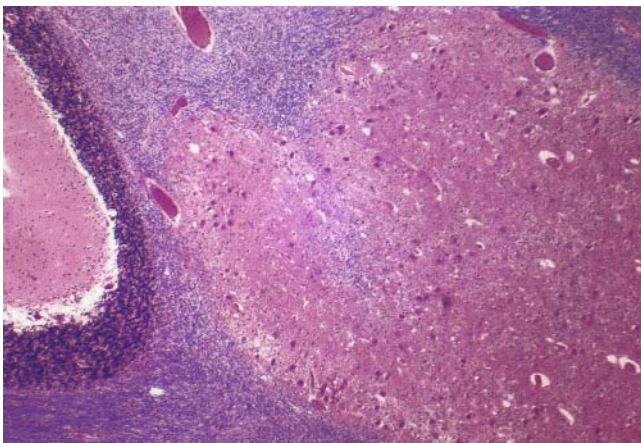


Fig. 2.11-5. Lissencephaly type 1, exhibiting dysplasia of the dentate nucleus in Miller-Dieker syndrome. H&E.

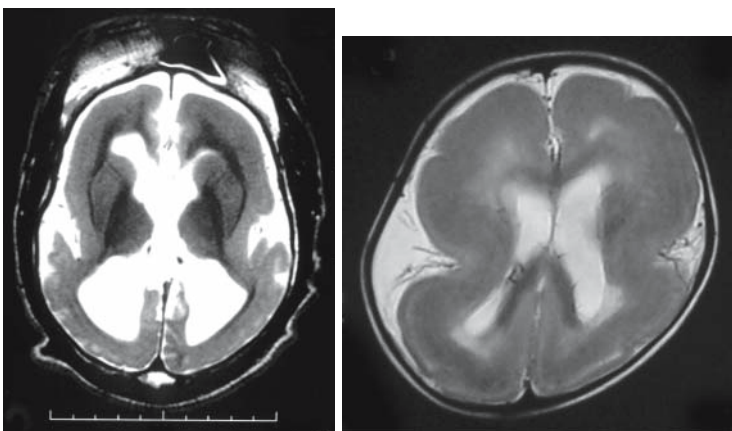


Fig. 2.11-6. Lissencephaly type I. MRI displays regional agyria, pachygyria, thick cortex, thin white matter, and colpocephalic lateral ventricles. (Courtesy of Dr. M. Kato.)

2.12 Miller-Dieker Syndrome, Double Cortex Syndrome, X-Linked Lissencephaly with Abnormal Genitalia

Miller-Dieker syndrome in an infant manifests as facial anomalies and type 1 lissencephaly with regional agyria, pachygyria, a thick four-layer cortex, thin white matter, colpocephalic lateral ventricles, olivary and dentate nuclear dysplasia, and heterotopia. There is mutation of the *LIS-1* gene (17p13.3), which codes for the protein platelet-activating factor acetylhydrolase (PAFAH), which is localized in Cajal-Retzius cells and neuroepithelium [34,35].

X-linked lissencephaly (XLIS) and *double cortex syndrome (DCX)*: Mutations of the *DCX* gene produce lissencephaly in male patients. The cortex is smooth (more so in the frontal lobes) and the cortex is thick with a prominent cell space zone. In female patients with *DCX* mutations there is a band heterotopia, or “double cortex” [36].

Autosomal recessive lissencephaly is associated with mutations of the reelin (*RELN*) gene. There is lissencephaly with cerebellar hypoplasia, and clinically a severe developmental delay, hypotonia, and seizures [36].

X-linked lissencephaly with corpus callosum agenesis and ambiguous genitalia in genotypic males is associated with mutations of the *ARX* gene located in human chromosome Xp22.13. *ARX* is expressed in interneurons of the forebrain and in the interstitium of the male gonad. It is involved in differentiation of the testes and the embryonic forebrain, especially in the proliferation of neural precursors and the differentiation and tangential migration of interneurons [37,38].



Fig. 2.12-1. Miller-Dieker syndrome. Fetal brain (with 17p-) at 19 GW. The fetal brain resembles a normal brain at this age, but fewer gyri are formed.



Fig. 2.12-2. Miller-Dieker syndrome: fetal brain coronal section. There are few gyri and the cortex is thick.

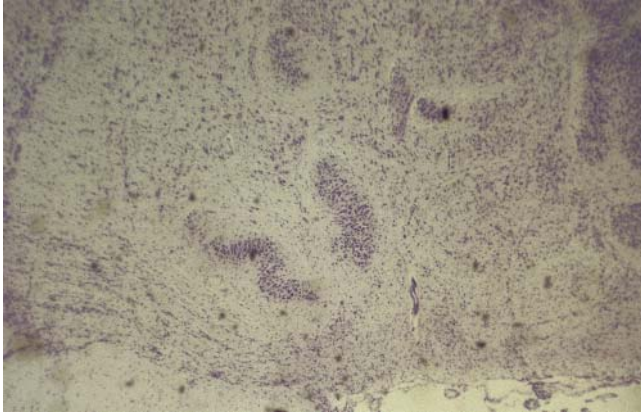


Fig. 2.12-3. Miller Dieker syndrome: fetal brain. Microscopy of the medulla oblongata shows abnormal olivary nuclei. Nissl stain.

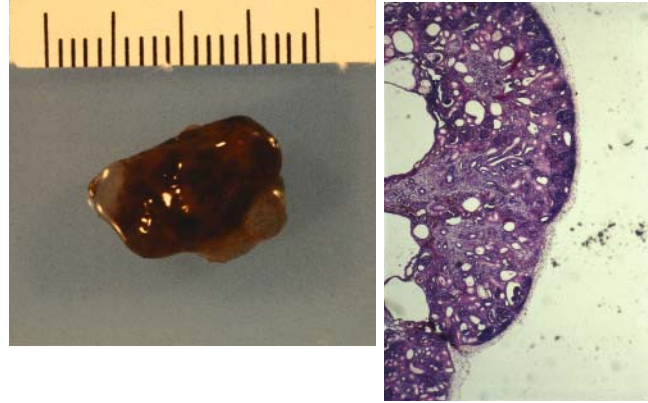


Fig. 2.12-4. Miller Dieker syndrome: fetal kidney. *Left.* The kidney is small and contains multiple cysts. *Right.* Microscopy of a cystic kidney. H&E.

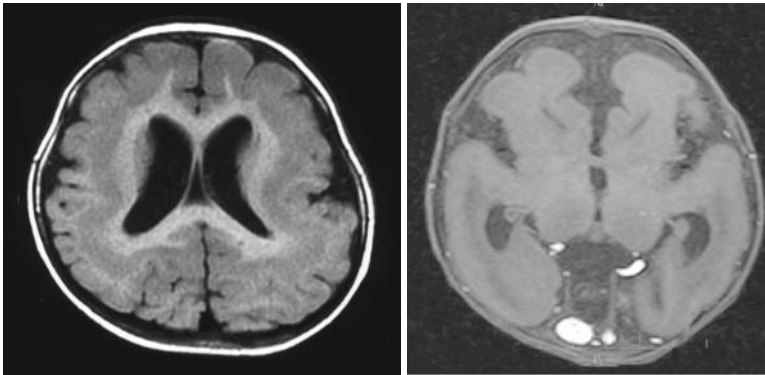


Fig. 2.12-5. Double-cortex syndrome: MRI. *Left.* T2-weighted MRI shows subcortical band heterotopia (double cortex). *Right.* Lissencephaly. (Courtesy of Dr. M. Kato.)

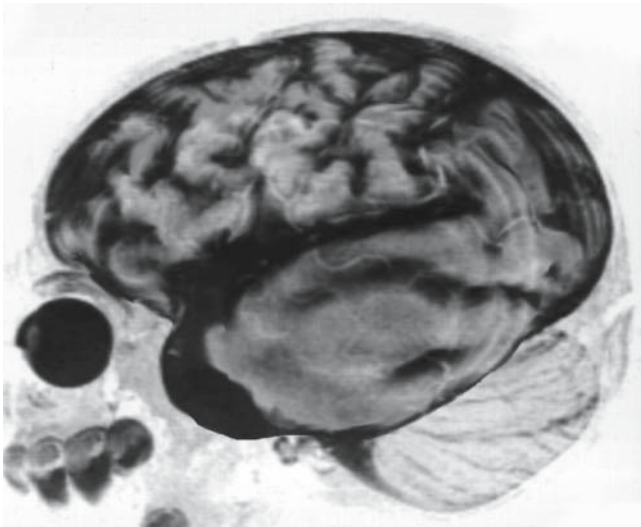


Fig. 2.12-6. MRI of X-linked lissencephaly with abnormal genitalia (XLAG). There is a moderately thick cortex, more severe in the posterior brain than the anterior brain regions. Colpocephaly is present. (Courtesy of Dr. M. Kato.)

2.13 Hemimegalencephaly and Focal Cortical Dysplasia

Hemimegalencephaly is associated with severe epilepsy, hemiplegia, and psychomotor delay. There are some associations with linear nevus, neurofibromatosis-1, tuberous sclerosis, and hemihypertrophy of the body. The brain exhibits hemimegalencephaly, and the cortex of the enlarged hemisphere exhibits regions with pachygyria-polymicrogyria and cortical dysplasia. The cortex may be thicker or thinner than normal, with disordered layering and large abnormal neurons. There may be balloon cells, intense gliosis, and selective neuronocytomegaly [42].

The cause is not known, and no genes have been identified. Selective alterations occur in distinct neurotransmitter receptors and the increased expression of some genes in hemimegalencephalic cortex [43]. MRI

reveals asymmetry of hemispheres, regions with a thick cortex, and high intensity in some parts of the cerebrum. There may be dilatation and deformity in the lateral ventricle.

Focal cortical dysplasia refers to a focal malformation of cerebral cortex, which shows loss of laminar organization, isolated abnormally large neurons, and/or balloon cells (see Chapter 26, Section 26.5). Balloon cells are often huge and characterized by abundant clear-staining cytoplasm lacking cellular processes and have peripherally positioned nuclei or multinuclei. They are pathognomonic and have astrocytic lineage, although some show dysplastic neuronal characteristics. They are epileptogenic and may have a reduction or immaturity of inhibitory neurons.

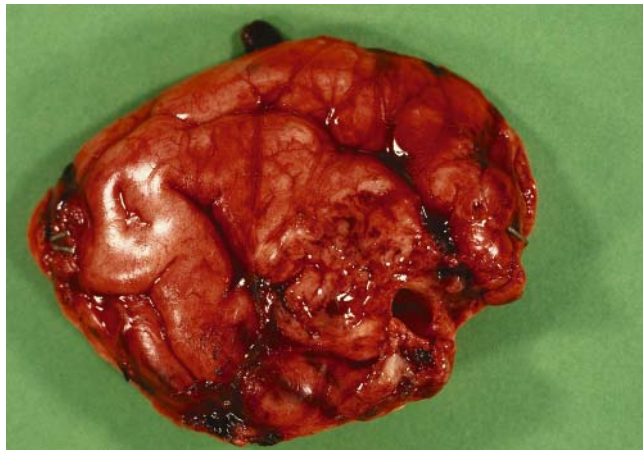


Fig. 2.13-1. Focal cortical dysplasia: surgically resected cerebral tissue.

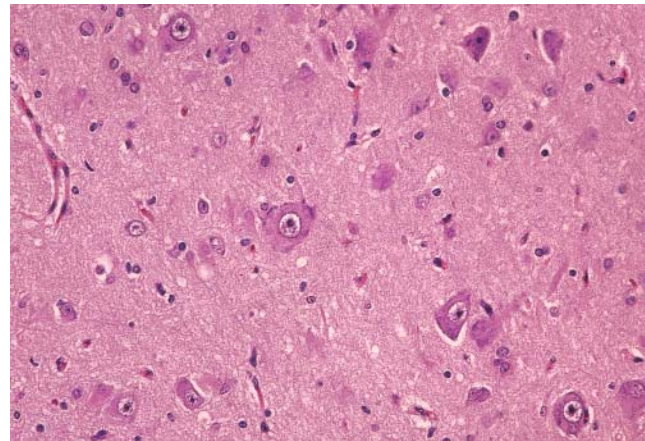


Fig. 2.13-2. Focal cortical dysplasia exhibiting several large neurons irregularly arranged in the cerebral cortex. H&E.

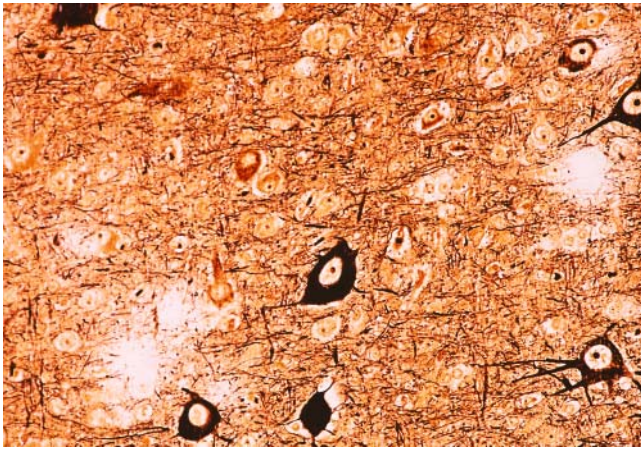


Fig. 2.13-3. Focal cortical dysplasia shown by the Bielchowsky method defining neuronocytomegaly. Some neurons contain neurofibrillary tangles.

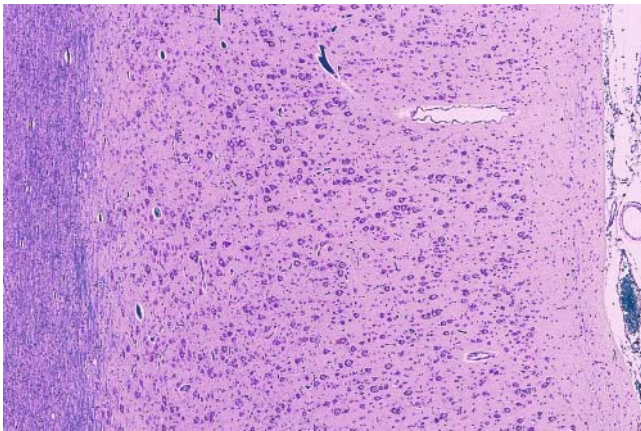


Fig. 2.13-5. Hemimegalencephaly. Microscopic appearance of dysplastic cortex exhibiting an absence of layering, increased cellularity, and neuronocytomegaly. LFB.

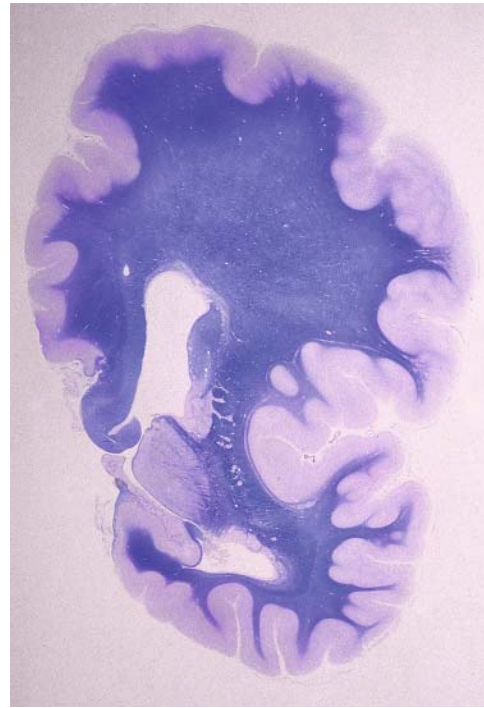


Fig. 2.13-4. Hemimegalencephaly: whole mount of a coronal section of cerebral hemisphere. LFB.

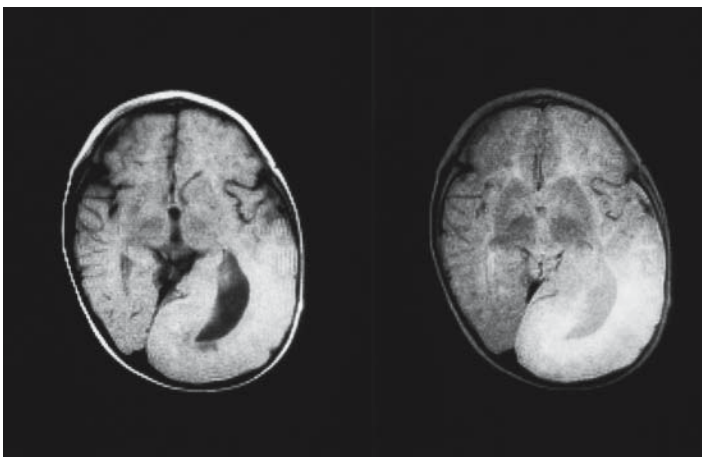


Fig. 2.13-6. Hemimegalencephaly. MRI reveals a large right hemisphere with focal regions of obvious dysplasia.

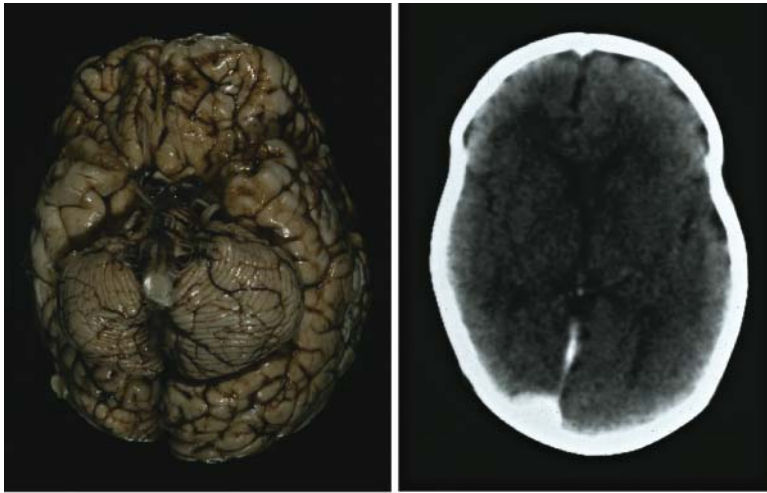


Fig. 2.13-7. Hemimegalencephaly. *Left.* Basal view of the brain. *Right.* CT findings. Left cerebral hemisphere is larger than the right one.



Fig. 2.13-8. Hemimegalencephaly. *Left.* Cerebral hemispheres. *Right.* Cerebellar hemispheres. Left hemisphere is larger than the right one in both cerebrum and cerebellum.

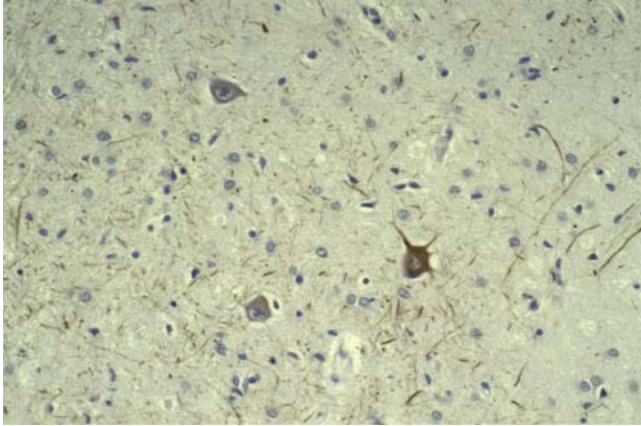


Fig. 2.13-9. Hemimegalencephaly. NF immunohistochemistry shows that large neurons are scattered in the subcortical white matter.

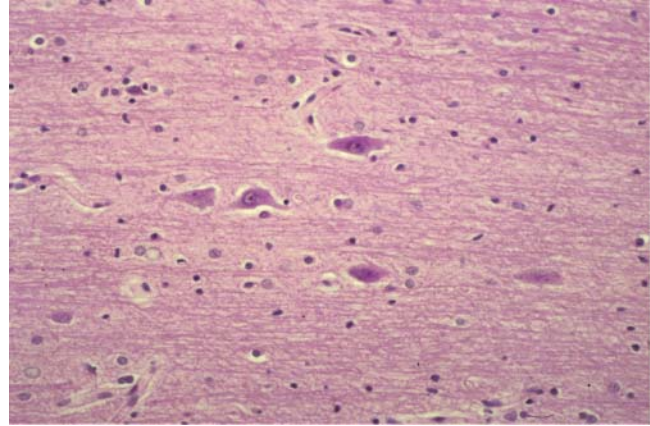


Fig. 2.13-10. Hemimegalencephaly. Isolated neurons are scattered in the white matter. H&E.

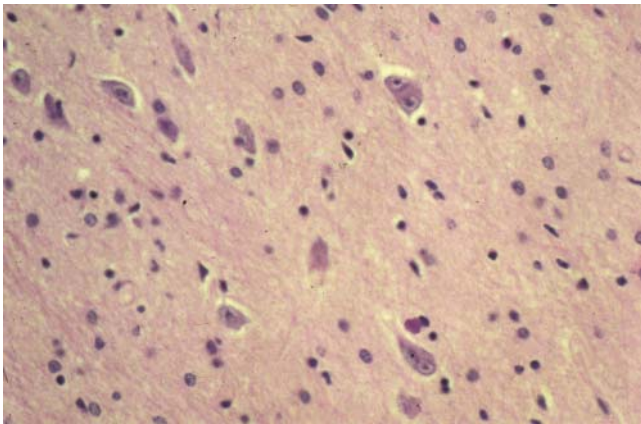


Fig. 2.13-11. Hemimegalencephaly. Irregularly arranged large neurons in the cortex. H&E.

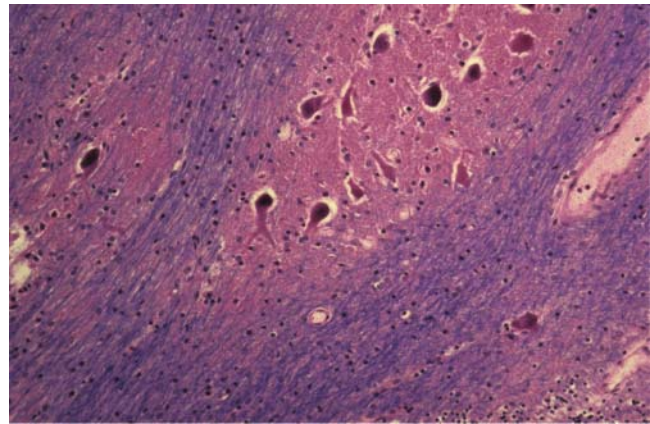


Fig. 2.13-12. Hemimegalencephaly. Heterotopic gray matter in the white matter. H&E/LFB.

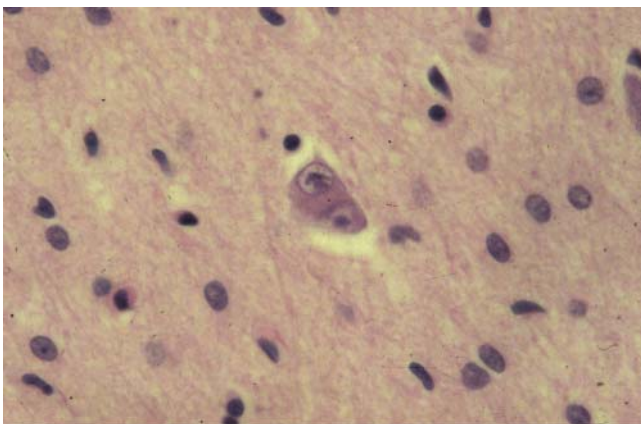


Fig. 2.13-13. Hemimegalencephaly Large neuron with two nuclei in the white matter. H&E.

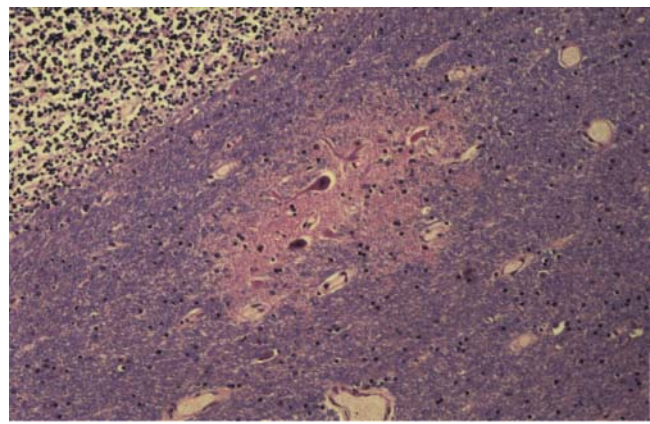


Fig. 2.13-14. Hemimegalencephaly. Heterotopic gray matter in the cerebellar white matter. H&E/LFB.

2.14 Cobblestone (Type 2) Lissencephaly: Fukuyama Congenital Muscular Dystrophy

In type 2 lissencephaly the cortex is agyric and irregular. The meninges exhibit mesodermal proliferation surrounding extensive glioneuronal heterotopias, which fuse with an abnormal unlayered cortex.

Fukuyama congenital muscular dystrophy (FCMD) is caused by mutations in *fukutin* [44–46]. FCMD is a form of congenital muscular dystrophy with psychomotor development delay. The mutated *fukutin* gene (9q31) causes an overmigration of cortical neurons through the

subpial membrane, producing cobblestone (type 2) lissencephaly [47] with polymicrogyria-pachygyria of the superficial cerebral cortical layers [48]. In the cerebellum there is a polymicrogyria with leptomeningeal cysts. The corticospinal tracts in the brain stem are in an abnormal location. MRI reveals polymicrogyria-pachygyria in the superficial cortical layer. CT reveals low density in the white matter and cerebellar hemispheric cysts.



Fig. 2.14-1. Fukuyama congenital muscular dystrophy (FCMD). Brain in the lateral view shows a microgranular (cobblestone) smooth cerebral surface.

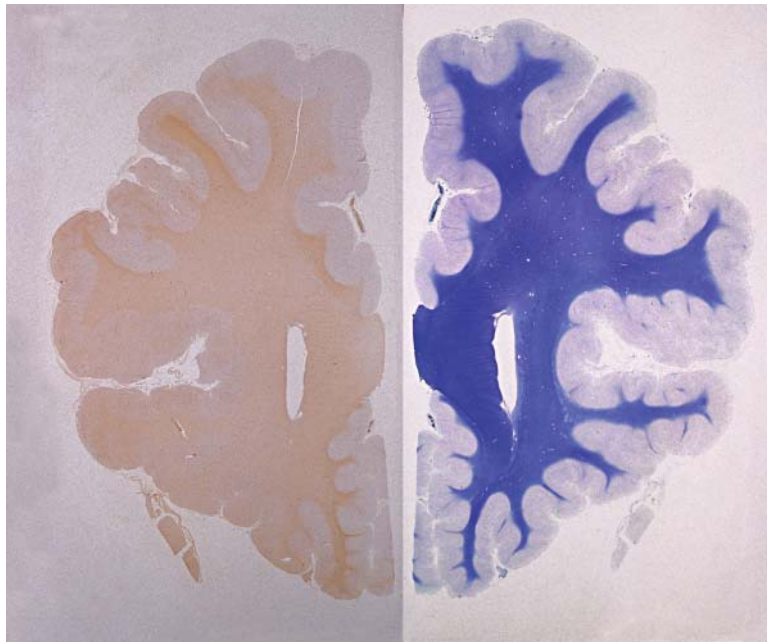


Fig. 2.14-2. Fukuyama congenital muscular dystrophy. Cerebral hemisphere whole mount from a coronal section exhibits polymicrogyria and pachygyria in the frontal and temporal cortices (*right*), and the cerebral cortex exhibits an increase in myelin basic protein (MBP)-positive fibers in the cerebral cortex (*left*).

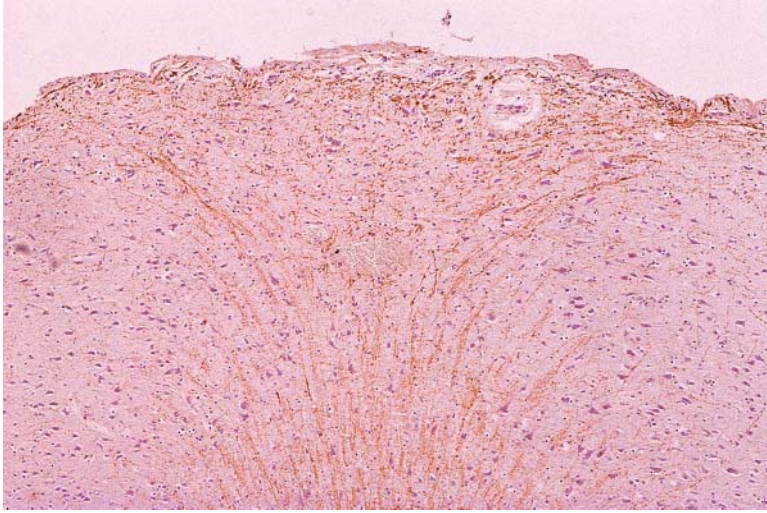


Fig. 2.14-3. Fukuyama congenital muscular dystrophy. Higher magnification of **2.14-2** shows the protrusion of myelin sheaths (marked with MBP immunohistochemistry) through the cortical cellular layers.

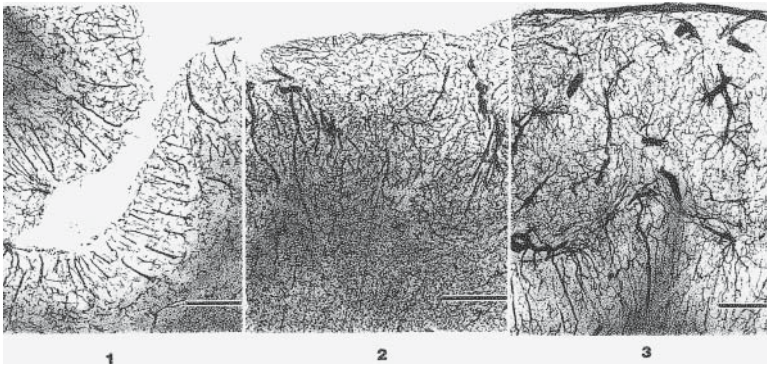


Fig. 2.14-4. Fukuyama congenital muscular dystrophy. Vascular staining shows mild, moderate, and marked irregularity in three grades of cortical dysplasia, respectively. The abnormal micro-angioarchitecture of the cerebral cortex is defined with a silver stain. (Courtesy of K. Takada.)

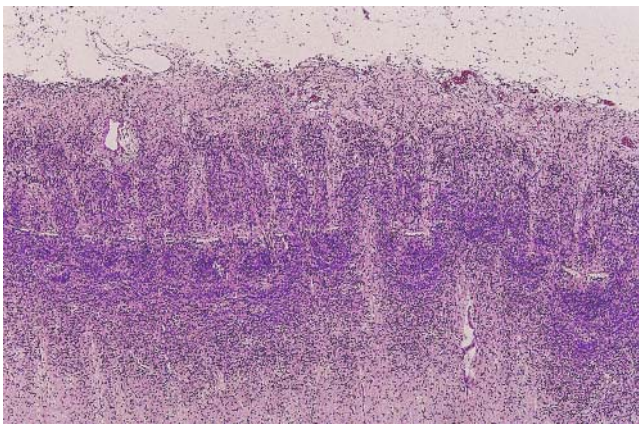


Fig. 2.14-5. Fukuyama congenital muscular dystrophy. Microscopic section of fetal brain shows the irregular superficial cortical layer, which may exhibit polymicrogyria or lissencephaly in the mature brain. H&E.

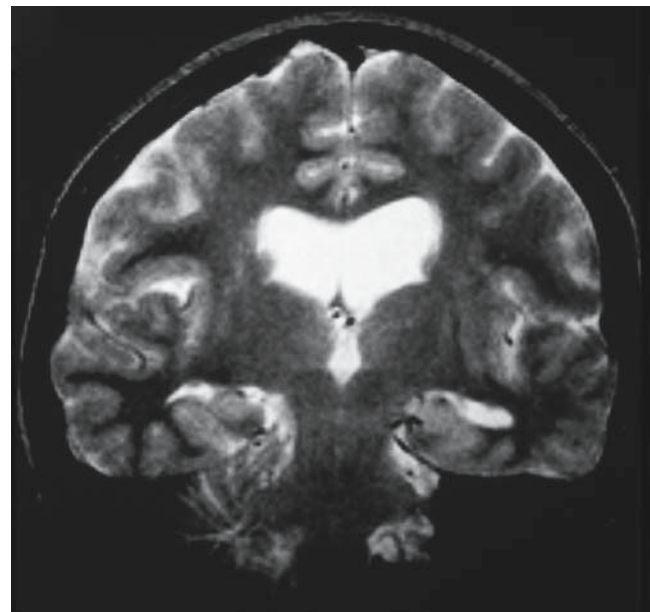


Fig. 2.14-6. Fukuyama congenital muscular dystrophy. MRI of the abnormal cortex shows an irregular intensity in the T2-weighted image.

2.15 Walker-Warburg Syndrome

Walker-Warburg syndrome was described as a cerebro-ocular disorder exhibiting type 2 lissencephaly, hydrocephalus, and eye abnormalities. The syndrome is also known as HARD+E (hydrocephalus, agryria, retinal dysplasia, encephalocele). The association with muscle disease was not made in early reports. Infants present with profound psychomotor retardation, hydrocephalus, and developmental defects; and they die during early infancy [2].

The brain exhibits a cobblestone (type 2) lissencephaly, polymicrogyria-pachygyria involving almost the whole cortical layer, overmigration of cortical neurons through the subpial membrane, diffuse polymicrogyria in the cerebellar hemispheres, aqueductal obstruction, hydro-

cephalus, and brain stem dysplasia. The disorder is autosomal recessive and is caused by mutations in the O-mannosyltransferase gene (*POMT1* [49]). This causes an O-mannosylation defect in muscle [50].

Muscle-eye-brain disease is a similar syndrome consisting of congenital muscular dystrophy, ocular abnormalities, and lissencephaly type 2. The autosomal recessive disorder is caused by a mutation in O-mannose beta-1,2-*N*-acetylglucosaminyl transferase gene (*POMGnT1*), which produces a defect in O-mannosyl glycan synthesis [51].

POMGnT1 and *POMT1* are involved in glycosylation of α -dystroglycan, which is one of the components of the dystrophin-glycoprotein complex [52].



Fig. 2.15-1. Walker-Warburg syndrome. Coronal section of the cerebrum in a child exhibits the lissencephalic surface, thick cerebral cortex, and dilated ventricles.

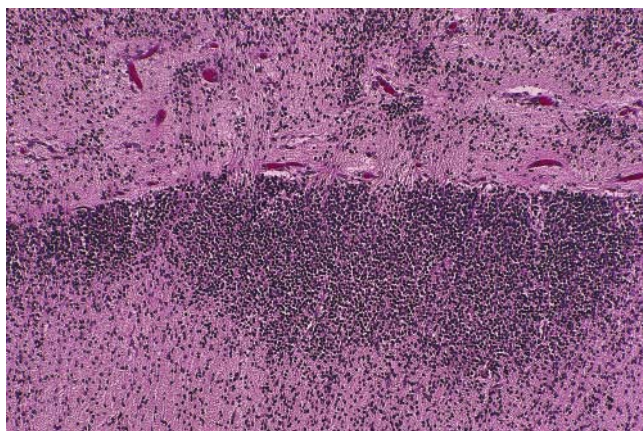


Fig. 2.15-2. Walker-Warburg syndrome in a fetus at 20 weeks' gestation. The abnormal cortex is made up of a superficial irregular layer and a thin deep cellular layer. The superficial layer protrudes through the boundary of the deeper layer. H&E.

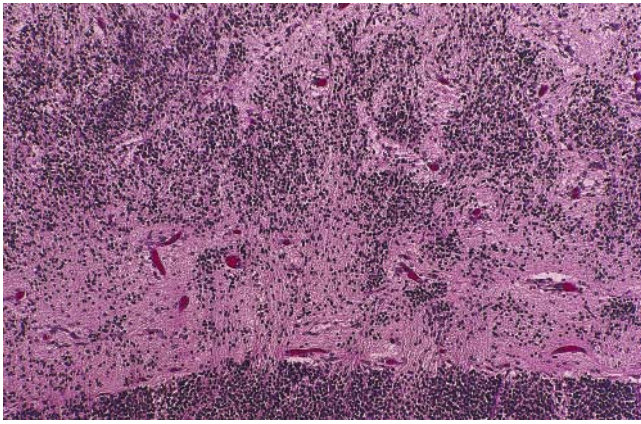


Fig. 2.15-3. Walker-Warburg syndrome. Higher power view of 2.15-2 revealing the irregular arrangement of the thick superficial cellular layer. H&E.

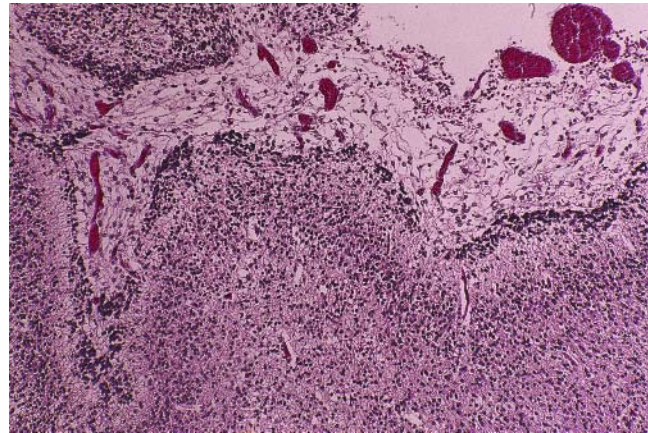


Fig. 2.15-4. Walker-Warburg syndrome (same case as in 2.15-2). Note the cerebellum with thick leptomeninges, with partial loss of the superficial granular cell layer. H&E.

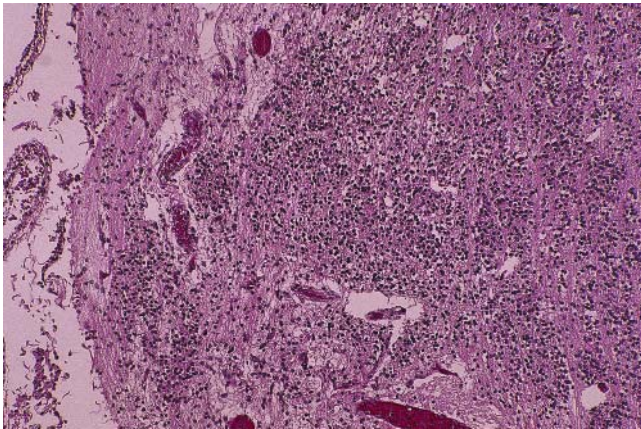


Fig. 2.15-5. Walker-Warburg syndrome at 20 weeks' gestation. The basis pontis is covered with irregular clusters of neural tissue in the leptomeninges and fiber bundles containing large vessels. H&E.

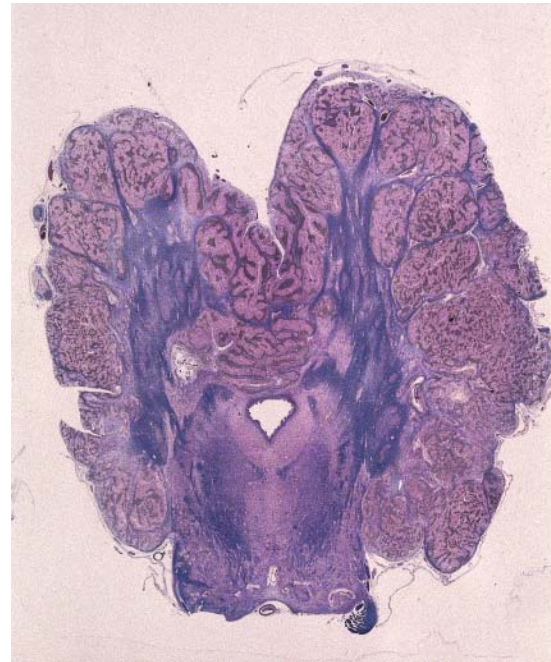


Fig. 2.15-6. Walker-Warburg syndrome. The cerebellum of a child exhibits diffuse, extensive polymicrogyria in the cerebellar cortex. LFB.

2.16 Malformations of Cortical Organization

Polymicrogyria, a relatively common malformation of cortical development, is characterized by multiple small gyri with abnormal cortical lamination. It is a thin layer of cortex that is folded and fused to produce an irregular surface composed of buried and fused gyri. Its various forms encompass a wide range of clinical, etiological, and histological findings and are thought to occur between 17 and 26 weeks' gestation.

Generalized Polymicrogyria

Generalized polymicrogyria may be the result of many etiologies, such as intrauterine cytomegalovirus infection, placental perfusion failure, or Zellweger syndrome.

Focal or Multifocal Polymicrogyria

Bilateral Symmetrical Polymicrogyria

Bilateral frontoparietal polymicrogyria. The polymicrogyria is predominantly in the frontoparietal lobes and

is associated with mental retardation, developmental delay, esotropia, and seizures. It is an autosomal recessive disorder with a locus at 16q12.2–21 (gene *GPR56*) [53,54].

Bilateral perisylvian polymicrogyria. This disorder is associated with mild mental retardation, epilepsy, and difficulties with expressive speech and feeding. The gene is located at Xq28 [55].

Bilateral posterior polymicrogyria. This category includes asymmetrical polymicrogyria and schizencephaly (see Section 2.20).

Focal or Multifocal Cortical Dysplasia

See Section 2.13 and Chapter 26 (Section 26.4) [56].

Microdysgenesis

See Chapter 26 (Section 26.2).

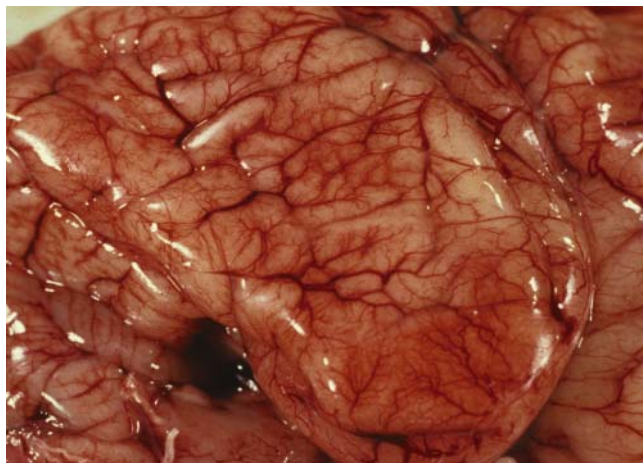


Fig. 2.16-1. Polymicrogyria: macroscopic view. There are many small gyri in the surface of the cerebral hemisphere.

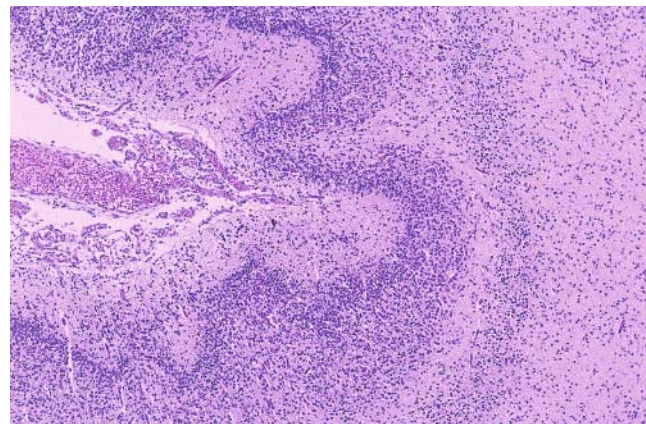


Fig. 2.16-2. Polymicrogyria. Microscopic demonstration of the folded four-layer cortical pattern. H&E.

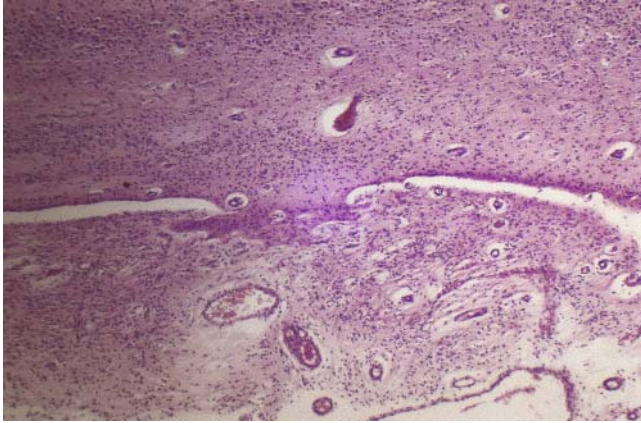


Fig. 2.16-3. Polymicrogyria associated with focal protrusion of germinal cells into the lateral ventricle. H&E.

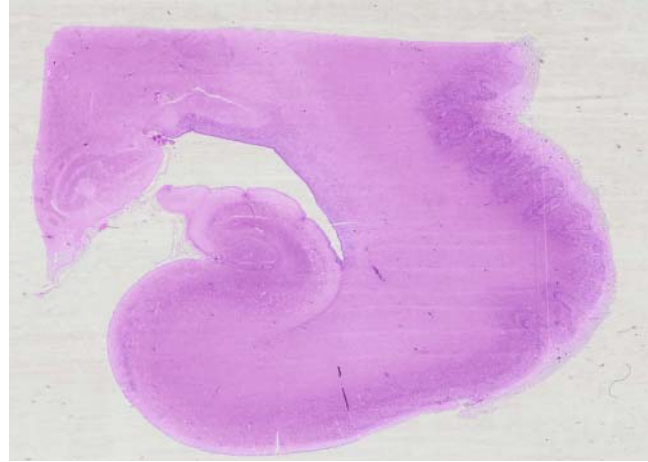


Fig. 2.16-4. Polymicrogyria. The cortex is made up of small fused gyri without cortical layers in the lateral temporal lobe. H&E.

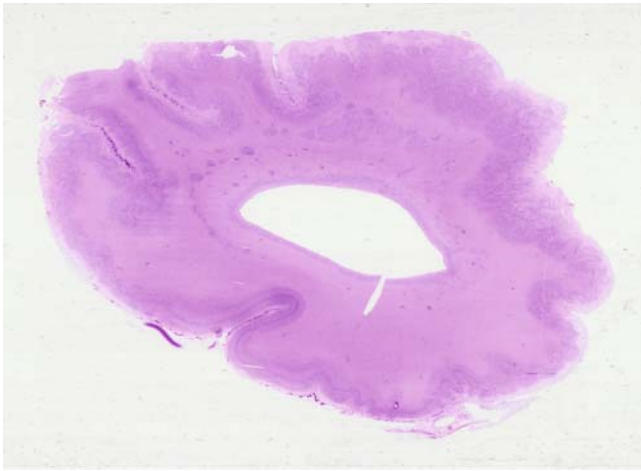


Fig. 2.16-5. Polymicrogyria in occipital lobe. The smoothed-out cortex is composed of small folded gyri. Whole mount stained with H&E.

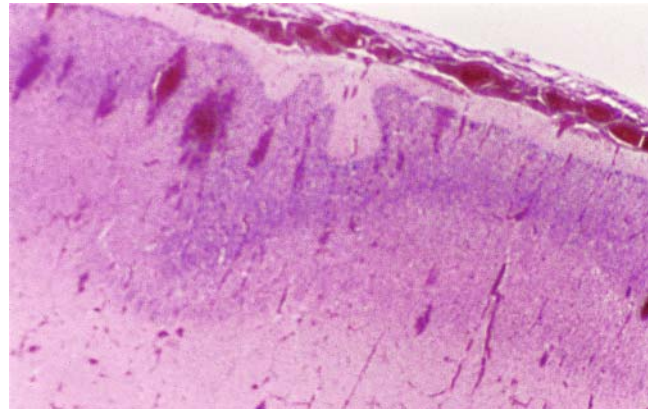


Fig. 2.16-6. Polymicrogyria in a neonate showing congestion and perivascular hemorrhage into the abnormal cortex. H&E.

2.17 Thanatophoric Dysplasia Type 1

Thanatophoric dysplasia is characterized by short limbs with bowed long bones, flat vertebrae, short ribs, a large cranium with a low nasal bridge, and a narrowed thorax. There are two major subtypes: A short, curved femur characterizes type 1; and a straight femur with cloverleaf skull characterizes type 2. The neuropathology includes megalencephaly with posterior fossa hypoplasia, deep sulci with polymicrogyria, and leptomeningeal

glioneuronal heterotopia. There is temporal lobe enlargement, a deep transverse sulcus across the inferior medial temporal surface, and hippocampal dysplasia. The basal ganglia and the dentate and olivary nuclei are also malformed.

Mutations in fibroblast growth factor receptor-3 (*FGFR3*) have been identified in both types of thanatophoric dysplasia [57,58].



Fig. 2.17-1. Thanatophoric dysplasia. Infant with short stature and short limbs.



Fig. 2.17-2. Brain exhibits abnormal formation of sulci associated with pachygyria, predominantly in the temporal lobes.

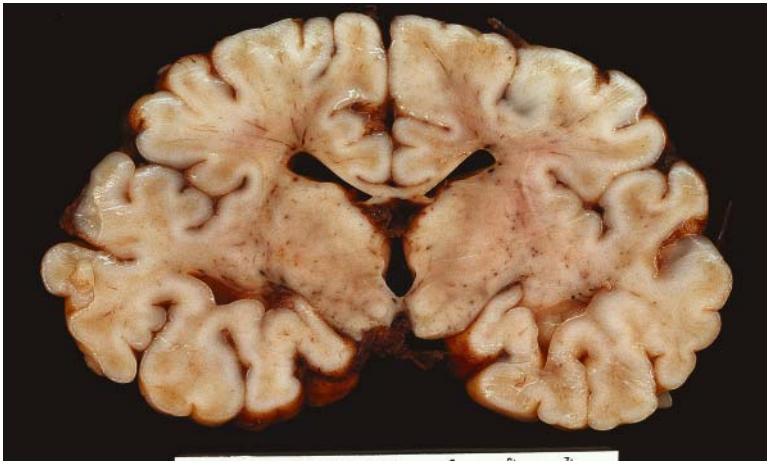


Fig. 2.17-3. Coronal section of the brain exhibits abnormal deep sulci in the temporal lobes.

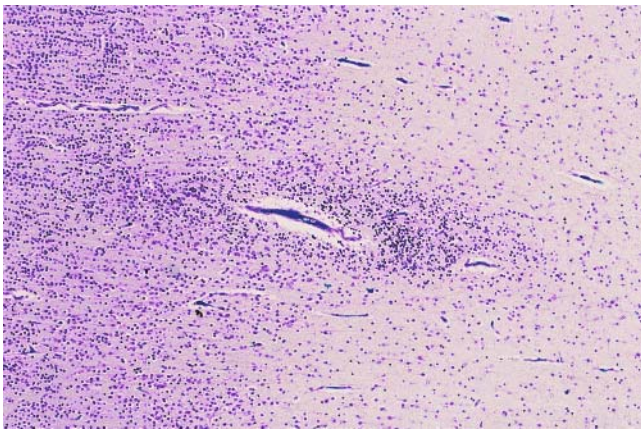


Fig. 2.17-4. Microscopic section of subcortical neuronal heterotopia encircling a small vessel. Nissl stain.

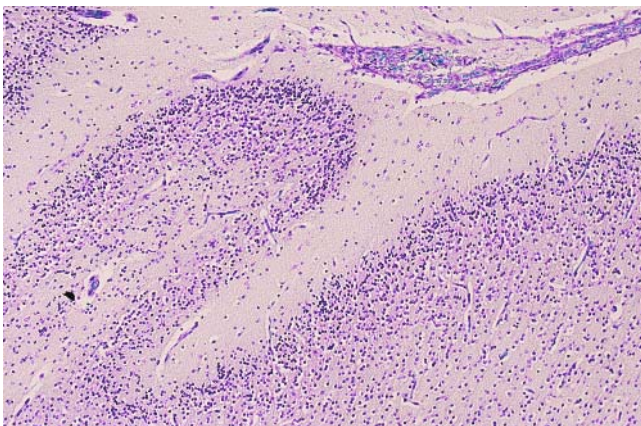


Fig. 2.17-5. Microscopic view of polymicrogyria. LFB.

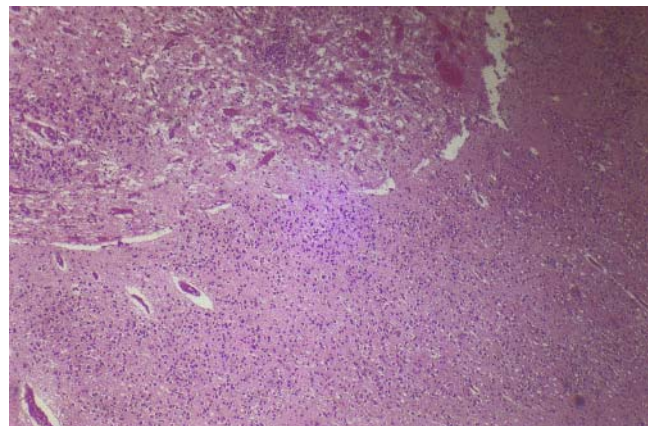


Fig. 2.17-6. Microscopic view of leptomeningeal glioneuronal heterotopia. H&E.

2.18 Hydrocephalus

Classification

Hydrocephalus caused by obstruction

 Congenital aqueductal occlusion

 Lesions in the ventricular system or subarachnoid space

Hydrocephalus caused by overproduction of CSF

 Choroid plexus hyperplasia or neoplasms

Hydrocephalus without obvious lesion

 Normal-pressure or low-pressure hydrocephalus

 Hydrocephalus ex vacuo

Hydrocephalus, type unspecified

 X-linked congenital hydrocephalus

The pathogenesis and classification of congenital aqueductal occlusion via stenosis, forking, gliosis, or membrane formation is controversial [59,60].

X-linked congenital hydrocephalus affects boys, 25% of whom have adduction-flexion deformity of thumbs. Mental deficiency may be associated; and other associations include agenesis of the corpus callosum and agenesis of the corticospinal fiber system. There is a mutation in L1 CAM at Xq28 [61]. Hydrocephalus due to stenosis of the aqueduct of Sylvius (HSAS); mental retardation, aphasia, shuffling gait, adducted thumbs (MASA); and corpus callosum hypoplasia, retardation, adducted thumbs, spastic paraplegia, hydrocephalus (CRASH) syndromes are allelic disorders [62]. Other inherited cases of congenital hydrocephalus have been reported [63].

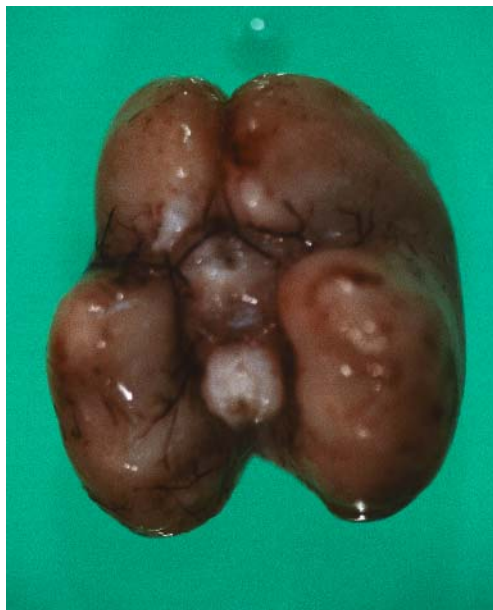


Fig. 2.18-1. Congenital hydrocephalus of a fetus: aqueductal stenosis.



Fig. 2.18-2. Congenital hydrocephalus in fetal brain. Coronal section shows marked dilatation of the ventricles.

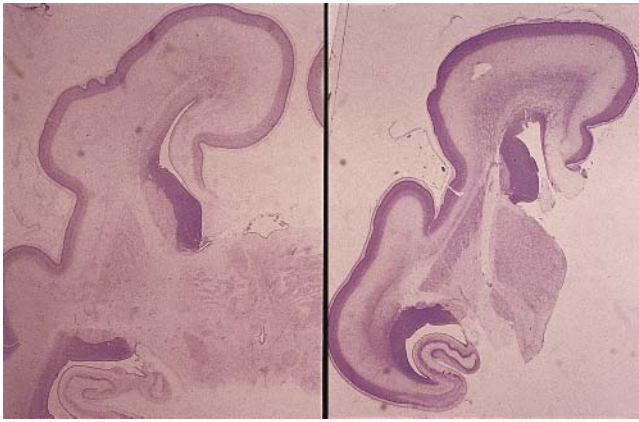


Fig. 2.18-3. X-linked hydrocephalus with dilatation of lateral ventricles, thalamic fusion, and hypoplasia of the white matter and pyramidal tracts in a fetus of 25 weeks' gestation. *Left.* The brain shows negative L1 CAM immunohistochemistry. This case is genetically determined. *Right.* The control.

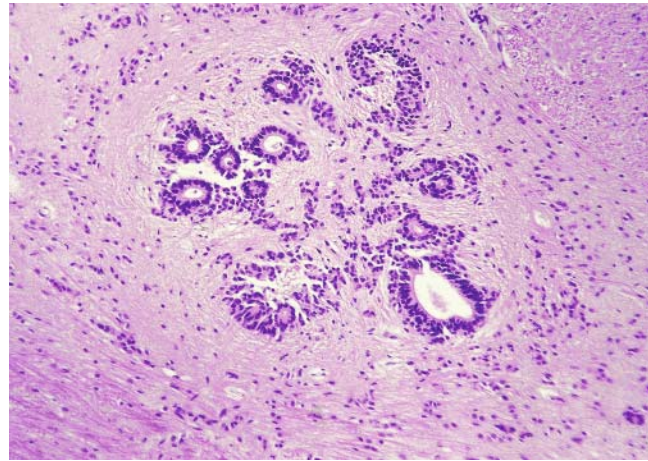


Fig. 2.18-4. Aqueductal stenosis with multiple forking. H&E.

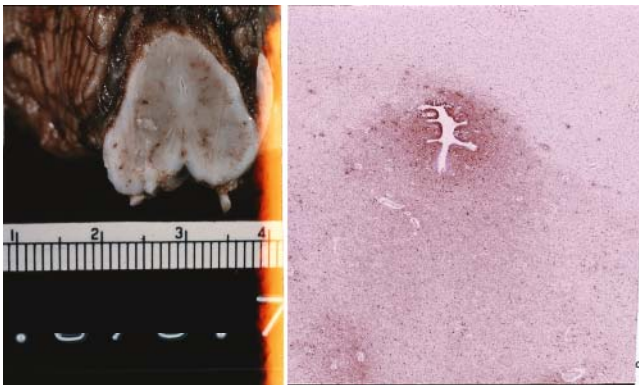


Fig. 2.18-5. Congenital hydrocephalus with aqueductal stenosis. *Left.* Macroscopic view. *Right.* Microscopic view. GFAP.

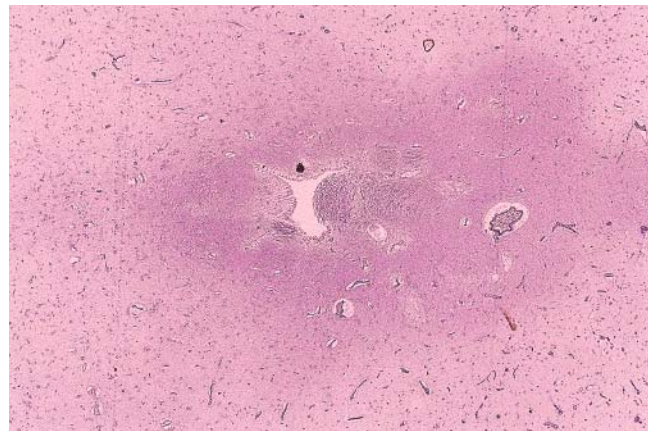


Fig. 2.18-6. Congenital hydrocephalus. Aqueductal stenosis with fibrillary astroglia. Holzer stain.

2.19 Porencephaly

Porencephaly is a cystic cavity within the brain with or without communication between the ventricle and subarachnoid space. It usually develops following a destructive process such as hemorrhage, infarction, or infection in fetal life. When porencephaly develops in the early fetal period, the cavity is smooth walled with a surrounding abnormal gyral pattern in the cortex; e.g. polymicrogyria or pachygyria.

Porencephaly may also develop in the perinatal period following hypoxia-ischemia or hemorrhage. It may appear multicystic, the cysts separated by trabeculae or the small cysts may expand into a single porencephalic cyst.

Fetal or neonatal thrombocytopenia, coagulopathies and hemophilia are reported as a possible pathogenesis [64,65].



Fig. 2.19-1. Congenital porencephaly. Note the large defect with internal trabecula and polymicrogyria in the adjacent cerebrum.

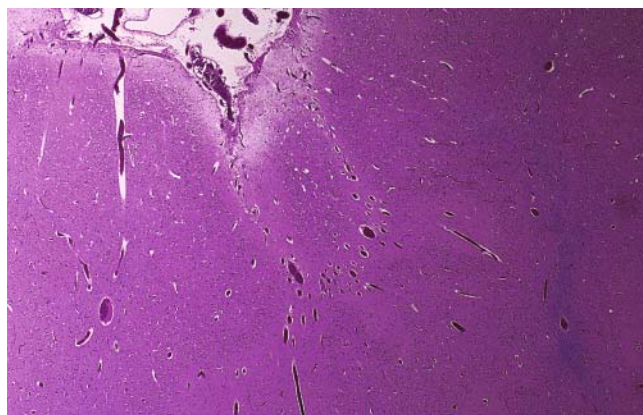


Fig. 2.19-2. Congenital porencephaly. Histology of polymicrogyria in the wall of the porencephalic cavity from 2-19-1. H&E.

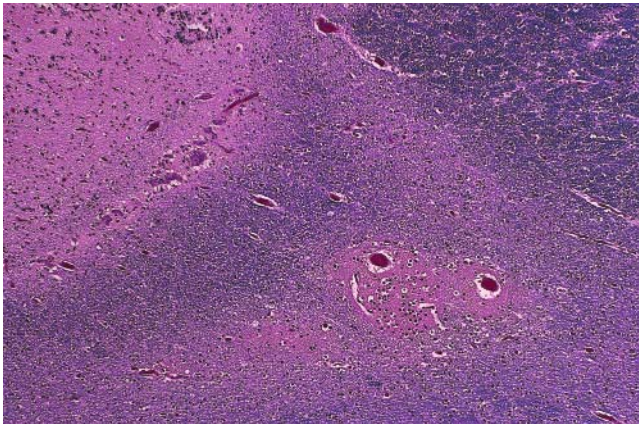


Fig. 2.19-3. Congenital porencephaly with neuronal heterotopia in subcortical white matter adjacent to the porencephalic cavity from 17-1. H&E/LFB.



Fig. 2.19-4. Congenital porencephaly in the left parietal lobe.



Fig. 2.19-5. Porencephaly. Note the large cavity formation in the left parietal lobe, which communicates with the subarachnoid space.



Fig. 2.19-6. Porencephaly. The cavity in the left temporal lobe is expanded, forming a porencephalic cyst.

2.20 Schizencephaly

Schizencephaly is a form of porencephaly that is usually bilateral and symmetrical. There is a narrow cleft in the cortex (narrower than the width of a gyrus) that may extend through to the ventricle. Schizencephaly can be classified as open or closed lip and communicating (with the ventricle) or noncommunicating, depending on whether the cleft is open or closed. The walls of the cleft have radially oriented gyri or polymicrogyria.

Antenatal cerebral infarcts in the middle cerebral artery distribution have been implicated in the patho-

genesis of schizencephaly. A very early onset is suggested when it is associated with neuronal heterotopia in ventricular walls, indicating disruption of neuronal migration. Familial occurrence is rarely reported but germline mutations in the homeobox gene *EMX2* have been found in patients with severe schizencephaly [66]. These genetic cases suggest developmental failure, although the genetic mechanism is heterogeneous.



Fig. 2.20-1. Schizencephaly. Lateral view of the fetal brain reveals a focal defect in the hemisphere.

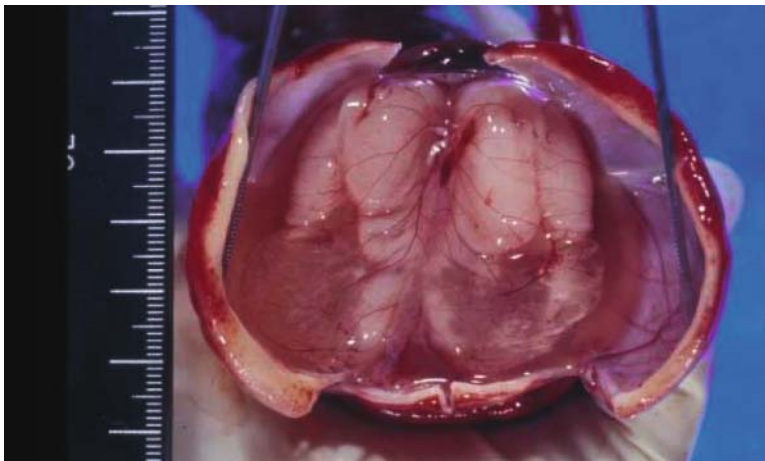


Fig. 2.20-2. Schizencephaly. Fetal brain at 23 weeks' gestation exhibiting bilateral symmetrical defects of parasagittal portions of the frontal and parietal lobes. (Courtesy of Dr. Kanaumi T.)

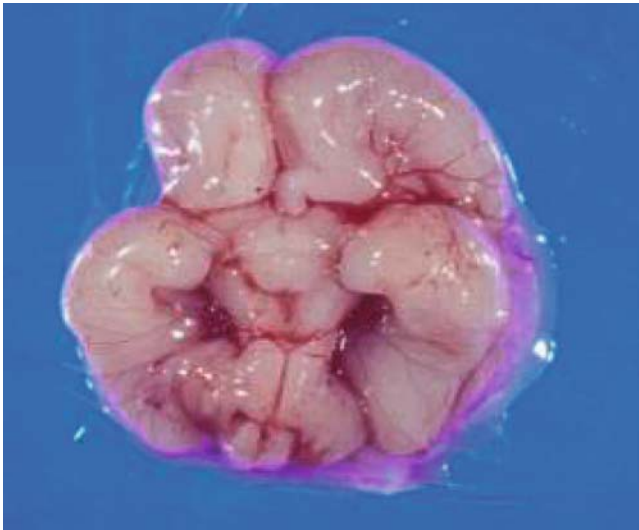


Fig. 2.20-3. Schizencephaly. Basal view of the same brain as in 2.19-2. The brain appears normal.

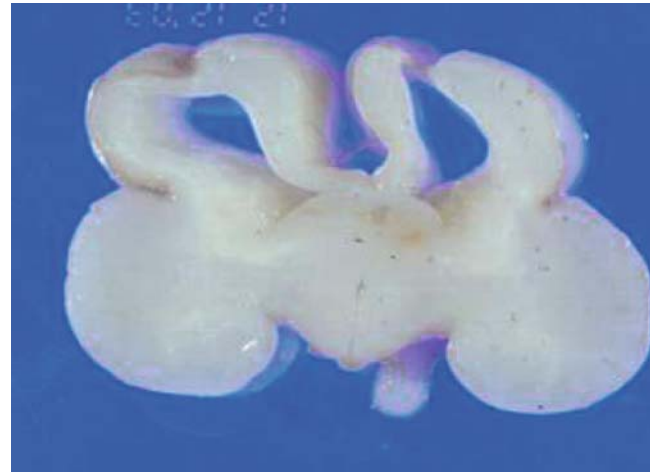


Fig. 2.20-4. Schizencephaly (same case as in 2.19-2). Coronal section of fetal brain at the level of the mammillary bodies. There are partial defects in parasagittal areas of the frontal lobes of both hemispheres.



Fig. 2.20-5. Schizencephaly (same case as in 2.19-2). There are large defects in parasagittal areas of the parietal lobes in the fetal brain.

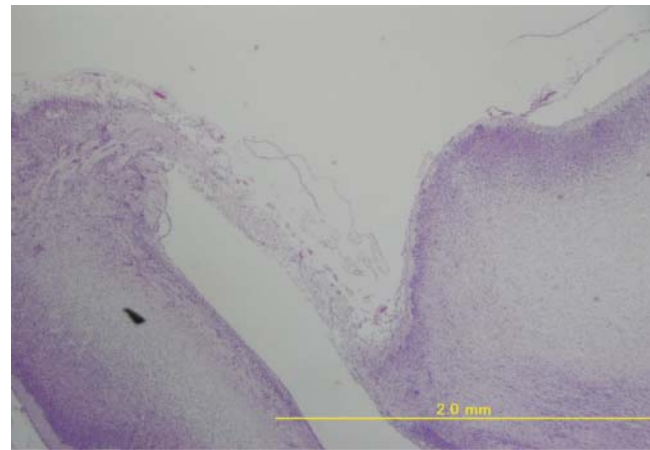


Fig. 2.20-6. Schizencephaly. Histology of frontal area shows a complete defect of the cortex and white matter of the parietal lobe, with polymicrogyria and cortical dysplasia bordering the defect. H&E. (Courtesy of Dr. Kanaumi T.)

2.21 Hydranencephaly

Hydranencephaly exhibits extreme ventricular dilatation, with most of the cerebral mantle replaced by a membrane of gliotic connective tissue containing an occasional neuron or ependymal cell. In some of the necrotic cerebral lesions there may be islands of cerebral tissue underneath the leptomeninges. The basal ganglia are relatively spared. The thalami are small. The lesion is the result of an early fetal destructive process that may be caused by ischemic necrosis secondary to vascular insufficiency, fetal hypoxia, accidental trauma, or CO intoxication or the result of a genetic malformation (Fowler's disease) [2,63]. Congenital

hydranencephalic-hydrocephalic syndrome with proliferative vasculopathy shows glomeruloid vessels, intracytoplasmic inclusions, and microcalcifications; and, it may be attributed to alterations in the mitochondrial respiratory chain.

Basket brain is considered to be a lesion intermediate between hydranencephaly and porencephaly. There is a bilateral large defect of both cerebral hemispheres with sparing of the cingulate gyri and adjoining tissues. This forms a medial-sagittal arch of brain connecting the occipital and frontal brain remnants [67].



Fig. 2.21-1. Hydranencephaly. Basal view of the brain and spinal cord shows a remnant of cerebrum, intact basal ganglia, and a normal-appearing cerebellum, brain stem, and spinal cord.

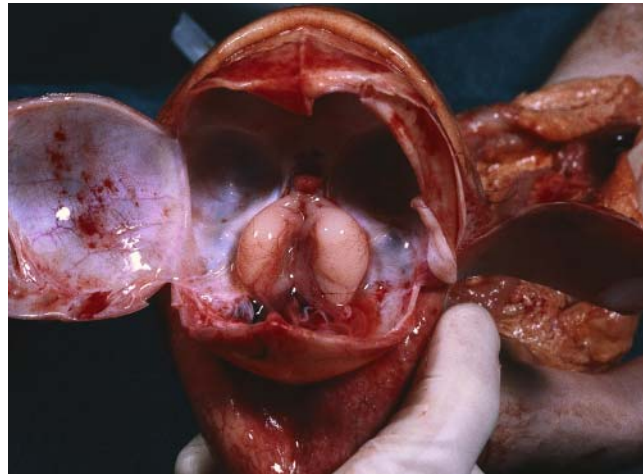


Fig. 2.21-2. Hydranencephaly at autopsy. The basal ganglia and thalamus are intact.

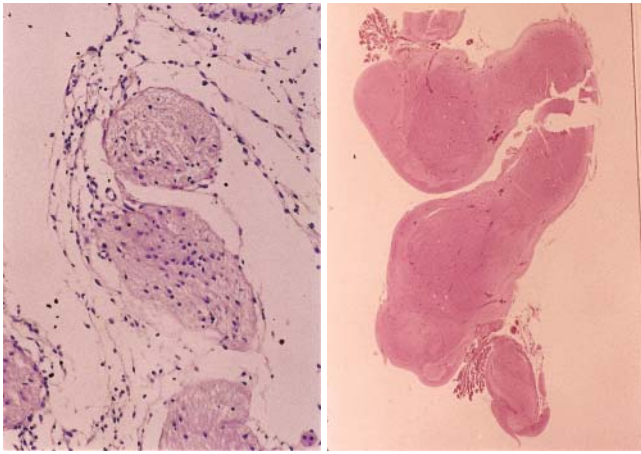


Fig. 2.21-3. Hydranencephaly. *Left.* Remains of the cortex with gliosis in the subpial region. *Right.* Histology of the cerebral hemispheres shows remnants of the diencephalon, midbrain, and part of the temporal cortex. H&E.

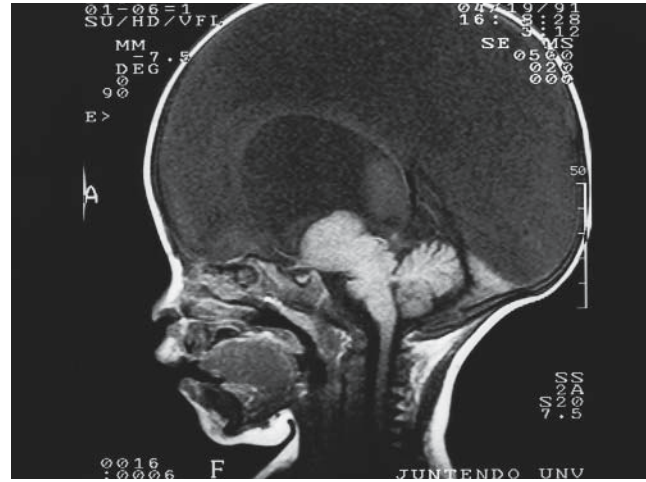


Fig. 2.21-4. Hydranencephaly. MRI sagittal view of the head, revealing a complete defect of the cerebrum with intact diencephalon, brain stem, and cerebellum.



Fig. 2.21-5. Hydranencephaly. Angiography shows few cerebral arteries.

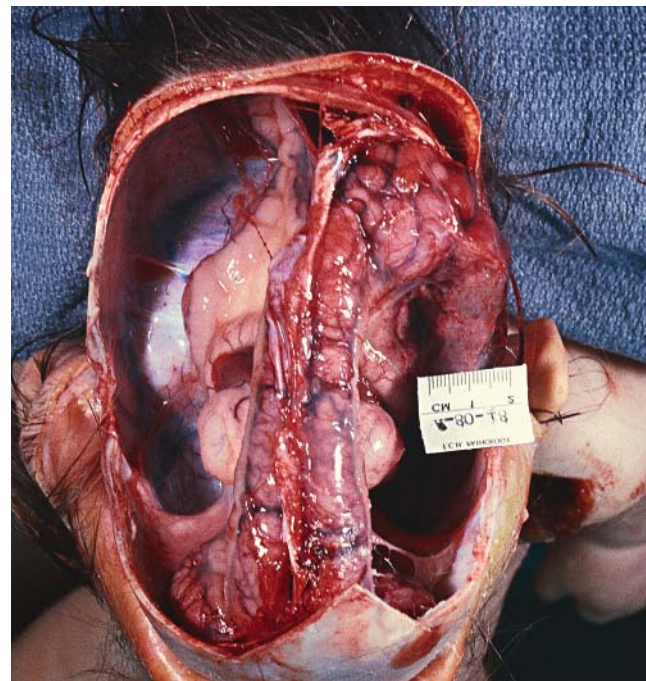


Fig. 2.21-6. Basket brain. Bilateral hemispheric defect with preservation of parasagittal areas such as the cingulate gyri and adjacent brain tissues supplied by the anterior cerebral artery.

2.22 Cysts: Subependymal Cysts, Colloid Cysts, Gliependymal Cysts

The *subependymal cyst* (SEC) is formed following focal necrosis or hemorrhage into the subependymal germinal layer. Prenatal SEC, called subependymal germinolysis, may be associated with congenital anomalies (e.g., heart disease and Zellweger syndrome) or with prenatal infections (e.g., rubella and cytomegalovirus infection). Neonatal SEC follows subependymal hemorrhage in preterm infants and is identified by hemosiderin-laden macrophages in the cyst wall [68].

The *colloid cyst* (neuroepithelial or parahypophyseal cyst) is rare in children and may be familial. It is usually

found in the third ventricle and contains thick mucinous amorphous debris. The lining has variable cells: cuboidal, flat, columnar ciliated, goblet, or multilayered [69].

The *gliependymal cyst* is less common. The microscopic structure of its wall is usually lined by ciliated ependyma, but it is variable. Some cysts have the epithelium situated on a basement membrane or on a sheet of reticulum fibers similar to the choroid plexus. This cyst derives from displaced neuroectodermal tissue.

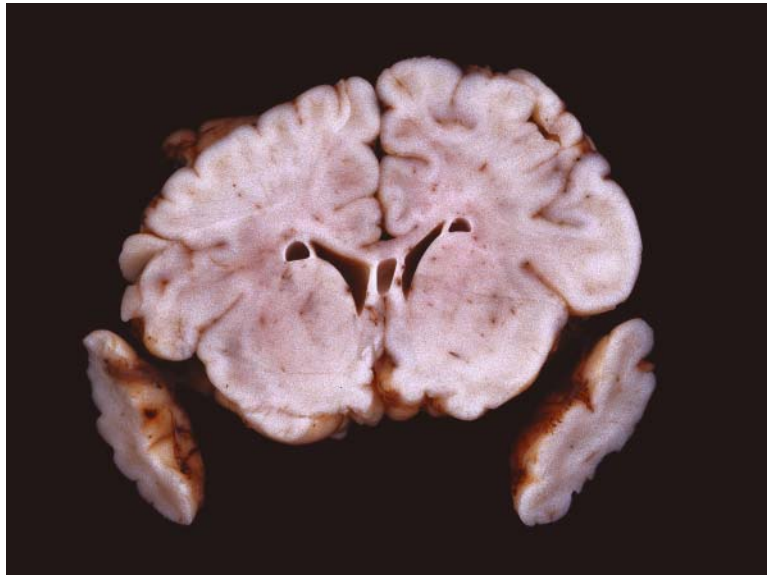


Fig. 2.22-1. Subependymal cyst (germinolysis) on the head of the caudate nucleus.

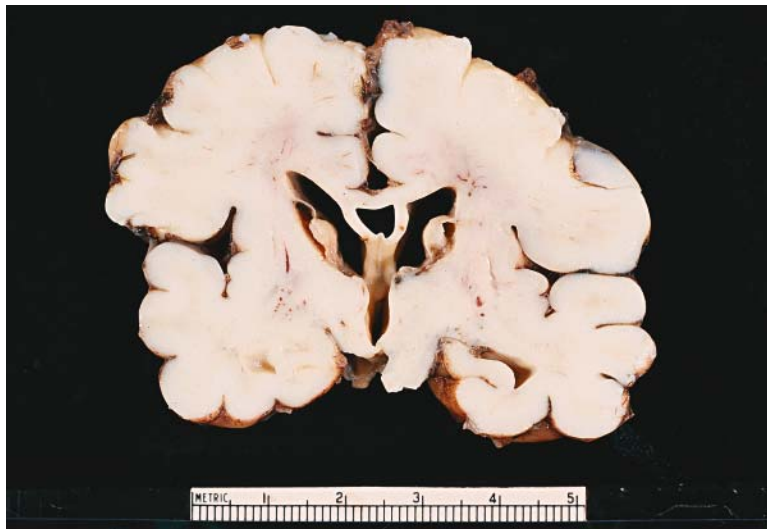


Fig. 2.22-2. Subependymal cyst (germinolysis) in the striae terminalis between the caudate nucleus and thalamus.

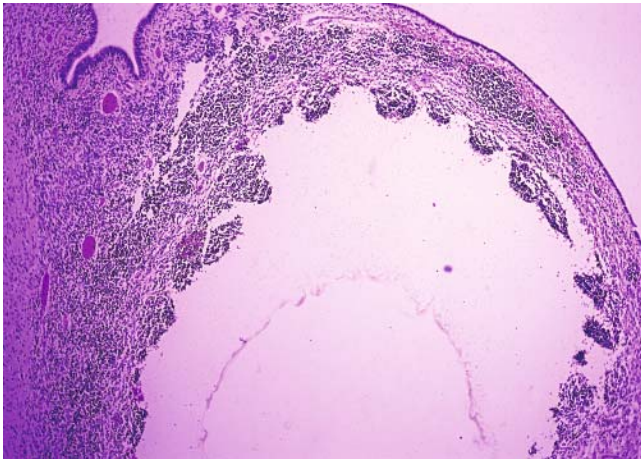


Fig. 2.22-3. Subependymal cyst exhibiting germinal cells in the wall of the cyst (germinolysis). H&E.

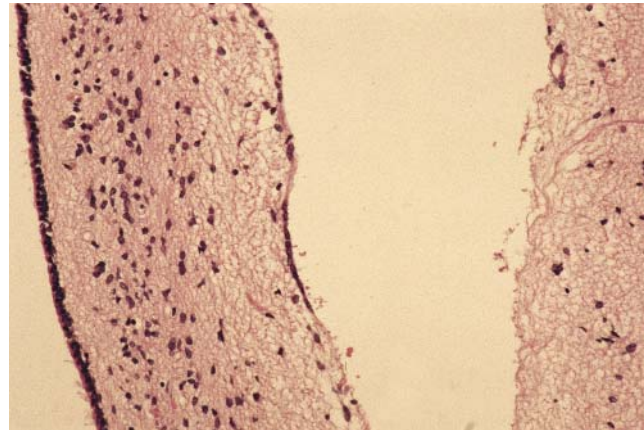


Fig. 2.22-4. Developmental ependymal cyst in the subependymal layer of the lateral ventricle lined by ependyma. H&E.

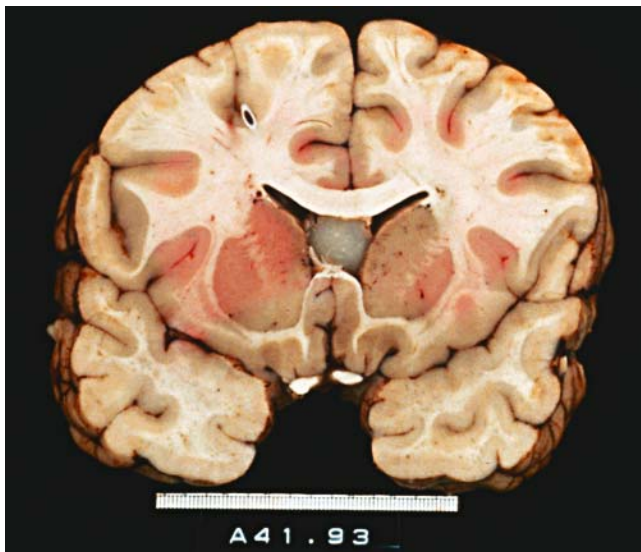


Fig. 2.22-5. Colloid cyst in the septum pellucidum.

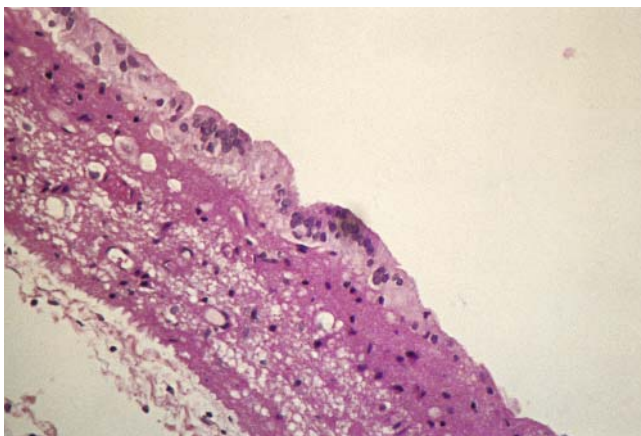


Fig. 2.22-6. Gliependymal cyst. Cyst wall shows ciliated ependymal cells. H&E.

2.23 Arachnoid Cyst, Neuroenteric Cyst

The congenital arachnoid cyst is formed by a developmental split in the arachnoid with loculated clear CSF between the brain and dura. It is lined by smooth tissue and often does not communicate with the rest of the subarachnoid space, causing pressure deformity of the underlying brain. The most common locations are in the sylvian fissure, interhemispheric fissure, and cisterna magna. The pathogenesis of the arachnoid cyst is not known, but infection and trauma have been suggested. The cortex under the cyst is usually intact but may be

deformed or displaced. If this is marked or causing symptoms, surgical resection of the cyst is performed.

Neuroenteric cysts are heterotopic intraspinal cysts lined with mucosa of the alimentary tract. They vary in size and in the type of mucosal lining. The cysts are most commonly found in the low cervical and upper thoracic segments at the ventral surface of the cord. Associated deformities of the spine are severe in infants and may include shortening of the neck or complete splitting of the spine [69].

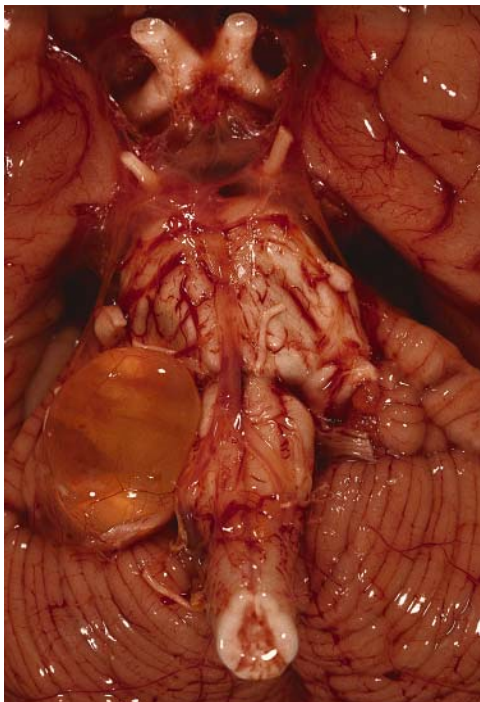


Fig. 2.23-1. Arachnoid cyst on the lateral side of the brain stem.

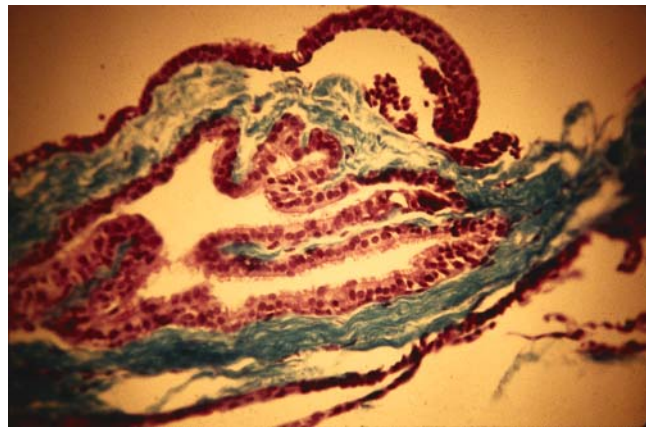


Fig. 2.23-2. Arachnoid cyst. Microscopy with trichrome stain.

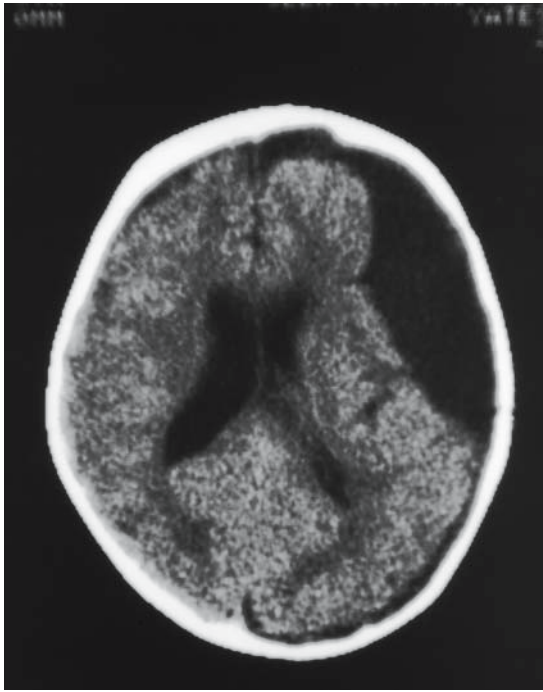


Fig. 2.23-3. Arachnoid cyst over the right frontal region with a compression deformity of the right cerebral hemisphere.

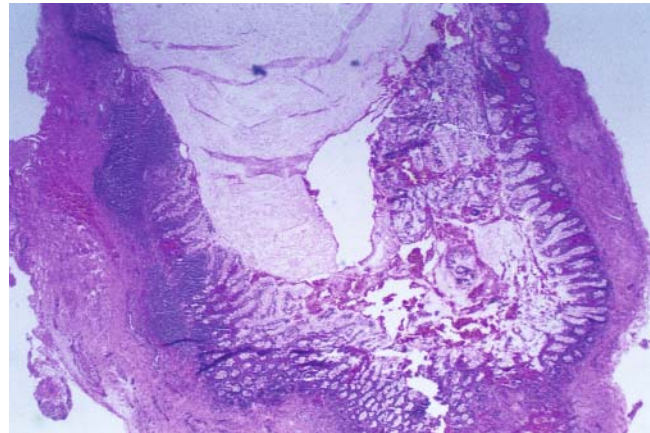


Fig. 2.23-4. Neuroenteric cyst. Microscopy reveals respiratory-type and gastrointestinal-type mucosa. H&E.

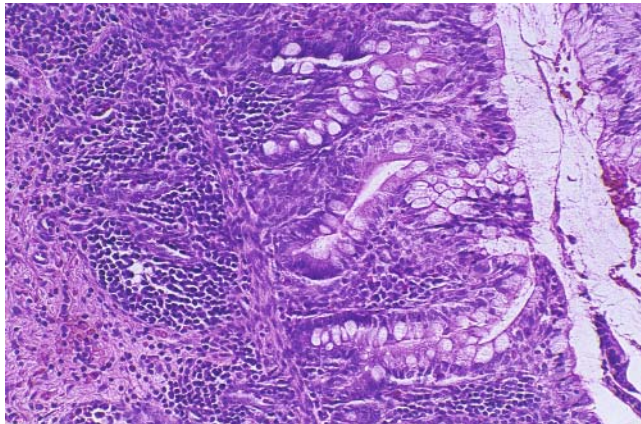


Fig. 2.23-5. Neuroenteric cyst. Microscopy reveals gastrointestinal-type mucosa. H&E.



Fig. 2.23-6. Teratogenous cyst. Simple epithelium found dorsal to the spinal cord without features of the neuroepithelial or neuroenteric cyst. H&E.

2.24 Malformation of the Cranium: Craniosynostosis, Meckel-Gruber Syndrome, Amniotic Band

Craniosynostosis is premature fusion of the cranial sutures. Mutations in the *FGFR* gene are present in several syndromes with craniosynostosis, such as Apert's, Crouzon's, and Pfeiffer's syndromes [70]. Apert's syndrome has variable degrees of cranial synostosis, syndactyly of the hands and feet, and may have a frontonasal encephalocele [71]. Crouzon's syndrome has craniosynostosis of coronal, lambdoid, and sagittal sutures; and it shows a deformed skull, exophthalmos, and mental retardation.

Meckel-Gruber syndrome is a combination of occipital skull defect with encephalocele, microcephaly, cerebral and cerebellar hypoplasia, and renal cysts. The locus heterogeneity has been demonstrated as MKS1 to chromosome 17q21-24, MKS2 to 11q13, and MKS3 to 8q24 [72–75].

Amniotic bands form when the amnion ruptures and creates bands that may compress or encircle and amputate parts of the developing fetus.



Fig. 2.24-1. Apert syndrome. This syndrome is characterized by craniosynostosis and severe syndactyly of the hands and feet (as acrocephalosyndactyly). The brain exhibits polygyria.



Fig. 2.24-2. Crouzon's syndrome. The cerebral hemispheres are normal. The narrowed cisterna magna crowds the brain stem and cerebellum.



Fig. 2.24-3. Meckel-Gruber syndrome. Note the skull defect and occipital encephalocele.

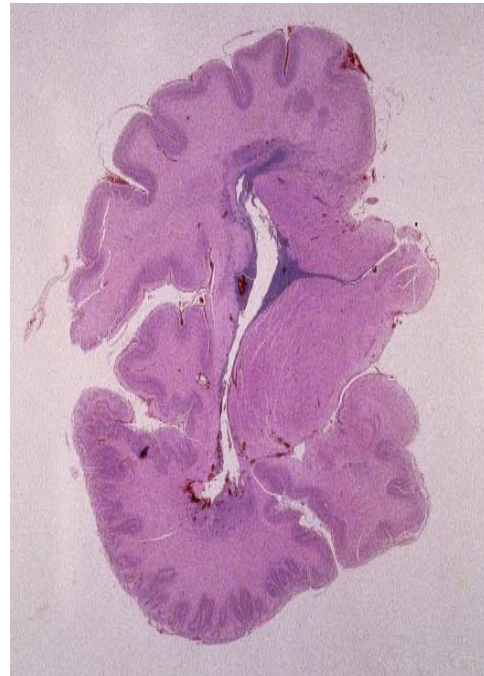


Fig. 2.24-4. Meckel-Gruber syndrome. Whole mount of cerebral hemisphere exhibits deformity of the lateral ventricle and polymicrogyria of the parietal and temporal cortex. H&E.

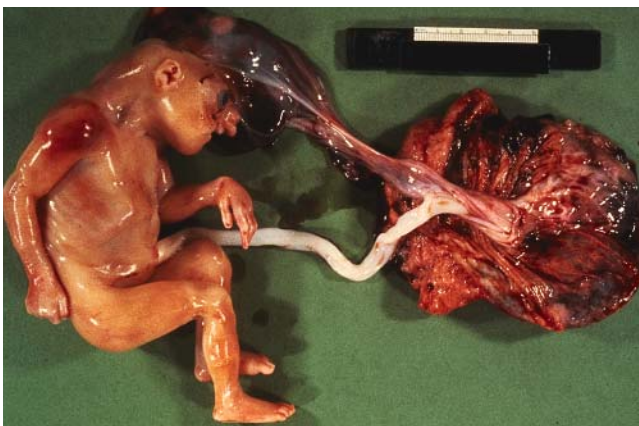


Fig. 2.24-5. Amniotic bands cause face and skull malformations.



Fig. 2.24-6. Amniotic bands are attached to the upper jaw and head, deforming the mouth, eye, nose, and forehead.

2.25 Malformation of the Brain Stem

The olivary nuclei may show various abnormal shapes: hypoconvoluted C-shaped structures, hyperconvoluted structures, thickening of the dorsal rami of the principal olive, a solid mass of cells, or a group of disconnected segments. Malformations of the dentate nucleus may also be associated with olivary dysplasias, and there are frequently other brain abnormalities such as those in the cortex in Zellweger's syndrome. Ectopic olivary segments situated along the migration path from the rhombic lip are also reported in Zellweger's syndrome.

Mobius syndrome is characterized by congenital facial diplegia associated with orofacial malformations and may be caused by cranial nerve nuclear aplasia,

hypoplasia, or ischemic necrosis [76]. Some or all of the IX, X, XI, and XII cranial nerves may be involved. The absence of the facial nerve can be diagnosed by MRI [77]. Most cases are sporadic, but familial cases are also reported.

Dentato-olivary dysplasia is often present in conditions with intractable infantile seizures such as Ohtahara syndrome. In this condition the inferior olives are hook-shaped, coarse, and lacking undulations; and dentate nuclei show a compact arrangement of interconnected islands [2]. The olivopontocerebellar atrophies or hypoplasias (see Section 2.28) are rare conditions with some genetic associations.

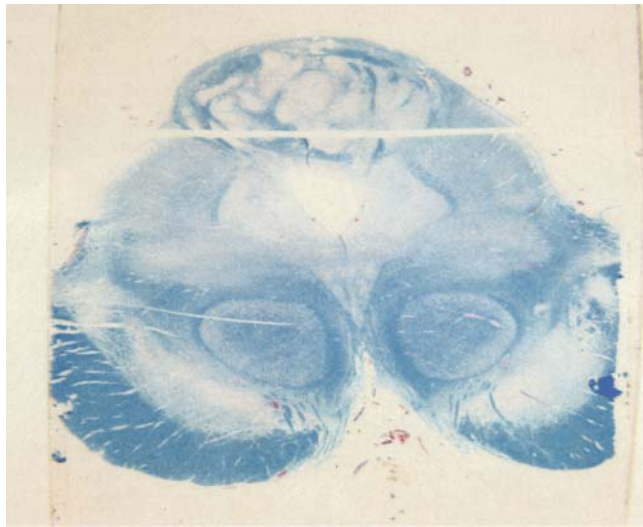


Fig. 2.25-1. Midbrain with gray matter heterotopia occupying the collicular plate. LFB.

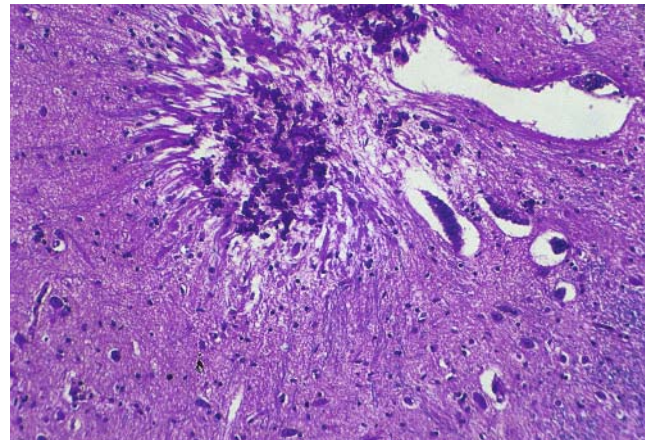


Fig. 2.25-2. Moebius syndrome with focal gliosis and calcification in the tegmentum of the brain stem. H&E.

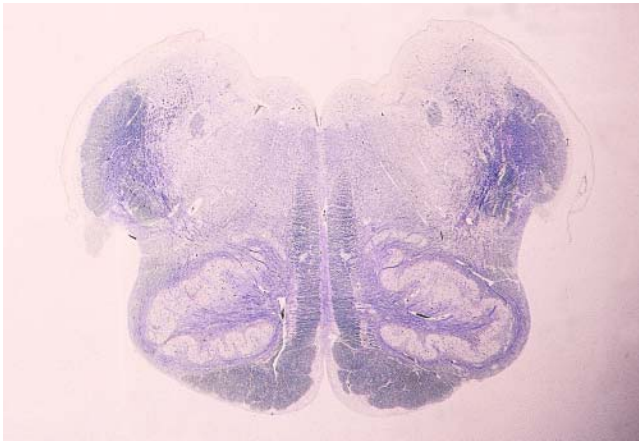


Fig. 2.25-3. Zellweger syndrome. Medulla has abnormally shaped principal olivary nuclei. LFB.

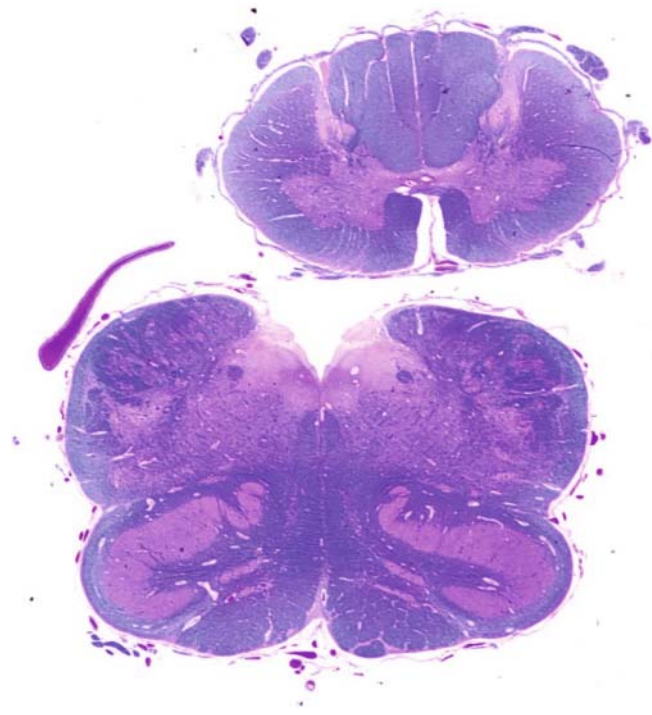


Fig. 2.25-4. Dentato-olivary dysplasia. Medulla oblongata shows poor convolutions and thickening of the principal olivary nuclei. H&E/LFB.



Fig. 2.25-5. Dentato-olivary dysplasia. Horizontal section of the pons and cerebellum shows enlarged dentate nuclei. The cerebellar folia and the pons are normal.

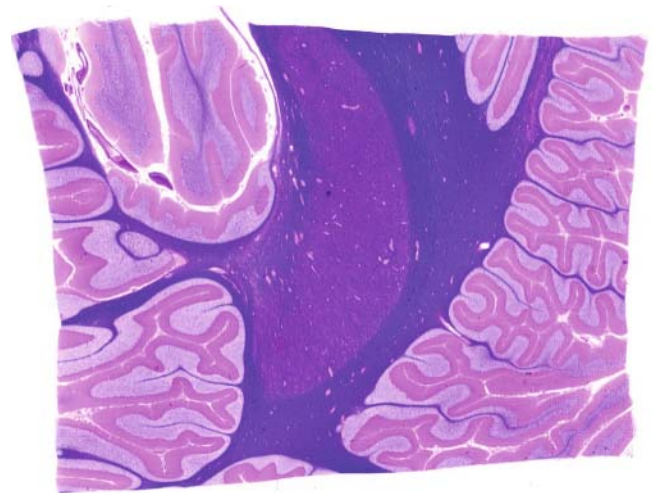


Fig. 2.25-6. Dentato-olivary dysplasia. Histology of the cerebellum shows a large, thickened dentate nucleus. H&E.

2.26 Agenesis of the Vermis of the Cerebellum and Joubert Syndrome

Agenesis of the vermis of the cerebellum has been used to designate different conditions. In the *Dandy-Walker malformation* (DWM) and *Dandy-Walker variant* (DWV), there is total or near-total agenesis of the vermis with separation of the cerebellar hemispheres (rhombencephaloschisis) with or without cystic dilatation of the cleft and fourth ventricle.

In cerebellum without vermis (also known as agenesis of the vermis with fusion of cerebellar hemispheres, rhombosynapsis, or rhomboencephalosynapsis) there is

a single lobed cerebellum without paired hemispheres or vermis.

Joubert syndrome is characterized by cerebellar vermis hypoplasia with prominent superior cerebellar peduncles (molar tooth sign on MRI), episodes of hyperpnea, abnormal eye movements, ataxia, and mental retardation. The *JS* gene, encoding joubertin protein, is expressed in embryonic hindbrain and forebrain [78,79]. There may be associated occipital meningoceles or meningoencephaloceles.

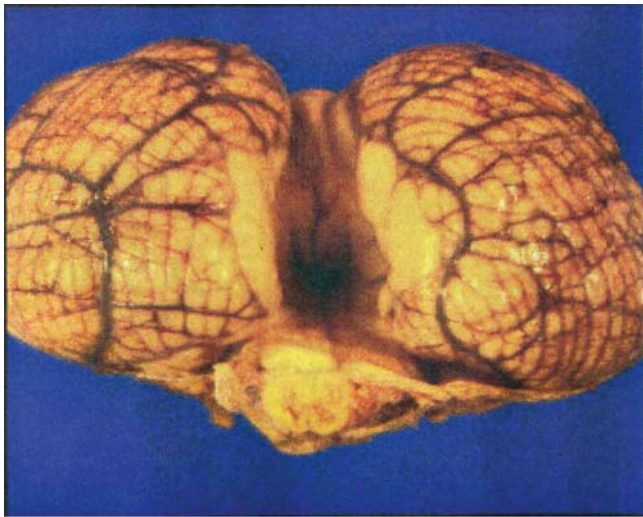


Fig. 2.26-1. Agenesis of the vermis with separation of cerebellar hemispheres without cystic dilatation of the cleft and fourth ventricle (rhombencephaloschisis).

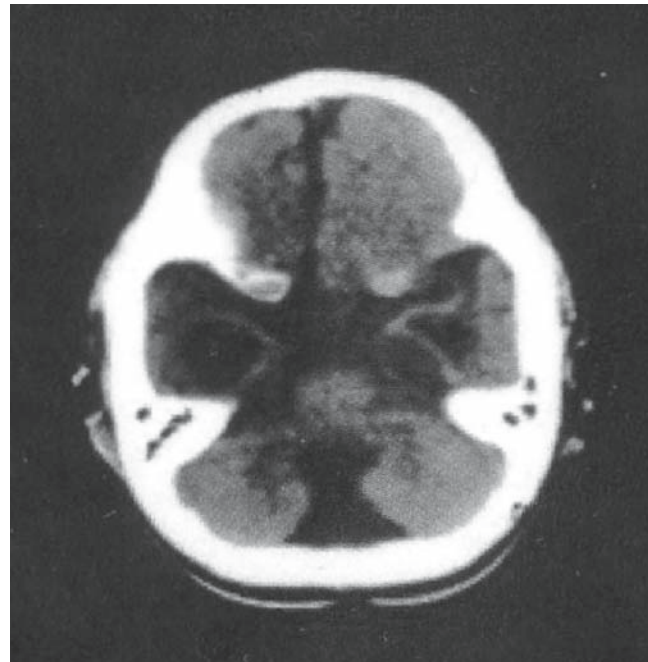


Fig. 2.26-2. Agenesis of the cerebellar vermis seen on a CT scan of an infant brain.



Fig. 2.26-3. Joubert syndrome. The superior cerebellar peduncles are separated and parallel to each other (molar tooth sign). H&E.

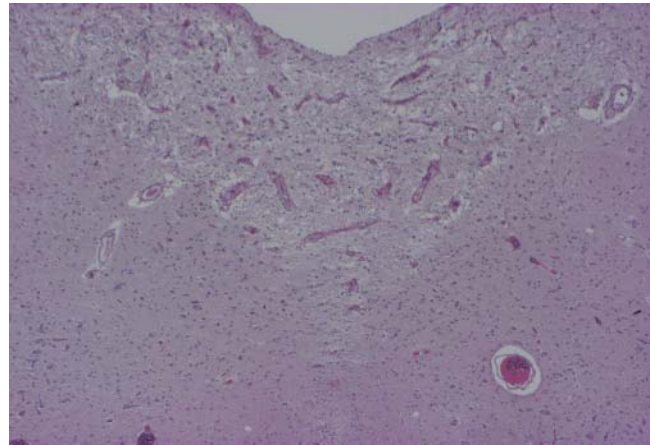


Fig. 2.26-4. Joubert syndrome. Periventricular areas of the medulla oblongata show gliosis with vascular dilatation. H&E.



Fig. 2.26-5. Rhombencephalosynapsis. The cerebellum is pear-shaped with a markedly shortened horizontal diameter and an increased anteroposterior diameter. The fourth ventricle is also elongated anteroposteriorly.

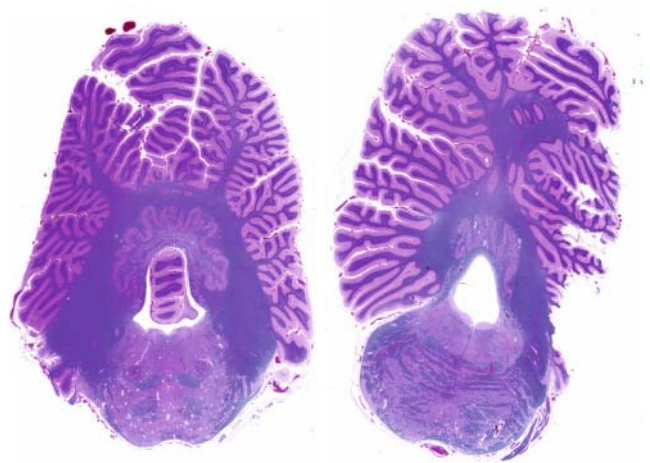


Fig. 2.26-6. Rhombencephalosynapsis. Histology of a horizontal section of the brain stem and cerebellum shows “agenesis of the vermis with fusion of cerebellar hemispheres.” The dentate nucleus is also fused, forming a central deep core. H&E/LFB.

2.27 Malformation of the Cerebellar Hemispheres and Spinal Cord

Total cerebellar aplasia is rare. Neocerebellar aplasia or hypoplasia of the cerebellum, also rare, is characterized by a small vermis and extremely small or absent cerebellar hemispheres [67]. Aplasia or hypoplasia of the cerebellum may coexist with malformations of cerebral hemispheres. For example, in lissencephaly type 2 there is cerebellar heterotopia, polymicrogyria, or disorganized cortex with lack of fissures and folia.

Syringomyelia and *syringobulbia* are cavitating lesions that may be primary or secondary to tumors or trauma or hemorrhage. The cavities are initially in the gray

matter and may arise from a dilated central canal in which abnormal CSF pressure produces enlargement [2,80].

Diastematomyelia consists of a division in two halves of the spinal cord. Its localization is often lumbar. It is frequently associated with other spinal cord and vertebral column malformations, such as spina bifida. The cleft between two hemicords is of variable size, and one or both of the cords may be hypoplastic. *Dimyelia* or *dipromyelia* consists of complete duplication of the spinal cord.



Fig. 2.27-1. Dandy-Walker-like lesion in Walker-Warburg syndrome with cerebellar hemispheres splayed by a midline cyst (not visible) and deformation of the occipital poles.



Fig. 2.27-2. Complete agenesis of the cerebellum: brain stem with midbrain dissected superiorly. The collicular plate partially covers the floor of the fourth ventricle from which blindly ending cerebellar peduncles extend.

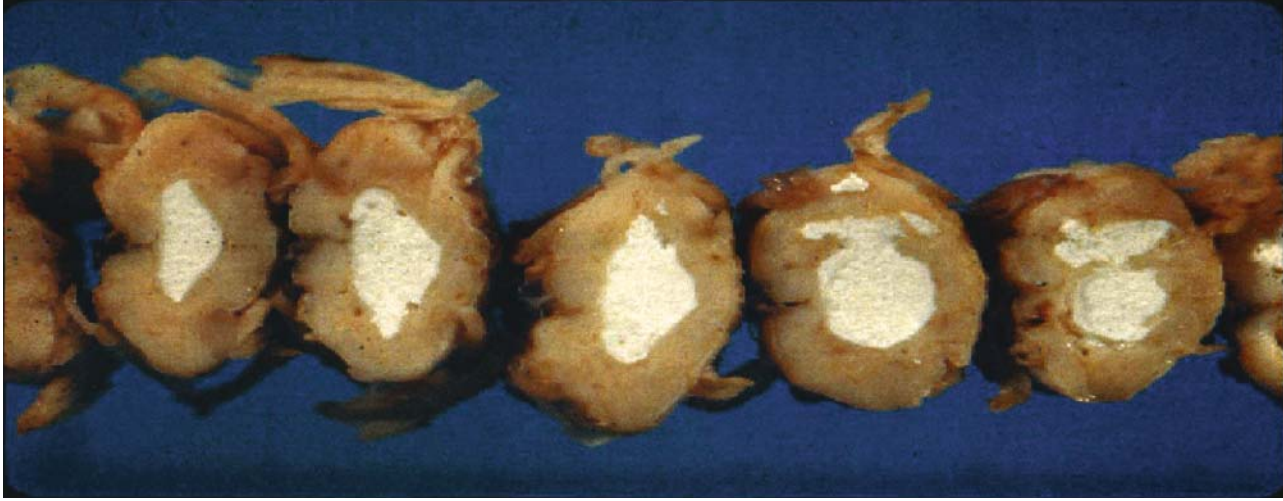


Fig. 2.27-3. Spinal cord syringomyelia from an adult following injection of barium and gelatin. The cavity extends over many segments and exhibits irregularities at some levels. H&E.



Fig. 2.27-4. Spinal cord syringomyelia. Histology reveals a slit-like cavity after collapse of the fluid-filled space following cord dissection. The cavity runs laterally in the cord, interrupting the ventral horns. LFB.

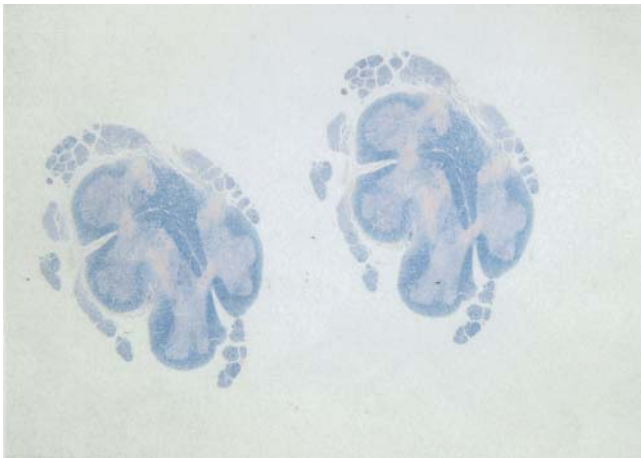


Fig. 2.27-5. Diastatomyelia. There is partial duplication of the spinal cord with union of the posterior horns at one side.



Fig. 2.27-6. Diplomyelia with two separate spinal cords at the lumbar level.

2.28 Infantile Olivopontocerebellar Atrophy/Hypoplasia, Pontocerebellar Hypoplasia

The terms infantile olivopontocerebellar atrophy (OPCA) or hypoplasia (OPCH) are applied to rare disorders presenting at birth with a reduced number of neurons in the olives and in the pons with an associated small cerebellum. It is not defined whether there is indeed loss of cells, or “hypoplasia.” The disorders are variously reported of families with OPCH, microencephaly, and white matter gliosis [81,82]. Another condition, the disialotransferrin developmental deficiency syndrome, is an autosomal recessively inherited disease with OPCA, failure to thrive, hypotonia, liver disease, and

retinal dystrophy [83]. Some infants with Werdnig-Hoffmann disease have OPCA [84]. A recent report suggests a classification of these complex disorders [85].

Pontocerebellar hypoplasia, a rare autosomal recessive disorder, is characterized by an abnormally small cerebellum and brain stem. Genetic studies in one family have shown a linkage to chromosome 7q11–21. It has been called cerebellar atrophy with progressive microcephaly (CLAM) [86].

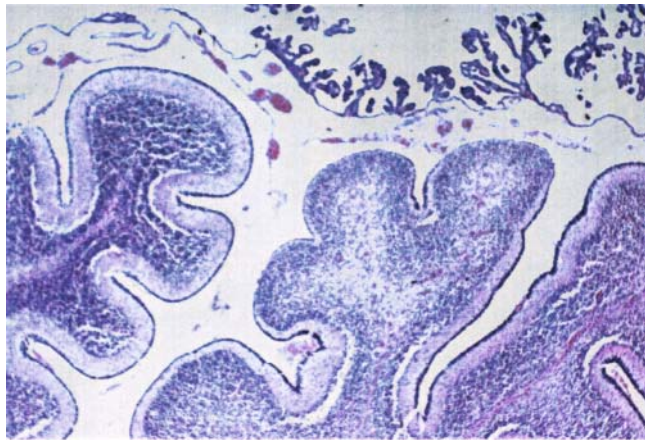


Fig. 2.28-1. Olivopontocerebellar atrophy (OPCA). Cerebellum with diffuse and focal atrophy of the folia. H&E/LFB.

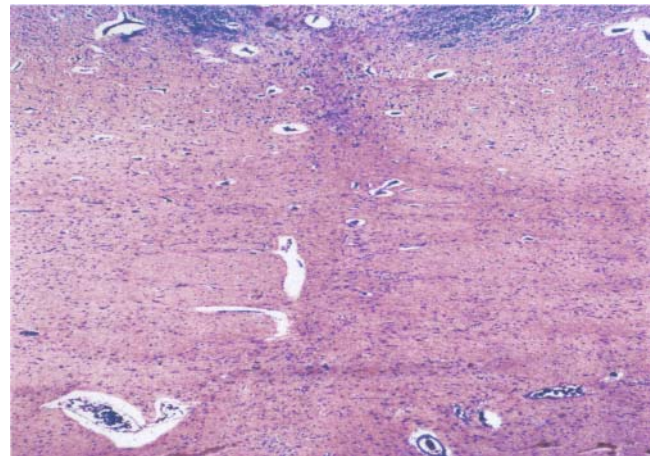


Fig. 2.28-2. OPCA. Histology of the pons (myelin stain) showing myelination of the medial longitudinal fasciculus and absence of myelin in pontocerebellar tracts. H&E/LFB.

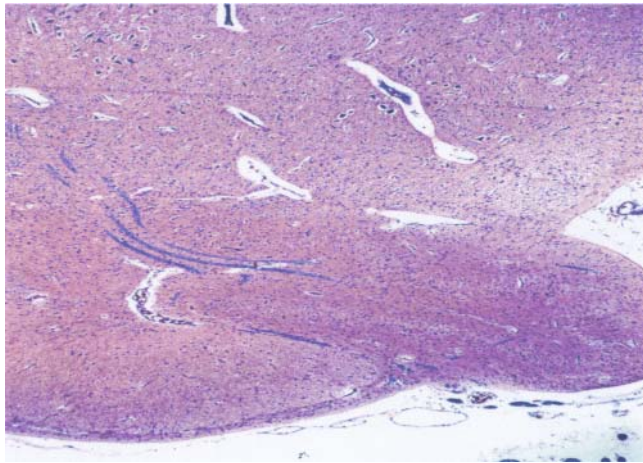


Fig. 2.28-3. OPCA. Histology of the ventral lateral medulla. Note the olive protruding laterally and a complete absence of neurons. Some myelinated axons leave the olivary hilus. H&E/LFB.

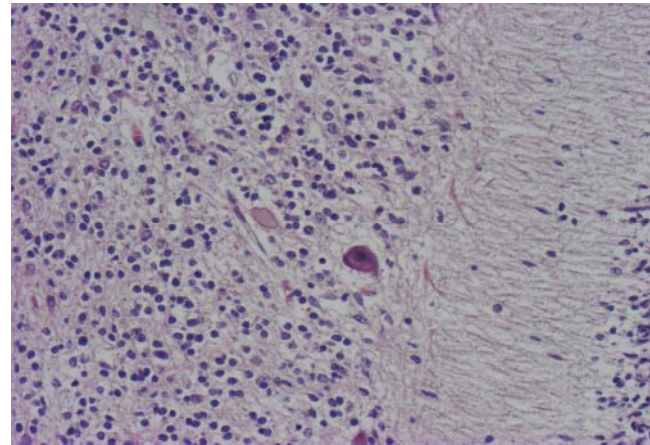


Fig. 2.28-4. Pontocerebellar hypoplasia. Microscopy reveals a loss of Purkinje cells and torpedo formation. H&E.

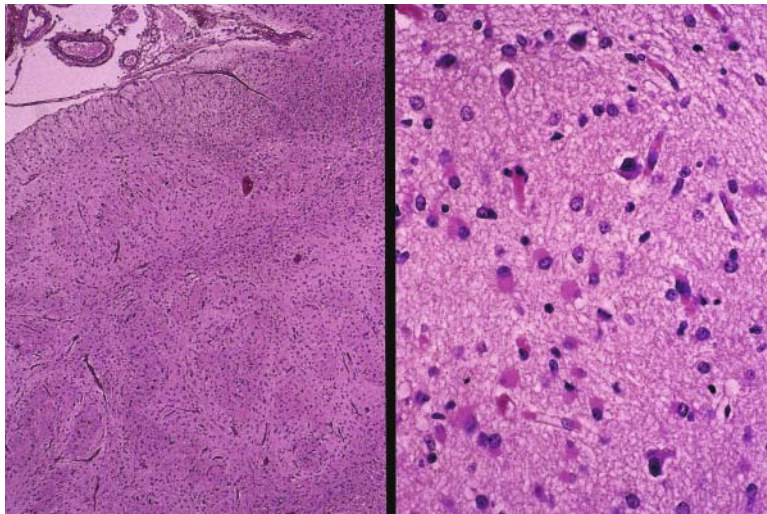


Fig. 2.28-5. Pontocerebellar hypoplasia. Microscopy reveals hypoplasia of the interior olivary nucleus in a case of pontocerebellar hypoplasia. H&E.

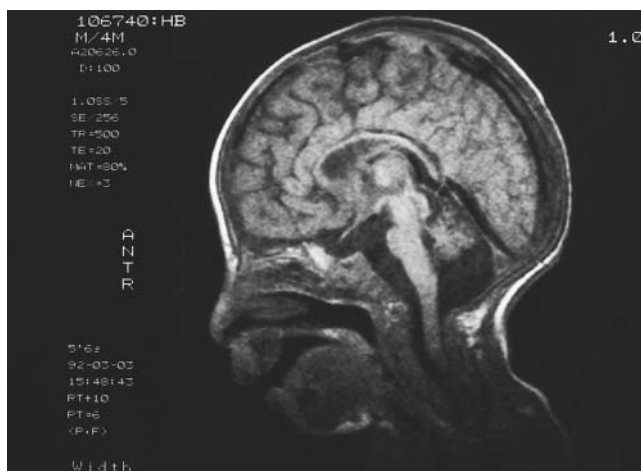


Fig. 2.28-6. Pontocerebellar hypoplasia. MRI shows a small basis pontis and cerebellar vermis.

3 Chromosomal Abnormalities

3.1 Down Syndrome

Down syndrome (DS), caused by trisomy 21, is characterized clinically by somatic abnormalities, intellectual disabilities in children, and Alzheimer-type dementia in adults. The phenotype may vary, with minor brain anomalies such as hypoplasia of the superior temporal gyrus, brain stem, and cerebellum, decreased brain weight and rounded occipital poles [1]. Basal ganglia calcification is more frequently found in the region of the globus pallidus and putamen, and its incidence increases with age [2]. Dendrites gradually show abnormal arborization and decreased spines after 4 months of age [3,4]. Alzheimer-type dementia with neuritic plaques and neurofibrillary tangles develops in young adults. Senile plaques and cerebrovascular amyloidosis involve β -

amyloid protein ($A\beta$). In Alzheimer-type dementia, $A\beta_{42}$, which aggregates more rapidly than $A\beta_{40}$, is a major component of diffuse (early) plaques, whereas $A\beta_{43}$ demonstrates early axonal damage in diffuse plaques [5].

The DS phenotypes are determined by a trisomy of the DS obligate region (DSOR) in the long arm of chromosome 21. Increased dosages of genes at DSOR cause pathological manifestations of DS by the overexpression of their products, including amyloid precursor protein (APP), S-100 protein, superoxide dismutase-1, BACE2, and DSCAM. The *APP* gene is related to the pathogenesis of Alzheimer-type dementia in DS [6].



Fig. 3.1-1. The brain of the newborn with Down syndrome shows slight dilatation of the sylvian fissure, a narrow superior temporal gyrus, and a small cerebellum and brain stem.

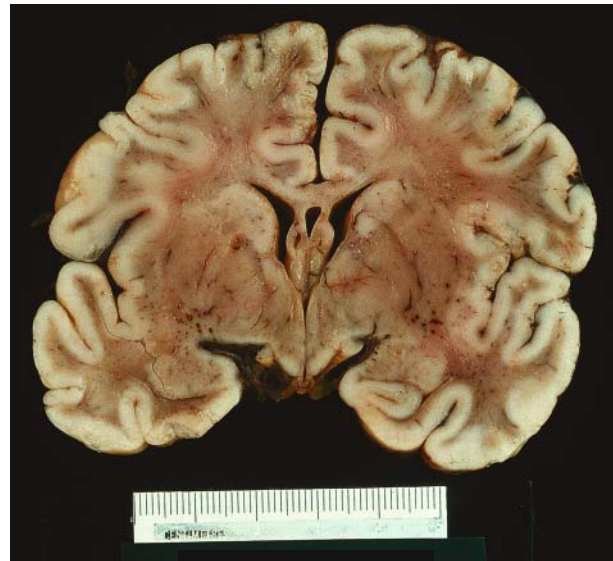


Fig. 3.1-2. Coronal section of the cerebrum exhibits a hypoplastic superior temporal gyri.

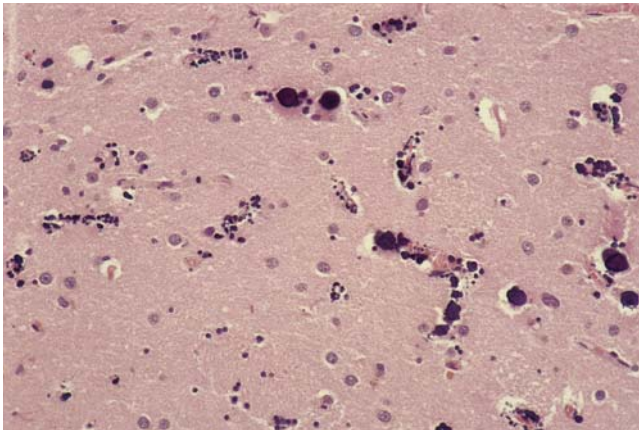


Fig. 3.1-3. Histology of basal ganglia exhibits multiple areas of calcification around the small vessels. Basal ganglia calcification is more frequent in the cases of Down syndrome than in controls. H&E.

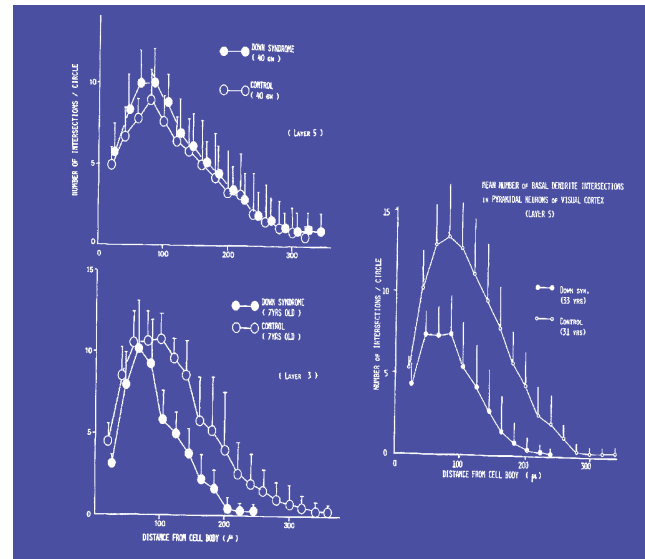


Fig. 3.1-4. Abnormal development of dendrites in the visual cortex of a patient with Down syndrome (closed circles) and a control (open circles) (Scholl analysis of dendritic branching).

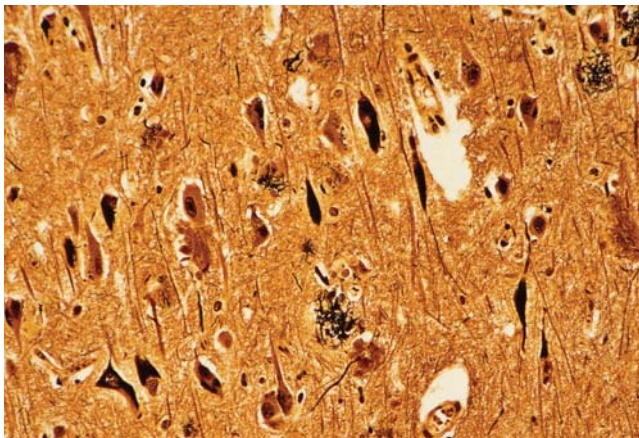


Fig. 3.1-5. Hippocampus with Bielschowsky stain defining the pathology of Alzheimer's disease. Note the neurofibrillary tangles in pyramidal neurons and several neuritic plaques in the neuropil. Bielschowsky stain.

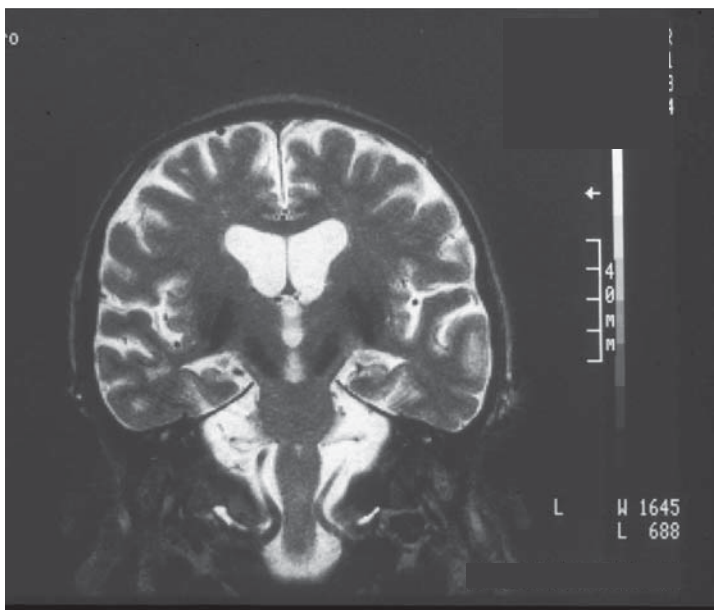


Fig. 3.1-6. Magnetic resonance imaging (MRI) of a 50-year-old patient showing atrophy of the hippocampus and dilatation of the lateral ventricle.

3.2 Trisomy 13 and Trisomy 18

Trisomy 13 (Patau syndrome) is characterized by malformations of microcephaly; microphthalmia, absent eye, or retinal dysplasia; cleft lip or palate in the face; and congenital heart and urogenital anomalies. The brain anomalies may include microcephaly, holoprosencephaly, thalamic fusion, polymicrogyria, and leptomeningeal glioneuronal heterotopia at the base of the cerebrum and brain stem. In the cerebellum, the heterotopias, including germinal cells in the dentate nucleus,

are extensive, and other dysplasia of the cerebellar gray matter are observed [7].

Trisomy 18 (Edwards syndrome) is associated with malformation of the face (dysmorphic) and extremities, neurological abnormalities, and minor malformations of the brain [8,9]. The latter include abnormalities in the histology of the hippocampus, inferior olivary nuclei, and lateral geniculate body.

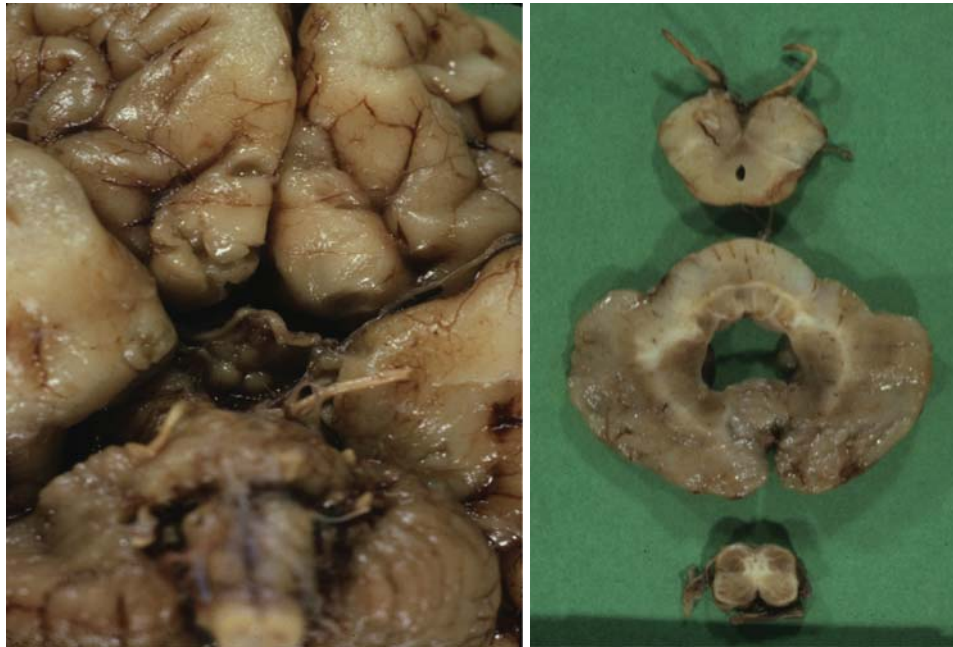


Fig. 3.2-1. Trisomy 13, *Left*. The base of the brain exhibits smooth gyri of the temporal lobe. *Right*. The brain stem and cerebellum are small with slight dilatation of the fourth ventricle.

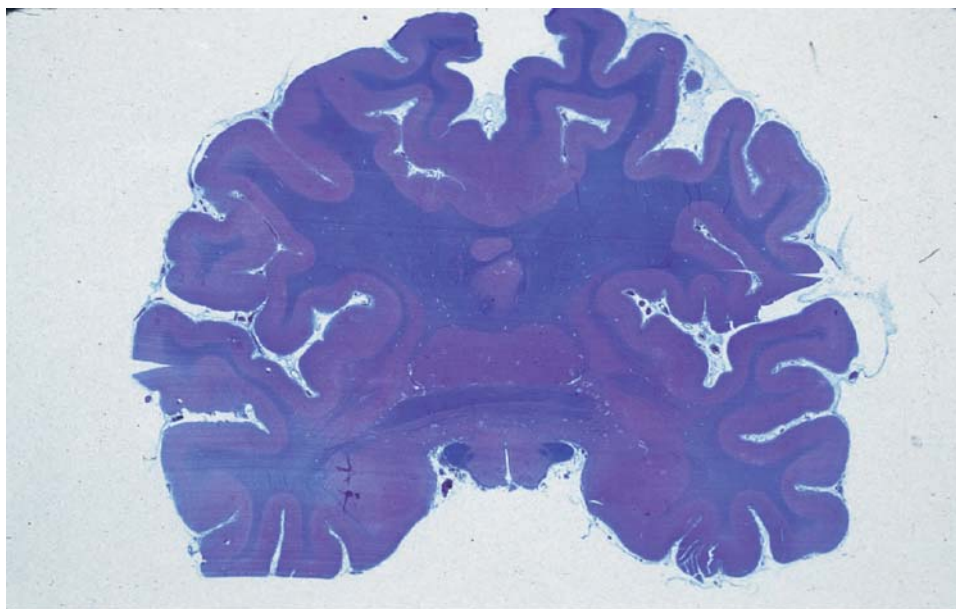


Fig. 3.2-2. Trisomy 13. Coronal section of the cerebrum exhibiting fusion of the cerebral hemispheres. LFB.

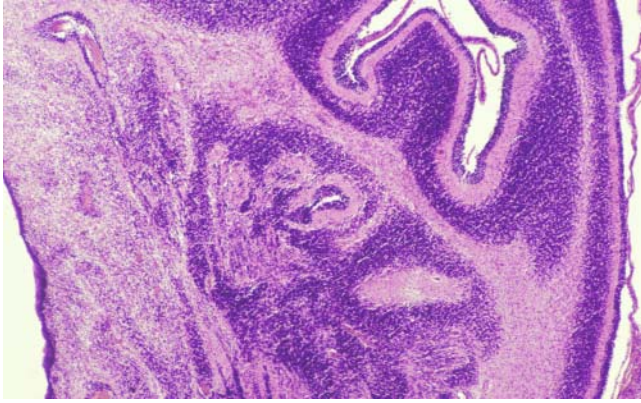


Fig. 3.2-3. Trisomy 13. Microscopic view of cortical dysplasia of the cerebellum in the same neonate as in 3.2-2. H&E.

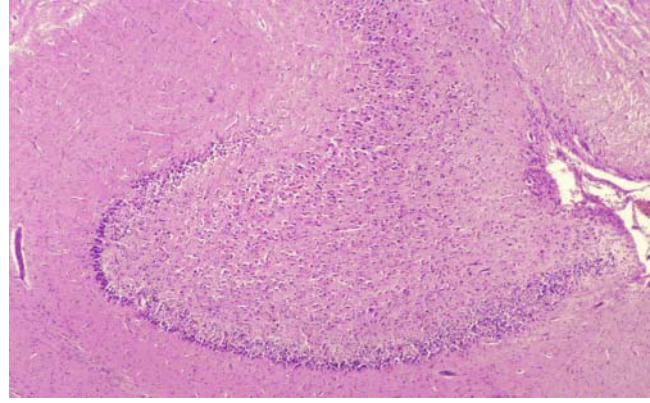


Fig. 3.2-4. Trisomy 18. Hippocampal dysplasia with incomplete rotation of the hippocampus and a small outwardly rotated fascia dentata in a neonatal brain. H&E.

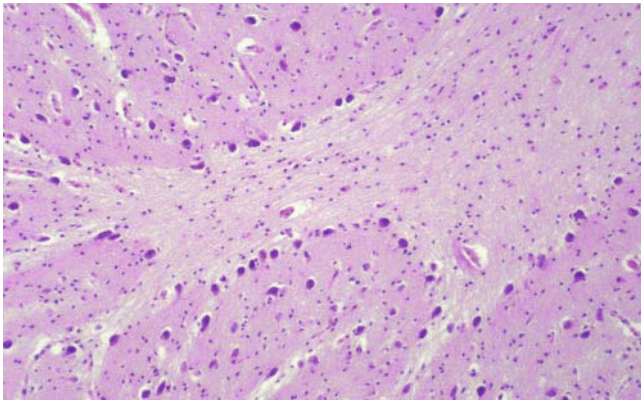


Fig. 3.2-5. Trisomy 18. Olivary dysplasia. The dorsal segment of the inferior olivary nucleus is thick, and the undulation of the nuclear profile is abnormal. The rows of neurons are characteristic. H&E.

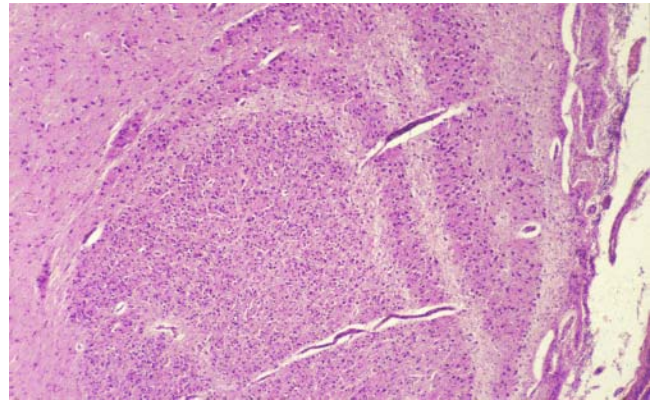


Fig. 3.2-6. Trisomy 18. Incomplete cellular lamination in the lateral geniculate body. There is vertical layering of cells with poor distinction of the magnocellular and parvocellular layers. H&E.

3.3 Chromosome 1q-

Chromosomal aberrations may present as a monosomy or a partial deletion of the chromosome. Deletion of the long arm of chromosome 1 (1q-) is a rare condition associated with malformations of many organs, including the central nervous system (CNS), heart, and kidney. Proximal deletion of the long arm 1q- [del (1)(q23-q25)] is characterized by pre- and postnatal growth retardation, psychomotor retardation, and a specific craniofa-

cial malformation (bilateral complete cleft of the lip and palate) as well as other systemic anomalies [10]. When there is an interstitial deletion of the long arm 1q- [1q25-32], the infant presents with severe intra- and extrauterine growth retardation, facial dimorphisms, multiple organ malformations, a hypoplastic hypophysis, and multiple endocrine deficiencies [11].



Fig. 3.3-1. Chromosome 1q-. Polymicrogyria, reduced thickness of white matter, and dilatation of lateral ventricles.

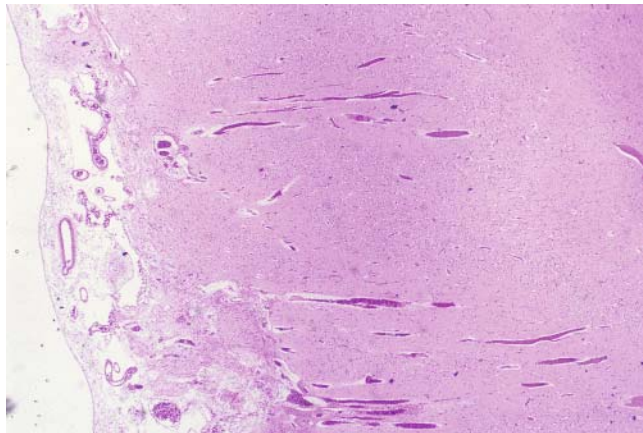


Fig. 3.3-2. Microscopy reveals cortical dysplasia with an irregular cortical surface and an irregular neuronal arrangement. The cortical vessels are abnormal, and subcortical heterotopias are present. H&E.

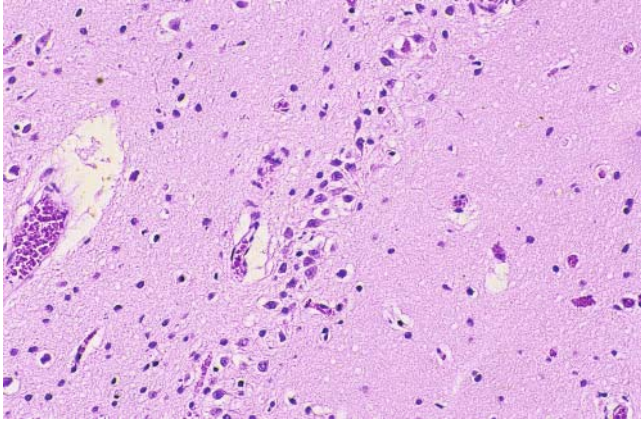


Fig. 3.3-3. Reduced number of granule cells in the thin dentate gyrus of the hippocampus. H&E.

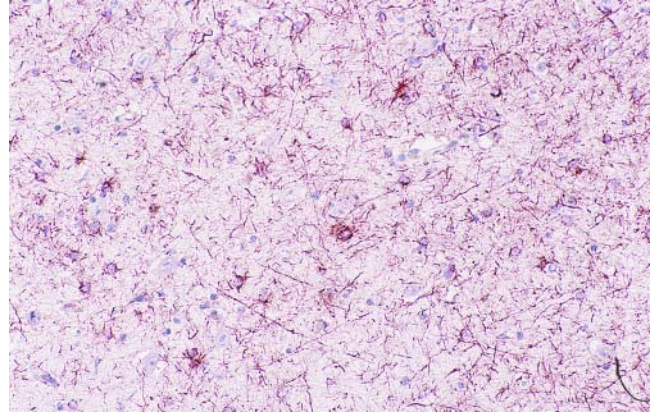


Fig. 3.3-4. Marked astrogliosis similar to status marmoratus in the thalamus. H&E.

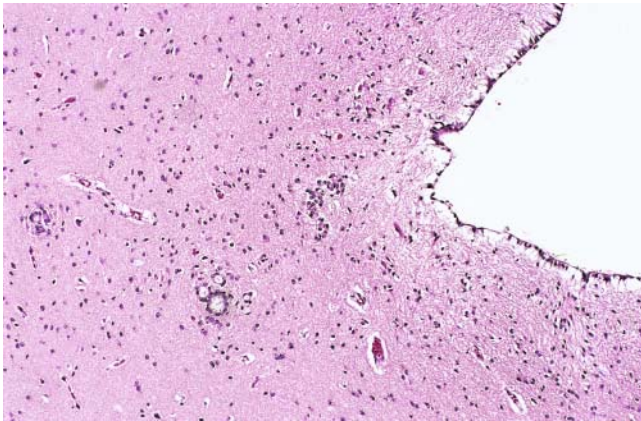


Fig. 3.3-5. Rosette formation of ependymal cells (duct formation) around the aqueduct. H&E.

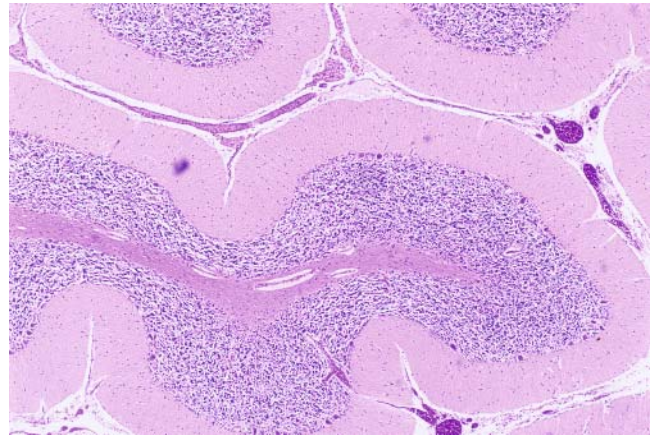


Fig. 3.3-6. Microscopic view of the cerebellum reveals hypocellularity in the granular cell layer, loss of Purkinje cells, and Bergman gliosis. There is atrophy of white matter in the cerebellar lobules. H&E.

3.4 Chromosome 4p-

The 4p- syndrome, or Wolf-Hirschhorn syndrome, is a chromosome disorder with a partial deletion of the short arm of chromosome 4 involving band 4 p16. There are typical craniofacial features consisting of a scalp defect (“Greek warrior helmet appearance”), widely spaced eyes, a saddle nose, microcephaly, and prominent glabella. There is intrauterine growth retardation,

mental retardation, intractable epilepsy, and hypotonia [12]. There are severe CNS abnormalities including microcephalus, microgyria, migration disorders, and hydrocephalus. There is hypoplasia of the cerebellum, a cavum or absent septum pellucidum, agenesis of the corpus callosum, and absence of olfactory bulbs.



Fig. 3.4-1. Chromosome 4p-. Lateral view of the brain, which exhibits mild microcephaly, a small cerebrum, and a large cerebellum.



Fig. 3.4-2. Sagittal section of the brain shows a thin corpus callosum and a small pons.



Fig. 3.4-3. Coronal sections of the cerebrum, showing hypoplasia of the cerebral white matter with moderate dilatation of the lateral ventricles.

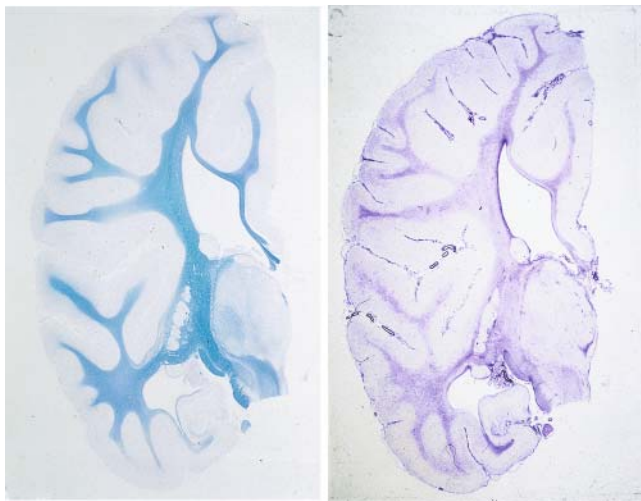


Fig. 3.4-4. Low-power histological view of the cerebral hemispheres shows slight hypomyelination (*left*) (LFB) and diffuse astrogliosis in the white matter and the hippocampus (*right*) (Holzer stain).

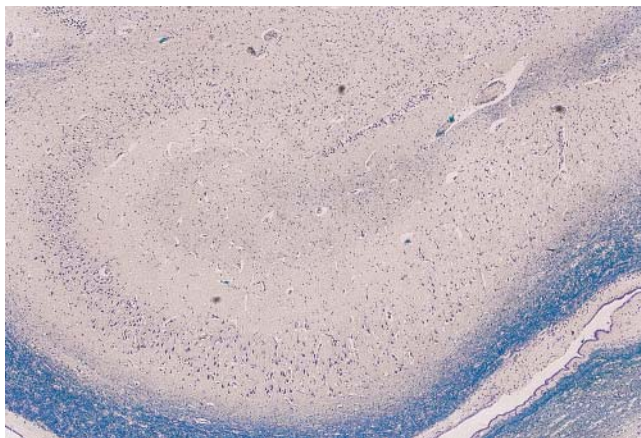


Fig. 3.4-5. Neuronal loss in CA1 of Ammon's horn and hypocellularity of granular cells of the dentate gyrus. LFB.

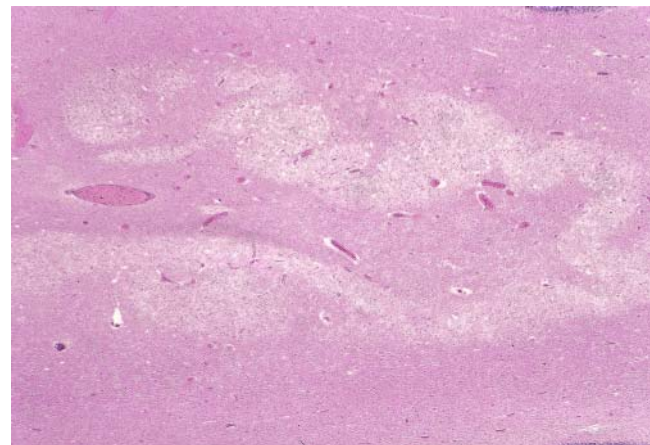


Fig. 3.4-6. Excessive convolution of the dentate nucleus in the cerebellum. H&E.

4. Perinatal Brain Damage

4.1 Birth Trauma in Term Infants

Perinatal brain damage includes all brain injuries that occur during the perinatal period in infants of all gestational ages, whereas injury from birth trauma per se occurs more frequently in full-term neonates. Important advances in perinatal care have decreased the incidence of birth trauma. Birth trauma of the nervous system may result in the following.

Extracalvarial hemorrhage (subgaleal hemorrhage, cephalohematoma)

Sinus injury or thrombosis

Intracranial hemorrhage

Epidural, intradural, or subdural hemorrhage

Subarachnoid or subpial hemorrhage

Cerebral, cerebellar, or brain stem hemorrhage

Intraventricular hemorrhage

Brain contusions

Secondary hypoxic or ischemic brain injury

Brachial plexus and peripheral nerve injuries

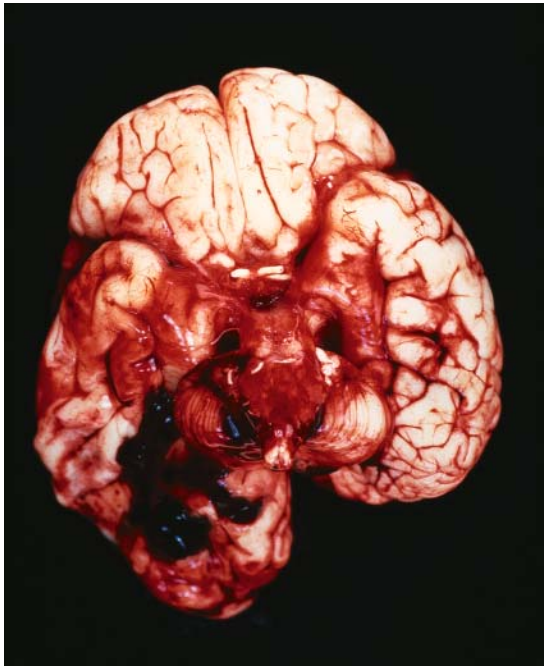


Fig. 4.1-1. Birth trauma. Subdural hemorrhage in the posterior fossa. The hematomas in the posterior fossa may compress the brain stem and cerebellum and cause obstructive hydrocephalus with cerebral swelling, as on the *right*.

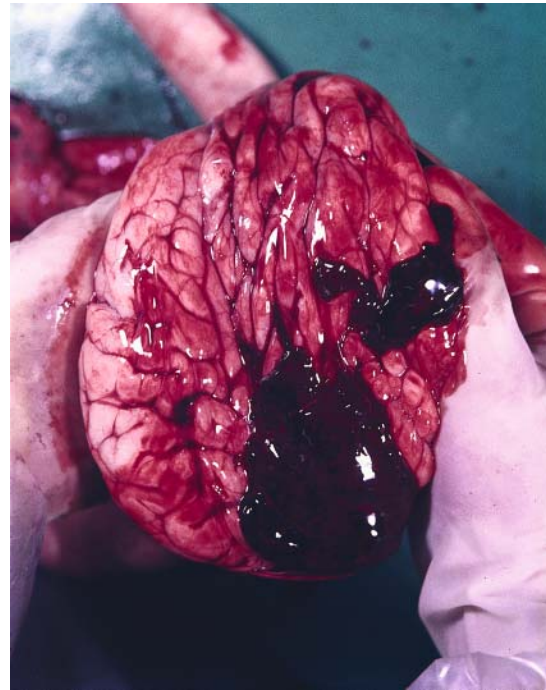


Fig. 4.1-2. Birth trauma. Marked subdural hematoma over the right cerebral hemisphere, which is markedly swollen with flattening of the gyri and narrowing of the sulci.

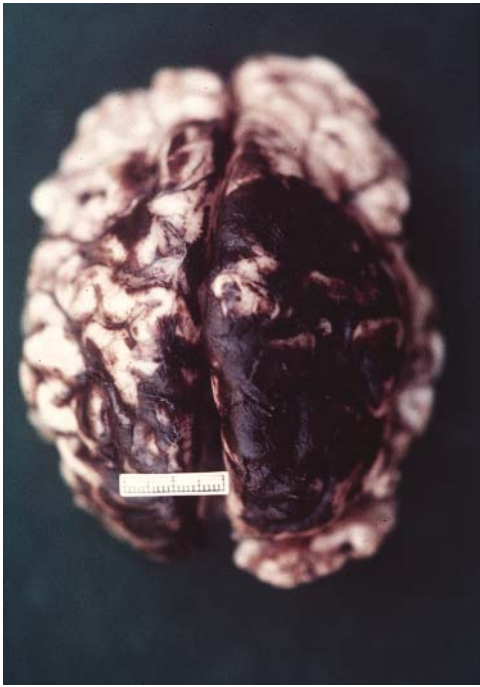


Fig. 4.1-3. Birth trauma. Subarachnoid hemorrhage partially involving both cerebral hemispheres.

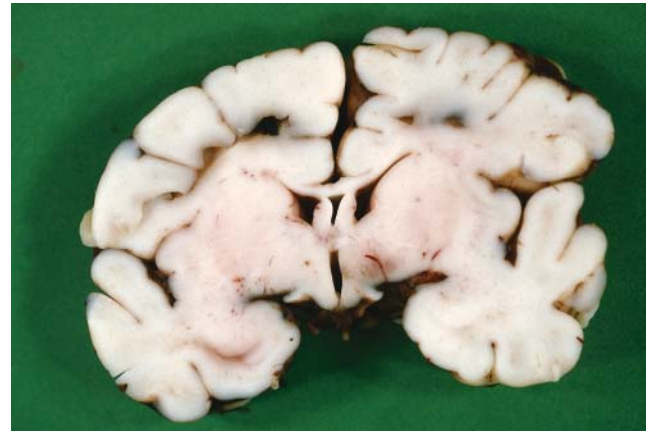


Fig. 4.1-4. Birth trauma. Cerebral white matter hemorrhage caused by birth trauma. The unmyelinated white matter is more vulnerable than cortex to shearing forces that develop when the brain is deformed by the flexible infant skull [1].



Fig. 4.1-5. Birth trauma. Extensive hemorrhage in the brain stem and spinal cord. The cervical and thoracic cord are most vulnerable if there is excessive traction (as with breech deliveries) or excessive head rotation (as with cephalic deliveries) [1].

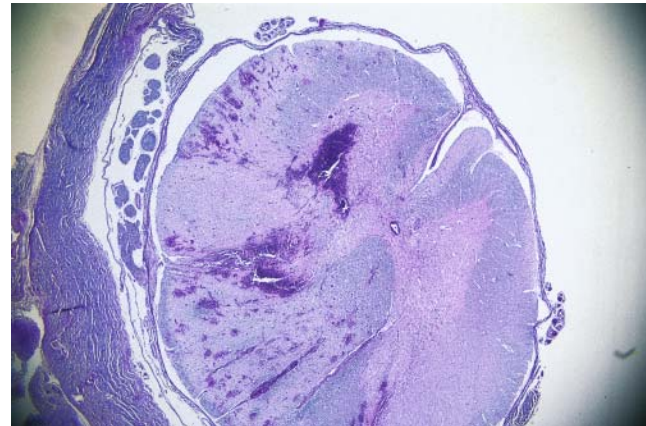


Fig. 4.1-6. Spinal cord traumatic hemorrhage. Cord ischemia and/or hemorrhage may be the result of compression by vertebral fractures, subdural hemorrhage, or stretching of the cord. H&E.

4.2 Periventricular/Intraventricular Hemorrhage and Cerebellar Hemorrhage in Preterm Infants

Periventricular/intraventricular hemorrhage (PVH/IVH) continues to exist in very low-birth-weight infants, although its incidence has been decreased by modifications in perinatal care. PVH/IVH develops after rupture of venules in the periventricular germinal epithelium (matrix), causing subependymal hemorrhage (SEH), which can expand into the ventricle causing IVH. This extends to the subarachnoid space producing subarachnoid hemorrhage (SAH) around the cerebellum and brain stem [1]. A very large IVH causes venous stasis in the deep medullary veins of the periventricular white matter and subsequent periventricular hemorrhagic infarction (PVHI). This is usually unilateral, although SEH often occurs bilaterally.

The pathogenesis of PVH and IVH is multifactorial.

1. Predisposing factors: anatomical, cellular, and physiological immaturity; high cellularity in the subependymal matrix and arterial end zone; and bush-like venous drainage [2]
2. Pathogenetic factors [3]
 - a. Intravascular factors: fluctuating cerebral blood flow, increased cerebral blood flow, increased cerebral venous pressure, decreased blood flow (followed by reperfusion), platelet and coagulation disturbances
 - b. Vascular factors: tenuous capillary integrity, vulnerability of matrix capillaries to hypoxic-ischemic injury
 - c. Extravascular factors: deficient vascular support, fibrinolytic activity, postnatal decrease in extravascular tissue pressure



Fig. 4.2-1. Subependymal hemorrhage (SEH), extending to intraventricular hemorrhage (IVH). Bilateral SEHs and periventricular white matter hemorrhage. Intraventricular blood flows to the fourth ventricle and the surface of the cerebellum through the foramina of Luschka and Magendie.



Fig. 4.2-2. Histological view of an SEH into the germinal matrix (epithelium) without rupture into the ventricle (grade 1 IVH). H&E.

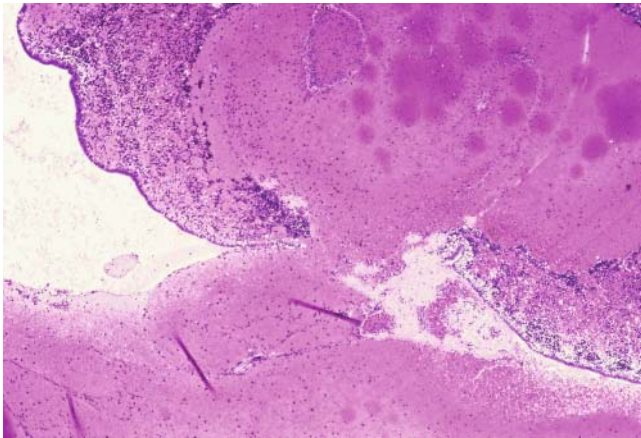


Fig. 4.2-3. SEH extending to IVH. Rupture of an SEH into the intraventricular space (grade 2 IVH). H&E.

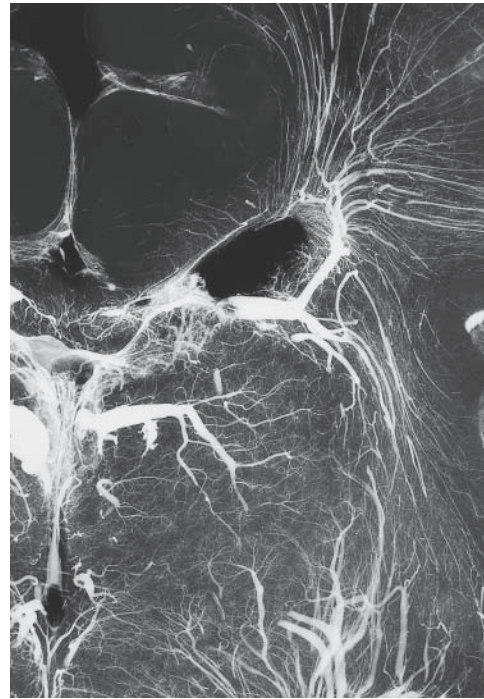


Fig. 4.2-4. Postmortem cerebral venography defines numerous venules contributing to the terminal branches of the internal cerebral veins in the subependymal matrix.



Fig. 4.2-5. Histology of cerebral hemispheres with SEH and periventricular white matter hemorrhage (grade 4 IVH). H&E.

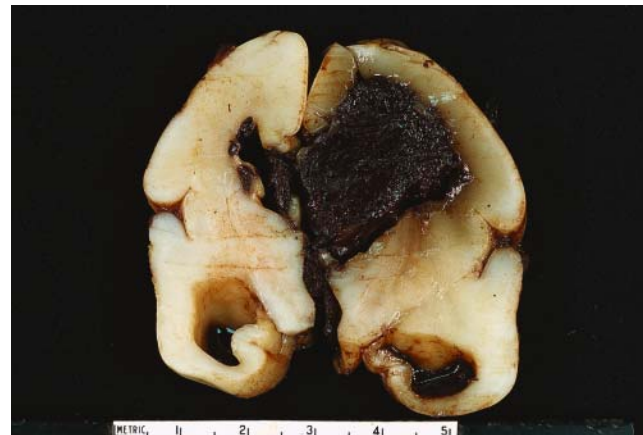


Fig. 4.2-6. Intraventricular hemorrhage/periventricular hemorrhage (IVH/PVH). Extensive venous infarction of the right cerebral periventricular white matter associated with a large right IVH (grade 4 IVH/PVH).

4.3 Sequelae of IVH and Other Hemorrhages in Preterm Infants

The IVH may predispose to posthemorrhagic hydrocephalus because of disturbed cerebrospinal fluid (CSF) flow and/or adsorption. Posthemorrhage hydrocephalus (PHH) is caused by aqueduct stenosis or obstruction with astrogliosis and hemosiderin deposits or by stenosis of the foramina of Magendi and Luschka with fibrosis and hemosiderin deposits. PHH is frequently associated with cerebellar subarachnoid hemorrhage and olivocerebellar pathology [4].

Subependymal cysts with hemosiderin deposits may define a residual SEH.

Cerebellar hemorrhages may develop in the immature external granular layer and/or adjacent internal

granular layer. The etiologies are many and include traumatic and asphyxial causes [1]. The hemorrhages are often multiple, and the hematomas may cause extensive tissue destruction. Olivocerebellar degeneration may be caused by cerebellar hemorrhage or subarachnoid hemorrhage producing loss of Purkinje cells and retrograde degeneration of inferior olivary neurons [1,5].

Cortical hemorrhagic necrosis, associated with traumatic or hypoxia-ischemia may be observed in very low-birth-weight infant brains.



Fig. 4.3-1. Cortical hemorrhage necrosis. Focal hemorrhages are found in the frontal, parietal, and temporal lobes in the brain of a very low-birth-weight infant.

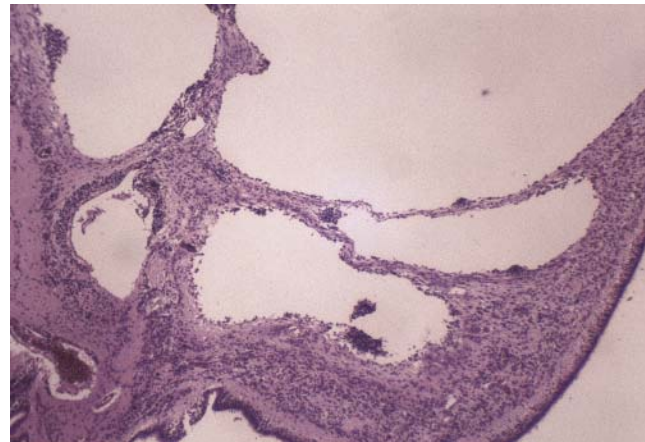


Fig. 4.3-2. Posthemorrhage subependymal cyst shows hemosiderin deposits in the wall and in macrophages. H&E.

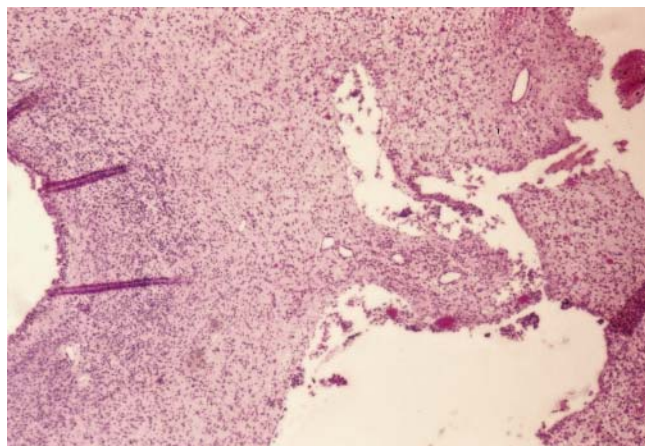


Fig. 4.3-3. Remote lesion of periventricular white matter hemorrhage. There are multiple cysts with hemosiderin deposits. H&E.

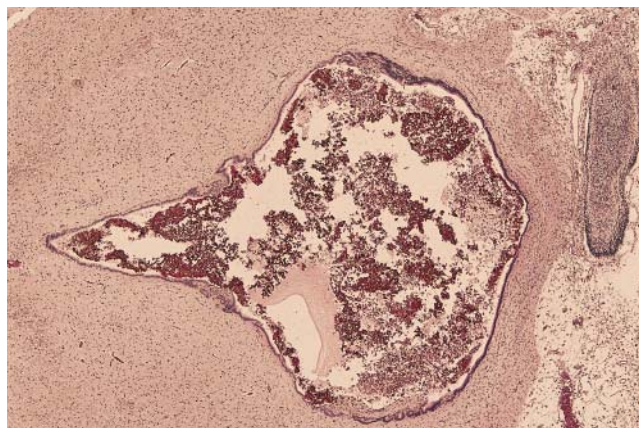


Fig. 4.3-4. Posthemorrhage hydrocephalus. The aqueductal dilatation contains blood from an intraventricular hemorrhage. H&E.



Fig. 4.3-5. Posthemorrhage hydrocephalus. There is marked dilatation of the lateral ventricles at 4 months of age following an intraventricular hemorrhage that had occurred previously in a very low-birth-weight infant.

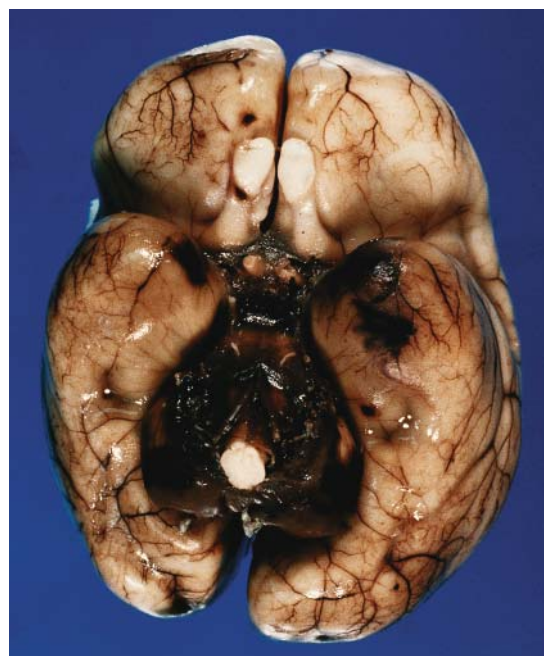


Fig. 4.3-6. Subarachnoid hemorrhage in the brain stem and cerebellum accumulating in the posterior fossa following periventricular and intraventricular hemorrhage in a very low-birth-weight infant.

4.4 Perinatal Hypoxic-Ischemic Encephalopathy

Fetal and neonatal hypoxia or ischemia produces cell or tissue necrosis or apoptosis in specific sites of the neonatal brain and spinal cord. The lesions of perinatal hypoxic-ischemic encephalopathy (HIE) are classified as follows.

Cerebral cortical (laminar) necrosis
 Basal ganglia and thalamic necrosis leading to status marmoratus
 Hippocampal necrosis, possibly causing hippocampal sclerosis
 Pontosubicular neuron necrosis (PSN)
 Periventricular leukomalacia (PVL)
 Subcortical leukomalacia (SCL)
 Parasagittal infarction
 Ulegyria
 Cingulate necrosis

Brain stem necrosis
 Cerebellar cortical necrosis
 Cerebellar cystic leukomalacia

Although these lesions can be found independently in specific regions, they often present together in the complicated lesions of perinatal brains. The location of the lesion is determined by the maturity of the brain (immature or mature) and the severity or duration of hypoxic-ischemic insults (total or partial).

Cortical laminar necrosis is seen in areas of cortical necrosis or around a cerebral infarction, predominantly in pyramidal cell layer III or V. Basal ganglia or thalamic necrosis is found alone in some neonates with perinatal asphyxia but is often associated with cerebral cortical or brain stem necrosis.

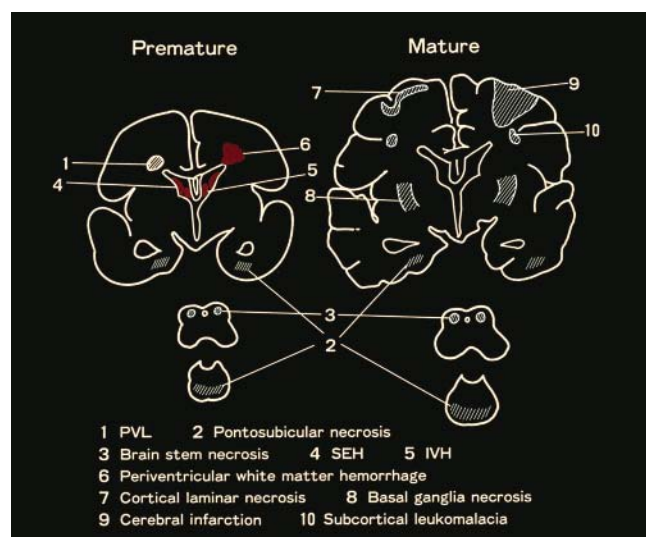


Fig. 4.4-1. Characteristic localization of lesions in hypoxic-ischemic encephalopathy (HIE) is compared for term and preterm infants.

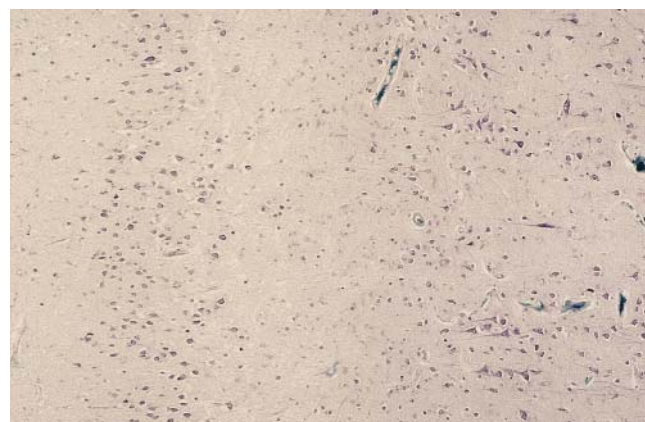


Fig. 4.4-2. Cortical laminar necrosis. There is laminar loss of neurons in the cerebral cortex of a 2-year-old child who had neonatal HIE and hypoglycemia. Nissl stain.

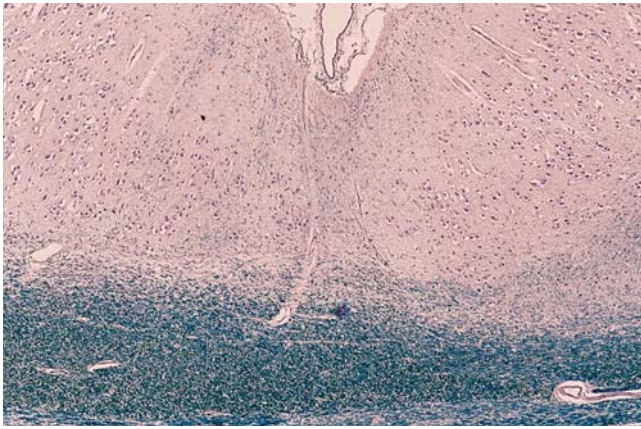


Fig. 4.4-3. Sequelae of cortical laminar necrosis. Note the cerebral cortical neuron loss and plaque fibromyelination in the cortex of a deep sulcus caused by remote cortical necrosis in a 6-year-old boy with cerebral palsy. LFB.



Fig. 4.4-4. Bilateral thalamic hemorrhage into areas of ischemic necrosis in the bilateral thalami of an infant with cyanotic congenital heart disease.



Fig. 4.4-5. Basal ganglia necrosis in a 21-day-old infant with neonatal asphyxia and cyanotic congenital heart disease. There is bilateral striatal necrosis exhibiting neuronal degeneration, neuronophagia, and calcification.



Fig. 4.4-6. Sequelae of basal ganglia necrosis. The Holzer stain defines an area of astrogliosis (purple) that may become abnormally myelinated (i.e., "status marmoratus") in a child with choreoathetotic-type cerebral palsy.

4.5 Parasagittal Infarction, Ulegyria, Lobar Sclerosis

Parasagittal infarction occurs in the cerebral cortex and white matter in the watershed zones of the blood supply located among the anterior, middle, and posterior cerebral arteries. It is more marked posteriorly [3]. Impaired cerebrovascular autoregulation or reduced cerebral perfusion pressure contribute to cerebral ischemia in these arterial border zones. Ischemia causes cerebral infarction, which may be diffuse (producing lobar sclerosis) or focal (resulting in ulegyria).

Ulegyria refers to an alteration in the shape of the affected gyrus. It is caused by neuronal loss and glial

scars involving the cortex at the bottom of the sulcus, at the site supplied by end-arteries. During the acute phase of ulegyria formation, there is diffuse pallor of the cortex at the depth of the sulci associated with vacuolization of the tissue, nuclear pyknosis, chromatolysis, dissolution, and dropping out of neurons [6]. Established lesions show dilatation of the subarachnoid space at the depth of the sulcus in one or several adjacent sulci.

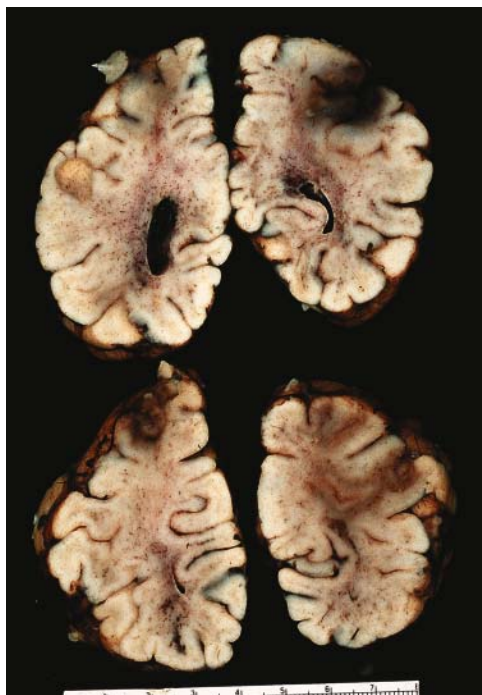


Fig. 4.5-1. Parasagittal watershed infarction in a term neonate.

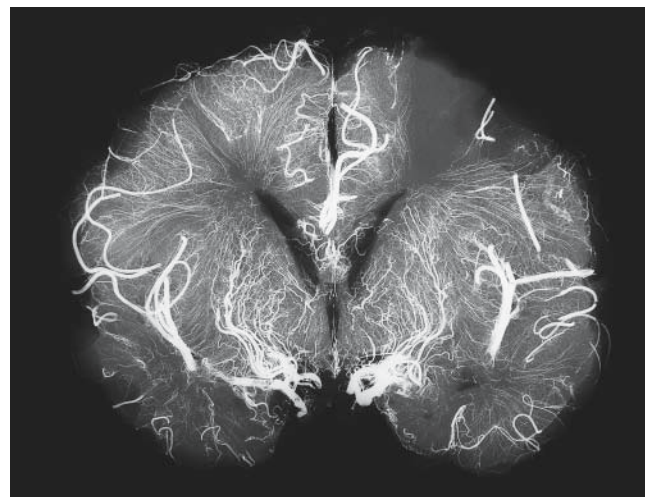


Fig. 4.5-2. Parasagittal watershed infarction, with cerebral infarction in hypoxic-ischemic encephalopathy. Postmortem angiography demonstrates parasagittal cerebral infarction at the border zone of the anterior and middle cerebral arteries in the right cerebral hemisphere.



Fig. 4.5-3. Multicystic leukomalacia. Appearance of the brain at age 2 years. There is cingulate gyrus destruction and cystic change in the white matter. The infant, born at term, experienced perinatal asphyxia; and at 10 days of age brain ultrasonography demonstrated a transient brightness.

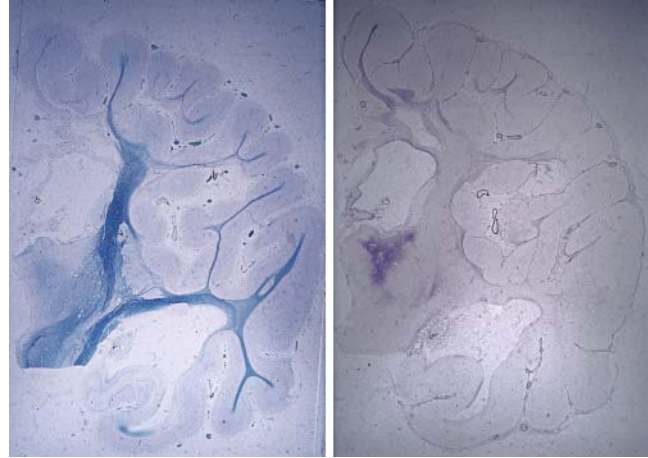


Fig. 4.5-4. Large section of the cerebral hemisphere seen in 4.5-3. *Left.* Decreased myelin in the white matter and destruction of cingulate gyri. LFB/Nissl stain. *Right.* Astrogliosis in the white matter and thalamus. Holzer stain.

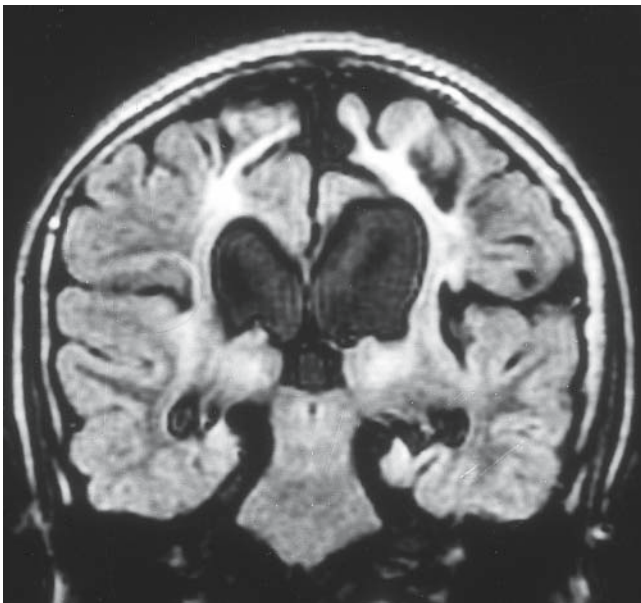


Fig. 4.5-5. FLAIR magnetic resonance imaging (MRI) shows high intensity in the superior parietal gyri and white matter, suggesting lobar sclerosis and ulegyria in a case of cerebral palsy.



Fig. 4.5-6. Brain stem necrosis in a term neonate.

4.6 Sequelae of Cerebral Necrosis in Fetal and Perinatal Hypoxia

The timing of a brain injury during the fetal period may be suggested by a history of an intrauterine insult or by the degree of glial reaction compared with the postnatal age. Fetal ultrasonography or MRI may also identify significant brain injury. In the brains of stillborn infants and neonates there may be recent lesions such as subependymal hemorrhage, intraventricular hemorrhage, periventricular leukomalacia, pontosubicular neuron necrosis, and other ischemic lesions. There may also be more remote lesions such as multicystic encephalomalacia, porencephaly, polymicrogyria, scars, and dysplasias.

Polymicrogyria grossly exhibits a pachygyric pattern with rare coarse and irregular gyri that appear granular. There are two major microscopic patterns: four-layer and unlayered polymicrogyria. The four-layer pattern

consists of molecular, superficial cellular, acellular (mostly glial), and deep cellular layers. This pattern may be focal and associated with other cortical abnormalities produced by a circulatory disturbance. Unlayered polymicrogyria displays a chaotic pattern of neurons. It may be caused by fetal encephalitis or be associated with another abnormal cortical pattern.

Multicystic encephalomalacia may develop prenatally when cortical and subcortical white matter necrosis produces multiple cavities of various size associated with neuron loss and astrogliosis. This may develop following hypoxic-ischemic insults (fetal hypoxia), toxic insults (carbon monoxide intoxication), infections (cytomegalovirus infection, toxoplasmosis, listeriosis), or metabolic disorders (mitochondrial encephalopathy).

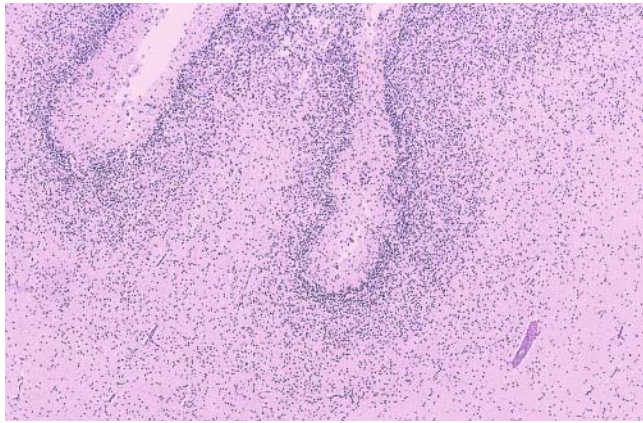


Fig. 4.6-1. Sequelae of fetal hypoxia: polymicrogyria and laminar neuron loss. Nissl stain.

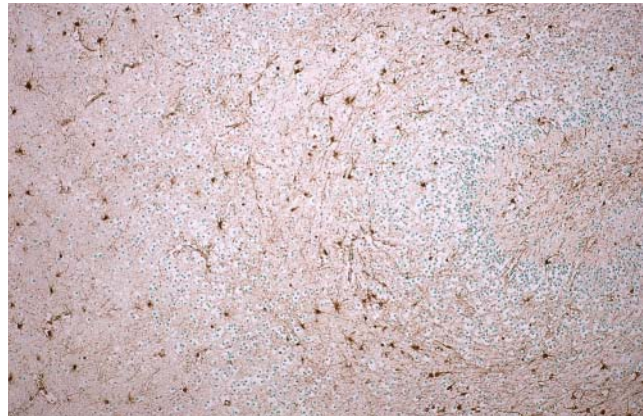


Fig. 4.6-2. Sequela of fetal hypoxia: gliosis marks a zone with loss of neurons in the cortex after fetal hypoxia. GFAP immunohistochemistry.



Fig. 4.6-3. Sequela of cerebral infarction during the fetal period: polymicrogyria.

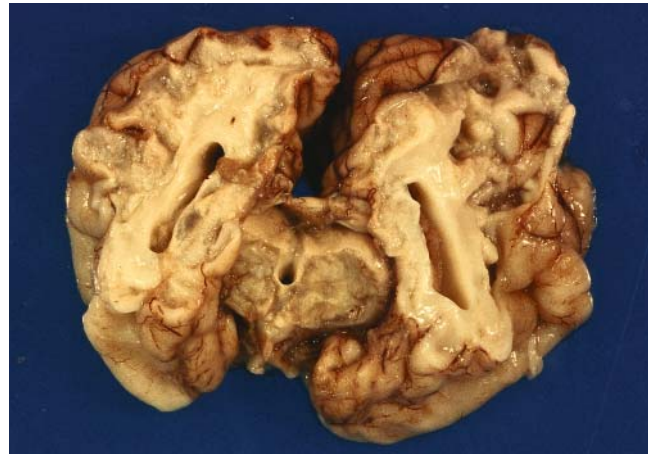


Fig. 4.6-4. Cortical necrosis accompanying multicystic encephalomalacia in an infant.

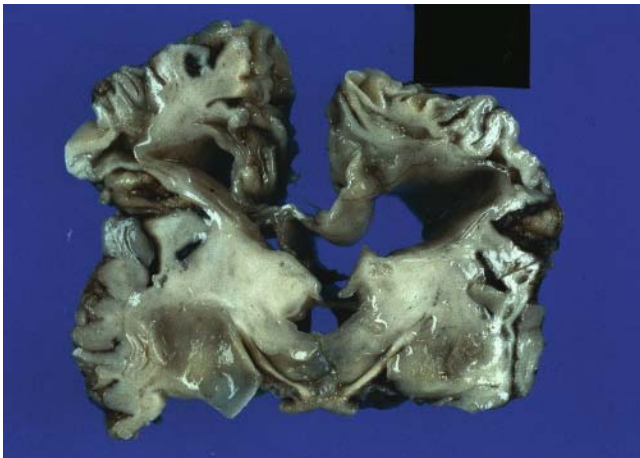


Fig. 4.6-5. Cortical necrosis and calcification associated with status marmoratus in the basal ganglia.

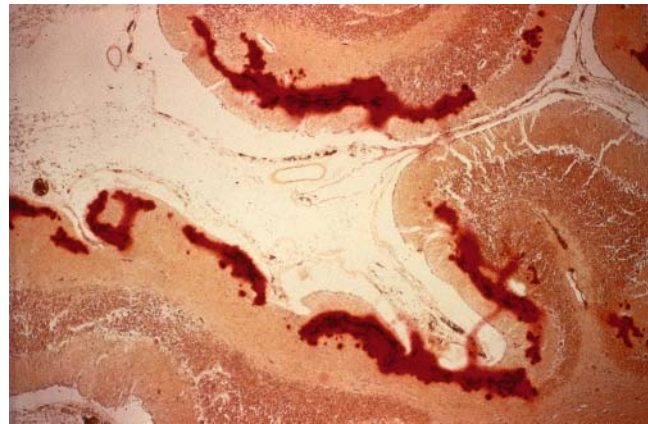


Fig. 4.6-6. Histology of cortical calcification secondary to hypoxic ischemic injury [7]. Von Kossa stain.

4.7 Periventricular Leukomalacia

Periventricular leukomalacia (PVL) is a major cause of cerebral palsy (particularly spastic diplegia) in low-birth-weight and some term infants.

Pathology

Predominantly in the parietal to occipital lobes, there is multifocal or widespread necrosis with or without cyst formation in the periventricular white matter (WM) [7,8]. Microscopically, there is axonal and cellular coagulative necrosis, microglial activation, foam cell infiltration, reactive astrogliosis, and neovascularization. This leads to WM atrophy with loss of axons and myelin [7–9].

Pathogenesis

Predisposing factors are as follows.

1. Vascular immaturity in the deep WM with characteristic end-arrests in the developing vasculature [5]
2. Vulnerability of differentiating glia (particularly pre-oligodendrocytes) to glutamate and cytokines
3. Prenatal infection, increasing the sensitivity to periventricular necrosis

Causal factors include (1) perinatal ischemia following reoxygenation, (2) axonal damage with release of excitatory amino acids, and (3) microglial activation with an increase of inflammatory cytokines [10,11].



Fig. 4.7-1. Periventricular leukomalacia (PVL). Note the multiple white spots (necrotic foci) in periventricular white matter.

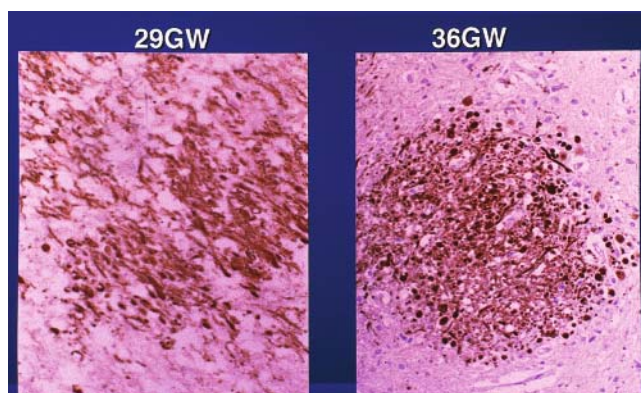


Fig. 4.7-2. Periventricular leukomalacia. A recent PVL lesion. Note the axonal swellings defined by amyloid precursor protein (APP) immunohistochemistry. *Left.* Note the wide distribution of axonal swellings. *Right.* Localized coagulation necrosis is evident with APP immunohistochemical stains.

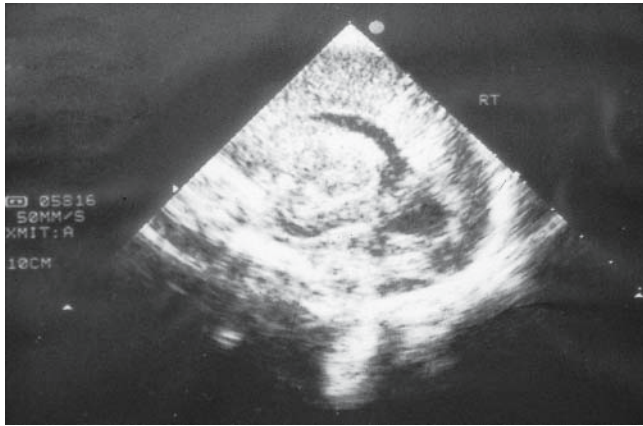


Fig. 4.7-3. Periventricular leukomalacia. There is high echo density in the deep white matter of a preterm infant with PVL, as seen by ultrasonography.



Fig. 4.7-4. Periventricular leukomalacia. Macroscopic appearance of the PVL lesions. There are white opaque lesions in the periventricular white matter in this brain 29 days after birth.

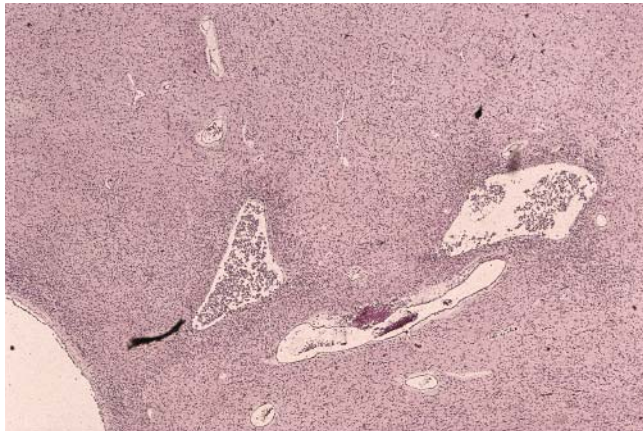


Fig. 4.7-5. Periventricular leukomalacia (same case as in 4.7-1). Histology of the periventricular white matter shows multiple microcysts containing foam cells surrounded by astrogliosis. H&E.

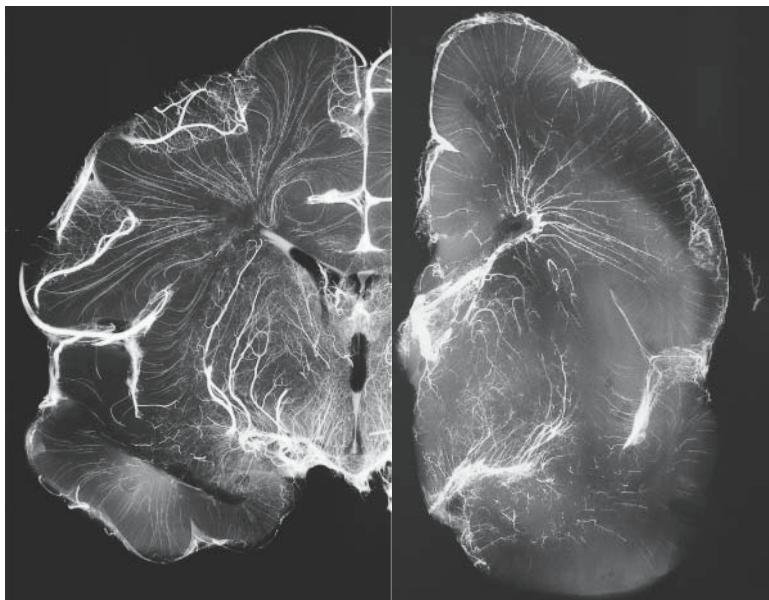


Fig. 4.7-6. Postmortem microangiography of the preterm infant brain using an injected gelatin-barium mixture and soft X-ray apparatus. *Left.* Arterial architecture. This defines the watershed of end-arteries in the periventricular white matter. *Right.* Venous architecture. Note different architecture between arteries and veins.

4.8 Sequelae of Periventricular Leukomalacia

Clinically, focal PVL results in spastic paraplegia or diplegia. Widespread PVL causes severe motor deficits of the lower and upper limbs and impaired cognitive function.

The older lesions of PVL appear chalky or cavitated and contain foam cells with surrounding zones of astrogliosis and encrustation of axons. There is loss of myelin in and around the lesions. The necrotic lesions of PVL are multifocal in the periventricular white matter, which causes a reduction in the amount of white matter. This is associated with a reduced population of oligodendrocytes. In mild cases of focal PVL there is localized astro-

gliosis, whereas severe cases PVL are associated with diffuse gliosis in the white matter. There is compensatory dilatation of the lateral ventricles, and the ventricular contour is irregular [9].

The progress of PVL is demonstrated by cranial imaging. Ultrasonography shows periventricular high echo density or cystic changes in acute lesions. MRI shows focal low or high intensity and atrophy of the periventricular white matter in chronic lesions. PVL exhibits low intensity on T1-weighted MRI and high intensity on T2-weighted and FLAIR MRI images in very low-birth-weight infants.

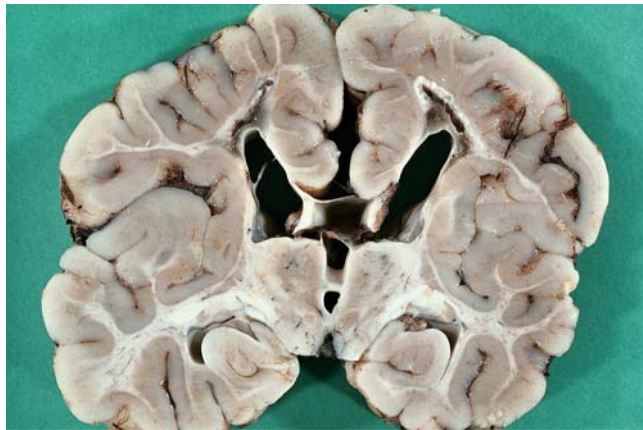


Fig. 4.8-1. Cystic lesions in periventricular leukomalacia (PVL). Note the dilated ventricles and reduced white matter volume in a case of cerebral palsy.

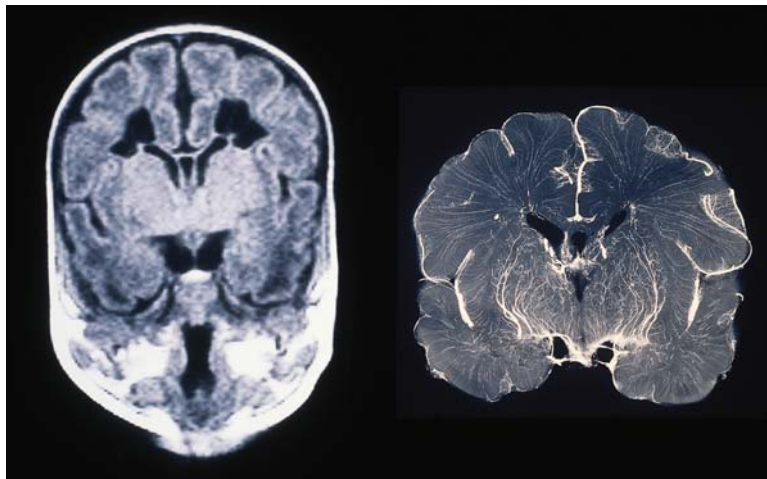


Fig. 4.8-2. Sequelae of periventricular leukomalacia. *Left.* MRI shows bilateral cystic lesions of PVL, white matter volume loss, and an irregular ventricular wall. *Right.* Postmortem angiography. Cystic lesions correspond to the end zone areas of medullary arteries.

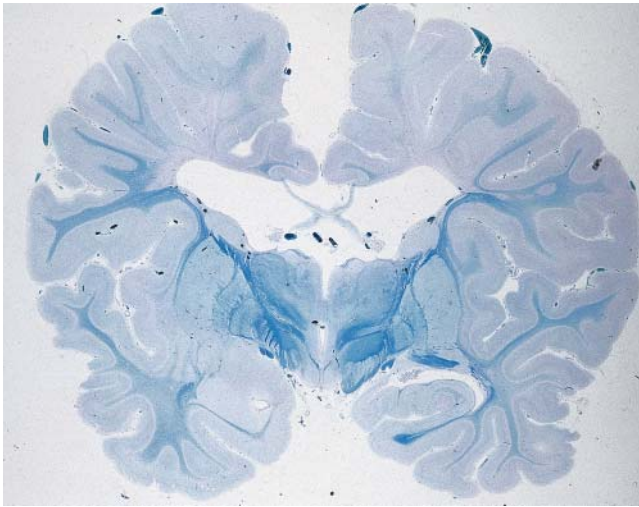


Fig. 4.8-3. Whole mount of the cerebral hemispheres shows dilatation of lateral ventricles and loss of myelin sheaths associated with PVL. LFB. The same case as in 4.8-2 left MRI.

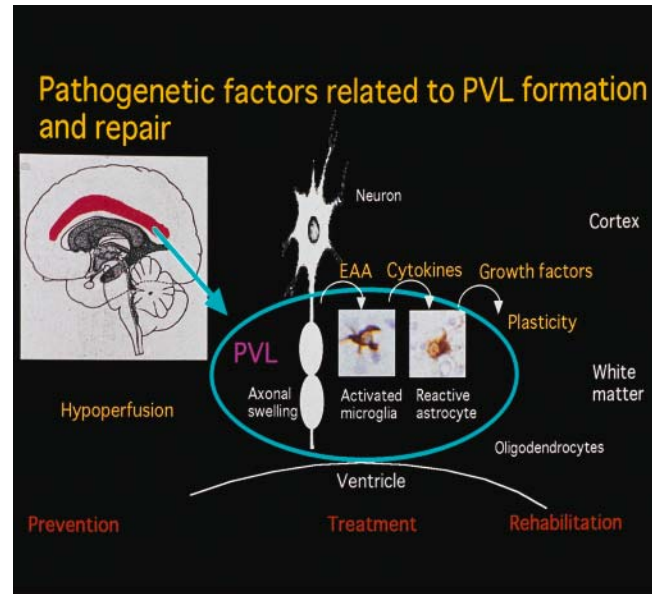


Fig. 4.8-4. Pathogenesis of PVL.

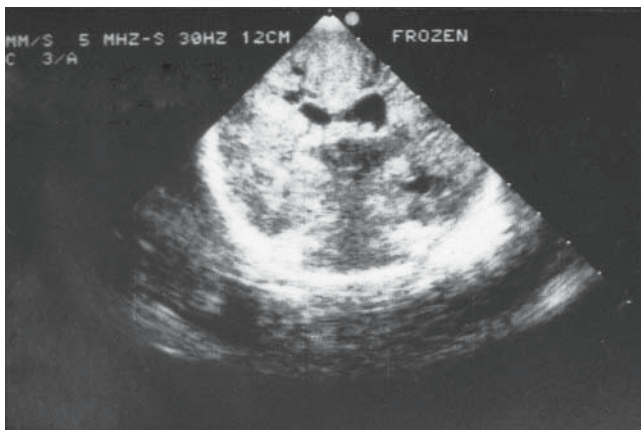


Fig. 4.8-5. Multicystic leukomalacia. Ultrasonography reveals multiple cystic lesions in subcortical white matter in a 1-day-old infant.



Fig. 4.8-6. Multicystic leukomalacia present in the brain of the same neonate as in 4.8-5 at the time of death (3 days of age). There is marked destruction of the white matter, which occurred before birth.

4.9 Subcortical Leukomalacia, Multicystic Encephalomalacia

Subcortical leukomalacia is a focal leukomalacia situated underneath the cortex of the deep sulci. It is located in the border zone of major cerebral arteries and is found in term or postterm infants who have experienced cerebral hypoperfusion. Focal subcortical leukomalacia is sometimes found in infants with sudden infant death syndrome or cyanotic congenital heart disease [12]. Widespread subcortical leukomalacia is seen in infants with hypoperfusion caused by hypoxic-ischemic encephalopathy or meningitis. The vulnerability of the develop-

ing microvasculature and premyelinating metabolic activity may be risk factors for the development of subcortical leukomalacia.

Multicystic encephalomalacia (also referred to as cystic encephalomalacia or multicystic encephalopathy) is a severe form of encephalomalacia. Large separated cavities occur throughout the cortex and white matter bilaterally [13]. The lesions develop as the result of a severe hypoxic-ischemic insult near the end of gestation or during the early postnatal period [12].



Fig. 4.9-1. Subcortical leukomalacia. There is focal white matter rarefaction at the depth of a sulcus associated with a paucity of axons and myelin and, rarely, swollen axons, macrophages, and reactive astrocytes.



Fig. 4.9-2. Subcortical leukomalacia. Whole mount with PTAH stains.

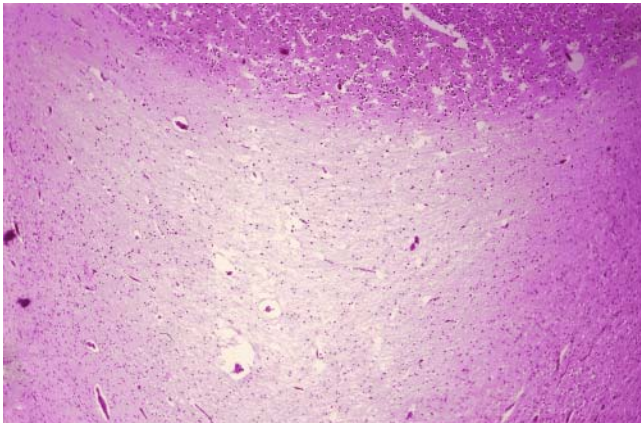


Fig. 4.9-3. Subcortical leukomalacia. Histology shows spongy changes associated with axonal swellings, foam cell infiltration, and astrogliosis. H&E.



Fig. 4.9-4. Microangiography of the frontal cortex and white matter shows the paucity of penetrating vessels underneath the sulcus in the term brain.

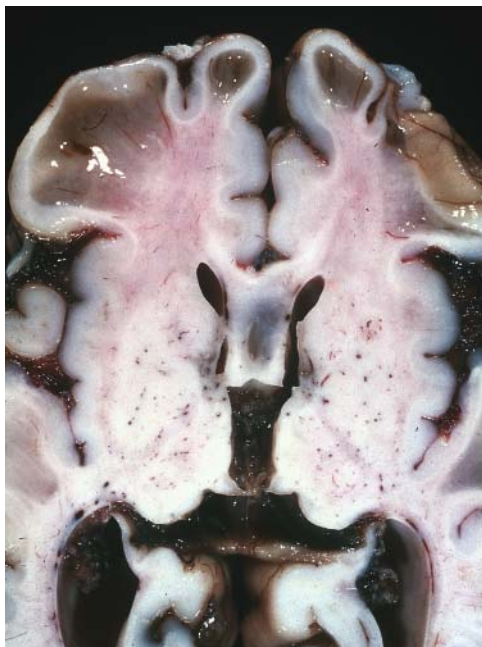


Fig. 4.9-5. Subcortical leukomalacia. There are multiple lesions in adjacent gyri in a prematurely born infant.

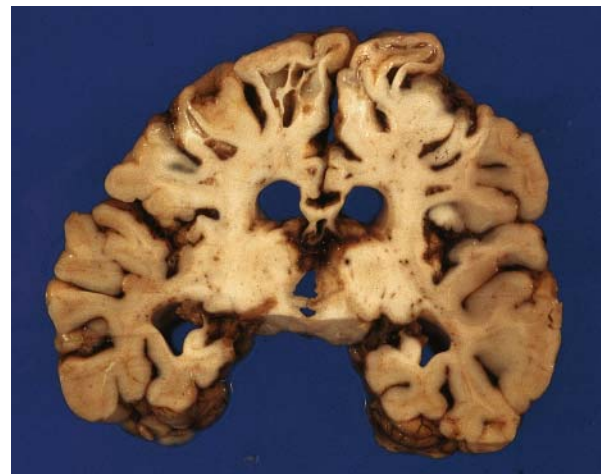


Fig. 4.9-6. Subcortical leukomalacia. There is cyst formation in the subcortical white matter of an infant with hypoxic-ischemic encephalopathy.

4.10 Hippocampal Necrosis and Pontosubicular Neuron Necrosis

In a neonate with acute perinatal asphyxia, hippocampal neuronal necrosis is expressed as neuronal eosinophilia. In chronic lesions there is loss of neurons and astrogliosis in CA1, CA3, and CA4 and the subiculum. The neuron loss of CA1 is similar to that produced with experimental delayed neuronal death.

In neonates 28 weeks to 2 months after birth, the subiculum of the hippocampal formation may exhibit (without involving CA1–CA4) the changes characteristic of pontosubicular necrosis (PSN) [1,13]. With PSN, neurons of the subiculum and the ventral pons show

karyorrhexis and cell shrinkage of cytoplasm. Acute PSN mimics the histology of apoptosis: karyorrhexis, cellular atrophy, DNA fragmentation in situ, and few reactive astrocytes [14–16]. In the basis pontis and the subiculum there is a developmental discrepancy between the early development of the vessels and the late maturation of the neurons, which may predispose fetuses and neonates to PSN [17]. Causal factors have been identified to include hyperoxemia, ischemia, hypocarbia, and hypoglycemia [18–21].

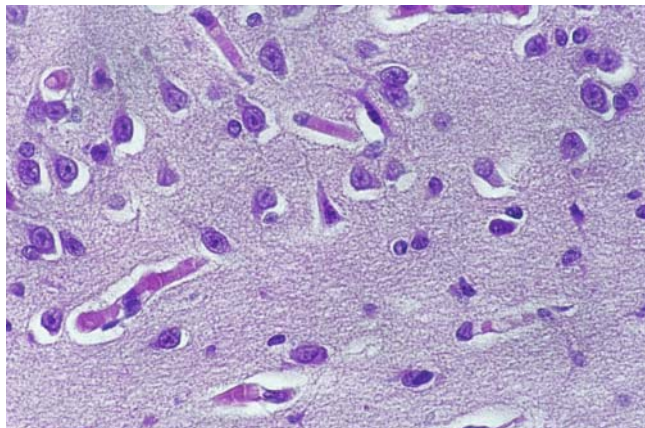


Fig. 4.10-1. Pontosubicular necrosis (PSN). Note the selective neuronal karyorrhexis in pontine nuclei. H&E stains. Karyorrhexis is disintegration of the nucleus into basophilic clumps with loss of nuclear membrane definition. H&E.

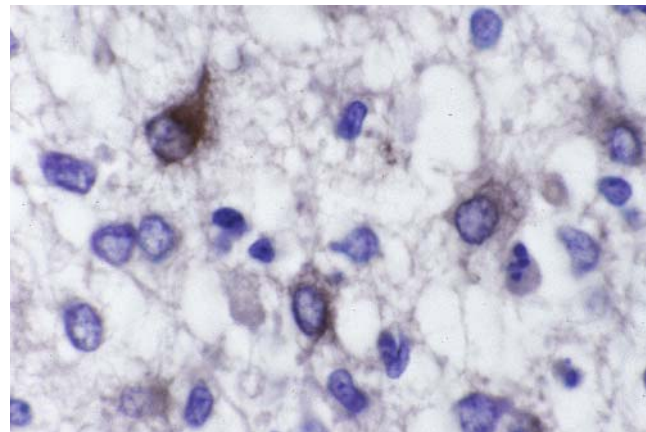


Fig. 4.10-2. PSN. Severe neuronal karyorrhexis is associated with reactive astrogliosis. GFAP. Three- to five-day-old lesions exhibit progressive dropout of neurons, astrocyte and microglial aggregation, and active macrophage proliferation.

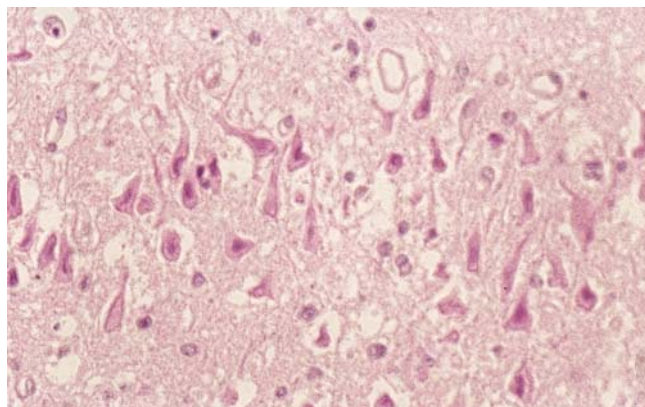


Fig. 4.10-3. Hippocampal necrosis. Note the marked eosinophilia of neurons in the pyramidal layer of the hippocampus. The necrosis involves Sommer's sector (CA1), where pyramidal neurons show eosinophilic cytoplasmic change. H&E.

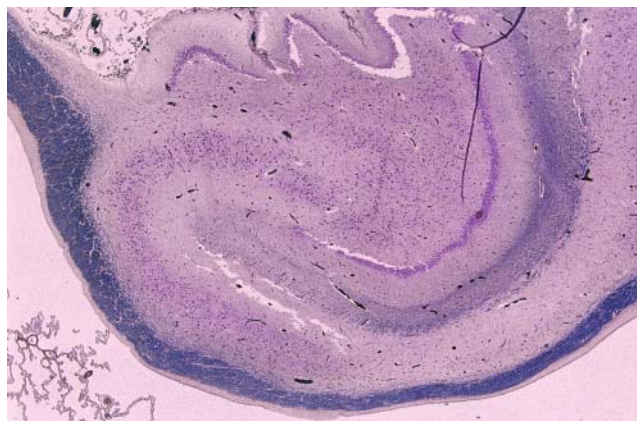


Fig. 4.10-4. Hippocampal necrosis. Neuron loss in the pyramidal cell layer CA1 of a patient with cerebral palsy, intellectual disabilities, and epilepsy. H&E. There is ongoing debate as to the relation of this lesion to Ammon's horn sclerosis associated with partial complex epilepsy of temporal origin.

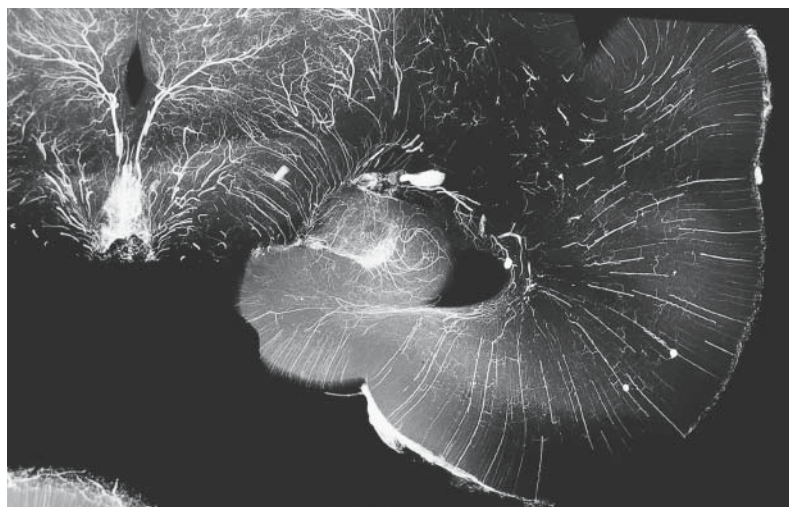


Fig. 4.10-5. Arterial architecture in postmortem microangiography of the hippocampus at 28 weeks' gestation. Ammon's horn and subiculum have well-developed vascularity.



Fig. 4.10-6. Arterial architecture in postmortem microangiography of the pons at 28 weeks' gestation. Pontine nuclei are located along the course of perforating arteries.

4.11 Perinatal Brain Stem Necrosis, Moebius Syndrome, Ondine's Curse

Selective symmetrical *necrosis of brain stem nuclei* is seen in infants, older children, and adults who have experienced cardiac arrest with profound hypotension (cardiac arrest encephalopathy, hypotensive brain stem necrosis) [1,22]. In neonates, brain stem necrosis is found predominantly in cranial nerve nuclei, the reticular formation of the tegmentum of the brain stem, and in the posterior colliculi of the tectum. Similar brain stem lesions are found after total asphyxia [23] and massive brain stem necrosis [24,25] and with chronic hypoventilation [2]. In acute lesions, neurons are eosinophilic in the center of the various nuclei. In remote lesions, neuronal loss, astrogliosis, and cavity formation are found in the nuclei. Brain stem necrosis is some-

times found alone but more commonly is associated with cerebral damage. High blood flow and oxygen demand in nuclei may be a predisposition for the pathogenesis of brain stem necrosis.

Moebius syndrome is a congenital malformation syndrome associated with facial diplegia and other cranial nerve deficits. Neuropathology shows cranial nuclei changes consisting of cellular hypoplasia or atrophy and foci of necrosis in the tegmentum. There are probably multiple etiologies, both developmental and destructive. Familial cases have been reported [26,27].

Ondine's curse, also called central alveolar hypoventilation, is associated with brain stem gliosis [28].

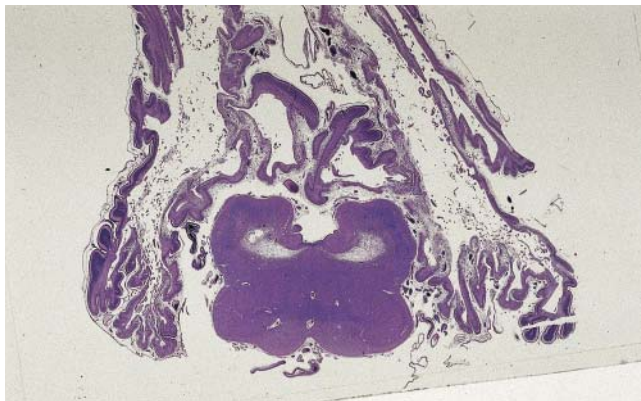


Fig. 4.11-1. Brain stem necrosis. Bilateral tegmental necrosis, sparing the inferior olivary nuclei, is associated with cerebellar white matter necrosis in a case of cardiac arrest encephalopathy. [29] H&E.

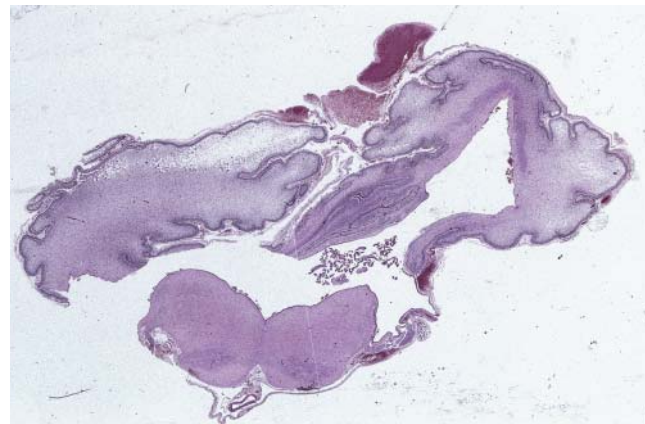


Fig. 4.11-2. Olivocerebellar degeneration in a very low-birth-weight infant with cerebellar cystic leukomalacia and remote subarachnoid hemorrhage following extensive intraventricular hemorrhage. H&E.



Fig. 4.11-3. Olivocerebellar degeneration. Unilateral atrophy of the right inferior olivary nucleus in the medulla oblongata, with a defect of the contralateral left cerebellar hemisphere, is seen in an infant with sudden death. Histology of the brain stem shows neuronal loss and astrogliosis in the contralateral inferior olivary nucleus.

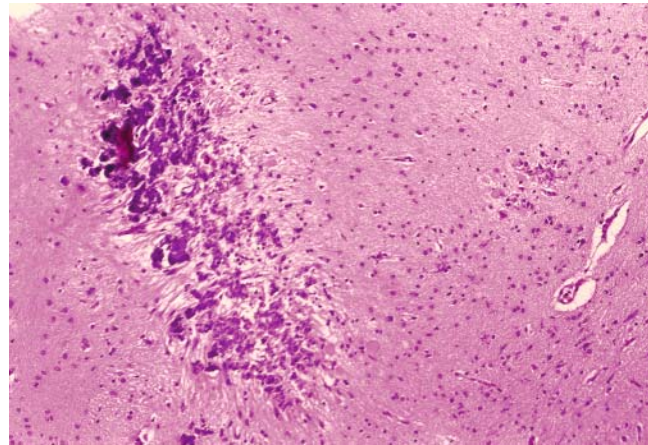


Fig. 4.11-4. Moebius syndrome. Note the calcification of foci in the tegmentum of the pons. H&E.

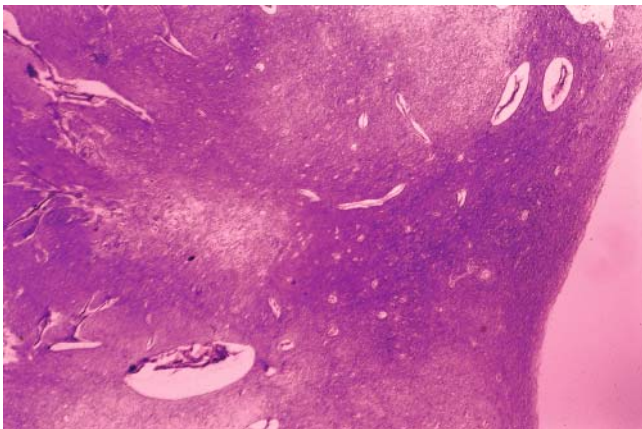


Fig. 4.11-5. Moebius syndrome. There is marked fibrillar astrogliosis in the tegmentum of the pons. Holzer stain.

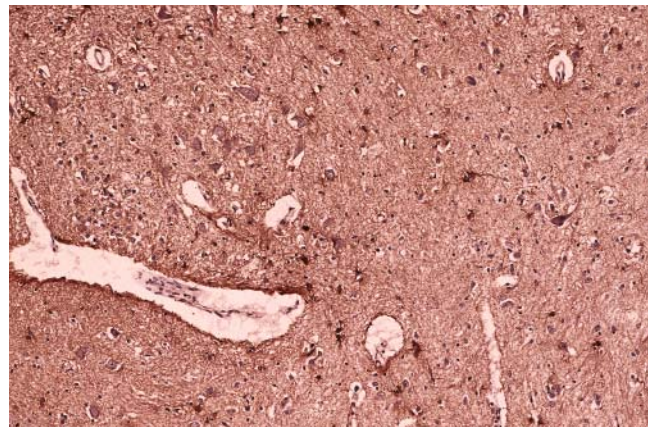


Fig. 4.11-6. Ondine's curse. There is marked astrogliosis in the tegmentum of the medulla oblongata. GFAP immunohistochemistry.

4.12 Cerebellar Hemorrhage, Olivocerebellar Transneuronal Degeneration, Cerebellar Infarction, Cerebellar Cystic Leukomalacia

Cerebellar hemorrhage and subarachnoid hemorrhage are more common in low-birth-weight preterm infants than in term infants. Subarachnoid hemorrhage in the cerebellum is often associated with intraventricular hemorrhage. Blood accumulates in the posterior fossa, and significant collections incite obliterative arachnoiditis, producing hydrocephalus and neuronal degeneration of Purkinje cells and granular cells. Hemorrhage in the cerebellum itself is frequently observed in very low-birth-weight infants and tends to occur in the internal and external granular cell layers of the cerebellar cortex. The hemorrhages may be multiple and small or focal and large, contiguous with blood in the subarachnoid

space. The pathogenesis of cerebellar hemorrhage is multifactorial, including trauma, hypoxia, infection, and bleeding disorders [1].

Isolated cerebellar hematomas or infarction are uncommon in the cerebellar hemisphere. They may produce Purkinje cell loss with Bergman glial proliferation, which induces olivocerebellar retrograde degeneration with neuron loss and astrogliosis in the contralateral inferior olivary nucleus [5,28].

The white matter of the cerebellum may be involved with ischemic insults that produce necrosis and cyst formation (cerebellar cystic leukomalacia) [30].

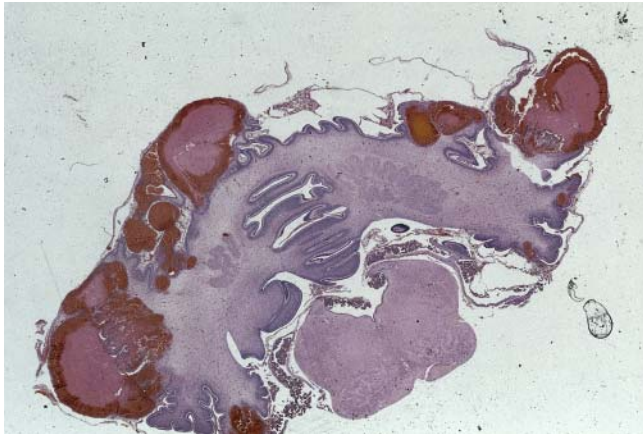


Fig. 4.12-1. Cerebellar hemorrhage. Note the multiple cerebellar hemorrhages in both cerebellar hemispheres. H&E.

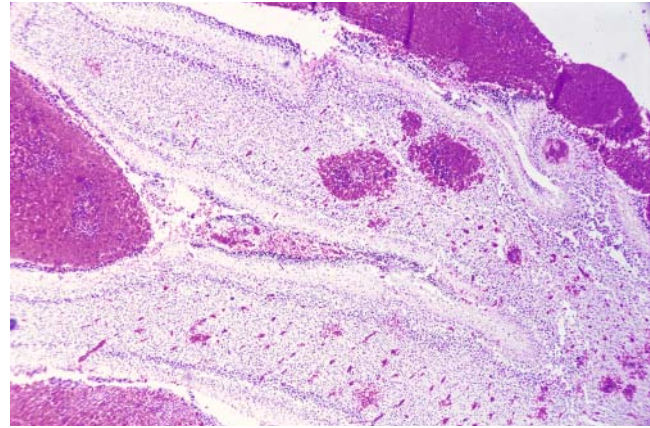


Fig. 4.12-2. Subarachnoid hemorrhage and cerebellar granular cell layer hemorrhage. H&E.

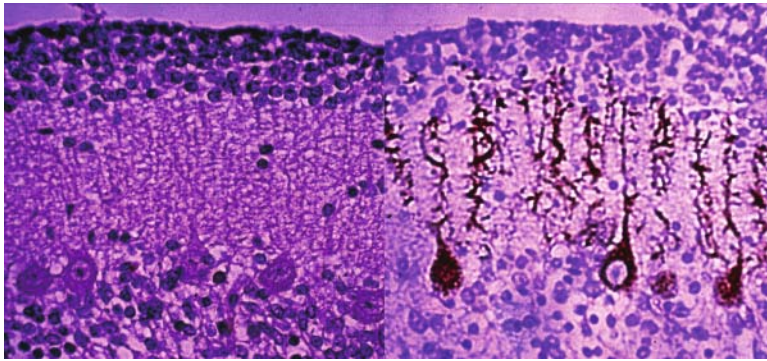


Fig. 4.12-3. Normal appearance of Purkinje cells in neonates. Dendritic trees of Purkinje cells have a few branches. *Left.* H&E. *Right.* Glutamate transporter (EAAT4) immunohistochemistry.

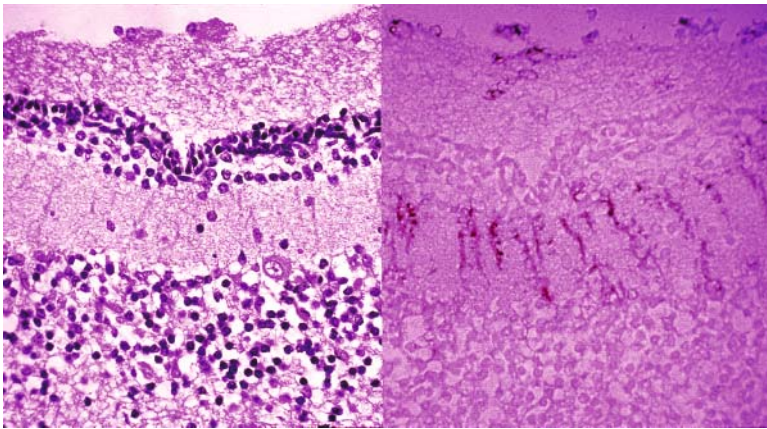


Fig. 4.12-4. Cerebellar subarachnoid hemorrhage may be associated with degeneration of Purkinje cells. *Left.* H&E. *Right.* Glutamate transporter (EAAT4) immunohistochemistry.

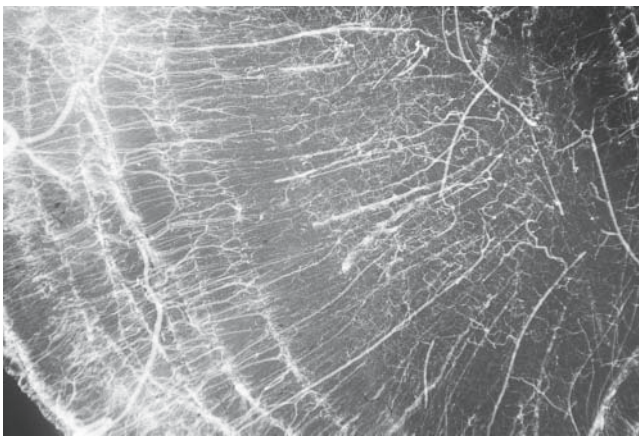


Fig. 4.12-5. Arterial vasculature of the cerebellum. Numerous perforating arteries from the fissures of the folia distribute to the white matter and provide branching small vessels to the cerebellar cortex.

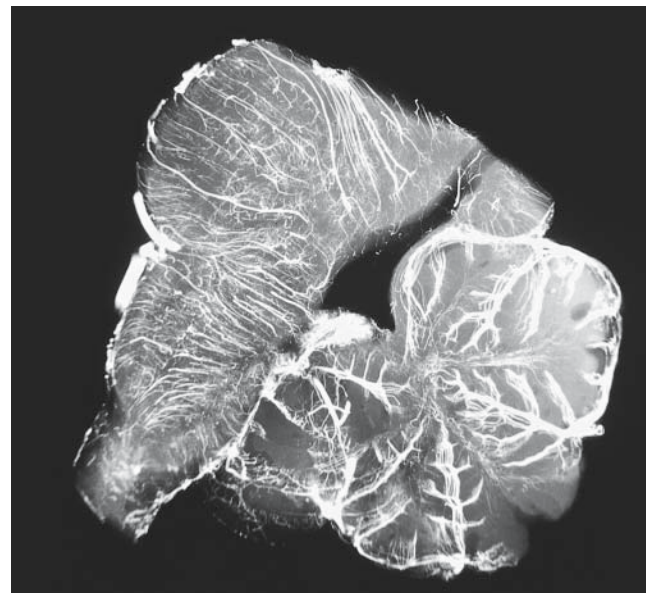


Fig. 4.12-6. Demonstration of arterial vasculature in the cerebellar vermis and the brain stem with characteristic branching patterns.

4.13 Kernicterus

The term kernicterus refers to both the clinical disease of bilirubin encephalopathy and the brain pathology. It is caused by excessively high levels of unconjugated bilirubin (hyperbilirubinemia). Infants have an immature liver and insufficient bowel enzymes for bilirubin metabolism; thus, at birth they have elevated “physiological” levels of unconjugated bilirubin. These levels may be increased by hemolysis, sepsis, hypoxia, drugs that displace bilirubin (which is normally bound to albumin), and by reduced levels of albumin. When unconjugated bilirubin levels are excessive, the cells (particularly cells of the brain) are unable to oxidize the bilirubin or transport it out of the cell. In the cell, the bilirubin binds to membranes (e.g., mitochondrial membranes), damaging them and impairing the cellular energy metabolism [31]. The hyperbilirubinemia is alleviated by phototherapy and an exchange blood transfusion.

Children surviving an acute episode of bilirubin encephalopathy may show cerebral palsy with choreoathetosis.

The gross pathology of kernicterus includes symmetrical yellow staining and neuronal necrosis of certain gray matter areas and nuclei. Most commonly involved are the globus pallidus, thalamus, subthalamus, cranial nerve nuclei, inferior olives, gracile and cuneate nuclei, and the roof nuclei of the cerebellum. Less frequently involved are the hippocampus (CA2), putamen, lateral geniculate body, and anterior horns of the spinal cord. Histology reveals shrunken neurons with pyknotic nuclei, eosinophilic neuronal necrosis, and bilirubin pigment in the acute lesions. Later, neuronal loss, astrogliosis, and hypermyelination appear in the basal ganglia (status marmoratus) and at other sites.



Fig. 4.13-1. Kernicterus. Note the yellow stain in the thalamus bilaterally.



Fig. 4.13-2. Kernicterus. There is a yellow change in the tegmentum of the medulla oblongata.



Fig. 4.13-3. Kernicterus. There is a yellow change in the tegmentum of the pons.

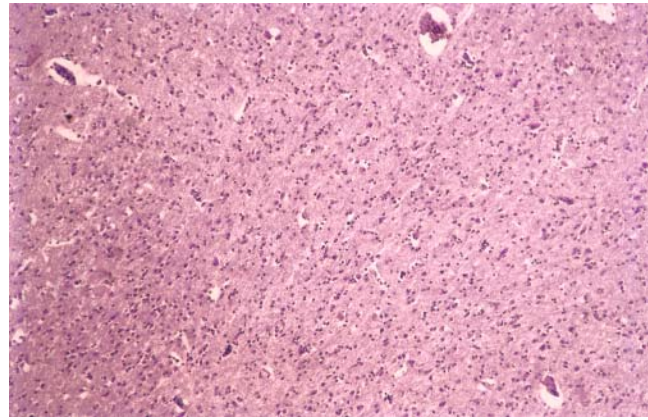


Fig. 4.13-4. Kernicterus. Note the neuronal loss and astrogliosis in a red nucleus. H&E.

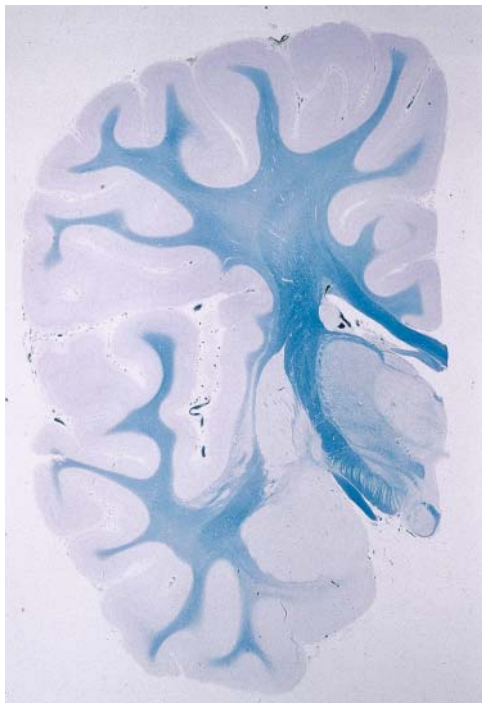


Fig. 4.13-5. Whole mount of the cerebral hemisphere with LFB stain defining the myelin (blue) with abnormal myelination of the thalamus (i.e., status marmoratus).

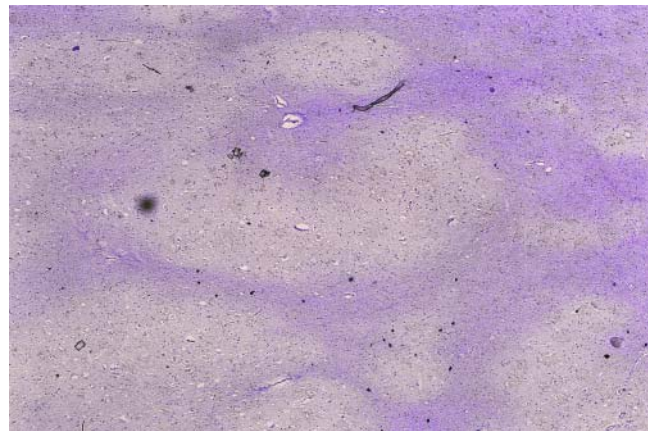


Fig. 4.13-6. Kernicterus. Sequelae of kernicterus, status marmoratus in the thalamus. Holzer stain, revealing the glial fibers which are abnormally myelinated in this condition.

5. Vascular Diseases

5.1 Arteriovenous Malformation

Vascular malformations are classified into four categories: (1) arteriovenous malformation (AVM); (2) cavernous hemangioma; (3) venous angioma and varix; and (4) capillary telangiectasis or telangiectasia. Symptoms of a vascular malformation may be secondary to rupture of the lesion, the vascular steal phenomenon (diversion of blood flow by the arteriovenous shunt from normal surrounding areas, which subsequently become ischemic), or to a mass effect.

The AVM is composed of abnormal arterial and venous channels without an intervening capillary network. The brain tissue surrounding the abnormal vessels frequently calcifies and shows hemosiderin-laden macrophages. There is frequently calcification of vessel walls that increases with age [1,2].

Vein of Galen aneurysm (VGA) is an aneurysmal dilatation of the vein of Galen caused by direct shunting of arterial blood through an AVM into the deep venous system. The VGA causes high-output cardiac failure in neonates; hydrocephalus and seizures in older infants; and hemorrhage in older children.

Cavernous hemangiomas (sometimes called “cavernomas” in the clinical literature) are a mesh of venous channels of various size, back to back, without intervening brain tissue. There may be multiple hemangiomas. The adjacent brain is gliotic and frequently shows hemosiderin-containing macrophages and eosinophilic granular bodies. Some cases are familial and are associated with mutations of *KRIT* [3–5].



Fig. 5.1-1. Arteriovenous malformation (AVM). Note the tangle of abnormal vessels on the brain surface.

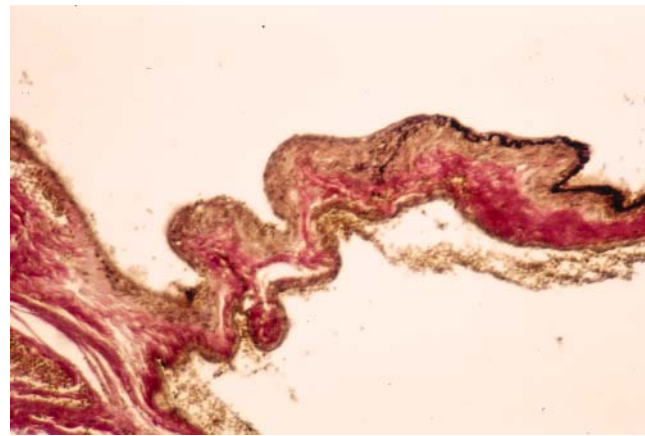


Fig. 5.1-2. AVM. Microscopic view of abnormal vessels, with arterialization of the vein in the arteriovenous shunt. Elastica-van Gieson.

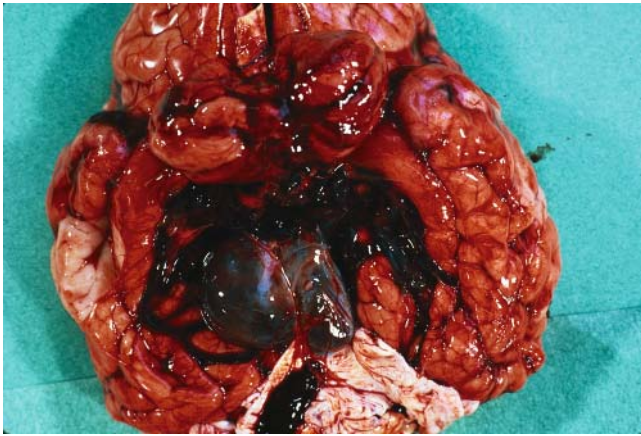


Fig. 5.1-3. Vein of Galen aneurysm (VGA). VGAs exhibit massive dilatation of the vein and of associated draining vessels. They show fibrous intimal hyperplasia and arterialization by elastic tissue. There are usually mural thrombi formed on their walls.



Fig. 5.1-4. VGA. Microangiography of a vein of Galen aneurysm shows associated abnormal draining veins.

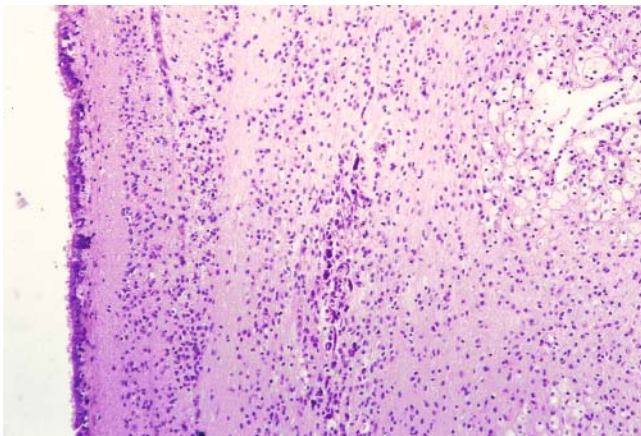


Fig. 5.1-5. VGA. Ischemic lesions (caused by the steal phenomena) with gliosis and calcification in periventricular white matter. H&E.

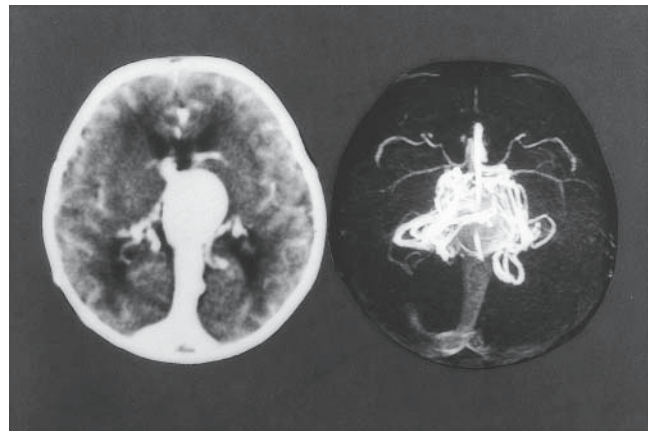


Fig. 5.1-6. VGA. Magnetic resonance imaging (MRI) angiography showing a vein of Galen aneurysm and associated abnormal draining veins. Ultrasonography also demonstrates VGA as an enlarged, echoic vessel in which pulsations are demonstrable in the mass.

5.2 Aneurysm

In adolescents and young adults (<20 years of age), *berry*, or *saccular*, *aneurysms* become more important than AVMs as a cause of primary intracranial hemorrhage. The aneurysm shows a deficiency of elastic and muscle tissue with dilatation of the collagenous vessel wall. There is an association between polycystic kidney, coarctation of the aorta, and cerebral aneurysms. Some are familial [6].

Dissecting aneurysms, with extravasation of blood into the arterial wall usually between the intima and the

media, may occur in the neck arteries following trauma or in intracerebral arteries near bifurcation sites where there are subintimal defects in the vessels walls.

Mycotic aneurysms originate when microbe-carrying emboli (usually from the heart) lodge in a cerebral vessel and produce a pyogenic infection in the arterial wall, causing weakness, distension, and rupture [7].



Fig. 5.2-1. Aneurysm in the origin of the right middle cerebral artery.

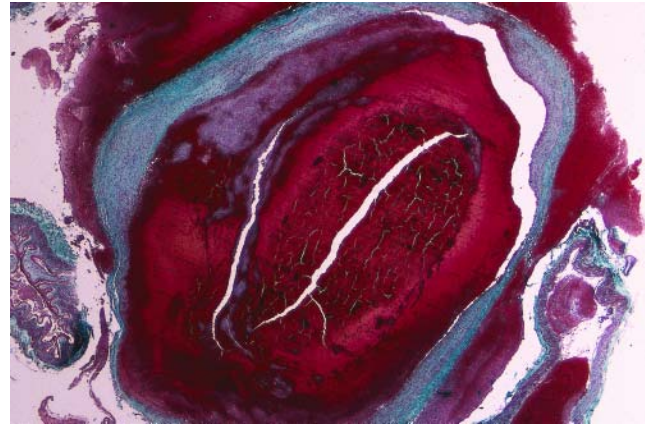


Fig. 5.2-2. Dome of a saccular aneurysm. Histology reveals vascular dilatation, irregular thinning of the wall, and absence of elastica in the wall. Gomori trichrome stain.



Fig. 5.2-3. Aneurysm (berry) at the bifurcation of the right middle cerebral artery.



Fig. 5.2-4. Aneurysm (berry) in the basilar artery.

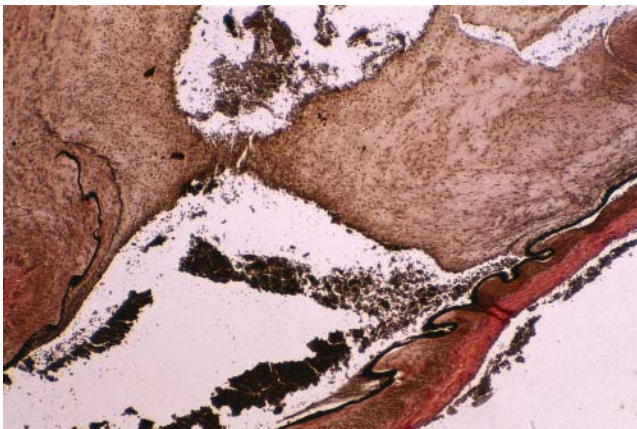


Fig. 5.2-5. The base of the aneurysm. Histology of the aneurysm in 5.2-4 shows intimal thickening and splitting of elastica. Elastica-van Gieson.

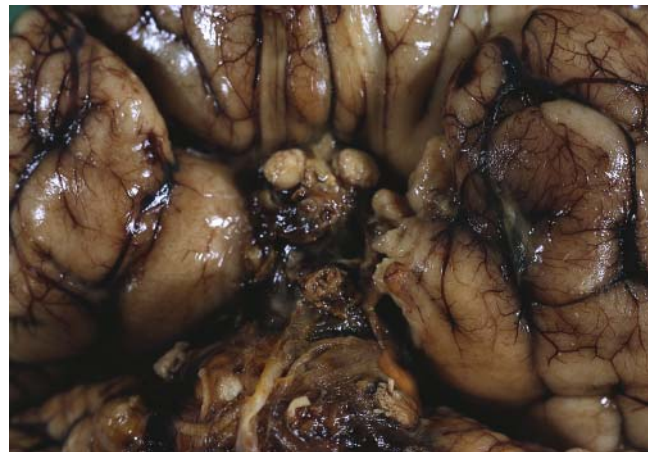


Fig. 5.2-6. Mycotic aneurysms occurring in intracerebral arteries following embolization of infected cardiac lesions. The aneurysms have ruptured producing subarachnoid hemorrhage.

5.3 Moyamoya Disease

Moyamoya disease, first noted in Japanese patients in 1957, is characterized by occlusive or stenotic lesions at terminal portions of the internal carotid arteries with prominent evolution of collateral vascular networks (moyamoya vessels) at the base of the brain [8]. It may occur as a primary or secondary phenomena (in neurofibromatosis-1, tuberous sclerosis, Marfan's syndrome, Alpert's syndrome, sickle cell anemia, Fanconi's anemia, and Schimke's immunosseous dysplasia). It presents as a hemispheric stroke in children and subarachnoid hemorrhage in older persons. Recent genetic studies suggest that some responsible genetic foci are in chromosomes 3, 6, 8, and 12 [9].

The neuropathology, of unknown pathogenesis, shows lesions in the circle of Willis. The walls of arteries are thick with marked fibrocellular thickening of the intima, splitting of the elastic lamina, and thrombus formation in the internal carotid arteries, posterior communicating arteries, and posterior cerebral arteries. There is no inflammation.

Fibromuscular dysplasia is a disease of arteries with anomalous increases and arrangements of elastic, collagen, and muscle, producing stenosis and poststenotic aneurysms. The etiology is not defined, although genetics, trauma, hormones, and viral factors have been implicated [10].

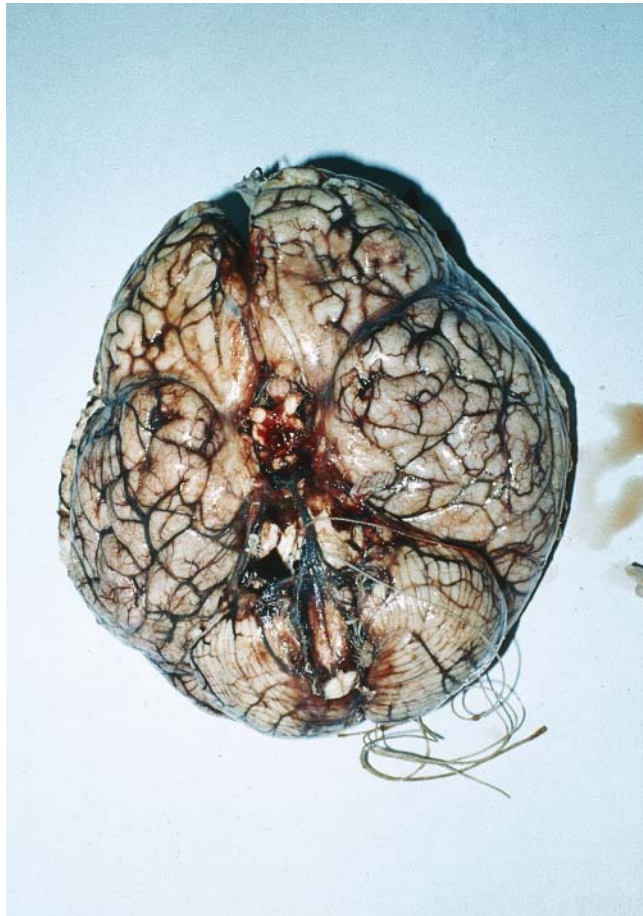


Fig. 5.3-1. Moyamoya disease, showing fatal brain swelling from edema.

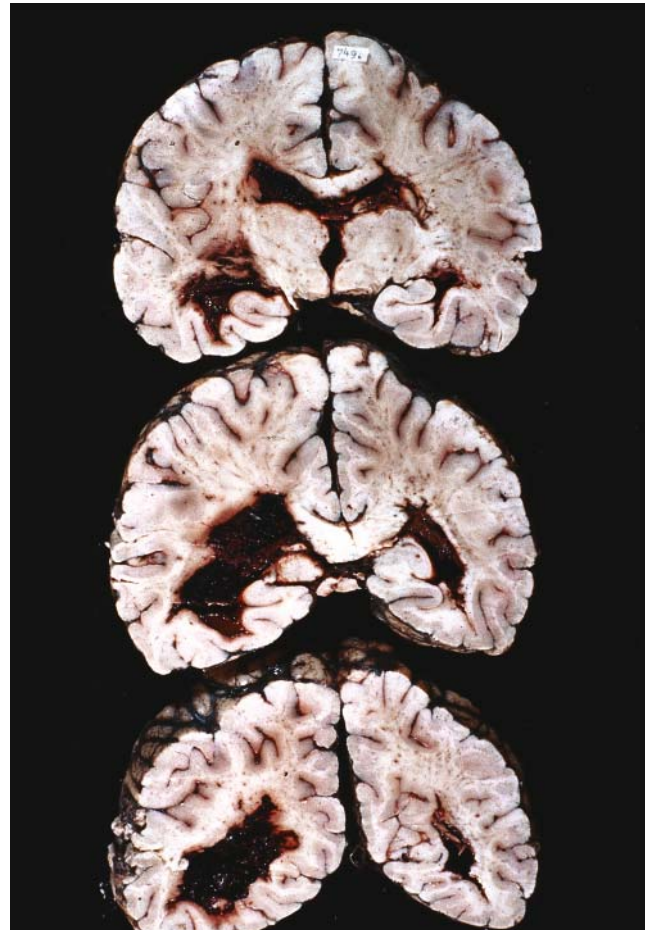


Fig. 5.3-2. Moyamoya disease with ischemia and hemorrhage in the ventricle and white matter.



Fig. 5.3-3. Moyamoya disease with stenotic middle cerebral arteries.

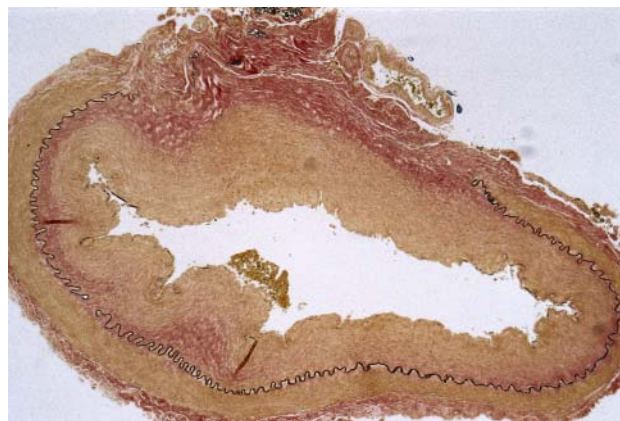


Fig. 5.3-4. Moyamoya disease. The artery of the circle of Willis exhibits thickening of the intima and lack of internal elastic lamina. Elastica-van Gieson.



Fig. 5.3-5. Moyamoya disease. Note the cortical necrosis in the occipital lobe.



Fig. 5.3-6. Moyamoya disease. Cerebral angiography shows marked moyamoya vessels (puff of smoke) in thalamostriatal regions on the left.

5.4 Cavernous Hemangioma and Pediatric Strokes

Infarcts and ischemic lesions in children usually present as strokes. Arterial ischemic stroke near birth is recognized in 1/4000 full-term infants, with seizures being a common presentation. In one study, 5.4% of 600 infants examined at autopsy showed cerebral infarcts. Some of the infarcts occur in utero; however, the histological evolution of the lesions is similar to that in the mature brain [11]. The most common causes of stroke include sepsis, embolization, and disseminated intravascular coagulation (DIC). Term neonates are more frequently affected than preterm babies. With survival, the child may exhibit clinical syndromes related to porencephaly, such as hemiplegia, seizures, or mental retardation. In older children, hematological and metabolic diseases (e.g., sickle cell disease and homocystinuria) are risk factors for stroke.

Classification of Vascular Diseases Responsible for Pediatric Strokes

1. Thromboembolic factors: moyamoya disease; cardiogenic embolism; fibromuscular dysplasia; venous thrombosis; atherosclerosis
2. Vasculitis: systemic vasculitis; drug-associated vasculitis; central nervous system (CNS) angitis; postinfectious vasculitis [12]
3. Human immunodeficiency virus (HIV)-associated vasculitis
4. Hematological and metabolic diseases inducing vascular disease (e.g., protein C deficiency, sickle cell disease, homocystinuria)

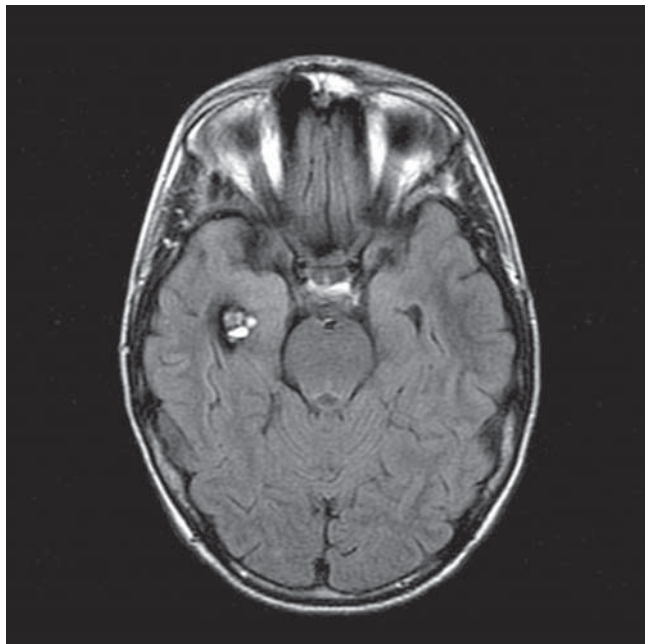


Fig. 5.4-1. A MRI (FLAIR) demonstrates a cavernous hemangioma in right temporal lobe of a patient being worked up for seizures.

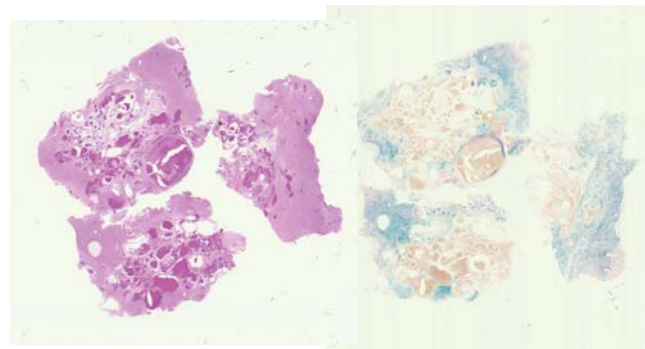


Fig. 5.4-2. Cavernous hemangioma. Whole mount of lesion in Fig. 5.4-1. *Left.* It shows the vascular malformation to be a “mulberry” of abnormal venous vessels. H&E. *Right.* Iron stain shows the hemosiderin deposition in the adjacent brain and correlating with the dark rim on MRI studies. Perls iron stain.

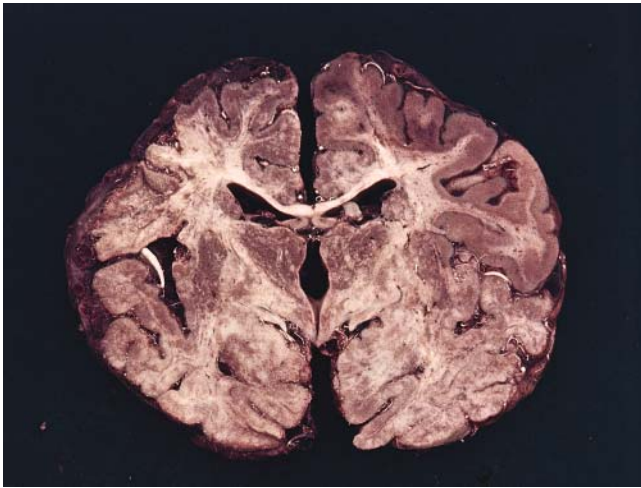


Fig. 5.4-3. Multiple infarctions in the brain associated with cyanotic congenital heart disease (tricuspid atresia) at 1 year of age.

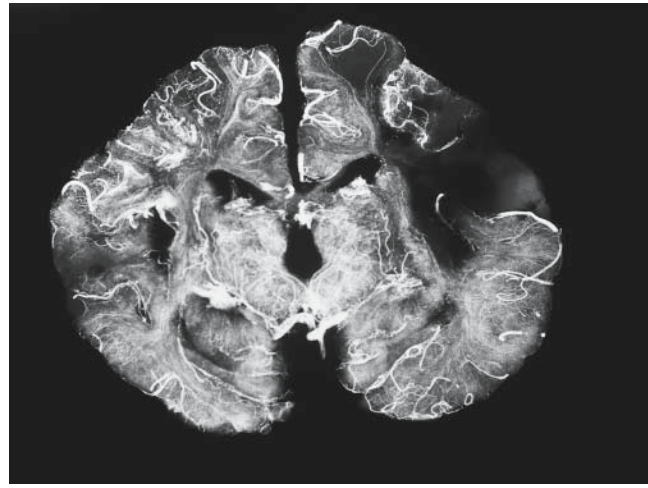


Fig. 5.4-4. Postmortem angiography (same case as in 5.4-3) reveals multiple infarctions. There are tortuous, enlarged vessels and an increased number of small vessels in the cerebral hemispheres.

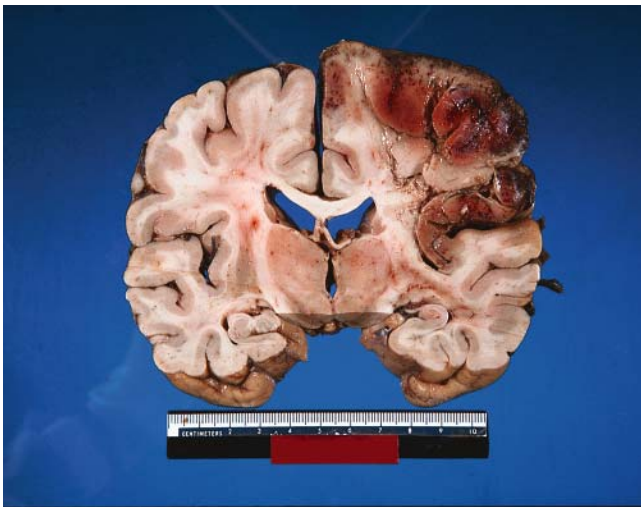


Fig. 5.4-5. Acute stroke in territory of right anterior and middle cerebral arteries.

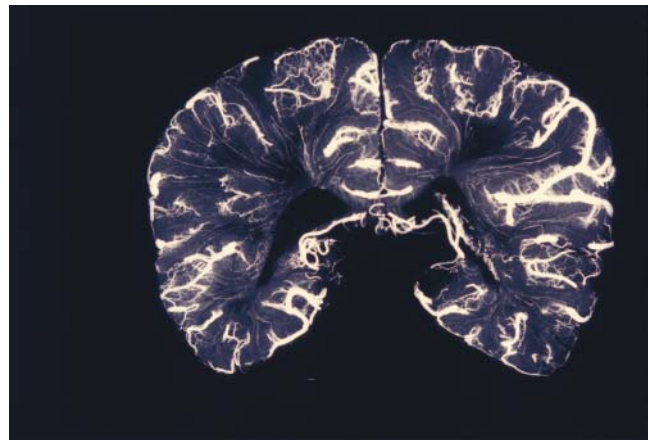
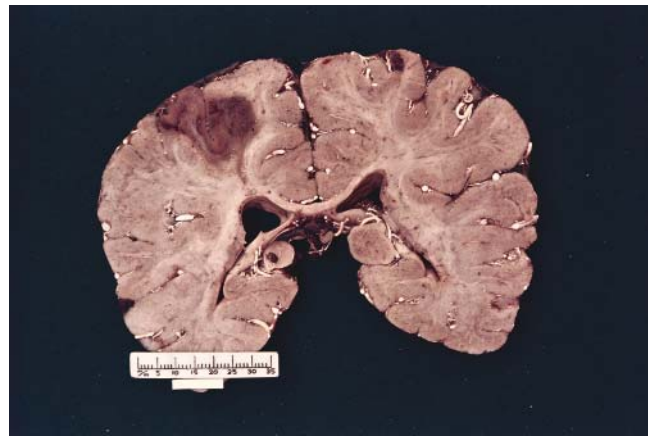


Fig. 5.4-6. Cerebral infarction in a case of a ventricular septal defect (upper). Postmortem angiography of the case. There are multiple foci of unfilled vessels in the cortex and white matter (bottom).

5.5 Venous Thrombosis (Septic/Other)

Venous thrombosis is usually secondary to electrolyte imbalance, leptomeningitis, disseminated intravascular coagulation, leukemia, sickle cell disease, congenital heart disease, or nutritional disturbances causing dehydration [13–15].

Thrombosis commonly occurs in the superior sagittal sinus (posterior part) with propagation into the adjacent superficial cerebral veins. When cerebral veins are involved, there is marked cerebral congestion, which may lead to subarachnoid hemorrhage and hemorrhagic infarction of the brain. Thrombosis of the deep cerebral veins is less common.

The pathogenesis of thrombosis or coagulation involves interaction of platelets with a platelet-

aggregating factor, factor VIII or von Willebrand's factor. When there is a deficiency of proteins that normally limit coagulation and promote fibrinolysis, dangerous thrombi may form. Such hypercoagulable states are present when infants have inherited deficiencies of protein C, protein S, or antithrombin III or when infants have anti-phospholipid antibodies.

Pathology shows microthrombi in small channels with microvascular endothelial proliferation in the cortex and deep central gray matter, sparing the white matter. Phlebothrombosis can involve both the cerebellar and cerebral hemispheres.



Fig. 5.5-1. Sagittal sinus thrombosis with subarachnoid hemorrhage.

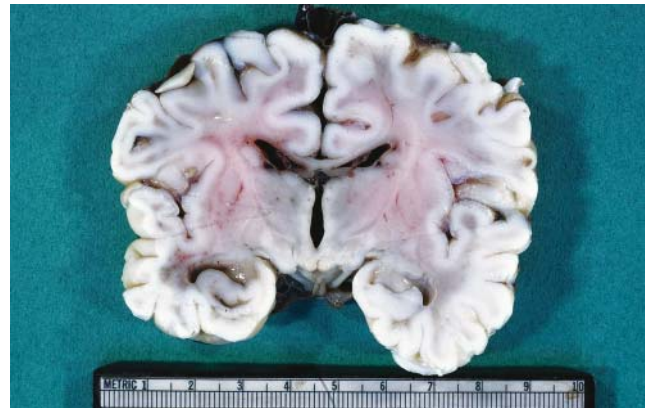


Fig. 5.5-2. Sagittal sinus thrombosis in a coronal section at the level of the mammillary body, showing edema and subependymal venous dilatation.



Fig. 5.5-3. Sagittal sinus with thrombus.

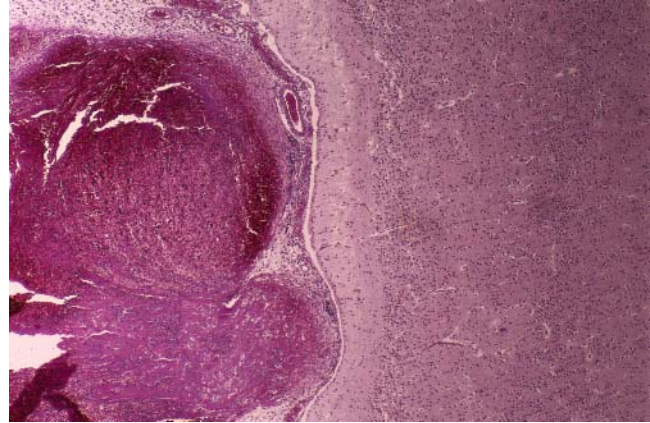


Fig. 5.5-4. Sagittal sinus thrombosis, microscopic view. H&E.



Fig. 5.5-5. Venous thrombosis, with a hematoma in the temporal lobe of a term neonate.

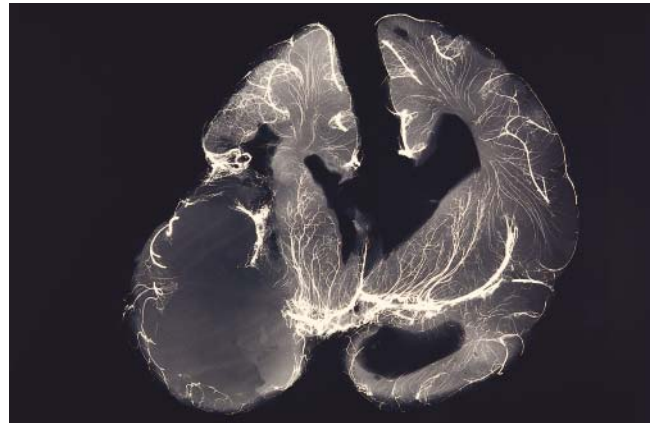


Fig. 5.5-6. Postmortem angiography of the case in 5.5-5 suggests loss of blood flow in the temporal lobe, deformity of the cerebral hemispheres, and dilatation of the lateral ventricle.

6 Increased Intracranial Pressure

6.1 Cerebral Edema

Cerebral edema, alterations in the amount or the site of brain water, is caused by brain injuries, infection, intoxication, and metabolic encephalopathies. It has been classified as being vascular/interstitial or toxic/cytoplasmic. Excessive brain edema produces increased intracranial pressure, which may cause brain herniation, with displacement of tonsillar, uncus, or cingulate brain tissues into the foramen magnum, posterior fossa, or below the falx, respectively. The herniated brain tissues can compress and interfere with regions of vital brain function (i.e., the brain stem). The gross deformations of brain herniations are not obvious in the brain of an infant with nonfused skull sutures, but the detrimental pressure effects of excessive brain edema may still operate [1].

Comparison of Vasogenic Edema and Cytotoxic Edema: Mechanism and Causes

Vasogenic edema: blood brain barrier is damaged by tumor, hematoma, abscess, contusion producing extravasation of plasma-like fluid, with swelling of astrocytic foot processes and myelin sheaths.

Cytotoxic edema: cellular membrane transporters are disturbed by ischemia causing impairment of cellular oxygenation, Na-K distribution, cytoplasmic, hydropic swelling and infarction



Fig. 6.1-1. Brain edema with swollen gyri and narrowed sulci.



Fig. 6.1-2. Brain edema with narrowing of the lateral and third ventricles and flattening of the gyri. There is grooving of the hippocampi.



Fig. 6.1-3. Brain edema with cerebellar tonsilar herniation.



Fig. 6.1-4. Brain edema with cerebellar tonsilar herniation.



Fig. 6.1-5. Sagittal section of the brain with brain edema. Note the narrowing of the fourth ventricle. Sudden death and resuscitation occurred at 6 months of age.

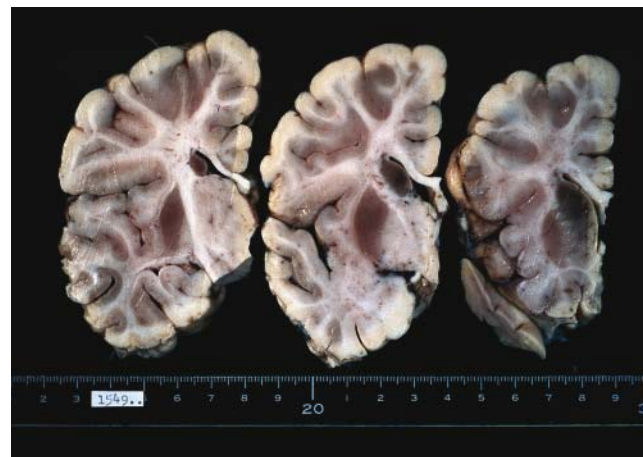


Fig. 6.1-6. Striatal necrosis in the case shown in 6.1-5.

6.2 Sequelae of Hypoxic Encephalopathy During Childhood

Hypoxia is defined as a reduction of oxygen supply or of its use so normal cellular metabolism is not maintained. Hypoxia is classified as *hypoxic* when the oxygen supply is impaired, *anemic* when the blood oxygen transport is impaired, or *histotoxic* when the tissue utilization of oxygen is impaired. The newborn brain is less vulnerable to hypoxia than the mature brain. The normal brain compensates for hypoxemia so if blood flow is maintained there may be little or no tissue damage. In children this may be observed in the brain of drowning victims and in those with sudden infant death syndrome. Hypoxia may also occur with allergic reactions or respiratory infections that produce respiratory arrest without cardiac arrest. The brain injury is at the synaptic level so good recovery is possible. When there is ischemia with impaired blood supply, tissue injury occurs. This is augmented if hypoxia is also present.

The tissue damage following a hypoxic/ischemic insult in the brain may be selective neuronal necrosis (related to excitotoxicity of glutamate on dendrites) or pan-

necrosis (when glia and blood vessels as well as neurons become necrotic). The extent of the injury determines the tissue response global or focal. Global ischemia results in damage in specific locations of the brains of children. In the cerebral cortex, *cortical laminar necrosis* (causing necrosis of neurons in the middle layers of the cortex) occurs predominantly in the arterial border zones of the cerebral hemispheres. In the hippocampus, neurons in *CA1* are first affected by the ischemic insults, sparing *CA2*. The basal ganglia are also damaged involving the corpus striatum or, specifically, the *globus pallidus*. The *cerebellum* can also show selected Purkinje cell death or necrosis in the boundary zone (watershed) between the cerebellar arteries.

Carbon monoxide (CO) poisoning combines anemic hypoxia (by occupying hemoglobin-binding sites) with histotoxic hypoxia (by binding to the iron in cells of the globus pallidus), with ischemic or stagnant hypoxia caused by the effect of CO on the heart [2].

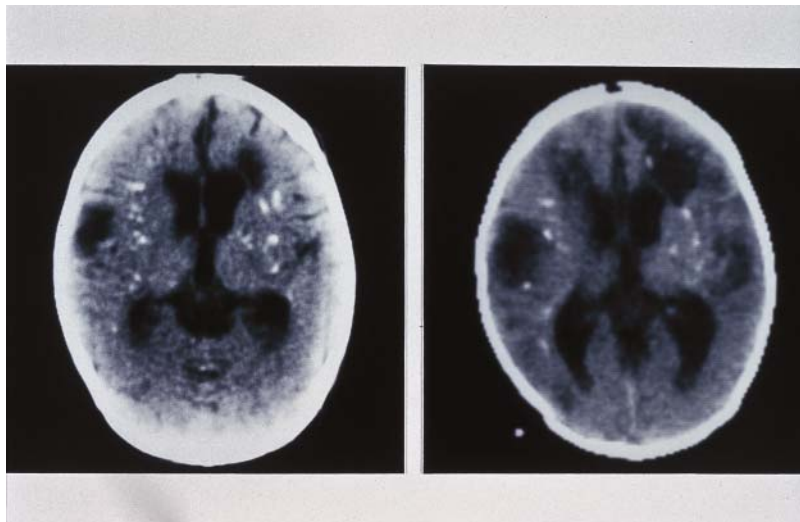


Fig. 6.2-1. Global ischemia. Computed tomography reveals calcification in injured areas.

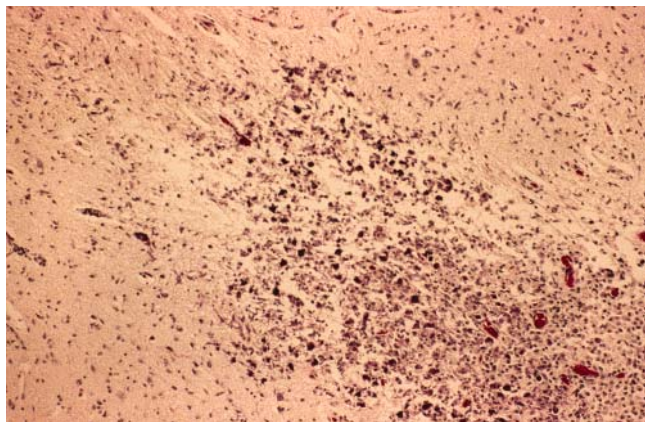


Fig. 6.2-2. Focal hypoxic-ischemic injury. The histological view shows calcification at the site of the injury. H&E.



Fig. 6.2-3. Focal hypoxic-ischemic injury. There is a vulnerable region of hemorrhagic necrosis at the depth of the sulcus.

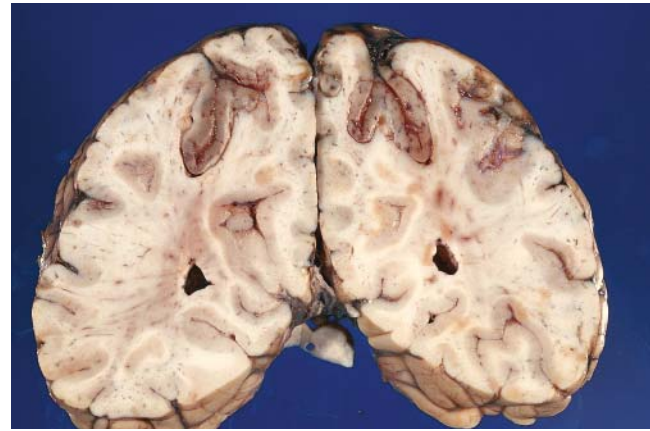


Fig. 6.2-4. Bilateral parasagittal infarction with cortical necrosis in the watershed between the anterior and middle cerebral arteries.



Fig. 6.2-5. Cortical atrophy after cerebral infarction, predominantly in the perisylvian area.

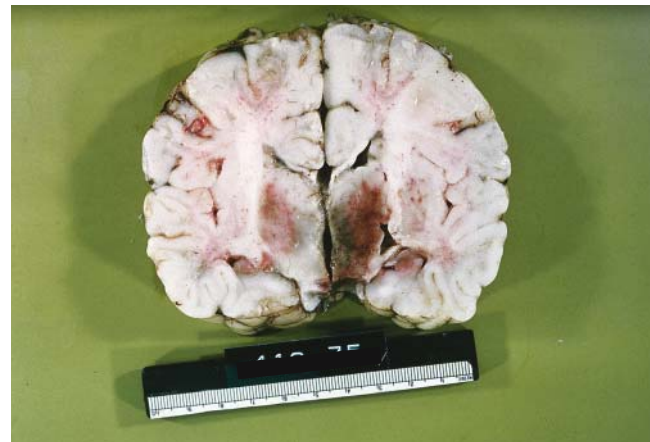


Fig. 6.2-6. Hemorrhagic infarction in the basal ganglia and thalamus in a sudden infant death case with failed attempts of resuscitation.

7 Neurocutaneous Syndromes

7.1 Tuberous Sclerosis Complex (Bourneville's Disease)

Tuberous sclerosis (TS) is a dominantly inherited disorder that affects multiple organ systems [1–3]. The current diagnostic criteria require TS complex-associated lesions of two or more organ systems or two dissimilar lesions of the same organ system. TS is sporadic in 60%–70% of cases. Two genes have been identified: *TSC1* (*hamartin*) located at 9q34 and *TSC2* (*tuberin*) located at 16p13.3 [4]. The genes have tumor-suppressing activity, but the pathogenesis of TS is not fully understood.

There are major and minor clinical features involving numerous systems: skin, retina, heart, kidney, lung, and

brain. Predominant neurological manifestations include mental retardation, epileptic seizures, and behavioral abnormalities, although there are also patients with no neurological impairment. The brain lesions, when present, probably result from altered migration of neurons and abnormal proliferation of glial elements. The lesions of TS include subependymal nodules, cortical hamartomas, areas of focal cortical hypoplasia, dysplasia, heterotopic gray matter, balloon cell changes in indeterminate astrocytes/neurons, and subependymal giant cell astrocytoma.

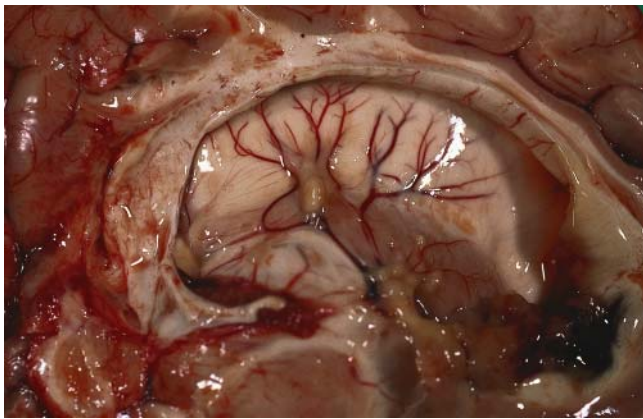


Fig. 7.1-1. Tuberous sclerosis. The nodules of tubers are seen on the ventricular wall.

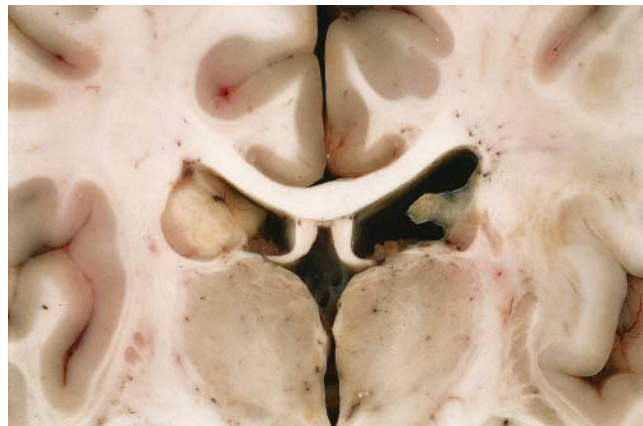


Fig. 7.1-2. Tuberous sclerosis with bilateral periventricular nodules on the wall and over the basal ganglia. They are composed of giant astrocytes or elongated fibrillary pilocytic astrocytes and interstitial calcifications.

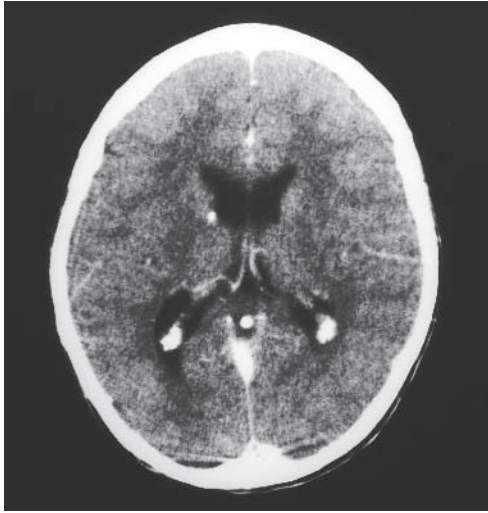


Fig. 7.1-3. Tuberous sclerosis. Computed tomography (CT) reveals the characteristic feature of multiple calcifications in the ventricular wall.

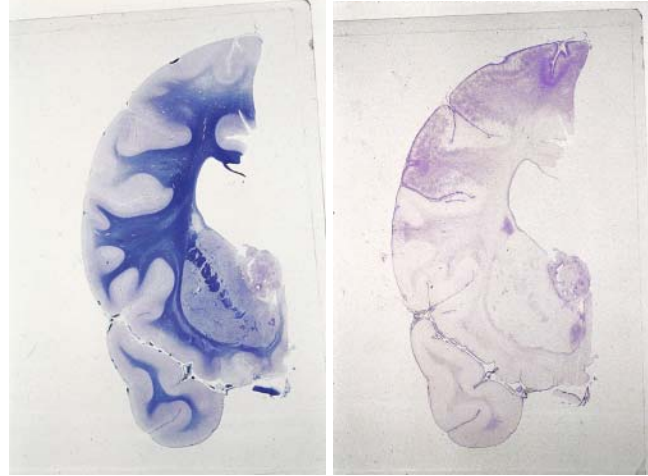


Fig. 7.1-4. Tuberous sclerosis. *Left.* Whole mount of cerebral hemisphere with cortical tubers and a periventricular giant cell astrocytoma. LFB stain reveals focal pallor of white matter and nonstaining of the nodule and tumor. *Right.* Holzer stain shows fibrillary astroglia in the cerebral cortex, white matter, and nodules with tumor in the ventricular wall.

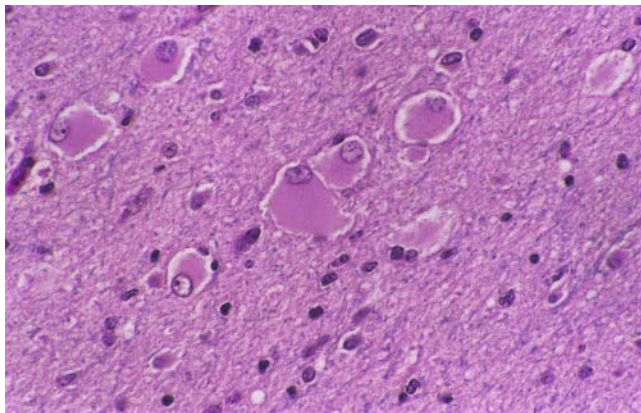


Fig. 7.1-5. Tuberous sclerosis. Balloon cells are in the cortical tuber, which is associated with giant astrocytes, gross disturbances of cell architecture, and dysplastic neurons of giant size.

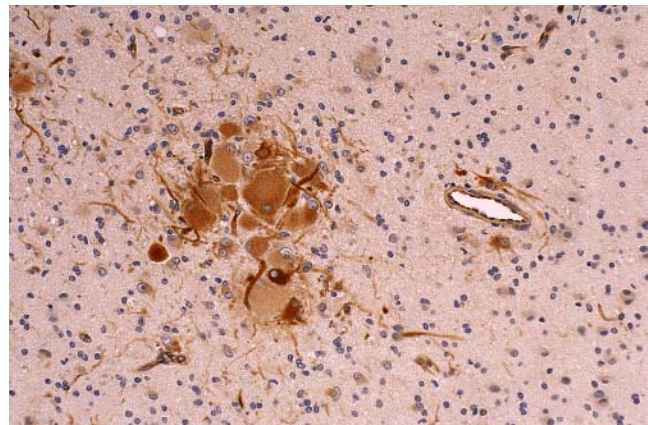


Fig. 7.1-6. Tuberous sclerosis. Nestin immunohistochemistry shows a positive reaction in balloon cells.

7.2 Neurofibromatosis 1 (von Recklinghausen's Disease)

Neurofibromatosis 1 (NF1) is a relatively common (about 1/3500–4000 persons) autosomal dominant neurocutaneous syndrome [5]. Approximately 50% of these NF1 individuals present with new mutations. The gene *NF1* is on 17q; and its protein, neurofibromin [6,7], has a complex role in intracellular signaling that is being actively investigated.

Cutaneous Manifestations

Cafe-au-lait spots are present.

Ocular Manifestations

Patients have pigmented iris hamartomas (Lisch nodules).

Neurological Manifestations

The lesions tend to develop over time: peripheral neurofibromas, plexiform neurofibromas, hamartomas, and

glial tumors of the central nervous system (CNS). Multiple neurofibromas grow along the major peripheral and autonomic nerves and near their terminations in the dermis and viscera. Peripheral nerve sheath tumors rarely progress to malignant peripheral nerve sheath tumors. The CNS tumors consist of optic nerve glioma, astrocytomas or glioblastomas in the third ventricle, cerebellum, or spinal cord. Periventricular “bright spots” are identified in imaging studies and may indicate dysplasia.

Osseous Lesions

Osseous lesions include dysplasias of the skull and long bones, absence of the sphenoid, vertebral scalloping, scoliosis, and thinning of long bones.

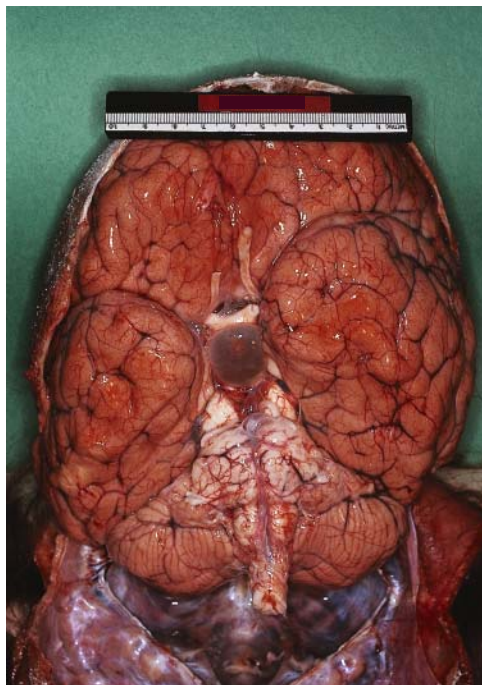


Fig. 7.2-1. Neurofibromatosis 1 (NF1). The brain of von Recklinghausen's disease is sometimes megalencephalic or associated with glioma.



Fig. 7.2-2. Deformed aqueduct and colliculi in the midbrain.

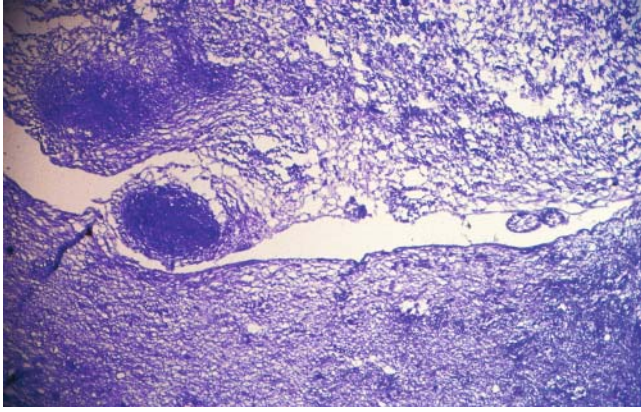


Fig. 7.2-3. Astrogliosis around the aqueduct in the same case as Fig. 7.2-2. Holzer stain.

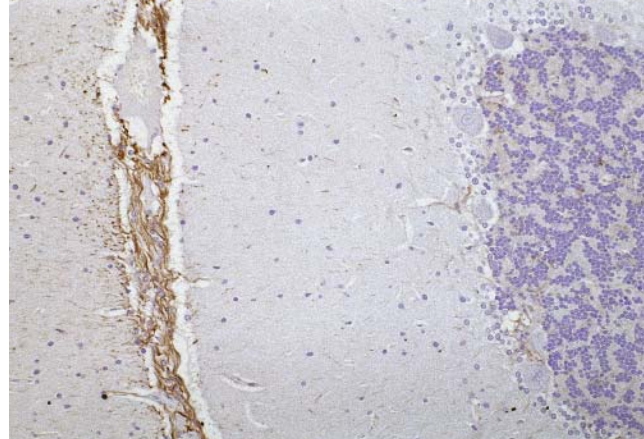


Fig. 7.2-4. Leptomenigeal astroglial heterotopia is demonstrated in the leptomeninges of the cerebellum. GFAP immunohistochemistry [2].

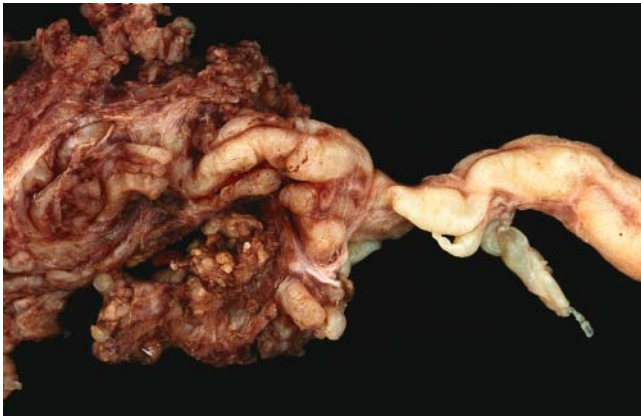


Fig. 7.2-5. Plexiform neurofibroma.



Fig. 7.2-6. Magnetic resonance imaging (MRI) in a 9-year-old child with von Recklinghausen's disease shows a high-intensity reaction (bright spots) in the thalamus. This high intensity may be identified in the basal ganglia, brain stem, or cerebellum.

7.3 Sturge-Weber Syndrome

Sturge-Weber syndrome is a neurocutaneous disorder that presents with a facial port-wine stain (a malformation of the blood vessels) in the ophthalmic division of the trigeminal artery (and sometimes other branches) and an angioma or capillary telangiectasia of underlying vessels in the leptomeninges [8]. A vascular steal of cerebral blood flow is created by these vessels of low resistance, and ischemia develops in the underlying brain, with the development of perivascular calcifica-

tions and laminar necrosis. There may be a severe seizure disorder, mental retardation, and/or glaucoma associated with this pathology. Hemispherectomy of the cortex with the hemangioma during infancy prevents seizures, hemiparesis, and intellectual disabilities. There is no known genetic association or family history of this disorder in patients with Sturge-Weber syndrome. Fibronectin expression is increased in fibroblasts and brain tissue of those with Sturge-Weber syndrome [9].



Fig. 7.3-1. Sturge-Weber syndrome. The cerebral hemisphere was removed by surgical hemispherectomy.

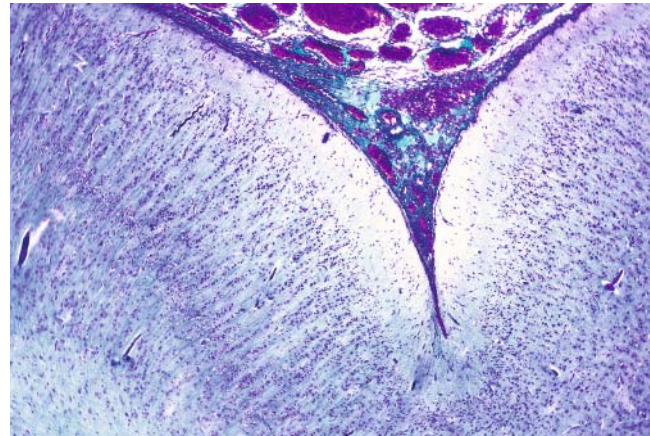


Fig. 7.3-2. Leptomeningeal angiomas.

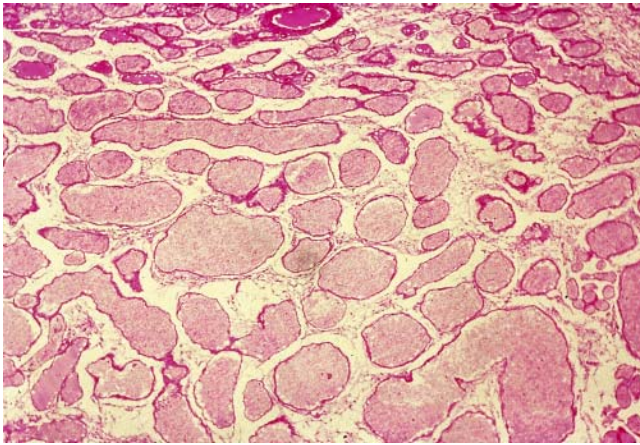


Fig. 7.3-3. Leptomeningeal angiomas (higher magnification). Note the increased numbers of thin-walled dilated capillary-like vessels. H&E.

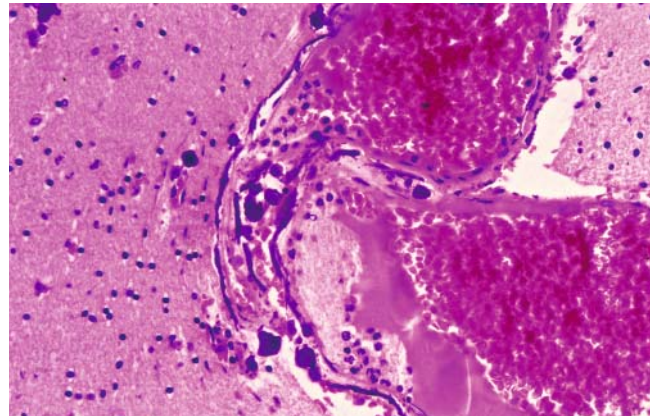


Fig. 7.3-4. Calcification in the walls of an intracortical vessel and neurophil. H&E.



Fig. 7.3-5. Radiograph of the brain exhibits calcification in the gyri.

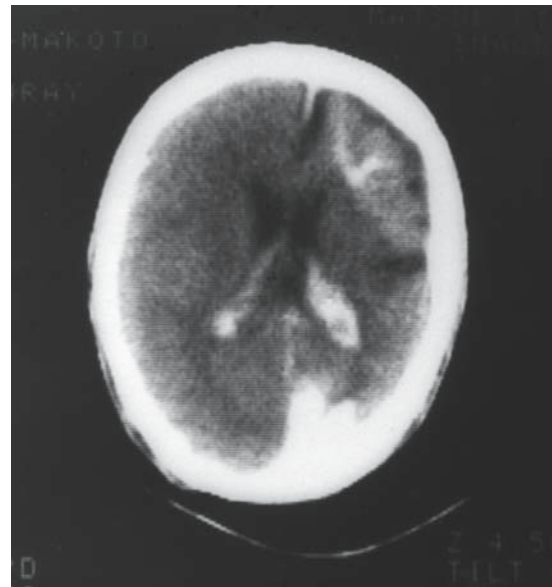


Fig. 7.3-6. Computed tomography demonstrates intracerebral calcifications.

7.4 Ataxia Telangiectasia

Ataxia telangiectasia is an autosomal recessive syndrome that begins during childhood. It is caused by a range of mutations of a gene on 11q called ataxia-telangiectasia mutated gene (*ATM*), which is normally involved in the sensing of DNA damage, leading to its repair. The clinical features include immunological abnormalities, increased liability to malignancies, progressive cerebellar ataxia, and cutaneous and conjunctival telangiectasias. There is increased α -fetoprotein and chromosomal fragility [10,11].

The pathology of the brain consists of atrophy of the cerebellar cortex, predominantly in the vermis. The Purkinje cells have cytoplasmic or dendritic inclusions,

anomalous dendritic arborization, and axonal swelling (torpedoes). There is gliosis in the cerebellar white matter and neuronal loss in the dentate nucleus and inferior olives. There is degeneration of the posterior columns and loss of satellite cells of the dorsal root ganglia. Most tissues exhibit bizarre, large irregular nuclei. There is a reduction of lymphoid tissue. ATM protein is normally detected in the cerebellar cortex, but not the cerebral cortex, at the late gestational stage. Cerebellar neurons, particularly Purkinje cells, express marked ATM immunoreactivity during the late prenatal and early postnatal periods, followed by persistent moderate reactivity [12].

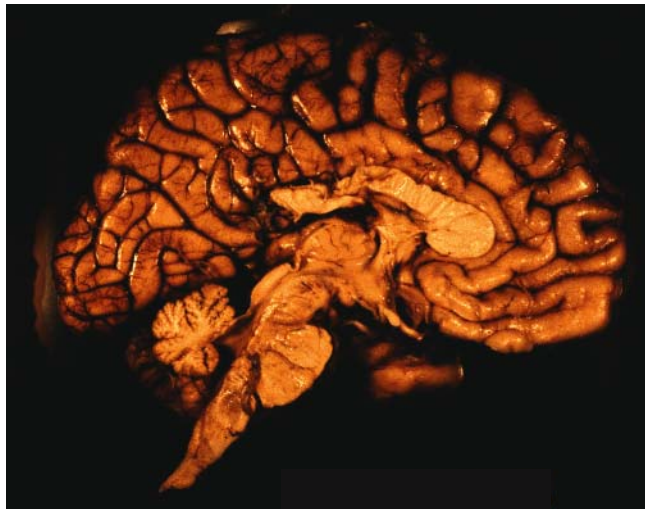


Fig. 7.4-1. Ataxia telangiectasia. Sagittal view from the midline of the brain revealing cerebellar atrophy.

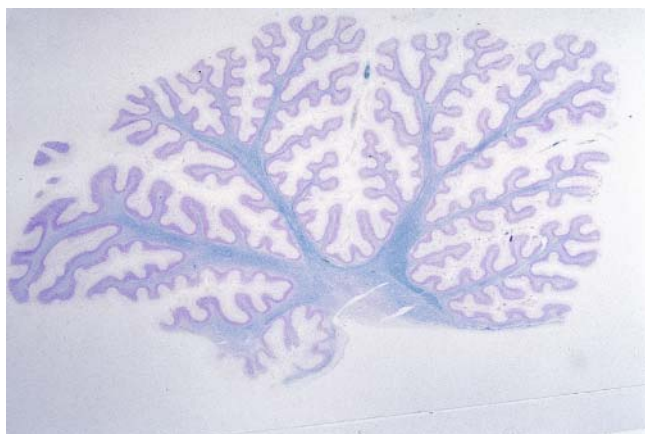


Fig. 7.4-2. Ataxia telangiectasia. This is the cerebellar vermis, demonstrating marked atrophy of the folia and decreased myelin in the white matter. LFB.

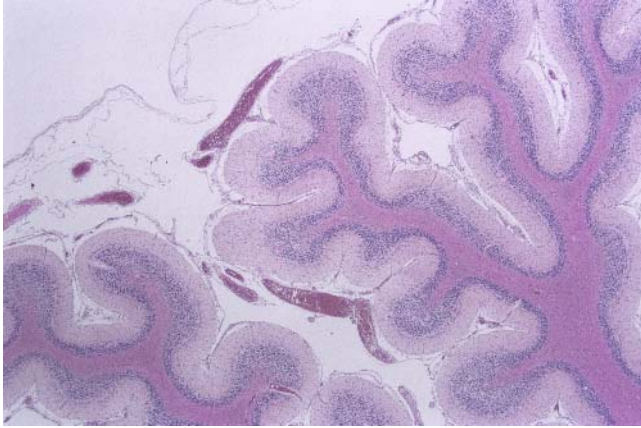


Fig. 7.4-3. Ataxia telangiectasia. There is Purkinje cell loss in the cortex, enlargement of sulci, and vascular dilatation in the leptomeninges. H&E.

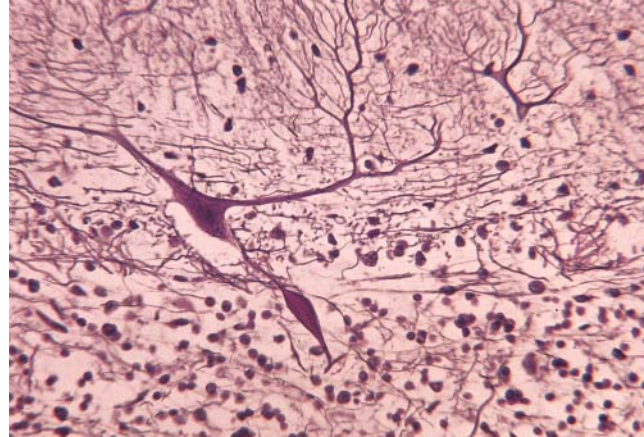


Fig. 7.4-4. Ataxia telangiectasia. Note the torpedo formation in the axon of a degenerating Purkinje cell. Bodian stain.

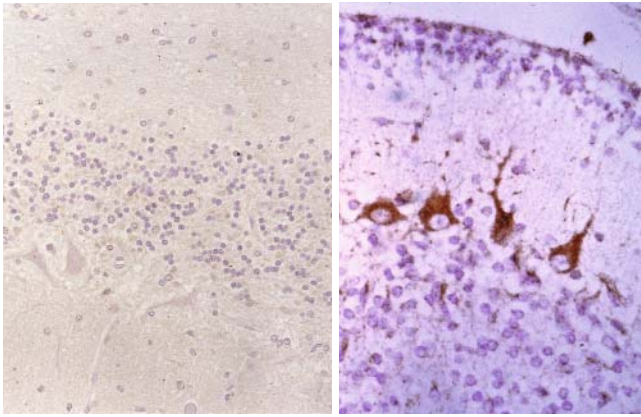


Fig. 7.4-5. Ataxia telangiectasia. Cerebellar hemisphere, ATM immunoreactivity. *Left.* Negative for ATM reactivity. *Right.* Normal for ATM reactivity.

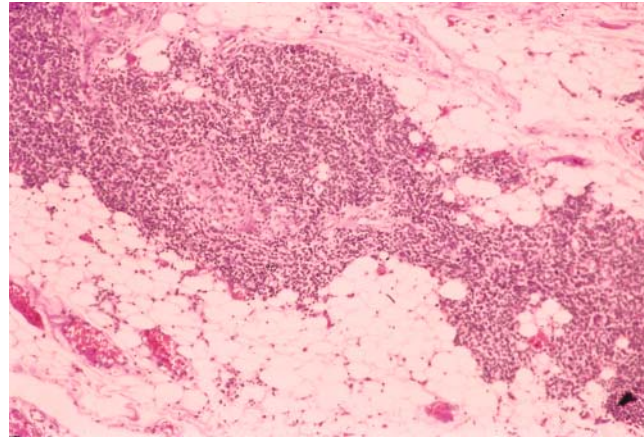


Fig. 7.4-6. Thymus shows marked atrophy with decreased thymus cells and absence of Hassel bodies. H&E.

8 Lipidosis

8.1 GM₁ Gangliosidoses

GM₁ gangliosides accumulate in lysosomes secondary to a deficiency of acid β -galactosidase. The increased GM₁ gangliosides in cell membranes cause abnormal neuronal growth and synaptic dysfunction. There is a severe infantile type (with bony and visceral involvement) and milder juvenile and adult types.

The disease is an autosomal recessive disorder. The locus for human β -galactosidase maps to chromosome 3q21. Its cDNA has been cloned, and many mutations are appreciated [1–3].

GM₁ Gangliosidosis Type 1 (Infantile: Norman-Landing Disease)

GM₁ gangliosidosis type 1 presents as failure to thrive, hepatosplenomegaly, skeletal and facial dysmorphism, psychomotor retardation, and death before the second birthday. Pathology examination reveals atrophy that is prominent in the cerebral cortex and cerebellar folia. There is ballooning of neuronal cytoplasm by the stored lipid. In the cerebellum, storage is in the dendrites of Purkinje cells. Later in the course, there is neuronal loss

with gliosis. EM reveals membranous bodies in the cytoplasm of neurons.

GM₁ Gangliosidosis Type 2 (Late-Infantile and Juvenile: Derry's Disease)

GM₁ gangliosidosis type 2, a late-infantile disorder, presents with progressive mental and motor retardation between 1 and 5 years of age. Seizures are common, and spastic quadriplegia develops with cerebellar and extrapyramidal signs. Decerebrate rigidity follows, with death occurring at 3–10 years of age. There are no visceral signs.

GM₁ Gangliosidosis Type 3 (Adult)

The adult form of the disease, GM₁ gangliosidosis type 3, begins during late childhood with weakness, ataxia, dysarthria, myoclonus, and parkinsonian signs. Cognitive impairment is lacking or mild. A common mutation has been described among type 3 cases [4].

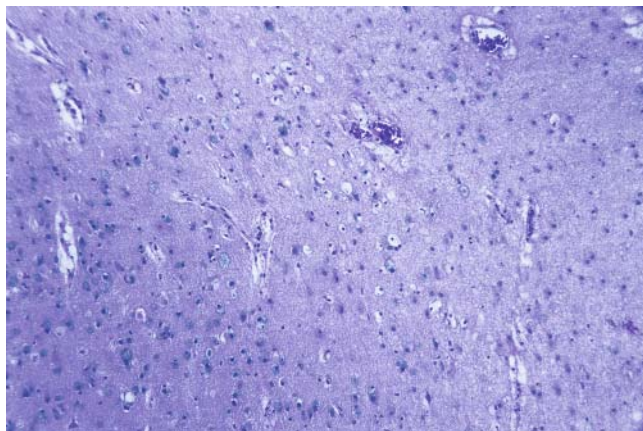


Fig. 8.1-1. GM₁ gangliosidosis type 1. The cortex (*left*) displays many ballooned neurons containing lipid. The white matter (*right*) shows a loss of myelin. LFB.

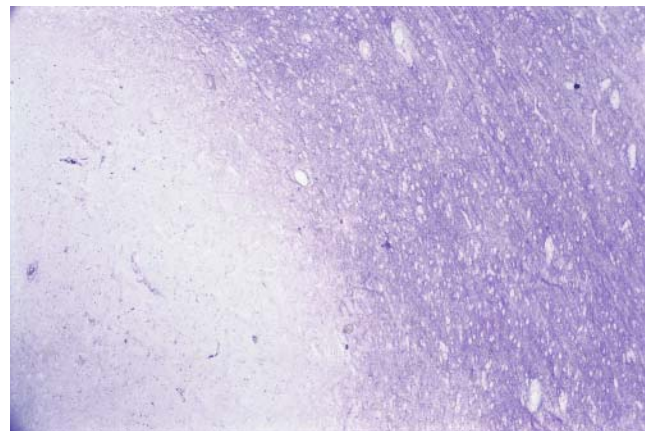


Fig. 8.1-2. There is marked fibrillary astroglia in the cerebral white matter. Holzer method.

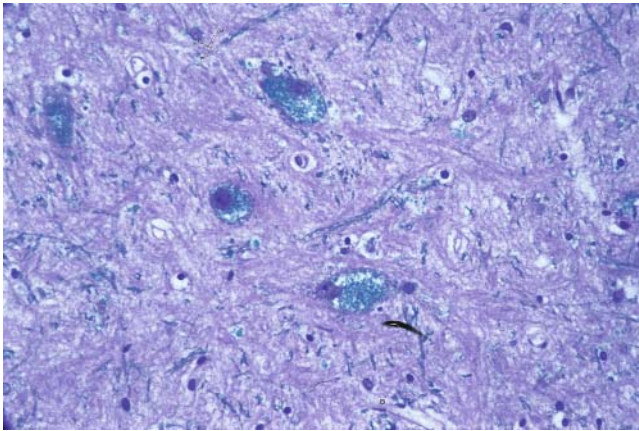


Fig. 8.1-3. Note the neuronal ballooning in the globus pallidus. Glial cells also contain stored lipid and are stained by LFB.

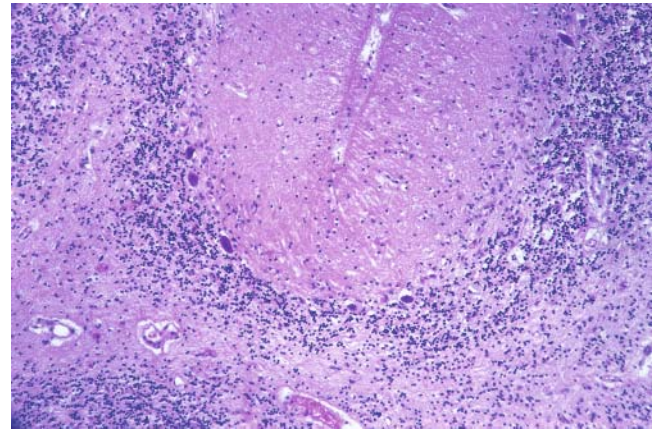


Fig. 8.1-4. The cerebellum exhibits neuronal loss and astrogliosis. The preserved Purkinje cells are atrophic. H&E/LFB.

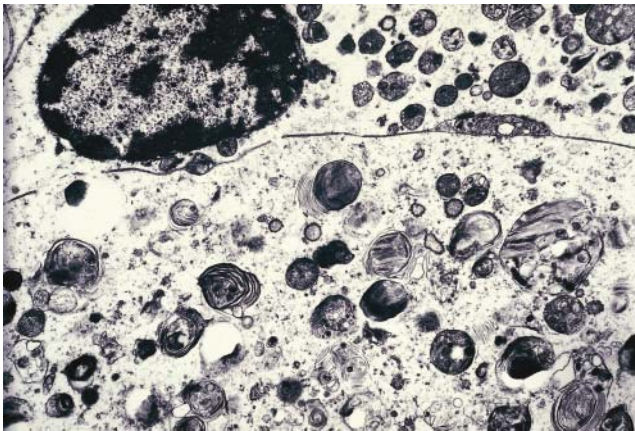


Fig. 8.1-5. Ultrastructure of neuronal cytoplasm shows abnormal curved laminar profiles of the stored lipid.

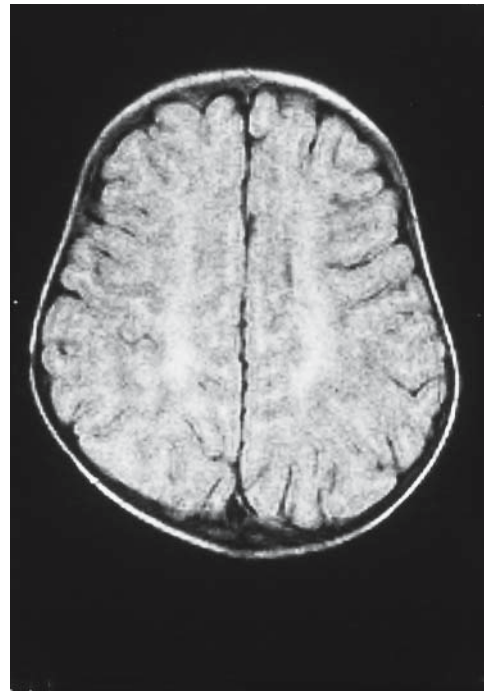


Fig. 8.1-6. Magnetic resonance imaging (MRI) shows the high intensity of the gliotic cerebral white matter on FLAIR imaging.

8.2 GM₂ Gangliosidosis

The GM₂ gangliosidoses are autosomal recessive disorders caused by failure of the β -hexosaminidase system. GM₂ accumulates in neurons, causing progressive mental and motor deterioration. There are three polypeptides in the β -hexosaminidase system: hexosaminidase A with α and β subunits; hexosaminidase B with two β subunits; and hexosaminidase S with two α subunits. Mutations in the subunits lead to various forms of GM₂ gangliosidosis. The clinical features are essentially identical [3,5].

GM₂ Gangliosidosis Type 2 (Tay-Sachs Disease)

A deficiency of the α -subunit causes severe psychomotor retardation beginning at 4–5 months. The subunit α locus maps to chromosome 15 (15q22-q25.1). Pathology evaluation shows that the firm cerebrum may be microcephalic or megalencephalic. There is neuronal swelling and astrocytic hyperplasia. The white matter degenerates, becoming gelatinous. Microglial cells stain strongly with LFB and Sudan black B.



Fig. 8.2-1. GM₂ gangliosidosis (Tay-Sachs disease). The cerebral hemisphere is atrophic and shows diffuse demyelination in the white matter. The cerebral cortex is thin with laminar necrosis. Ventricles are dilated.

GM₂ Gangliosidosis Type 0 (Sandhoff Disease)

A deficiency of the subunit β affects hexosaminidase A and B. Hexosaminidase β -subunit locus maps to chromosome 5 (5q13).

GM₂ Gangliosidosis Type AB

With GM₂ gangliosidosis type AB, there is a deficiency of the GM₂ activator protein. Hexosaminidase A and B are normal or elevated. The GM₂ activator protein is encoded on chromosome 5.

GM₂ Gangliosidosis Type B₁

With GM₂ gangliosidosis type B₁ there is normal synthesis of α subunits, but catalysis of GM₂ is defective and storage results.

GM₂ Gangliosidosis: Adult Form

The adult form of GM₂ gangliosidosis is caused by marked deficiency of hexosaminidase associated with point mutations in the α subunit coding region.

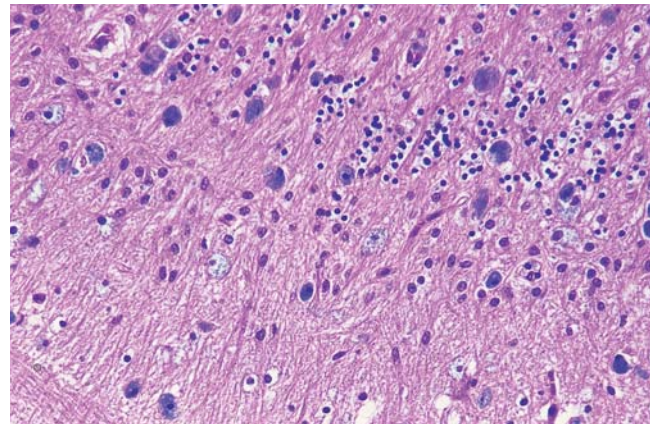


Fig. 8.2-2. The cerebellum shows distended lipid-containing granular neurons and axons, loss of Purkinje cells, and Bergman glia proliferation in the cortex. H&E/LFB. The cerebellum and brain stem are atrophic.

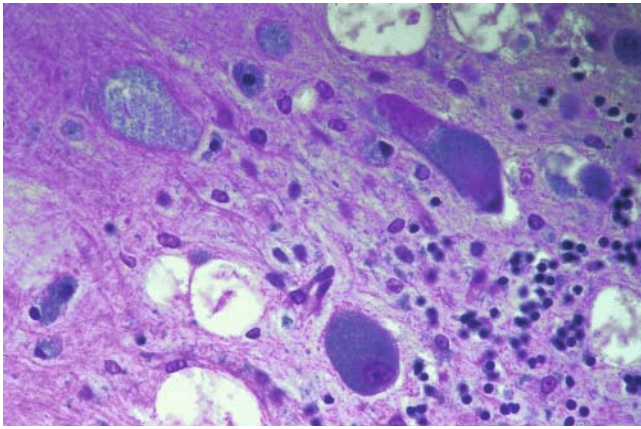


Fig. 8.2-3. Cerebellar cortex, at higher magnification, displays ballooned neurons and axons. H&E/LFB.

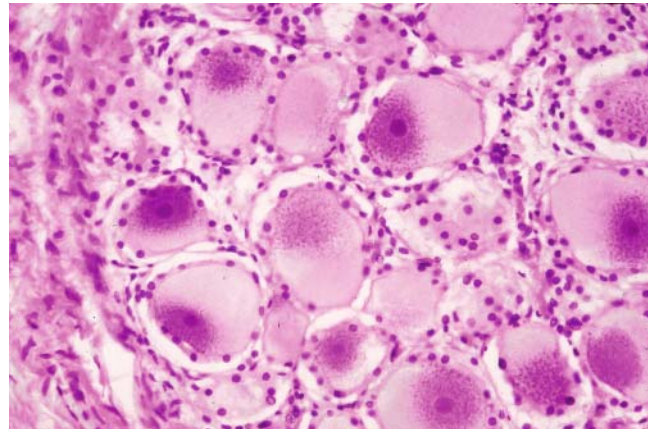


Fig. 8.2-4. Ballooned neurons in the sensory ganglion. H&E.



Fig. 8.2-5. Golgi stain defines the abnormal ballooned neurons of the "meganeurites." There is aberrant dendrite formation. Golgi stain.

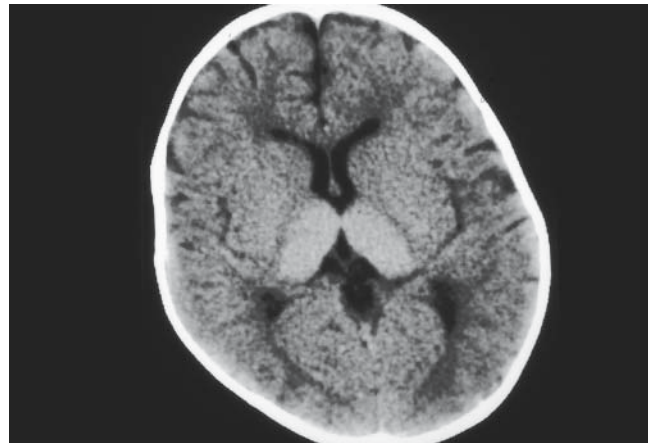


Fig. 8.2-6. Computed tomography (CT) of a patient with Tay-Sachs disease exhibiting atrophy of gyri and low density in the cerebral white matter.

8.3 Gaucher's Disease

Gaucher's disease is caused by a deficiency of glucocerebrosidase, with resulting storage of glucocerebroside. Clinically, there are neuropathic and nonneuropathic forms. Type 1 (*chronic or adult nonneuronopathic*), the most prevalent form, occurs from birth to adulthood, presenting with splenomegaly, hypersplenism, and bone necrosis. Type 2 (*acute or infantile neuronopathic*) is a rapidly progressive neurovisceral storage disease that occurs before 6 months of age. It presents with spasticity, extrapyramidal signs, and cranial nerve involvement. Type 3 (*subacute or juvenile neuronopathic*) develops during the first decade of life with hepatosplenomegaly, ataxia, myoclonus, seizures, and spasticity.

Pathology

In *type 1*, there may be perivascular Gaucher cells in Virchow-Robin spaces. In *type 2*, there is no evidence

of neuronal storage; but prominent neuronal loss, neuronophagia, and gliosis are present in the basal ganglia and brain stem. There is mild neuronal loss in cortical layers 3 and 5. Electron microscopy (EM) has revealed tubular and fibrillary inclusions in neurons. In *type 3*, the changes described in type 2 are present but less severe.

Genetics

This disorder is autosomal recessive. The gene locus for human glucocerebrosidase is located on chromosome 1q21–q31 [6,7].

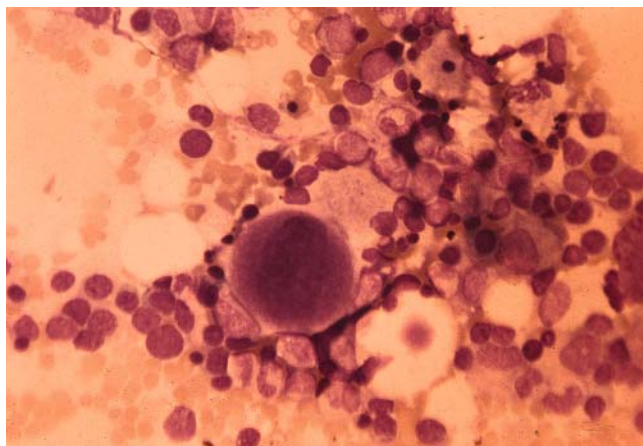


Fig. 8.3-1. Gaucher's disease type 1. Gaucher cells in bone marrow. H&E.

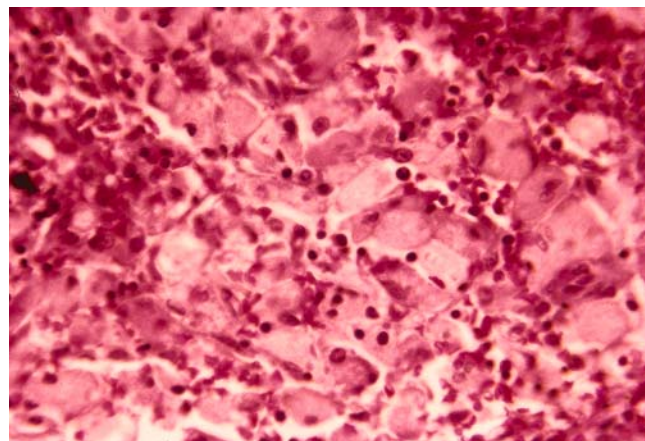


Fig. 8.3-2. Gaucher cells in spleen. H&E.

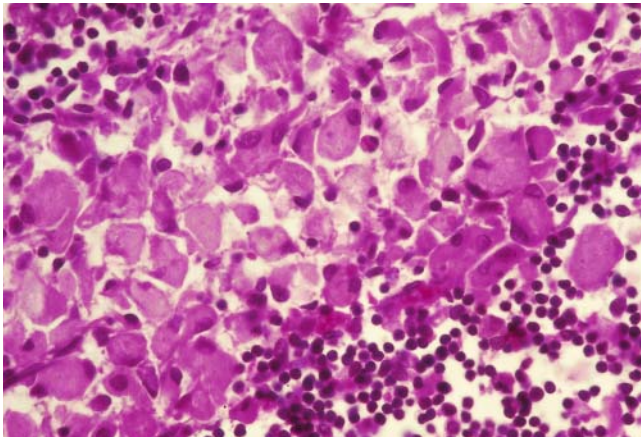


Fig. 8.3-3. Gaucher cells in lymph node tissue. H&E.

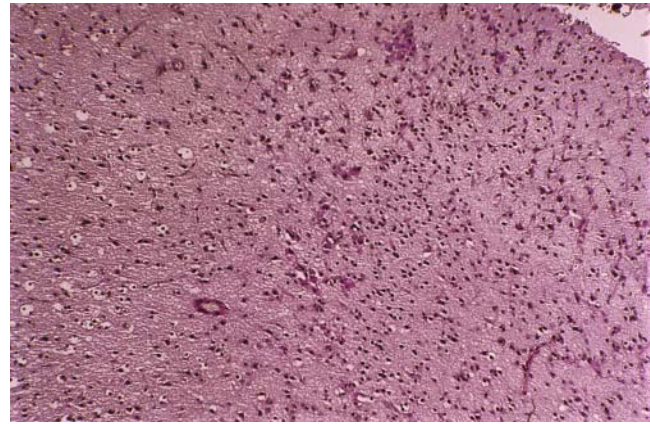


Fig. 8.3-4. Isolated Gaucher cells in vessels of the cerebral cortex. PAS.

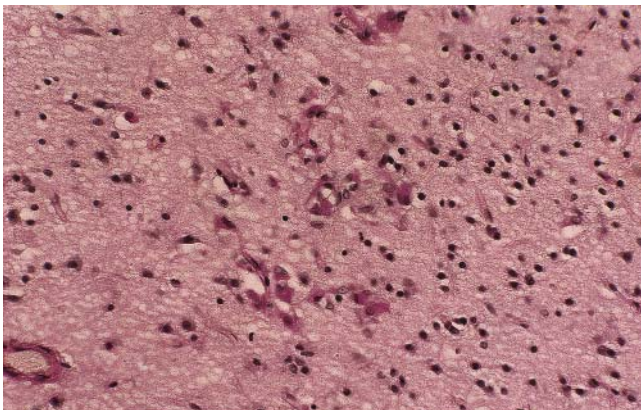


Fig. 8.3-5. Higher magnification of Gaucher cells in the cortex. PAS.

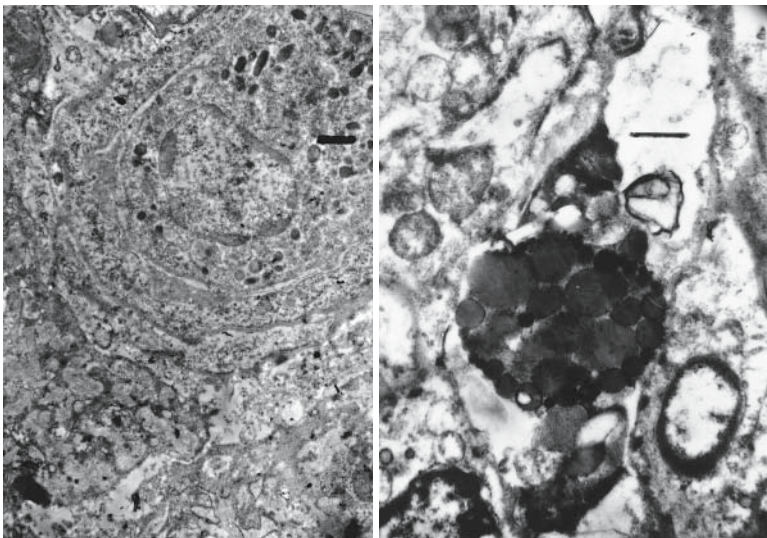


Fig. 8.3-6. EM of a 9-month-old boy shows twisted tubular structures in a Gaucher cell. Other storage materials appear as variously sized membrane-bound round to ovoid inclusions.

8.4 Niemann-Pick Disease

There are four types of Niemann-Pick disease, a sphingomyelin-cholesterol lipidosis. Types A and B have deficient sphingomyelinase activity [8], whereas types C and D have normal or mildly reduced activity [9]. Type A disease has infantile, late infantile or juvenile, and juvenile forms with massive hepatosplenomegaly; lung, eye, and bone storage; and rapidly progressive neurological symptoms. Type B has hepatosplenomegaly but no central nervous system (CNS) involvement.

Pathology

With type A, the brain is atrophic with neuronal storage and foam cells in the leptomeninges and perivascular spaces. There is neuronal loss in the cerebral and cerebellar cortex, basal ganglia, brain stem, and spinal cord. There may be neuroaxonal dystrophy and white matter degeneration. Lipid-containing foam cells are found in most organs. EM shows cytoplasmic inclusions. Type B has severe visceral involvement but no CNS changes.

Genetics

Type A and B are autosomal recessive, caused by mutations in the acid sphingomyelinase gene at 11p15.1–15.4.

Niemann-Pick type C (NPC) is caused by abnormal trafficking of intracellular cholesterol. Two genetic groups, *NPC1* and *NPC2*, are defined. The gene *NPC1* is on chromosome 18q11.

Niemann Pick type D (Nova Scotia variant) is allelic with type C. The ages and presentations vary. The commonest presentation is a late-infantile/juvenile disorder with visceromegaly, ataxia, poor school performance, seizures, and supranuclear gaze palsy.

Pathology

Enlarged organs contain foamy macrophages, which may contain basophilic granules (sea-blue histiocytes). The liver in infantile cases resembles that seen with giant cell hepatitis. The brain is atrophic, particularly the cerebellum. Neurons are swollen with PAS- and LFB-positive storage products and may exhibit neurofibrillary tangles and neuroaxonal dystrophy. EM shows polymorphous cytoplasmic bodies [3].

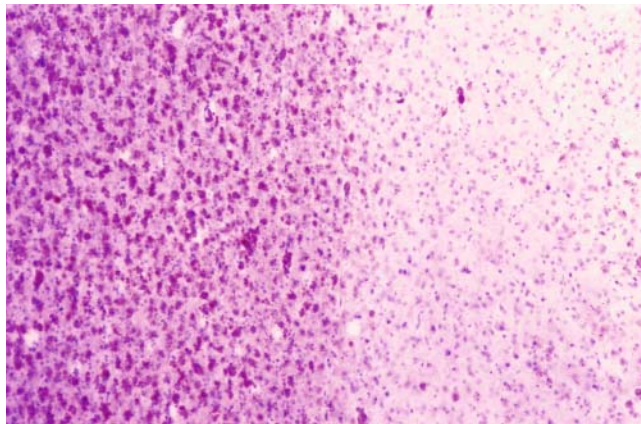


Fig. 8.4-1. Niemann-Pick disease. Cerebral cortex and white matter show PAS-positive storage material. The stored material stains as a lipid.

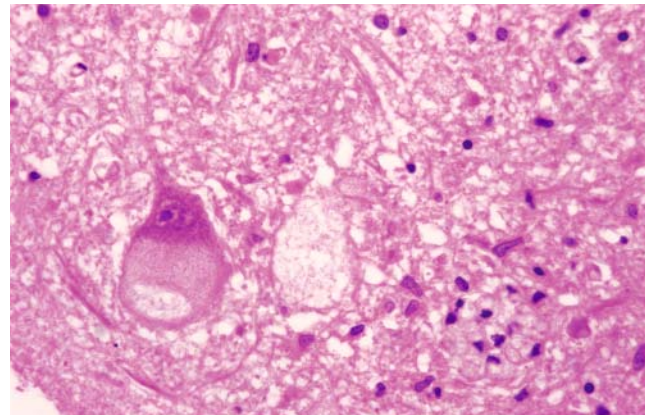


Fig. 8.4-2. Niemann-Pick cells in neurons of a nucleus of the medulla. H&E.

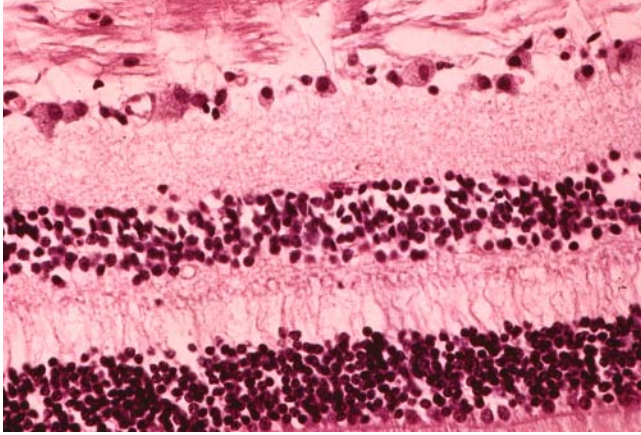


Fig. 8.4-3. The retina, with storage and loss of ganglion cells. The spinal ganglia, roots, autonomic ganglia, and peripheral nerves may undergo morphological changes similar to those of the CNS. H&E.

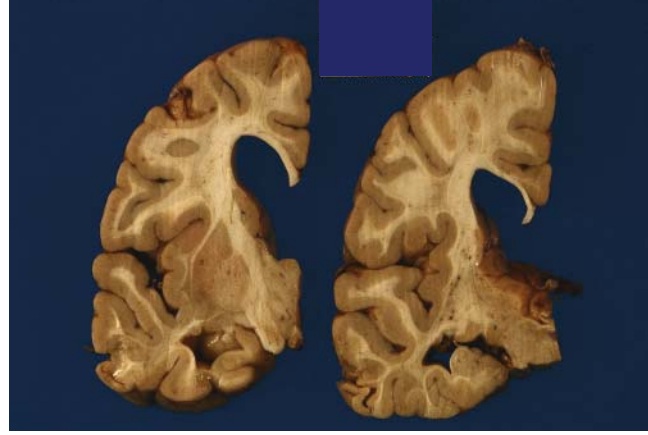


Fig. 8.4-4. Gross brain shows atrophy with ventricular dilatation.

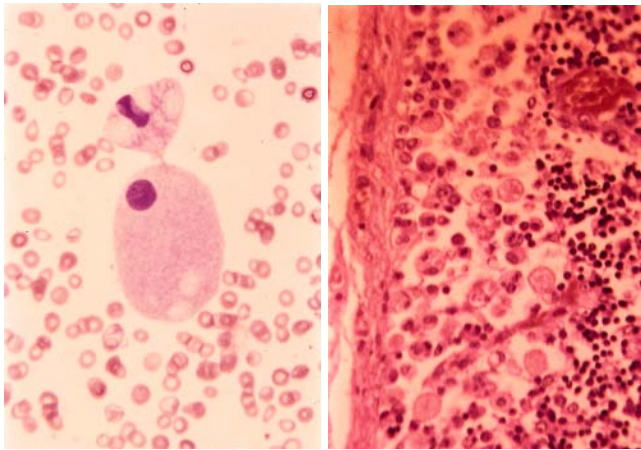


Fig. 8.4-5. Niemann-Pick foam cells in the spleen. H&E.

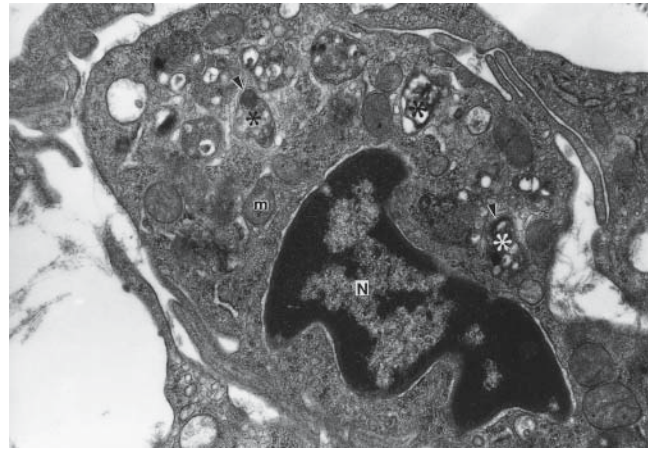


Fig. 8.4-6. EM shows cytoplasmic inclusions described as polymorphic cytoplasmic bodies, oligomembranous bodies, spherical membranous sacs, or multilamellar bodies consisting of laminated membranes with some electron-dense cores and amorphous electron-dense material similar to lipofuscin.

8.5 Neuronal Ceroid Lipofuscinosis

The commonest storage disorder affecting the brain and eyes results from storage of ceroid/lipofuscin material. Neuronal ceroid lipofuscinosis (NCL) is autosomal recessive, and its genetic classification includes eight loci.

Infantile NCL1 (Haltia-Santavuori Disease, Infantile Batten Disease)

Infantile NCL1 begins during infancy as psychomotor retardation, blindness, and seizures. There is brain atrophy (weight is 200–400 g) with shrinkage of the cortical gyri and cerebellar folia. The brain stem is spared.

Skull and dura are thick with a subdural gelatinous layer. Neurons contain autofluorescent granular material in the cytoplasm with histochemical characteristics of lipofuscin or ceroid. EM of all organs shows osmophilic globules with a granular matrix (granular osmophilic deposits, or GRODs). They may be a single globule (0.5 μ m) or aggregates of globules (3 μ m) surrounded by a unit membrane with acid phosphatase activity. GRODs differ from lipofuscin in that they have no electron-lucent vacuoles. The defective gene is on chromosome 12p32. The gene product is palmitoyl-protein thioesterase, and the GRODs contain sphingolipid activator proteins A and D and fatty acid thioesters [3,10,11].

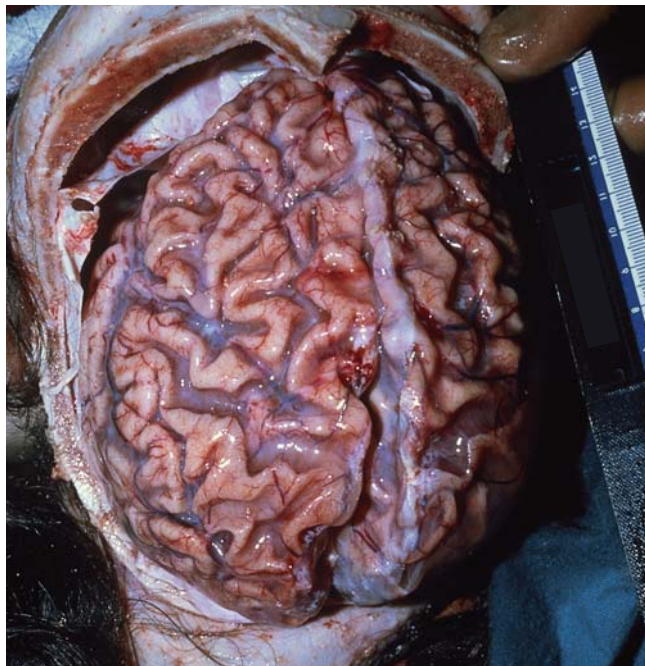


Fig. 8.5-1. Ceroid lipofuscinosis. Late infantile type. The brain shows diffuse, marked atrophy.



Fig. 8.5-2. Late infantile type. Coronal sections of the cerebrum show marked atrophy with sulcal and ventricular dilatation.

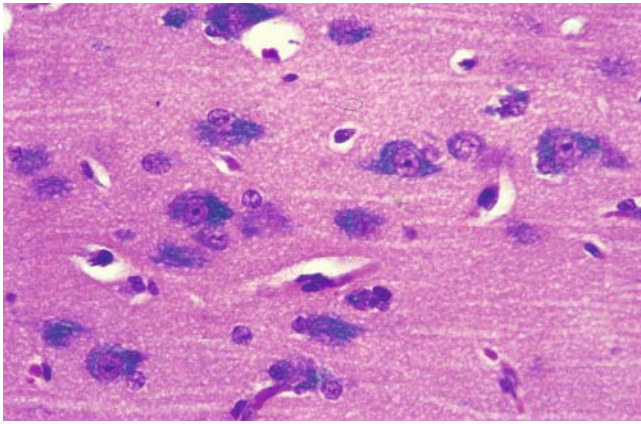


Fig. 8.5-3. Late infantile type. There is an accumulation of lipid in the cytoplasm of cortical neurons. H&E/LFB. Cortical neurons show accumulation of granular material in the neuronal cytoplasm without a ballooning effect.

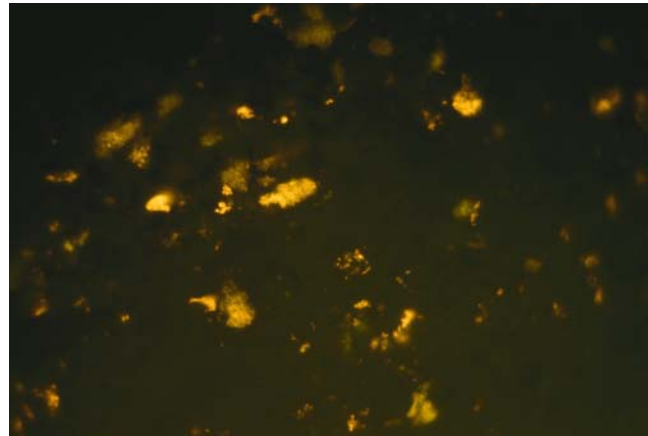


Fig. 8.5-4. Late infantile type. Neurons exhibit autofluorescence.

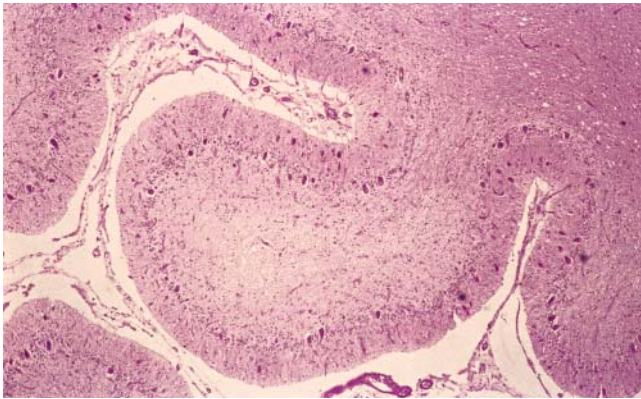


Fig. 8.5-5. Late infantile type. The cerebellar cortex shows loss of Purkinje cells and granular cells with astroglia. H&E.

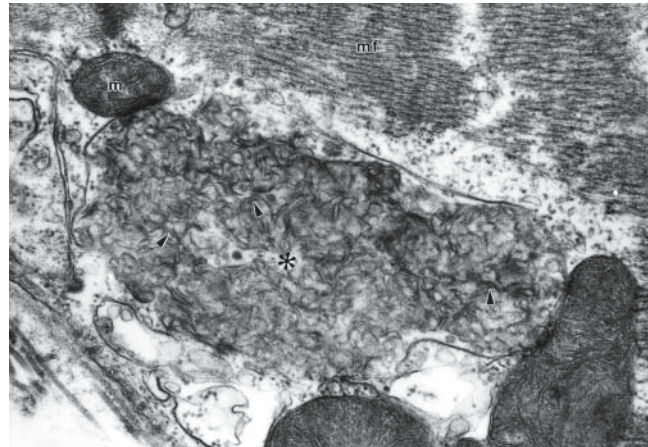


Fig. 8.5-6. Juvenile type. EM of sclera shows fingerprint inclusions.

8.6 Neuronal Ceroid Lipofuscinosis

Late Infantile CLN2, CLN5, CLN6, and CLN7 (Jansky-Bielshowsky Disease or Late-Infantile Batten Disease)

With late infantile CLN2, CLN5, CLN6, and CLN7 disease, regression begins at 18 months to 4 years, with refractory seizures, impaired vision, spastic tetraplegia, and bulbar paralysis; death occurs at 4–10 years. The cerebellum is most affected. The deposits are yellow with H&E and are PAS-, Sudan black-, and luxol fast blue-positive. Autofluorescence is yellow, not the normal orange. EM reveals curvilinear bodies (0.2–1.0 μ m) in membrane-bound clusters. Granular or fingerprint inclusions may be present. There is storage of subunit C of mitochondrial ATP synthetase caused by defects in (1) *CLN2* (11p15), associated with gene product pepstatin-insensitive peptidase; (2) *CLN5* (13q22), with the gene product membrane protein; or *CLN6* (15q-21-23), coding for unknown product or defects in *CLN7*, an unknown gene.

Juvenile CLN3 (Batten-Spielmeyer-Vogt Disease, Juvenile Batten Disease)

With juvenile CLN3, the degree of atrophy is proportional to the disease duration. There are vacuolated lymphocytes. EM reveals that all cells show fingerprint inclusions. The involved gene is on chromosome 16p12; the product is lysosomal membrane protein. The storage material is also subunit C.

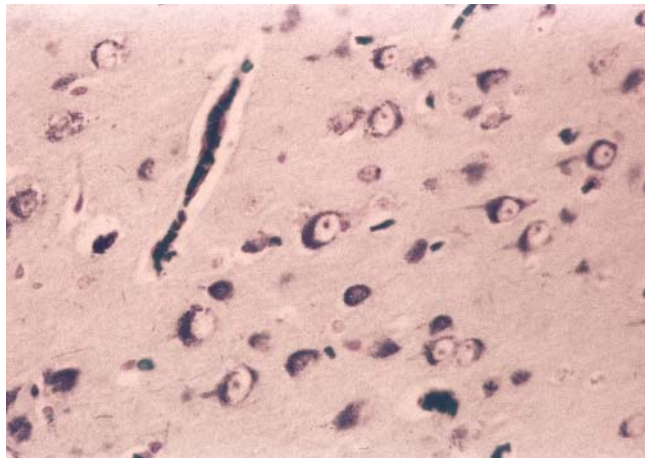


Fig. 8.6-1. Ceroid lipofuscinosis, juvenile type. The cerebral cortex shows cytoplasmic ceroid lipid (ceroid lipofuscin) deposition. LFB.

Adult CLN4 (Kufs' Disease; Adult Batten Disease)

With adult CLN4 type A, there is progressive myoclonic epilepsy with ataxia, behavioral disturbances, and late dementia with rigidity. With adult CLN4 type B, there is progressive dementia with cerebellar and extrapyramidal disease.

Pathology

Cerebral atrophy occurs predominantly in the frontal lobes; there are no vacuolated lymphocytes. EM reveals curvilinear bodies, fingerprint bodies, and rectilinear profiles.

Genetics

There are two forms: autosomal recessive and autosomal dominant. Northern epilepsy CLN8 (variant NCL) develops during childhood and has a genetic defect at 8p22. The storage materials are subunit C and sphingolipid activator proteins A and D [3,10,11].

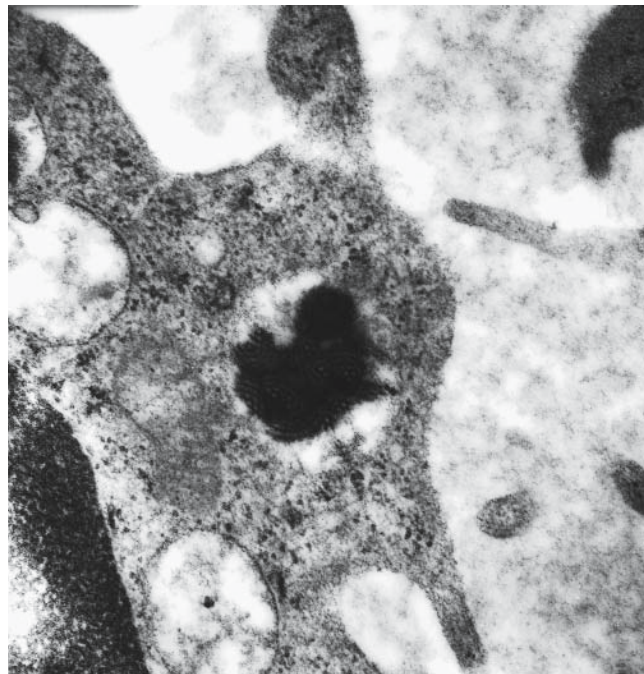


Fig. 8.6-2. Ceroid lipofuscinosis, juvenile type. EM shows curvilinear osmophilic inclusions.

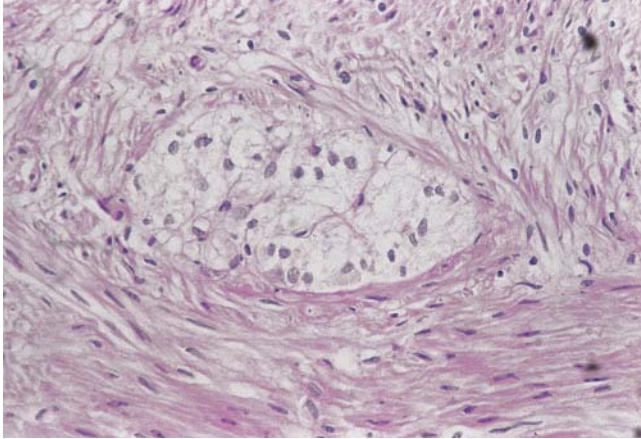


Fig. 8.6-3. Ceroid lipofuscinosis, late infantile type. The rectum shows foamy changes of Auerbach plexus neurons. H&E.

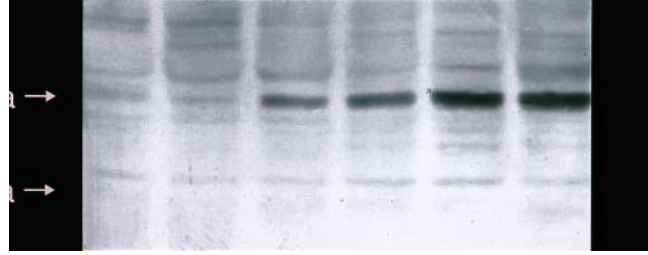


Fig. 8.6-4. Western blotting of CLN2 in the developing cerebral cortex of human brains reveals a gradual increase of CLN2 after 39 weeks' gestation [10].

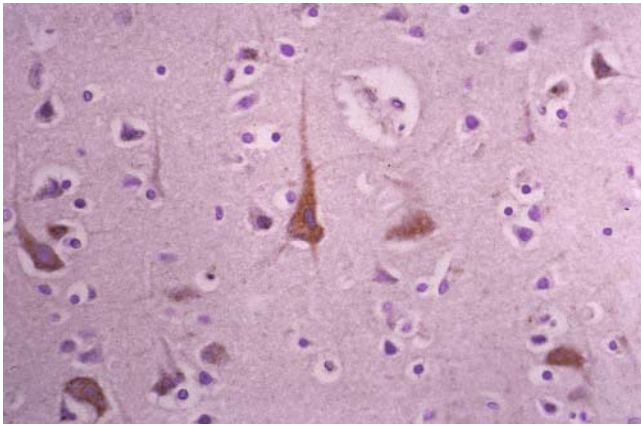


Fig. 8.6-5. Normal cerebral cortex shows positive expression of CLN2 in neurons.

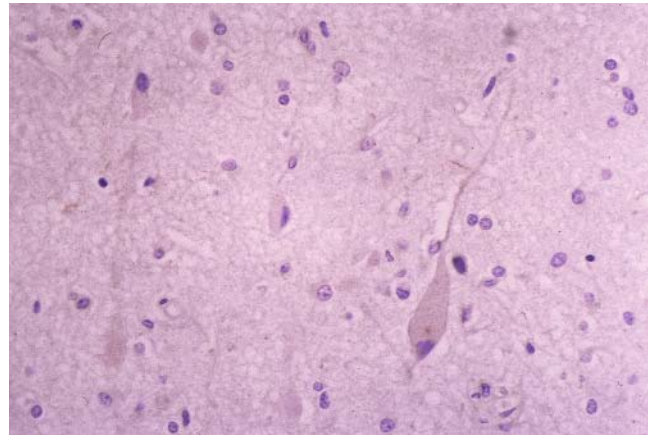


Fig. 8.6-6. Ceroid lipofuscinosis, late infantile. The cortex shows negative expression of CLN2 in neurons [1].

8.7 Farber's Disease, Wolman's Disease, Fabry's Disease

Wolman's Disease

With Wolman's disease, acid lipase deficiency, cholesterol esters and triglycerides accumulate in cells. It is symptomatic during the first weeks. Adrenals are calcified. There is sudanophilic storage in the capillary endothelium, neurons of the medulla, retina, Purkinje cells, microglia, periadventitial macrophages, and astrocytes; and there are foamy histiocytes in the leptomeninges and choroid plexus. There is loss of cortical neurons, delayed myelination, and diffuse gliosis. The disease is autosomal recessive (10q23.2–q23.3).

Farber's Disease (Lipogranulomatosis)

A deficiency of acid ceramidase causes accumulation of ceramide, producing five types of disease: *type 1* (classic), with deformed joints, subcutaneous nodules, and hoarseness beginning at age 2 weeks to 4 months; *types 2 and 3* (intermediate and mild), in which the nervous system is slightly affected; *type 4* (neonatal visceral), with hepatosplenomegaly and severe psychomotor impairment

develop during the first weeks of life; *type 5* (neurological, progressive), with ataxia, loss of speech, progressive quadriparesis, and seizures at 1.0–2.5 years. PAS-positive material is stored in the neuronal cytoplasm of the spinal cord, brain stem nuclei, basal ganglia, cerebellum, cerebral cortex, retina, autonomic ganglia, and histiocytes.

Electron microscopy reveals (1) a Farber body: a curvilinear tubular (ceramide) structure consisting of two dark lines separated by a clear space; (2) a Zebra body caused by secondary accumulation of other lipids.

Ceramidase deficiency is autosomal recessive. The acid ceramidase gene is at 8p22–21.2.

Fabry's Disease

Fabry's disease is an X-linked lysosomal disorder with deficiency of β -galactosidase, causing storage of glycosphingolipids, especially globotriaosylceramide, in cells with resulting renal, cardiac, and cerebrovascular complications in homozygous males and some heterozygous females [3,12].

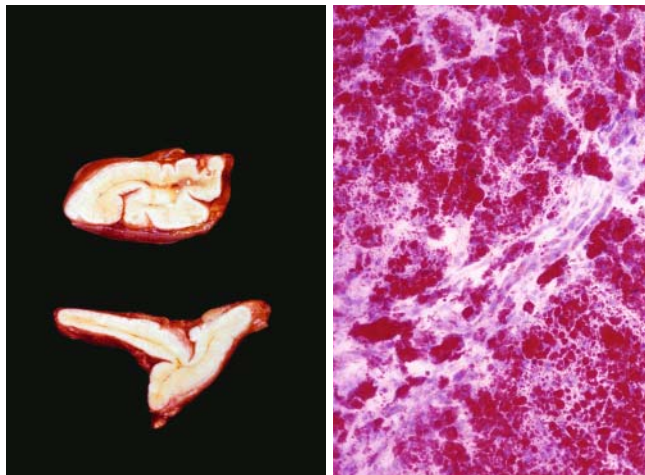


Fig. 8.7-1. Wolman's disease. Adrenal glands (*left*). Cholesterol storage in the liver (*right*). Sudan III. Lipid storage has been ultrastructurally demonstrated in oligodendrocytes, Schwann cells, and perineural and endoneural cells.

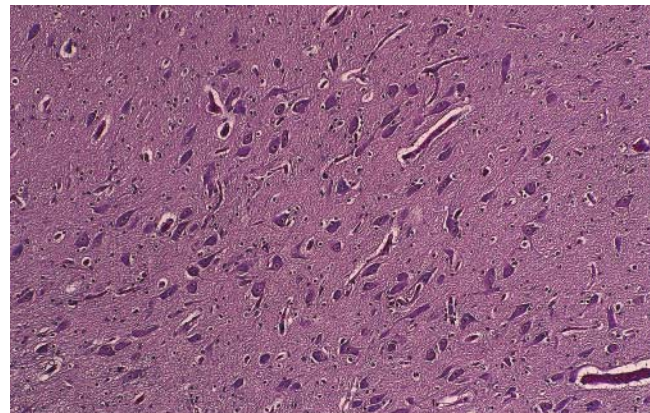


Fig. 8.7-2. Wolman's disease. Storage in the deep nucleus in the medulla oblongata. H&E.

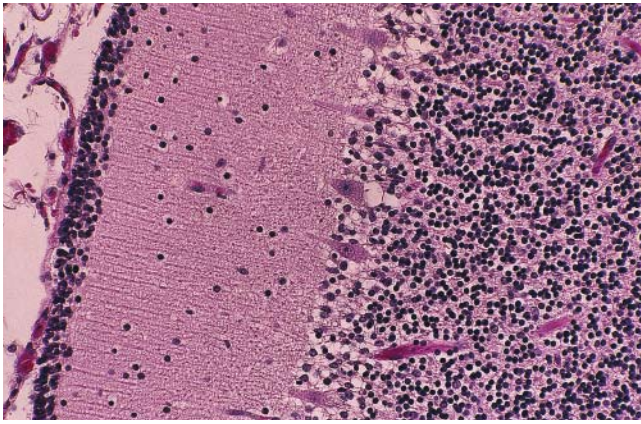


Fig. 8.7-3. Wolman's disease. Storage in Purkinje cells of the cerebellar cortex. H&E.

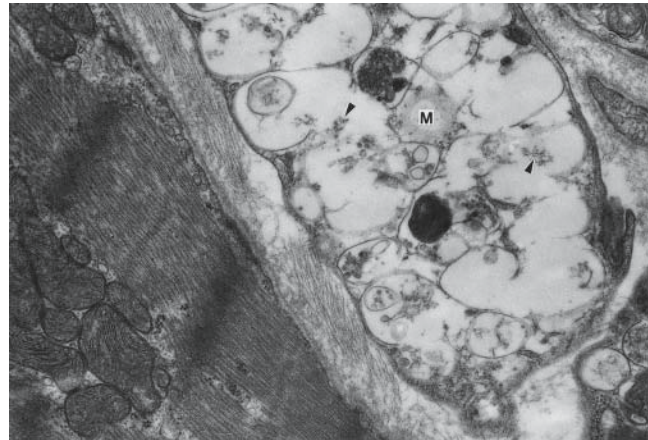


Fig. 8.7-4. Farber's disease. EM of endomyocardial tissue. Visceral involvement with accumulation of storage material in macrophages, which is usual in types 1 and 4 but inconstant in type 5.



Fig. 8.7-5. Fabry's disease. Angiokeratoma.

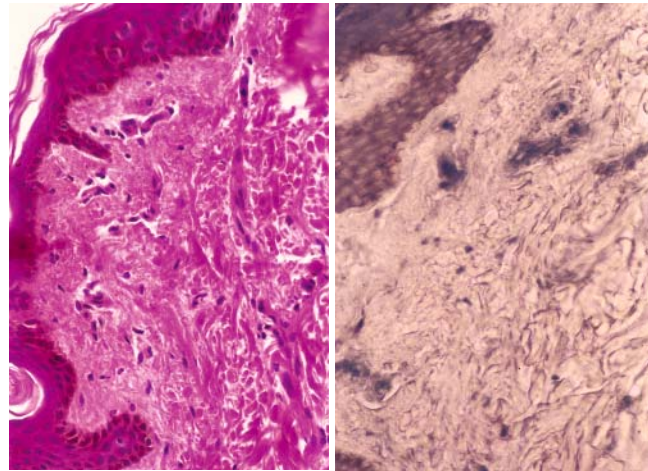


Fig. 8.7-6. Fabry's disease. Skin biopsy shows Sudan black B (SBB)-positive glycosphingolipid storage. *Left.* H&E. *Right.* SBB.

9 Mucopolipidosis

9.1 Galactosialidosis

Galactosialidosis (α -neuraminidase deficiency + galactosidase deficiency with defective protective protein) has *congenital* (severe resembling sialidosis type 2), *infantile* (mild), and *juvenile-adult* forms. There are dysmorphic features, hepatosplenomegaly, psychomotor retardation, macular cherry-red spots, and myoclonus. There is cytoplasmic vacuolization of many cell types. Rare brain reports suggest atrophy and neuronal

loss in optic nerves, thalamus, globus pallidus, brain stem, and cerebellum with neuronal storage in Betz cells, basal forebrain, cranial nerve nuclei, anterior horns, and ganglia. Electron microscopy (EM) shows variable shapes of storage material. The disorder is caused by a defective “protective protein” encoded on chromosome 20q13.1 and a resulting deficiency of β -galactosidase and α -neuraminidase [1].

Table 9.1. Sialic acid disorders and oligosaccharidoses

Disease	Enzyme defect	Accumulating material	Gene
Galactosialidosis	Protective protein 1	Sialyl oligosaccharide, cathepsin A, PPCA	20q13.1
Infantile sialic storage disease, Salla disease	Sialin (transporter protein)	<i>N</i> -Acetylneuraminic acid, free sialic acid	6q14–15
Sialuria	UDP-GlcNAc2-epimerase	Free sialic acid	
α -Mannosidosis	α -Mannosidase	Mannose-rich	19p13.2–12
β -Mannosidosis	β -Mannosidase	Mannose-rich	4q21–q25
Fucosidosis	α -Fucosidase	Glycoproteins, glycolipids oligosaccharide	1p34
Aspartylglucosaminuria	Aspartylglucosaminidase	Glycoasparagine	FUCA1
Schindler disease	α - <i>N</i> -Acetylgalactosaminidase	Glucoconjugates	4p34–35 22q13.1–13.2

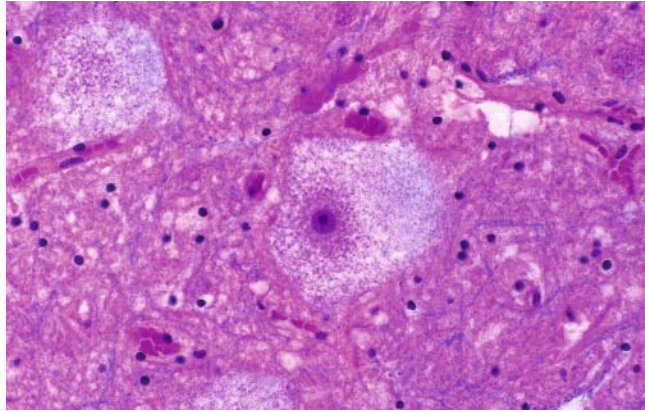


Fig. 9.1-1. Galactosialidosis. Neuron with ballooning and accumulation of PAS-positive material in glial cells.

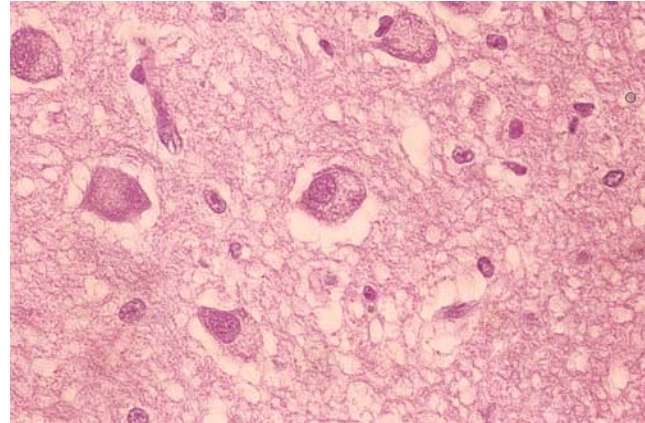


Fig. 9.1-2. Neurons with ballooning of cytoplasm in the inferior olivary nucleus. H&E.

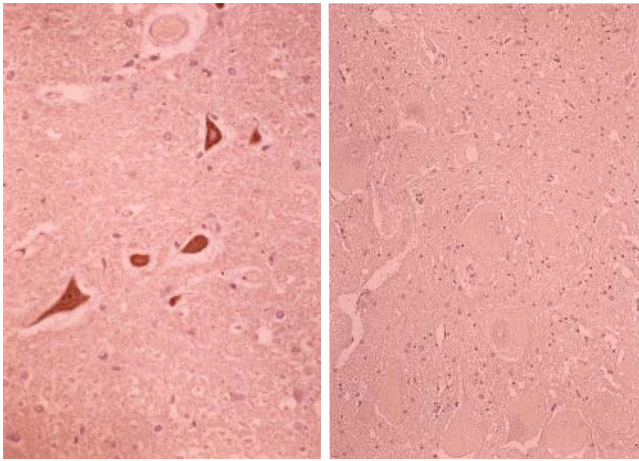


Fig. 9.1-3. *Left.* Protective protein immunoreactivity is positive in the anterior horn neurons of a normal spinal cord. *Right.* Protective protein immunoreactivity is negative in the anterior horn cells of the spinal cord from a 16-year-old child with galactosialidosis.

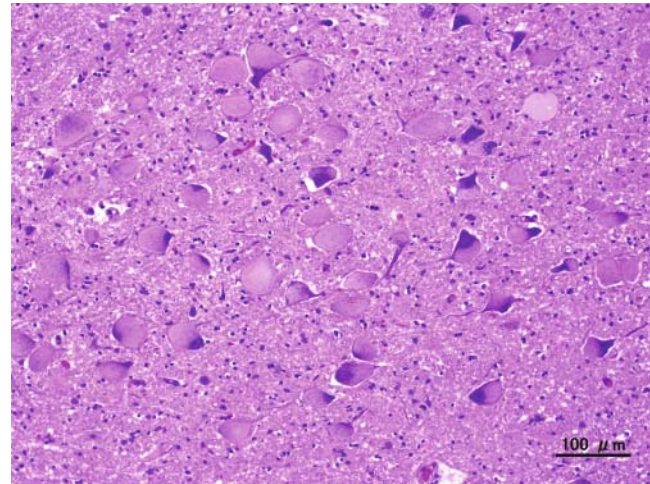


Fig. 9.1-4. Neurons showing lipid storage. H&E/LFB.

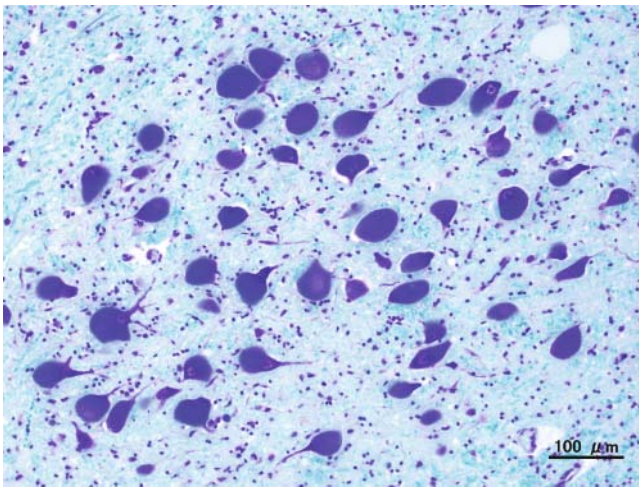


Fig. 9.1-5. Lipid storage in the neurons of V motor nucleus. (Courtesy of Dr. A. Kakita.)

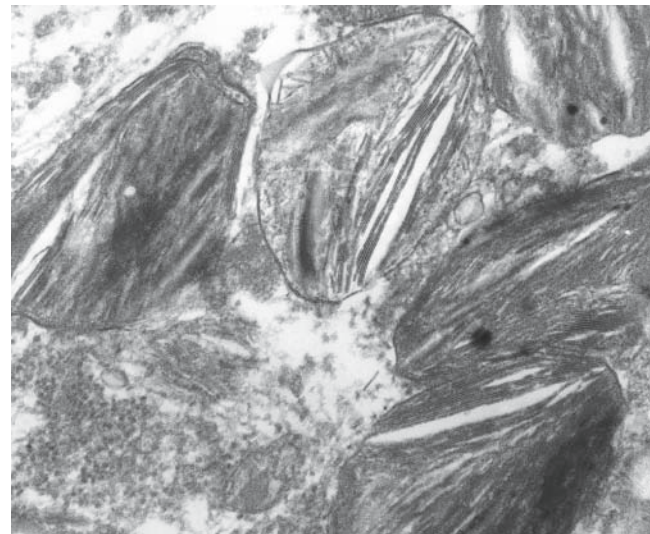


Fig. 9.1-6. EM of parallel lamellar inclusions. (Courtesy of Dr. A. Kakita.)

9.2 I Cell Disease, Mucopolysaccharidosis Type 2

With I cell disease, the lysosomal enzymes are synthesized normally but lack a recognition marker that targets them to the lysosome so the enzymes are secreted into body fluids. There is a defect in *N*-acetylglucosamine-1-phosphotransferase, which normally attaches a phosphate group to a mannose chain of the lysosome enzymes. Clinical and radiological features are similar to those in Hurler syndrome, with early onset of an abnormal face, thick skin, hernia, limited movements, clubfeet, dislocated hips, kyphosis, hypotonia, hirsutism, and mild to severe psychomotor retardation. There is gingival hypertrophy, hepatosplenomegaly, frequent cardiomegaly, and corneal opacities. There is a rapid progressive course to death at 5–8 years of age.

Pathology

Intraneuronal lamellar bodies (inclusions) are found in the spinal ganglia and anterior horn, and there are vacu-

olated fibroblasts in the heart valves, kidney, lung, spleen, glomerular epithelium, vascular walls, and periportal spaces in the liver.

Genetics

The disorder is inherited as an autosomal recessive disease. Three genetically distinct forms of I cell disease have similar phenotypes. Mutations in the *N*-acetylglucosaminyl-1-phosphotransferase gene at 4q21–q23 have been reported in one form [2,3].



Fig. 9.2-1. I-cell disease. Gross brain shows slight dilatation of the sulci.



Fig. 9.2-2. Coronal section of the cerebrum at the mammillary bodies shows normal ventricles.



Fig. 9.2-3. The brain stem and cerebellum appear normal.

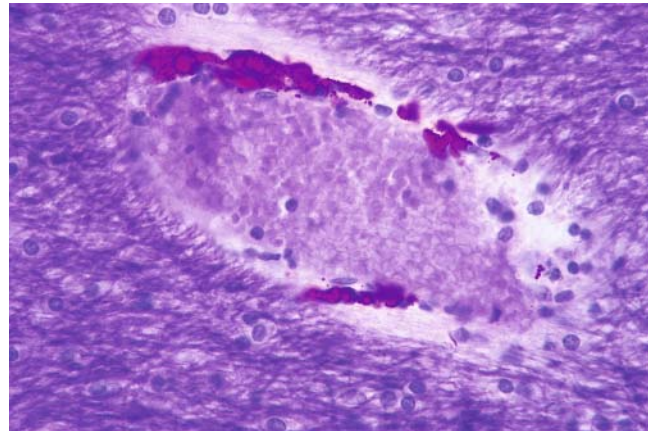


Fig. 9.2-4. Perivascular PAS-positive macrophages in the white matter.

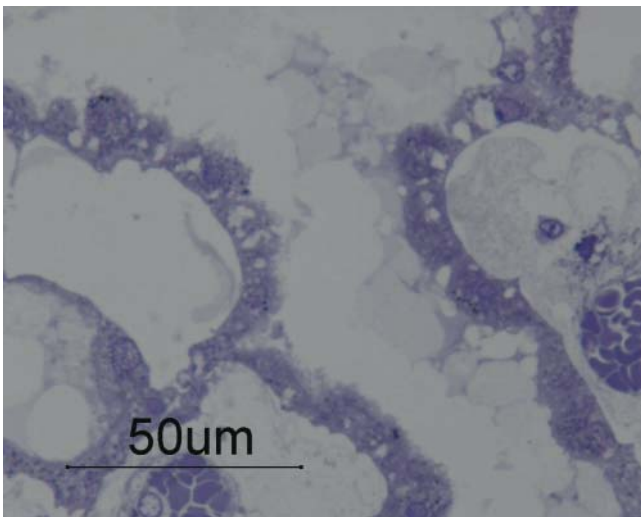


Fig. 9.2-5. Vacuolated cells in the choroid plexus. Toluidine blue stain of a thin section.

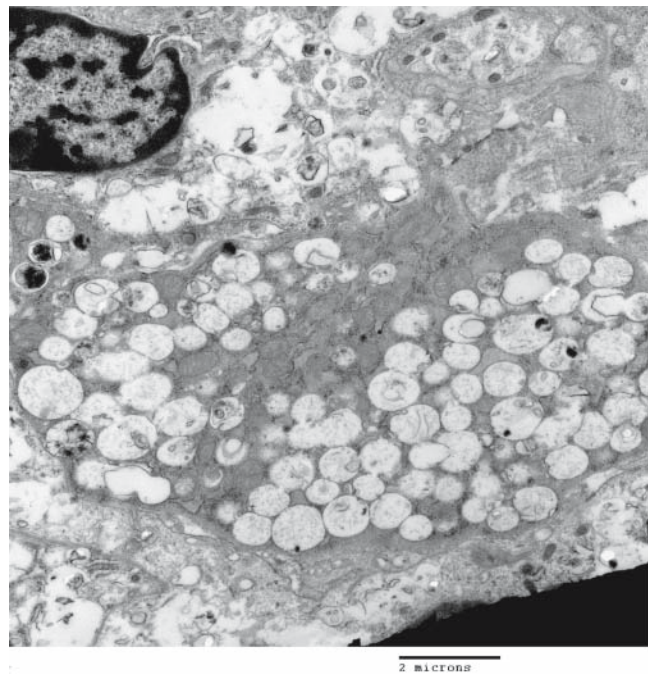


Fig. 9.2-6. EM of cells showing vacuoles in the cytoplasm.

9.3 Multiple Sulfatase Deficiency

The phenotype of multiple sulfatase deficiency (MSD) is a combination of mucopolysaccharidosis and metachromatic leukodystrophy. It is caused by deficiency of arylsulfatase A, B, and C and other sulfatases required for the degradation of mucopolysaccharides. Sulfatides and mucopolysaccharides accumulate in brain, liver, kidney, and urine. Clinical features begin at age 1 with neurological regression, unsteadiness, weakness, pyramidal signs, and peripheral neuropathy. The children develop squints, decreasing higher cortical function, myoclonus, and generalized seizures, quadriplegia, optic atrophy, and pigmentary degeneration of the retina by age 4 years. The face becomes coarse, and there is hepatomegaly and dysostosis.

Pathology

There are the same lesions as metachromatic leukodystrophy and a mucopolysaccharidosis. There is symmetri-

cal demyelination in the white matter, massive neuronal loss, and ballooned neurons containing PAS-positive material, with zebra bodies seen on EM. There may be meningeal thickening and hydrocephalus with cerebral and cerebellar atrophy. Peripheral blood cells contain metachromatic inclusions.

Genetics

There is a deficiency of arylsulfatase A (mapped to chromosome 5), and iduronate and steroid sulfatase (mapped chromosome X). Combined deficiencies in various sulfatases could be explained by a defect in some common post-translational process [2,3].



Fig. 9.3-1. Multiple sulfatase deficiency. The cerebrum exhibits atrophy and demyelination.

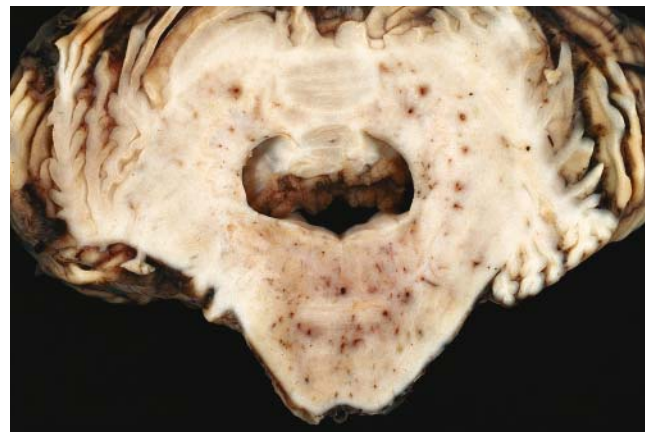


Fig. 9.3-2. Multiple sulfatase deficiency. Note the atrophic pons and cerebellum with dilatation of the fourth ventricle and obvious enlargement of the perivascular spaces.

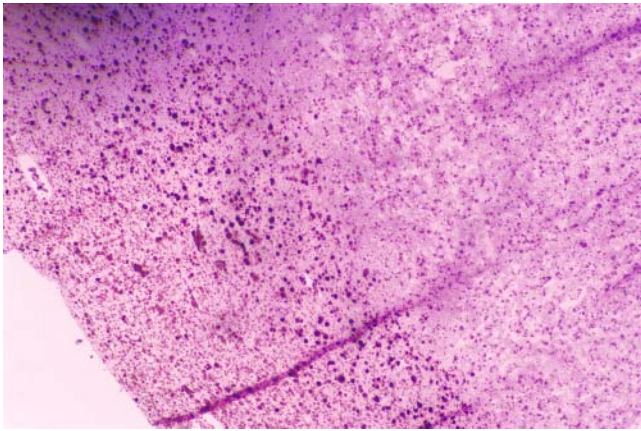


Fig. 9.3-3. Multiple sulfatase deficiency. The cerebral white matter exhibits deposition of metachromatic substance stained with acidic cresyl violet.

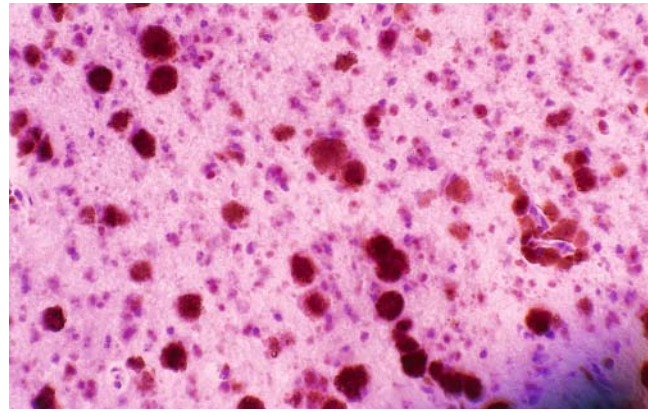


Fig. 9.3-4. Multiple sulfatase deficiency. Note the metachromatic substance deposits in the white matter. Acidic cresyl violet stain.

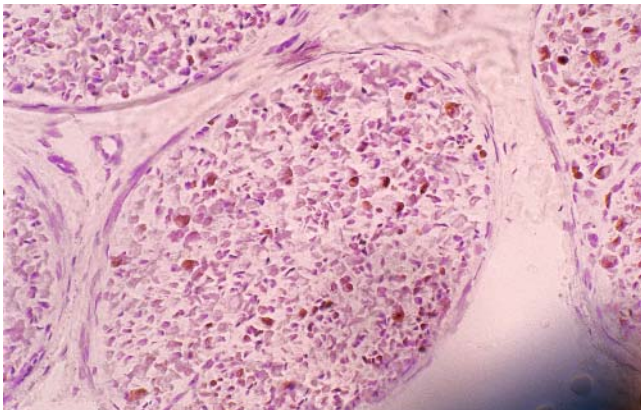


Fig. 9.3-5. Multiple sulfatase deficiency. The peripheral nerves exhibit deposition of metachromatic substance stained with acidic cresyl violet.

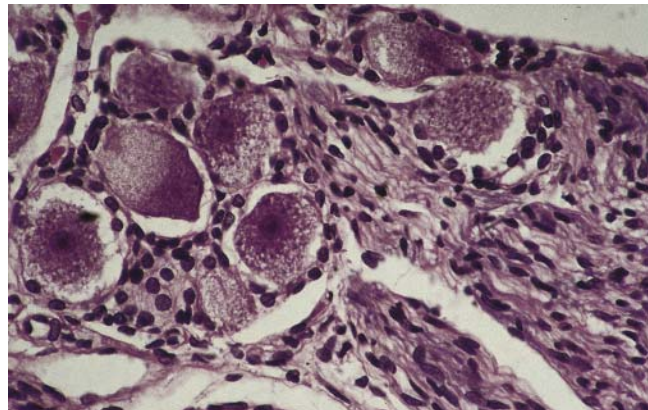


Fig. 9.3-6. Sialic storage disease. Note the neurons with ballooning of cytoplasm in the lumbar ganglion. H&E.

9.4 Mucopolysaccharidoses

The mucopolysaccharidoses are inherited disorders caused by specific enzyme defects in the degradation of the glycosaminoglycans (mucopolysaccharides, or MPS). The enzyme deficiencies result in the accumulation of glycosaminoglycans in lysosomes of various tissues and in excessive excretion of partially degraded glycosaminoglycans in urine. There is multisystem involvement, with organomegaly, dysostosis, abnormal hearing, corneal clouding, joint stiffness, and cardiac dysfunction.

Pathology

There is storage of MPS in the lysosomes of lymphocytes (Reilly bodies) and of liver. In the brain there is both MPS storage in the perivascular space and ganglioside storage in neurons (mucopolidosis). Storage of MPS in the connective tissue leads to hyalinization of collagen, which leads to joint deformities, thickened meninges, hydrocephalus, and compression of peripheral nerves [3].

Table 9.2. Enzyme defects in the mucopolysaccharidoses

Disease	Enzyme defect	Glycosaminoglycan	Gene
Hurler-Scheie	α -L-Iduronidase	Dermatan, heparan sulfates	4p16.3
Hunter	Induronate sulfatase	Dermatan, heparan sulfates	Xq28
Sanfilippo A	Heparan sulfamidase	Heparan sulfate	17q25.3
Sanfilippo B	α -N-Acetylglucosaminidase	Heparan sulfate	17q21
Sanfilippo C	Acetyl-CoA- α -glucosamide-N-acetyltransferase	Heparan sulfate	
Sanfilippo D	N-Acetylglucosamine-6-sulfate sulfatase	Heparan sulfate	12q14
Morquio A	Galactose-6-sulfatase	Keratan, chondroitin sulfate	16q24.3
Morquio B	β -Galactosidase	Keratan sulfate	3p21.33
Maroteaux-Lamy	Acetylglucosamine-4-sulfatase	Dermatan sulfate	5q13-14
Sly	Hyaluronidase	Hyaluronan	3p21.-21.3



Fig. 9.4-1. Hurler's syndrome. There is marked atrophy of the cerebral hemispheres with ventricular dilatation. The perivascular space is enlarged in the gray and white matter.

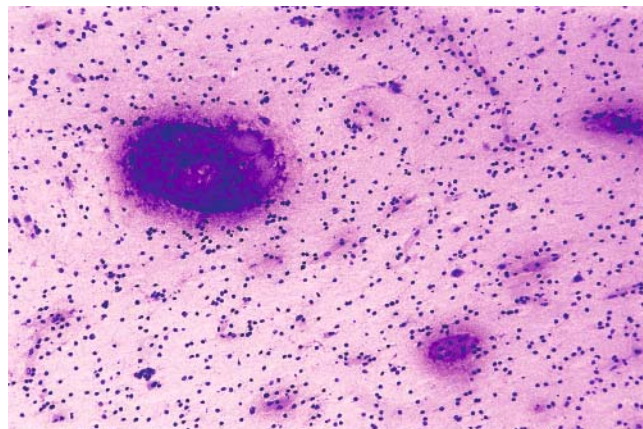


Fig. 9.4-2. Hurler's syndrome. There is metachromatic substance in the dilated perivascular space of the cerebrum. Toluidine blue.

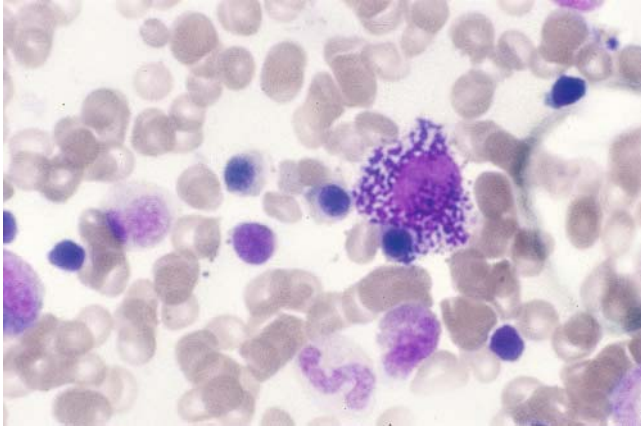


Fig. 9.4-3. Hurler's syndrome. Note the storage in bone marrow macrophages.

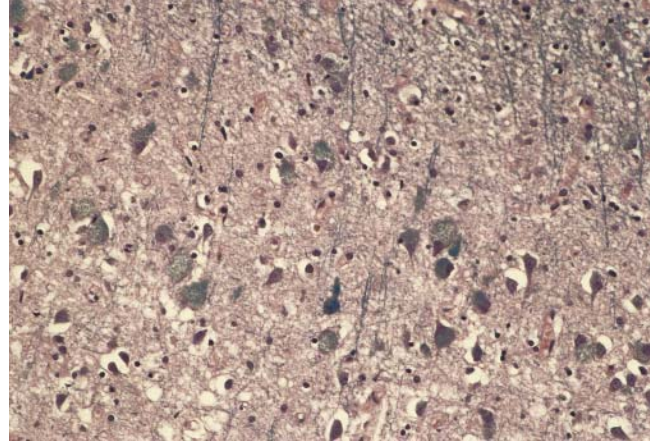


Fig. 9.4-4. Sanfilippo's syndrome. There is neuronal ballooning with lipid in the cerebral cortex. LFB.

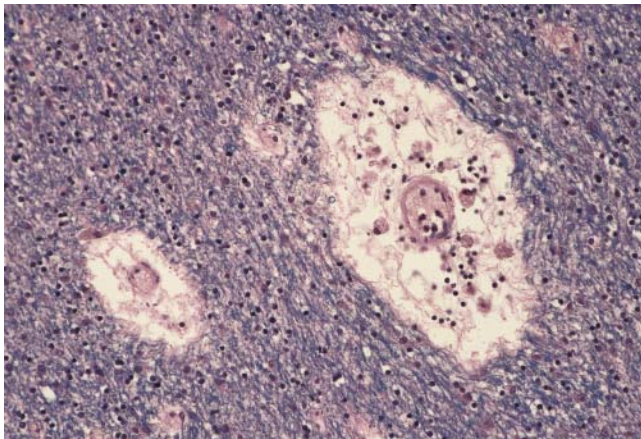


Fig. 9.4-5. Sanfilippo's syndrome. Note the enlarged perivascular space in the cerebral white matter. LFB.

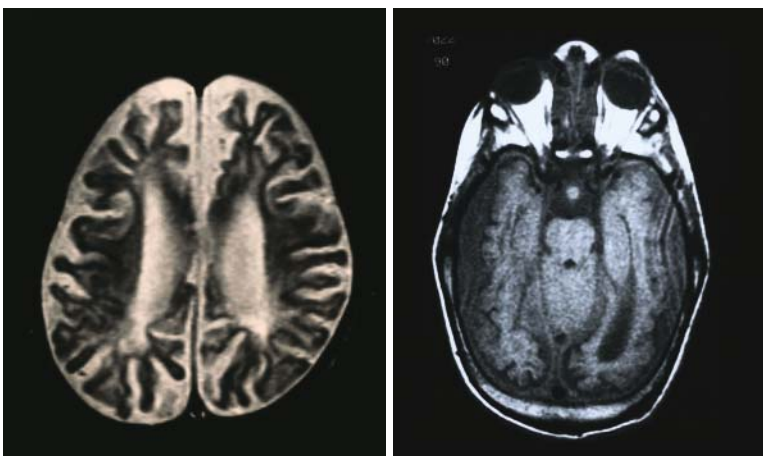


Fig. 9.4-6. Sanfilippo's syndrome (*left*) and Hurler's syndrome (*right*). Magnetic resonance imaging (MRI) shows brain atrophy and linear high intensity in the cerebral white matter, which demonstrates an enlarged perivascular space in the cerebral white matter. *Left.* Sanfilippo's syndrome (T₂-weighted). *Right.* Hurler's syndrome (T₁-weighted).

9.5 Sialidosis Type 2

Sialidosis Type 1 (Cherry Red Spot–Myoclonus Syndrome)

Sialidosis type 1, caused by α -neuraminidase deficiency, is classified as mucopolipidosis type 1. The disorder begins during late childhood with polymyoclonus, generalized seizures, macular cherry red spot, visual difficulties, gait disturbance, and delayed intellectual decline. Computed tomography (CT) shows cerebral and cerebellar atrophy.

Sialidosis Type 2 (Dysmorphic Group or Lipomucopolysaccharidosis)

Sialidosis type 2 is an autosomal disorder with marked α -neuraminidase deficiency characterized by neurological, ocular, visceral, skeletal, and facial abnormalities. There are three forms. The *congenital* form presents as a stillborn infant with hydrops or as an infant with hepatomegaly, skeletal dysplasia, ocular abnormalities, and telangiectatic skin rash. In the *infantile* form, the dysmorphic infant with organomegaly and severe psycho-

motor retardation may survive into the second year. There are *juvenile* forms in which the child survives with action myoclonus and myoclonic seizures, ataxia, macular cherry red spots, and corneal clouding.

Pathology

There is cytoplasmic vacuolization in neurons, oligodendrocytes, vascular endothelial cells, and some cells of visceral organs. The vacuoles are membrane-bound and may contain a floccular material. Stacked lamellae or myelin figures are reported in neurons of the brain stem, spinal cord, and myenteric plexus. Other ultrastructure reports include electron-dense bodies, lamellar inclusions, reticulogranular materials, and lipofuscin. Loss of neurons in brain and cerebellum has been described.

Genetics

Sialidosis is autosomal recessive, and its gene, *NEU1*, is located on 6p21.3 [4].



Fig. 9.5-1. Sialidosis type 2. Facial appearance (note the depressed nasal bridge).



Fig. 9.5-2. Periventricular calcification.

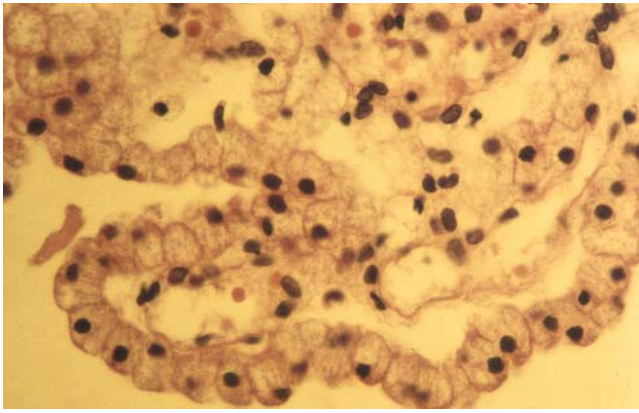


Fig. 9.5-3. Choroid plexus with some vacuolated cells. H&E.



Fig. 9.5-4. Cut surface of the kidney, which may show storage in the tubular epithelium.

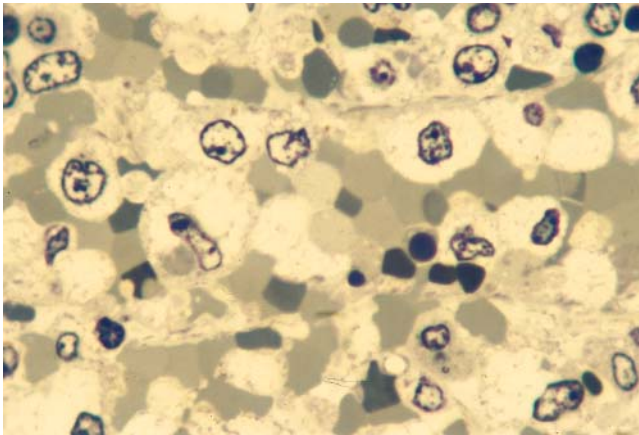


Fig. 9.5-5. Spleen showing foamy histiocytes and lymphocytes. Toluidine blue. The vacuoles are stained with PAS and Alcian blue. The storage material is oligosaccharide with *N*-acetylneuraminic acid.

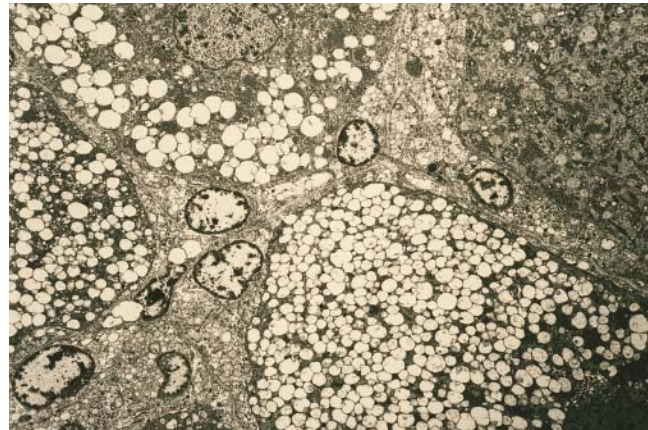


Fig. 9.5-6. EM shows multiple vacuoles in the dorsal root ganglia, some containing floccular material. $\times 4000$.

10 Glycogen Storage Disease

10.1 Pompe's Disease

Pompe's disease, the infantile form of generalized glycogenesis (infantile type II glycogenesis), is an autosomal recessive lysosomal glycogen storage disease. It presents with early onset of cardiomegaly, hypotonia, cerebral dysfunction, failure to thrive, and early death. Lysosomal glycogen storage affects practically all the tissues in the body and results from a defect of acid α -1,4-glucosidase (or acid maltase). The acid α -glucosidase locus has been localized on chromosome 17.

In Pompe's disease, a large excess of glycogen is seen in most tissues. Peripheral blood displays disease-specific lysosomal inclusions in lymphocytes. PAS staining with Best's carmine reveals small, discrete cytoplasmic vacuoles, which disappear with diastase treatment.

Both the central nervous system (CNS) and peripheral nervous system (PNS) are involved in Pompe's

disease. In the PNS, neuronal glycogen storage is most prominent in the dorsal root ganglia, autonomic ganglia, myenteric plexus neurons, and retinal ganglia cells. Electron microscopy (EM) demonstrates lysosomal glycogen in Schwann cells, mesenchymal cells, mural cells of the vasculature, and perineural cells. Lipofuscin accumulates with lysosomal glycogen in Schwann cells of unmyelinated axons and choroidal macrophages of the retina. In the CNS, neuronal glycogen storage is most severe in anterior horn cells of the spinal cord and motor nuclei of the brain stem (III to XII). The neurons are ballooned. The perikaryon has a PAS-positive granular appearance. Free and membrane-bound glycogen is present in the cerebellum and parts of the basal ganglia. The cerebral cortical neurons, Purkinje cells, and granule neurons are relatively spared [1].

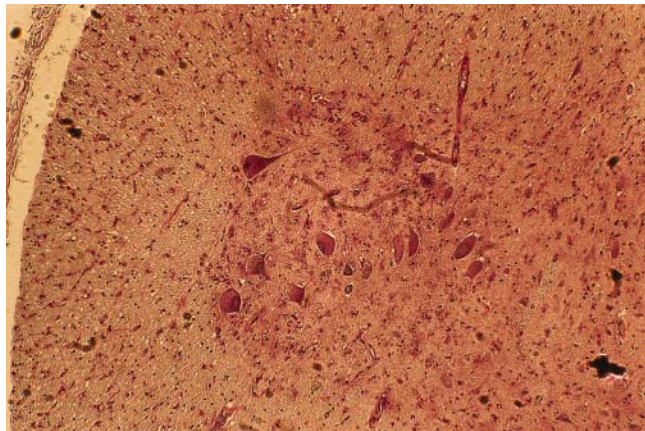


Fig. 10.1-1. Pompe's disease. Spinal cord with PAS-positive glycogen storage in the anterior horn cells.

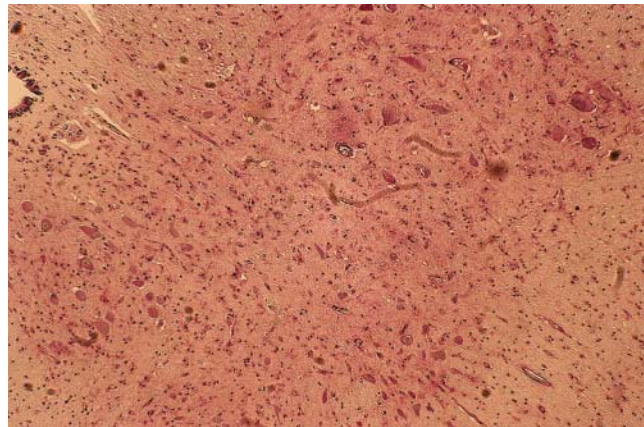


Fig. 10.1-2. PAS glycogen storage in deep nuclei of the cerebrum.

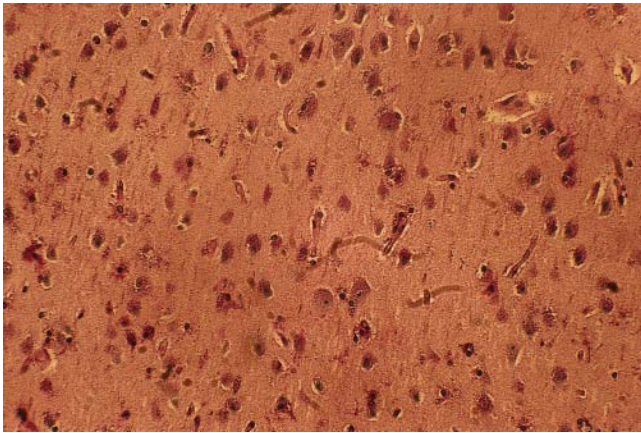


Fig. 10.1-3. PAS-positive glycogen storage in cortical neurons.

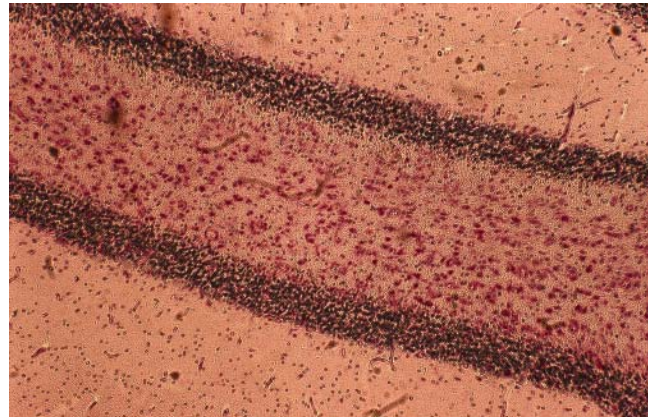


Fig. 10.1-4. PAS-positive glycogen storage in neurons of the molecular and internal granular cell layers of the cerebellum.

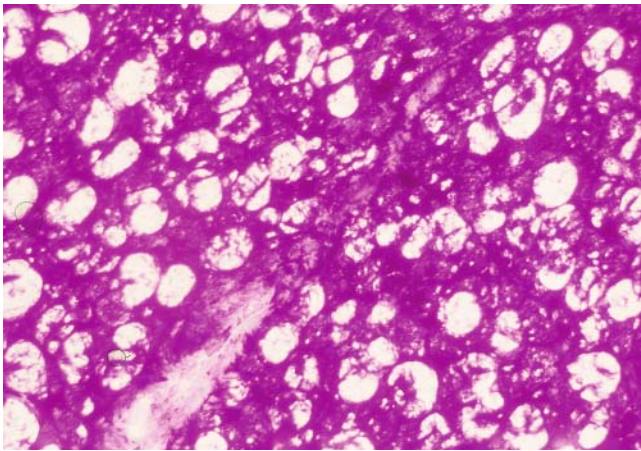


Fig. 10.1-5. Muscle showing increased glycogen accumulation. PAS.

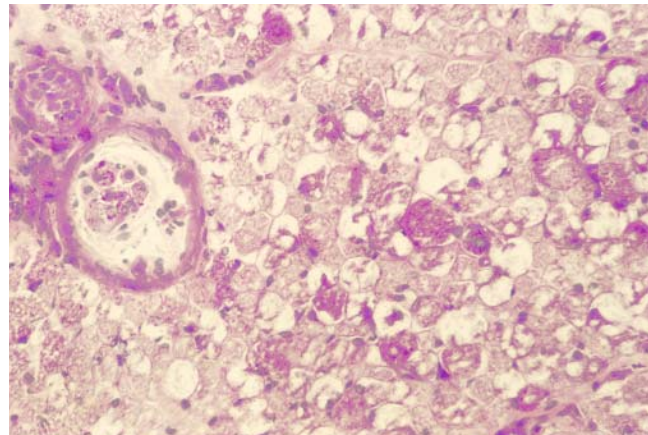


Fig. 10.1-6. Glycogen deposits in muscle fibers disappear with diastase treatment. PAS after digestion.

11 Peroxisomal Disorders

Table 11.1. Classification of peroxisomal disorders [1]

Peroxisome biogenesis disorders (PBDs)
Zellweger spectrum
Zellweger syndrome (ZS)
Neonatal adrenoleukodystrophy (NALD)
Infantile Refsum disease (IRD)
Rhizomelic chondrodysplasia punctata (RCDP)
Single peroxisomal enzyme deficiencies
β -Oxidation of fatty acids
X-linked adrenoleukodystrophy (ALD)
Acyl-CoA oxidase (AOX) deficiency
D-Bifunctional protein (DBP) deficiency
Racemase deficiency
Ether phospholipid biosynthesis
Dihydroxyacetone phosphate (DHAP) acyltransferase deficiency
Alkyl-DHAP synthase deficiency
α -Oxidation of fatty acids
Refsum disease (phytanoyl-CoA hydroxylase deficiency)
Hydrogen peroxide metabolism
Acatalasemia (catalase deficiency)
Glyoxylate detoxification
Hyperoxaluria type 1 (alanine glyoxylate aminotransferase deficiency)
Glutaryl-CoA metabolism
Glutaric aciduria type 3 (glutaryl-CoA oxidase deficiency)
Isoprenoid biosynthesis
Mevalonate kinase deficiency
Contiguous gene syndrome
Contiguous ABCD1 DXS1357E deletion syndrome (CADD5)

11.1 Zellweger's Syndrome

Zellweger's syndrome is an X-linked autosomal recessive disorder of peroxisomal biogenesis with an absence of the peroxisome. There is a wide range of characteristic dysmorphic features and cerebrohepatorenal involvement. Laboratory studies characteristic of Zellweger's syndrome include (1) elevated levels of pipecolic acid in plasma, cerebrospinal fluid (CSF) and urine; (2) elevated levels of saturated (C26) and monosaturated (C26:1) VLCFA in plasma, body fluids, and tissues with an elevated C26:0/C22:0 ratio; (3) decreased (<10% of normal) tissue level of phosphatidyl ethanolamine plasmalogen, a phospholipid constituent of myelin and platelet-activating factor; and (4) deficient activity of dehydroxyacetone phosphate acyltransferase, the key enzyme in the pathway for plasmalogen synthesis (located in the peroxisomal membrane).

Pathology

There is hepatomegaly with fibrosis, renal cysts, neuronal migration defects, and degenerative changes. In the

cerebellum, Purkinje cell heterotopias are concentrated at the base of the ansiform lobule. Cerebral degenerative changes include (1) cysts in the subependymal regions; (2) sudanophilic leukodystrophy involving periventricular white matter, corpus callosum, optic nerves, and the posterior columns; (3) neuroaxonal dystrophy predominantly in the dorsal nucleus of Clarke and lateral cuneate nucleus; and (4) degenerative changes of the retina.

Electron Microscopy

Electron microscopy (EM) studies of neurons and axons show striated inclusions of large electron-lucent clefts and lamellar lipid profiles.

Genetics

Defects in at least 12 *PEX* genes, which are required for normal peroxisome assembly, have been identified [1,2].

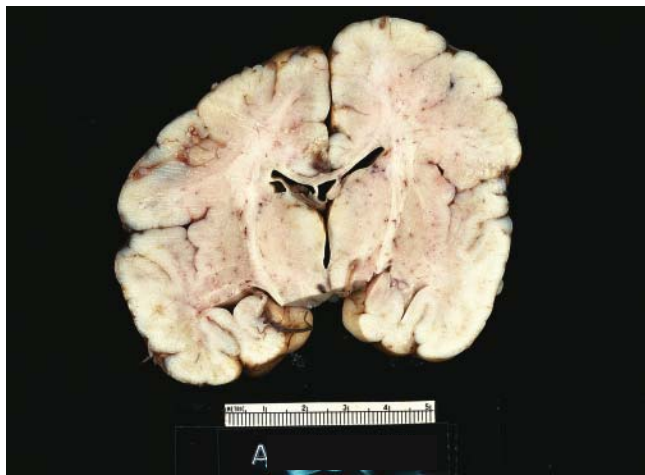


Fig. 11.1-1. Zellweger's syndrome. Note the microgyria and a subependymal cyst (germinolysis) of the left lateral ventricle.

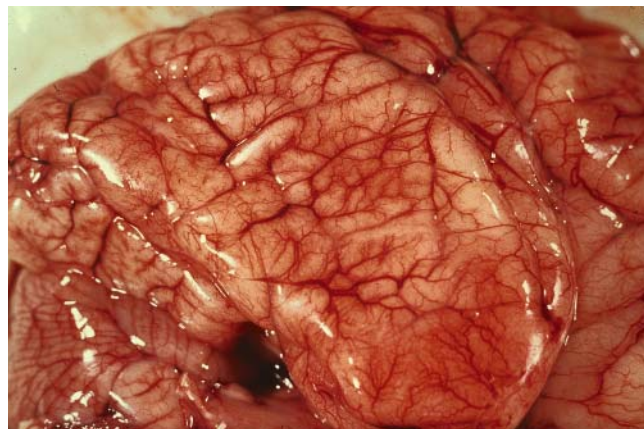


Fig. 11.1-2. There is polymicrogyria on the surface of the brain. Polymicrogyria is usually limited to regions of the lateral parietal, frontal, and temporal convexity. It is more prominent superiorly over the frontoparietal convexity.

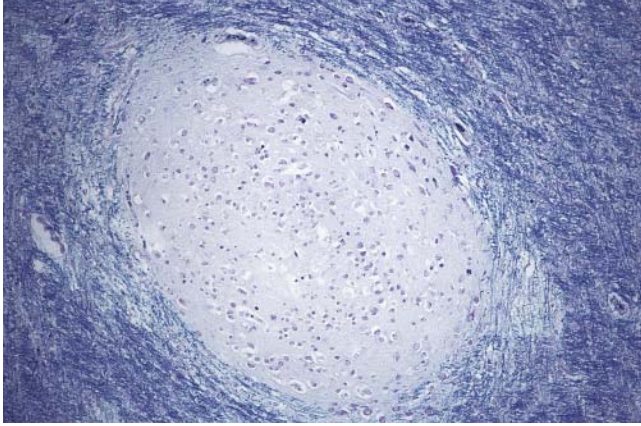


Fig. 11.1-3. Neuronal heterotopias in the cerebral white matter underneath the polymicrogyral regions. LFB.

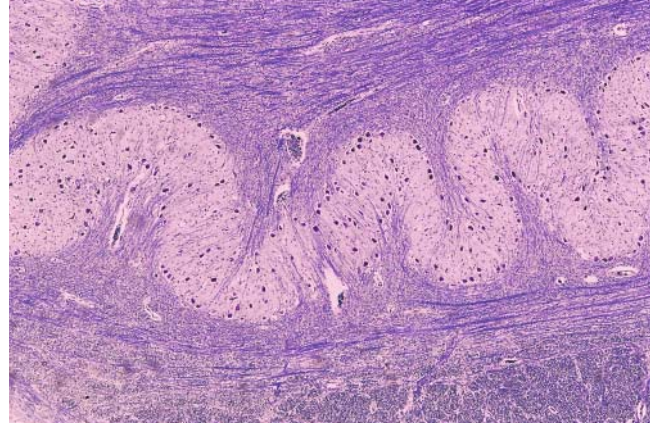


Fig. 11.1-4. The inferior olivary nucleus is dysplastic. There is discontinuity in the cellular lamella of the principal olivary nucleus. The degree of convolutional folding of the lamella is reduced. LFB.

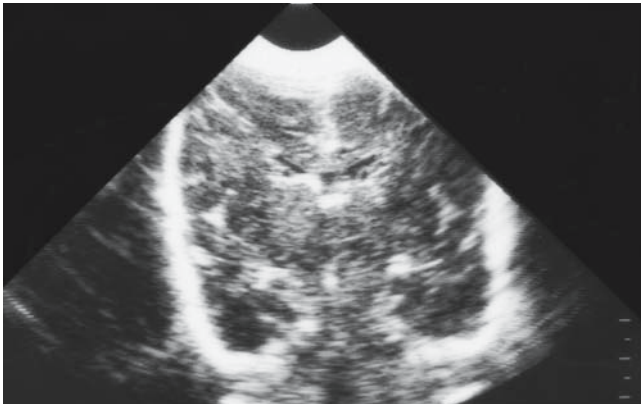


Fig. 11.1-5. Ultrasonography of the brain revealed a subependymal cyst.

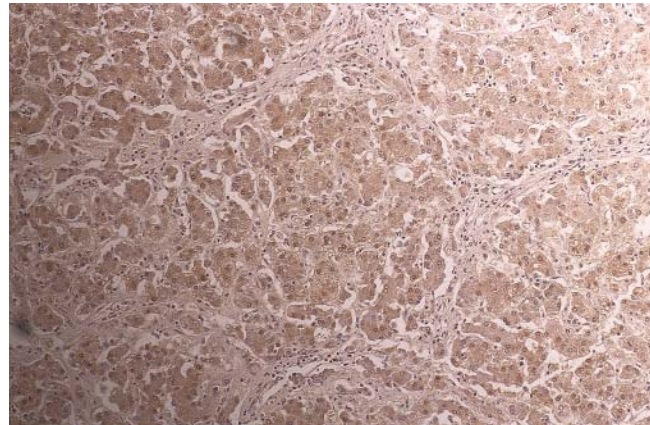


Fig. 11.1-6. Liver fibrosis. Hepatocytes lack positive granules in cytoplasm stained by catalase immunohistochemistry. Negative staining with this method suggests the absence of peroxisome in the cytoplasm and is diagnostic.

11.2 Neonatal Adrenoleukodystrophy

Neonatal adrenoleukodystrophy (NALD) and infantile Refsum's disease are milder phenotypes of peroxisome biogenesis disorders and are caused by an absence of peroxisomes. There is a pseudo-form of NALD that has peroxisomes but lacks acyl-CoA oxidase. NALD resembles X-linked adrenoleukodystrophy disease and Zellweger's syndrome, but the course is slower, with death at 2–3 years. Clinically, there is liver involvement, peripheral neuropathy, facial dysmorphism, adrenal insufficiency, extreme hypotonia and neurological dysfunction, ocular abnormalities, and a hearing deficit.

Pathology

The pathology includes sudanophilic leukodystrophy with lymphocytic cuffing and neuronal migration defects with polymicrogyria and heterotopias. The peripheral nerves may exhibit demyelination. There are subtle adrenal lesions and biochemical changes similar to those in Zellweger's syndrome [3,4].



Fig. 11.2-1. Neonatal adrenoleukodystrophy. The external brain may exhibit polymicrogyria.

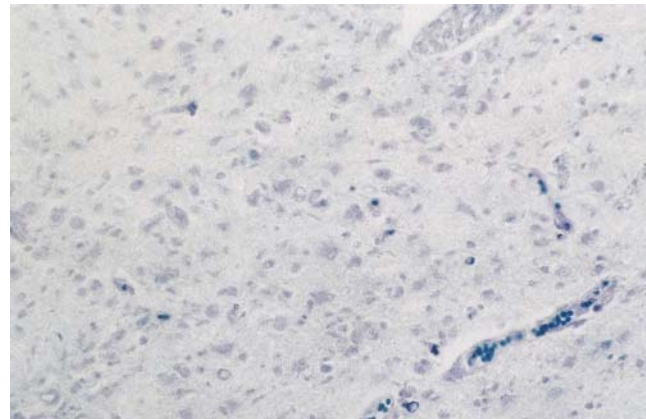


Fig. 11.2-2. There is reduced myelination in the cerebral white matter. LFB.

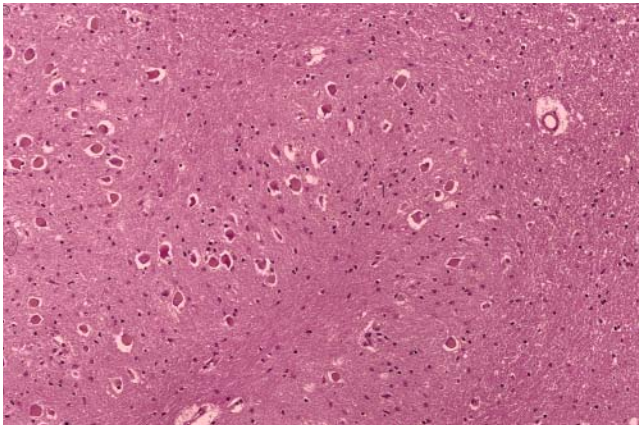


Fig. 11.2-3. Inferior olivary dysplasia. H&E.

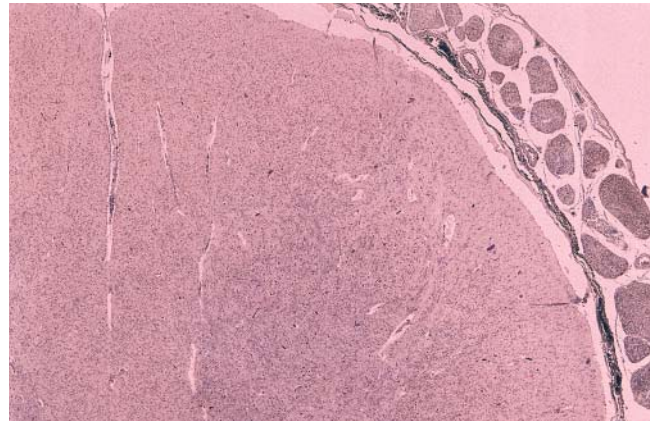


Fig. 11.2-4. The spinal cord and nerve roots show hypomyelination. LFB.

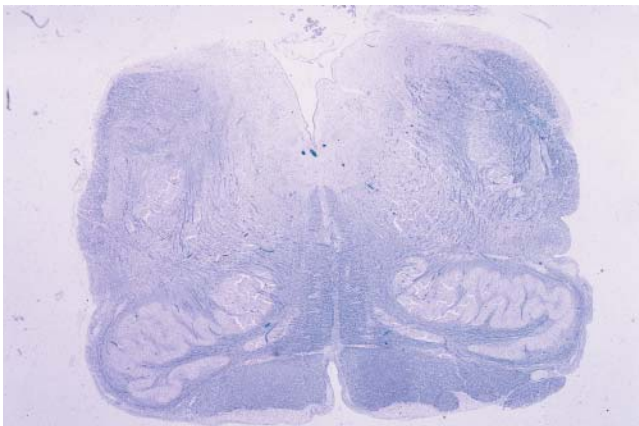


Fig. 11.2-5. At 7 months of age, there is hypomyelination in the pyramids and inferior olivary dysplasia. LFB.

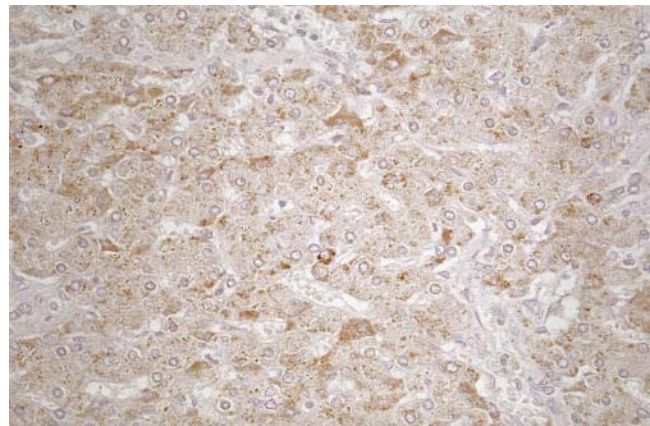


Fig. 11.2-6. Negative immunoreactivity of bifunctional protein in the liver.

11.3 Adrenoleukodystrophy

With the classic childhood form of adrenoleukodystrophy, there is an onset of behavioral, intellectual, and motor deterioration between 4 and 10 years of age. There is also loss of vision and hearing and progressive hemiplegia with parietooccipital demyelination. Adrenal insufficiency occurs. There is progressive demyelination and accumulation of very long-chain fatty acids (VLCFAs) because of defective oxidation by peroxisomes. In addition, there is a deficiency of a peroxisomal membrane protein (ALDP) needed for active transport of enzyme cofactors or substrates required for β -oxidation of VLCFAs.

There are variant phenotypes. In males there is slowly progressive paraparesis and adrenomyeloneuropathy. Some females present with myeloneuropathy.

Pathology

The brain lesion is in the white matter with symmetrical demyelination accompanied by foam cells and perivas-

cular inflammatory cells. There is associated myelin degeneration descending into the brain stem and spinal cord. The adrenal gland shows cytoplasmic striated inclusions in adrenocortical cells in the zona fasciculata.

Magnetic resonance imaging (MRI) shows focal bilateral low intensity in white matter on T1-weighted images and high intensity on T2-weighted images, predominantly in the parietooccipital lobes. Calcifications are evident on computed tomography (CT).

Genetics

The Xlinked *ALD* gene (an ATP-binding cassette-transporter gene) is located on Xq28 [4].

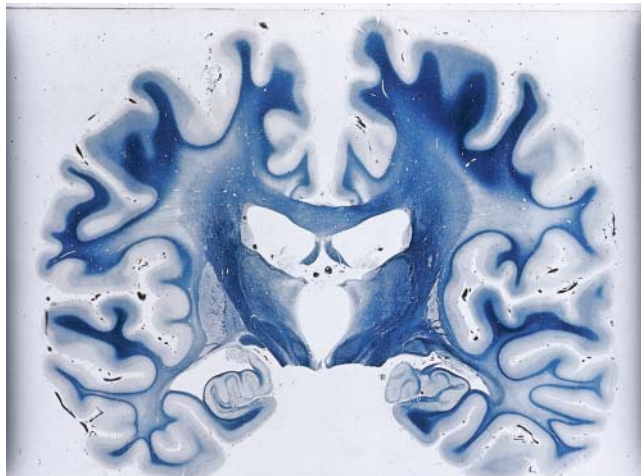


Fig. 11.3-1. Adrenoleukodystrophy. The cerebral hemispheres with myelin stain show marked symmetrical demyelination, with sparing of U fibers.

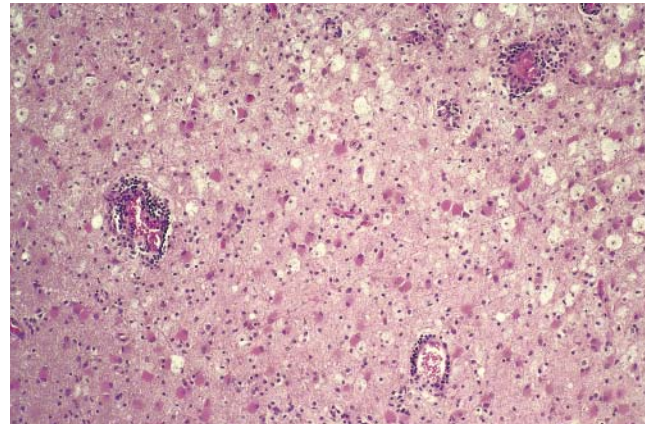


Fig. 11.3-2. The white matter shows marked astrogliosis, foam cell appearance, and perivascular inflammatory round cell infiltration. H&E.

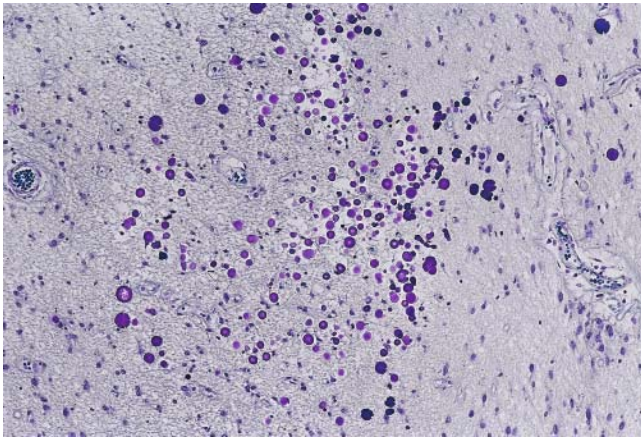


Fig. 11.3-3. The white matter exhibits demyelination with calcification. KB stains.

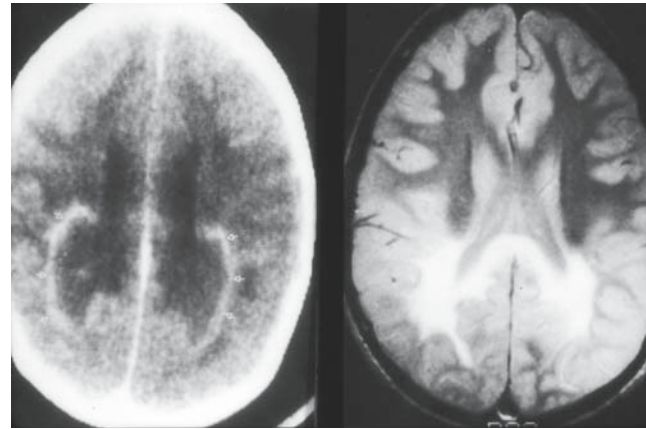


Fig. 11.3-4. Enhanced CT shows white matter high density in the parietooccipital regions outlining low-density foci, suggesting demyelination. MRI shows high-intensity areas in the occipital white matter on T2-weighted imaging.

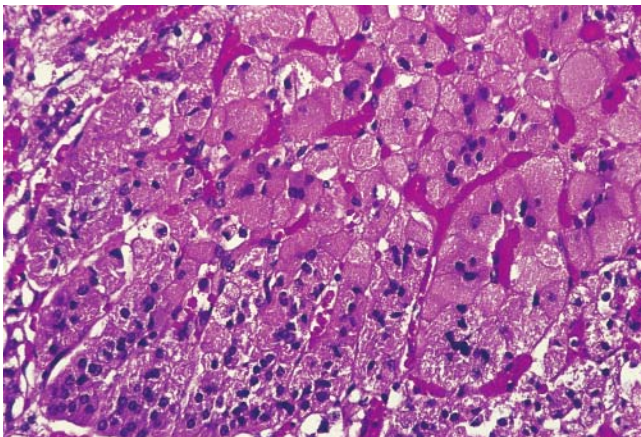


Fig. 11.3-5. Balloon cells with striated inclusions in the cortex of the adrenal gland.

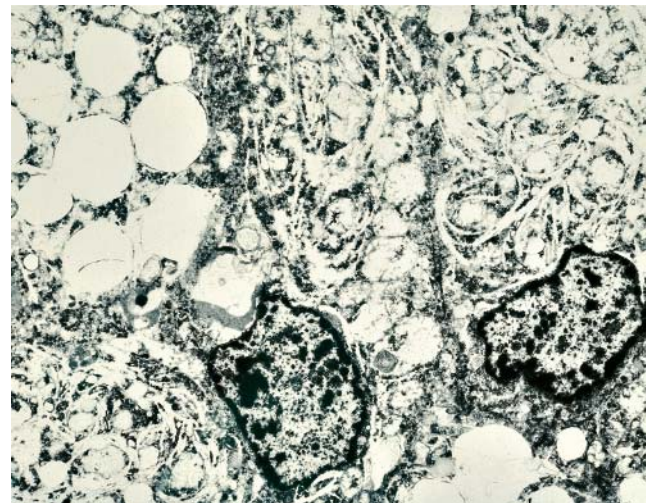


Fig. 11.3-6. EM picture of adrenal cortex. The adrenal cortical cells contain striated inclusions.

12 Urea Cycle Disorders

12.1 Argininosuccinic Aciduria

In the urea cycle, six enzymes are required to convert ammonia to urea: *N*-acetylglutamate synthetase (NAGS), carbamoylphosphate synthetase (CPS), ornithine transcarbamylase (OTC), argininosuccinate synthetase (ASS), argininosuccinate lyase, and arginase. Deficiency of any of these enzymes may cause disease. Such infants are asymptomatic for 1–5 days but then feed poorly, vomit, and become lethargic. They may be irritable, rigid, and convulse. They exhibit hyperpnea and respiratory alkalosis, hepatomegaly, and jaundice; and they may have brain edema with bulging fontanelles. Death ensues without treatment.

Pathology

The brain is swollen with flat gyri, narrow sulci, and reduced ventricular size. The protoplasmic astrocytes

are swollen (Alzheimer type II glia) possibly due to accumulation of intracellular glutamine and water. In chronic cases the brain may be atrophic.

Genetics

Argininosuccinic aciduria is an autosomal recessive disorder with a deficiency of argininosuccinate lyase. The gene has been cloned [1].

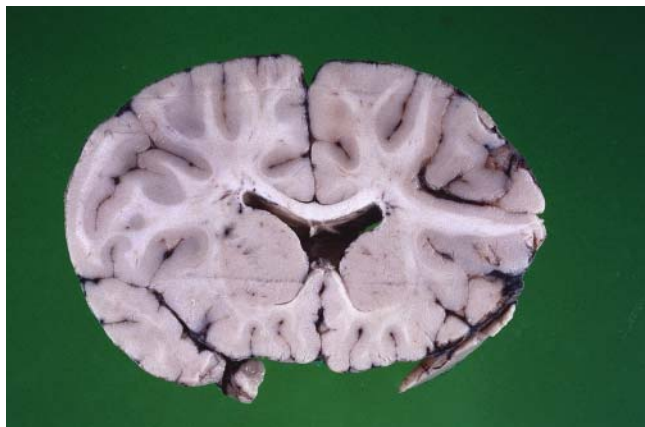


Fig. 12.1-1. Argininosuccinic aciduria. The brain in a case of argininosuccinic aciduria with swollen gyri and obliterated sulci.

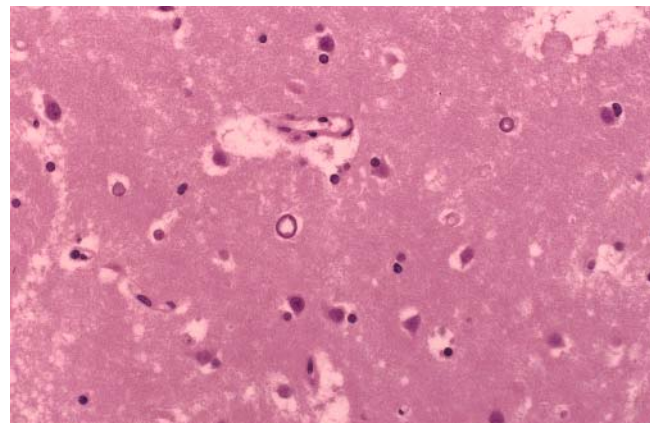


Fig. 12.1-2. Alzheimer type 2 glia in the putamen. Note the swollen cleared-out appearance of the astrocyte nucleus. H&E.

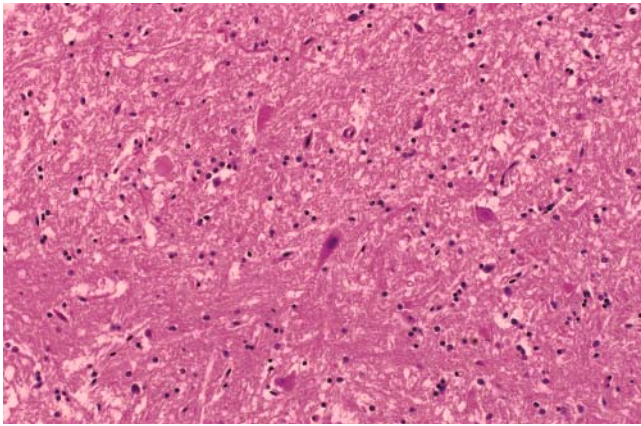


Fig. 12.1-3. There are axonal swellings in the globus pallidus. H&E.

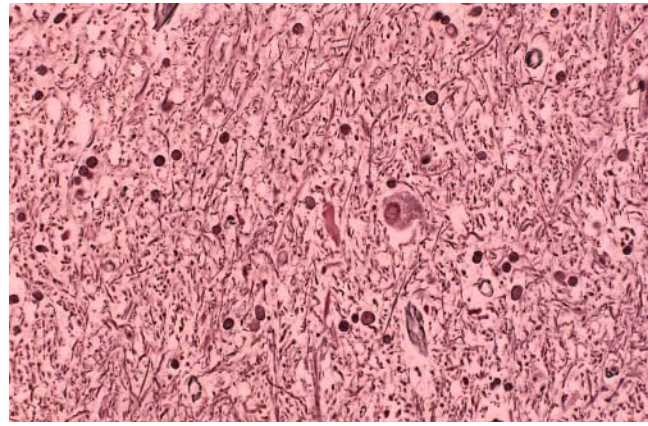


Fig. 12.1-4. Note also axonal swellings in the medulla oblongata. H&E.

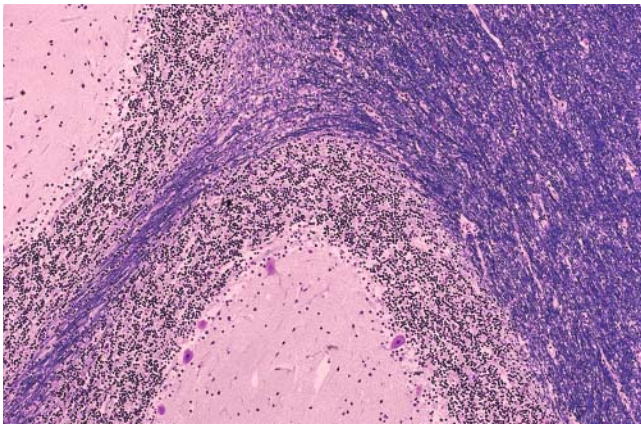


Fig. 12.1-5. There is a mild loss of Purkinje cells and granular cells in the cerebellum. LFB/Nissl.

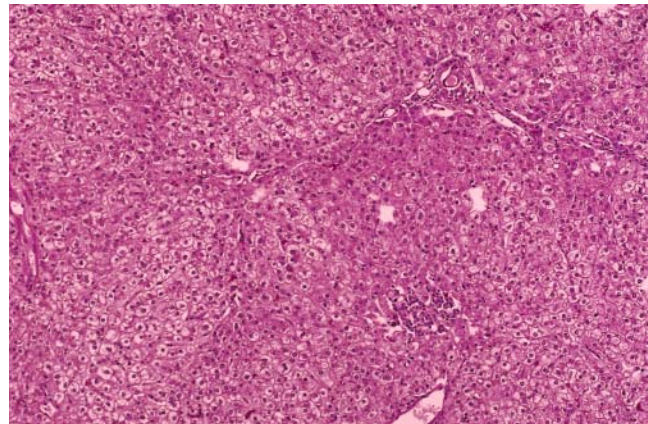


Fig. 12.1-6. There is fibrosis in the liver. H&E.

12.2 Glutaric Aciduria

Glutaric aciduria type 1 is an autosomal recessive disorder resulting from a deficiency of glutaryl-CoA dehydrogenase. This leads to an accumulation of glutaric and 3-hydroxyglutaric acids and secondary carnitine deficiency. Severe metabolic encephalopathies occur at age 6–18 months, causing necrosis of the striatum and stroke-like events, resulting in a dystonic dyskinetic movement disorders. Computed tomography (CT) or magnetic resonance imaging (MRI) shows severe leukoencephalopathy and striatal necrosis.

Pathology evaluation shows degeneration of the putamen and globus pallidum, frontotemporal cerebral

atrophy, and mild status spongiosis in the cerebral white matter [2]. Genetic study shows compound heterogeneity with a mutation of the glutaryl-CoA dehydrogenase gene.

Glutaric aciduria type 2 is transmitted by an autosomal recessive trait and is caused by a deficiency of either electron transport flavoprotein or electron transport flavoprotein oxyreductase. It is characterized by acidosis, hypoglycemia, organic aciduria and sweat-sock odor. The pathology shows symmetrical hypoplasia of the temporal cerebral lobes with axon loss and hypomyelination [3].



Fig. 12.2-1. Glutaric aciduria type 1. Coronal section of the brain shows marked atrophy of the striatum in the basal ganglia.

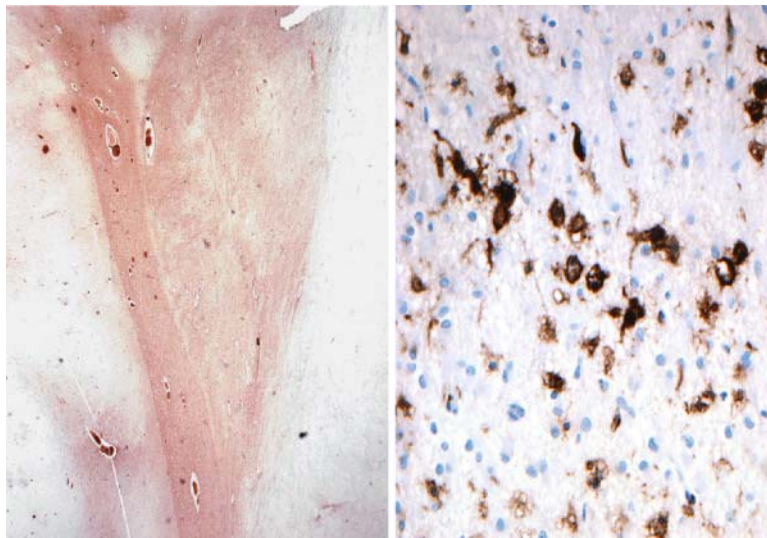


Fig. 12.2-2. *Left.* Histology of the basal ganglia shows marked atrophy and astrogliosis. GFAP. *Right.* Histology of the putamen shows an increase of GFAP-positive reactive astrocytes.

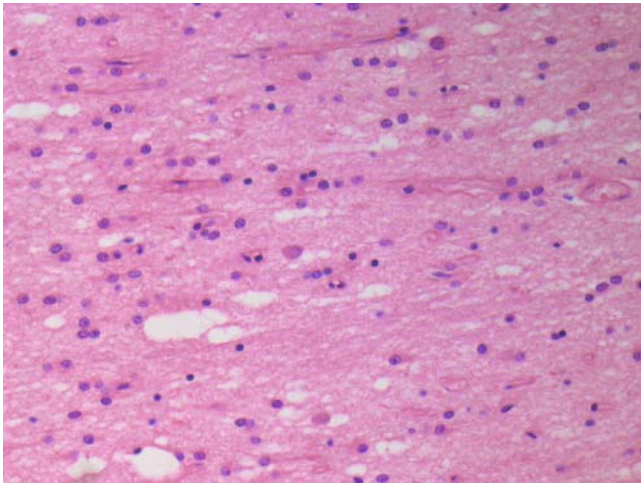


Fig. 12.2-3. Histology of the putamen shows neuronal loss, mild spongy changes, and astrogliosis. H&E.

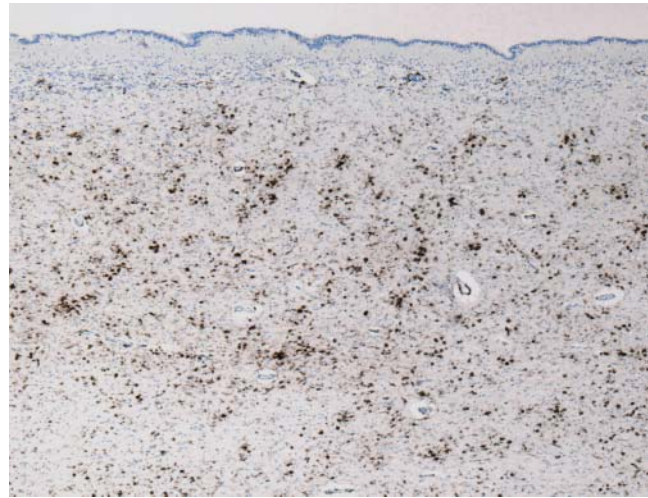


Fig. 12.2-4. Histology of the caudate nucleus shows an increase of microglial cells and/or macrophages. HLA-DR.

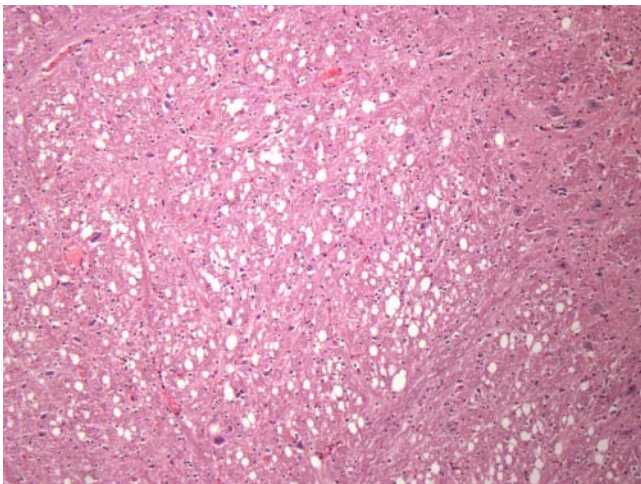


Fig. 12.2-5. There are vacuoles in the central tegmentum. H&E.

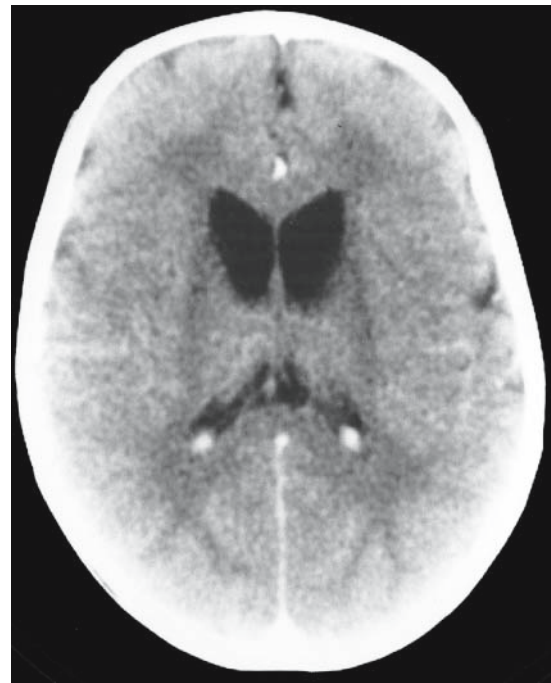


Fig. 12.2-6. CT shows marked atrophy of the basal ganglia.

12.3 Ornithine Transcarbamylase Deficiency

Ornithine transcarbamylase (OTC) deficiency is an X-linked disorder and the most common inherited cause of hyperammonemia. Clinical manifestations are more severe in hemizygous males, who often present during the neonatal period. Heterozygous females may be asymptomatic until later childhood or adulthood. Fluctuating concentrations of ammonia, glutamine, and other excitotoxic amino acids result in a chronic or episodically recurring encephalopathy.

Pathology

There are nonspecific findings in brains after acute death, including brain swelling and spongy changes in

the white matter with basal ganglia and cortical neuronal loss. Alzheimer type II astrocytes may be present. In survivors there has been massive destruction of the cerebral hemispheres, producing a “walnut brain” appearance. Cerebellar heterotopias and hypomyelination suggest a prenatal onset of lesions.

Genetics

Ornithine transcarbamylase (OTC) is a urea cycle enzyme coded by a gene located at Xp21.1. The genetic deficiency may be caused by a wide spectrum of mutations, most of them occurring de novo [4].



Fig. 12.3-1. Ornithine transcarbamylase deficiency. Gross brain showing swelling and hemorrhage.



Fig. 12.3-2. Coronal section at the mammillary bodies with massive left intracerebral hemorrhage.

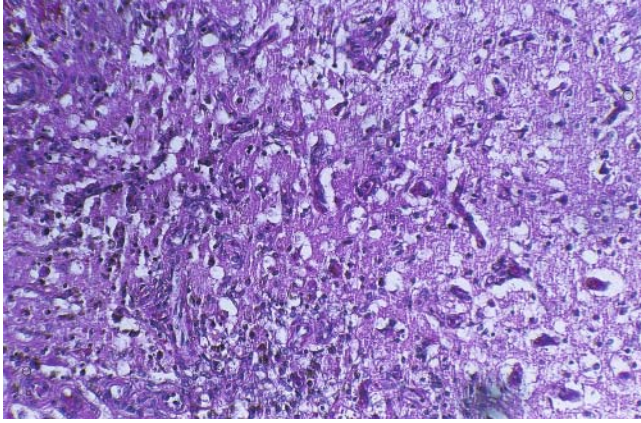


Fig. 12.3-3. Cerebral cortex shows edema and an early infarct with vascular proliferation. H&E.

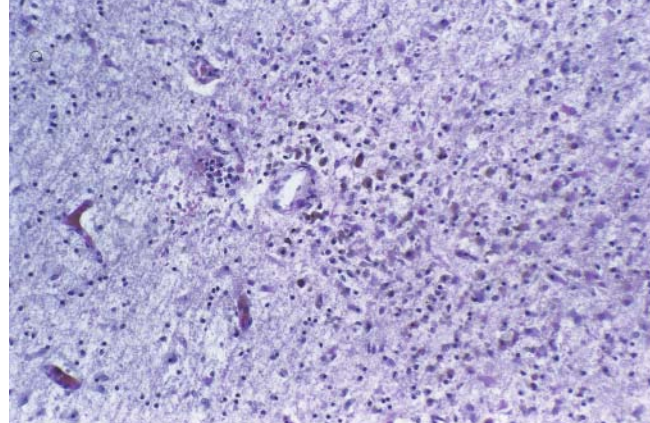


Fig. 12.3-4. White matter shows necrosis with gliosis, including hemosiderin-containing macrophages. H&E.

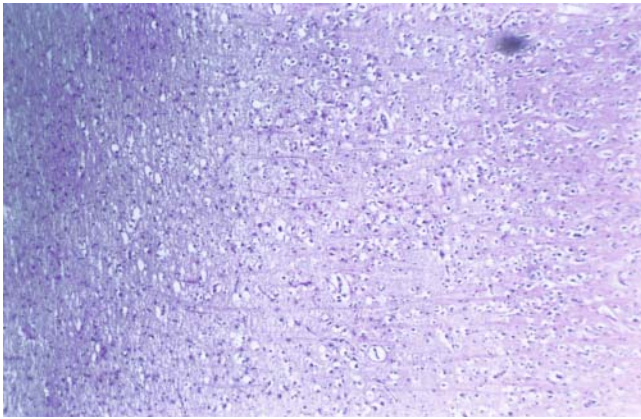


Fig. 12.3-5. White matter shows spongy changes with edema. H&E.

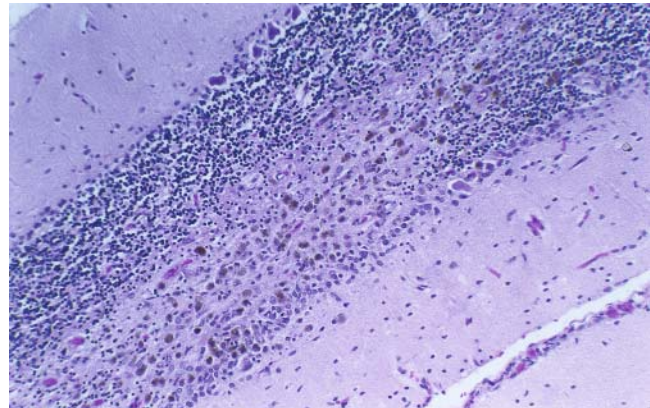


Fig. 12.3-6. Cerebellum has decreased myelin sheaths and internal granular cell loss with gliosis. There are hemosiderin-laden macrophages. H&E.

13 Amino Acid Metabolism Disorders

13.1 Homocystinuria

Several genetic abnormalities can produce excessive excretion of urinary homocystine. Cystathionine β -synthase deficiency (CBS) is the most common. Others include 5,10-methylene tetrahydrofolate reductase deficiency, defects in cobalamine and folate metabolism, and nutritional deficiencies of vitamin B₁₂ and folate.

Pathology

The accumulation of homocystine is postulated to alter platelet adhesiveness, vascular endothelium, and oxidation of cholesterol. Thus, vascular occlusions and infarcts

characterize the pathology of homocystinuria. Intimal fibrosis and other vascular abnormalities are found in the brain.

Genetics

Classic homocystinuria is due to cystathionine β -synthase (CBS) deficiency. The gene for CBS is located on 21q22.3. More than 130 mutations, which differ in prevalence and severity, have been described at the CBS gene. Mutation p.I278T is extremely prevalent [1]

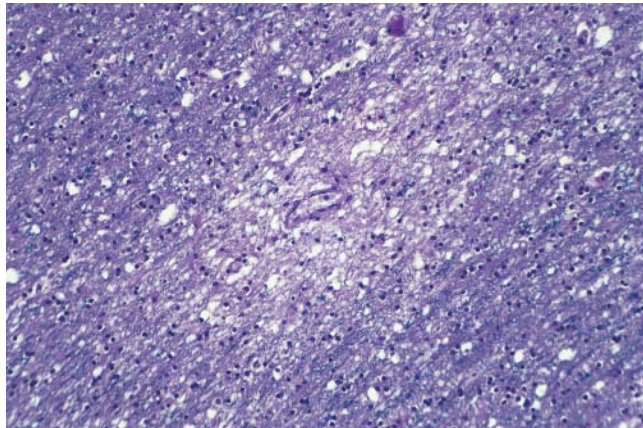


Fig. 13.1-1. Homocystinuria. Loss of myelin sheaths and spongy changes in the cerebral white matter. H&E/LFB.

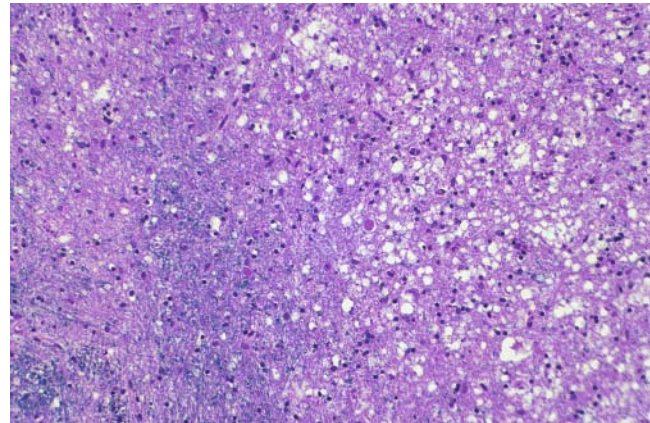


Fig. 13.1-2. Spongy changes in the dentate nucleus. H&E/LFB.

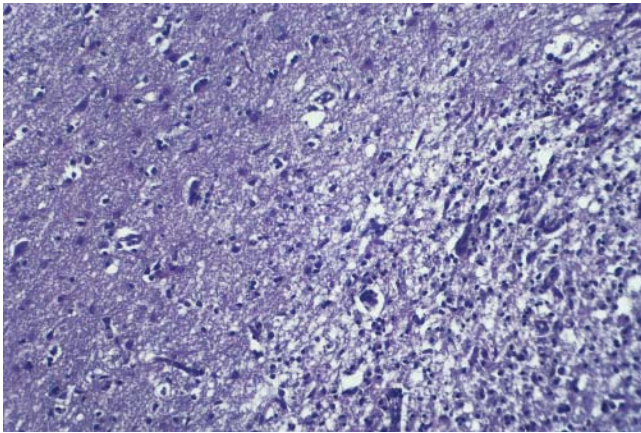


Fig. 13.1-3. Necrosis with astroglia in the inferior colliculus. H&E/LFB.

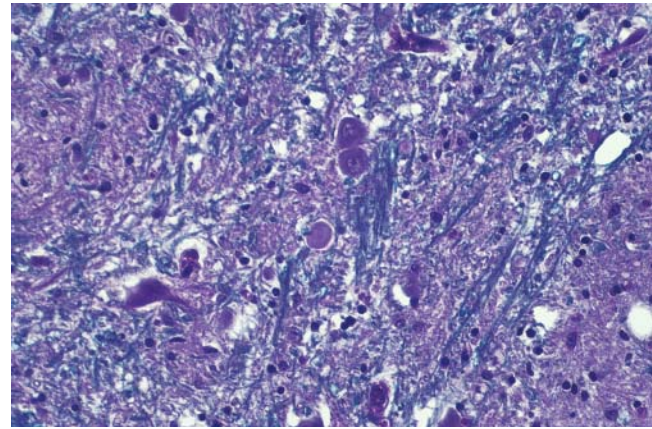


Fig. 13.1-4. Axonal swellings in the nucleus cuneatus of the medulla oblongata. H&E/LFB.

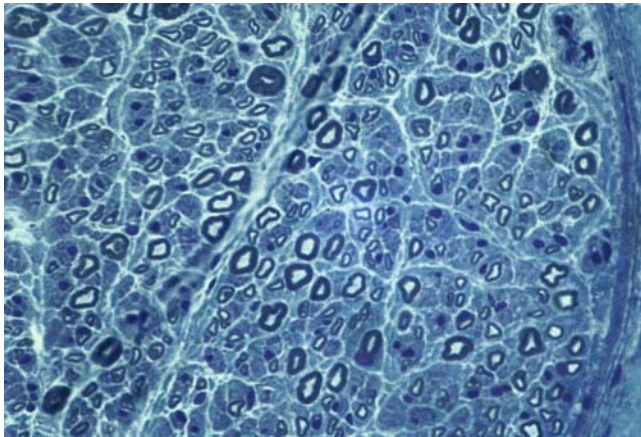


Fig. 13.1-5. Decrease of myelinated axons in the sural nerve. Toluidine blue stain of a thin section.

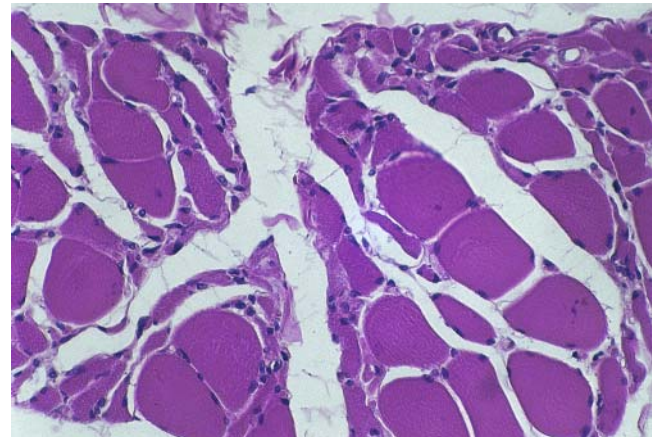


Fig. 13.1-6. Psoas muscle showing denervation group atrophy. H&E.

13.2 Phenylketonuria and Maple Syrup Urine Disease

Phenylketonuria

The classic form of phenylketonuria (PKU-I) results from phenylalanine reductase deficiency, whose gene locus is 12 (g22-12q24.2). This form of hyperphenylalanemia causes intellectual disabilities if it is not treated during the first few weeks after birth. Dihydropterin reductase deficiency (PKU II) and bipterin deficiency (PKU III) are rare variants of PKU. They exhibit progressive neurological disease associated with impaired synthesis of the neurotransmitters epinephrine, norepinephrine, and dopamine.

Pathology

Neuropathology findings are variable, although microcephaly and generalized myelin pallor are common. Histology suggests a delay of neuronal and myelin maturation. The cerebral white matter, exhibiting widespread demyelination or dysmyelination, dis-

plays various changes: status spongiosus, myelin necrosis, macrophage infiltration, or extensive gliosis [1].

Maple Syrup Urine Disease

Maple syrup urine disease is an autosomal recessive disorder caused by defects in the mitochondrial branched chain α -keto acid dehydrogenase multienzyme complex. There are several forms of the disorder. The commonest presents during the neonatal period. Infants are normal at birth but within 2 weeks have feeding problems and become unresponsive. They have breathing irregularities, apnea, myoclonic jerks, convulsions, and opisthotonic spasms. Metabolic acidosis, ketonemia, ketonuria, and a characteristic odor are present. The toxic effect of branched-chain amino acids on the brain is not understood. Treatment may prevent death and neurological handicap in survivors. The neuropathology consists of edema and a delay in myelination, which are similar to the manifestations of PKU [1].



Fig. 13.2-1. Phenylketonuria II. Note the slight congestion in the base of the pons in a case of dihydropterin reductase deficiency (PKU II).

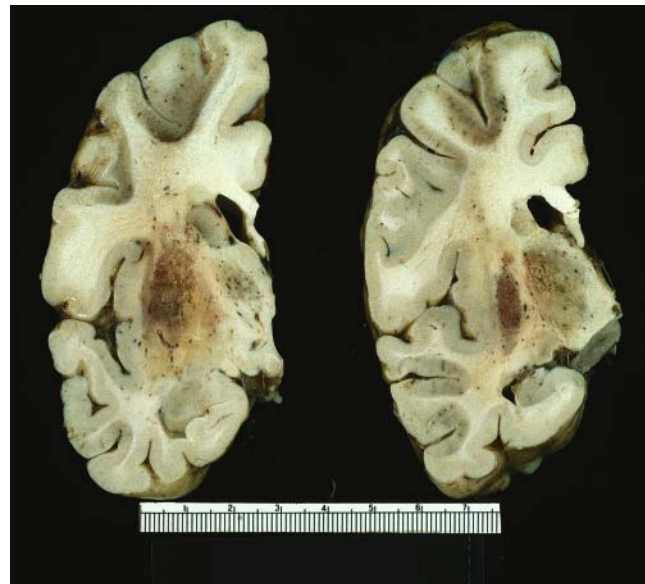


Fig. 13.2-2. Phenylketonuria II. There are congestion and necrosis in the basal ganglia, thalamus, and deep white matter.

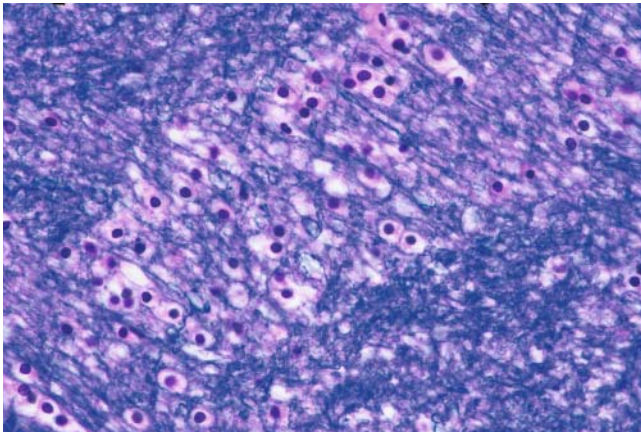


Fig. 13.2-3. Maple syrup urine disease. Note the spongy changes of edema in the cerebral white matter. H&E/LFB.

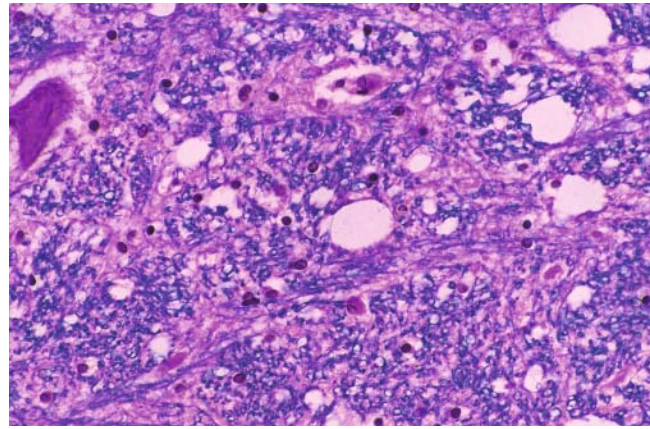


Fig. 13.2-4. Maple syrup urine disease. There are spongy changes in the reticular formation of the midbrain. H&E/LFB.

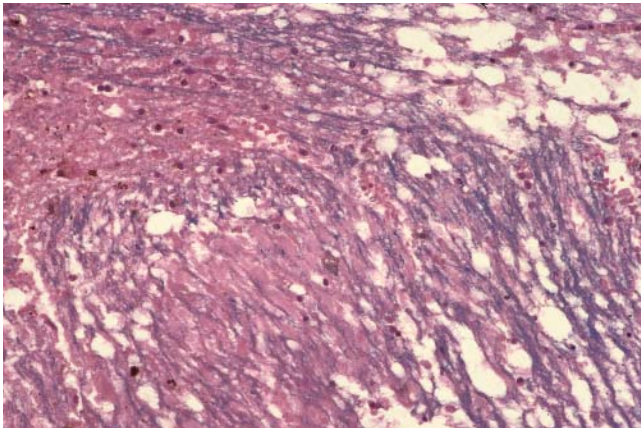


Fig. 13.2-5. Maple syrup urine disease. Note the spongy changes in the pons. H&E/LFB.

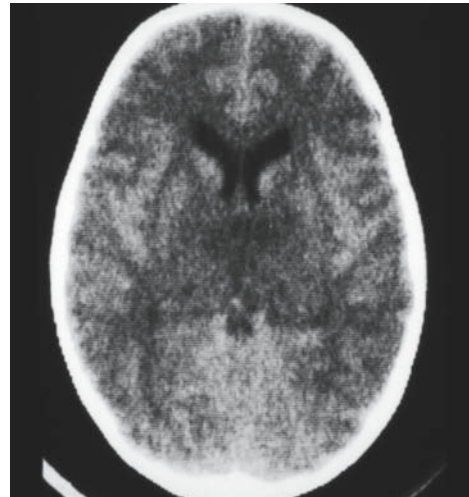


Fig. 13.2-6. Maple syrup urine disease. Computed tomography (CT) shows diffuse low density in the cerebral white matter. The third ventricle is narrowed, and the anterior horns of the lateral ventricles are relatively enlarged.

14 Mitochondrial Cytopathy

14.1 Wernicke's Encephalopathy

Wernicke's encephalopathy is a serious neurological disorder caused by vitamin B₁ or thiamine deficiency, chiefly in chronic alcoholics and rarely in children. It may be associated with starvation, prolonged intravenous treatment without vitamin supplementation, hemodialysis, and gastric stapling. The classic triad of clinical symptoms described by Wernicke (gait ataxia, ophthalmoplegia, confusion) are found in only one-third of patients during the initial examination.

Thiamine is a helper molecule required by three enzymes involved in two pathways of carbohydrate metabolism. Because intermediate products of these pathways are needed for the generation of other essential molecules in the cells, a reduction in thiamine can interfere with numerous cellular functions, leading

to serious brain disorders, including Wernicke's encephalopathy. Typical findings upon magnetic resonance imaging (MRI) show signal intensities in the medial thalami and periaqueductal regions of the midbrain. Single photon emission computed tomography (SPECT) shows bilateral frontal and frontoparietal hypoperfusion as well as basal ganglia hypoperfusion. Pathology is located in the mammillary bodies and periventricular regions of the third and fourth ventricles and aqueduct. There may be an acute hemorrhagic lesion, followed by with acute necrosis, vascular proliferation with endothelial hypertrophy, and relative sparing of neurons. Loss of myelin and gliosis is present in chronic lesions. Thalamic lesions are common [1].

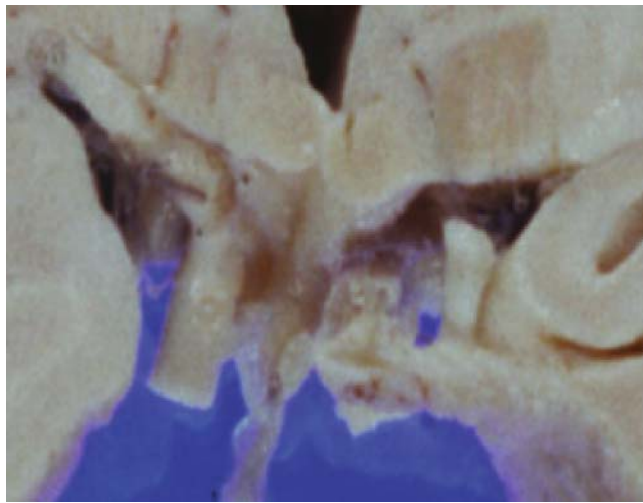


Fig. 14.1-1. Wernicke's encephalopathy. Mammillary bodies are slightly pigmented from previous hemorrhage in a child. (Courtesy of Dr. Kanaumi T.)

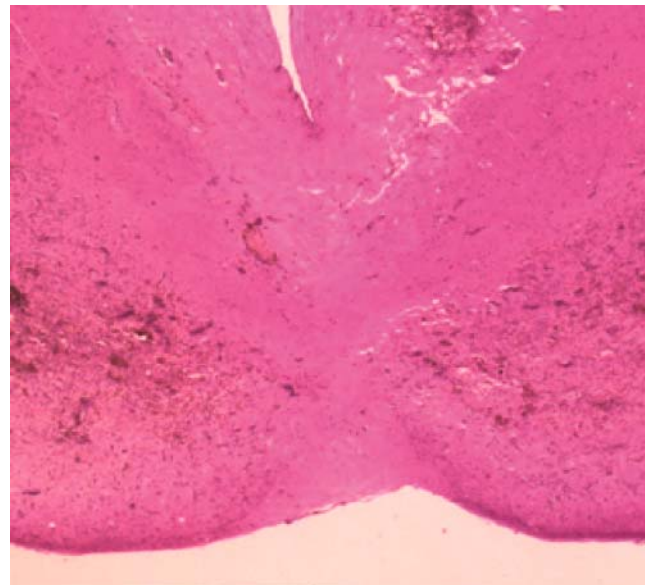


Fig. 14.1-2. Multiple perivascular hemorrhages are evident in both mammillary bodies of the case in 14.1-1. H&E.

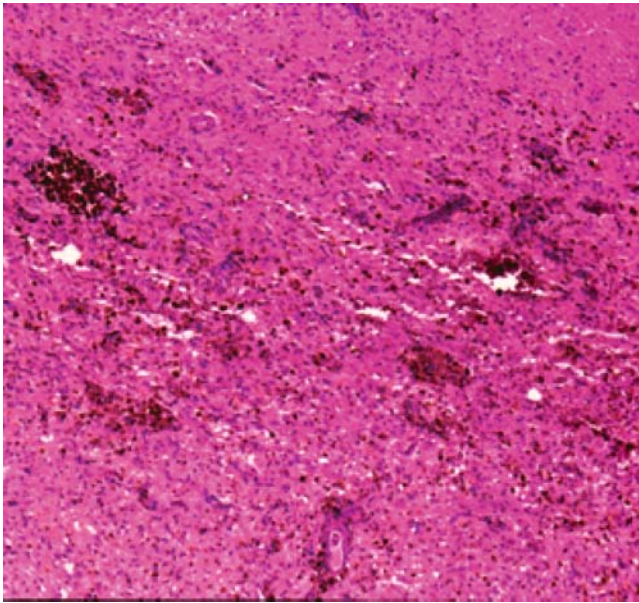


Fig. 14.1-3. Higher magnification of histology in the same case shows perivascular hemorrhage and gliosis. H&E.

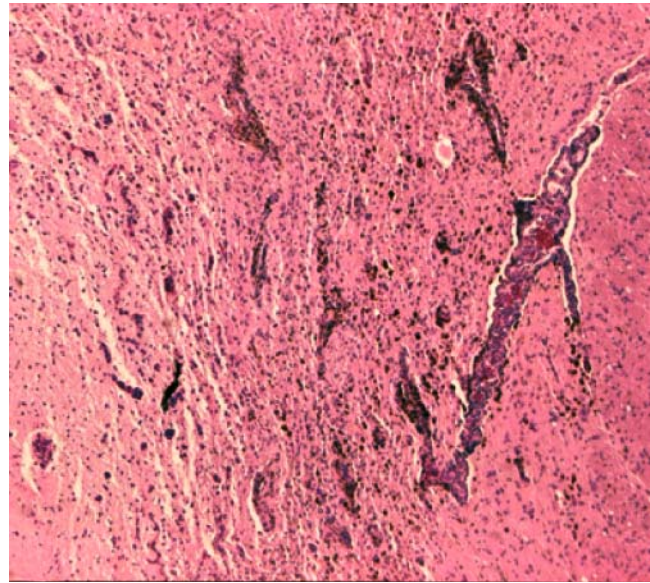


Fig. 14.1-4. There are perivascular hemosiderin-laden macrophages and gliosis in the medial part of the thalamus. H&E.

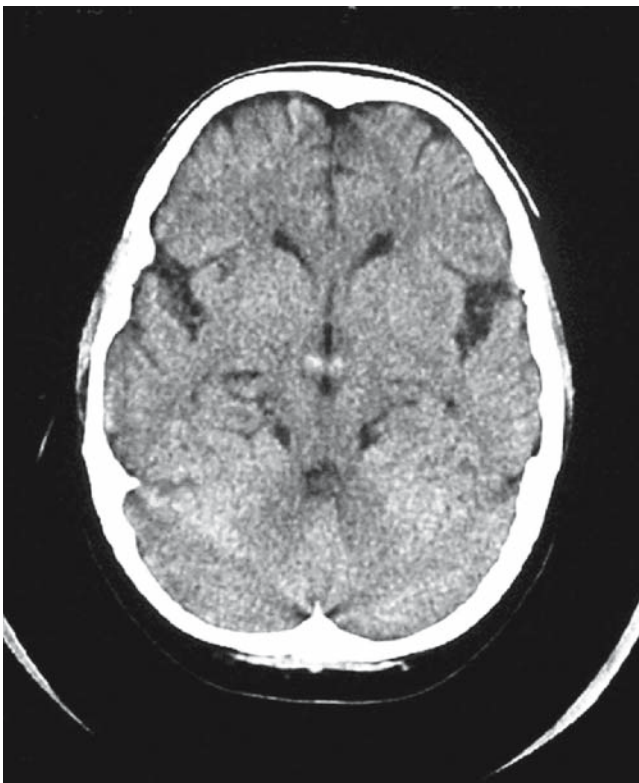


Fig. 14.1-5. CT shows high density in both mammillary bodies.

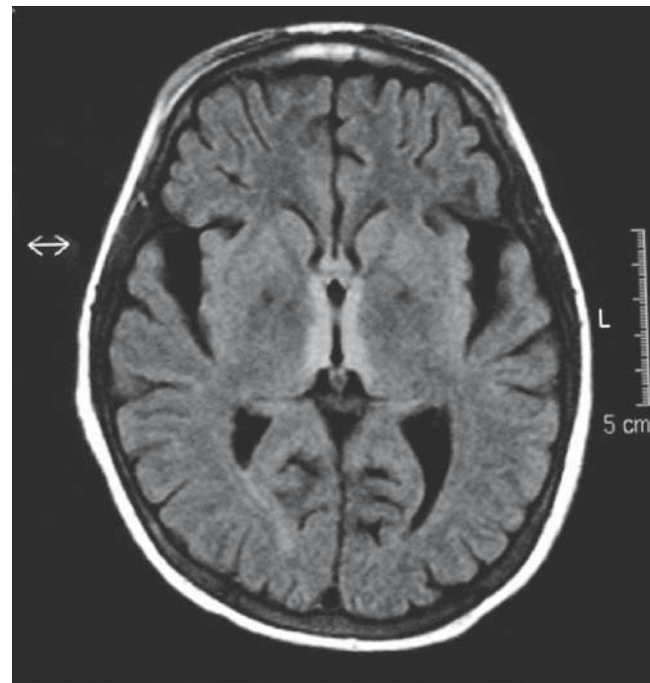


Fig. 14.1-6. T1-weighted MRI shows high intensity in periventricular parts of the bilateral thalami.

14.2 Subacute Necrotizing Encephalopathy of Leigh (Leigh's Syndrome)

Leigh's syndrome results from genetic abnormalities that produce defects of the pyruvate dehydrogenase complex, pyruvate carboxylase, cytochrome C oxidase (complex IV), NADH-dehydrogenase (complex I), or biotinidase deficiency. Altogether, 18% of the patients have mitochondrial DNA (mtDNA) mutations [2]. All ages may be affected, but it usually presents in infants, with hypotonia, failure to thrive, nystagmus, respiratory difficulties, ataxia, and psychomotor retardation.

Pathology

In the central nervous system (CNS), there are bilateral, symmetrical areas of gray and white matter softening, predominantly in the putamen and periaqueductal gray matter of the midbrain and often in the thalamus, substantia nigra, red nuclei, corpora quadrigemina, dentate nucleus of the cerebellum, inferior olives, and tegmentum of the pons and medulla. There are symmetrical

foci of partial necrosis, spongy changes, capillary proliferation, and isolated intact neurons. The lesions resemble those of Wernicke's disease; however, subacute necrotizing encephalopathy of Leigh (SNE) rarely has mammillary body lesions, and Wernicke's disease does not involve the substantia nigra. Demyelination may occur in the optic nerves and tracts and the dorsal spinal columns. Electron microscopy (EM) reveals abnormal mitochondria in Purkinje cells, granule cells, and choroid plexus epithelium [2].

Muscle tissue in pyruvate dehydrogenase complex deficiency shows lipid droplets adjacent to mitochondria and an excess of primitive type IIC fibers, suggesting arrested development. There are rarely ragged red fibers, but ultrastructural examination frequently shows mitochondrial changes: increased size, bizarre shapes, osmophilic inclusions, and disoriented cristae. Hypertrophic cardiomyopathy, renal tubulopathy, liver steatosis, and retinal pigmentary degeneration may be present.

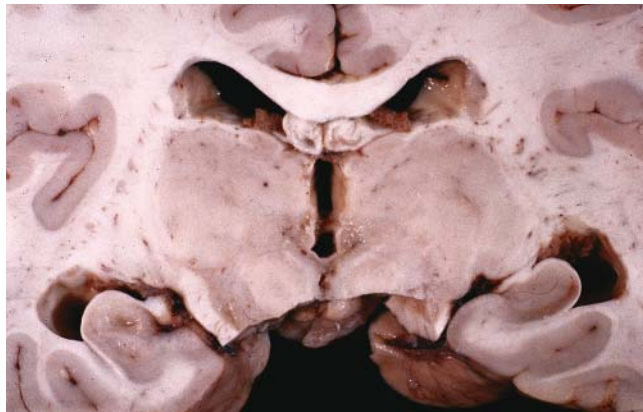


Fig. 14.2-1. Leigh's syndrome. There is necrosis in the caudate nucleus, medial parts of thalamus, and substantia nigra.

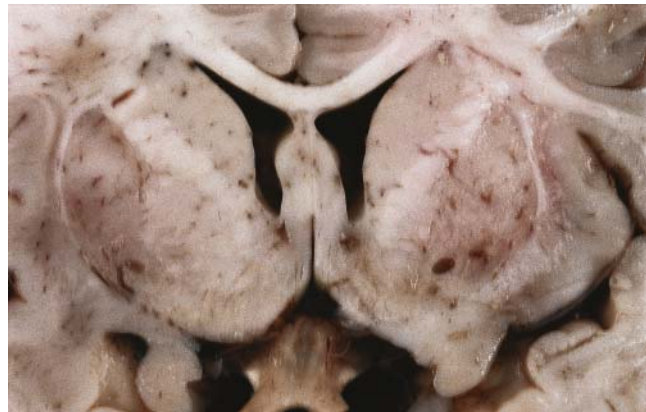


Fig. 14.2-2. The putamen shows necrosis with congestion.

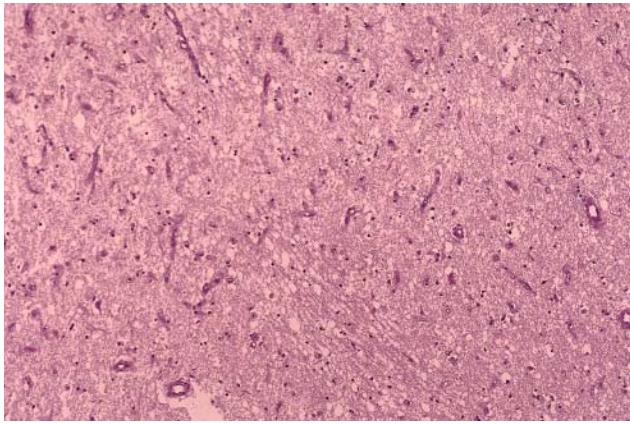


Fig. 14.2-3. The basal ganglia, thalamus, and midbrain exhibit spongy changes, increased vascularity, and relatively preserved neurons. H&E.

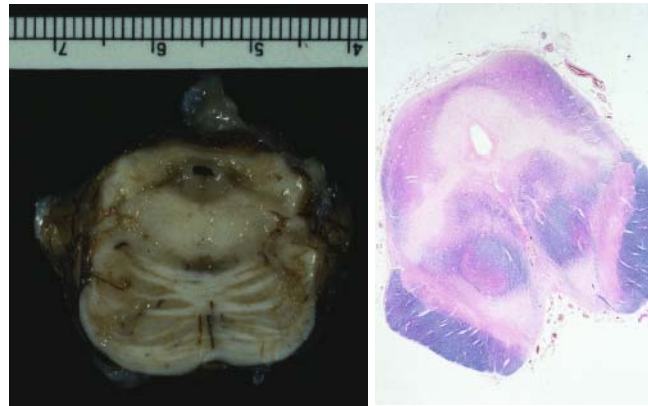


Fig. 14.2-4. Note the necrosis in the periaqueductal gray matter (*left*) and spongy changes in the periaqueductal gray matter and substantia nigra of the midbrain (*right*).

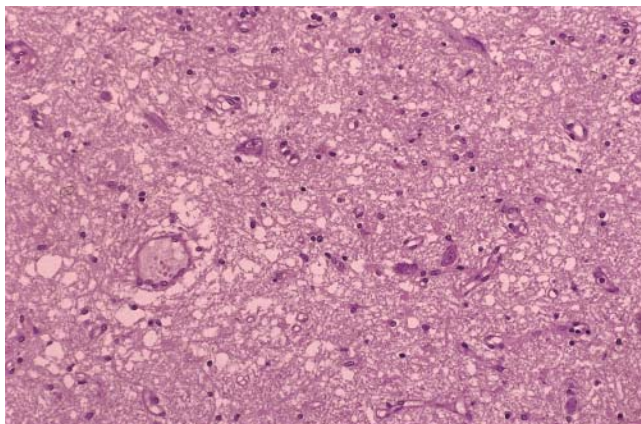


Fig. 14.2-5. Spongy changes, increased vascularity, and relatively preserved neurons are seen in the midbrain. H&E.

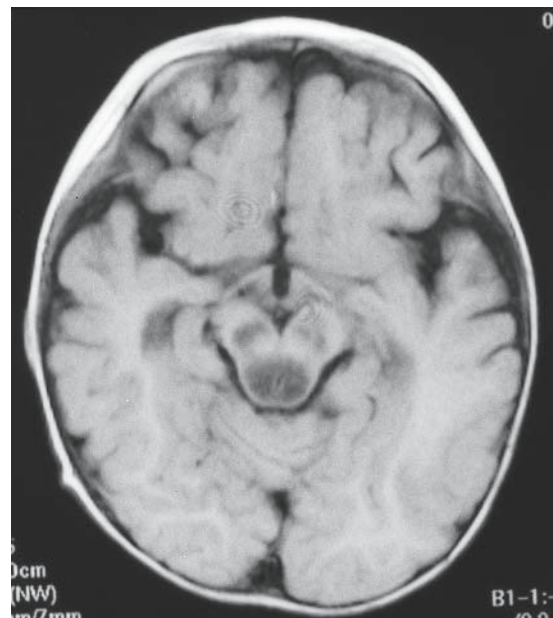


Fig. 14.2-6. MRI shows low intensity in the periaqueductal gray matter and substantia nigra of the midbrain.

14.3 Mitochondrial Encephalomyopathy, Lactic Acidosis, and Stroke-like Episode (MELAS) Syndrome

In the mitochondrial encephalomyopathy/lactic acidosis/stroke-like episode (MELAS) syndrome, early development is normal. Muscle weakness begins before central neurological dysfunction, which is apparent between 2 years of age and young adulthood. Most patients have partial or generalized seizures.

Pathology

There are multiple solitary or confluent foci of necrosis in both cerebral cortices and occasionally in the thalami and basal ganglia. These infarct-like lesions vary in size and age and are located at the top of the cerebral gyri, not in the sulci. Microscopy reveals loss of neurons and prominence of capillaries. Layer IV may be preferentially involved. Older lesions cavitate and tend to be in the occipital cortex. Neurons in Sommer's sector of Ammon's horn are preserved. Gliosis is prominent in the subcortical white matter. The deep white matter is normal. Deposits of calcium (seen on neuroimaging) is

present in capillary walls of the caudate nuclei, globus pallidus, thalamus, and midbrain. In the cerebellum, Purkinje cells and granular neurons are focally absent. The dentate nucleus exhibits neuronal loss, astrocytosis, capillary proliferation, and calcium deposits in the capillary walls. Ultrastructural studies fail to show mitochondrial abnormalities in neurons or glial cells, but marked accumulation of mitochondria (with occasional structural abnormalities) is observed in the smooth muscle cells, pericytes, and endothelial cells of small cerebral arteries. The pathogenesis of the lesions is still being debated.

Genetics

About 80% of MELAS patients have a mutation (A3243G) in the tRNA leucine gene that affects the activities of complexes I and IV of the respiratory chain. There is overlap with Leigh syndrome [3–5].

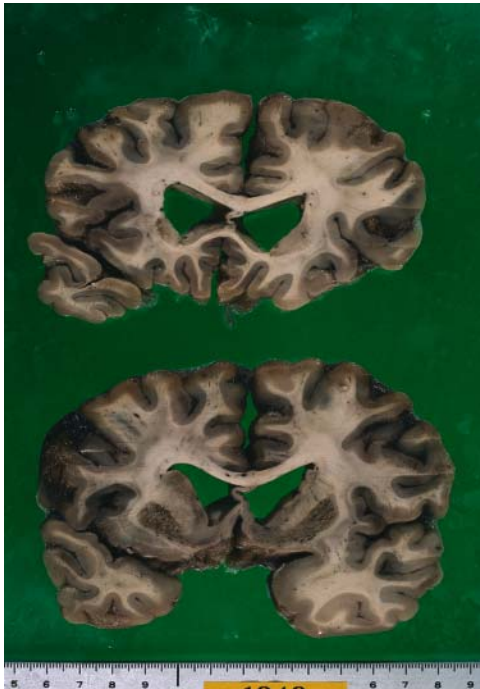


Fig. 14.3-1. MELAS syndrome. The brain shows mild atrophy with ventricular dilatation and focal softening in the left inferior frontal gyrus.

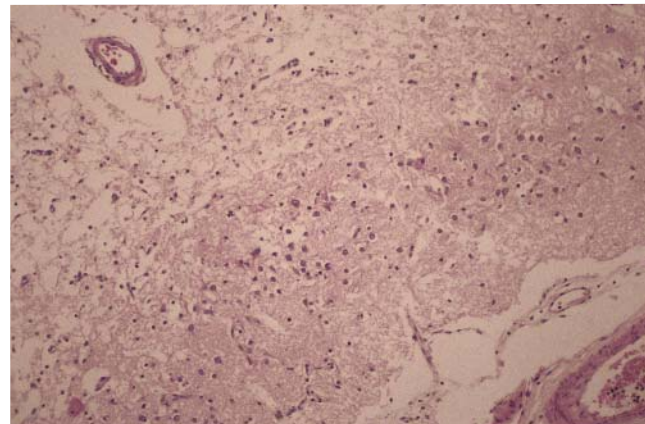


Fig. 14.3-2. Neuronal loss and spongy changes in the cortex. H&E.

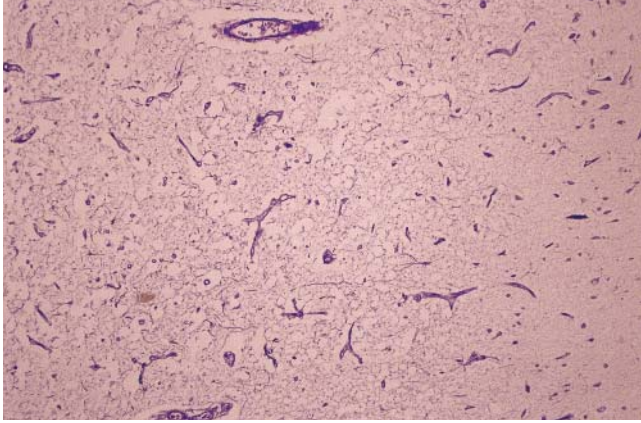


Fig. 14.3-3. Spongy change, mild fibrillary astrogliosis, and increased vascularity in the cortex. Holzer stain.

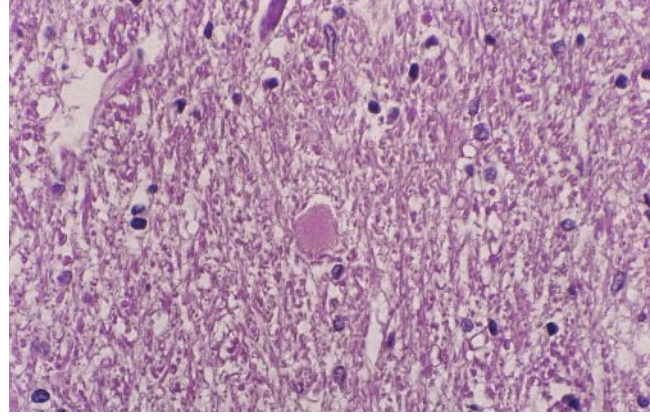


Fig. 14.3-4. Axonal swelling in the cerebral white matter. H&E.

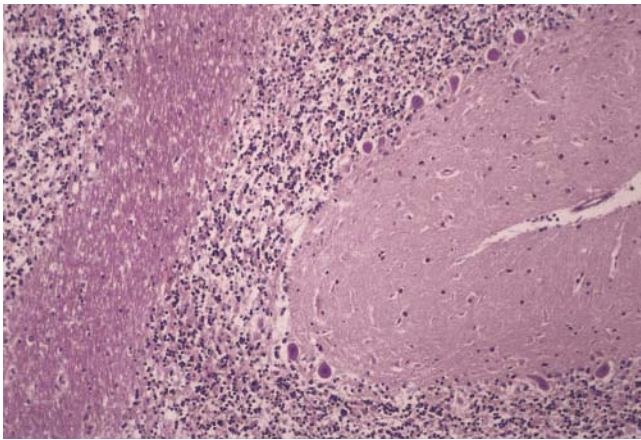


Fig. 14.3-5. The cerebellar cortex shows some loss of Purkinje and granular cells. H&E.

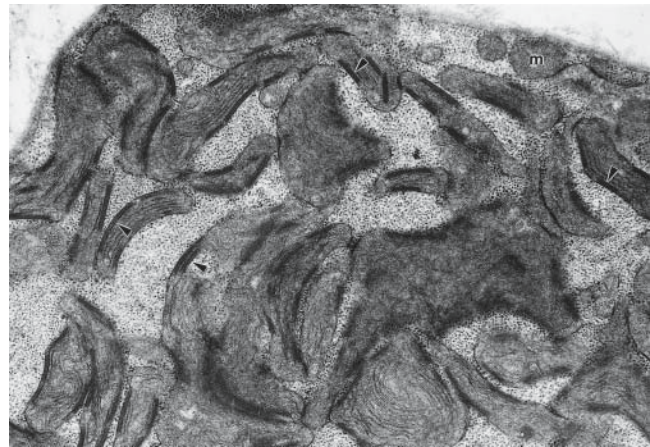


Fig. 14.3-6. EM of a muscle biopsy shows altered subsarco-plasma mitochondria. These mitochondria exhibit variability in size, shape, and substructure. Most contain crystalline curvilinear structures reminiscent of "parking lot" inclusions, which are in continuity with the cristae. $\times 24\,000$.

14.4 Alpers-Huttenlocher Syndrome (Progressive Neuronal Degeneration in Childhood With Liver Disease)

Alpers-Huttenlocher syndrome presents with seizures (sometimes as status epilepticus) during the first 2 years of life. Development stagnates, and seizures become prominent, sometimes with *epilepsia partialis continua*. Spasticity, dementia, and blindness ensue. Brain imaging reveals progressive brain atrophy. The liver disease may progress to liver failure.

Pathology

The brain shows characteristic regions of thinned, granular, discolored cortex. The medial occipital cortex is frequently involved. Histological studies reveal characteristic widespread, patchy involvement of the cortex, where astrocytosis, vacuolization, neuronal loss,

hypertrophic astrocytes, and capillary proliferation replace the cortex. Alzheimer type II astrocytes are seen when there is liver failure. The liver shows severe diffuse microvesicular fatty change, hepatocyte necrosis, bile duct proliferation, and nodular cirrhosis.

Genetics

The disorder is rare, and its pathogenesis is controversial. There have been familial cases with autosomal recessive inheritance, and there is increasing evidence of a mitochondrial disorder. Complex IV deficiency, mtDNA depletion, and mtDNA polymerase deficiency have been described [4,6].



Fig. 14.4-1. Alpers-Huttenlocher syndrome. Coronal sections of anterior cerebrum showing focal discoloration and atrophy in the cortex.

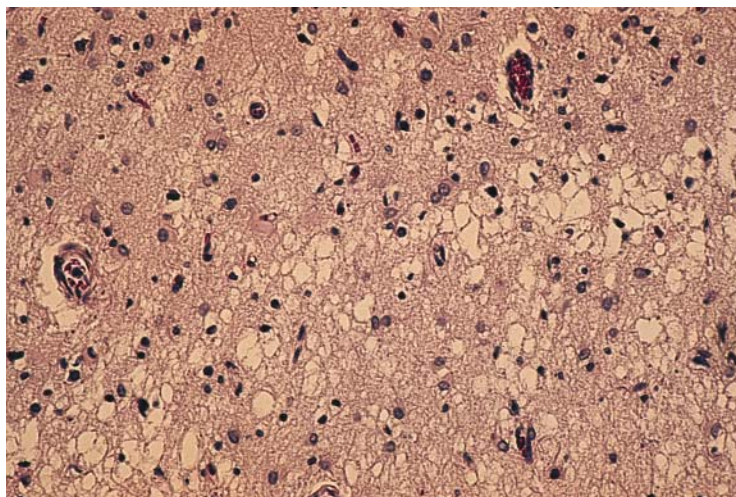


Fig. 14.4-2. Neuronal loss and gliosis in the cortex. H&E.

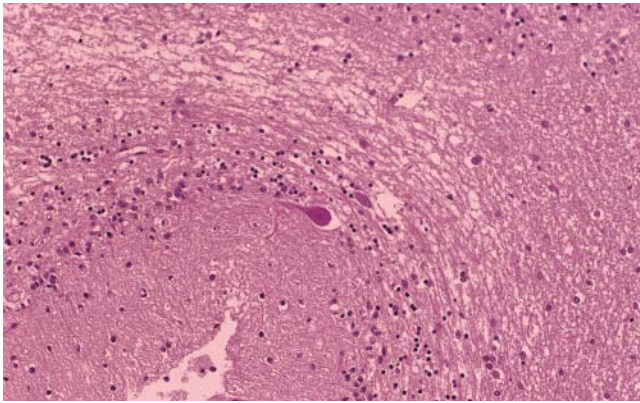


Fig. 14.4-3. Cerebellum. Note the loss of Purkinje cells and granular cells. H&E.

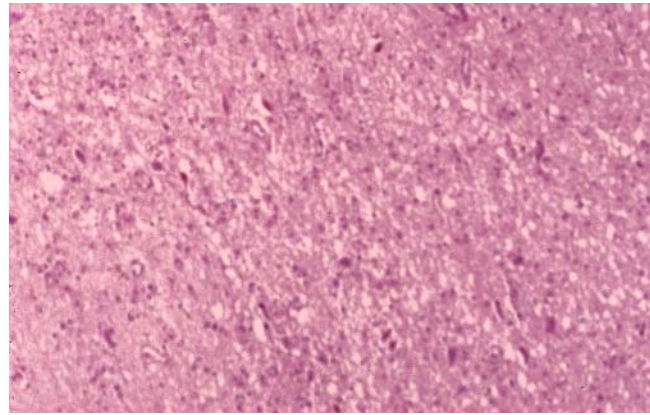


Fig. 14.4-4. Substantia nigra exhibits neuron loss and spongy changes. H&E.

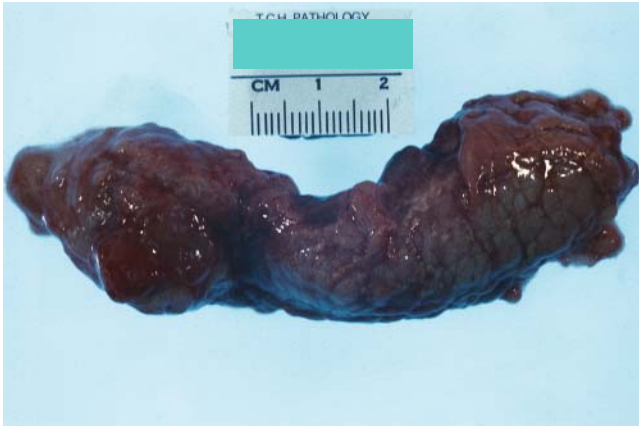


Fig. 14.4-5. Liver cirrhosis.

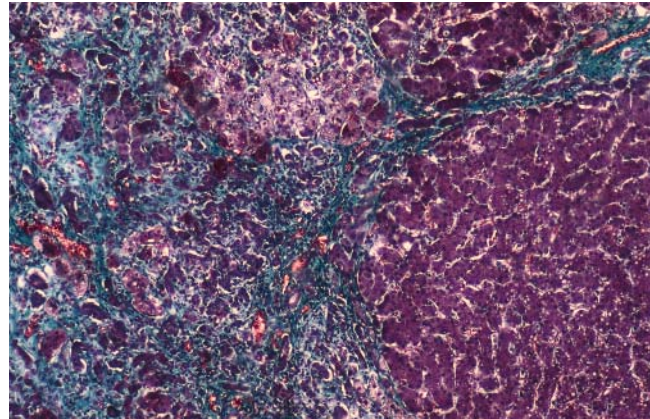


Fig. 14.4-6. Liver cirrhosis with marked fibrosis and regenerating nodules. Trichrome stain.

15 Other Heredodegenerative Diseases

15.1 Dentato-Rubro-Pallido-Luysian Atrophy

Dentato-rubro-pallido-luysian atrophy (DRPLA) is a rare familial disorder comprising degeneration of the cerebellar efferent system and of the pallido-luysian tracts. Ataxic choreoathetoid, pseudo-Huntington, and myoclonic epilepsy forms of this syndrome have been described. The disorder begins between 7 and 20 years of age.

Pathology

Gross examination discloses a reduction in the size of the brain stem and the superior cerebellar peduncles. Histopathological changes consist of atrophy affecting the dentate nucleus, the globus pallidus (particularly in

the external segment), the corpus Luysii, tegmentum of the midbrain and pons, superior colliculi and red nucleus, the reticular formation, and the central gray matter. Neuronal loss in the fastigial nucleus and degeneration of the fastigiovestibular system have been described. There are ubiquitinated neuronal and glial intranuclear inclusions.

Genetics

The disorder is dominantly inherited. It is caused by a mutation in the gene for atrophin-1 (located at 12p13p31), which produces a CAG repeat expansion [1].



Fig. 15.1-1. Dentato-rubro-pallido-luysian atrophy (DRPLA) Decreased neurons in the dentate nucleus. KB stain.

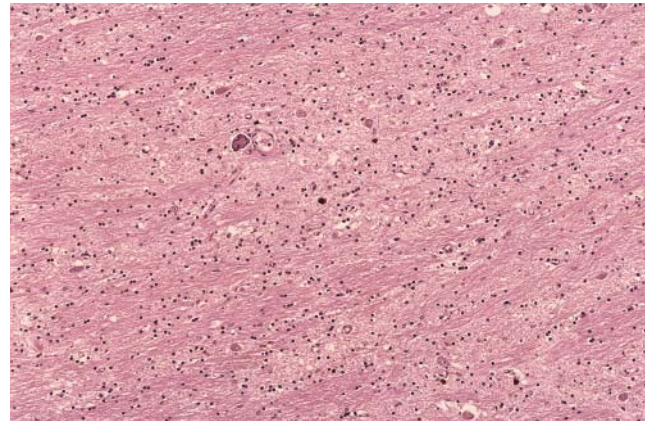


Fig. 15.1-2. Decreased neurons in the red nucleus. H&E.

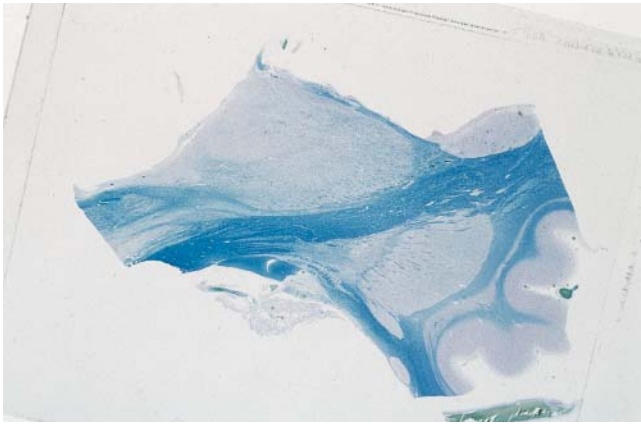


Fig. 15.1-3. Atrophy of the basal ganglia, thalamus, and mid-brain. KB stain.

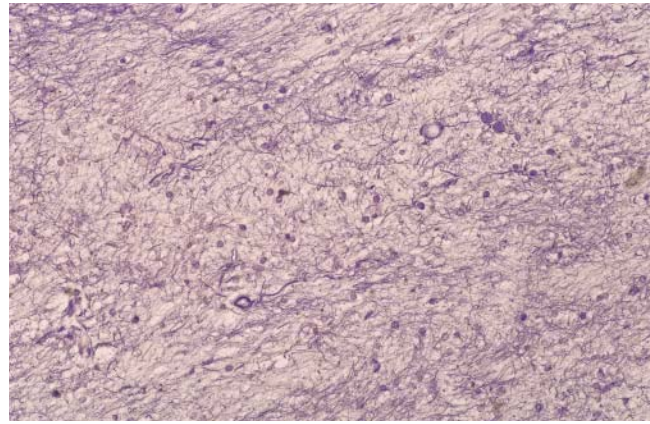


Fig. 15.1-4. Gliosis in the atrophic globus pallidus. Holzer stain.

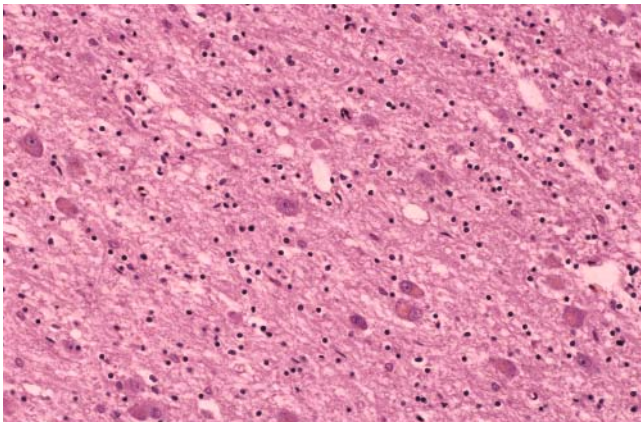


Fig. 15.1-5. Neuronal loss and spongy change in the Luysian body. H&E.

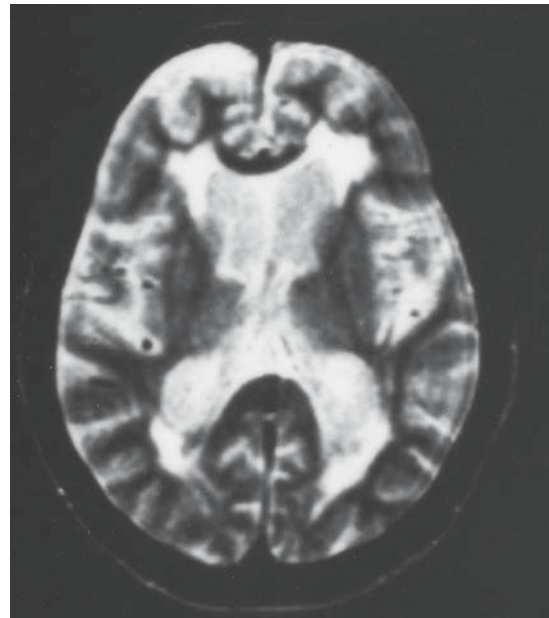


Fig. 15.1-6. T2-weighted magnetic resonance imaging (MRI) shows atrophy of the cerebrum, dilatation of the lateral and third ventricles, and focal high intensity of periventricular white matter.

15.2 Friedreich's Ataxia

Friedreich's ataxia is an autosomal recessive degenerative disorder characterized clinically by an early onset of progressive spinocerebellar ataxia, corticospinal tract signs, skeletal involvement, and cardiomyopathy.

Pathology

Friedreich's ataxia affects both the central nervous system (CNS) and peripheral nervous system (PNS). In the CNS, the characteristic lesions are in the spinal cord. The posterior columns and the dorsal spinocerebellar tract of Flechsig are shrunken with pale myelin. Neurons of Clarke's column disappear. There is fiber loss in the gracile fasciculus and less in the cuneate fasciculus. The ventral spinocerebellar tract of Gowers is less severely involved. The pyramidal tract axons exhibit a dying-back process showing progressive loss as they descend in the cord. In the brain stem, there is gliosis and loss of neurons in the gracile and cuneate nuclei. In the cerebellum, there is marked cell loss, with gliosis in the

dentate nuclei associated with degeneration of the superior cerebellar peduncles. The cerebellar white matter is gliotic. Variable pathology of the optic nerves and cerebral hemispheres has been reported.

In the PNS, there is a decrease in the density and total number of myelinated fibers. The density of small myelinated fibers is normal, but the axonal size and myelin thickness are reduced. There is loss of large myelinated fibers in the posterior roots, and some fibers have reduced myelin sheaths for the axonal diameters. In the spinal ganglion, there is moderate loss of ganglion cells, with proliferation of capsule cells [1].

Genetics

The disease is an autosomal recessive cerebellar ataxia caused by a mutation in the gene for frataxin (a mitochondrial protein) in the centromeric region of chromosome 9.



Fig. 15.2-1. Friedreich's ataxia. Spinal cord, with regional loss of myelin. H&E/LFB.

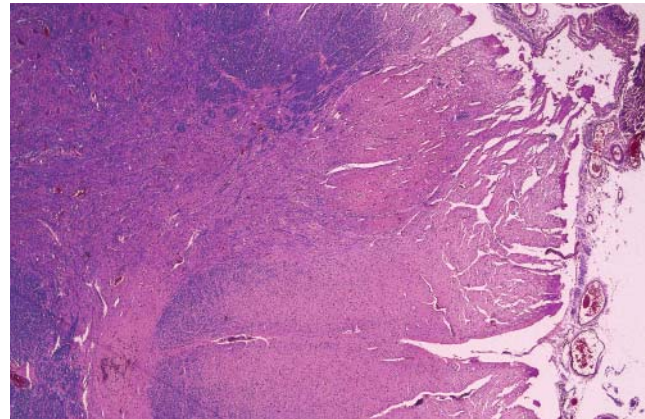


Fig. 15.2-2. Spinal cord, with loss of myelin sheaths in the spinocerebellar tract and posterior column. H&E/LFB.

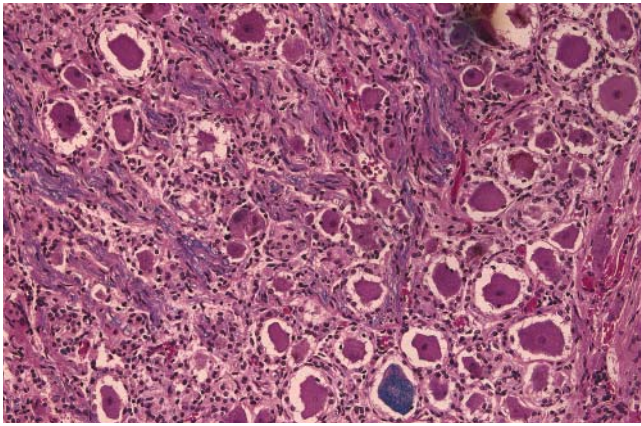


Fig. 15.2-3. Dorsal root ganglion, with loss of neurons and proliferation of capsule cells. H&E/LFB.

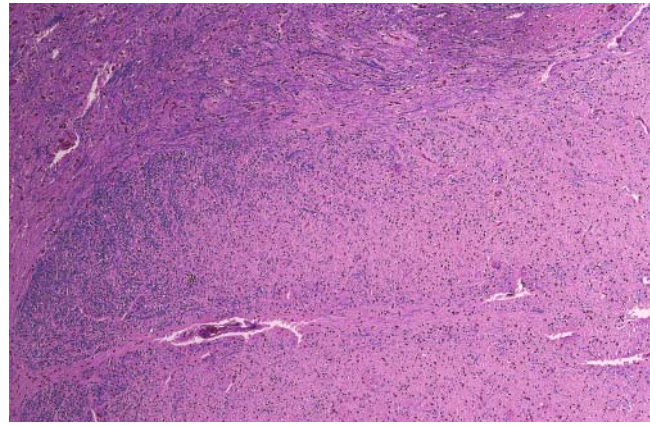


Fig. 15.2-4. Loss of myelin sheaths in the posterior column. H&E/LFB. In some cases, neuronal cell loss is seen in the nuclei of cranial nerves VIII, XI, and XII.

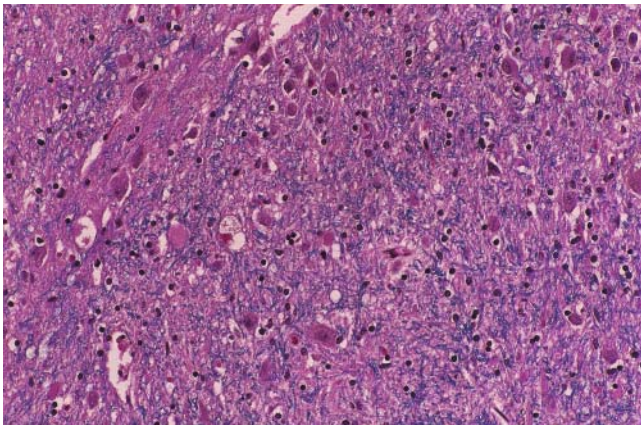


Fig. 15.2-5. Axonal swellings in the nucleus gracilis. H&E/LFB.

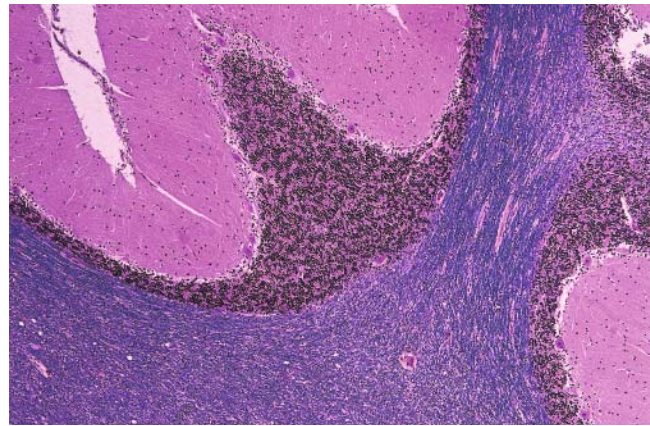


Fig. 15.2-6. Cerebellum shows a partial decrease of Purkinje cells and myelin sheaths. Depletion of Purkinje cells in the superior vermis and in neurons in corresponding parts of the inferior olivary nuclei has been described in some cases. H&E/LFB.

15.3 Lafora Body Disease

Lafora body disease is an autosomal recessive inherited form of progressive myoclonus epilepsy. It has abnormalities of carbohydrate metabolism with the accumulation of glucose phosphate polymers (polyglucosan) in various cells in the body. The first manifestations begin between 6 and 19 years of age, with decreased scholastic performance, behavior disorder, visual and mental deterioration, and seizures. Antemortem diagnosis may be made by demonstrating PAS-positive, diastase-resistant, basophilic, and variably metachromatic inclusion bodies (Lafora bodies) in liver, striated muscle, or sweat gland biopsies.

Pathology

The brain shows diffuse cortical atrophy, mostly in the globus pallidus and thalamus. Lafora bodies range in size from 1 to 30 μm in diameter. They have a concentric organization: a basophilic core surrounded by a pale zone. They may appear as single or multiple inclusions in the perikaryon, where they displace the nucleus and Nissl substance to the side. They may be free in the

tissue. They are scattered in the gray matter and accumulate in the substantia nigra, dentate nuclei, superior olive, pontine reticular nuclei, basal ganglia, and cerebral cortex.

Electron microscopy (EM) reveals that Lafora bodies lack a limiting membrane except in striated muscles. The core contains a dense bundle of fibrils about 6–8 nm in diameter. Some of the fibrils have a bead-like appearance. The fibrils are arranged in whorls at the center and radiate out at the periphery. Between the fibrils are dense, granular structures about 15–50 nm in diameter. Lafora bodies contain insoluble aggregates of glucose phosphate polymers (polyglycosans) [2–5].

Genetics

A gene locus is mapped to chromosome 6q. Many cases of Lafora body disease are caused by mutations in the *EPM2A* gene, which codes for the protein laforin, a protein tyrosine phosphatase, and some in the *EPMA2B* gene, which encodes malin, the laforin-interacting ubiquitin E3 ligase.

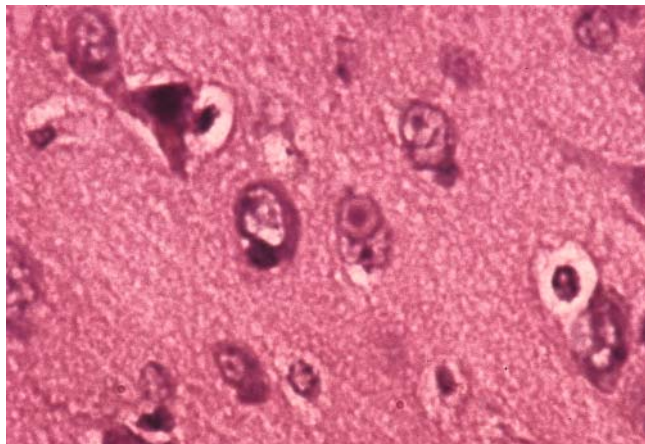


Fig. 15.3-1. Lafora body disease. Cerebral cortex exhibiting concentric Lafora bodies. H&E.

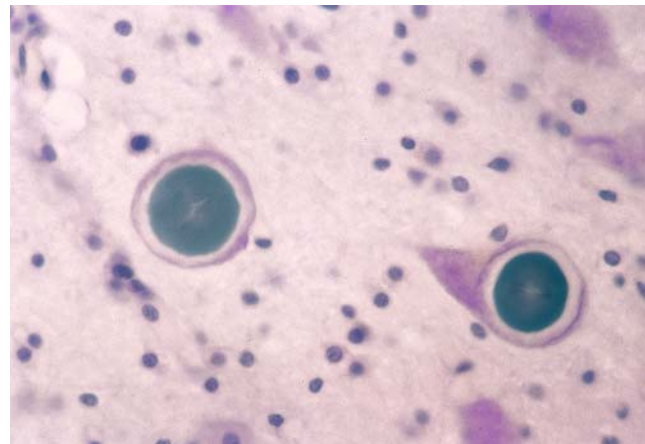


Fig. 15.3-2. Lafora body in the dentate nucleus. Alcian blue.

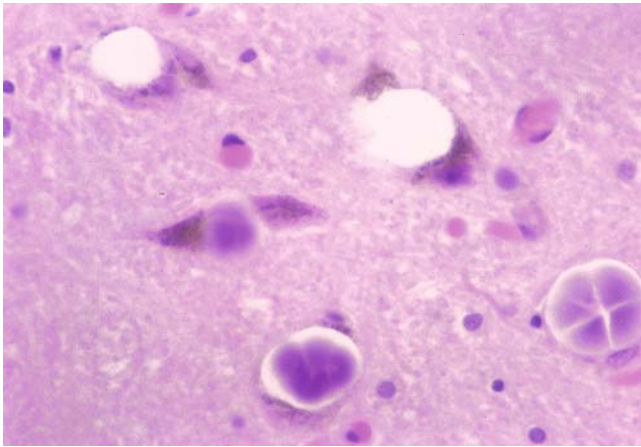


Fig. 15.3-3. Lafora body in the substantia nigra. H&E.

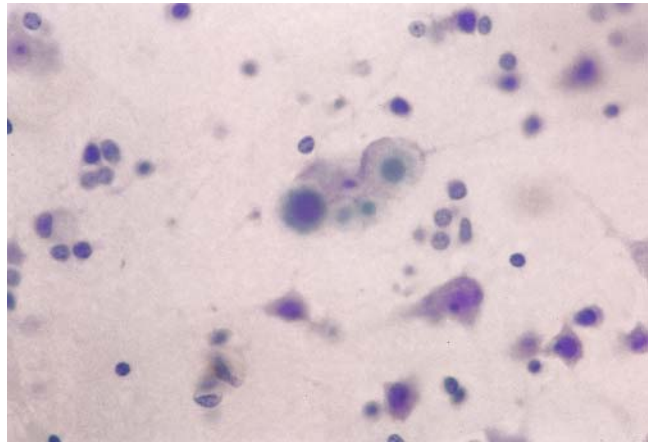


Fig. 15.3-4. Lafora body in the precentral gyrus. Alcian blue.

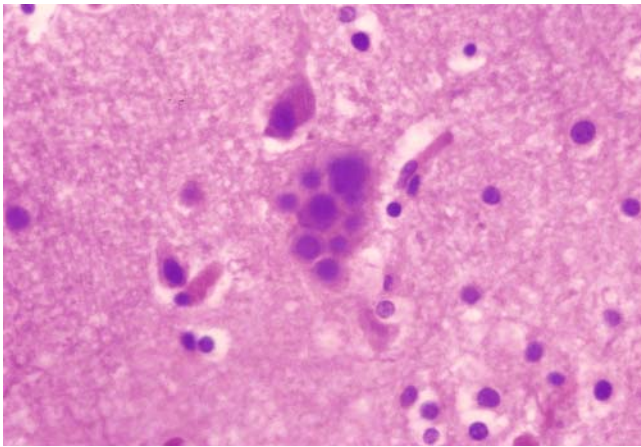


Fig. 15.3-5. Multiple Lafora bodies in the precentral gyrus. H&E.

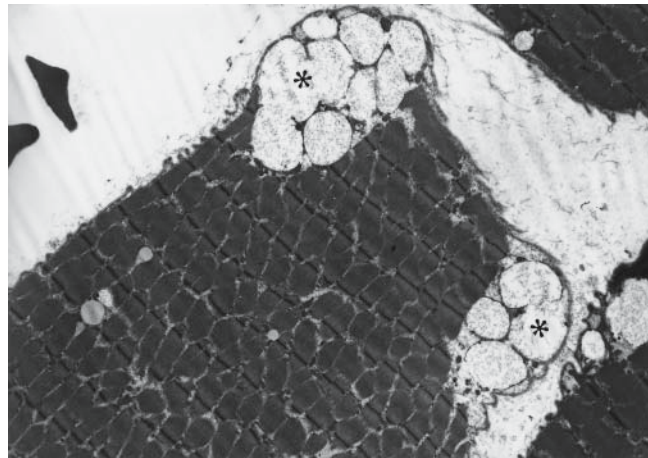


Fig. 15.3-6. EM of a Lafora body in skeletal muscle.

15.4 Rett Syndrome

Rett syndrome [6] is a disorder of the nervous system caused by abnormalities in the *MeCP2* gene [7,8], which is involved in the regulation of gene translation. Most cases are sporadic, although there are rare familial cases. The classic disorder affects girls, who appear normal at birth but have delayed motor and cognitive function that becomes obvious during the first 2 years of life. The girls develop characteristic hand stereotypies, abnormal gait, a delay in head growth, and loss of hand use and speech. Some girls never walk. They usually develop seizures, severe autonomic malfunction, and scoliosis. There are Rett variants; some girls retain some speech

or hand use. The disorder occurs in males sometimes presenting as a severe developmental delay, encephalopathy, and early death. In some boys the phenotype is that of Angelman syndrome or of mental retardation. Rett girls may survive for decades, requiring total care. There is an increased incidence of sudden death during their teen-age years [9]. The pathology is concentrated in the nervous system. The brain is microcephalic, weighing about 900 g. There is maturation failure of individual neurons, which exhibit a paucity of dendrites and dentritic spines [10]. As yet there is no specific therapy [8].



Fig. 15.4-1. Rett syndrome. Coronal sections of a small Rett brain showing no obvious malformation and a normal cortex, white matter, and basal ganglia.



Fig. 15.4-2. Section of Rett cortex and myelin shows normal staining of the myelin with LFB/H&E.



Fig. 15.4-3. Rett brain (*right*) and trisomy 21 brain (*left*). The brains are approximately the same weight. The cerebellum in the Rett brain is relatively larger than that in the trisomy 21 brain.

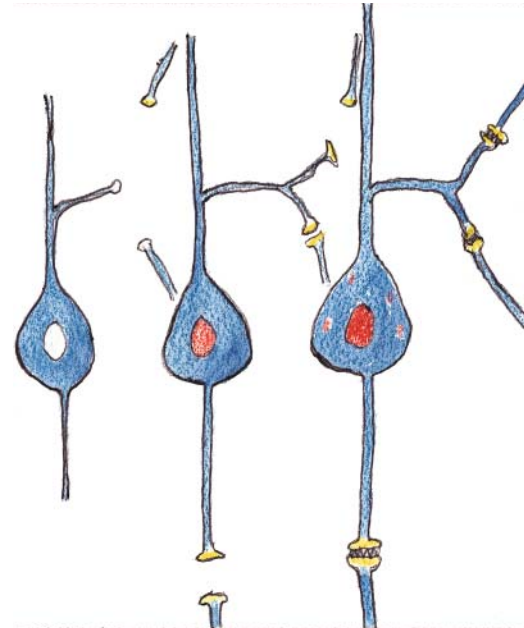


Fig. 15.4-4. Cartoon of MeCP2 expression. (in red) is expressed in the neuronal nucleus before the first synapses occur and it continues to be expressed in increasing amounts in the nucleus as the neuron matures, developing more dendritic branches and synapses. There is a small amount of MeCP2 in the cytoplasm.

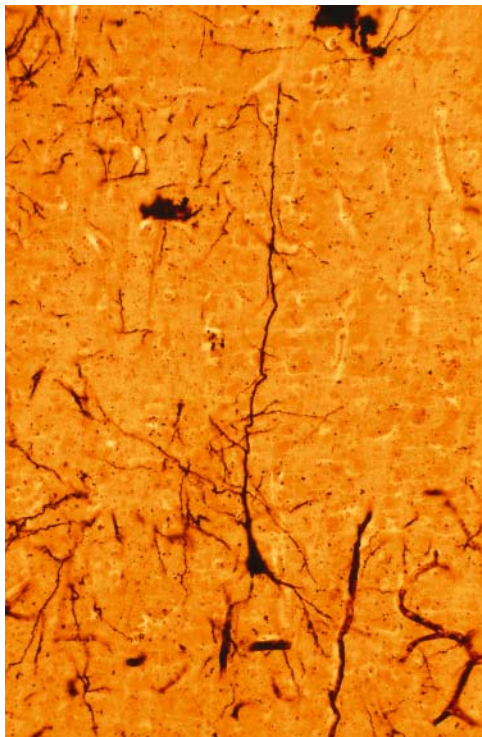


Fig. 15.4-5. Golgi impregnation of a pyramidal neuron in Rett syndrome. Note the paucity of apical dendritic branches.

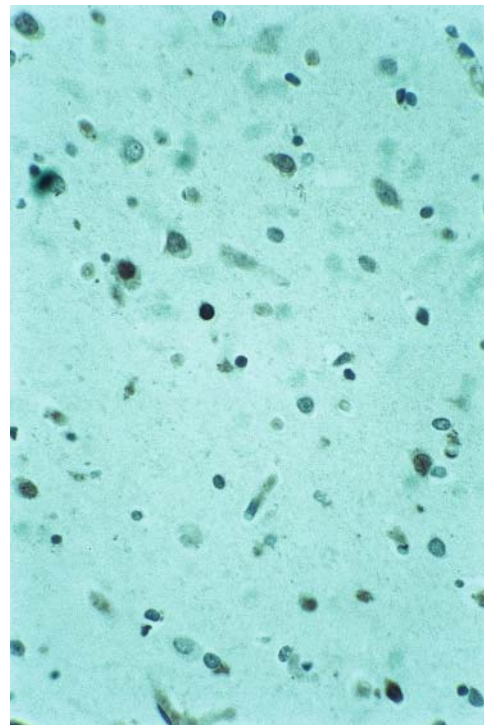


Fig. 15.4-6. Cortex in a Rett syndrome brain stained with antibody to MeCP2. Some neurons are negative; others have a low degree of expression; and still others have a high degree of expression. There is a small amount of reactivity in the cytoplasm. The glia and endothelium are negative.

15.5 Autism

Autism is a persistent neuropsychiatric syndrome of early childhood with a prevalence of 5–10/10 000 population. Males are more often affected than females. The diagnosis is clinical, based on behavior: failure of social development, lack of eye contact, delay in verbal or other communication skills, and stereotypic behavior. The presentation and clinical progression vary over a wide spectrum. In Asperger's syndrome, language skills are maintained.

Genetics

No single gene has been identified, but several have been suggested, some involving serotonin and

dopamine metabolism. Concordance in monozygotic twins is >90%. The pathology studies are confusing. MRI suggests a range of findings: normal brain or megalencephaly; reduced or enlarged lobules VI and VII of the cerebellum; enlarged or reduced parietal lobe; reduced size of the midbrain and medulla. Neuropathology reports are equally confusing; normal brain size or megalencephaly; reduced numbers of Purkinje and granular neurons in the neocerebellar cortex; increased neuronal numbers in the amygdala and other limbic regions; reports of aberrant cortical lamination and malformed inferior olivary nuclei. SPECT studies suggest that autism is associated with anomalous cerebral asymmetry and left hemispheric dysfunction [11].



Fig. 15.5-1. Autism. Gross brain is usually reported to be normal.

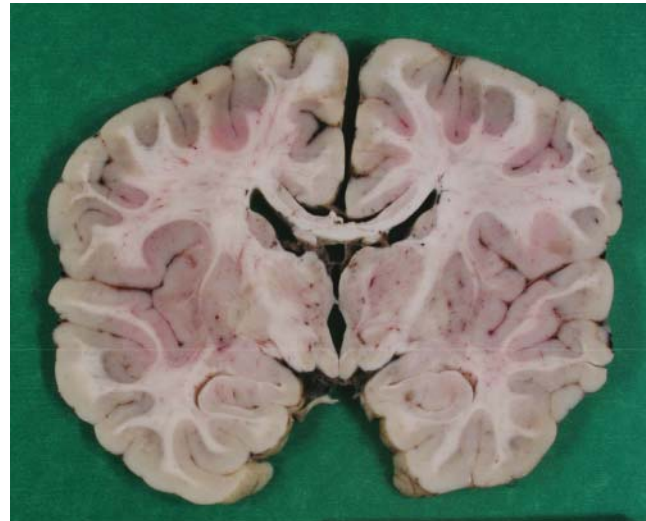


Fig. 15.5-2. Coronal section reveals a persistent cavum pellucidum.

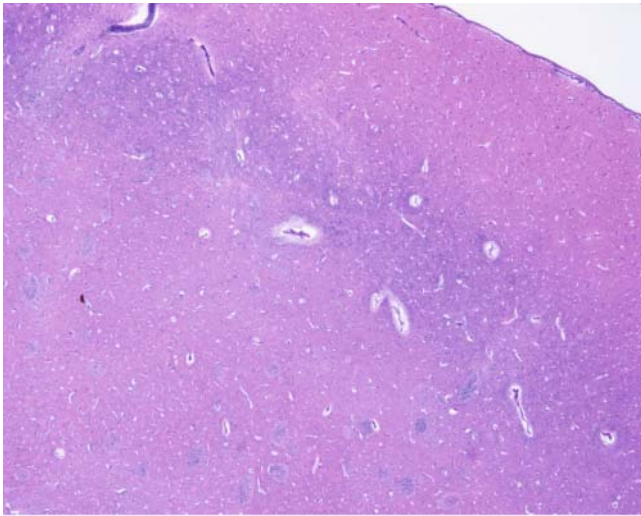


Fig. 15.5-3. The caudate nucleus shows dysplasia, with diffusely increased myelination. H&E/LFB.

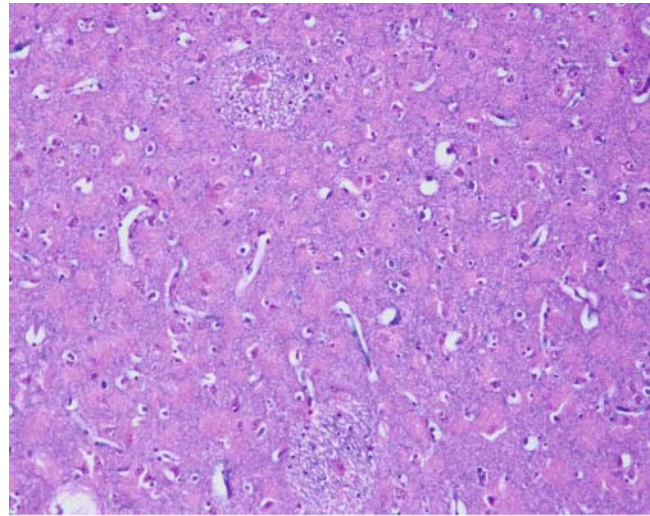


Fig. 15.5-4. Slightly myelinated fibers are found around the neurons. H&E/LFB.



Fig. 15.5-5. The central part of the corpus callosum is thin and irregular.

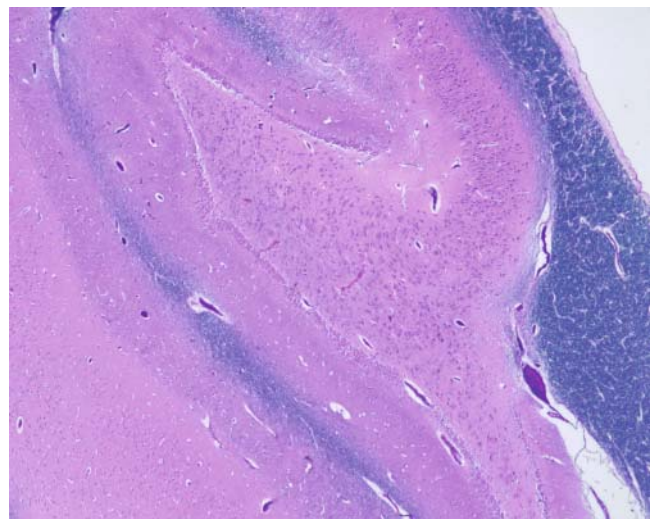


Fig. 15.5-6. In the hippocampus, the pyramidal cell layer is thick with increased neuronal density, predominantly in CA3 and CA4. H&E/LFB.

15.6 Congenital Myotonic Dystrophy

Congenital myotonic dystrophy (DM1) is a dominantly inherited disease of muscle, heart, brain, and lens. Its symptoms are evident from birth. The mother has myotonic dystrophy and passes it on to the child in a more severe form. Congenital myotonic dystrophy is associated with developmental delay and intellectual disabilities. The neonate born from a mother with myotonic dystrophy (see Chapter 25, Section 25.5) usually shows marked hypotonia, respiratory distress, hydrocephalus, and periventricular leukomalacia (PVL) [12].

Neuroimages of congenital DM1 shows characteristic hyperintensity of the white matter at the posterosuperior trigone, and ventricular dilatation. Classic DM1 shows hyperintense lesions in the bilateral frontal and/or temporal regions [13].

The brain in congenital myotonic dystrophy sometimes shows hydrocephalus, and there is frequently evidence of ischemic injury, such as periventricular leukomalacia. The pathogenesis of intellectual disabilities is unknown. The role of the expansion of CTG or CCTG repeats is poorly understood.

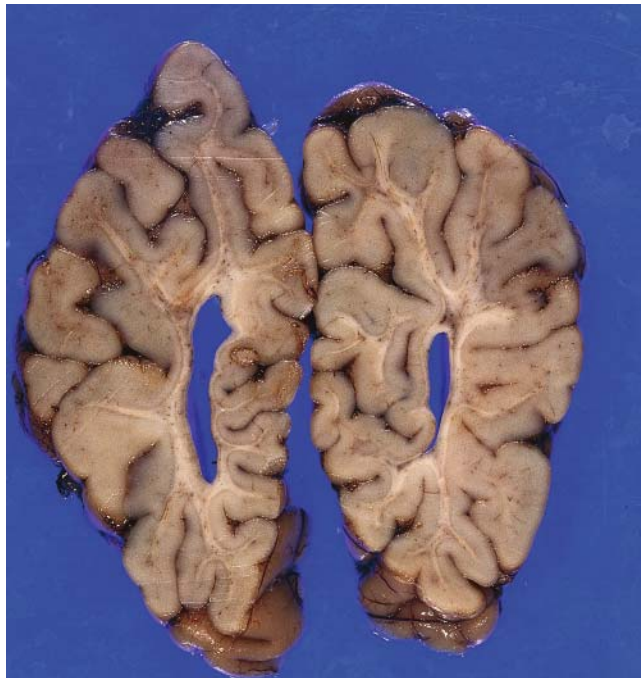


Fig. 15.6-1. Congenital myotonic dystrophy. There is atrophy of the cerebral white matter with periventricular leukomalacia (PVL).

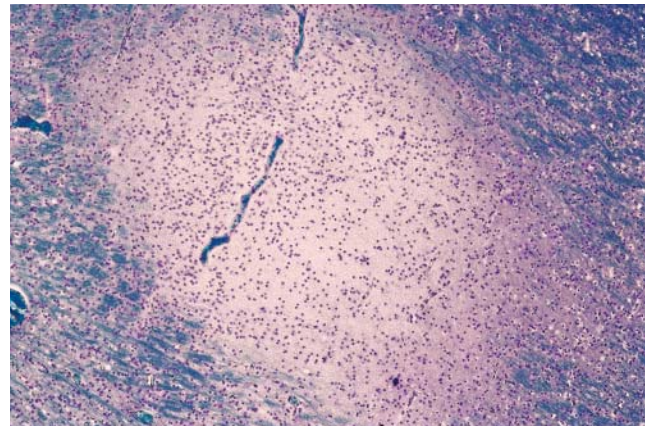


Fig. 15.6-2. Histology of PVL shows loss of myelin sheaths and gliosis in the periventricular white matter. LFB/Nissl.

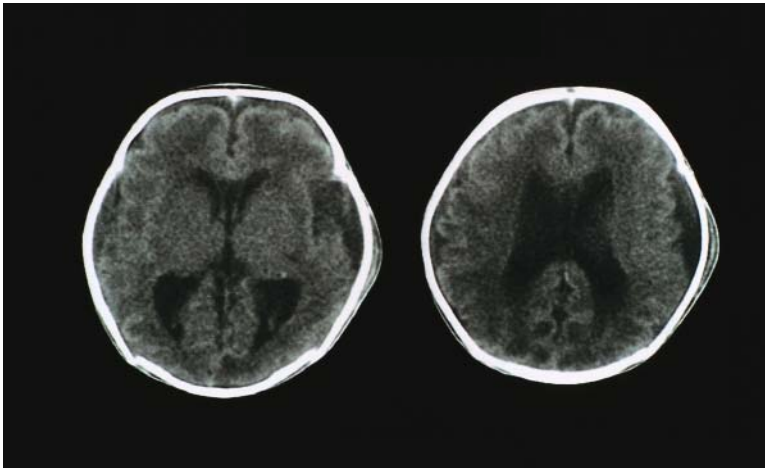


Fig. 15.6-3. CT of a neonate shows slight dilatation of the lateral ventricles and low density of the cerebral white matter. In this case, focal lesions of PVL are found in the periventricular white matter.

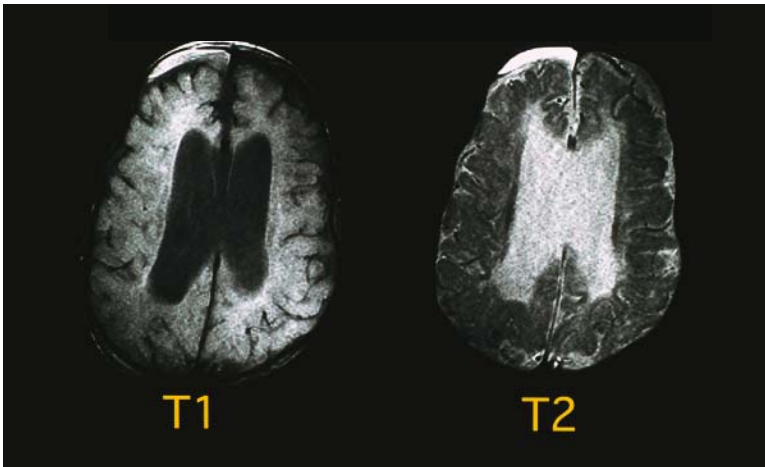


Fig. 15.6-4. T1-weighted and T2-weighted MRI at 11 months of age shows dilatation of the lateral ventricles and white matter atrophy with PVL.

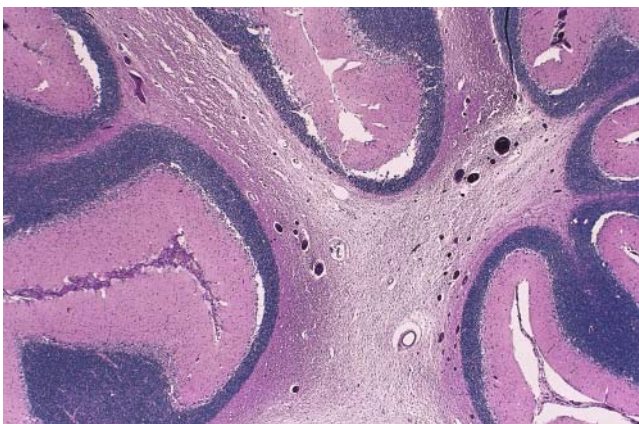


Fig. 15.6-5. There are areas of softening in the cerebellar white matter. H&E/Nissl.

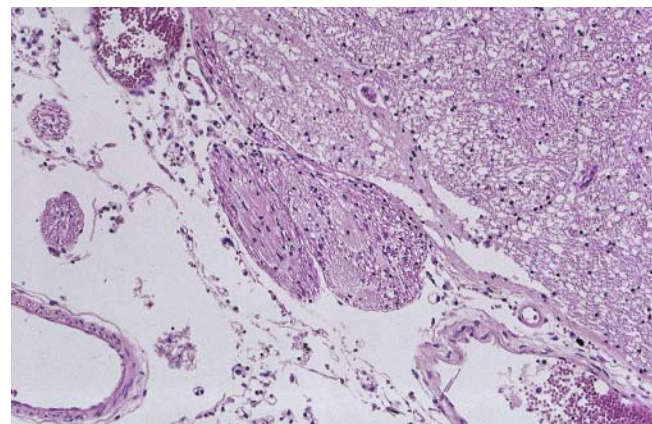


Fig. 15.6-6. Leptomeningeal glioneuronal heterotopia (LGH) is seen at the base of the cerebrum. H&E.

16 Basal Ganglia Diseases

16.1 Wilson's Disease

Wilson's disease is an autosomal recessive disorder in which excessive amounts of copper accumulate in body tissues, particularly in the liver, kidneys, cornea, and brain. It presents initially at ages 8–12 with hepatic, neurological, or psychiatric disturbances including movement disorders (dysarthria, rigidity, tremor) and psychotic behavior. There are characteristic Kayser-Fleischer rings caused by copper in the limbus of the cornea. Serum ceruloplasmin and copper levels are low, and urinary copper is increased.

Magnetic resonance imaging (MRI) shows hyperintense T2-weighted images of the caudate nuclei, lenticular nuclei, thalamus, and dentate nuclei. Patients with long-standing cases have brain and cerebellar atrophy.

Pathology

Macroscopically, the putamen, globus pallidus, and caudate appear reddish brown and atrophic. The

putamen is most severely affected, with cavitation or spongy changes. The process may involve the cerebral or cerebellar white matter, with atrophy of the overlying cortex. There is neuronal loss, chiefly in the putamen, subthalamic nucleus, and dentate nucleus. The caudate and globus pallidus are less affected. There is accumulation of Alzheimer's type II astrocytes in the gray matter of the cerebrum, brain stem, and cerebellum. There is vacuolation or loss of myelin and formation of large cells with foamy or granular cytoplasm called Opalski cells in the globus pallidus, thalamus, subthalamus, and brain stem nuclei. Cirrhosis of the liver is present.

Genetics

Wilson's disease is an autosomal recessive disorder with mutation in the gene (13q14.3) that encodes for a copper-binding p-type ATPase [1].



Fig. 16.1-1. Wilson's disease. Brown pigmentation in the putamen.



Fig. 16.1-2. Necrosis and atrophy of the putamen. H&E/LFB.

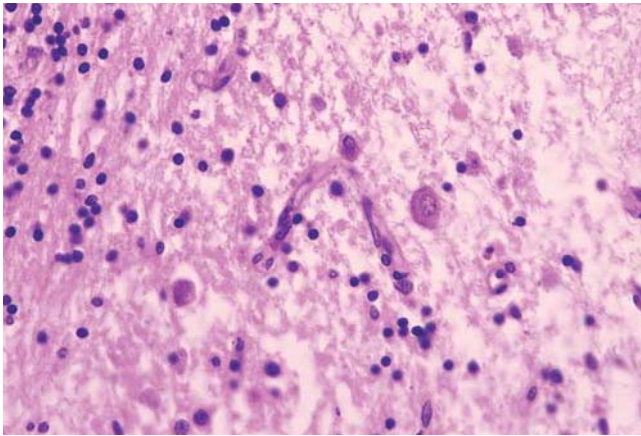


Fig. 16.1-3. Necrosis and gliosis in the putamen. H&E.

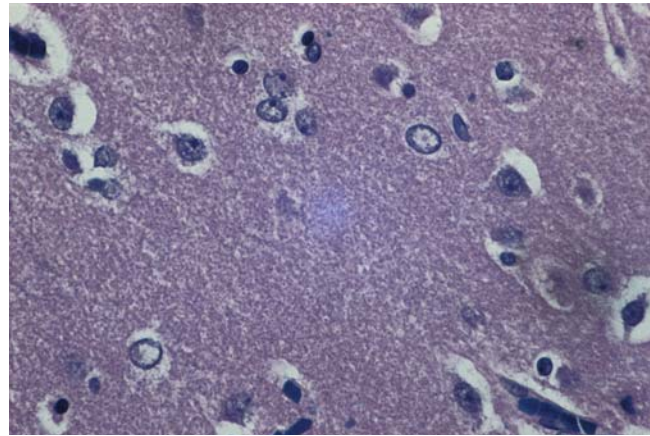


Fig. 16.1-4. Alzheimer type 2 glia in the putamen. H&E.

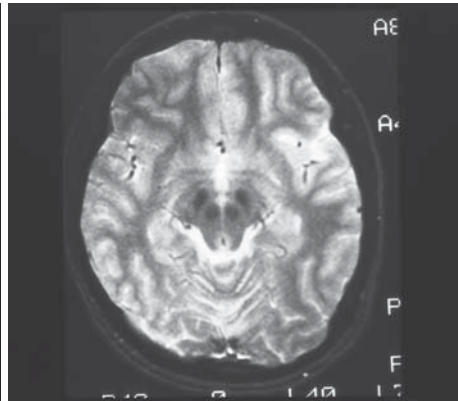
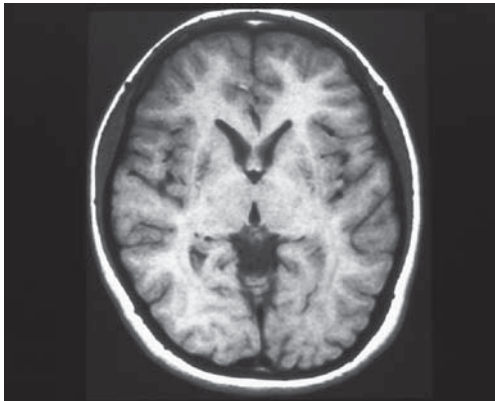


Fig. 16.1-5. T1-weighted MRI shows low intensity in the putamen and globus pallidus.

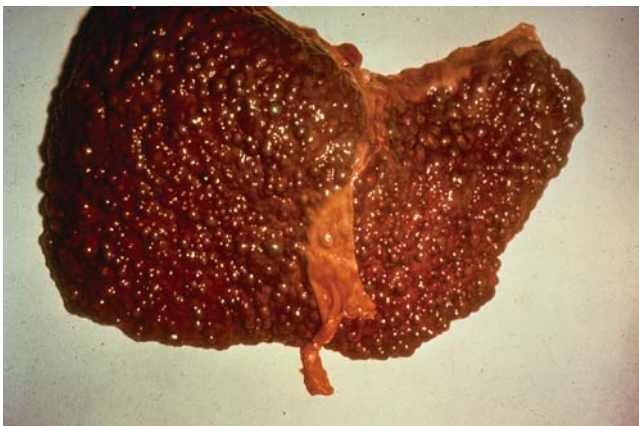


Fig. 16.1-6. The liver shows cirrhosis.

16.2 Menkes Syndrome

Menkes disease is an X-linked recessive copper transport deficiency. It is characterized clinically by seizures, psychomotor retardation, failure to thrive, temperature instability, connective tissue findings, and peculiar hair. The lactate/pyruvate ratio in blood and cerebrospinal fluid (CSF) is elevated, copper and ceruloplasmin levels are decreased, and there is norepinephrine deficiency.

Pathology

There is sparse, wiry, hypopigmented hair that is twisted (pili torti) and broken (trichorrhexis nodosa). Skeletal muscle shows enlarged mitochondria with irregular cristae in a disorderly pattern. The brain shows dilated, tortuous cerebral arteries, with fragmentation of the internal elastic lamina. There is diffuse cerebral atrophy with loss of neurons in the cortex and heterotopic neurons in the white matter. There is fibrillary gliosis of

the cerebral hemispheres and basal ganglia. Lipid droplets accumulate in glial cells and macrophages. In the cerebellum, the vermis is atrophic, with atrophy of molecular and inner granular layers. There are signs of maldevelopment and degeneration: ectopic Purkinje cells in molecular and granular layers with Purkinje cells displaying somatic sprouts, dendritic aberrations, swollen dendrites, weeping willow formations, and medusa head formations. Electron microscopy (EM) shows mitochondrial enlargement with increased matrix, matrix pallor, and loss of cristae.

Genetics

Menkes disease is an X-linked disorder with the mutant gene close to the centromere of the long arm of the X chromosome (q13.3) [2].



Fig. 16.2-1. Menkes' syndrome. The brain with hemorrhages in the left cerebral white matter and lateral ventricle.



Fig. 16.2-2. Circle of Willis and related arteries exhibit focal dilatation.

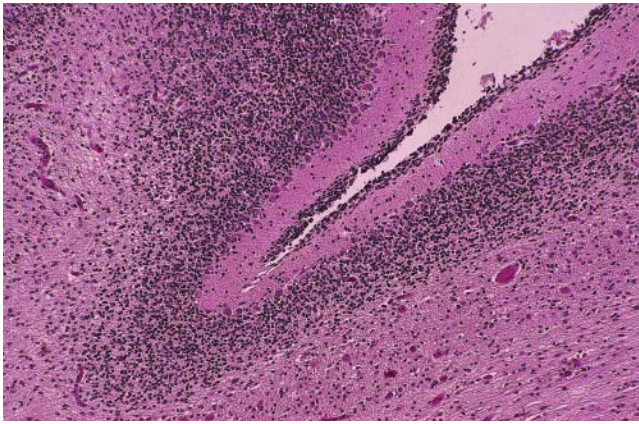


Fig. 16.2-3. Cerebellum in neonate showing thin cortex with poor cellular arrangement. H&E.

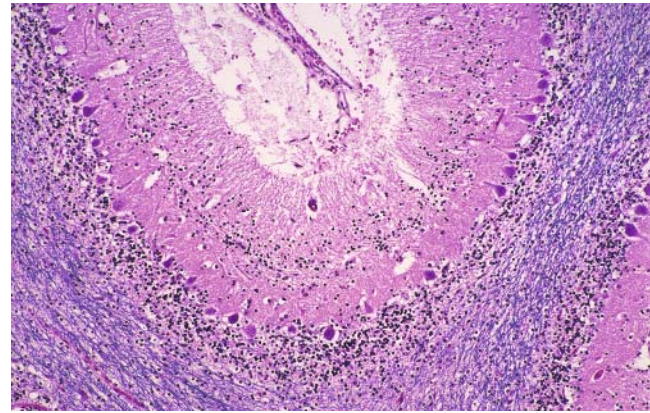


Fig. 16.2-4. Cerebellum of an infant showing an irregular row of Purkinje cells and glial proliferation in the superficial molecular layer. H&E/LFB.

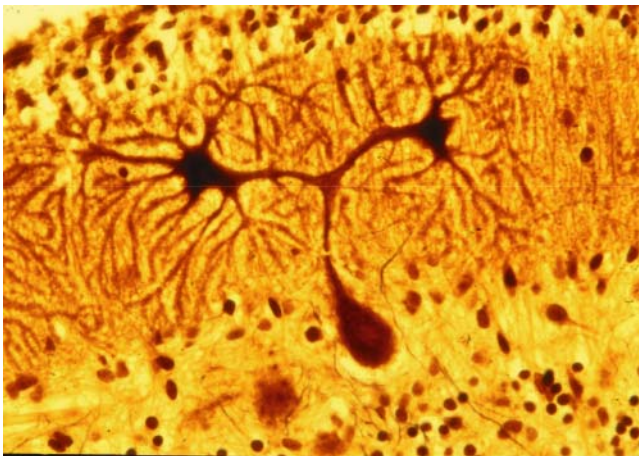


Fig. 16.2-5. Dendritic branchings of a Purkinje cell are abnormal.

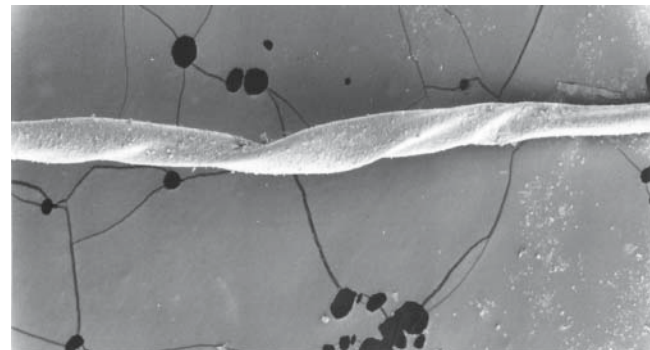


Fig. 16.2-6. Hair. Scanning microscopy shows the hair characteristically twisted around its axis (pili torti) with a variety of breaks (trichorrhexis nodosa).

16.3 Juvenile Huntington Disease

Juvenile Huntington disease usually begins during the fourth decade with chorea and personality changes; however, there are also juvenile and early- and late-onset cases. The clinical and neuropathological features of Huntington's disease in children differ from those in adults, and the average duration of the disease is shorter in children. During the initial stages of the childhood illness, ataxia, rigidity, dementia, and seizures are common neurological features.

Pathology

There is cerebral atrophy and a selective decrease in the size of the caudate, putamen, and globus pallidus. There is gliosis and a marked loss of medium-sized spiny projecting neurons (substance P-, enkephalin-, and GABA-

containing neurons) in the caudate and putamen. There is astrocytosis of the globus pallidus. In some children the cerebellum is atrophic, associated with loss of Purkinje cells and dentate neurons. Neuronal nuclear inclusions may be seen with antibodies to ubiquitin.

Genetics

Huntington's disease is an autosomal dominant disorder caused by mutations in the gene on chromosome 4 encoding the protein huntingtin and causing accumulations of polyglutamine. Predictive testing for relatives of the patients with Huntington's disease can be carried out with a DNA marker that is closely linked to the defective Huntington's gene. The mutated gene causes expansion of the CAG repeats [3].

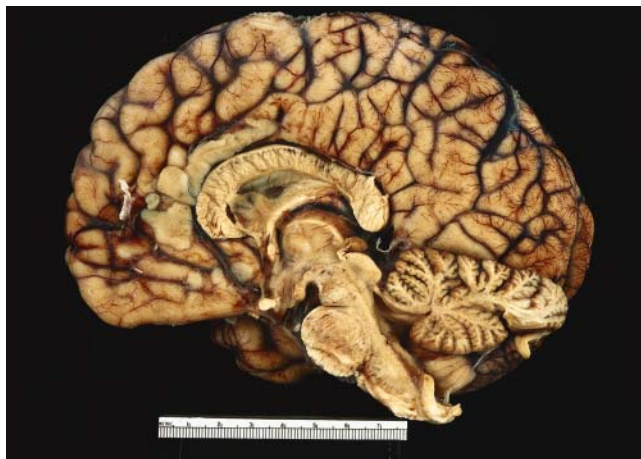


Fig. 16.3-1. Juvenile Huntington disease. Brain of a case of juvenile Huntington's disease exhibits marked cerebellar atrophy.

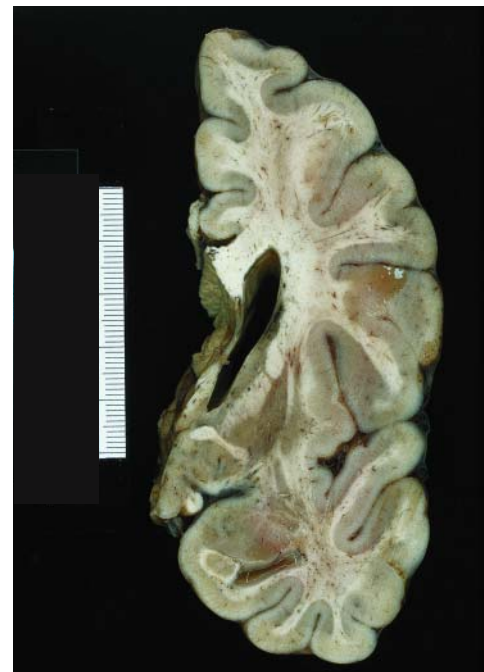


Fig. 16.3-2. Cerebral hemisphere, with atrophy of the caudate nucleus.



Fig. 16.3-3. Whole mount of cerebral hemisphere. Note atrophy of the caudate nucleus. H&E/LFB.

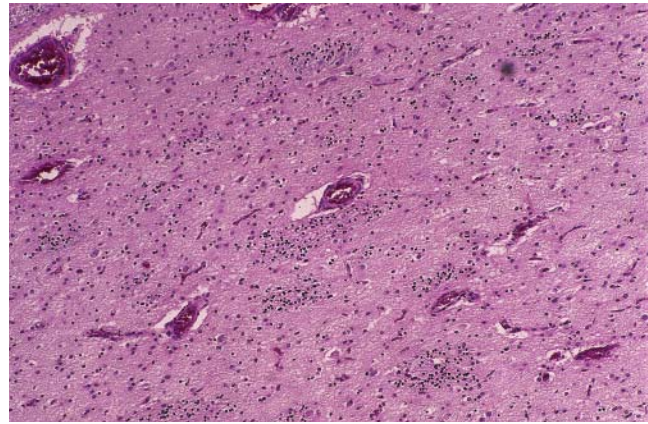


Fig. 16.3-4. Caudate nucleus with loss of medium-sized neurons and gliosis. H&E.

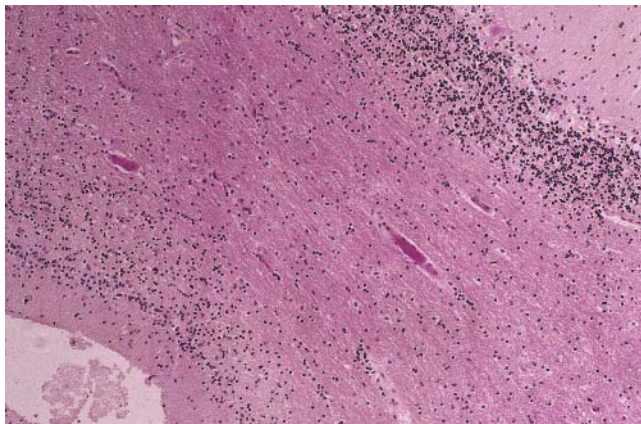


Fig. 16.3-5. Cerebellum shows loss of Purkinje cells and granular cells with increased Bergman cells. H&E.

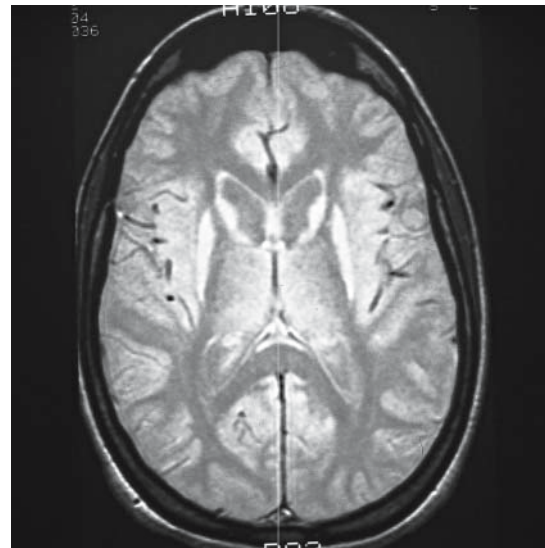


Fig. 16.3-6. MRI reveals atrophy of the caudate nucleus.

17 Neuroaxonal Degeneration

17.1 Infantile Neuroaxonal Dystrophy (Seitelberger's Disease)

Infantile neuroaxonal dystrophy is an autosomal recessive neurodegenerative disorder characterized by dystrophic changes involving mainly the terminal axons. The dystrophic axons result from a defective retrograde axonal transport, but the underlying metabolic defect is unknown. A disorder with similar axonal pathology called schindler's disease is caused by *N*-acetylgalactosaminidase deficiency. It has been reported in two siblings with clinical and neuropathological features of infantile neuroaxonal dystrophy [1]. The both disorder present during the first 2 years of life with psychomotor deterioration, hypotonia, pendular nystagmus, and symmetrical pyramidal tract signs.

Axonal dystrophy is a feature, of several other diseases; Hallervorden-Spatz disease, late infantile and juvenile neuroaxonal dystrophy.

Pathology

Gross examination of the brain shows marked atrophy and sclerosis of the cerebellum, bulbar pyramids, and

optic nerves. The cerebral cortex and white matter are moderately atrophic, and the globus pallidus is faintly yellow-brown. The pathognomonic lesion is axonal swelling in the neuropil of the cortex, basal ganglia, brain stem, and spinal cord. There is Purkinje and granular neuronal loss in the cerebellum associated with torpedoes [2]. Also present is cell loss in the lateral geniculate and dense collections of neutral fat and cholesterol-filled macrophages in the basal ganglia [3]. Peripheral nerve biopsy and nerves in other tissue biopsies are diagnostic.

Electron microscopy (EM) shows that the cytoplasm of spheroid bodies contains several types of abnormal organelle: clusters of branched tubular or vesicular profiles and occasionally crystalloid inclusions. Adjacent to clusters, filamentous structures can be disoriented or organized in beaded and lattice-like works, forming concentric or spiral structures. Mitochondria and synaptic vesicles are usually found close to these structures, suggesting the proximity of axonal terminals.



Fig. 17.1-1. Infantile neuroaxonal dystrophy. Cerebral hemisphere of infantile neuroaxonal dystrophy exhibiting pallor of the white matter. KB stain.

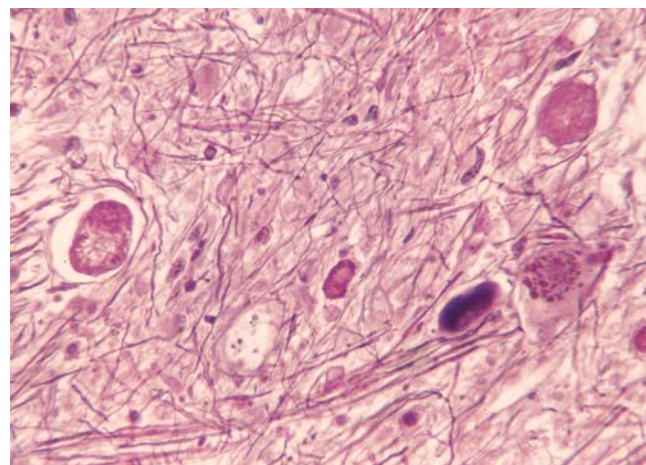


Fig. 17.1-2. Spheroids in the nucleus cuneatus of the medulla oblongata. The accumulation of spheroids is more intense in the posterior horns of the spinal cord, dorsal columns of the lower medulla. Bodian stain.

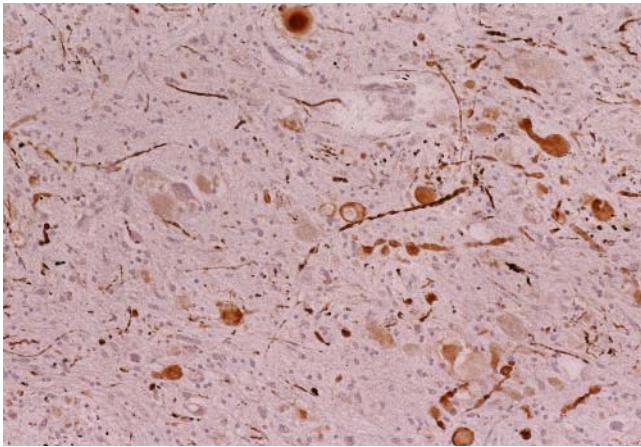


Fig. 17.1-3. Axonal swellings in the vestibular nucleus of the medulla oblongata. Neurofilament immunohistochemistry.

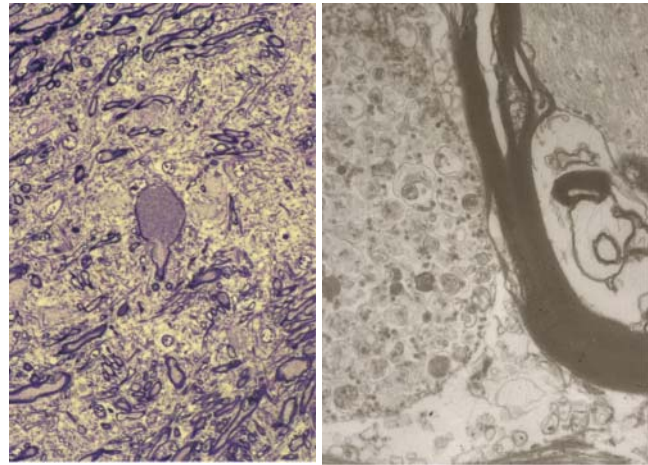


Fig. 17.1-4. Epon thin section shows spheroid of axonal swelling in the white matter, and EM reveals several types of abnormal organelle in the spheroid.



Fig. 17.1-5. Cerebellar hemispheres exhibit atrophy of the cerebellar cortex and fibrillary astrogliosis. Holzer stain.

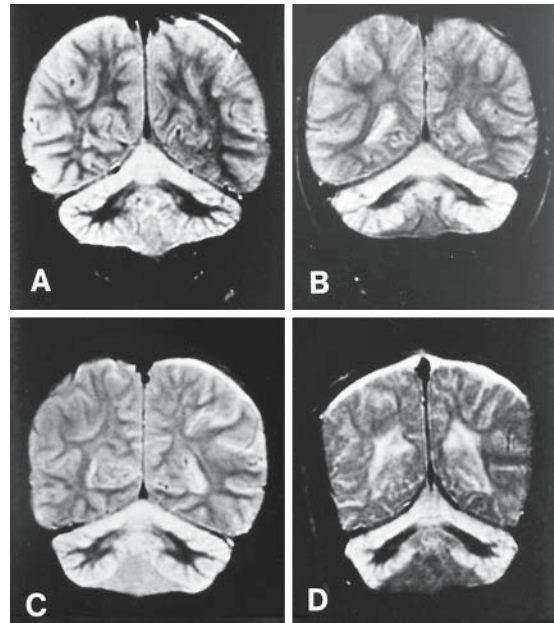


Fig. 17.1-6. Magnetic resonance imaging (MRI). Note the marked high intensity of the cerebellum and brain stem on T2-weighted imaging [2].

17.2 Hallervorden-Spatz Disease

Hallervorden-Spatz disease is an autosomal recessive disorder with mutations in the gene encoding pantothenate kinase 2 (*PANK2*). There are two clinical forms.

Pathology

There is atrophy of the globus pallidus and brown discoloration of both the globus pallidus and the pars reticulata of the substantia nigra. Microscopically, there is neuronal loss in the pallidonigral system, cerebellum, and lateral geniculate body, with a large number of spheroid bodies in most central nervous system (CNS) structures and deposits of iron, lipofuscin, and melanin

in the globus pallidus and substantia nigra. These findings are similar to those of the aged brain; and in adult cases neurofibrillary tangles (NFTs) are found in the hippocampus, neocortex, nuclei of basal forebrain, subthalamic nucleus, and brain stem reticular formation [4].

Electron Microscopy

EM has shown that the dystrophic axons contain various combinations of degenerating organelles, smooth membranous profiles, neurofilaments, microtubules, and dense granules [5].

Table 17.1. Phenotypic features of pantothenate kinase-associated neurodegeneration

Feature	Early-onset, rapidly progressive (classic) disease	Late-onset, slowly progressive (atypical) disease
Age at onset	First decade	Second or third decade
Major neurological features	Extrapyramidal dysfunction, corticospinal tract involvement	Speech disorders, psychiatric disorders, extrapyramidal dysfunction, corticospinal tract
Pigmentary retinopathy	Very common	Rare
Rate of disease progression	Loss of independent ambulation within 10–15 years after onset	Loss of independent ambulation within 15–40 years after onset
Brain MRI	Eye of the tiger	Eye of the tiger

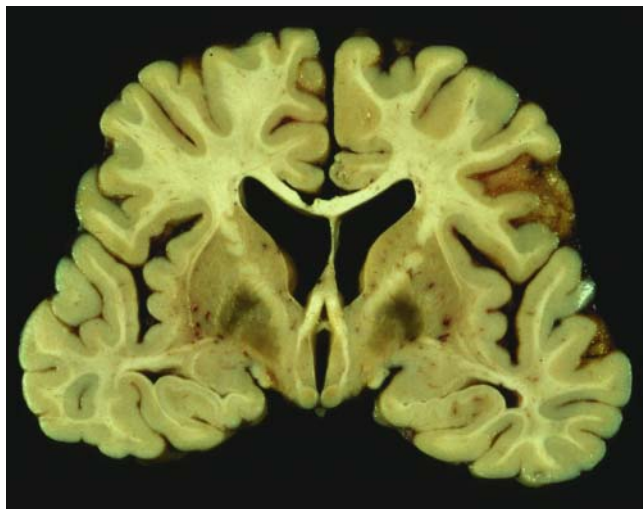


Fig. 17.2-1. Hallervorden-Spatz disease. Cerebral hemisphere. Brown pigmentation in the globus pallidus.



Fig. 17.2-2. Midbrain. Brown pigmentation in the pars reticulata of the substantia nigra.

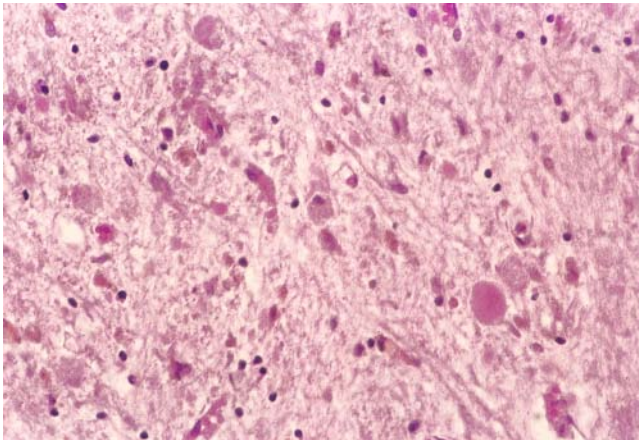


Fig. 17.2-3. Globus pallidus shows neuronal loss, axonal swelling, deposits of pigments, and gliosis in the whole area. H&E.

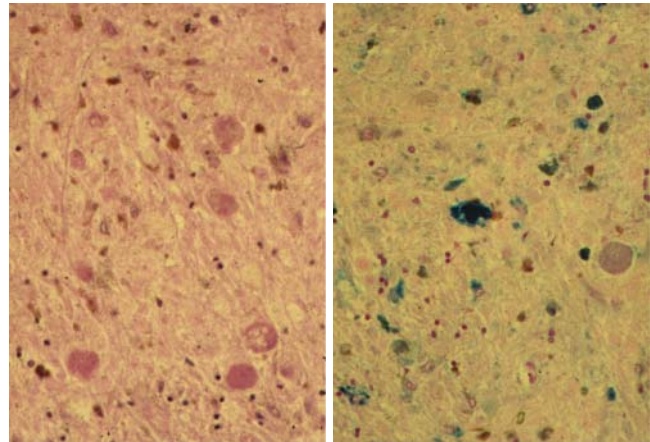


Fig. 17.2-4. Deposits of iron-positive pigments are found in the cytoplasm of astrocytes, neurons, and microglia around vessels. Iron stain of globus pallidus.

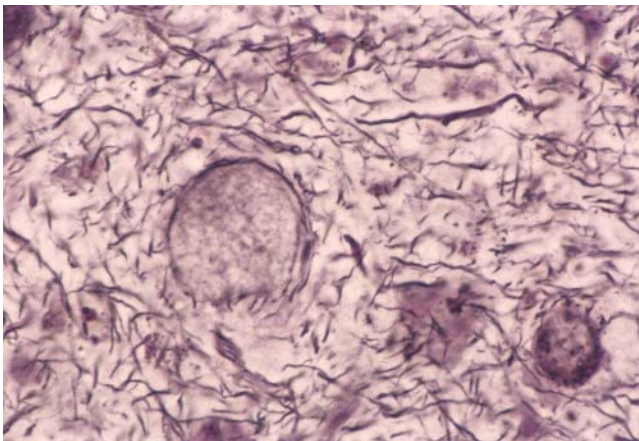


Fig. 17.2-5. Spheroids of swollen axons in the globus pallidus. Bodian stain.

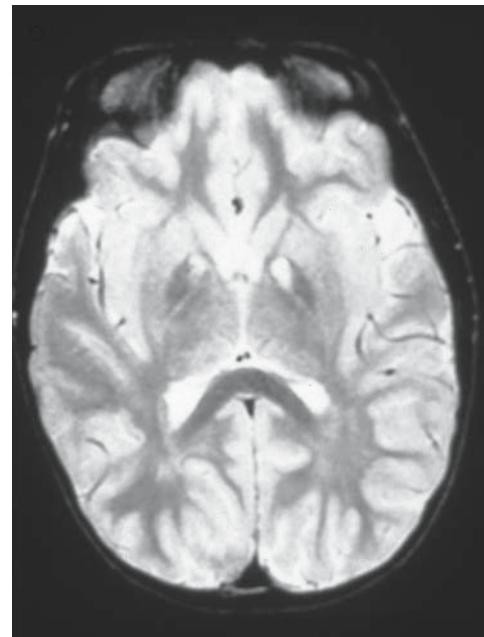


Fig. 17.2-6. MRI with iron accumulation and tissue changes pigments producing the characteristic "eye of the tiger" sign.

18 Leukodystrophy

18.1 Vanishing Leukoencephalopathy (Childhood Ataxia with Central Hypomyelination Syndrome)

Vanishing leukoencephalopathy is a vacuolating leukoencephalopathy with subcortical cysts. Symptoms develop at 18 months to 5 years of age with slowly progressive cerebellar ataxia, spasticity, variable optic atrophy, late development of bulbar symptoms, and preserved mental capacities. There are adult cases.

Pathology

The brain is soft, with widespread swelling and sponginess of the cerebral white matter with gelatinous subcortical cysts. These are present in the anterior temporal regions and sometimes in frontal and parietal lobes. U fibers and projection fibers are variably involved. The cortex and basal ganglia are not involved. Cerebellar white matter and the brain stem are shrunken. Microscopy reveals preserved gray matter with the exception of cerebellar Purkinje cells. Surrounding the cysts are naked axons, some myelin fragments, reactive astrocytes, macrophages with sudanophilic material, and increased oligodendrocytes. The lesion of the white matter is characterized by splitting of the outer lamellae of the myelin sheaths. The myelin splitting leads to

slowly progressive neurological dysfunction. The cortex remains intact [1,2].

Magnetic Resonance Imaging

During the early stage, MRI reveals that there is extensive involvement of the white matter of the cerebral hemispheres with signal abnormality and considerable swelling. The posterior limb of the internal capsule and cerebellar white matter usually show abnormal signals without swelling. The corpus callosum and the brain stem are largely spared, and the cortex and basal ganglia are always spared [3].

Genetics

One gene found on chromosome 3q27 (*EIF2B5*), which encodes one of five subunits of the translation factor eIF2B, has been found to be mutated in some patients with vanishing white matter disease [4]. Other patients have mutations in one of the other genes that encodes eIF2B subunits.



Fig. 18.1-1. Vanishing leukoencephalopathy. The brain exhibits its normal-appearing cerebral cortex.



Fig. 18.1-2. Whole mount of cerebral hemisphere demonstrates the lucency of the white matter.

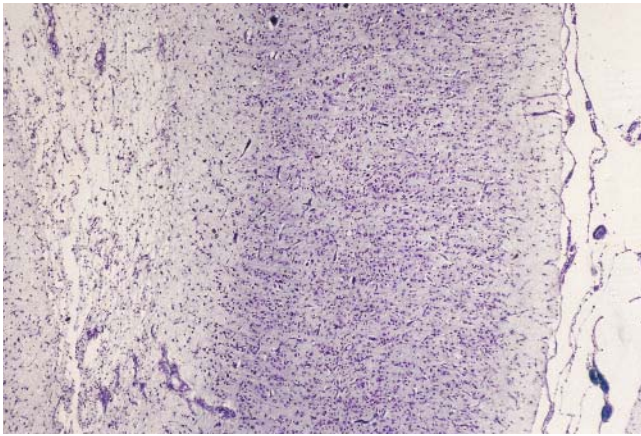


Fig. 18.1-3. Microscopy shows normal cortex overlying spongy white matter. Nissl stain.

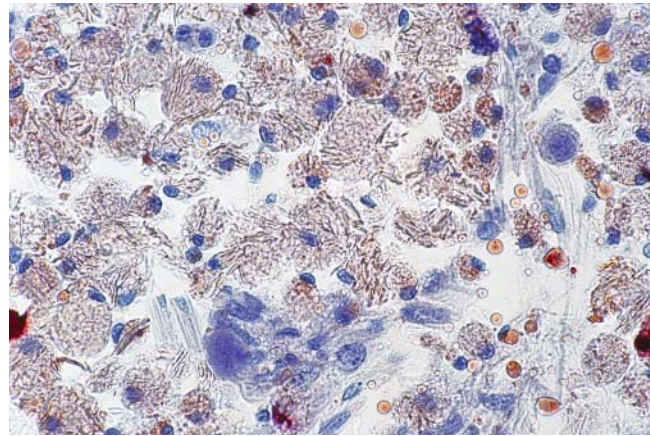


Fig. 18.1-4. Microscopy with sudanophilic macrophages infiltrating the white matter. Sudan III.

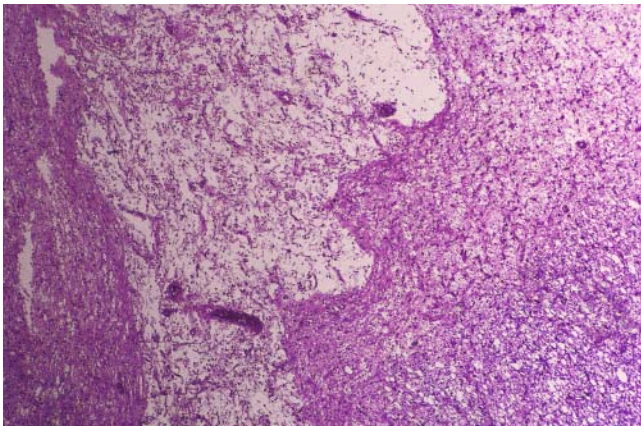


Fig. 18.1-5. Microscopy demonstrates cystic changes and marked gliosis in white matter. H&E.

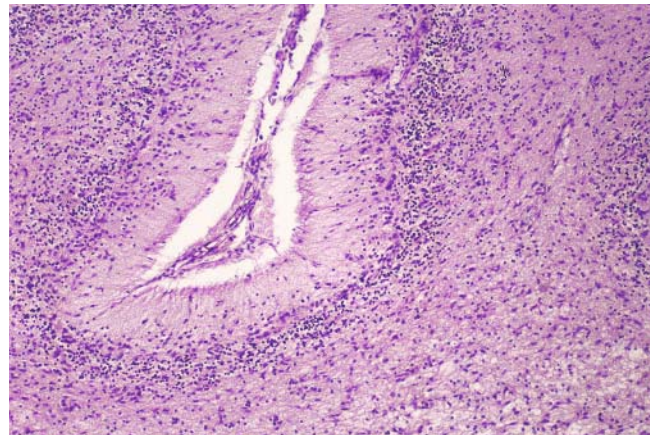


Fig. 18.1-6. The cerebellum exhibits loss of Purkinje cells and granular cells with gliosis. H&E.

18.2 Metachromatic Leukodystrophy

Metachromatic leukodystrophy (MLD) is an autosomal recessive sphingolipid storage disease with sulfatide storage in the central nervous system (CNS), peripheral nervous system (PNS), and some viscera. It is caused by a deficiency of arylsulfatase A (gene on 22q13). A similar disorder is caused by genetic deficiency of sphingolipid activator protein1 (saposin-B) on chromosome 10. There are late infantile, juvenile, and adult forms, with a rare congenital-infantile case. With the infantile form, there is normal early development, then falling and spasticity with loss of motor function and language and spastic quadriplegia and blindness. In the other forms, progression is slower, and symptoms are milder. Adult forms may present with a peripheral neuropathy.

Pathology

There is symmetrical demyelination in the CNS and PNS with sulfatide storage (metachromatic material) in the CNS, PNS, kidneys, gallbladder, liver, pancreas, adrenals, ovaries, and testes. electron microscopy (EM) of storage materials shows variously described inclusions: prismatic, tuffstone, herringbone, or honeycomb patterns.

Magnetic Resonance Imaging

MRI reveals diffuse low intensity in white matter on T1-weighted images and high intensity on T2-weighted images [5].



Fig. 18.2-1. Metachromatic leukodystrophy (MLD). Coronal section of brain through the thalamus with symmetrical demyelination and preserved U fibers.

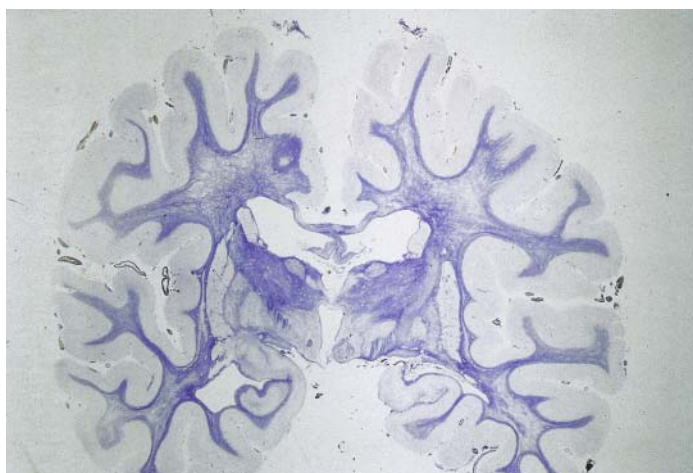


Fig. 18.2-2. Marked demyelination and fibrillary astroglia. Holzer stain.

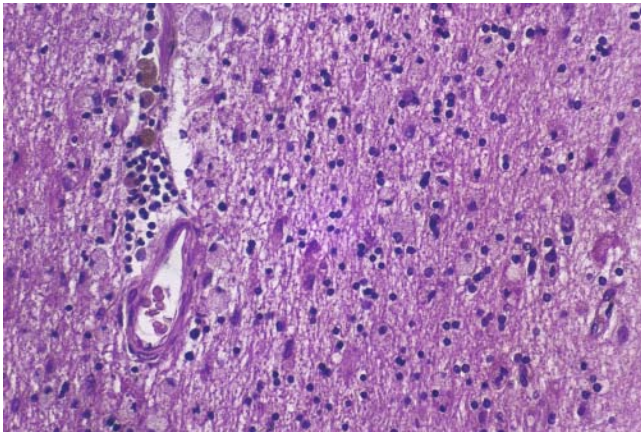


Fig. 18.2-3. Microscopic section of white matter exhibiting marked astrogliosis and microglial proliferation. H&E.

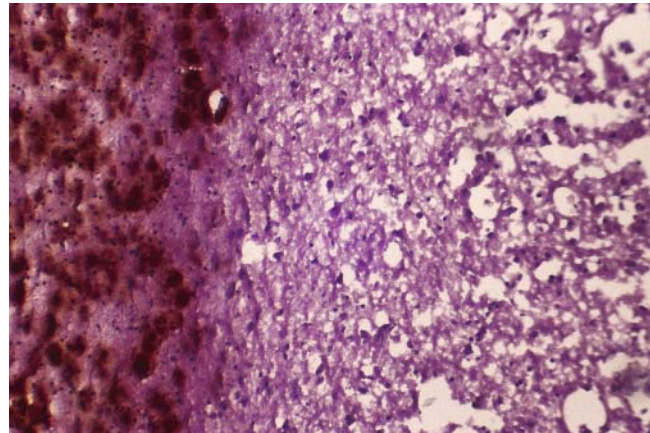


Fig. 18.2-4. Metachromatic substance in macrophages stained brown with acidic cresyl violet.

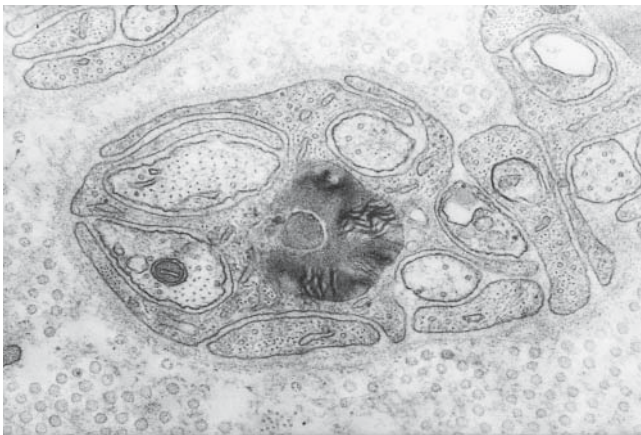


Fig. 18.2-5. EM of sural nerve biopsy shows tuffstone bodies in Schwann cell cytoplasm.

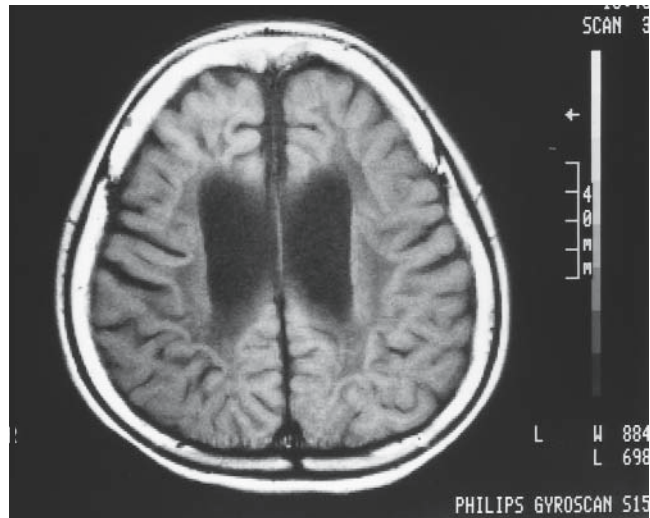


Fig. 18.2-6. T1-weighted MRI in a case of juvenile MLD showing marked atrophy, low intensity of cerebral white matter, and dilated ventricles.

18.3 Krabbe's Disease (Globoid Cell Leukodystrophy or Galactosylceramide Lipidosis)

Krabbe's disease is an autosomal recessive lysosomal storage disease caused by a deficiency of galactocerebroside β galactosidase (gene on chromosome 14). The *infantile form* begins at 3–6 months of age with irritability, rigidity, and tonic spasms. Death is at 1–18 months. The *juvenile form* begins at 3–10 years of age with slow development of gait disturbance, spastic paraparesis, and visual and intellectual decline. The *adult form* presents as asymmetrical limb weakness, spastic gait, poor coordination, and tremor.

Pathology

In the commonest infantile form, the brain is atrophic with gliotic firm white matter. There is loss of myelin

(except U fibers) and some axonal degeneration as well as gliosis and accumulation of globoid cells (macrophages containing PAS-positive materials). EM of globoid cells reveals slender tubular structures of galactocerebroside. Oligodendrocytes are reduced, and there are fewer neurons in the thalamus, cerebellum, dentate nucleus, and brain stem. Peripheral nerves show onion bulb formation and loss of large axons.

Magnetic Resonance Imaging

MRI shows low intensity in white matter on T1-weighted images and high intensity on T2-weighted images as well as atrophy of the caudate nucleus [5].

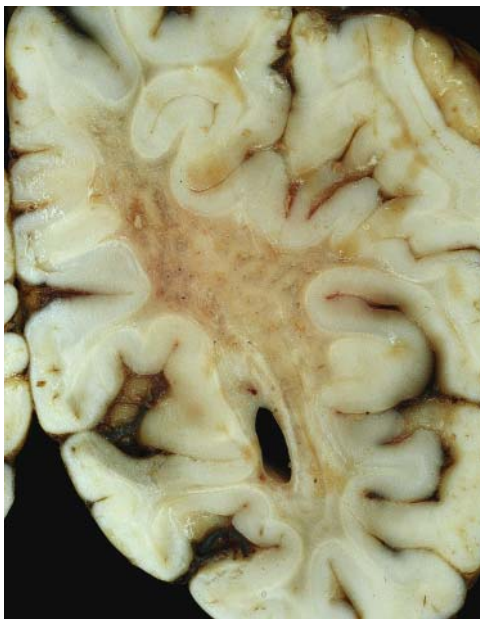


Fig. 18.3-1. Krabbe's disease. Demyelination with preserved U fibers in white matter.

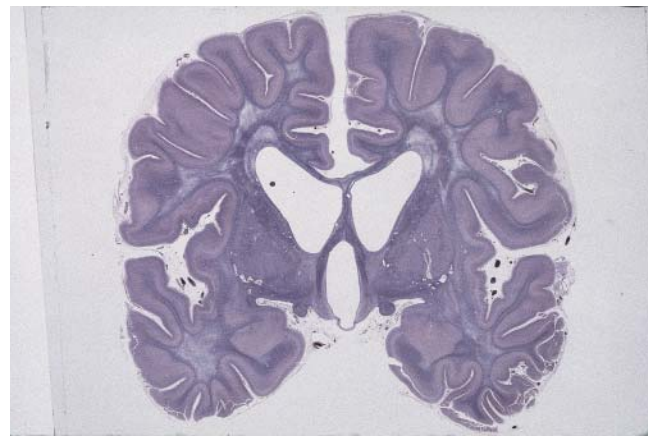


Fig. 18.3-2. Demyelination and astroglia in white matter. PTAH.

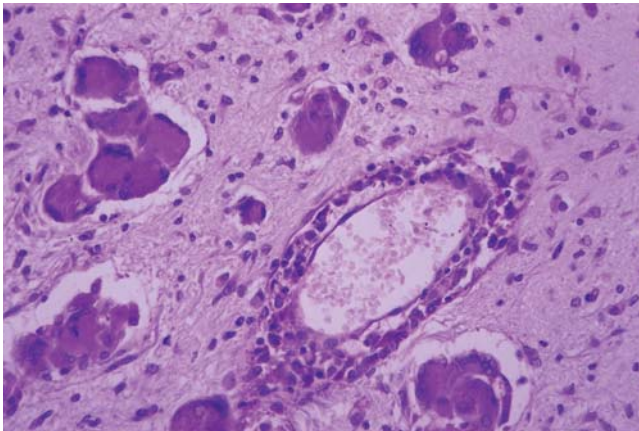


Fig. 18.3-3. Microscopy showing globoid cells and perivascular microglial cells. PAS.

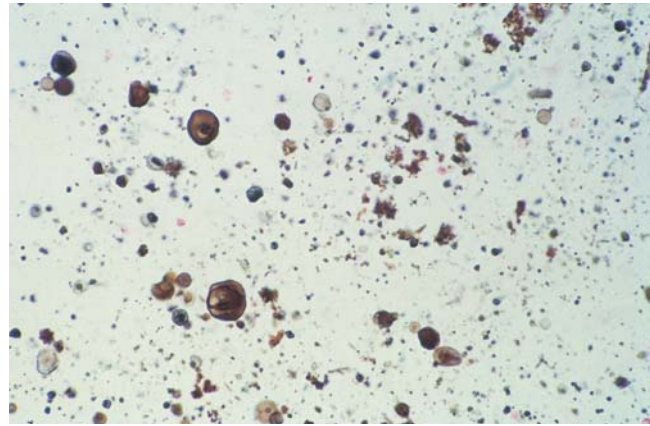


Fig. 18.3-4. Calcification in the white matter.

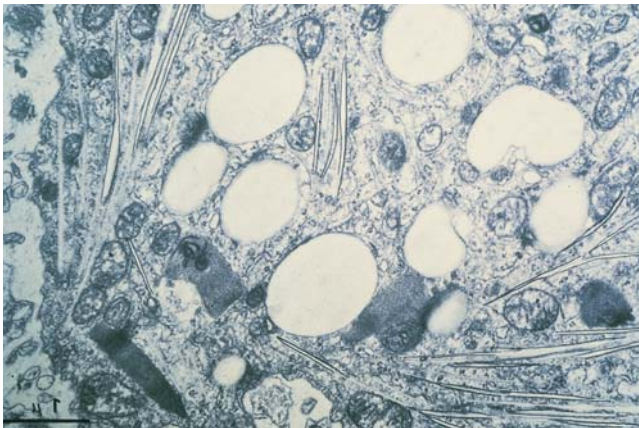


Fig. 18.3-5. EM shows characteristic polygonal or tubular structures.

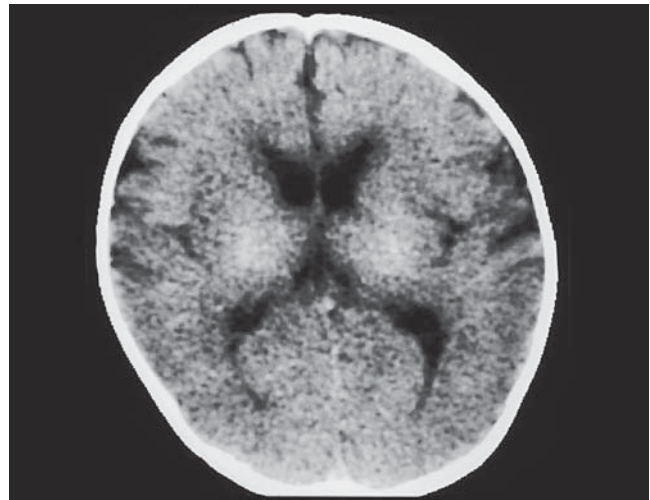


Fig. 18.3-6. Computed tomography (CT) shows slight dilatation of the lateral ventricle and slightly low density in periventricular white matter.

18.4 Alexander's Disease

The *infantile* form of Alexander's disease begins at 6 months to 2 years of age with megalencephaly and/or hydrocephalus, seizures, developmental delay, and spastic paresis. Death occurs at 2 months to 7 years. The *juvenile* form begins at 7–14 years of age with bulbar weakness, spasticity, ataxia, and mental deterioration. The *adult* form is variable, with bulbar symptoms, spastic paraparesis or quadriparesis, and cognitive dysfunction.

Pathology

Brain appearance depends on the duration of the disorder. Early cases are megalencephalic; later cases show atrophy. There may be hydrocephalus with aqueduct occlusion and atrophic, yellow discolored granular white matter. Histology shows accumulation of Rosenthal fibers in subpial and perivascular locations with dysmyelination. Rosenthal fibers are eosinophilic, refractile, rod-shaped bodies (0.5 μm up to 25 μm in width and up to 30 μm in length). They are intracellular, non-membrane-bound osmophilic deposits that are intimately associated with skeins of intermediate filaments composed of GFAP and vimentin filament proteins. The major protein component of Rosenthal fibers is αB -crystallin (a 27-kDa heat shock protein) and ubiquitin.

In the CNS, αB -crystallin is normally expressed at low levels in astrocytes and oligodendrocytes, but it can accumulate in glia and neurons in numerous other neurological disorders [6].

Computed Tomography

CT reveals dilation of the lateral and third ventricles as well as diffuse, symmetrical, low density of the white matter, particularly in the frontal lobes.

Magnetic Resonance Imaging

There are prolonged T1- and T2-weighted MRI relaxation times in a distribution identical to that of the CT abnormalities. MRI may demonstrate more white matter disease than CT [7].

Genetics

The gene responsible for Alexander's disease is the one encoding glial fibrillary acid protein. In Alexander's disease there is a *de novo* dominant gain of function mutation [1].

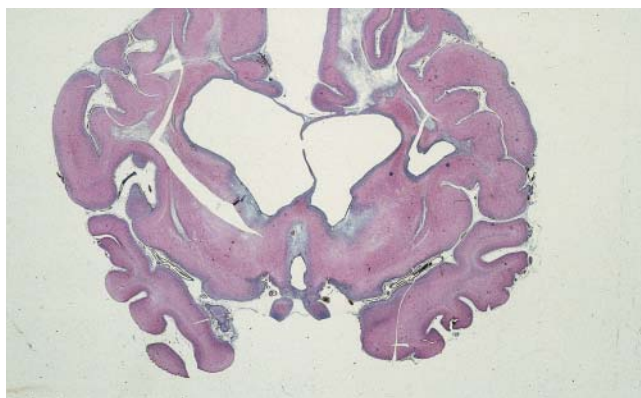


Fig. 18.4-1. Alexander's disease. Whole mount of the cerebral hemispheres shows megalencephaly, dilated ventricles, and poor myelination. H&E/LFB.

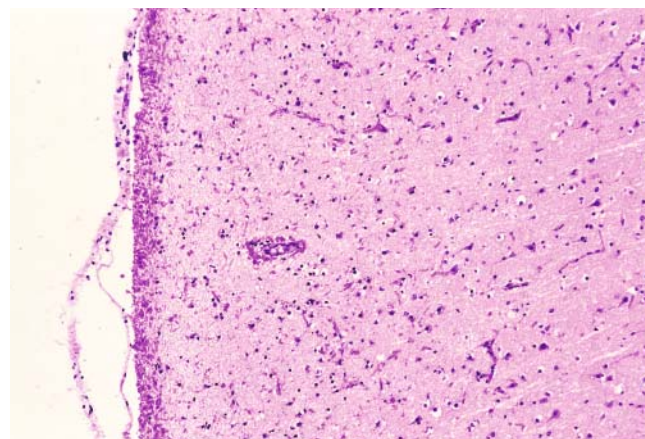


Fig. 18.4-2. Section of cerebral cortex stained with PAS, which defines the Rosenthal fibers. Note the PAS-positive processes in subpial and perivascular areas.

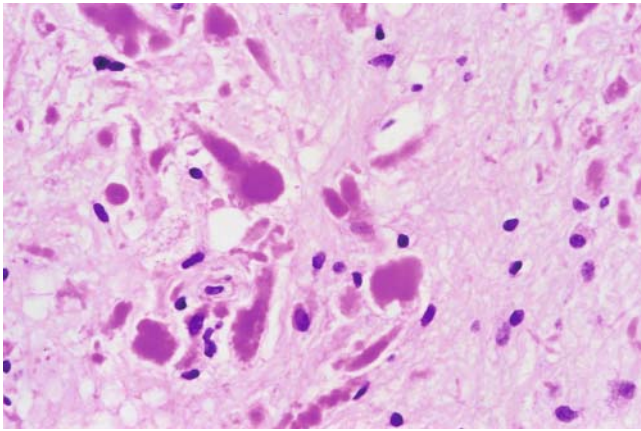


Fig. 18.4-3. Higher power view of PAS-positive Rosenthal fibers.

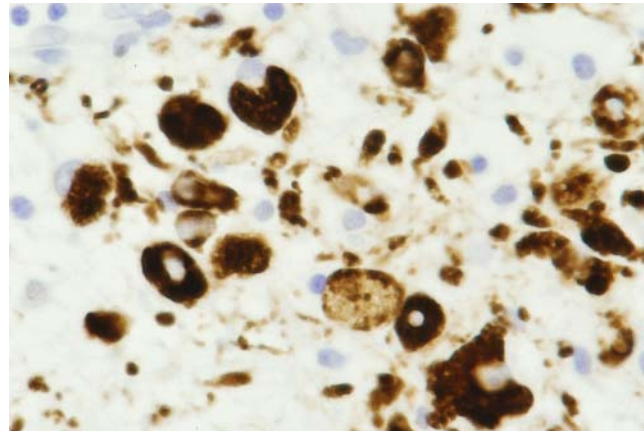


Fig. 18.4-4. GFAP-positive Rosenthal fibers.

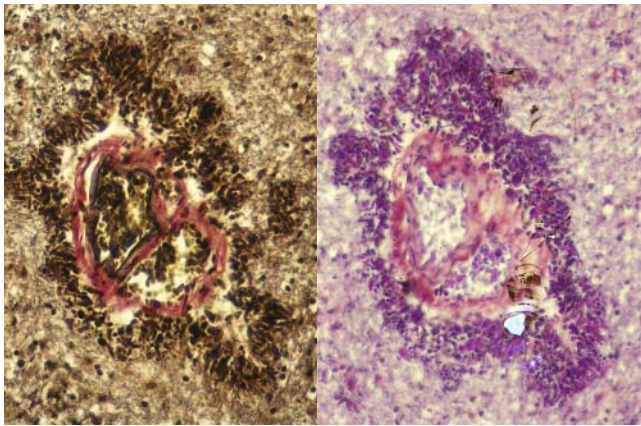


Fig. 18.4-5. Perivascular materials are defined with elastica-van Gieson (*left*) and PTAH stains (*right*).

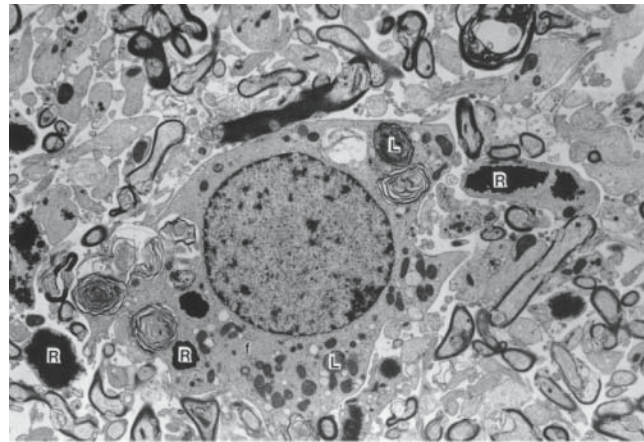


Fig. 18.4-6. EM ($\times 6825$) of a piece of cortex and white matter from a 3-year-old child. An astrocyte containing filaments (*f*), lysosomes (*L*), and Rosenthal fibers (*R*) is surrounded by numerous cell processes, some of which contain Rosenthal fibers.

18.5 Canavan's Disease, Spongy Degeneration of the Neuraxis (Canavan–van Bogaert–Bertrand Disease)

Canavan's disease is an autosomal recessive disorder caused by aspartoacylase (ASPA) deficiency, an enzyme required for myelin formation. A neonatal form of the disease presents with lethargy, crying, decreased spontaneous movements, hypotonia, feeding difficulties, and early perinatal death. The infantile form shows loss of head control and, frequently, megalencephaly during early infancy, hypotonia followed by spasticity, optic atrophy, coarse nystagmoid eye movement, seizures, and autonomic instability. Most patients die before 5 years of age.

N-Acetylaspartate (NAA) is increased in urine, bone, and cerebrospinal fluid. ASPA activity in fibroblasts of individuals with spongy degeneration of the neuraxis can be absent or reduced. More than 40 gene mutations for ASPA have been described [2].

Pathology

Megalencephaly is seen in the younger patients. The hemispheres show poor definition of gray and white matter, which is gelatinous with the texture of a wet sponge. Microscopically, there is vacuolization of the deep cortical layers and most of the white matter including the arcuate fibers (U fibers), with relative sparing of the centrum ovale. Myelin is absent. There is proliferation of Alzheimer's type II astrocytes. Spongy change may be present in the cerebellum between Purkinje cells and the granular layer. Other structures frequently involved include the optic nerve, basal ganglia (Pallidum), nuclei of the brain stem, and the gray and white matter of the spinal cord [4,8].

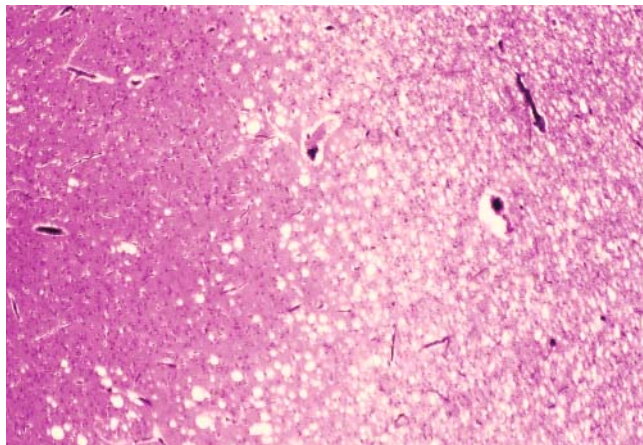


Fig. 18.5-1. Canavan's disease. Spongy changes in the white matter. H&E.

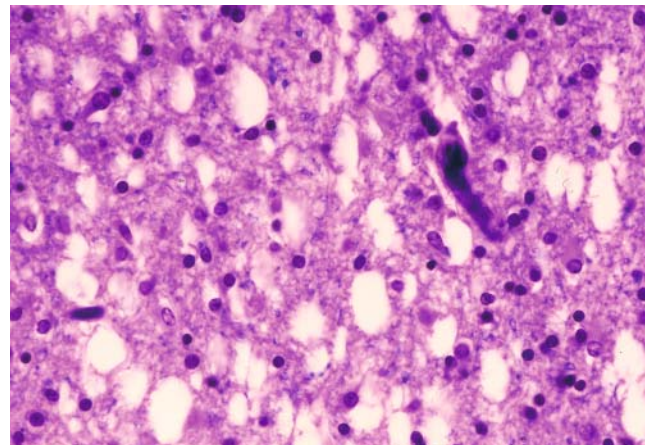


Fig. 18.5-2. Spongy change and loss of myelin sheaths. H&E.

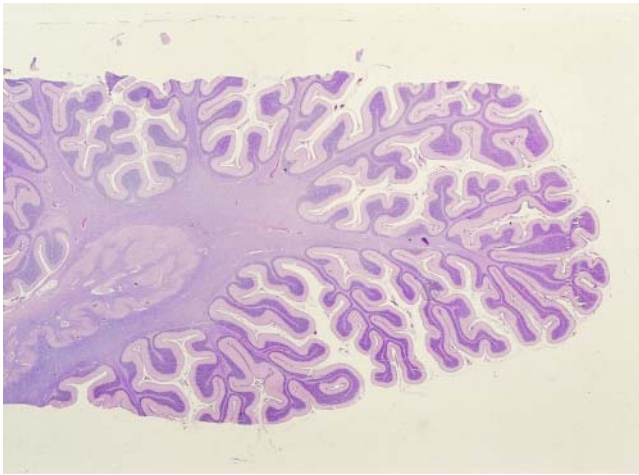


Fig. 18.5-3. Myelin pallor in the cerebellar white matter. H&E/LFB.

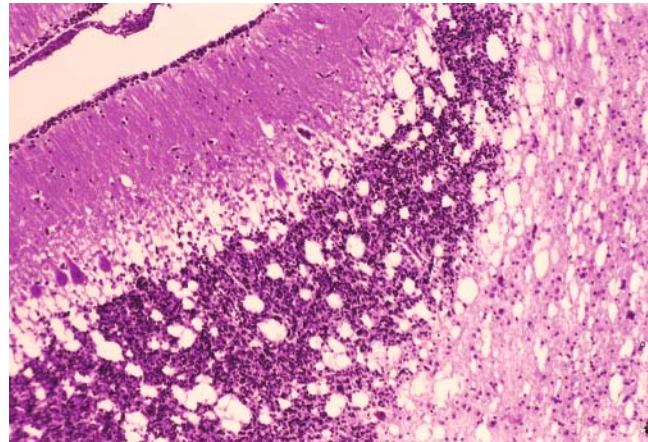


Fig. 18.5-4. Cerebellum showing spongy change in the granular cell layer and white matter. In the cerebellum, Alzheimer's type II astrocytes and vacuolization are seen in the subcortical white matter and in the molecular and Purkinje cell layers of the cortex. H&E.



Fig. 18.5-5. EM reveals abnormal mitochondria, splits in myelin lamellae, swelling of the astrocytic perikaryon and processes, and gigantic abnormal mitochondria with a dense filamentous matrix and distorted cristae.

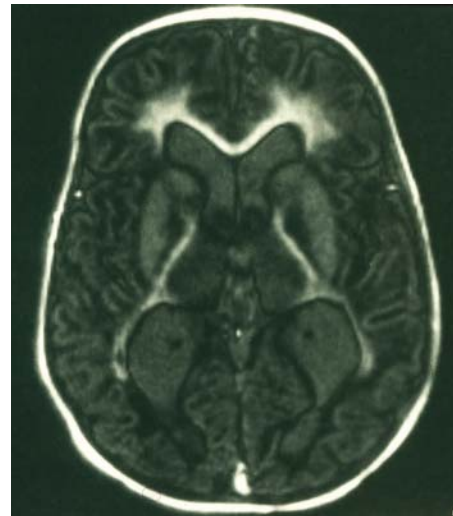


Fig. 18.5-6. MRI reveals the presence of reduced gliotic white matter. CT and MRI reveal symmetrical subcortical white matter change at an early stage.

18.6 Cockayne's Syndrome, Connatal Cockayne's Syndrome

Cockayne's syndrome is an autosomal recessive disorder with signs of premature aging, cachectic dwarfism, photosensitive dermatitis, and progressive neurological defects including retinopathy, deafness, peripheral neuropathy, psychomotor retardation, and pyramidal and cerebellar signs. There are *connatal* and *infantile* forms. The disorder can be diagnosed by demonstrating hypersensitivity of cultured fibroblasts to the lethal effects of ultraviolet (UV) light and a defective recovery of post-UV DNA synthesis. It is hypothesized that the lesions in Cockayne's syndrome result from impaired repair of DNA associated with multiple gene defects. One is DNA helicase (*ErcG6* gene) located at 10q11-q21.

Pathology

There is marked microcephaly, basal ganglia and cortical capillary calcifications, atrophy of the cortical mantle,

and reduced white matter. Lipofuscin accumulation, neurofibrillary tangles, Hirano bodies, and nuclear atypia have been described in cortical neurons. In the white matter, there is patchy loss of myelinated fibers in a tigroid fashion. The corpus callosum is thin, and the lateral ventricles are enlarged. The cerebellum is frequently atrophic with white matter loss; and there is a diffuse paucity of Purkinje and granule cells with proliferation of Bergman astroglia. Purkinje cells may display axonal swellings (torpedoes), dendritic expansions (cactus flowers), and mineralization of the dendrites. Nuclear abnormalities also occur in cerebellar neurons. The patchy demyelination with nerve cell loss may involve the brain stem and spinal cord. EM of peripheral nerves may show onion bulb formation and Schwann cells containing granular material [4,9].

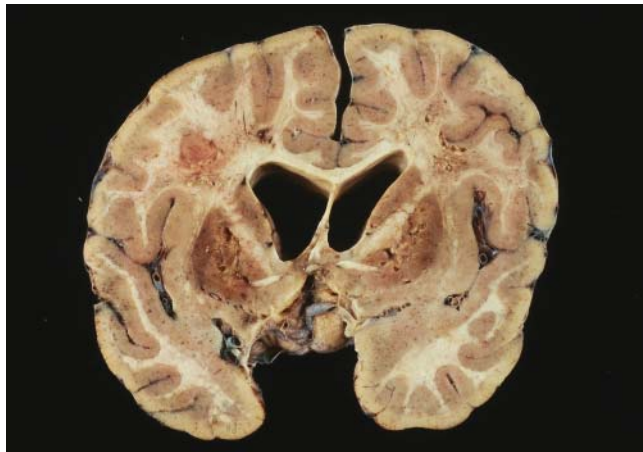


Fig. 18.6-1. Cockayne's syndrome. Coronal section of cerebral hemispheres showing patchy demyelination (calcification in white matter), discoloration, and shrinkage of the basal ganglia (which contain calcific deposits) as well as minimal hydrocephalus.

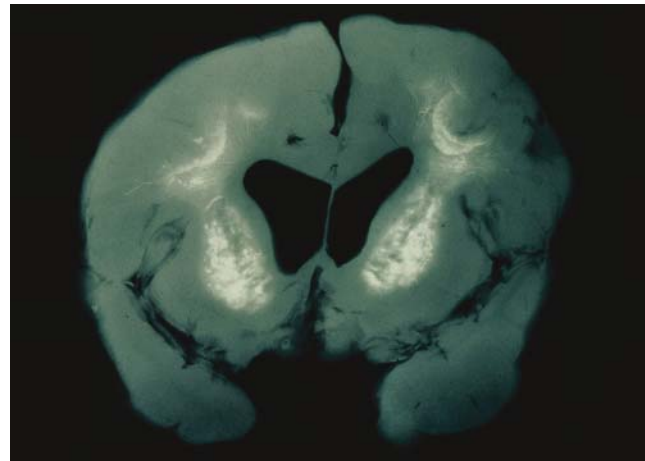


Fig. 18.6-2. Radiograph of the case in 18.6-1 shows calcification in the basal ganglia and cerebral white matter.



Fig. 18.6-3. Coronal section through basal ganglia exhibits calcification.

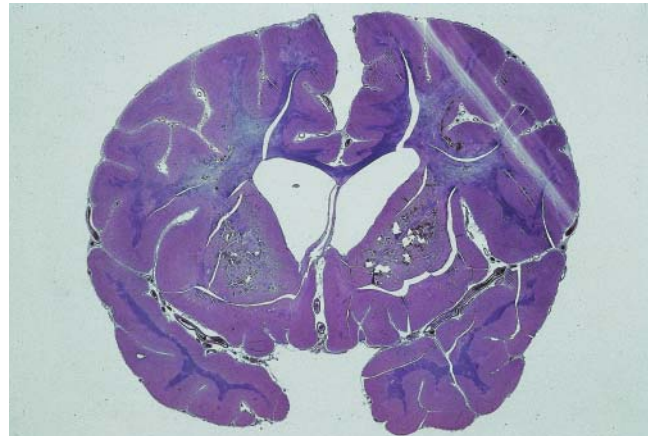


Fig. 18-6-4. Whole mount exhibits calcification in the basal ganglia and demyelination in the white matter. LFB/H&E.

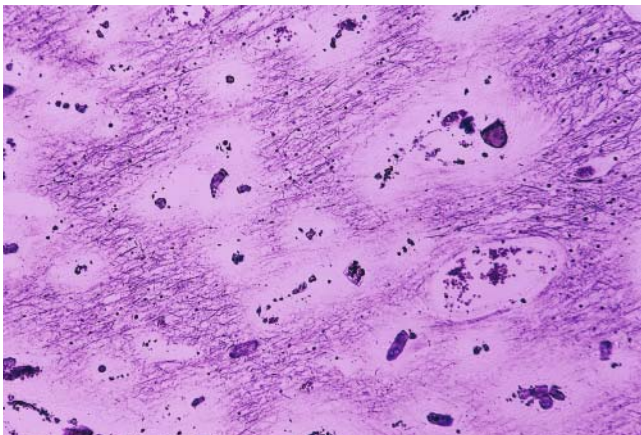


Fig. 18.6-5. White matter exhibits tigroid-state demyelination. LFB.

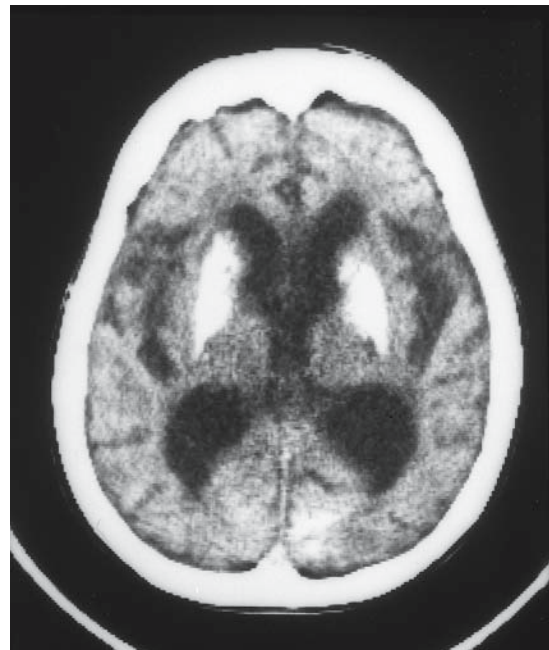


Fig. 18.6-6. CT with basal ganglia calcification.

18.7 Pelizaeus-Merzbacher Disease

Pelizaeus-Merzbacher disease (PMD) is an X-linked recessive disorder characterized by almost complete absence of central myelin and sparing of the peripheral nervous system. In some cases the disorder begins during the neonatal period with abnormal eye movements, microphthalmia, optic atrophy, head titubation, and hypotonia. This form is rapidly progressive, leading to involuntary movements, spasticity of the legs, intellectual failure, and early death. In other cases, the rate of progression is slower.

Pathology

The brain is atrophic with sulcal widening and ventricular enlargement. The corpus callosum is thin and hypoplastic, and the cortex is preserved; however, a diffuse lack of myelin staining is characteristic of the disorder. There are rare islands of preserved myelin in the pro-

tracted cases, giving a “tigroid” appearance. The cerebellum is atrophic with Purkinje cell (PC) and granular cell loss. Axons are preserved. There are perivascular macrophages with sudanophilic lipid and variable degrees of gliosis. There may be associated heterotopias and microgyria. MRI findings are variable; brain stem auditory and visual evoked potentials are abnormal.

Genetics

Most cases of Pelizaeus-Merzbacher disease are caused by a defect of the proteolipid protein (PLP) with abnormalities in the gene at Xq21-22. Pelizaeus-Merzbacher disease (PMD) and familial spastic paraplegia type 2 (SPG2) are also caused by a mutation of the *PLP* gene [9–11].



Fig. 18.7-1. Pelizaeus-Merzbacher disease. Gross brain showing normal-appearing cortex.

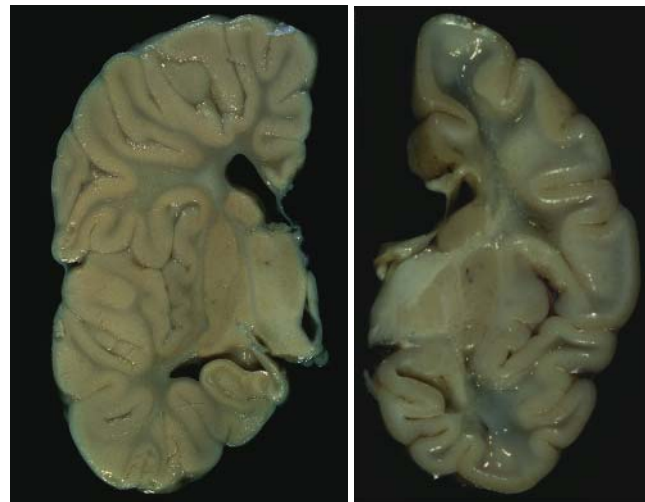


Fig. 18.7-2. Coronal sections show discolored, shrunken white matter.

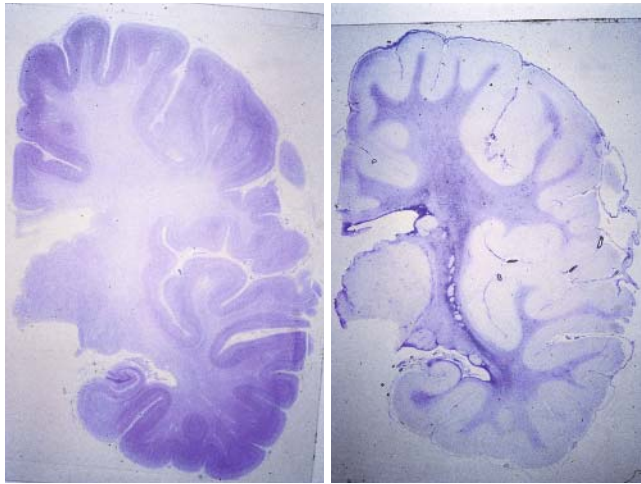


Fig. 18.7-3. *Left.* Poor staining of myelin sheaths in the cerebral hemisphere. LFB. *Right.* Whole mount with a glial stain showing diffuse white matter gliosis. Holzer stain.

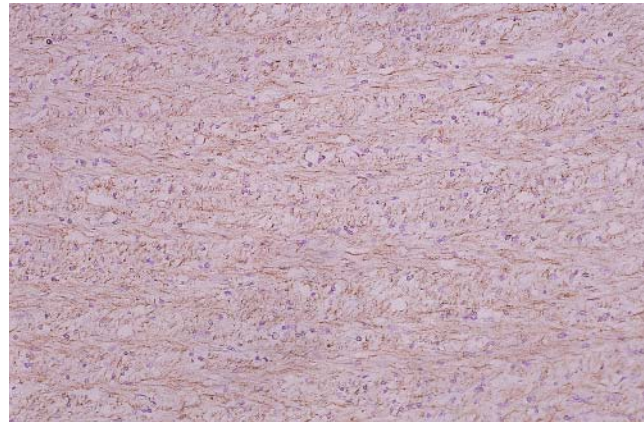


Fig. 18.7-4. White matter shows an absence of proteolipid protein (PLP). Immunohistochemical preparation.

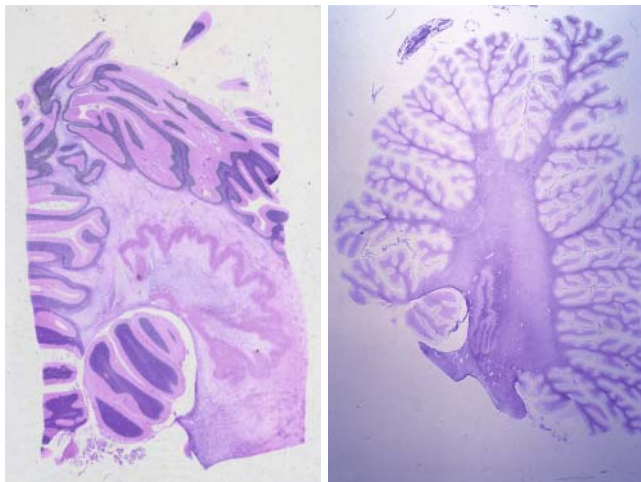


Fig. 18.7-5. Cerebellum shows atrophy and white matter hypomyelination and gliosis. *Left.* LFB. *Right.* Holzer stain.

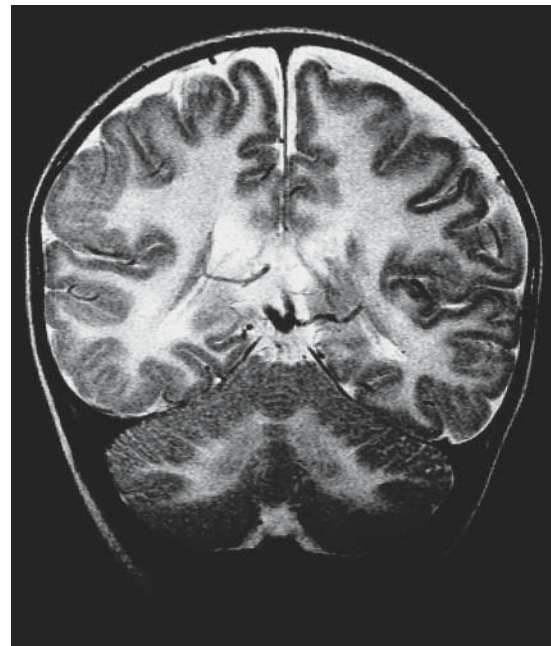


Fig. 18.7-6. MRI reveals cerebral atrophy and an absence of white matter myelination.

19 Demyelination

19.1 Acute Disseminated Encephalomyelitis (Postinfectious/Postvaccination Perivenous Encephalomyelitis)

Acute disseminated encephalomyelitis (ADEM) is a demyelinating disease that affects all ages, except children less than 2 years. It occurs during the course of various infections, particularly the acute exanthematous diseases of childhood (measles, rubella, chickenpox, and smallpox immunization), other common viral infections (i.e., Epstein-Barr virus, adenovirus, cytomegalovirus, influenza, rhinoviruses, coronaviruses), and following vaccination against smallpox, measles, and rabies. The clinical features are the same regardless of the inciting event. The symptoms develop days to weeks after the onset of the predisposing cause. The symptoms and signs of acute disseminated encephalomyelitis are related to the portion of the central nervous system (CNS) that is most severely damaged. Death occurs in 20%–30%. There are neurological deficits in survivors.

Pathology

The brain shows mainly involvement of the white matter with numerous small foci of demyelination. Histologically, there is a destructive inflammatory reaction with lymphocytes and occasional plasma cells around small veins throughout the cerebrum, brain stem, cerebellum, and spinal cord. Phagocytic microglial cells are present in the lesions. There is relative sparing of axons and nerve cells. There is a sharp margin between the foci of demyelination and normal areas. At later stages, the extent of gliosis exceeds the area of demyelination. In ADEM the tissue reaction is the same age everywhere reflecting the monophasic nature of the disease. This differs from multiple sclerosis in which lesions are of differing ages [1].



Fig. 19.1-1. ADEM. Multiple sites of demyelination in the white matter of the cerebrum.



Fig. 19.1-2. Multiple lesions of demyelination in the cerebellar white matter.

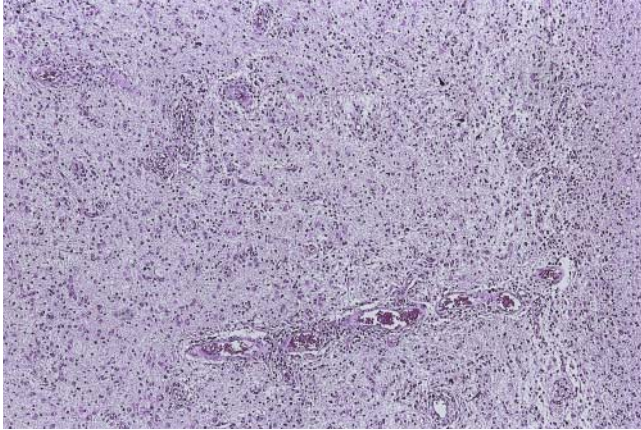


Fig. 19.1-3. Perivascular small round cell infiltration in the cortex and white matter. H&E.

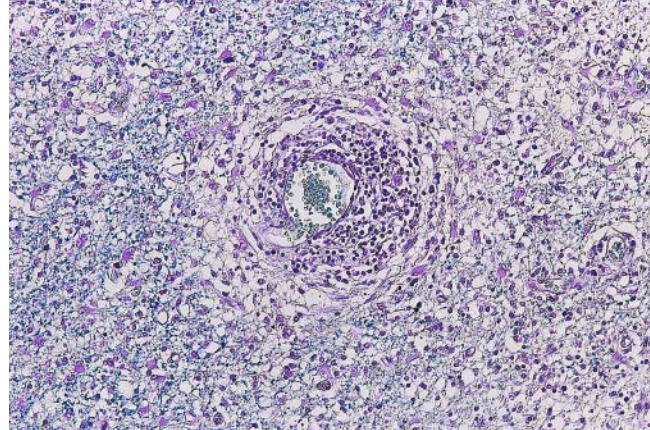


Fig. 19.1-4. Perivascular cuffing with astrogliosis and loss of myelin sheaths in the same case. LFB.

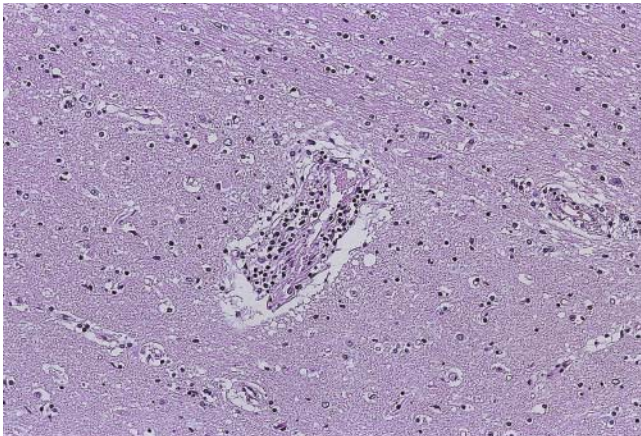


Fig. 19.1-5. Perivascular cuffing in the white matter in the same case. H&E.

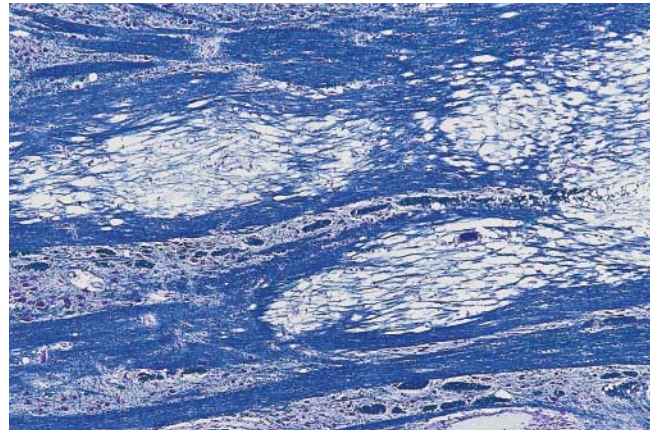


Fig. 19.1-6. Microscopic multifocal demyelination in the same case. LFB.

19.2 Acute Necrotizing Encephalopathy

Acute necrotizing encephalopathy (ANE) is a type of acute encephalopathy that affects young children following febrile viral diseases such as influenza and exanthema subitum [2]. ANE is most prevalent in East Asia but is also present in other regions of the world. The clinical course of ANE is fulminant, with a rapid decrease of consciousness, variable degrees of hepatic dysfunction, and severe neurological sequelae in the survivors [3].

Pathology

The lesions of ANE exhibit edema, petechial hemorrhage, and necrosis, suggesting local breakdown of the blood–brain barrier. Both the gray and white matter are involved. The parenchymal lesions have a laminar

pattern surrounding vessels, which exhibit excessive permeability, producing an area of “vasogenic edema.” This increases, moving deep into the brain away from the cerebral surface [4].

Magnetic Resonance Imaging

Cranial computed tomography (CT) and magnetic resonance imaging (MRI) show characteristic bilateral brain lesions in which the multiple, symmetrical brain lesions affect the bilateral thalami, putamina, cerebral periventricular white matter, cerebellum, and brain stem tegmentum. Images of the lesions often exhibit a concentric structure, such as is seen in the tissue pathology. The periphery of the lesions shows positive contrast enhancement [4].

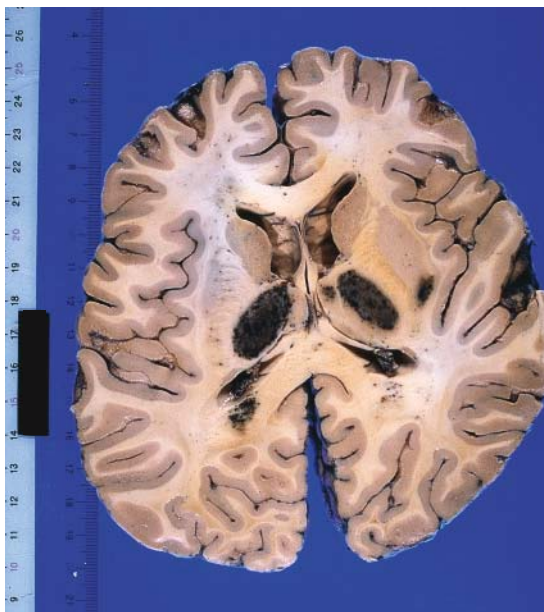


Fig. 19.2-1. Acute necrotizing encephalopathy (ANE). Note the cavity formation with hemorrhagic necrosis in the thalamus and white matter of both cerebral hemispheres. (Courtesy of Dr. Mizuguchi M.)

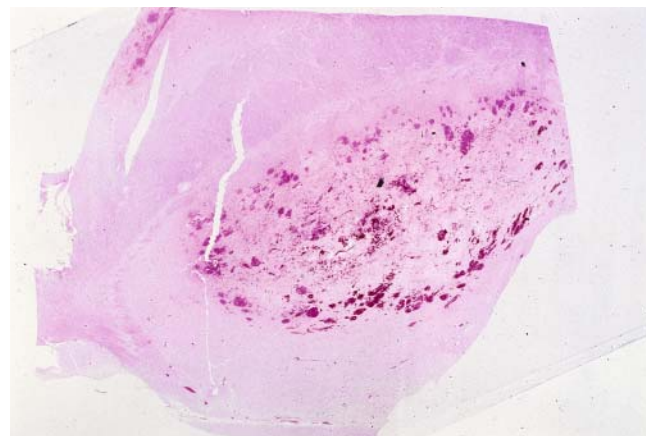


Fig. 19.2-2. Whole mount of thalamus shows a focus of hemorrhagic necrosis. H&E.

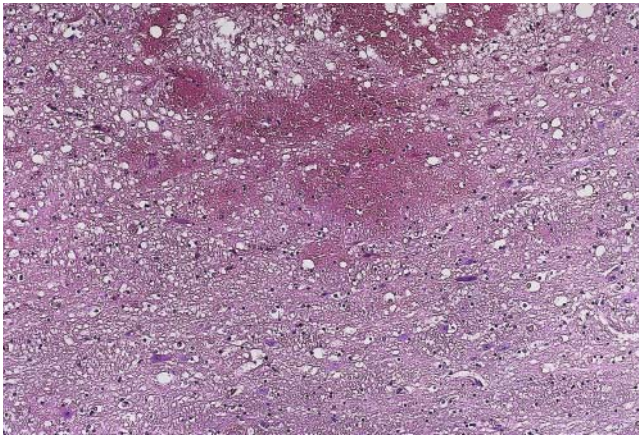


Fig. 19.2-3. Hemorrhage and necrosis in the thalamus. H&E.

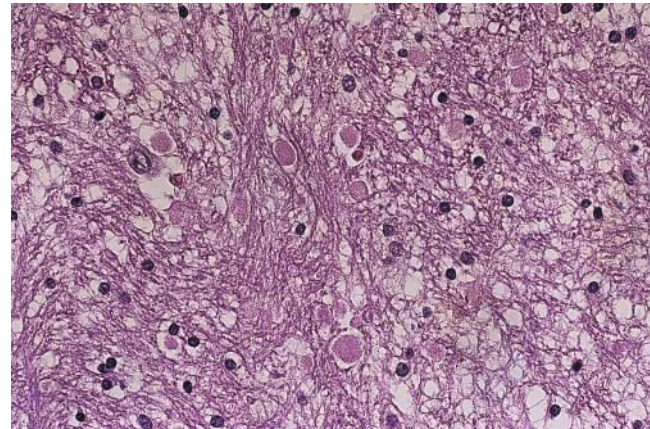


Fig. 19.2-4. Axonal swelling in white matter. H&E.

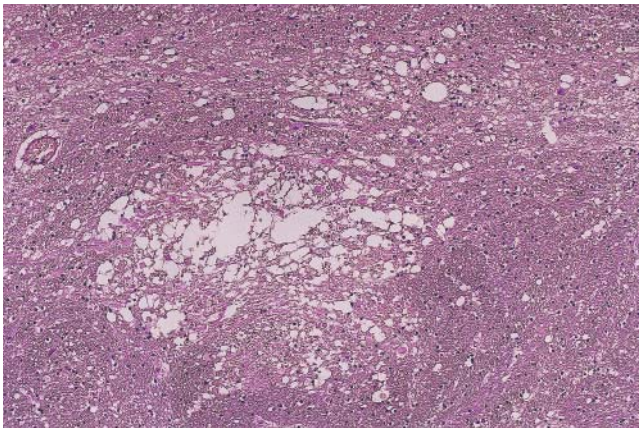


Fig. 19.2-5. Focal necrosis with spongy changes in white matter. H&E.



Fig. 19.2-6. Cystic necrosis in the midbrain tegmentum. *Left.* H&E. *Right.* Holzer stain.

20 Infection

20.1 Congenital Cytomegalovirus Infection

The viruses known to be responsible for significant intrauterine infections include rubella virus, measles virus, mumps virus, enteroviruses (coxsackie virus, echovirus, hepatitis A, poliovirus), lymphocytic choriomeningitis virus, human immunodeficiency virus (HIV), herpes viruses (cytomegalovirus, varicella, herpes simplex), Epstein-Barr virus, and arboviruses.

Newborns who were infected in utero may present with: (1) acute or subacute signs of infection; (2) multiple organ system malformation (congenital viral syndromes);

(3) intrauterine growth retardation; (4) prematurity; or (5) no immediately evident signs of disease.

Cytomegalovirus (CMV) infection may cause hepatitis, pneumonitis, cutaneous petechiae, chorioretinitis, meningoencephalitis, and myositis during the acute or subacute stage. Chronic signs of CMV infection are microcephalus, brain malformation, periventricular calcification, hearing loss, and dental defects. An encephaloclastic process that occurs during neuronal migration leads to polymicrogyria or schizencephaly [1].

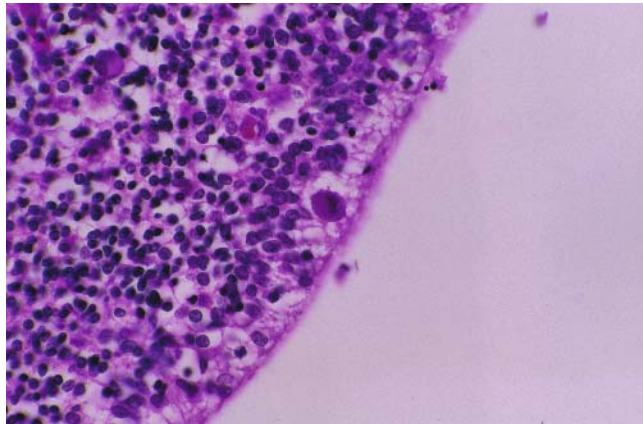


Fig. 20.1-1. Congenital cytomegaloviral (CMV) infection. Cytomegalic cells in the subependymal germinal layer. H&E.

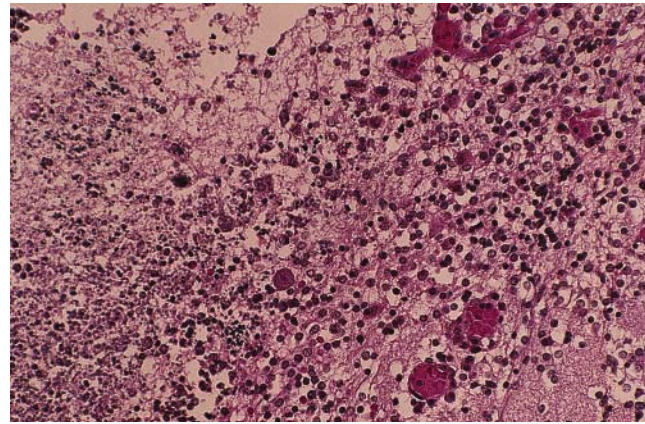


Fig. 20.1-2. Cytomegalic cells and calcification in the subependymal germinal layer. H&E.

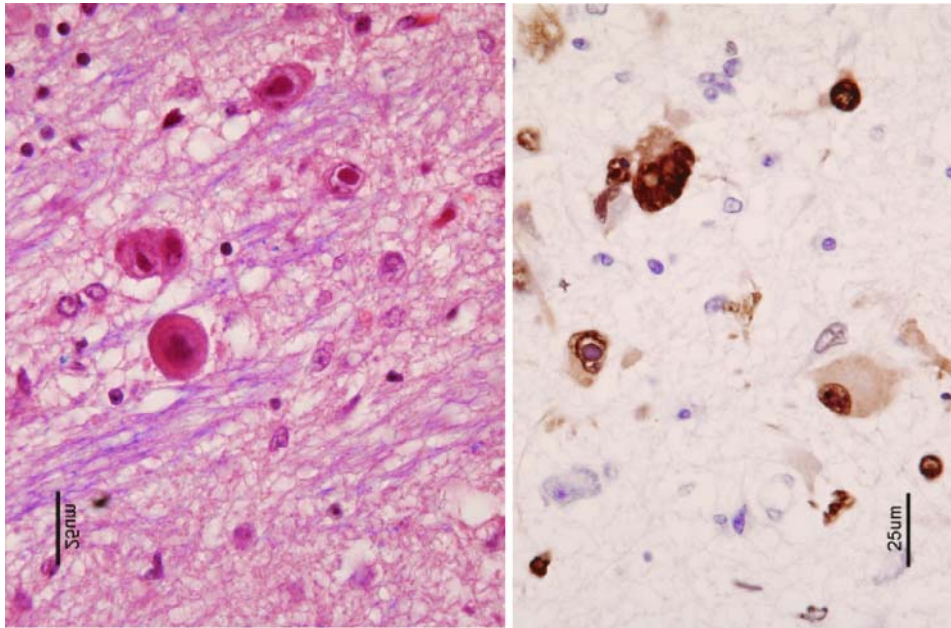


Fig. 20.1-3. CMV in situ hybridization shows positive cells in the subependymal layer. CMV immunohistochemistry.

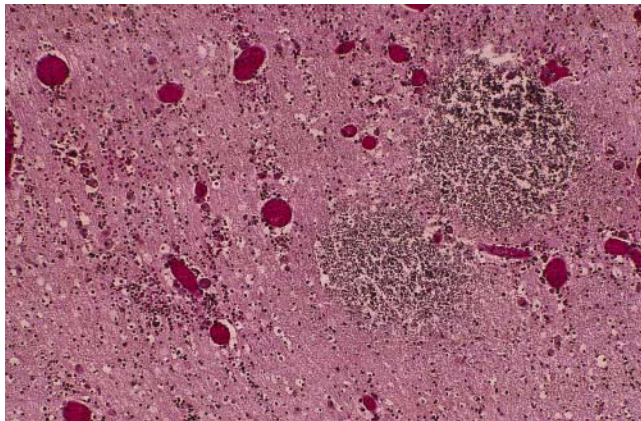


Fig. 20.1-4. Calcification in the white matter. H&E.

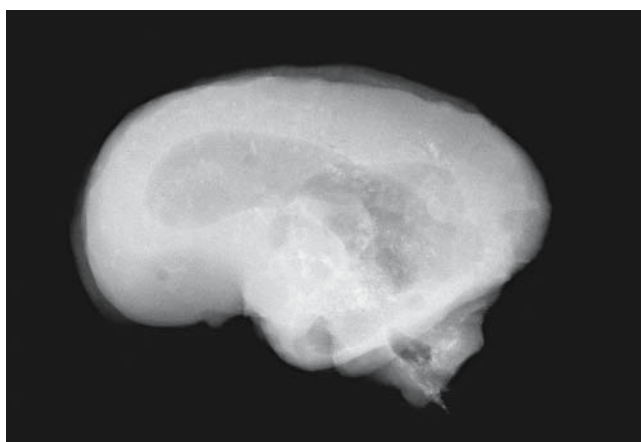


Fig. 20.1-5. Radiograph of fetal brain shows calcification in periventricular areas.

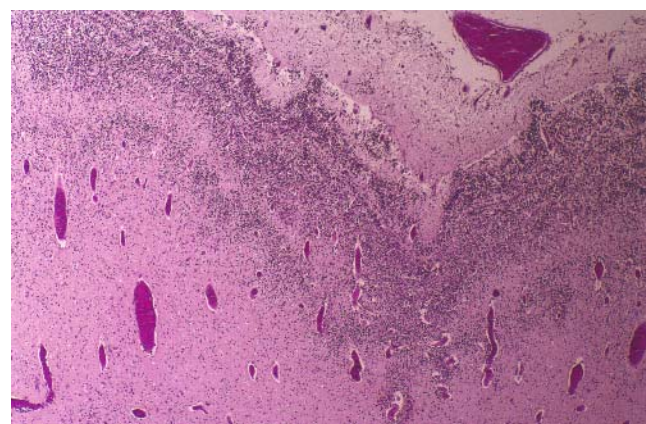


Fig. 20.1-6. Heterotopic glioneuronal tissue in the leptomeninges and polymicrogyria in a four-layer pattern. H&E.

20.2 Disseminated Varicella Zoster

Varicella infection is sometimes associated with neurological complications, including acute cerebellar ataxia, acute encephalopathy (Reye syndrome), acute necrotizing encephalopathy [2], or a postinfectious encephalitis or lacunar infarction after varicella infection in children [3]. Prenatal infection in the mother may result in acute neonatal encephalitis.

Neuropathology shows acute encephalopathy with fatty degeneration of the liver (Reye syndrome) in most

cases; in a few cases the liver exhibits disseminated focal necrotic foci with chronic inflammatory cell infiltration and inclusion bodies. Acute encephalitis produces multiple disseminated necrotic foci in neonates and a focal necrotic area in injured regions of the brain in children [4].

Congenital varicella syndrome includes cicatricial skin lesions (80%), limb deformities (70%), and ocular deformities (60%)



Fig. 20.2-1. Disseminated varicella zoster. Coronal section of the cerebrum exhibits brain purpura (multiple petechiae in the cerebri).



Fig. 20.2-2. Disseminated varicella zoster in the pons and cerebellum with multiple hemorrhages.

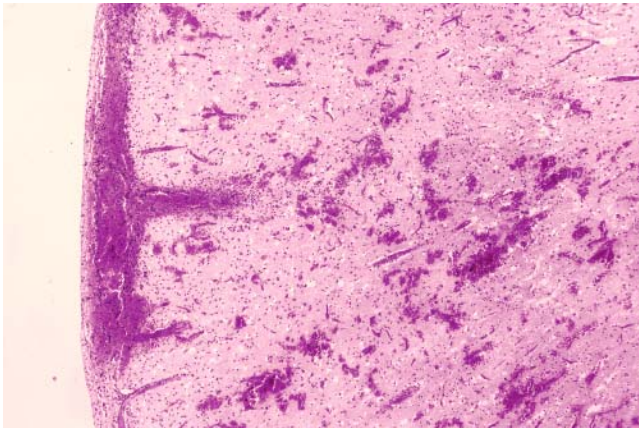


Fig. 20.2-3. Disseminated varicella zoster. Multiple hemorrhages in the cerebrum. H&E.

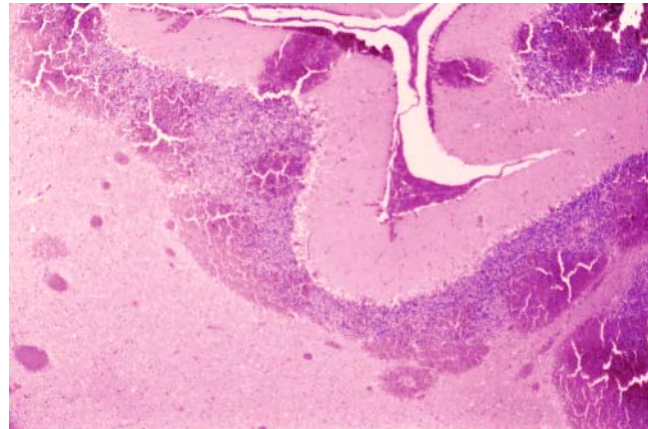


Fig. 20.2-4. Disseminated varicella zoster. Multiple hemorrhages in the cerebellum. H&E.

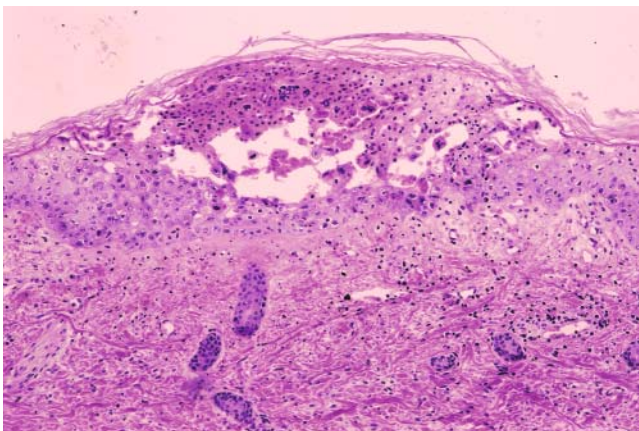


Fig. 20.2-5. Congenital varicella syndrome. Bullae on skin containing cells with viral inclusions and necrotic cells. H&E.

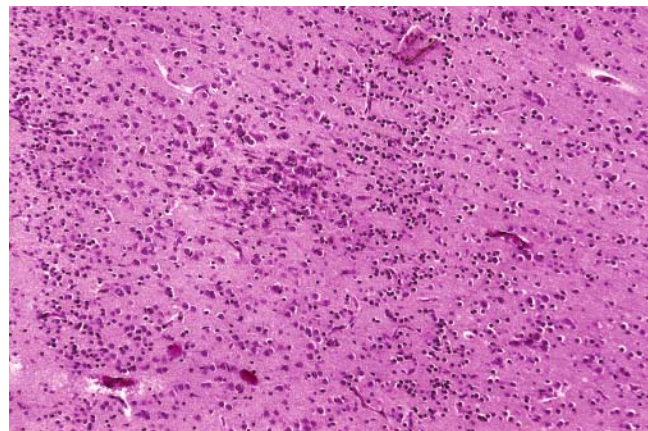


Fig. 20.2-6. Congenital varicella syndrome. Focal inflammatory foci and necrosis in the cerebral cortex. H&E.

20.3 Herpes Simplex Type 1 Encephalitis

Herpes simplex type 1 is the most common cause of nonepidemic encephalitis. The incidence in the general population is estimated to be 1/500 000. Herpes simplex type 1 encephalitis can be seen at any age.

Pathology

The lesions produced by herpes simplex type 1 are characteristically localized to the inferior frontal and medial temporal regions of the brain. Occasionally, the virus also damages the brain stem, producing necrotizing encephalitis. Necrosis is usually asymmetrical. Microscopically, there are perivascular lymphocytic infiltrates

and microglial nodules. In severe acute lesions there may be granulocytes, necrosis, microhemorrhages, and macrophages. Eosinophilic Cowdry's type A intranuclear inclusions are seen in neurons, oligodendrocytes, and astrocytes. Viral antigens can be identified by immunohistochemistry and by electron microscopy (EM), and virus particles can be identified in nuclei. Virus can be isolated from brain tissue by cell culture procedures. Virus DNA in paraffin sections of human brains can be detected at necropsy by use of the polymerase chain reaction (PCR).

Subacute herpes simplex virus type 2 meningoencephalitis produces acute encephalitis in the neonate or aseptic meningitis in adults [5].



Fig. 20.3-1. Herpes simplex type 1 encephalitis. Brain with temporal subarachnoid hemorrhage associated with focal herpes simplex encephalitis in a child.

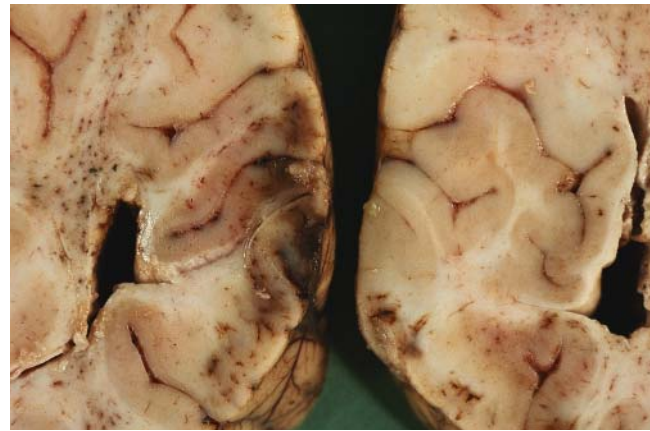


Fig. 20.3-2. Hemorrhagic necrosis in the cortex of the occipital lobes.

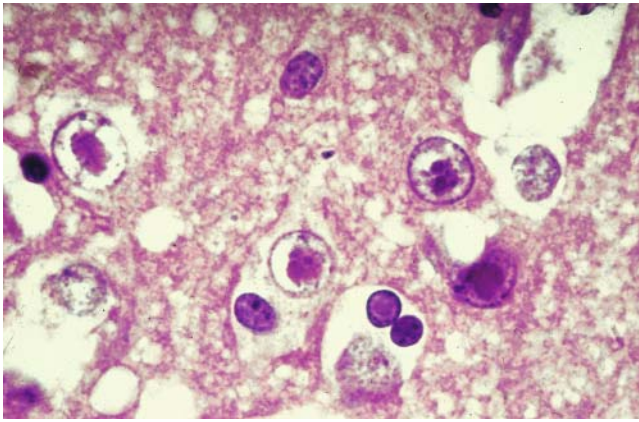


Fig. 20.3-3. Intranuclear inclusion in brain cells. H&E.

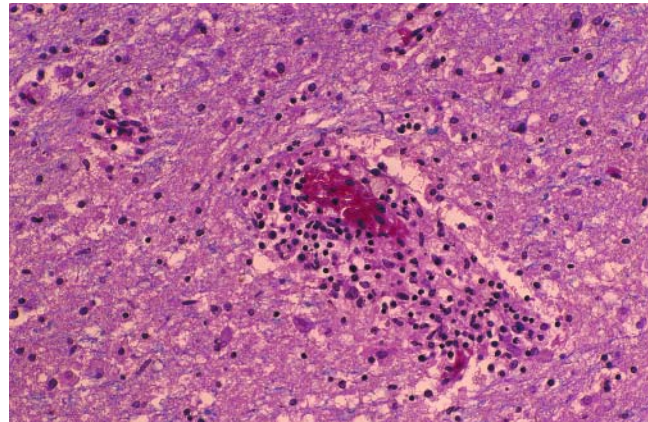


Fig. 20.3-4. Perivascular cuffing in the white matter. H&E.

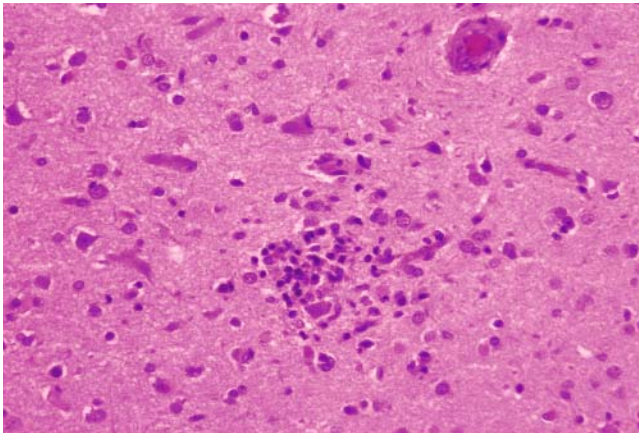


Fig. 20.3-5. Small foci of inflammatory cells; microglial nodule. H&E.

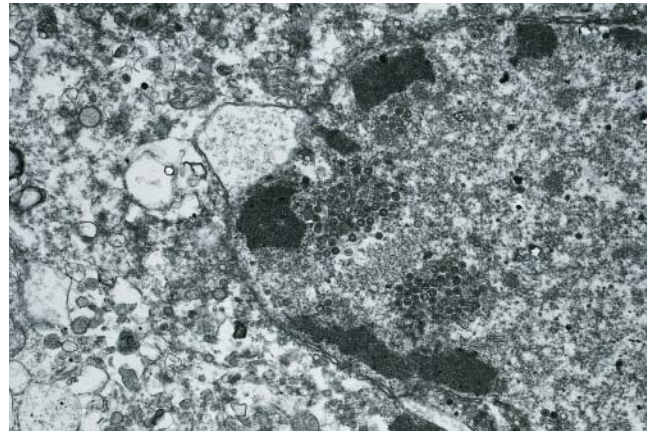


Fig. 20.3-6. EM shows viral inclusions in the nucleus.

20.4 Japanese Encephalitis

The most frequently occurring epidemic encephalitides are caused by arthropod-borne viruses (arboviruses). Japanese encephalitis virus is the most common cause of human arboviral encephalitis worldwide. The common arboviruses causing encephalitis in the United States belong to three families: (1) *Togaviridae* (Eastern equine and Western equine viruses); (2) *Flaviviridae* (St. Louis encephalitis virus, Japanese encephalitis virus, West Nile virus); and (3) *Bunyaviridae* (La Crosse virus). Mosquitoes are the arthropod vectors for most arboviral encephalitides.

Pathology

Gross examination of the brain shows diffuse or focal brain edema at the acute stage. Microscopically, the meninges show granulocytosis during the early phase and lymphocytosis and monocytosis during later phases. The lesion of Japanese encephalitis occurs primarily in the gray matter, similar to St. Louis encephalitis; and it predominantly involves the thalamus, brain stem, and cerebellum [5].

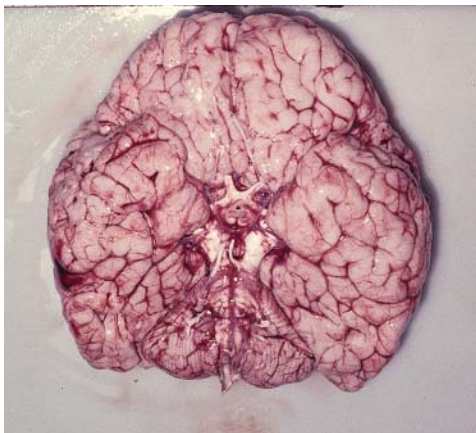


Fig. 20.4-1. Japanese encephalitis. Gross brain showing edema.

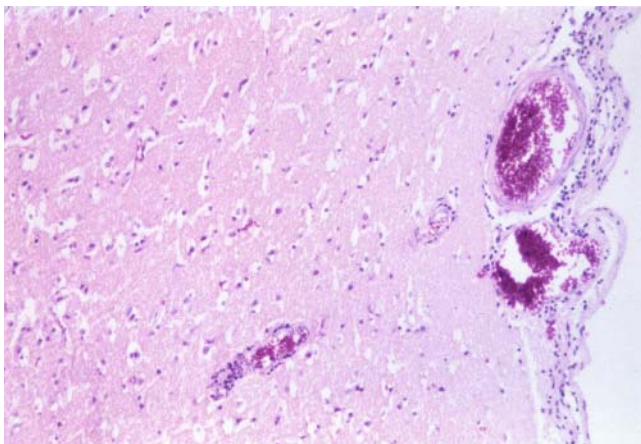


Fig. 20.4-2. Meningoencephalitis with leptomeningeal and perivascular inflammatory cell infiltration in the cerebral cortex.

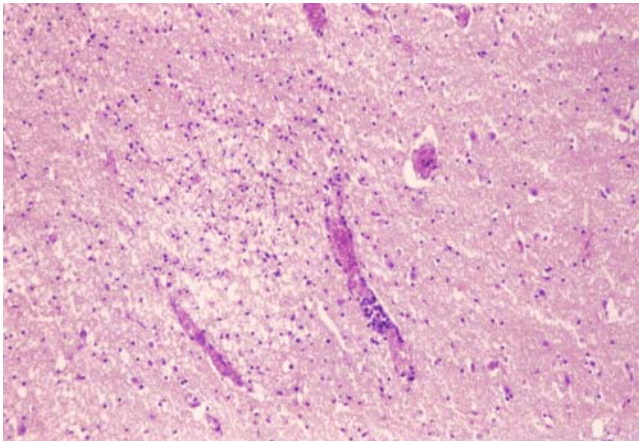


Fig. 20.4-3. Perivascular cuffing and necrosis in the thalamus.

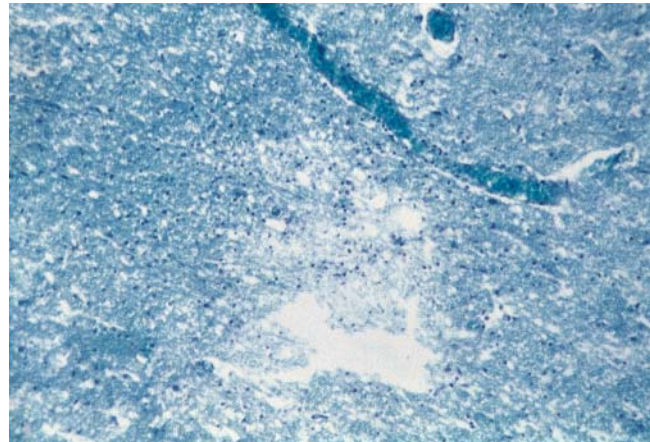


Fig. 20.4-4. Breakdown of myelin sheaths in the cerebral white matter. LFB.

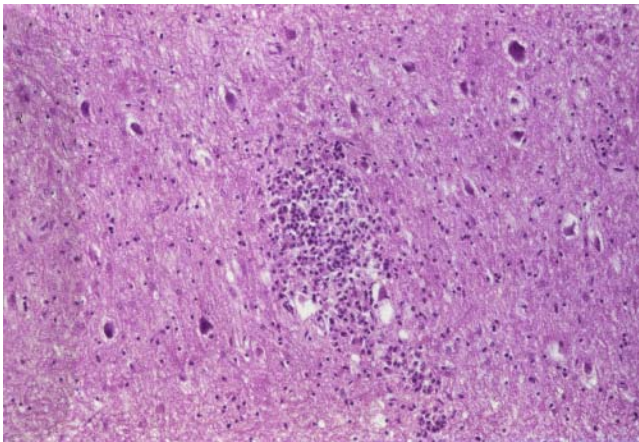


Fig. 20.4-5. Focal inflammatory cell infiltration in the dentate nucleus of the cerebellum. H&E.

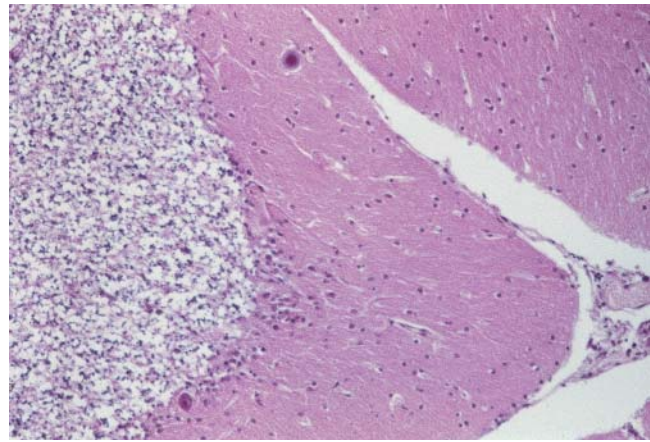


Fig. 20.4-6. Loss of granular cells and Purkinje cells as well as cell infiltration in the molecular cortex of the cerebellum. H&E.

20.5 Pediatric Human Immunodeficiency Virus (HIV) and Opportunistic Infection

Congenital HIV infection results from vertical transmission of maternal HIV infection. Transfusion-acquired HIV infection is acquired with transfusion of HIV-contaminated blood or blood products. After a long incubation period, both acquired and congenital infections lead to clinical immunodeficiency, which gradually worsens and is usually fatal [5].

Pathology

The neuro-pathogenesis of HIV-1 infection involves a cascade of viral products, cytokines and chemokines, and neurotransmitters. These lead to neuronal injury and deaths secondary to apoptosis or neurosis, and astrocytosis, as well as dendritic and synaptic damage.

Table 20.1. Clinical neurological manifestations of pediatric HIV infection

Manifestation	Common	Uncommon
Neurological abnormalities	Developmental delay	Seizures
	Encephalopathy	Movement disorders
	Microcephaly	Cerebellar signs
	Pyramidal tract neuromotor deficits	Peripheral neuropathy
	Cognitive impairment	
	Mental regression	
Neuroradiological findings	Basal ganglia calcifications	Low-density mass lesions in cases of opportunistic CNS infections or CNS tumors
	Brain atrophy with ventricular dilatation and cortical atrophy	
	Brain edema of variable degree	



Fig. 20.5-1. Congenital HIV infection. Gross brain showing dilatation of vessels in the base of the brain.

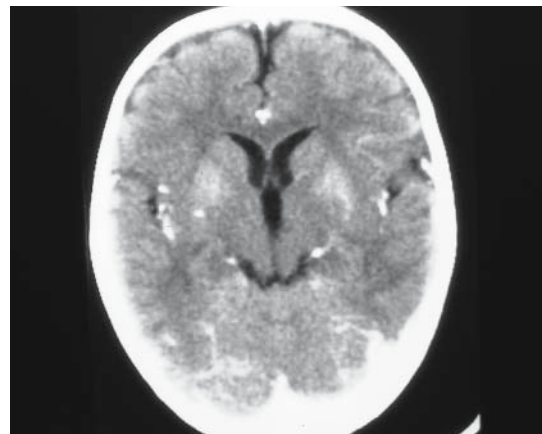


Fig. 20.5-2. Enhanced computed tomography (CT) shows multiple enhancement of lesions in the brain, including basal ganglia calcification.

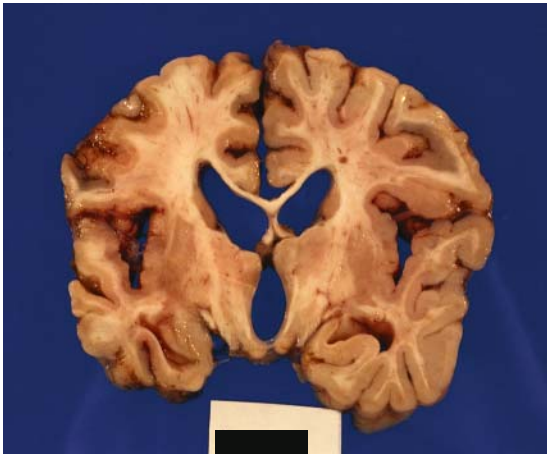


Fig. 20.5-3. Brain atrophy is predominantly in the gray matter.

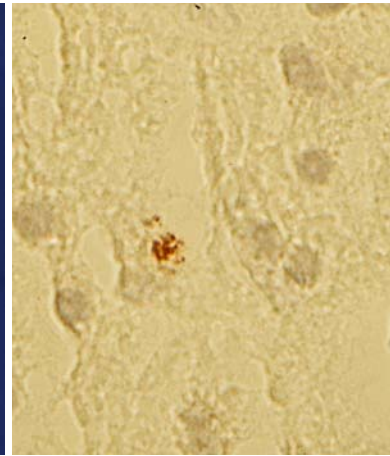


Fig. 20.5-4. *Left.* Focal cystic lesion in the periventricular area. *Right.* Immunohistochemistry identification of HIV antigen.



Fig. 20.5-5. Cerebellar atrophy.



Fig. 20.5-6. Golgi study shows poor dendritic development in the visual cortex of a child.

20.6 Progressive Multifocal Leukoencephalitis and Acute Hemorrhagic Leukoencephalitis (Hurst's Disease)

Progressive Multifocal Leukoencephalitis

Progressive multifocal leukoencephalitis (PML) occurs as an infrequent complication of a wide variety of conditions that compromise the immunological status of the host. It is rare in children.

Pathology

Multifocal demyelination occurs most prominently in the subcortical white matter and less commonly in the cerebellar, brain stem, or spinal cord white matter. PML is characterized by a triad of findings in demyelinating areas: (1) oligodendrocytes with enlarged nuclei (two to three times their normal size); (2) loss of oligodendroglia with relative sparing of axons; and (3) giant astrocytes with irregular lobulated hyperchromatic nuclei. There is little evidence of inflammation.

Electron Microscopy

There is a large number of 28- to 45-mm diameter papovavirus particles in dense crystalline arrays in the swollen oligodendroglial nuclei. The virus is identified by immune EM of purified viruses, immunofluorescence, or the immunoperoxidase test in a paraffin section of the brain [5].

Acute Hemorrhagic Leukoencephalitis

Acute hemorrhagic leukoencephalitis is one type of postinfectious encephalomyelitis. A mild viral infection precedes the onset of neurological symptoms (headache, vomiting, unconsciousness, seizures) by 1 to 3 weeks. Pathology includes perivascular petechial hemorrhages, necrotizing changes of the vessel wall, and inflammatory cells around vessels in the white matter. Demyelination is diffuse or multifocal [6].



Fig. 20.6-1. Progressive multifocal leukoencephalitis (PML). Note the numerous small foci of demyelination in the frontal lobe white matter. LFB.

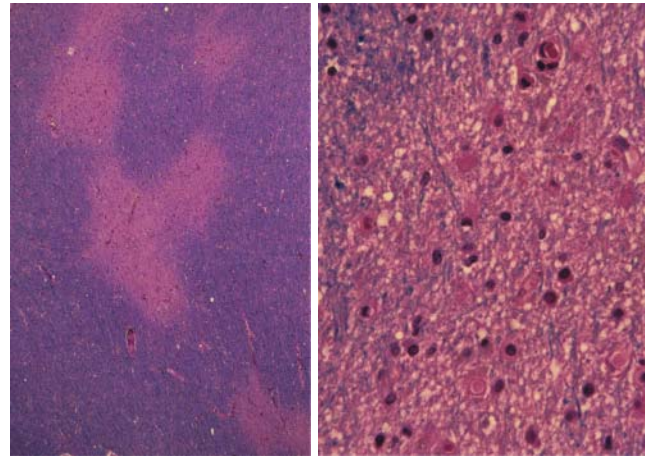


Fig. 20.6-2. Progressive multifocal leukoencephalitis. Giant astrocyte with multiple nuclei. (H&E). *Left.* Small foci of demyelination, *Right.* Close up of demyelinated area showing loss of myelin and reactive astrocytes (LFB/H&E).

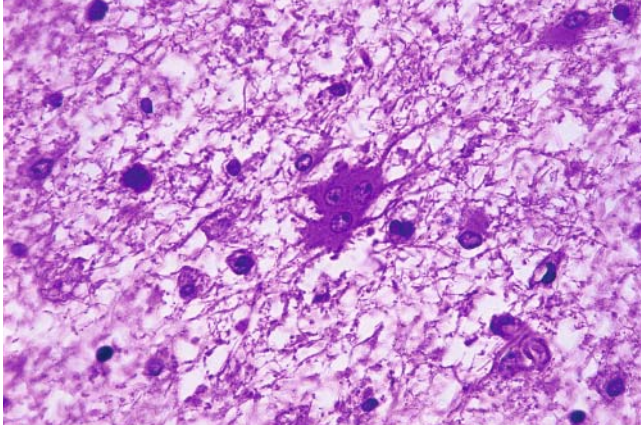


Fig. 20.6-3. Progressive multifocal leukoencephalitis. Oligodendrocytes with enlarged nuclei and astrocytes with multiple nuclei (H&E).

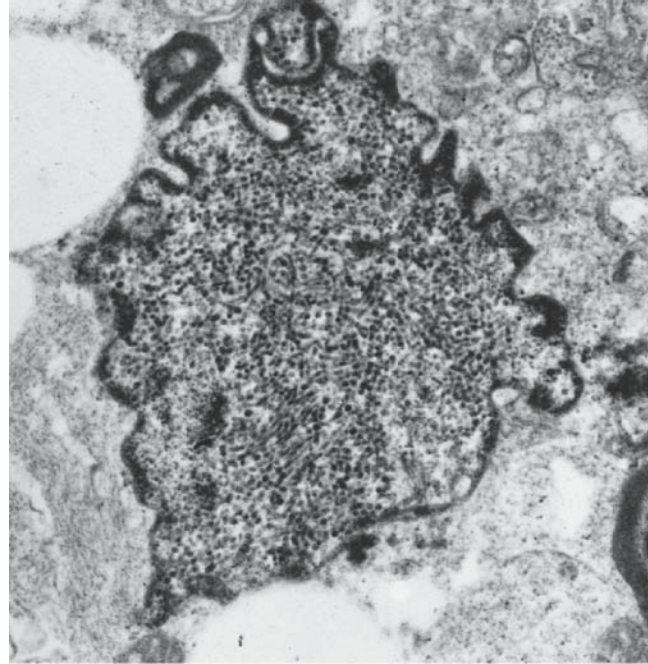


Fig. 20.6-4. Progressive multifocal leukoencephalitis. EM shows characteristic intranuclear inclusions.

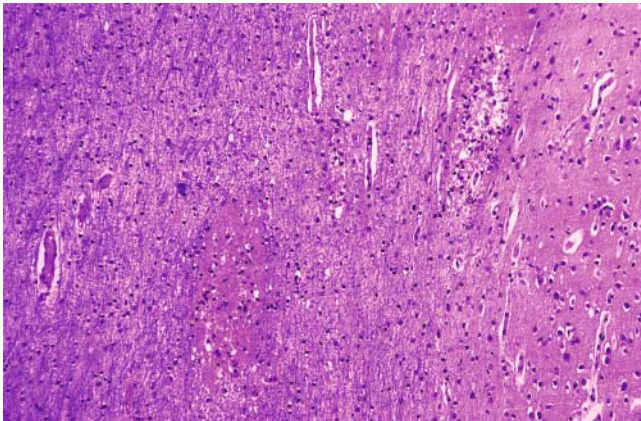


Fig. 20.6-5. Hemorrhagic leukoencephalomyelitis. Multifocal necrotic foci with perivascular hemorrhages in the cerebral white matter. KB stain.

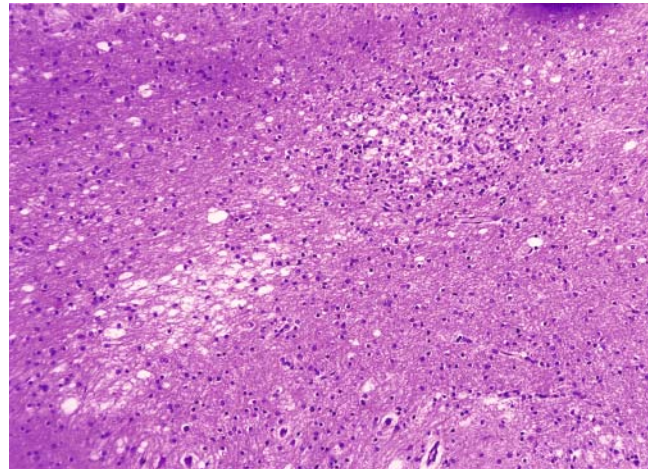


Fig. 20.6-6. Hemorrhagic leukoencephalomyelitis. Multifocal necrotic foci with spongy changes, inflammatory cell infiltration, and diffuse gliosis in the cerebral white matter. KB stain.

20.7 Rabies, Poliomyelitis, Parvovirus B19 Infection

Rabies is essentially a disease of animals. Most of the infections in animals and humans are caused by bites of rabid animals. The incubation time (stage I) is 1–3 months. The prodromal period of nonspecific symptoms (stage II) is 2–10 days. The acute neurological period of stage III causes “furious and paralytic” rabies. The brain and spinal cord show edema and petechial hemorrhages. Microscopically, there is lymphocytic perivascular cuffing in various regions of the central nervous system (CNS), especially in the basal ganglia. Rabies is characterized by the presence of Negri bodies [5].

Acute poliomyelitis is caused mainly by poliovirus and sometimes by other viruses (coxsackie virus, echovirus, and enterovirus). Anterior horn cells are selectively vulnerable to poliovirus. Nerve cells show chromatolysis and neuronophagia (neuron death) accompanied by inflammatory cell infiltration, edema, and microglial and macrophage proliferations [5].

Intrauterine parvovirus B19 infection is one of the causes of hydrops fetalis. Postmortem examination of a fetus may reveal the multinucleated giant cells of the macrophage/microglia [7].

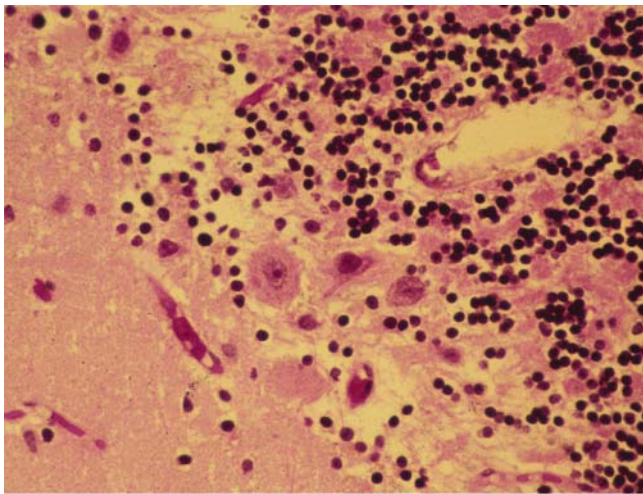


Fig. 20.7-1. Rabies. Histology of Negri bodies, eosinophilic inclusions, and an organized basophilic central core in the cytoplasm of large neurons.

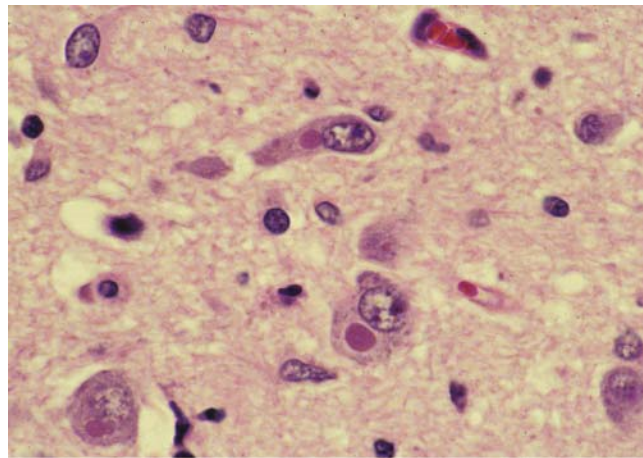


Fig. 20.7-2. Rabies. Negri bodies in intact neurons of the hippocampus. H&E.

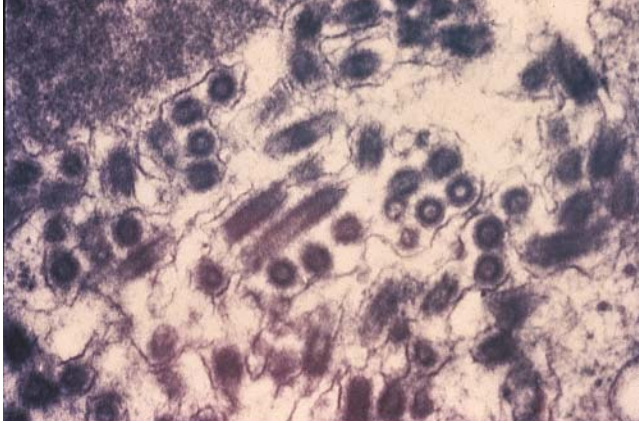


Fig. 20.7-3. Rabies. EM reveals bullet-like viral inclusions.

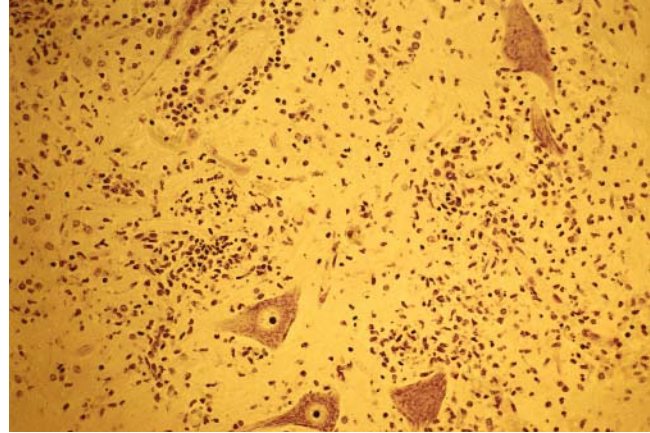


Fig. 20.7-4. Acute poliomyelitis. There is inflammatory cell infiltration around small vessels. Some neurons are atrophic or have disappeared.



Fig. 20.7-5. ParvoB19 infection. *Left.* This fetal brain shows focal atrophy in the insular area of right cerebral hemisphere. *Right.* There is a cavity formation in right insular region.

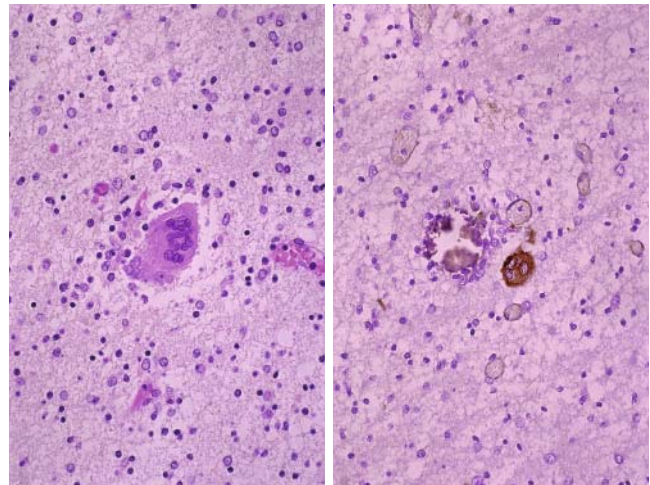


Fig. 20.7-6. ParvoB19 infection. *Left.* Polynuclear giant cells in perivascular areas of the fetal brain, with reactive astrocytes and microglia around the lesion. (H&E). *Right.* Macrophages and calcification in the cerebral white matter.

20.8 Subacute Sclerosing Panencephalitis

Subacute sclerosing panencephalitis (SSPE) is a rare childhood disease occurring in approximately 1/300 000 cases of measles. Typically, the patient has a history of initial contact with measles at a young age, usually less than 2 years of age. Neurological symptoms slowly develop between 5 and 15 years of age.

Pathology

In the early stages, the brain frequently has a normal weight and gross appearance. In later stages the brain becomes grossly atrophic. The pathological process follows a rostrocaudal progression with prominent involvement of the cortex and subcortical white matter. Perivascular inflammatory infiltrates consisting of lymphocytes and plasma cells are present in both the gray and white matter. In the gray matter, there is proliferation of “rod cells”; and inclusion bodies are found in neuronal and glial nuclei (Cowdry’s type A variety) and in the cytoplasm of neurons. The inclusion bodies are difficult to find during later stages of SSPE. Nerve cell loss is commensurate with the duration and severity of

the illness. In the white matter, there is diffuse demyelination and gliosis. In addition to the significant astrocyte proliferation there are intranuclear inclusions in the glial cells. EM shows that the inclusions are composed of measles nucleocapsids. Viral antigens may be identified in brain tissue by an immunofluorescence technique.

Similar Diseases

Subacute measles encephalitis (measles inclusion body encephalitis) occurs as an opportunistic infection in immunosuppressed or immunodeficient children with primary defects in cell-mediated immunity or who are under treatment with immunosuppressive drugs for lymphocytic malignancies (leukemia or lymphomas) or nephrosis. *Progressive rubella panencephalitis* also represents a slowly progressive encephalopathic disease with onset usually during the juvenile period. The disorder follows either congenital rubella syndrome or naturally acquired rubella in early life [5].



Fig. 20.8-1. Subacute sclerosing panencephalitis (SSPE). Brain with ventricular dilatation and marked atrophy.

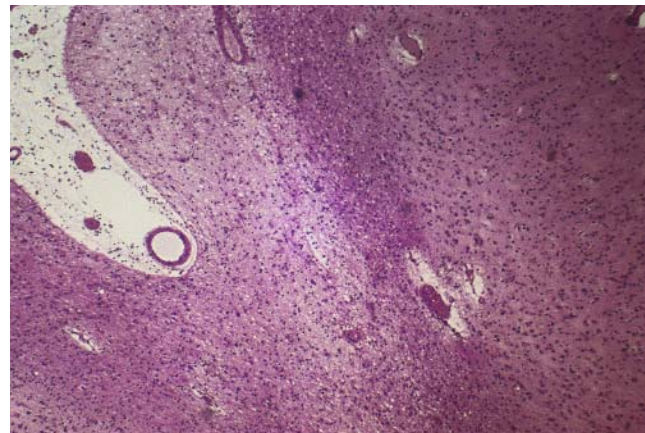


Fig. 20.8-2. Lesion of the cortex and white matter. Note the loss of neurons and astrogliosis in the thin cortex and astrogliosis in the white matter. H&E.

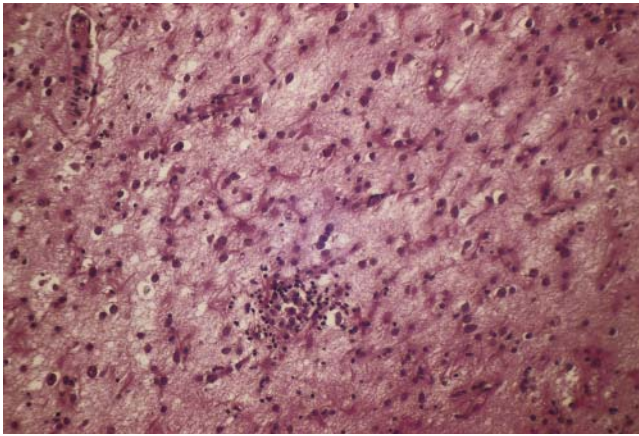


Fig. 20.8-3. Cortex exhibits inflammatory cell aggregates, neuronal loss, and astrogliosis. H&E.



Fig. 20.8-4. Focal demyelination in the frontal lobe.

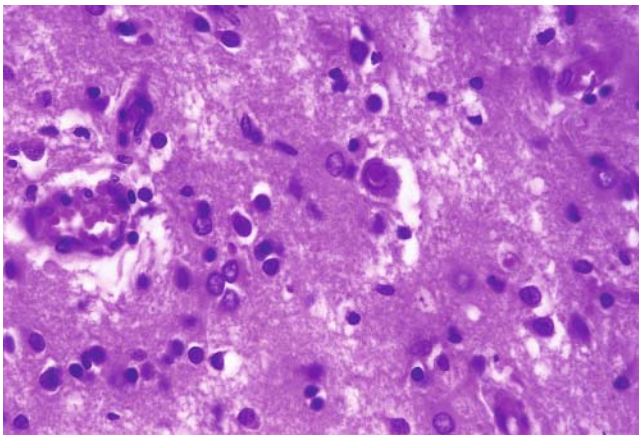


Fig. 20.8-5. Intranuclear inclusion in the cortex. The inclusion is often found in a degenerating part of the lesion.

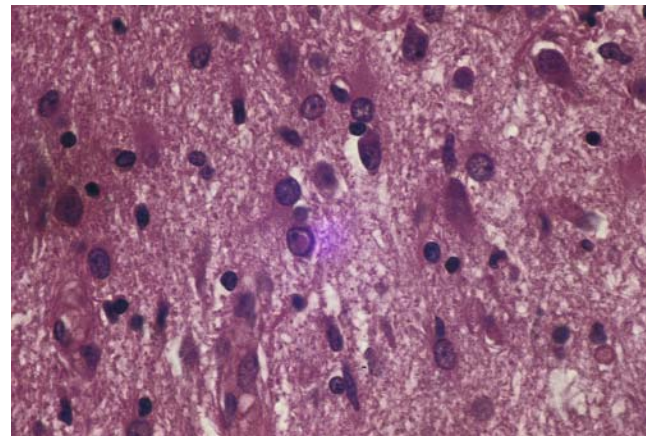


Fig. 20.8-6. Intranuclear inclusion in glial cells in the white matter. H&E.

20.9 Tuberculosis

The incidence of CNS tuberculosis is generally low, although in some regions with HIV infection it is more common. The prognosis is poor, and early diagnosis and treatment are essential. CNS infection with *Mycobacterium tuberculosis* usually results in both leptomeningitis and intraparenchymal lesions. PCR based on DNA sequence-specific tuberculosis with cerebrospinal fluid (CSF) and other tissues is a useful diagnostic test, but it may be negative in the tuberculoma itself.

Pathology

Tuberculous meningitis shows a whitish exudate about the base of the brain, surrounding the circle of Willis

and cranial nerves. The brain shows ventricular dilatation (hydrocephalus) and infarcts in the thalamus or basal ganglia. The gross tuberculoma is usually an irregular, round, firm mass with yellow/tan/white discoloration and a soft caseous center. Microscopically, the necrotic caseous region is surrounded by epithelioid cells, macrophages, lymphocytes, plasma cells, and multinucleated giant cells [8].

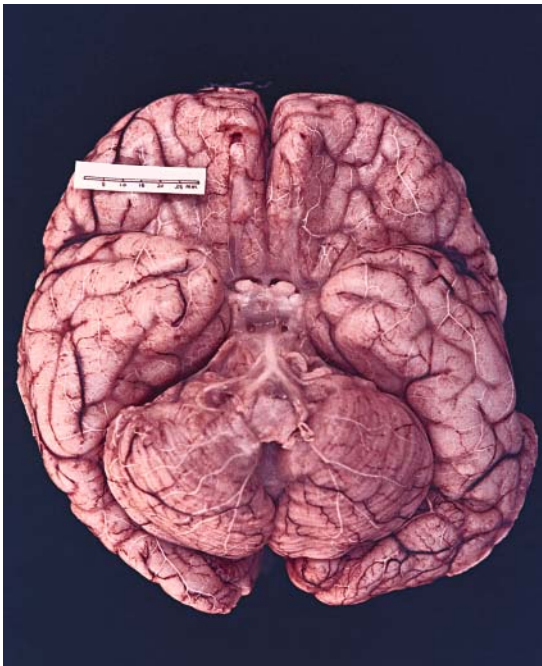


Fig. 20.9-1. Tuberculous meningitis. Gross brain. Leptomeningeal thickening in the base of the brain.

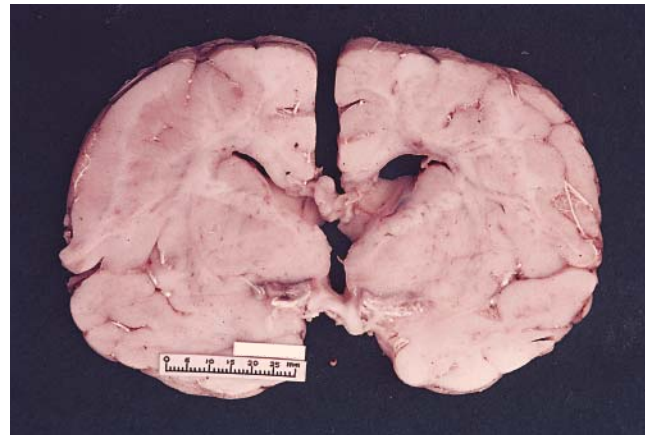


Fig. 20.9-2. Coronal section of brain through the basal ganglia shows edematous cerebral hemispheres.

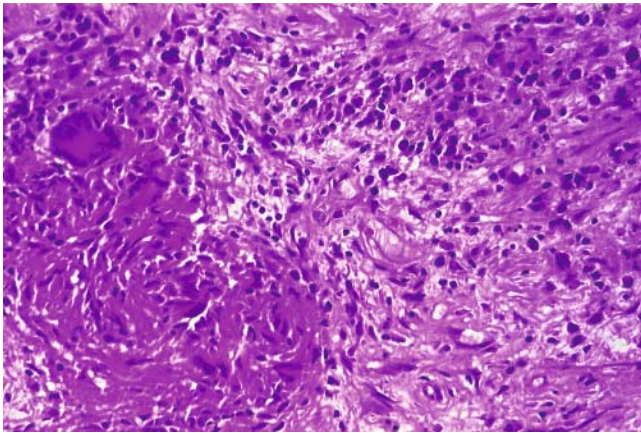


Fig. 20.9-3. Granuloma of tuberculosis composed of central necrosis, epithelioid cells, and Langhan's giant cells. H&E.

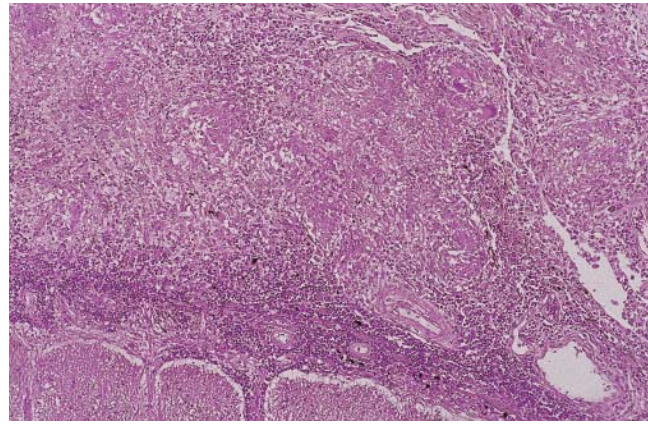


Fig. 20.9-4. Tuberculoma in the leptomeninges. H&E.

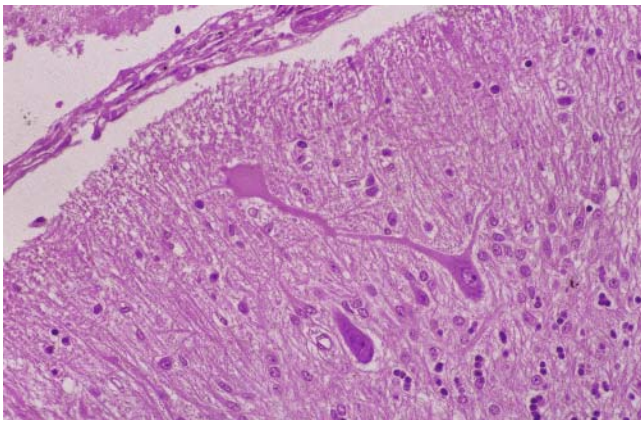


Fig. 20.9-5. Cerebellar cortex showing dendritic degeneration in the molecular layer. H&E.

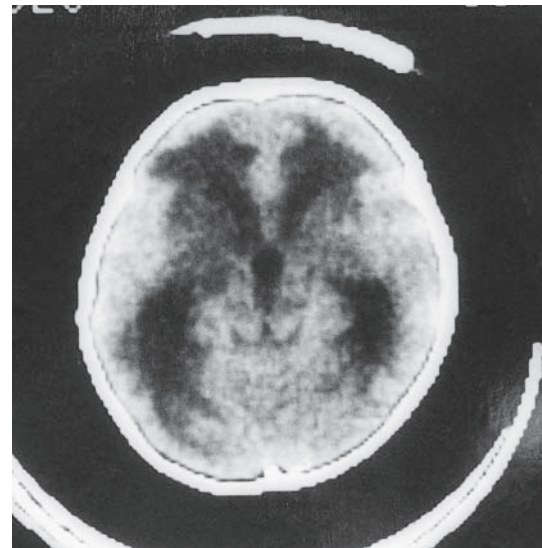


Fig. 20.9-6. CT shows diffuse low density in the cerebral white matter and dilatation of the third ventricle.

20.10 Acute Bacterial Meningitis and Brain Abscess

Acute Bacterial Meningitis

Acute bacterial meningitis is a common serious disease in neonates, who have poor protection against potential meningeal pathogens because of the absence of transplacentally acquired antibodies. Their exposure to meningeal pathogens in amniotic fluid or the maternal birth canal produces colonization of gastrointestinal or respiratory mucosal surfaces. If there is sustained high-level bacteremia, it may progress to leptomeningitis. If the meningitis is not treated early in the infection there is a risk of vascular occlusions and the production of permanent CNS damage.

Brain Abscess

Brain abscesses may develop when pyogenic organisms are introduced into the brain parenchyma. Both the

etiology and location of the abscess are influenced by the mode of infectious inoculation into the brain, which include (1) metastatic cerebral abscess from infected thromboemboli; (2) direct extension cerebral abscesses from adjacent infected foci, such as the ear, mastoid, or paranasal sinuses; (3) trauma-related cerebral abscesses; and (4) idiopathic or cryptogenic cerebral abscess in which the originating infectious focus is undetermined.

Cerebral abscesses occur in all age groups, with peak frequencies in the young (4–7 years of age) and in older adults. Cerebral abscesses in children are associated with cyanotic congenital heart disease, infective endocarditis, and contiguous ear, nose, and throat infections in approximately equal percentages. Cerebral abscesses are rare during the perinatal period, except when associated with gram-negative bacillary meningitis [8].



Fig. 20.10-1. Acute bacterial meningitis. There is purulent material in the subarachnoid space.

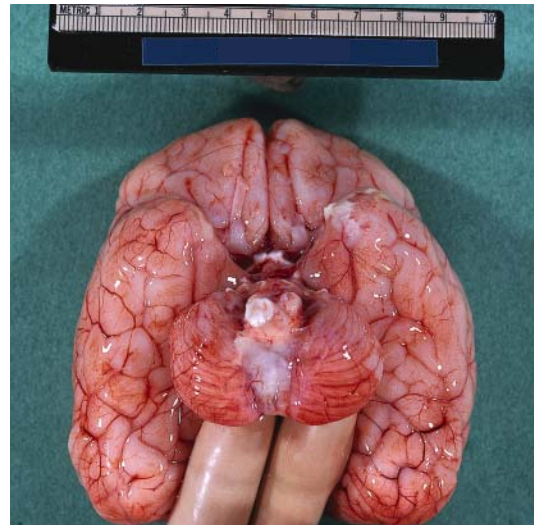


Fig. 20.10-2. Acute bacterial meningitis. Purulent meningitis in the meninges at the base of the brain.

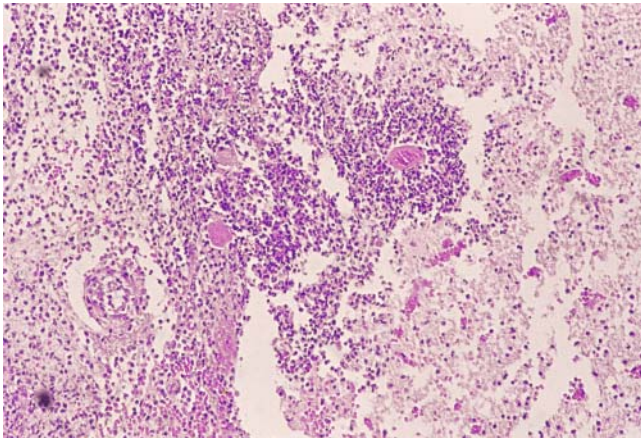


Fig. 20.10-3. Acute bacterial meningitis. There is acute leptomeningitis with acute inflammatory neutrophils invading the cortex. The vessels are obstructed with fibrin. H&E.

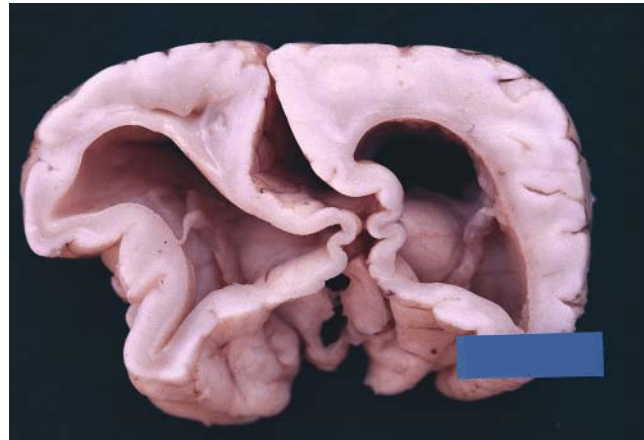


Fig. 20.10-4. Acute bacterial meningitis, the sequela of which is hydrocephalus.



Fig. 20.10-5. Brain abscess. Note the multifocal lesions in the periventricular area.

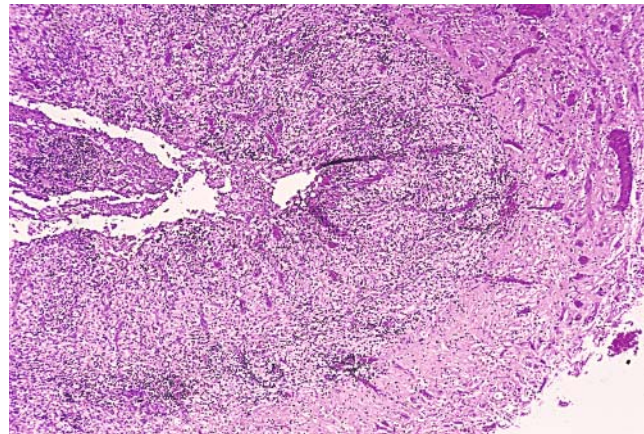


Fig. 20.10-6. Brain abscess. There is a central cavity of necrotic tissue surrounded by acute and chronic inflammatory cells with vascular proliferation. H&E.

20.11 Fungal Infections

Mycotic lesions in the CNS vary according to the underlying health or immunologic status of the host (see table below). The symptoms are usually minimal and the diagnosis is difficult. Hyphal fungi produce septic infarcts when the hyphal masses obstruct the arteries. The inflammatory response in the brain becomes granulomatous as the fungal infection persists. Organisms may be demonstrated with PAS or Grocott methenamine silver stain.

The most common cerebral mycosis is caused by *Candida albicans*. CNS candidiasis occurs primarily in immunocompromised patients who have been exposed to broad-spectrum antibacterial agents. Candidiasis is the most common neonatal fungal infection, developing in utero from an ascending vaginal infection or postnatally via passage through an infected/colonized birth canal.

Cryptococcus neoformans is the most common cause of childhood mycotic leptomeningitis. It may develop spontaneously in children without underlying illness, but it is more common in immunodeficient patients [9].

Table 20.2. Fungal infections

Organisms	CNS Lesions (Location)	Victims
<i>Candida</i> spp.	Leptomeningitis (rare), microabscess, granuloma	Neonates, immunosuppressed, prior antibacterial therapy
<i>Aspergillus</i> spp.	Cerebral infarcts, abscess	Immunosuppressed
<i>Cryptococcus neoformans</i>	Leptomeningitis	Immunosuppressed

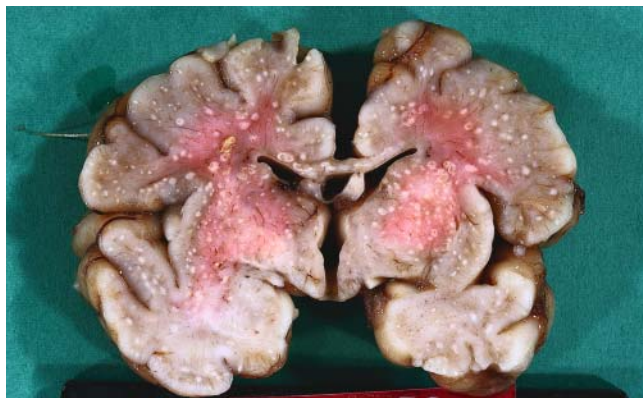


Fig. 20.11-1. *Candida* infection. The infection is in the brain of a neonate, with multiple widespread areas of focal necrosis.

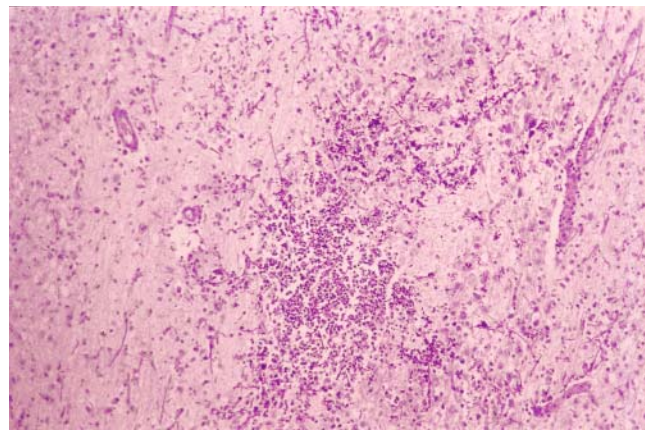


Fig. 20.11-2. *Candida* infection of the brain. Inflammatory cells surround the *Candida*. Calcification is present. H&E.

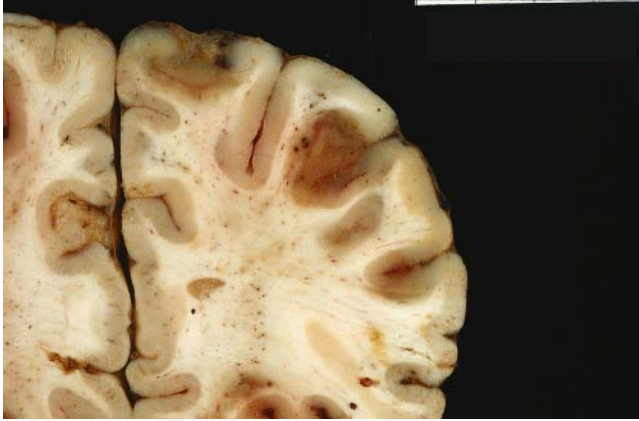


Fig. 20.11-3. *Aspergillus* infection. Focal necrosis in the cortex of the right middle frontal gyrus.

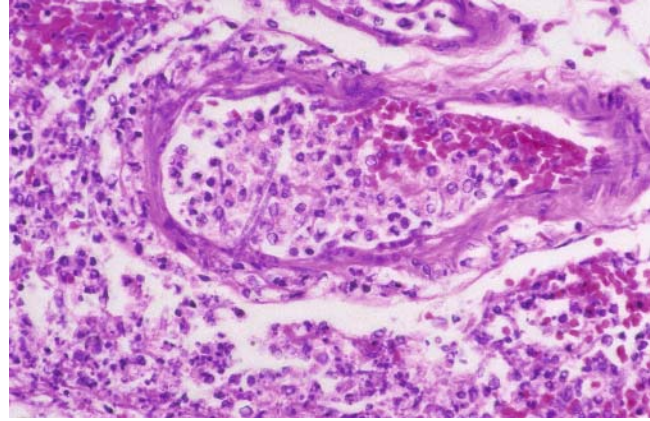


Fig. 20.11-4. *Aspergillus* vasculitis. Organisms in the CSF and tissues can be seen with the Ziel-Nielsen stain.

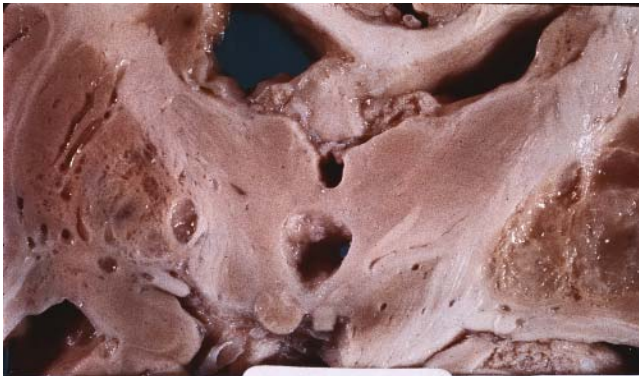


Fig. 20.11-5. *Cryptococcus* infection. There are multiple cavities in the basal ganglia, which are *Cryptococcus* abscesses.

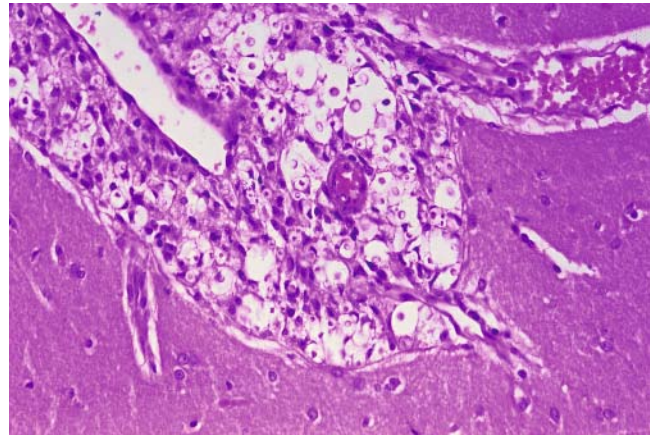


Fig. 20.11-6. *Cryptococcus* meningitis. Organisms are surrounded by clear spaces in the subarachnoid space and superficial cortex.

20.12 Toxoplasmosis, Congenital Toxoplasmosis

Congenital toxoplasmosis results when *Toxoplasma gondii* crosses the placental barrier. It may occur at any time during pregnancy, but the greatest risk is during the second trimester. The organism causes septicemia in the susceptible fetus, which results in encephalomyelitis. Parasites proliferate in the ependyma and subependymal region and spread through the brain, which may result in death in utero. The surviving neonate presents with seizures, brain calcification, hydrocephalus, and chorioretinitis. The neurological sequelae include microcephalus, hydrocephalus, and psychomotor retardation.

Acquired toxoplasmosis in children and adults usually follows a subclinical or benign course. However, in

immunocompromised patients it may result in *Toxoplasma* encephalitis.

Pathology

The lesions of encephalomyelitis, which are usually acute or subacute, consist of variously sized areas of granulomatous inflammation containing a central zone of necrosis. With congenital toxoplasmosis, brain atrophy may be associated with cystic cavities (porencephaly), ventricular dilation (obstructive hydrocephalus), and calcified foci throughout the brain, particularly around the ventricles.



Fig. 20.12-1. Toxoplasmosis. Note the necrosis in the pons and cerebellum.

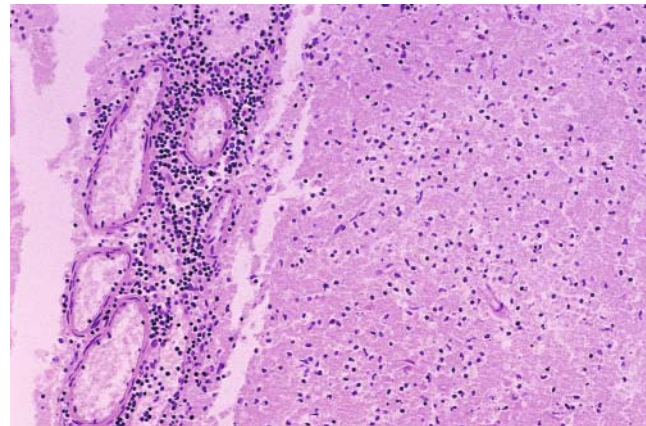


Fig. 20.12-2. Toxoplasmosis infection causing leptomenigitis with lymphocyte infiltration. H&E.

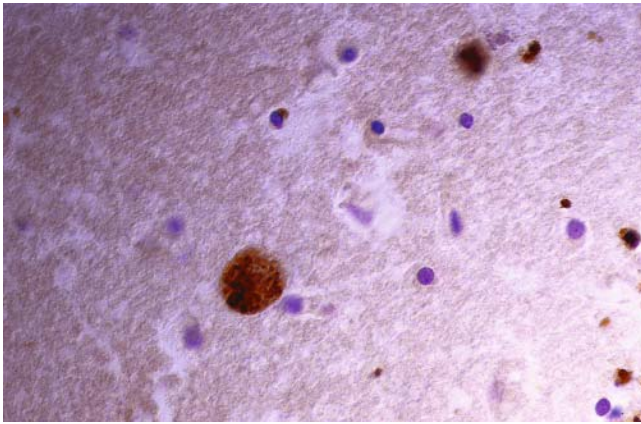


Fig. 20.12-3. *Toxoplasma* cyst with positive immunohistochemistry.

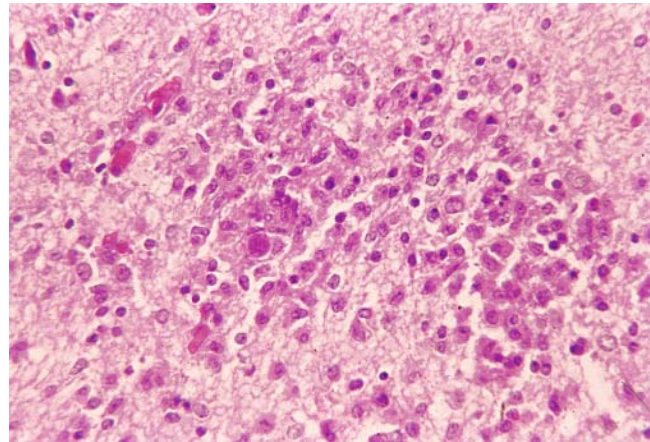


Fig. 20.12-4. Congenital toxoplasmosis infection in the brain. Note the cyst and epithelioid cells. H&E.

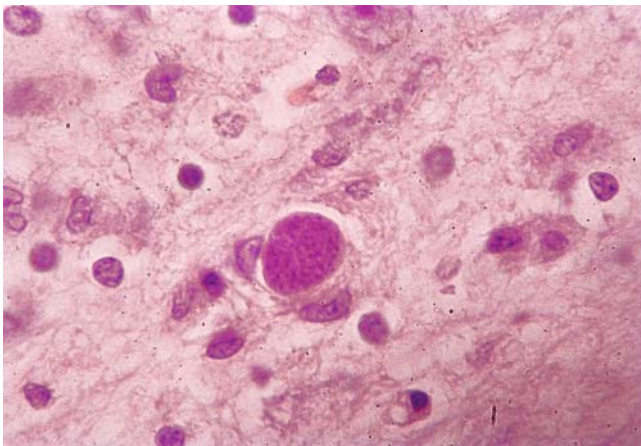


Fig. 20.12-5. Congenital toxoplasmosis infection in the brain. Note the cyst. H&E.

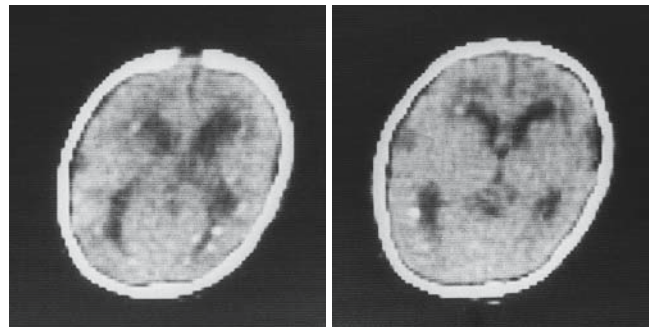


Fig. 20.12-6. Congenital toxoplasmosis. CT shows periventricular calcifications.

20.13 Amebiasis

Free-living amoebae invade the CNS in humans and produce encephalitis. Primary amebic meningoencephalitis (PAM) is caused by *Naegleria fowleri*, and granulomatous amebic encephalitis (GAE) is caused by *Acanthamoeba* and *Balamuthia*.

PAM is usually fatal within 2–7 days. Lesions can be found anywhere in the CNS in the form of acute necrotizing and hemorrhagic meningoencephalitis with swelling of affected regions [9].

Table 20.3. Free-living amoebae pathogenic to humans

Disease	Age	Immune status	Incubation	Course
<i>Naegleria</i> meningo encephalitis (PAM)	Children	Normal	2–15 Days	Fulminant
<i>Acanthamoeba</i> granulomatous encephalitis (GAE)	Children, adults	Compromised	Unknown	Days to months
<i>Leptomixid</i> granulomatous Amebic encephalitis	Children Adults	Compromised	Unknown	Days to months

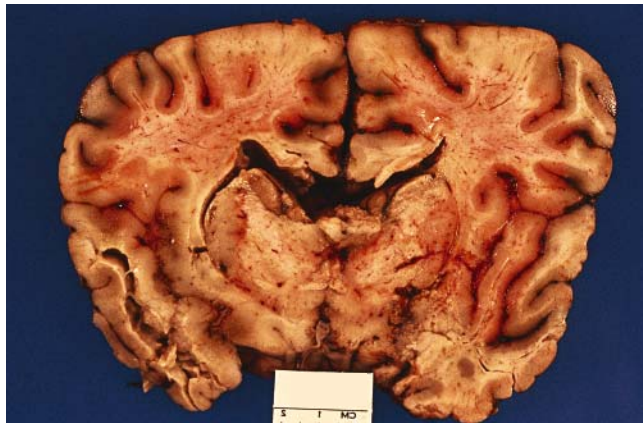


Fig. 20.13-1. *Naegleria fowleri* infection. Acute meningoencephalitis with marked brain edema and congestion. Inflammation and softening are more marked in the lower parts of the hemispheres.

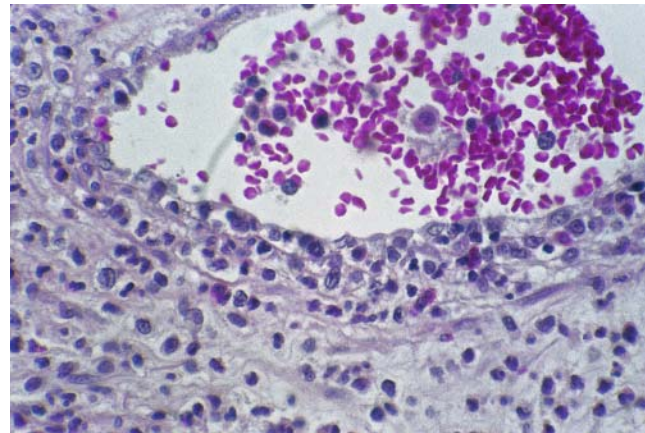


Fig. 20.13-2. Acute *Naegleria* meningitis. Subarachnoid phlebitis with polynuclear and mononuclear inflammatory cell infiltration. H&E.

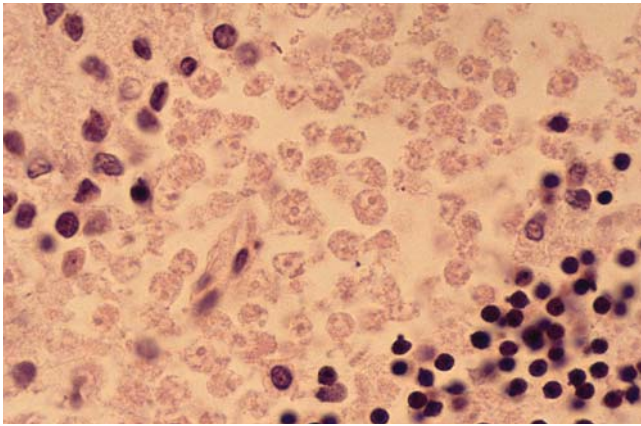


Fig. 20.13-3. *Naegleria* encephalitis with amebae in the cerebellar internal granular layer but no inflammatory response.

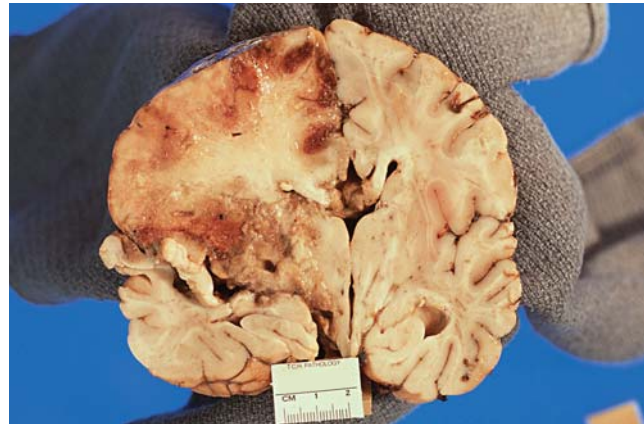


Fig. 20.13-4. Chronic amebic encephalitis in the left frontal lobe. Focal swelling of the frontal lobe is associated with marked congestion and hemorrhagic necrosis in the surrounding peripheral areas.

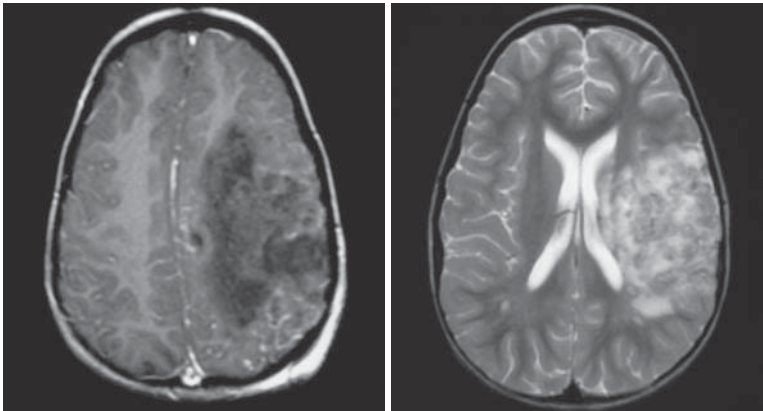


Fig. 20.13-5. Chronic *Acanthamoeba* encephalitis. T1-weighted MRI shows a localized low-intensity necrotic lesion in the left centrum semiovale; and T2-weighted MRI shows high intensity in the same area.

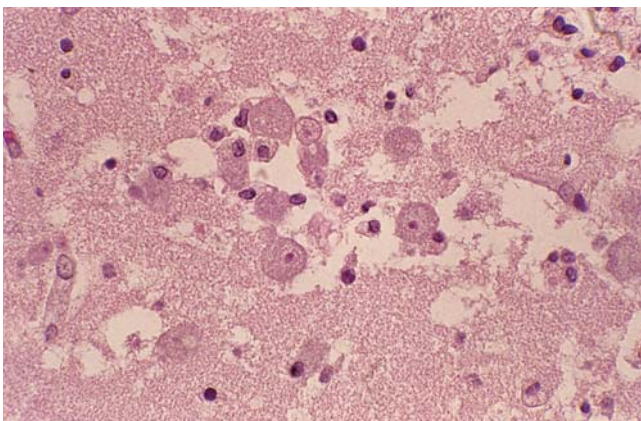


Fig. 20.13-6. Chronic *Acanthamoeba* encephalitis. Note the organisms in a necrotic zone.

20.14 Echinococcus, Trichinella Spiralis, Cysticercus

Echinococcosis occurs wherever humans live in close proximity to sheep and dogs (the definitive hosts). Humans are infected by eggs of the mature worm, which reside in the intestine of the animals. In humans, after ingestion of eggs, the eggs hatch in the intestine and produce oncospheres, which spread via the bloodstream to other organs, especially the liver and brain. Brain cysts are usually single and may be asymptomatic [9].

Trichinosis in humans is caused by ingestion of *Trichinella spiralis* larvae in infected meat of wild animals or pigs. Larvae can enter the circulation after penetrating the epithelium of the bowel. They survive primarily in muscle after producing an acute disorder of diarrhea, vomiting, abdominal pain, fever, myalgia, and facial and orbital edema. CNS infection is rare.

Cysticercosis is an important public health problem. Taeniasis occurs when humans ingest undercooked pork, wild boar, or wart hog meat that is contaminated with the larval stage of *Taenia solium*. The mature worm develops in the intestine of humans, and eggs are excreted in feces. This is the source of infection for the animals and also for humans. From the ingested eggs the oncospheres spread via lymphatics and vessels to the brain and other organs.

The larval form (*Cysticercus cellulosae*) produces cysts of various sizes that may produce symptoms, such as seizures, or create an obstructive hydrocephalus or focal brain and meningeal inflammation.

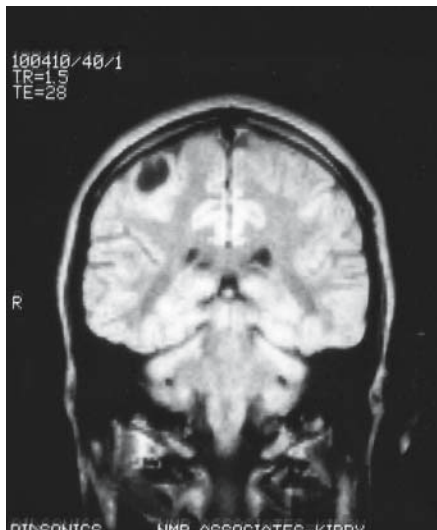


Fig. 20.14-1. Cysticercosis. T1-weighted MRI shows cavity formation surrounded by high intensity.

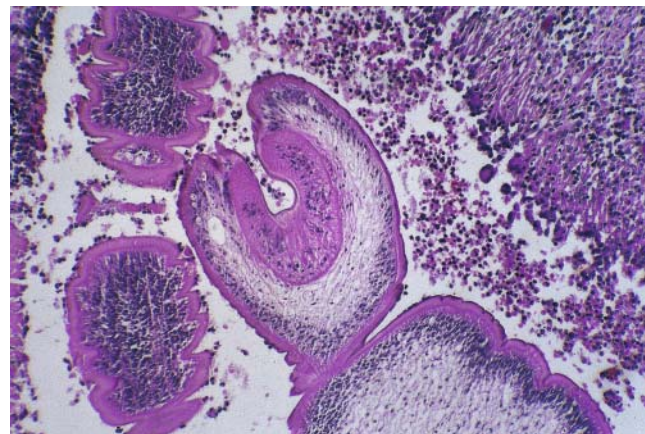


Fig. 20.14-2. Cysticercosis. Histology shows the scolex of the viable larvae.

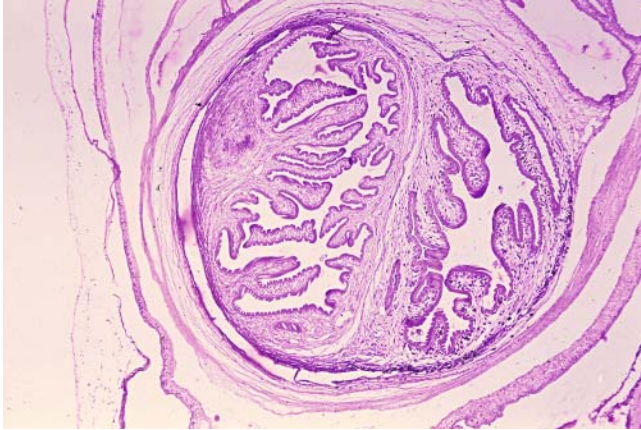


Fig. 20.14-3. *Cysticercus* larvae in a cerebral cyst.



Fig. 20.14-4. *Trichinella spiralis* in mucosa, showing the histology of the organism.

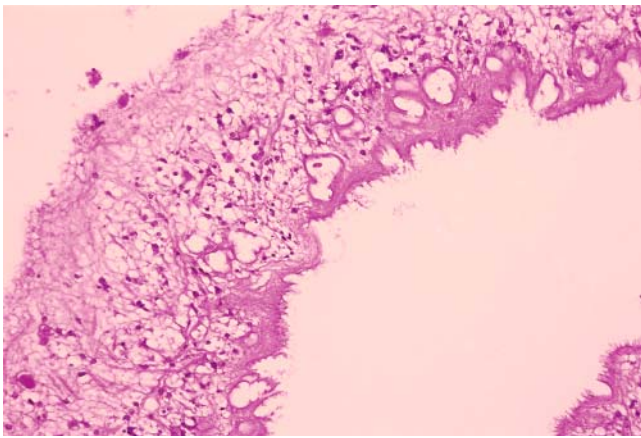


Fig. 20.14-5. Cysticercosis. Inflammatory changes in blood vessels consist of lymphocytes and plasma cell infiltration of the arterial lumen and adventitia. There is endothelial proliferation with progressive development of endarteritis.



Fig. 20.14-6. Cysticercosis. Note the cyst in the cerebral cortex.

21 Intoxication

21.1 Minamata Disease

Minamata disease (methylmercury poisoning) can affect all ages. In *adults* all the organs contain increased mercury, but lesions occur mainly in the nervous system, particularly the brain. The neurons, especially nonpyramidal cells in the cerebral and cerebellar cortices, are destroyed. In the cerebrum, there is selective involvement of the calcarine and precentral regions involving neurons in the second and upper third layer and predominantly in the depth of the sulci. In the cerebellum, the granular cells are most susceptible and are lost in the deeper regions of the folia of both hemispheres. In

nonfetal infantile Minamata disease there is hypoplasia of various organs, including the brain. There is widespread disintegration of cortical neurons and secondary degeneration of myelin sheaths.

Fetal Minamata disease shows hypoplastic and dysplastic changes. The germinal matrix persists in the ventricular walls, and the corpus callosum is underdeveloped. The cytoarchitecture of neurons in the cerebral and cerebellar cortices is abnormal, exhibiting hypoplastic and dysplastic changes. There is poor myelination [1–3].



Fig. 21.1-1. Infantile Minamata disease. Medial view of cerebral hemisphere showing brain atrophy and thin corpus callosum, especially in the posterior part (Courtesy of Dr. Eto K.)

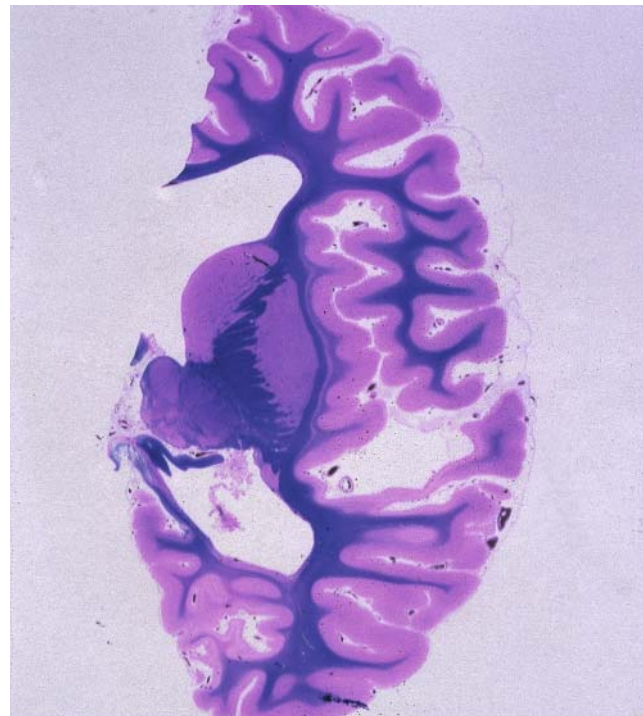


Fig. 21.1-2. Infantile Minamata disease. KB staining of a coronal section of the cerebral hemisphere shows atrophy of the cerebral hemisphere (Courtesy of Dr. Eto K.)

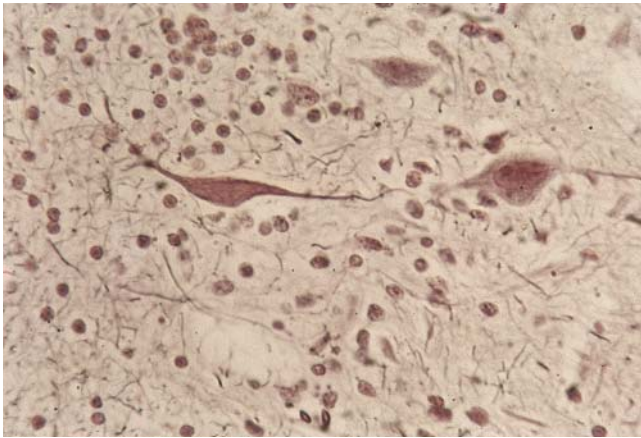


Fig. 21.1-3. Infantile Minamata disease. Bodian stain of the cerebellum shows degeneration of Purkinje cells with torpedo formation (Courtesy of Dr. Eto).



Fig. 21.1-4. Fetal Minamata disease. The cerebral cortex of the frontal lobe shows an irregular cellular arrangement in the superficial cortex (Courtesy of Dr. Eto).

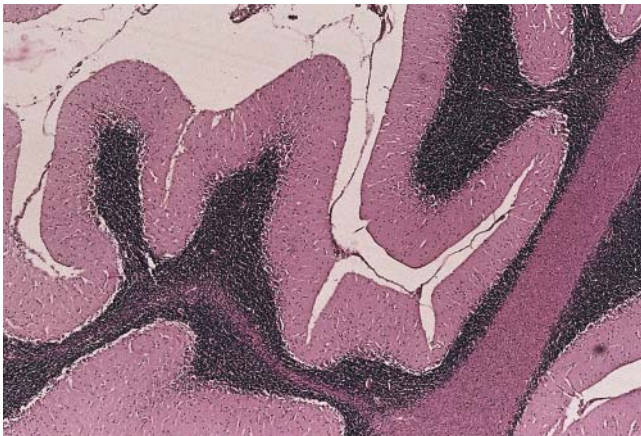


Fig. 21.1-5. Fetal Minamata disease. The folia of the cerebellum show focal reduction of the granular cell layer (Courtesy of Dr. Eto).

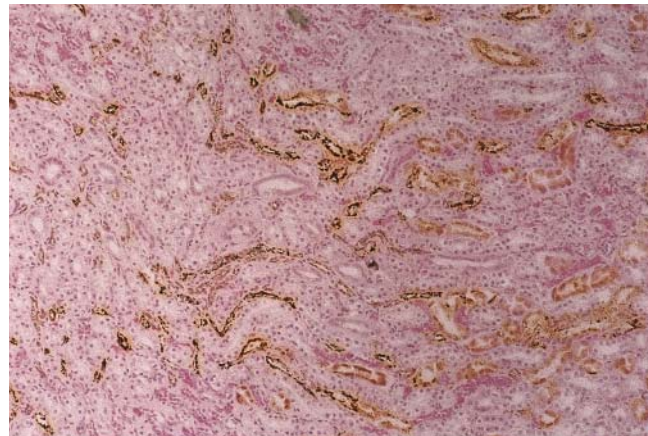


Fig. 21.1-6. Fetal Minamata disease. Mercury stain shows positive granules in epithelial cells of the renal tubules (Courtesy of Dr. Eto).

21.2 Fetal Alcohol Syndrome, Other Drug Intoxication

Alcohol can affect the immature nervous system through chronic in utero exposure or acute maternal intoxication. Numerous variable factors such as nutrition, vitamins, smoking, and drug intake may play a role in the production of this syndrome. The neuropathological features include leptomeningeal glioneuronal heterotopia, lissencephaly, agenesis of corpus callosum, and migration anomalies in the cerebellum, brain stem, and cerebrum.

Trimethadione (an anti-epileptic drug) is an important teratogen causing fetal trimethadione syndrome, and spontaneous abortion. Significant malformations include anencephaly, microcephaly, and meningocele [4].

Fetal hydantoin syndrome includes hypoplastic nail, microcephaly, craniofacial anomalies, and abnormal

motor and mental development. Acute intoxication of diphenylhydantoin (phenytoin) shows cerebellar signs, and chronic intoxication is also reported.

Table 21.1. Drugs and toxicants associated with adverse effects on the developing brain

Antiepileptic drugs	Trimethadione, diphenylhydantoin (phenytoin), valproic acid
Anticoagulants	Coumarin, warfarin
Drugs of habituation and abuse	Cocaine, ethanol, heroin, methadone
Folic acid antagonists	Aminopterin, methotrexate



Fig. 21.2-1. Fetal alcohol syndrome with facial dysmorphic features including a saddle-shaped nose, maxillary hypoplasia, absent philtrum between the nose and upper lip, and a short, thin upper lip.

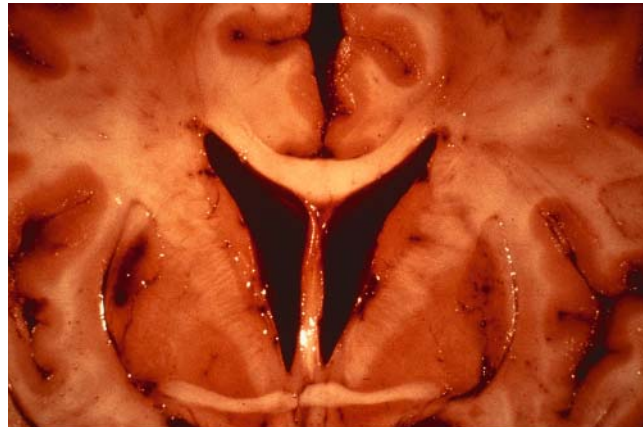


Fig. 21.2-2. Alcohol intoxication with thin corpus callosum and a small caudate nucleus and putamen.

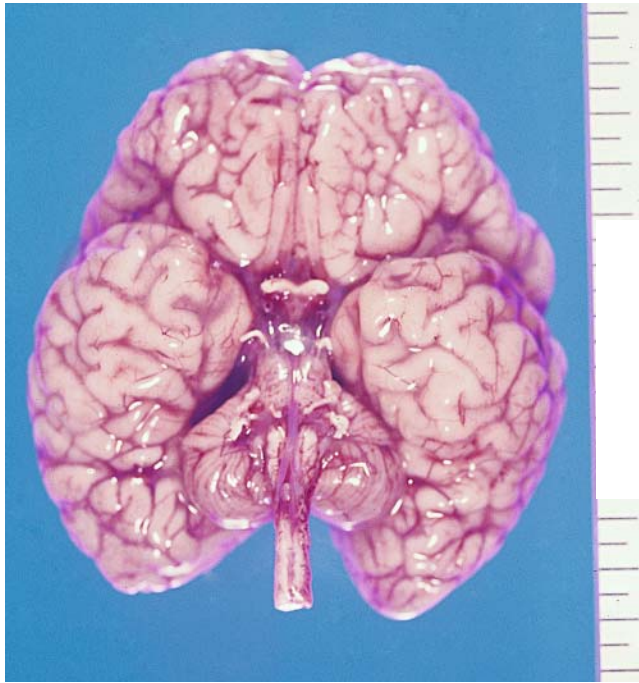


Fig. 21.2-3. Fetal trimethadione syndrome. Gross brain shows hypoplasia of the cerebellar hemisphere.

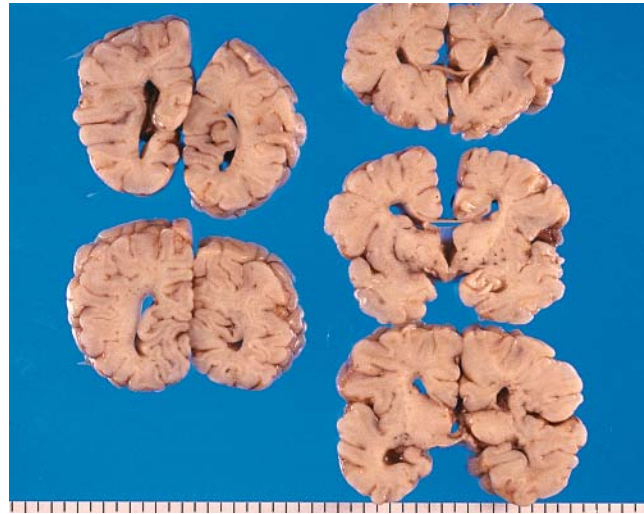


Fig. 21.2-4. Fetal trimethadione syndrome. These 1-cm sections of the cerebral hemispheres show partial agenesis of the corpus callosum. Microscopically, leptomeningeal heterotopia and polymicrogyria are apparent.

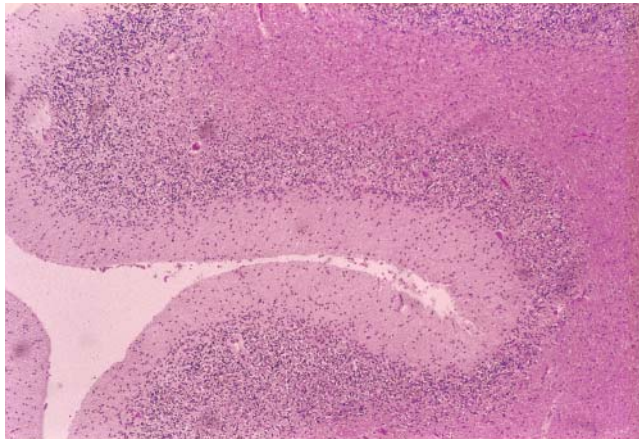


Fig. 21.2-5. Chronic diphenylhydantoin (DPH) intoxication. Note the loss of Purkinje cells, reduced number of granular cells, and increased Bergman glia in the cerebellum of a child. H&E.

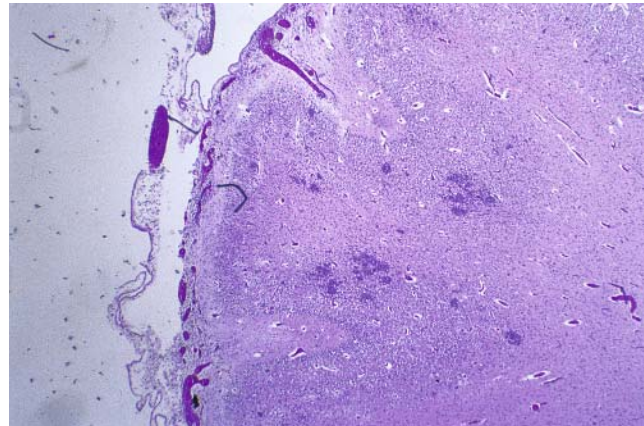


Fig. 21.2-6. Congenital cocaine syndrome. Polymicrogyria, residual immature cell groups, and diffuse leptomeningeal glioneuronal heterotopia are present in a neonate. H&E.

21.3 Carbon Monoxide Intoxication; Other Chemical and Drug Intoxication

Carbon monoxide binds to hemoglobin and to brain regions rich in iron, especially the globus pallidus and pars reticularis of the substantia nigra. CO exposure may cause demyelination of cerebral white matter or a delay in the myelin formation.

The injury in cadmium intoxication depends on many factors, including the dose and route of exposure and the ability to complex with metallothioneine. It interferes with neurotransmitter release and calcium channel function.

In Methotrexate intoxication, the combination of intrathecal administration of methotrexate and cranial irradiation produces a synergistic detrimental effect with resultant CNS damage. Toxic effects of methotrexate on oligodendrocytes lead to demyelination. It also acts as a folic acid antagonist, inhibiting dehydrofolate reductase, which may cause cell death. In the fetus, CNS malformations may be caused by methotrexate intoxication [5].

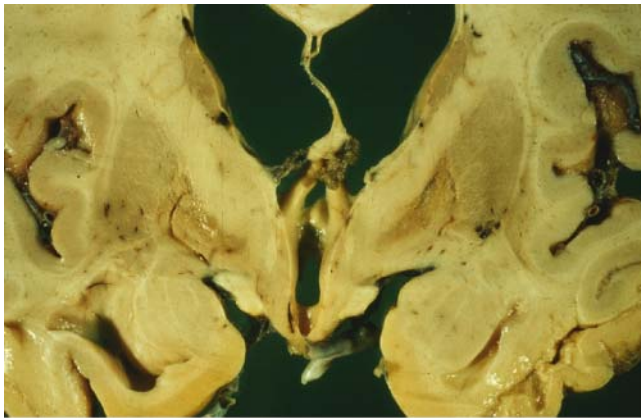


Fig. 21.3-1. Carbon monoxide intoxication in a fire victim. There is a toxic effect on the cells of the globus pallidus. The globus pallidus is atrophic.

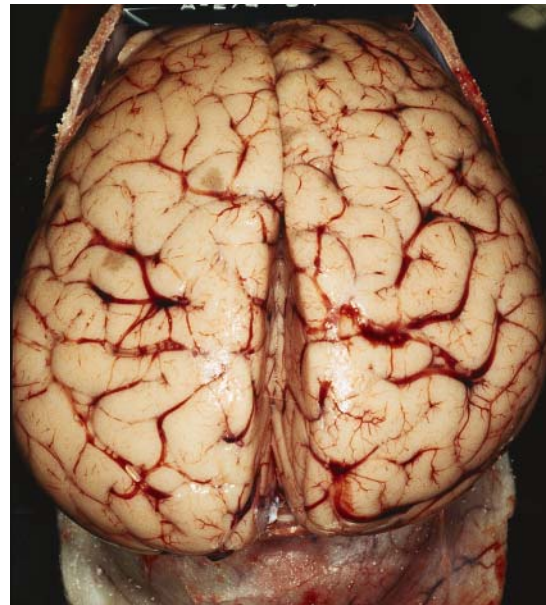


Fig. 21.3-2. Cadmium encephalopathy with marked brain swelling.

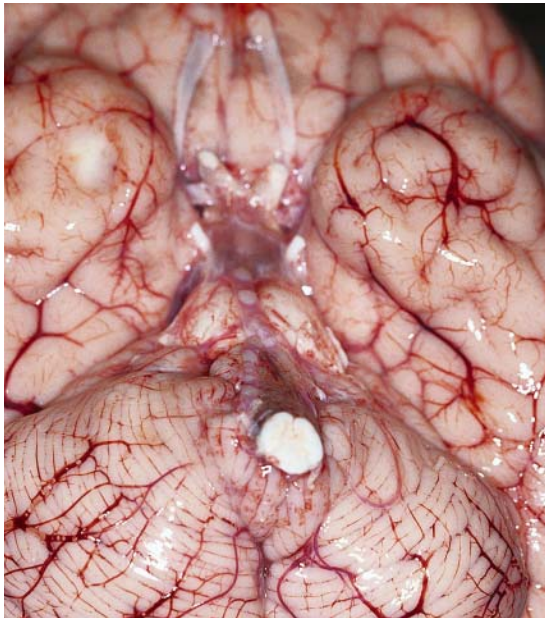


Fig. 21.3-3. Cadmium encephalopathy with tonsillar herniation caused by marked brain edema.

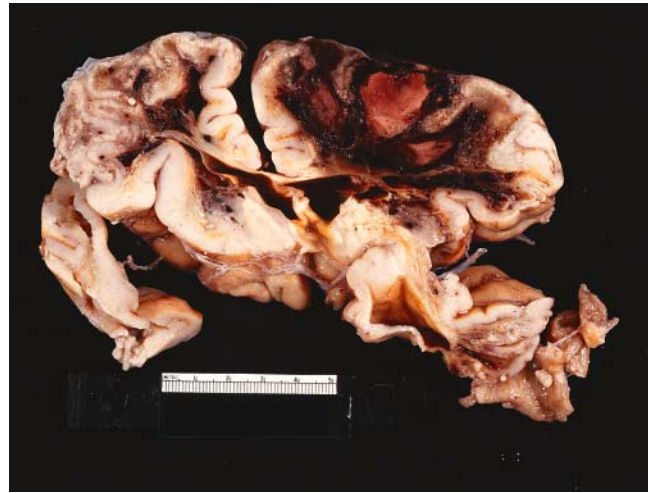


Fig. 21.3-4. Methotrexate intoxication and radiation. Marked necrosis and cavity formation are present in the white matter of both cerebral hemispheres. There is associated hemorrhagic infarction in the right hemisphere.

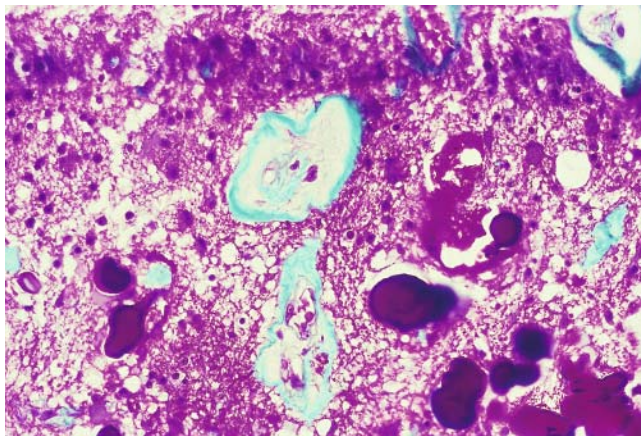


Fig. 21.3-5. Methotrexate intoxication and radiation. Note the marked necrosis associated with thick vascular walls and calcification. Masson trichrome stain.

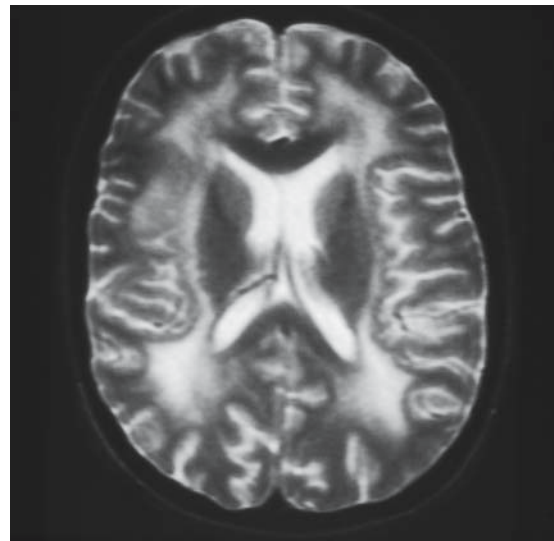


Fig. 21.3-6. Methotrexate intoxication and radiation. T2-weighted MRI shows high intensity in the cerebral white matter in a child, suggesting leukoencephalopathy.

22 Tumors

Table 22.1.

WHO classification of brain tumors.

Tumors of Neuroepithelial Tissue

Astrocytic tumors

Diffuse astrocytoma

Fibrillary

Protoplasmic

Gemistocytic

Anaplastic astrocytoma

Glioblastoma

Giant cell

Gliosarcoma

Pilocytic astrocytoma

Pleomorphic xanthoastrocytoma

Subependymal giant cell astrocytoma

Oligodendroglial tumors

Oligodendroglioma

Anaplastic oligodendroglioma

Mixed gliomas

Oligoastrocytoma

Anaplastic oligoastrocytoma

Ependymal tumors

Ependymoma

Cellular

Papillary

Clear cell

Tanocytic

Anaplastic ependymoma

Myxopapillary ependymoma

Subependymoma

Choroid plexus tumors

Choroid plexus papilloma

Choroid plexus carcinoma

Glial tumors of uncertain origin

Astroblastoma

Gliomatosis cerebri

Choroid glioma of the 3rd ventricle

Neuronal and mixed neuronal-glial tumors

Gangliocytoma

Dysplastic gangliocytoma of cerebellum

Desmoplastic infantile astrocytoma/ganglioglioma

Dysembryoplastic neuroepithelial tumor

Ganglioglioma

Anaplastic ganglioglioma

Central neurocytoma

Cerebellar liponeurocytoma

Paraganglioma of the filum terminale

Neuroblastic tumors

Olfactory neuroblastoma

Olfactory neuroepithelioma

Neuroblastomas of the adrenal gland and sympathetic nervous system

Pineal parenchymal tumors

Pineocytoma

Pineoblastoma

Pineal parenchymal tumor of intermediate differentiation

Embryonal tumors

Medulloepithelioma

Ependymblastoma

Medulloblastoma

Desmoplastic medulloblastoma

Large cell medulloblastoma

Medullomyoblastoma

Melanotic medulloblastoma

Supratentorial primitive neuroectodermal tumor

Neuroblastoma

Ganglioneuroblastoma

Atypical teratoid/rhabdoid tumor

Tumors of Peripheral Nerves

Schwannoma

Neurofibroma

Perineurioma

Malignant peripheral nerve sheath tumor

Tumors of the Meninges

Tumors of meningotheial cells

Meningioma

Mesenchymal, non-meningothelial tumors

Primary melanocytic lesions

Lymphomas and Haemopoietic Neoplasms

Germ Cell Tumors

Germinoma

Embryonal carcinoma

Yold sac tumor

Choriocarcinoma

Teratoma

Mature

Immature

with malignant transformation

Mixed germ cell tumor

Tumors of the Sellar region

Craniopharyngioma

Adamantinomatous

Papillary

Granular cell tumor

Metastatic Tumors

22.1 Astrocytic Tumors

Brain tumors are the commonest solid tumors of childhood. They range from hamartomas to pleomorphic, highly aggressive, undifferentiated neoplasms, many of which are unique to childhood. Their behavior depends on several factors: cell type, location in the brain, and age of the child. Despite scientific and technical advances, their treatment remains a challenge. Exceptional outcomes challenge molecular biologists, geneticists, oncologists, and surgeons to better understand and treat these common lesions.

In this chapter the classification and description of tumors are those of the World Health Organization [1]. The more common tumors of childhood are illustrated. Developmental lesions and cysts that may present as mass lesions have also been included in this chapter.

Five groups of astrocytic tumors are identified by their morphology and/or site. They include the diffusely infiltrating astrocytoma, the pilocytic astrocytomas, the

pleomorphic xanthoastrocytoma (see Section 22.3), the desmoplastic cerebral astrocytomas of infancy (see Section 22.8) and the subependymal giant cell astrocytoma (see Section 22.3).

In the *diffuse infiltrating astrocytoma* there is evidence that there is transformation from the grade II astrocytoma to a higher grade. The transformation may be associated with multiple genetic alterations. In grade II astrocytomas, *TP53* mutations and overexpression of *PDGFR* may occur. Anaplastic astrocytomas (grade III) often show loss of homozygosity (LOH) on 19q. Progression to glioblastoma multiforme (grade IV) may be associated with LOH on 10q and sometimes alterations in *PDGFRA*. In the diffuse astrocytoma, the higher histological grade is defined by an accumulation of aggressive features, such as nuclear atypia, mitoses, vascular endothelial proliferation, and necrosis.

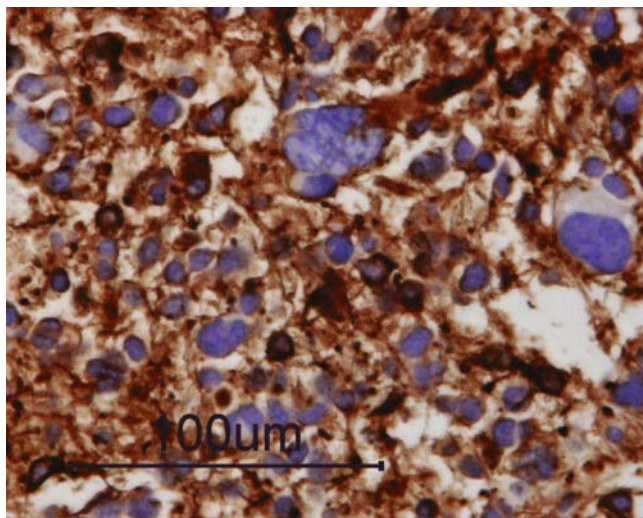


Fig. 22.1-1. Astrocytic tumors. Astrocytic cell. GFAP.

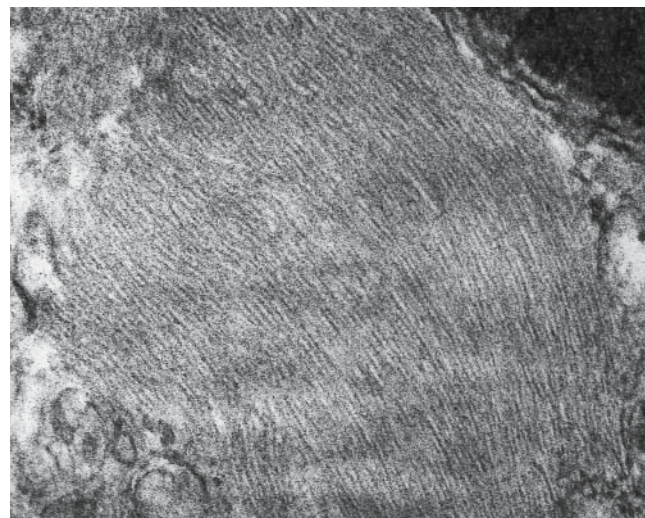


Fig. 22.1-2. Electron microscopy (EM) of characteristic intermediate filaments.

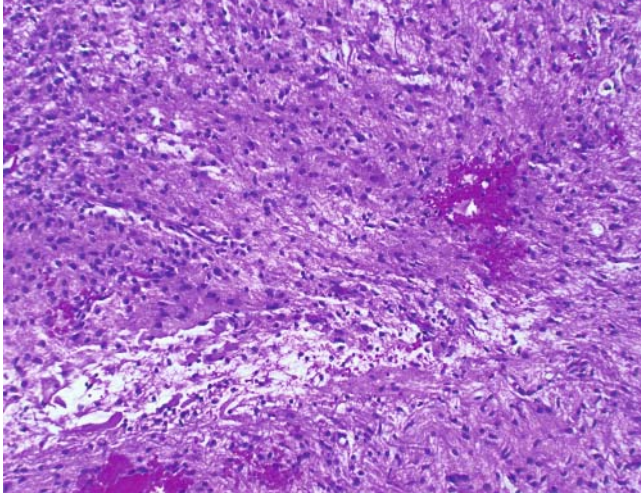


Fig. 22.1-3. Diffusely infiltrating astrocytoma. H&E.

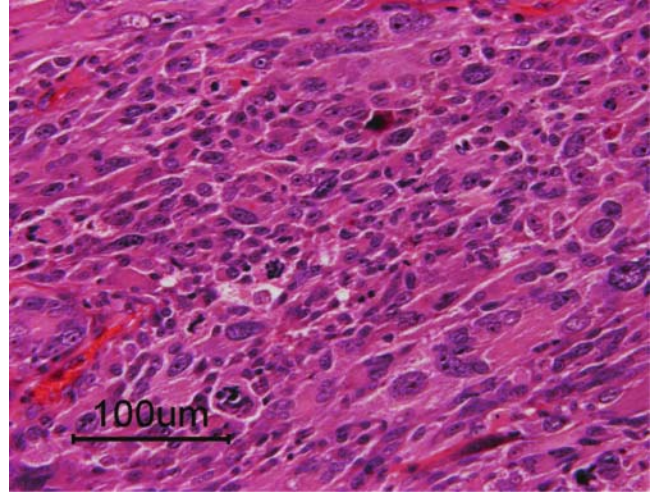


Fig. 22.1-4. Grade III astrocytoma (anaplastic astrocytoma). Note the prominent cellularity, nuclear atypia, and mitoses. H&E.

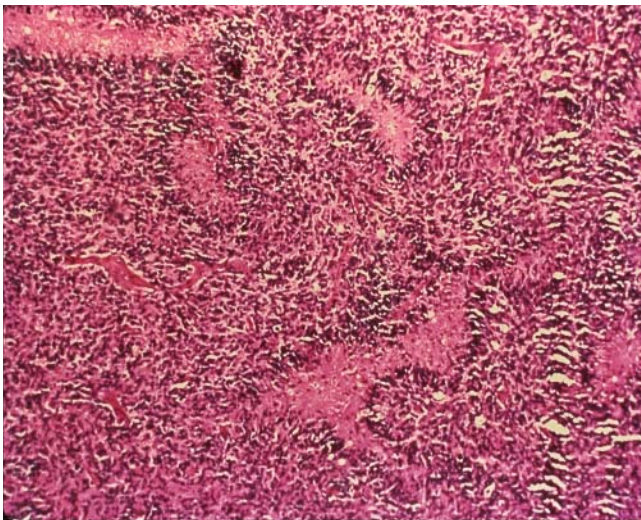


Fig. 22.1-5. Grade IV astrocytoma (glioblastoma multiforme). Note the foci of necrosis surrounded by pseudopalisades of poorly differentiated tumor cells. H&E.

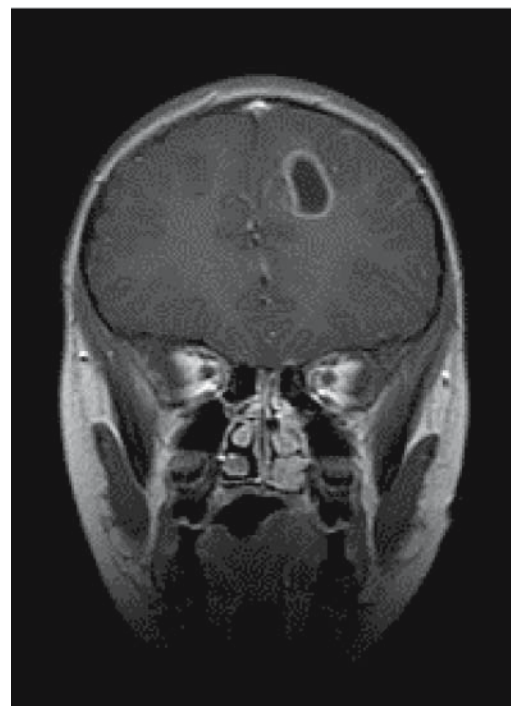


Fig. 22.1-6. Glioblastoma multiforme. T1-weighted magnetic resonance imaging (MRI) with contrast shows it as a ring enhancing lesion in the left frontal lobe.

22.2 Pilocytic Astrocytoma

The pilocytic astrocytoma, the most common glioma in children, usually occurs along a highway that goes from the optic nerve (optic nerve glioma, see also Section 22.22) posteriorly to include the hypothalamus, thalamus, and basal ganglia, down into the brain stem (exophytic brain stem glioma), and out into the cerebellum. The cerebral hemispheres and spinal cord can also be involved. It is grossly circumscribed, often cystic, and

composed of bipolar cells with a biphasic, loose, compact pattern. Rosenthal fibers and eosinophilic granular bodies (EGBs) are present in variable numbers. It has a prominent delicate vasculature that at the margin of the tumor may have a proliferative histology. It is slowly growing with MIB-1 labeling of 0%–3% and is classified as grade I. Malignant transformation is rare.

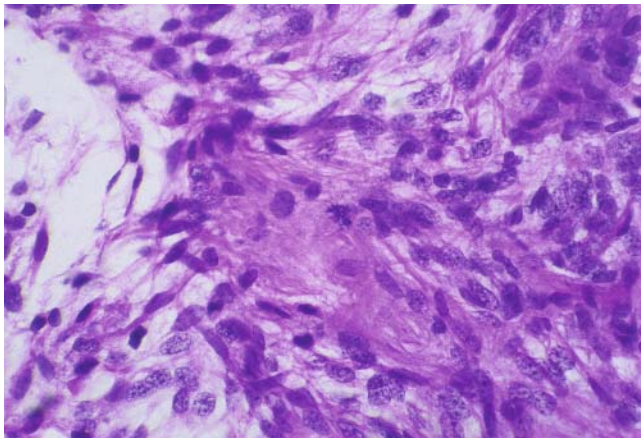


Fig. 22.2-1. Pilocytic astrocytoma. Touch preparation shows bipolar extension of the cellular cytoplasm. H&E.

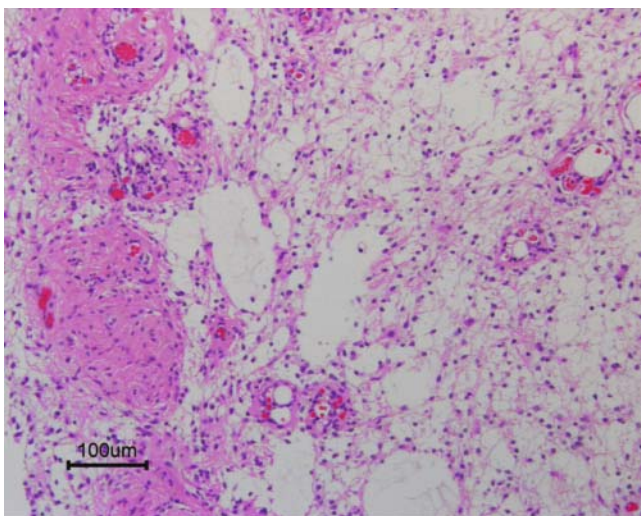


Fig. 22.2-2. Note the biphasic pattern centrally within a compact region. H&E.

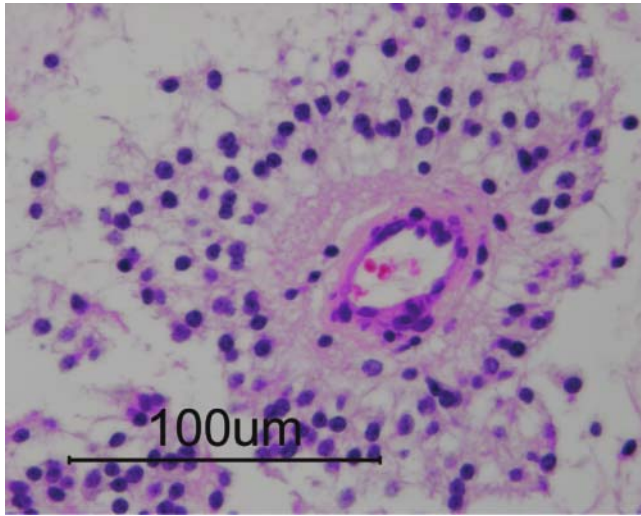


Fig. 22.2-3. This pilomyxoid astrocytoma (which lacks the usual biphasic pattern, Rosenthal fibers, and EGBs) forms a loose perivascular collar of tumor cells. H&E.

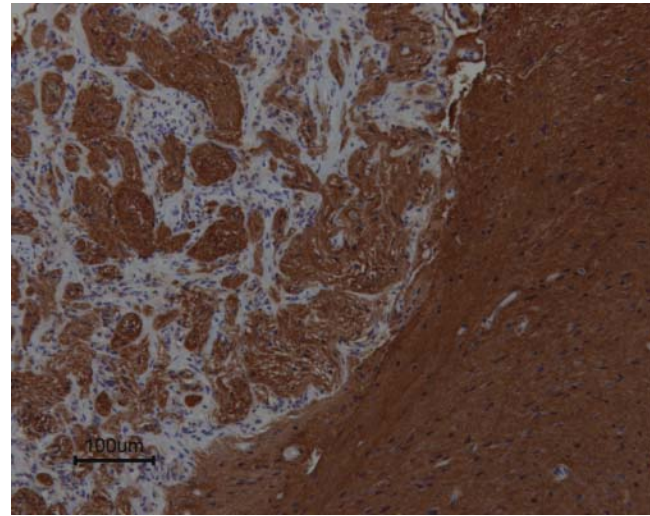


Fig. 22.2-4. The pilocytic astrocytoma extends into the sub-arachnoid space. GFAP.

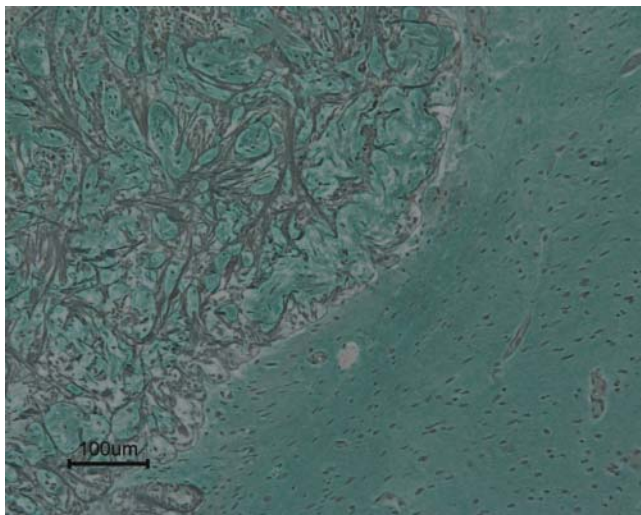


Fig. 22.2-5. The same features as seen in 22.2-4 are shown here with a reticulin stain.

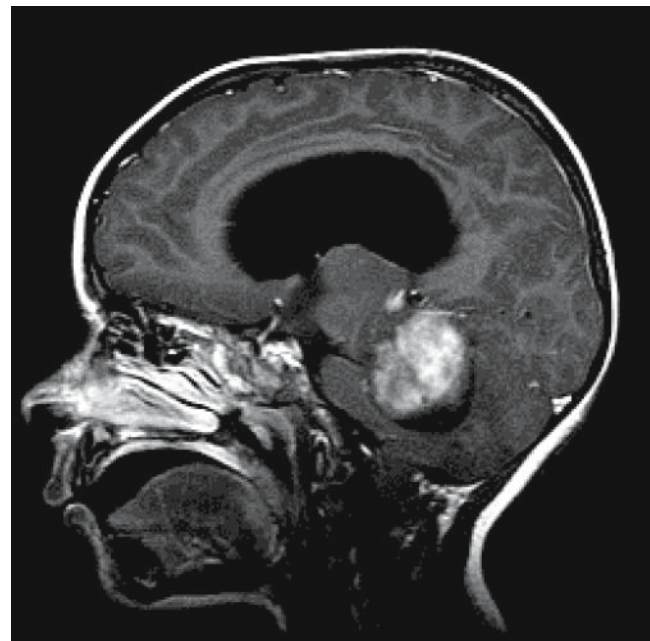


Fig. 22.2-6. T1-weighted MRI with contrast shows a circumscribed enhancing pilocytic astrocytoma extending into the fourth ventricle, producing obstructive hydrocephalus.

22.3 Miscellaneous Astrocytomas

Optic nerve gliomas are pilocytic astrocytomas that occur alone or as a manifestation of neurofibromatosis type I. They are usually a tumor of childhood with a favorable course; adult tumors are more aggressive. The tumor may arise in the optic nerve or in the chiasm, where it carries a worse prognosis. In the optic nerve, the tumor grows into the subarachnoid space (see Section 22.22), causing hyperplasia of the arachnoid cells [2].

Brain stem gliomas of childhood and adolescence are classified as intrinsic or exophytic tumors. The intrinsic type arises within the brain stem, usually the pons, causing diffuse expansion by a diffusely infiltrating astrocytoma with a potential for transformation to a high-grade tumor. The less aggressive exophytic and pilocytic tumor arises focally from a portion of the brain

stem and extends dorsally in an exophytic growth pattern [3].

Pleomorphic xanthoastrocytoma (PXA) is a grade II astrocytic tumor of children and young adults. It occurs usually in the superficial cerebrum and involves the meninges. It has pleomorphic, lipidized GFAP-reactive astrocytes. There is a rich reticulin network, and lymphocytes and eosinophilic granular bodies can be seen. Some PXAs have anaplastic features [4].

Subependymal giant cell astrocytoma (SEGA) is a benign, slowly growing grade I tumor in patients with tuberous sclerosis (see Section 22.22). It arises in the wall of the lateral ventricle and is composed of large pleomorphic cells that exhibit both astrocytic and neuronal phenotypes [5].



Fig. 22.3-1. Optic nerve glioma. Gross specimen shows the tumor expanding the optic nerve.

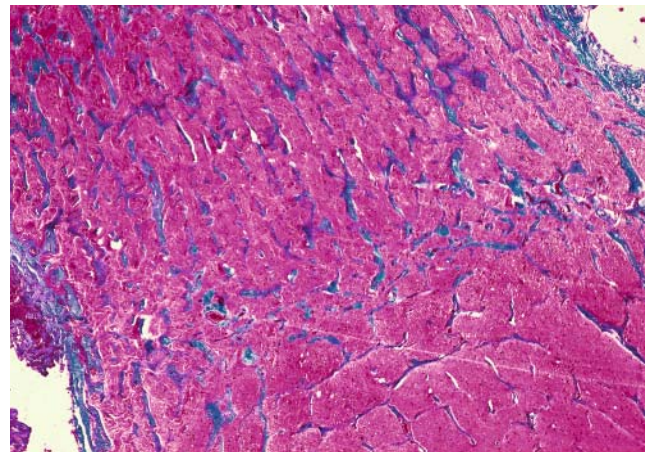


Fig. 22.3-2. Optic nerve glioma. Histology of the tumor that is expanding the optic nerve adjacent to the normal optic nerve.

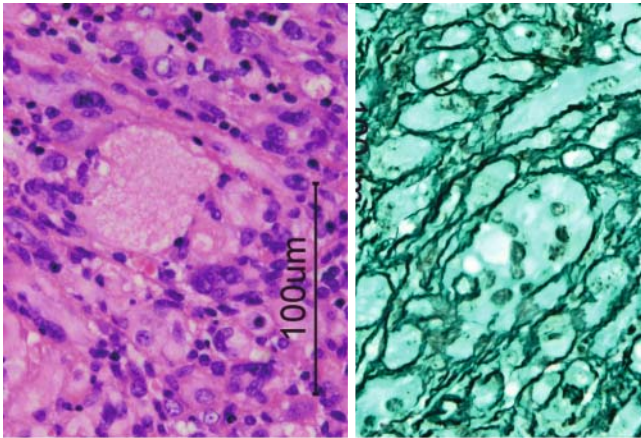


Fig. 22.3-3. Pleomorphic xanthoastrocytoma. *Left.* Pleomorphic tumor cells. H&E. *Right.* They tend to be surrounded by reticulin.



Fig. 22.3-4. Brain stem glioma. Transverse section shows recent hemorrhage in the tumor that has expanded and distorted the brain stem.

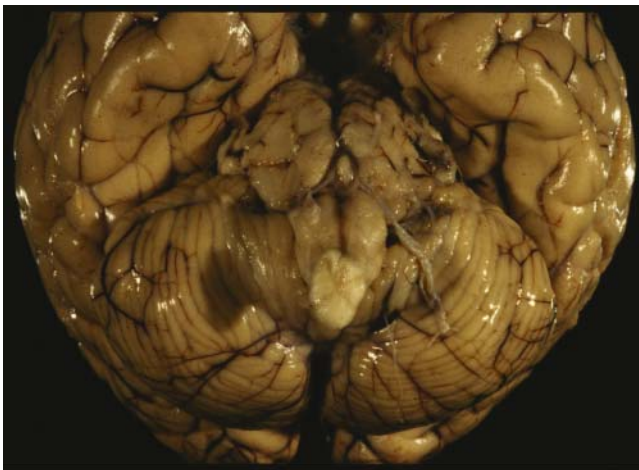


Fig. 22.3-5. Brain stem glioma (same case as in 22.3-4). Base of brain projection shows distortion of external anatomical landmarks by the expanding brain stem.

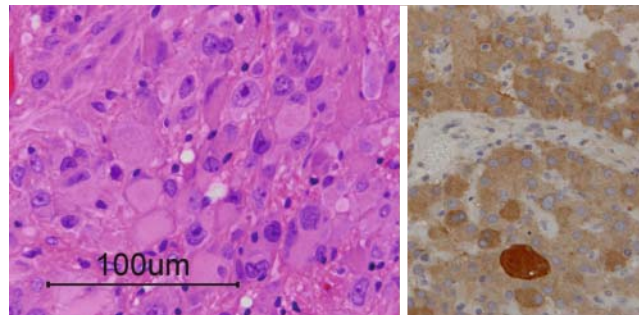


Fig. 22.3-6. Subependymal giant cell astrocytoma (SEGA). *Left.* Large tumor cells. H&E. *Right.* They frequently show reactivity for α,β -crystallin.

22.4 Ependymomas and Oligodendrogliomas

Ependymomas [6] typically arise from the ependymal lining of the cerebral ventricles and the spinal cord in young children and young adults. The ependymoma (grade II) accounts for up to 30% of intracranial tumors under the age of 3 years. It is common in the fourth ventricle and spinal cord. The cells are regular and associated with perivascular pseudorosettes (tumor cells around blood vessels) and/or true ependymal rosettes (tumor cells around a central lumen). Histological variants include cellular ependymoma, papillary ependymoma, clear cell ependymoma, and tanycytic ependymoma. Tumor cells express GFAP, S100, and epithelial membrane antigen (EMA) immunoreactivity. EM reveals cilia, microvilli, and junctional complexes. About 30% of ependymomas show changes in chromosome 22. Rare low-grade cortical tumors with ependymal features have been reported and represent a nosological challenge [7,8].

- *Anaplastic ependymoma* is an ependymal tumor of children with a high mitotic index, and microvascular proliferation; necrosis with pseudopalisading cells may be present.
- *Myxopapillary ependymoma* (grade 1) is a slowly growing tumor of young adults usually located in the caudal spinal cord.
- *Subependymomas* (grade 1) are composed of clusters of glial cells in a fibrillary matrix. They are usually found incidentally in adults at autopsy.

Representing only about 6% of all oligodendrogliomas, pediatric oligodendrogliomas are rare [9]. When compared to adult tumors, molecular studies of chromosomes 1 and 19 suggest that pediatric oligodendrogliomas may arise from different molecular alterations [10,11]. A common differential diagnostic consideration is DNET (see Section 22.9).

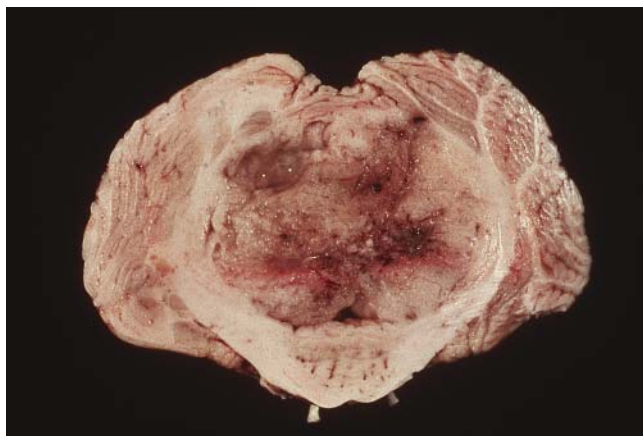


Fig. 22.4-1. Ependymoma. Gross specimen of an ependymoma arising within and expanding the fourth ventricle.

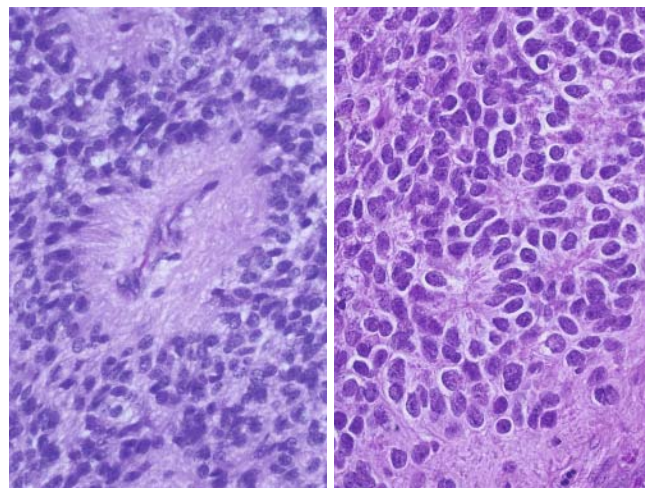


Fig. 22.4-2. Microscopy showing a perivascular pseudorosette (left) and a true rosette (right). H&E.

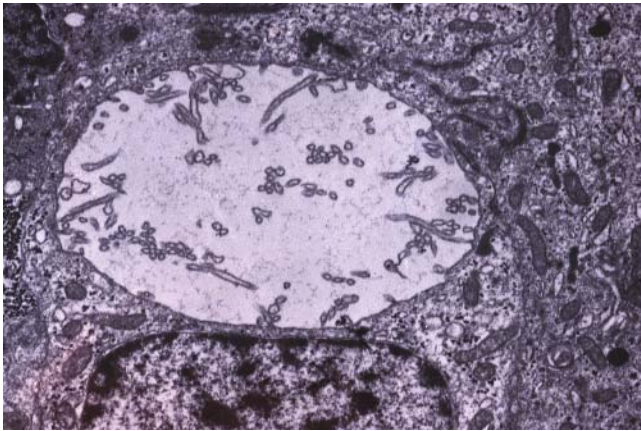


Fig. 22.4-3. EM shows microvilli.

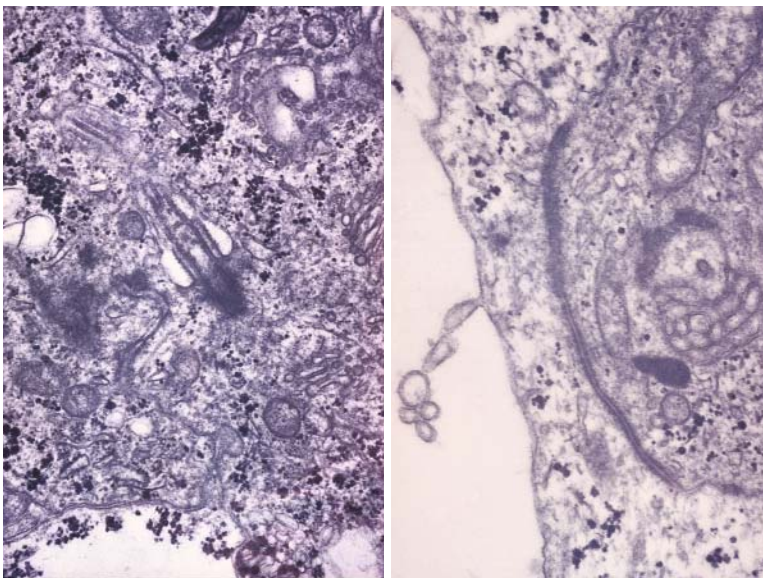


Fig. 22.4-4. EM shows cilia (*left*) and junctional complexes (*right*).

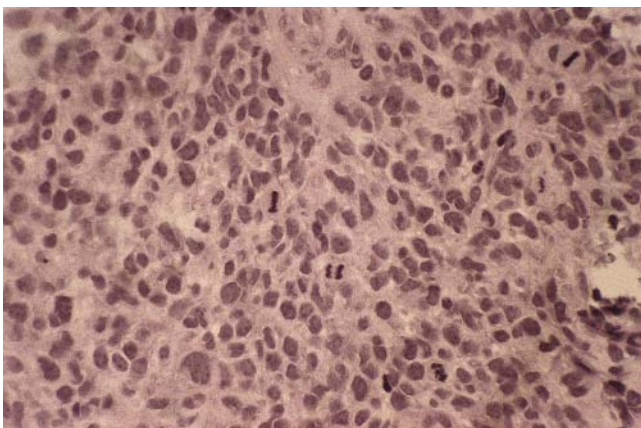


Fig. 22.4-5. Anaplastic ependymoma. Microscopy shows pleomorphic nuclei and prominent mitotic figures. H&E.

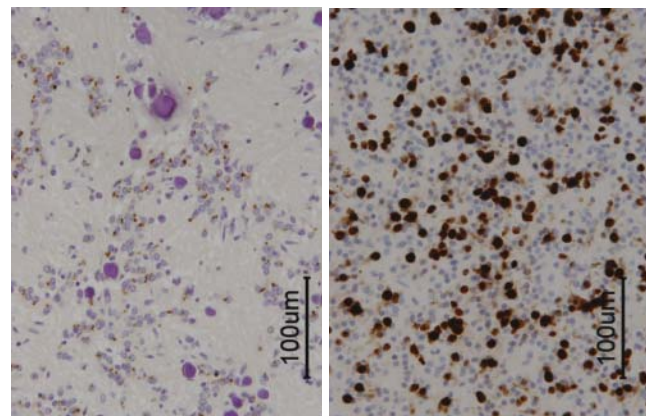


Fig. 22.4-6. Anaplastic ependymoma. EMA immunoreactivity (*left*) and MIB labeling (*right*). Note that the EMA is “dot-like reactivity”.

22.5 Choroid Plexus Tumors

Choroid plexus tumors, which arise from the epithelium of the choroid plexus, are the commonest brain tumor during the first year of life. The *choroid plexus papilloma* (grade I) is a papillary “cauliflower”-like growth composed of a delicate fibrovascular stroma covered by a single organized layer of cuboidal-to-columnar epithelium. The cells are immunoreactive for vimentin and cytokeratins and are variably reactive for S-100 and transthyretin. They grow into the ventricle and may cause hydrocephalus.

The *choroid plexus carcinoma* (grade III) may display solid sheets of pleomorphic cells, with loss of papillary structure. They have a high mitotic index and show brain invasion. There is an intermediate “atypical choroid plexus papilloma” of undefined behavior. Recently, two tumor suppressor genes, *TP53* and *hSNF5/INI-1*, have been implicated in the tumor’s biology. Choroid plexus tumors have been reported in two familial cancer syndromes: Li-Fraumeni syndrome (*TP53*) and rhabdoid predisposition syndrome (*INI-1*) [12].

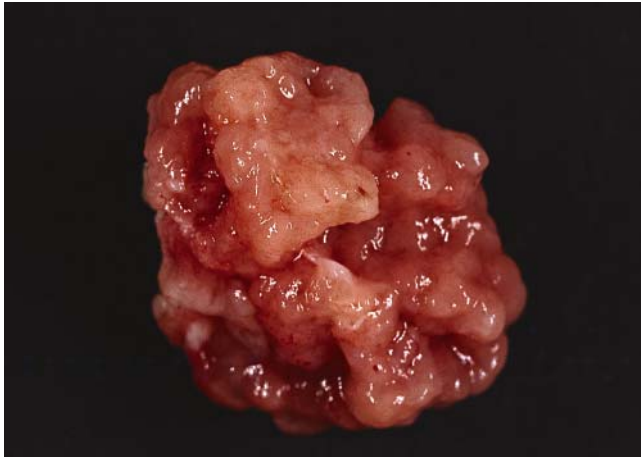


Fig. 22.5-1. Choroid plexus papilloma. Gross appearance of the papillary lesion.

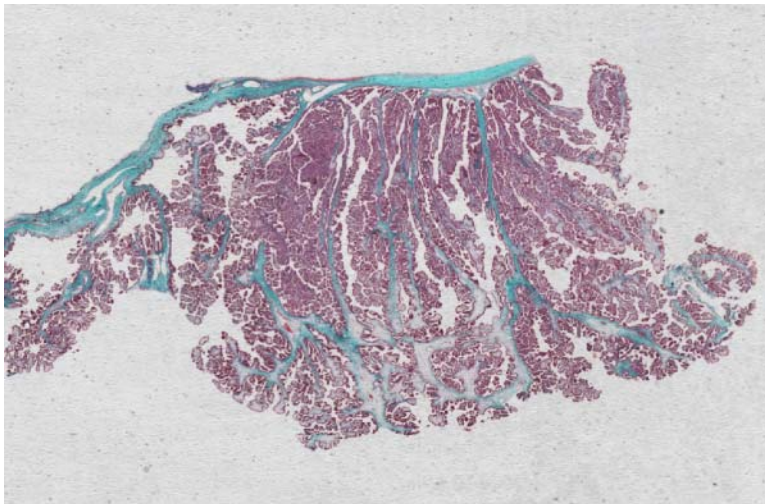


Fig. 22.5-2. Choroid plexus papilloma. Whole mount shows the delicate papillary structure. Trichrome.

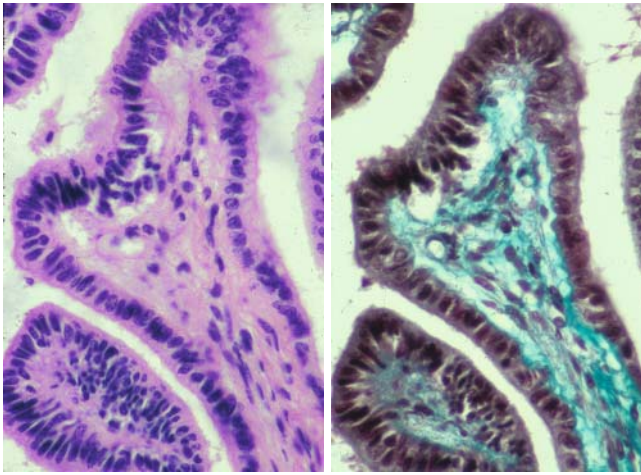


Fig. 22.5-3. Choroid plexus papilloma. Microscopy shows a single layer of epithelium on a delicate vascular core. H&E (left)/Trichrome (right). This is the same case as Fig. 22.5-2.

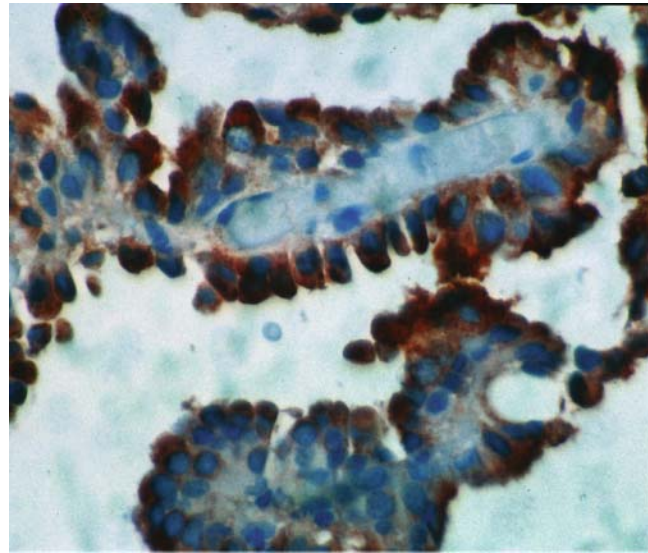


Fig. 22.5-4. Choroid plexus papilloma. Transthyretin immunoreactivity.

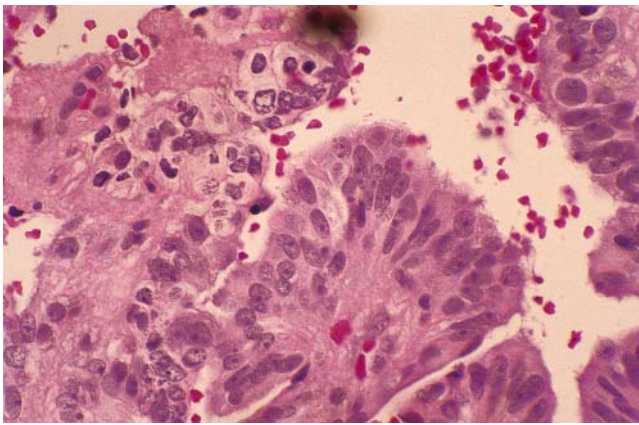


Fig. 22.5-5. Atypical choroid plexus papilloma microscopy shows loss of a single layer of epithelium and pleomorphic nuclei. H&E.

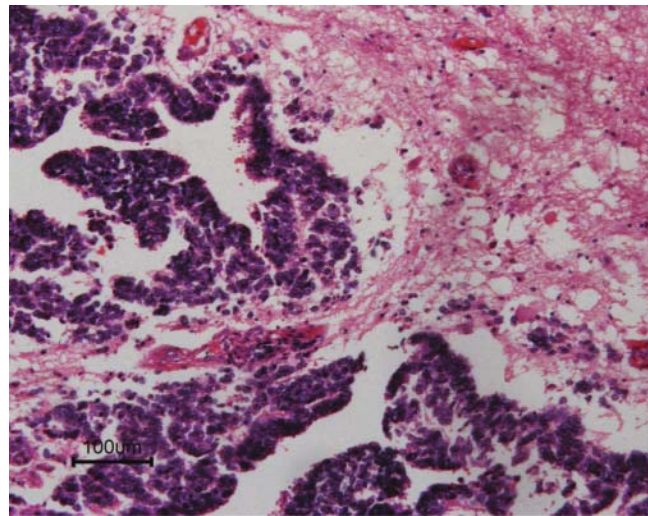


Fig. 22.5-6. Choroid plexus carcinoma. Microscopy shows brain invasion. H&E.

22.6 Neuroepithelial Tumors of Uncertain Origin

Neuroepithelial tumors of uncertain origin [13] are rare neuroepithelial tumors with a unique histology.

The *astroblastoma* (not graded) has rarely been reported in infants or young adults. It is composed of GFAP-positive perivascular astrocytes radiating to a central blood vessel. Its behavior is unpredictable.

Gliomatosis cerebri (grade III) is a diffuse glial tumor showing involvement of at least two lobes of the brain, often spreading to the posterior fossa and spinal cord.

It produces diffuse enlargement without destruction of the brain and is difficult to diagnosis even with imaging. It may present as a diffuse lesion without a tumor mass (type I) or as a diffuse lesion with a tumour mass (type II). The tumor cells usually resemble elongated astrocyte that grows between brain cells and along fiber tracts. However, there are some reports of an oligodendroglial appearance. The genetic data are inconclusive as to the cell of origin.

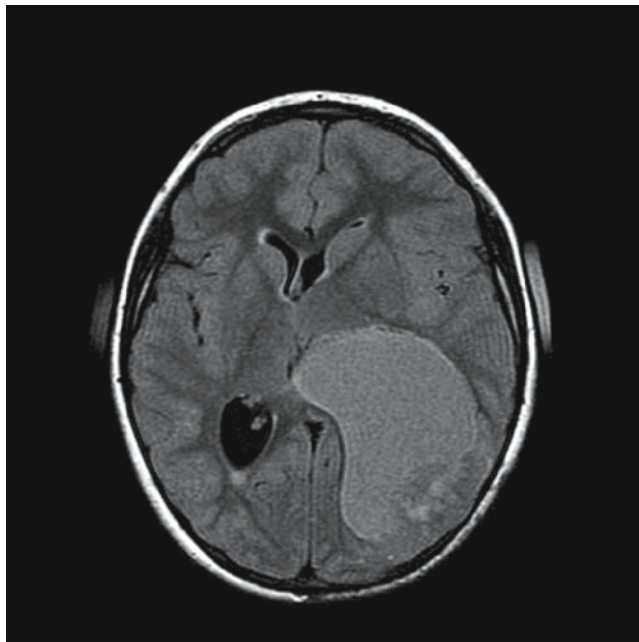


Fig. 22.6-1. Astroblastoma. MRI (axial FLAIR) shows a superficial tumor and cyst extending from the cortex to the posterior lateral ventricle and distorting the thalamus.

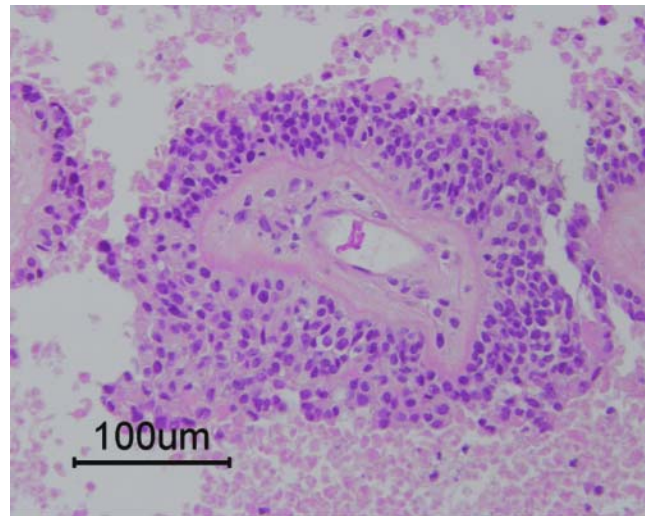


Fig. 22.6-2. Astroblastoma. Histology of a papillary region. H&E.

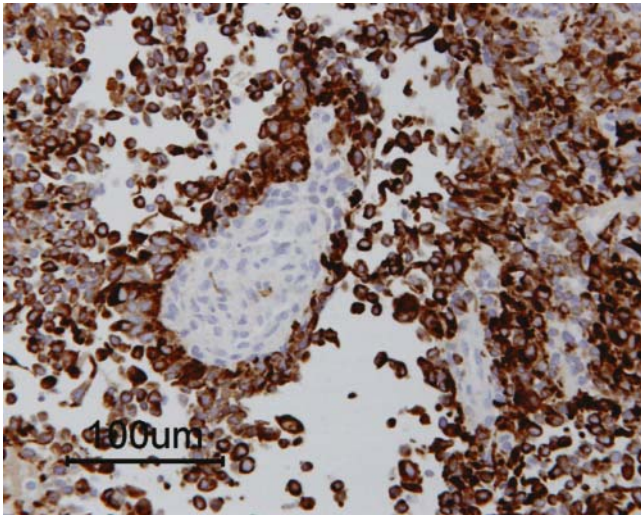


Fig. 22.6-3. Astroblastoma. Histology. GFAP immunohistochemistry.

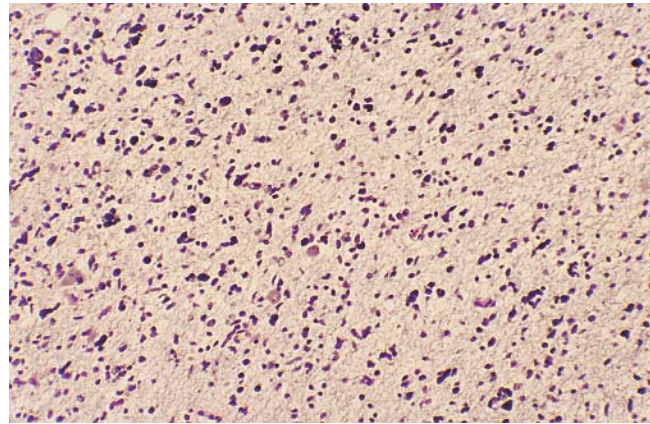


Fig. 22.6-4. Gliomatosis cerebri. Microscopy shows diffusely infiltrating tumor cells in white matter of the cerebral hemisphere. H&E.

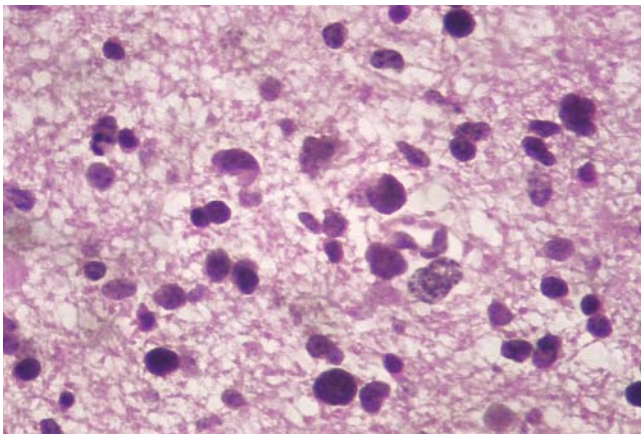


Fig. 22.6-5. Gliomatosis cerebri. Microscopy shows a cluster of tumor cells. H&E.

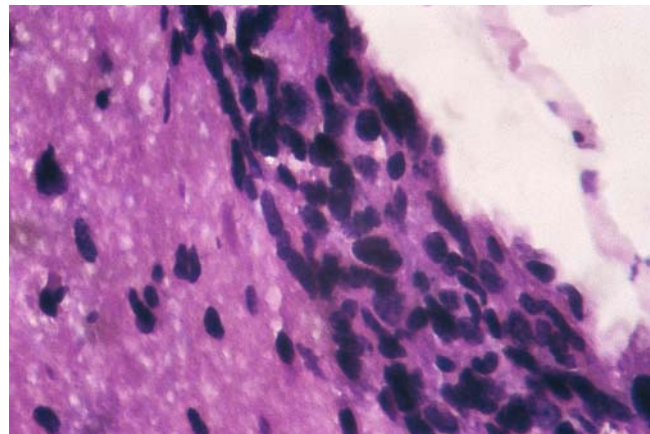


Fig. 22.6-6. Gliomatosis cerebri. Microscopy shows spread of tumor cells to the subpial region.

22.7 Neuronal and Mixed Neuronal-Glial Tumors

Gangliogliomas and *gangliocytomas* contain mature neoplastic neurons (ganglion cells) with glial cells (ganglioglioma) or without glial cells (gangliocytoma). Gangliocytomas are considered grade I, and most gangliogliomas are grade I or II. They may be found throughout the neuroaxis, including the pineal and pituitary glands. Most are in the temporal lobe, where they are associated with temporal lobe epilepsy. The ganglioglioma contains dysplastic ganglion cells accompanied by tumor astrocytes. There is a delicate vascular pattern, and lymphocytes commonly cuff the vasculature.

Eosinophilic granular bodies may be present. There is reticulin throughout the tumor. The malignant variants show anaplastic changes in the astrocytic component of the tumor, with increased mitotic activity, vascular endothelial proliferation, and necrosis [14].

Papillary glioneuronal tumor is low-grade brain neoplasm classified as variant of ganglioglioma. Its morphology shows pseudopapillary structures composed of blood vessels, after hyalinized, lined by uniform small astrocytes and proliferation of neurocytic cells.

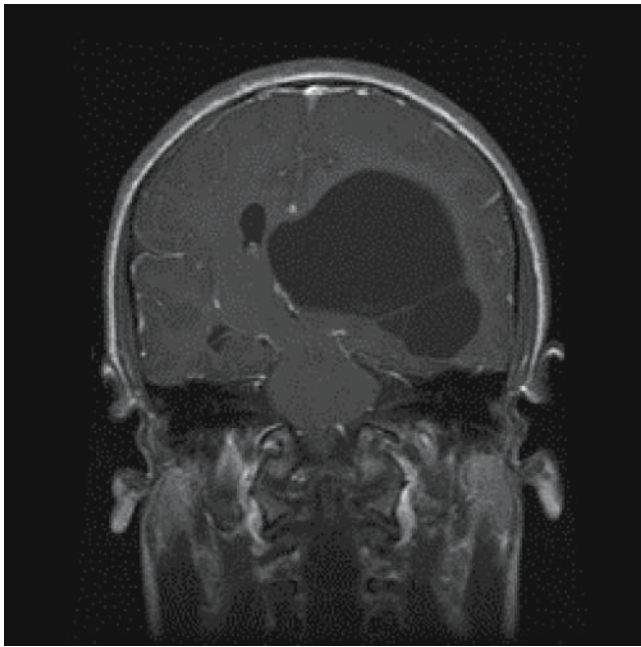


Fig. 22.7-1. Ganglioglioma. T1-weighted MRI with contrast shows a tumor with a large cystic component in the left temporal lobe.

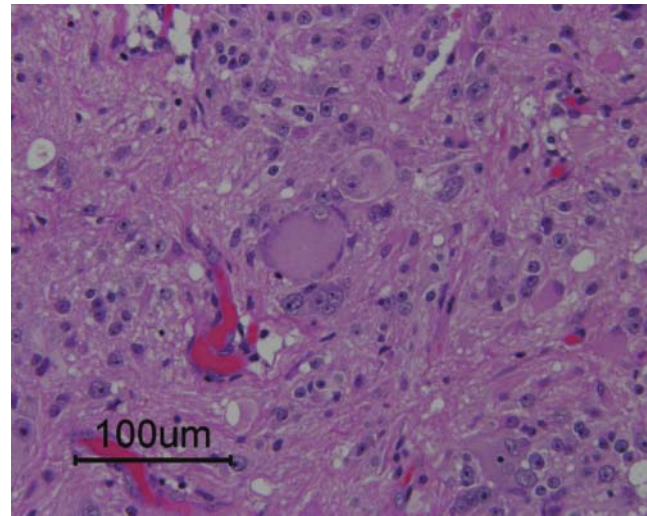


Fig. 22.7-2. Ganglioglioma. Histology shows the features described in the text. H&E.

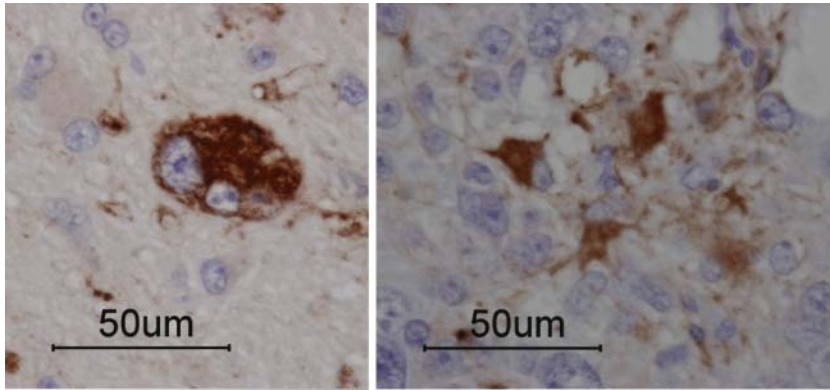


Fig. 22.7-3. Ganglioglioma. Immunohistochemistry with chromogranin (*left*) and GFAP (*right*).

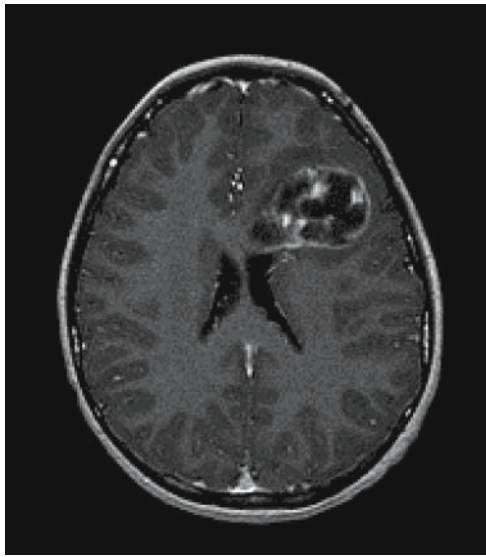


Fig. 22.7-4. Papillary glioneuronal tumor. MRI shows a multicystic low-intensity lesion in the left frontal lobe.

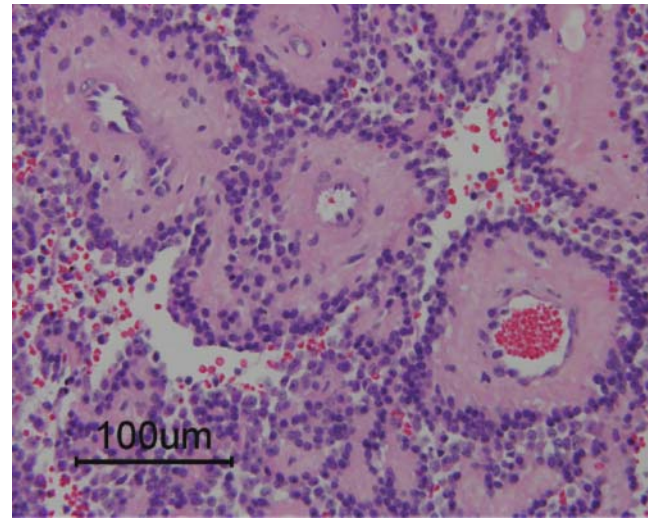


Fig. 22.7-5. Papillary glioneuronal tumor. Histology. H&E.

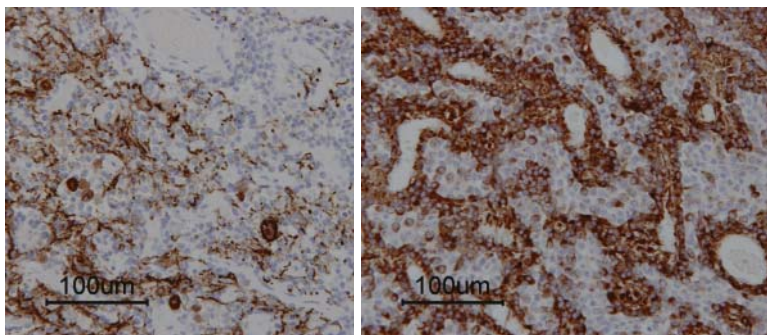


Fig. 22.7-6. Papillary glioneuronal tumor. Immunohistochemistry with neurofilament (*left*) and GFAP (*right*).

22.8 Desmoplastic Infantile Astrocytoma and Desmoplastic Infantile Ganglioglioma

Desmoplastic infantile astrocytomas and gangliogliomas [9] are large cystic grade I tumors seen primarily in infants. They are located in the cerebral hemisphere attached to the dura. These tumors are composed of

neuroepithelium (astrocytes with or without ganglion cells) with desmoplastic stroma and poorly differentiated cells. The neoplastic cells have basal lamina, suggesting that they are derived from subpial cells.

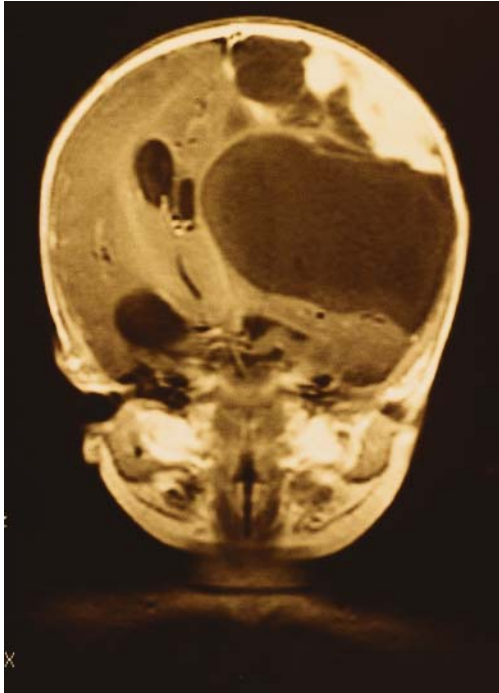


Fig. 22.8-1. Desmoplastic infantile ganglioglioma (DIG). Computed tomography (CT) shows a huge superficial cystic tumor.



Fig. 22.8-2. Gross appearance of the tumor associated with the meninges.

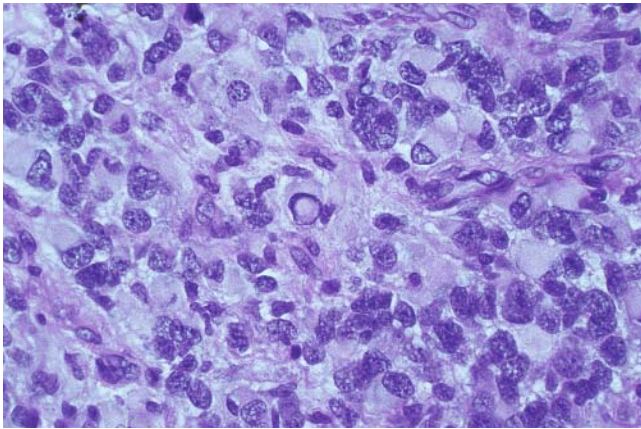


Fig. 22.8-3. Microscopy shows the mixture of neuroglial elements. H&E.

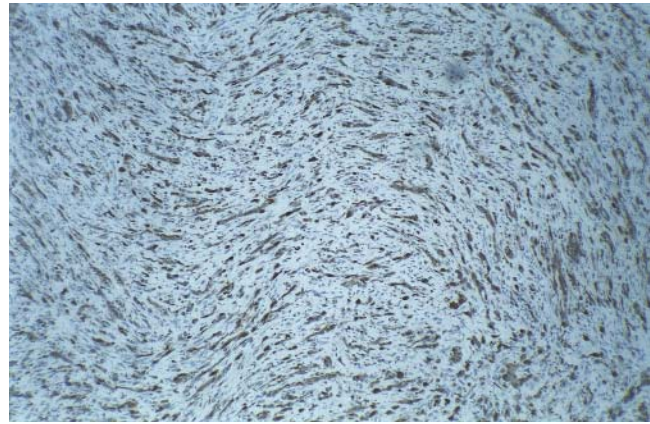


Fig. 22.8-4. Desmoplastic component shows GFAP-reactive spindle cells.

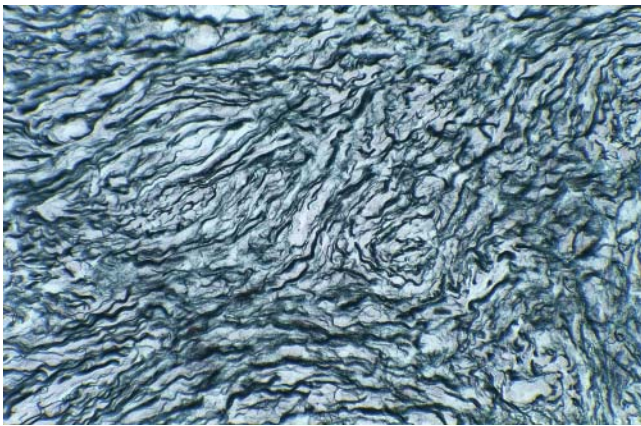


Fig. 22.8-5. Reticulin-rich desmoplastic component.

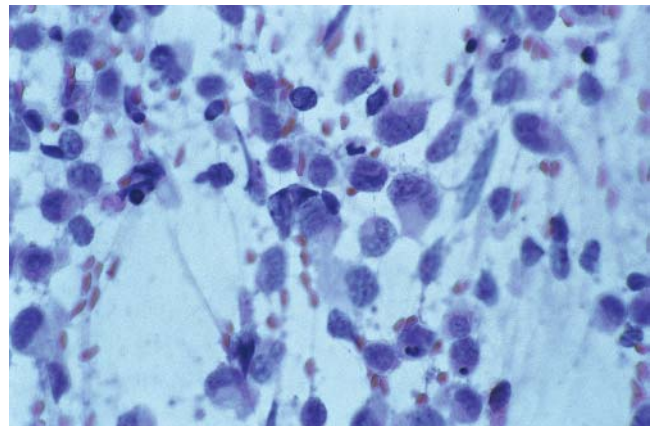


Fig. 22.8-6. Touch preparation shows astrocytic and spindle components. H&E.

22.9 Dysembryoplastic Neuroepithelial Tumor (Grade I)

Dysembryoplastic neuroepithelial tumor (DNET) (grade I) [14] is a benign glial-neuronal neoplasm thought to arise at sites of secondary germinal layers. It is usually found in the cerebral cortex in children and young adults, causing drug-resistant seizures. A “complex form” is in the cortex and is multinodular, with a characteristic glioneuronal element composed of columns of axons lined by “oligodendroglia-like cells (S-100-positive, GFAP-negative). Between the columns, normal-appearing neurons float in a pale (Alcian blue staining) mucinous matrix. The “simple form” of DNET is com-

posed of only the glioneuronal element. Cortical dysplasia may be associated with the DNET.

The central neurocytoma (grade II) is usually seen in young adults, although it has been reported in infants. It is found in the lateral and third ventricles. A similar-appearing lesion elsewhere is called an extraventricular central neurocytoma. The tumor resembles an oligodendroglioma, with regular cells surrounding delicate vessels. It usually has immunohistochemical and EM features of a neuronal tumor.

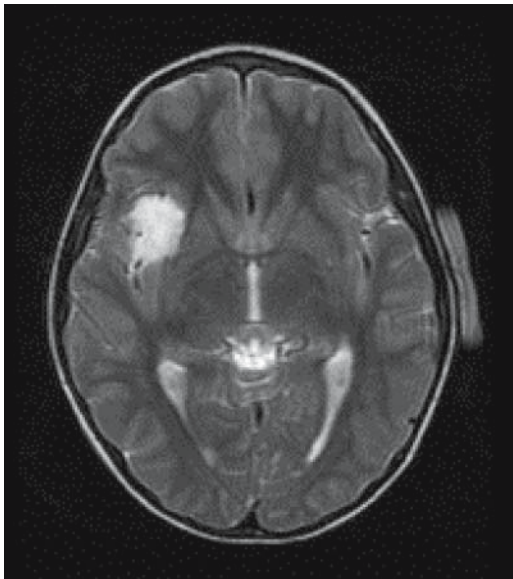


Fig. 22.9-1. Dysembryoplastic neuroepithelial tumor, grade I (DNET). T2-weighted fast spin echo MRI shows a multinodular lesion of the right medial temporal lobe.

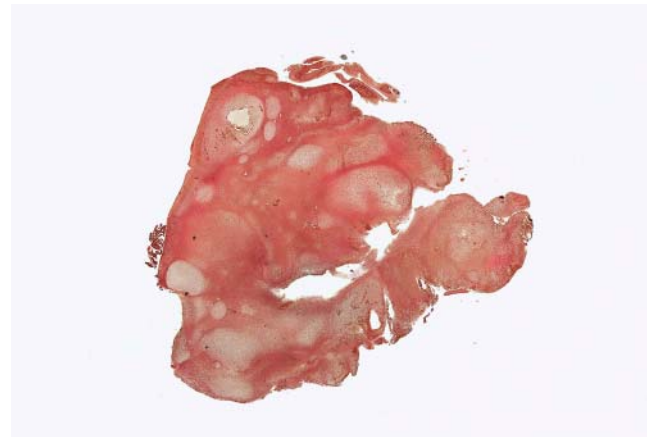


Fig. 22.9-2. Whole mount of the resected tumor displaying its multinodular nature. Trichrome.

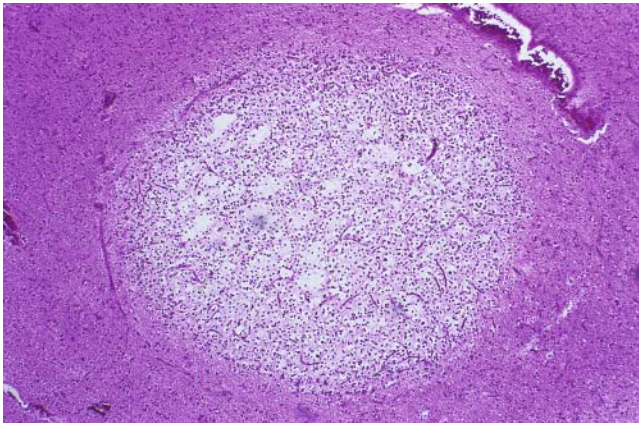


Fig. 22.9-3. Microscopy of one nodule that displays a microcystic appearance. H&E.

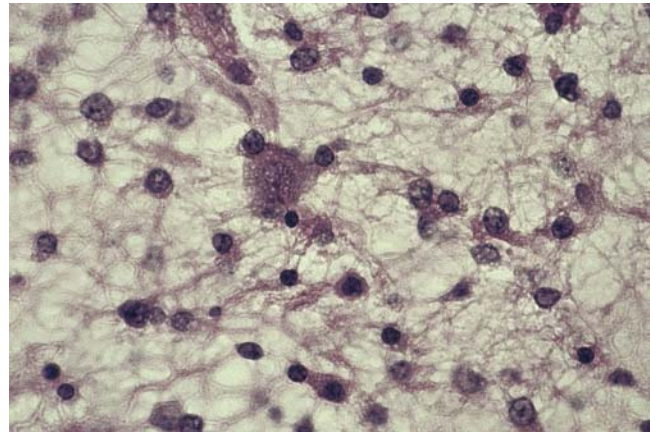


Fig. 22.9-4. High-power view of the glioneuronal element. H&E.

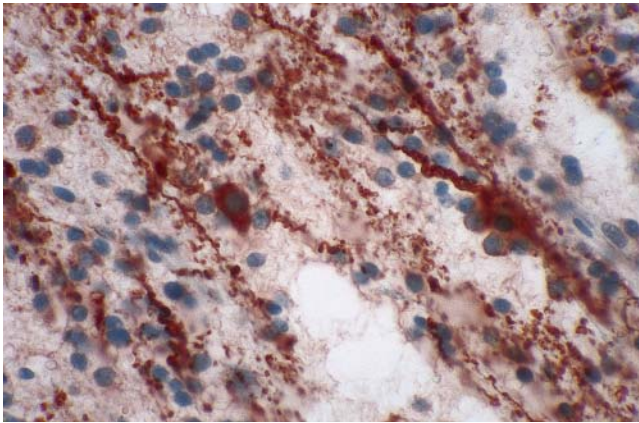


Fig. 22.9-5. Glioneuronal element stained with neurofilament reveals the columns of axons with associated small oligodendroglia-like cells and floating neurons.

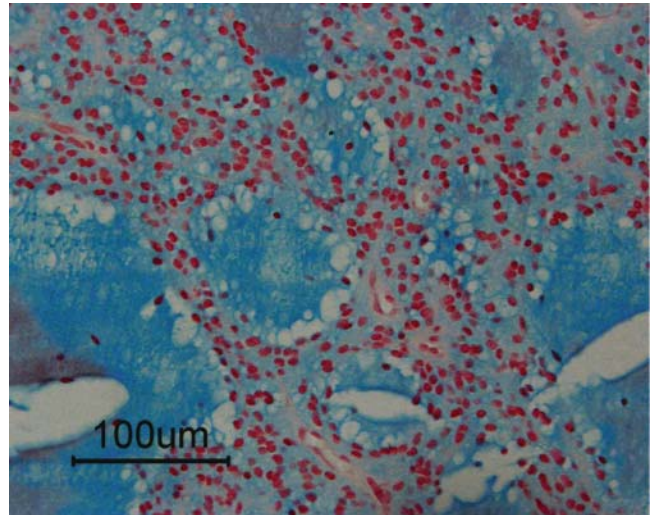


Fig. 22.9-6. The mucinous material in the cystic spaces stains with Alcian blue.

22.10 Embryonal Tumors

Embryonal tumors [15] account for a large portion of pediatric brain tumors. Three of them—ependymoblastoma, medulloblastoma (Fig. 22.11), supratentorial primitive neuroectodermal tumor (PNET) (Fig. 22.12)—have a similar undifferentiated round cell histology that exhibits divergent patterns of differentiation. The medulloepithelioma (Fig. 22.10) and the atypical teratoid/rhabdoid tumor (Fig. 22.13) have distinctive histologies.

The *medulloepithelioma* (grade IV), a rare malignant tumor in young children, is composed of neoplastic neuroepithelium. It has a papillary or trabecular arrangement of cells with an external limiting membrane (PAS-positive). There is a pseudostratified epithelium with many mitoses; and, characteristically, the mitotic activity is at the top of the epithelium, adjacent to the

lumen. In addition, there may be sheets of cells with astrocytic, neuronal, ependymoblastic, and oligodendroglial differentiation. There are ependymoblastomatous and ependymal rosettes. The epithelium marks with nestin, vimentin, and MAP5. Regions show immunoreactivity to antigens characteristic of each cell type.

Ependymoblastoma (grade IV) occurs in infants and young children. The tumors are usually supratentorial, near the ventricle, well circumscribed, but with microscopic invasion and cerebrospinal fluid (CSF) spread. Microscopy reveals a primitive neuroectodermal tumor with multilayered rosettes around a central lumen. The mitotic rate is high. The cells express S100, vimentin, cytokeratin, GFAP, and carbonic anhydrase isoenzyme II. EM reveals junctional complexes and cilia.

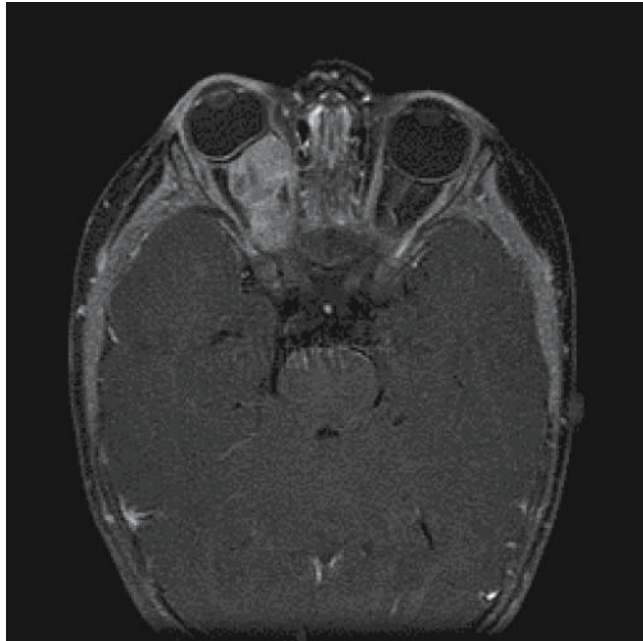


Fig. 22.10-1. Medulloepithelioma. T1-weighted MRI with contrast shows a large optic nerve tumor.



Fig. 22.10-2. Gross mass in the optic nerve region.

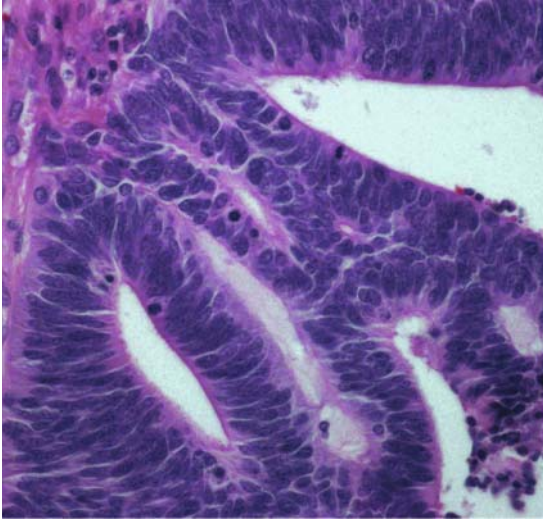


Fig. 22.10-3. Histology shows the primitive neuroepithelium and characteristic placement of mitoses. H&E.

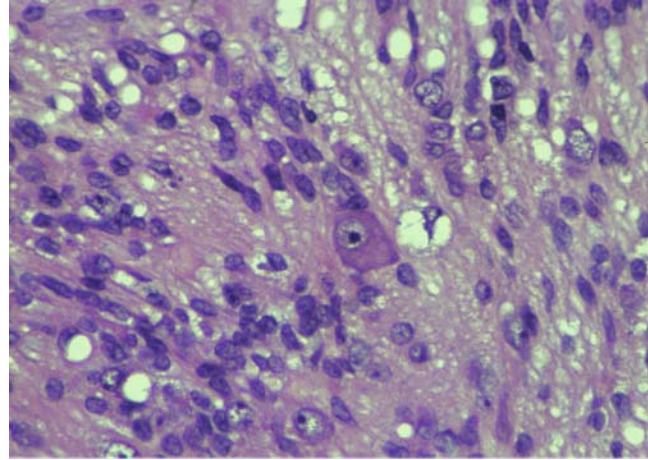


Fig. 22.10-4. Histology shows neuronal differentiation. H&E.

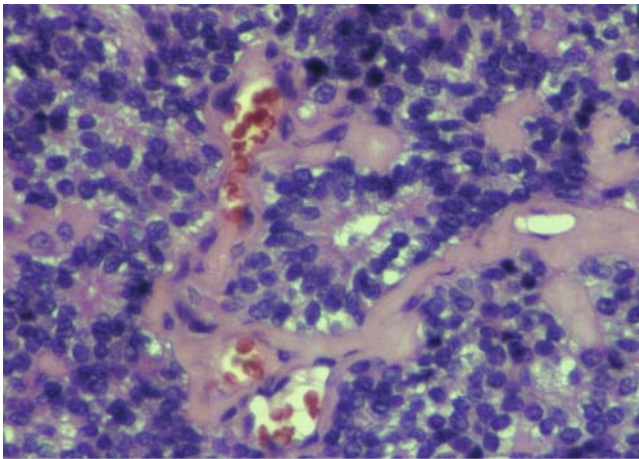


Fig. 22.10-5. Histology shows ependymal differentiation, including an ependymal rosette. H&E.

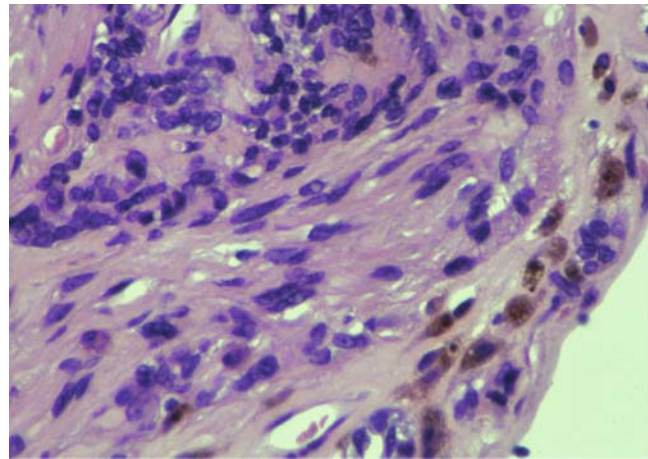


Fig. 22.10-6. Histology showing glial cells adjacent to pigment-containing cells. H&E.

22.11 Medulloblastoma (Grade IV)

Medulloblastoma (grade IV) [15] is an embryonal tumor of the cerebellum showing primitive neuroectodermal cells with neuronal differentiation. The classic form has neuroblastic rosettes (tumor cell nuclei around cytoplasmic processes). Mitoses and apoptoses may be frequent. Giant cells, vascular proliferation, and massive hemorrhage are rare. The desmoplastic medulloblastoma has nodules of tumor cells surrounded by densely packed cells that produce an intercellular reticulin network. The nodules may contain advanced neuronal differentiation.

The large cell medulloblastoma [16] has large pleomorphic nuclei with prominent nucleoli and more cytoplasm than the classic form. There is nuclear molding, areas of necrosis, and regions with apoptosis and high mitotic activity.

Medulloblastomas express synaptophysin and vimentin; and some cells express GFAP. Some tumors express NF proteins and retinal S antigen as well as the nerve growth factors NGF, BDNF, and NT3 and their receptors TrkA, TrkB, and TrkC. Electron microscopy reveals neuronal and astrocytic features. Cytogenetic studies have shown that 50% of tumors have isochromosome

17q. Chromosome 1 abnormalities are frequently identified. About 30%-40% of medulloblastomas have LOH on 17p and a loss of genetic material on 1q and 10q; 20% of medulloblastomas have amplification of *MYC*. Some medulloblastomas have abnormalities in the hedgehog/patched, APC, and Wnt signaling pathways.

This common tumor has been extensively studied; and the combined use of surgery, chemotherapy, and radiotherapy has improved the 5-year survival from 30% during the 1960s to 50%–70% currently. There is some correlation of survival with histology. The nodular variant has a better prognosis than the classic medulloblastoma. The large cell variant has the worst prognosis.

The *medulloblastoma* (grade IV) is a rare embryonal cerebellar tumor composed of medulloblastoma with a striated muscle component.

The *melanotic medulloblastoma* (grade IV) is a rare childhood tumor reported in the cerebellum and pineal regions. It is composed of medulloblastoma with a small pigmented epithelial component forming tubules or clusters.

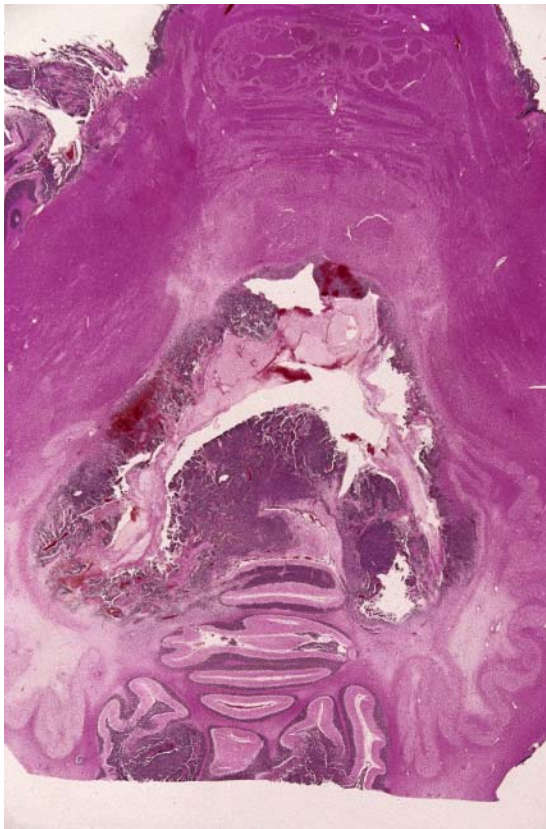


Fig. 22.11-1. Medulloblastoma. Whole mount of tumor expanding from the cerebellum into the fourth ventricle.

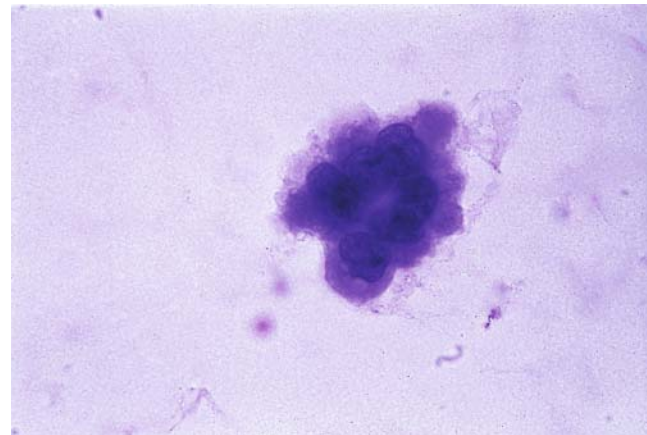


Fig. 22.11-2. CSF showing cytology, positive for a malignant cells. Wright stain.

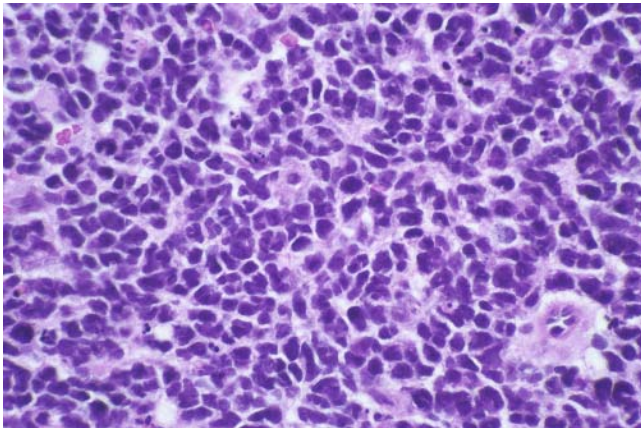


Fig. 22.11-3. Histology of classic medulloblastoma composed of round to elongated nuclei, little cytoplasm, and delicate vessels. H&E.

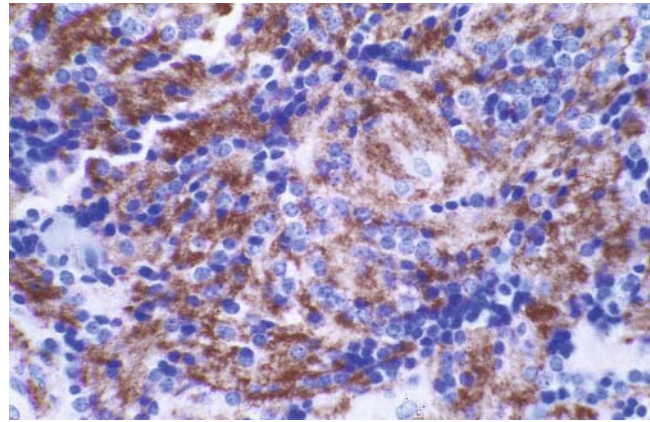


Fig. 22.11-4. Many tumor cells show synaptophysin immunoreactivity.

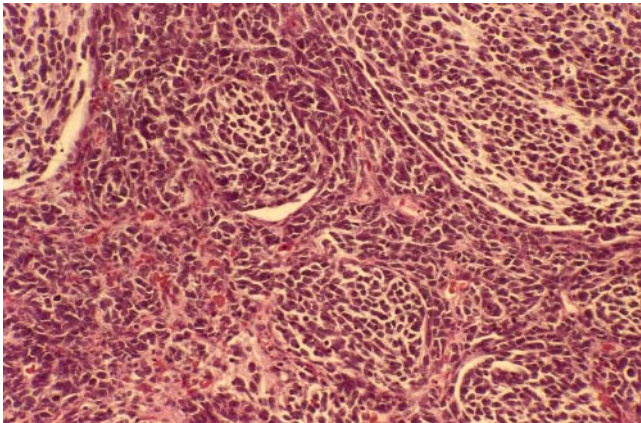


Fig. 22.11-5. Nodular type with tumor cells arranged in small and large nodules separated by less organized tumor stroma.

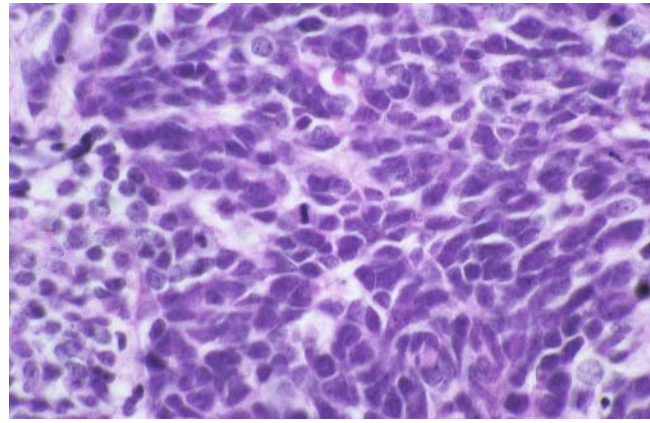


Fig. 22.11-6. Large cell type showing large irregular nuclei with molding and prominent mitoses.

22.12 Supratentorial Primitive Neuroectodermal Tumors

The *supratentorial primitive neuroectodermal tumor* (sPNET) is a grade IV embryonal tumor of poorly differentiated neuroepithelial cells that may display divergent differentiation: neuronal, astrocytic, ependymal, muscular, or melanocytic. Those with definite neuronal differentiation are called cerebral neuroblastomas. If ganglion cells are present, they are called ganglioneuroblastomas. They are found in the cerebrum or suprasellar region. They may be massive with cysts or hemorrhages. The histology resembles that of the classic

medulloblastoma. The cells vary from round to pleomorphic with little cytoplasm. Homer-Wright rosettes, ependymal canals, or cells containing melanin can be found. There is a variable desmoplastic component. Immunohistochemistry and EM reveal the components of the individual tumor. The proliferation index is high. Genetic studies suggest that sPNETs differ from medulloblastomas, and their prognosis is worse than that for medulloblastoma.

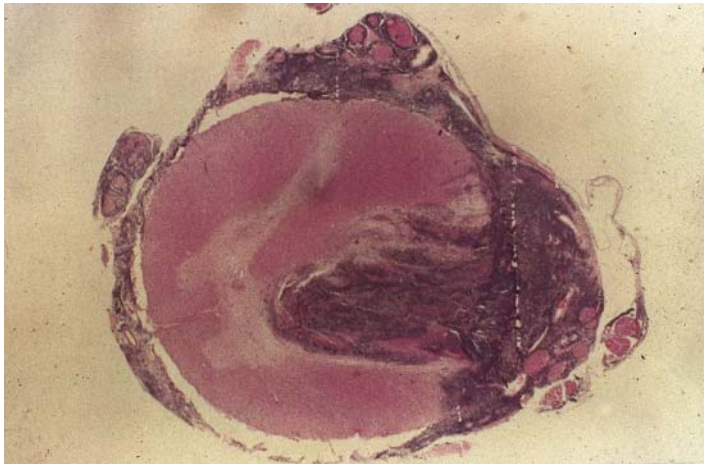


Fig. 22.12-1. Supratentorial primitive neuroectodermal tumor (sPNET). Whole mount of spinal cord surrounded by metastasizing PNET.

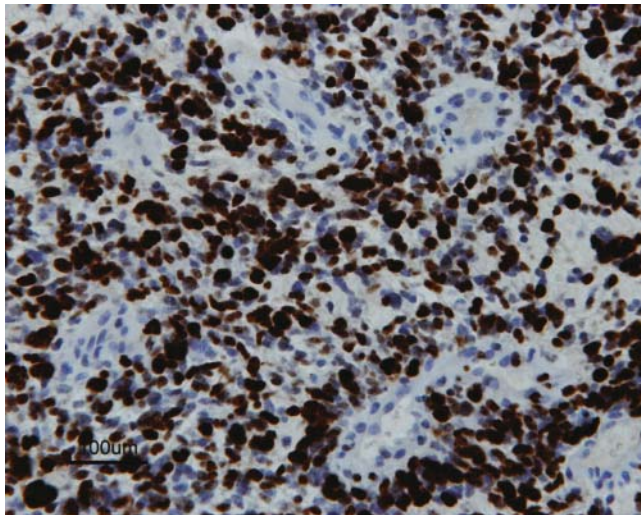


Fig. 22.12-2. sPNET. MIB-1 immunohistochemistry shows a high proliferative index.

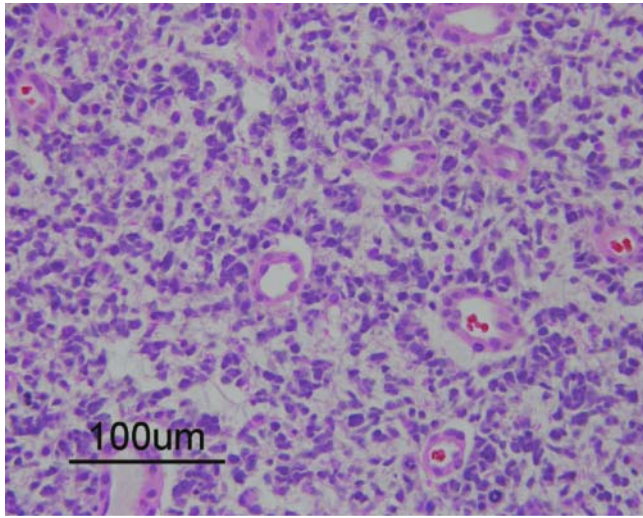


Fig. 22.12-3. sPNET. Histology of regular tumor cells infiltrating brain fascicles. H&E.

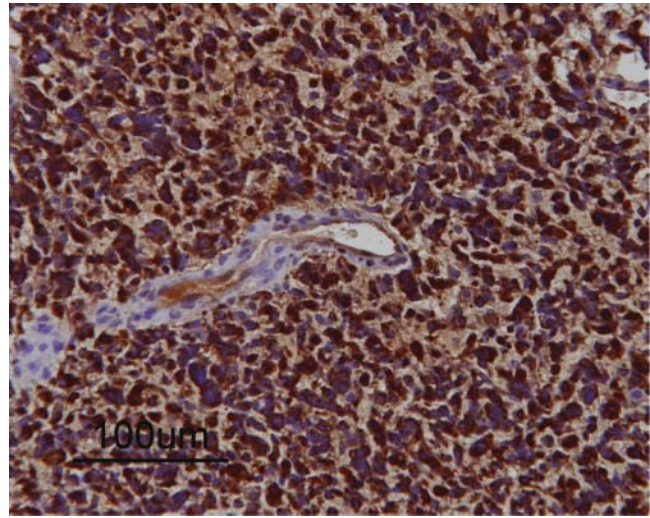


Fig. 22.12-4. sPNET. Immunohistochemistry for neuron-specific enolase.

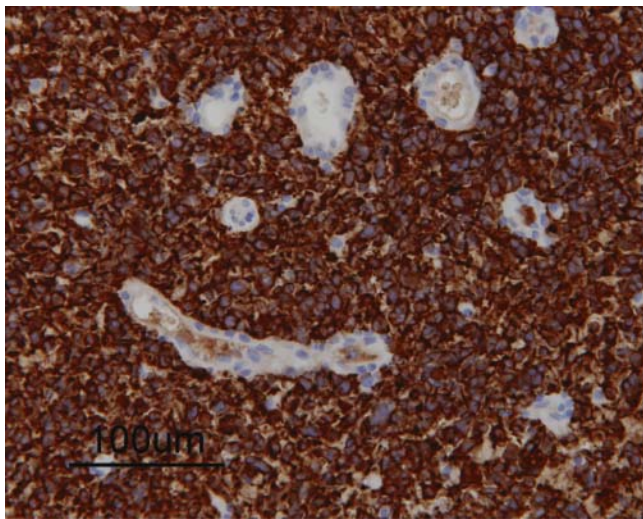


Fig. 22.12-5. sPNET. Immunohistochemistry for MAP2.

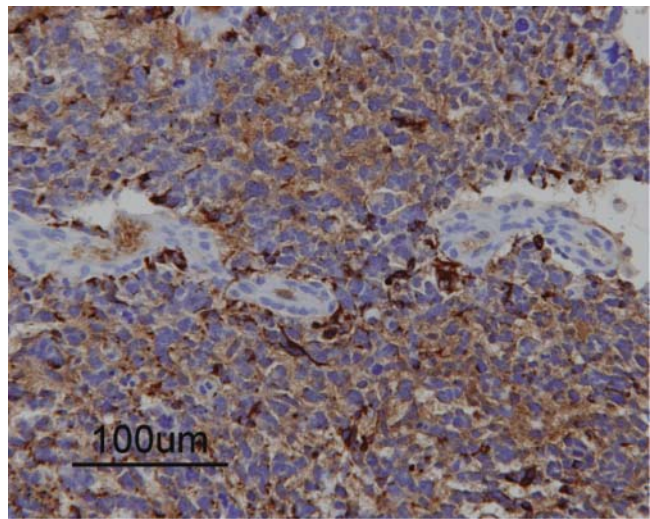


Fig. 22.12-6. sPNET. Immunohistochemistry for GFAP.

22.13 Atypical Teratoid/Rhabdoid Tumor (Grade IV)

Atypical teratoid/rhabdoid tumor (AT/RT) is an embryonal childhood tumor with rhabdoid cells with or without areas of PNET, epithelial tissue, and neoplastic mesenchyme. AT/RT usually occurs in the cerebello-pontine angle but also in the cerebrum, pineal region, or spinal cord or at multiple sites. It metastasizes through the CNS axis early. Typical rhabdoid cells are round-to-oval, medium-sized cells with a fine granular cytoplasm that may contain a denser pink body, which, as seen by EM, is composed of whorled bundles of intermediate filaments. Cell borders are distinct, and mitoses are common. The PNET component may display rosettes.

The mesenchymal element may appear as spindle cells or as denser areas of sarcoma. There may be an epithelial component that resembles adenocarcinoma or squamous epithelium. The rhabdoid cells express EMA, vimentin, and sometimes SMA. They may express GFAP, NFP, and keratin. They are negative for germ cell tumor markers. About 90% of CNS AT/RTs demonstrate monosomy or deletion of chromosome 22. The affected gene is *hSNF5/INI* found on chromosome 22q11.2. This gene has also been identified to be inactive in choroid plexus tumors (see Section 22.5) [12]. Prognosis for survival beyond 1 year is bleak.

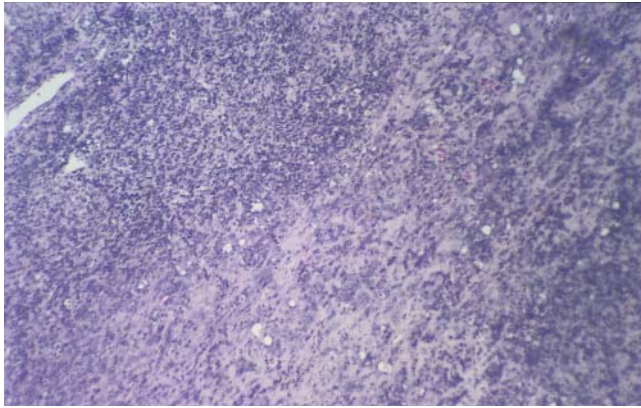


Fig. 22.13-1. Atypical teratoid/rhabdoid tumor (AT/RT). Histology shows a mixture of rhabdoid cells and undifferentiated cells. H&E.

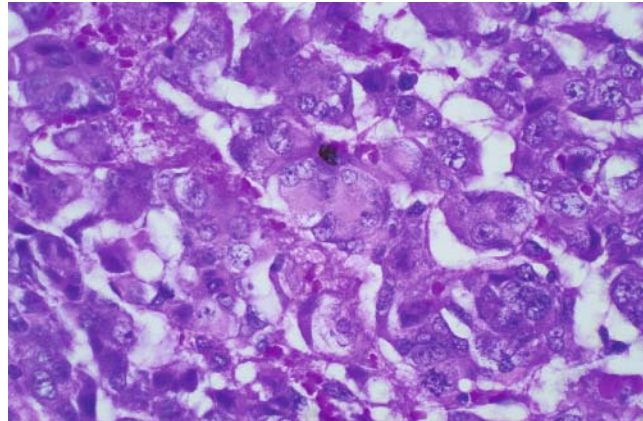


Fig. 22.13-2. Microscopy shows rhabdoid cells.

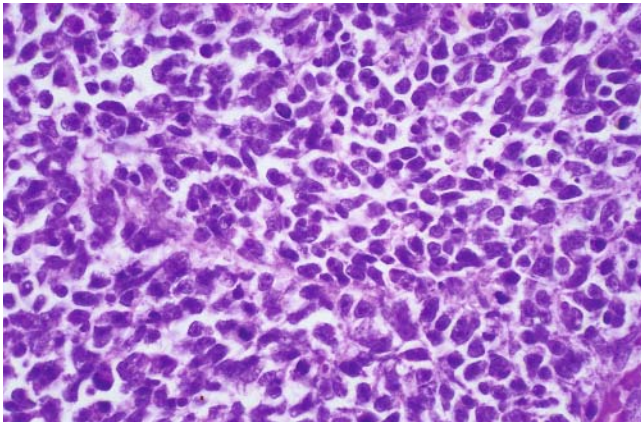


Fig. 22.13-3. Microscopy shows undifferentiated cells.

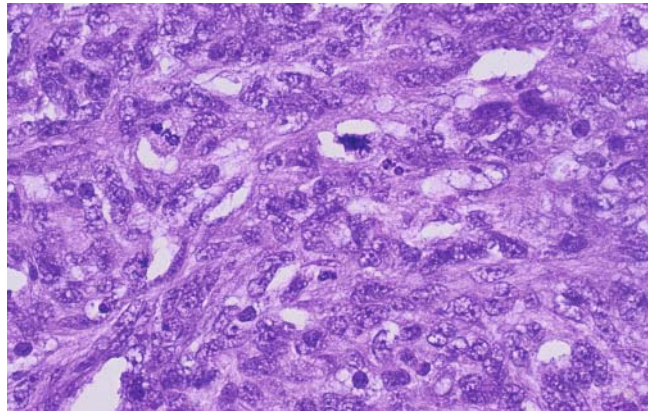


Fig. 22.13-4. Histology shows malignant epithelial cells.

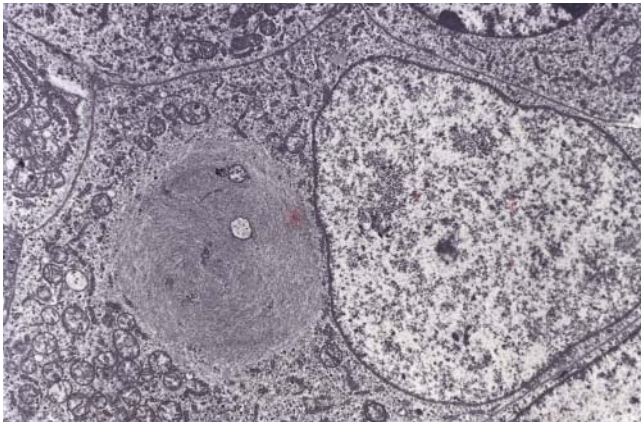


Fig. 22.13-5. EM shows dense cytoplasmic whorls of intermediate filaments.

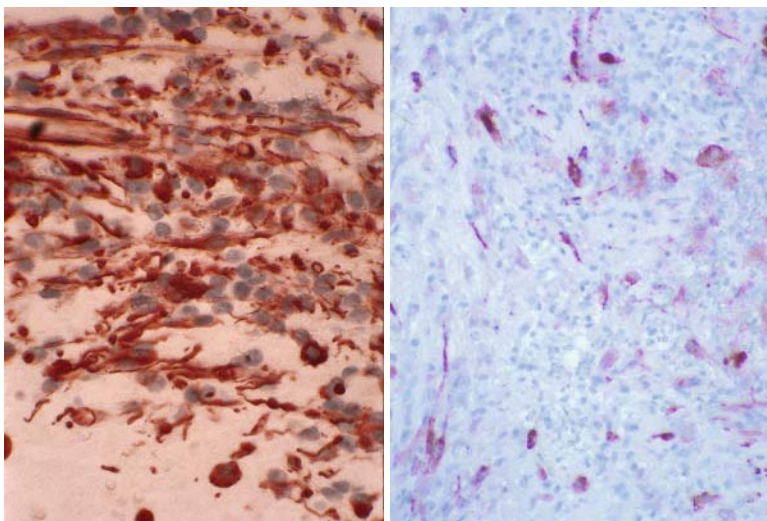


Fig. 22.13-6. Immunohistochemistry for EMA (*left*) and SMA (*right*).

22.14 Peripheral Neuroblastic Tumors

The neuroblastic tumors outside the central nervous system (CNS) are important tumors during childhood.

Olfactory neuroblastoma is a rare malignant neuroectodermal tumor possibly arising from the olfactory receptor neurons. It invades the cribriform plate and other nasal structures, the skull, and the brain. It may contain neuroendocrine elements and secrete ACTH. There are two histological patterns: neuroblastoma-like and neuroendocrine carcinoma-like. The first has small round tumor cells (which may show Flexner rosettes) and ganglion cells. A variant of the neuroblastoma type has large epithelial-like cells in a lobular pattern resembling a paraganglioma. The neuroendocrine carcinoma variant resembles carcinoid or small cell carcinoma of the lung. The tumor cells stain for neuronal or epithelial markers, depending on the type. Molecular genetics suggest that it differs from a classic neuroblastoma.

Neuroblastic tumors of the adrenal gland and sympathetic nervous system. These tumors are the most common extracranial solid tumor of childhood and are derived from the neural crest cells of the adrenal medulla or

sympathetic nervous system. They are located in the adrenal gland and in abdominal, thoracic, cervical, and pelvic sympathetic ganglia. There are four histological types: neuroblastoma (schwannian stroma-poor); ganglioneuroblastoma containing neuroblastic elements at various stages of maturation with >50% of volume comprised of schwannian stroma (schwannian stroma-rich); ganglioneuroblastoma composed of a neuroblastic nodular component mixed with ganglioneuroblastoma or ganglioneuroma components (schwannian stroma-rich/stroma-dominant and stroma-poor); and ganglioneuroma composed of schwannian stroma with maturing or mature ganglion cells (schwannian stroma-dominant). There are some genetic associations with this tumor: deletion of the short arm of chromosome 1p, loss of chromosome 11q, amplification of *MYCN* and overexpression of its RNA and protein, trisomy for 17q. There are numerous prognostic factors that have been identified related to patient age, tumor morphology, and gene expression.

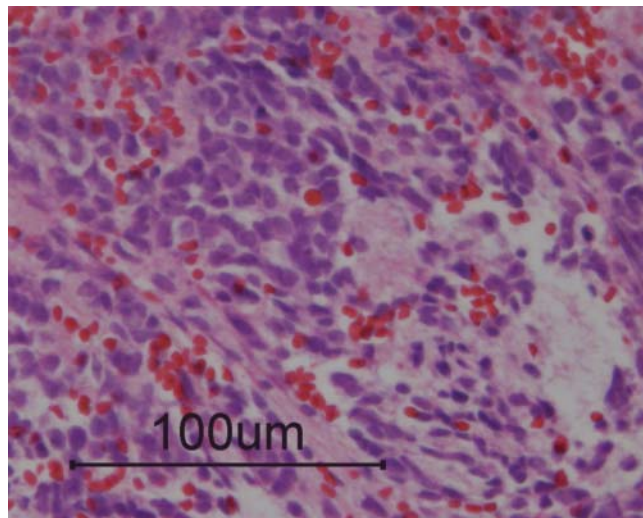


Fig. 22.14-1. Olfactory neuroblastoma. Histology shows loose lobules of tumor cells. H&E.

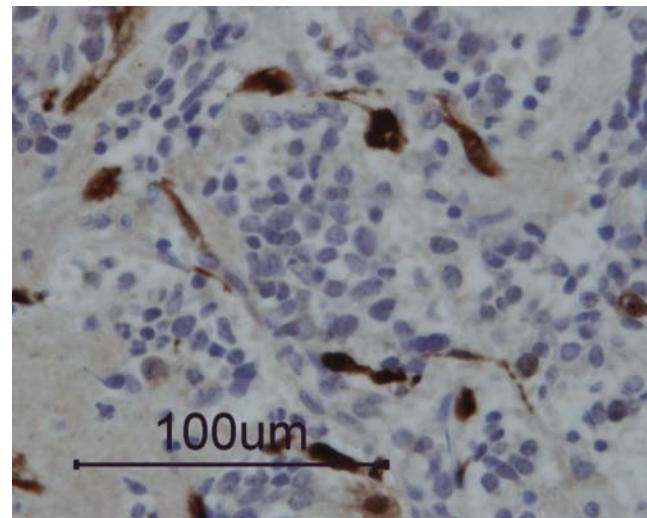


Fig. 22.14-2. Olfactory neuroblastoma. S100 immunohistochemistry, showing the S100 reactive sustentacular cells.

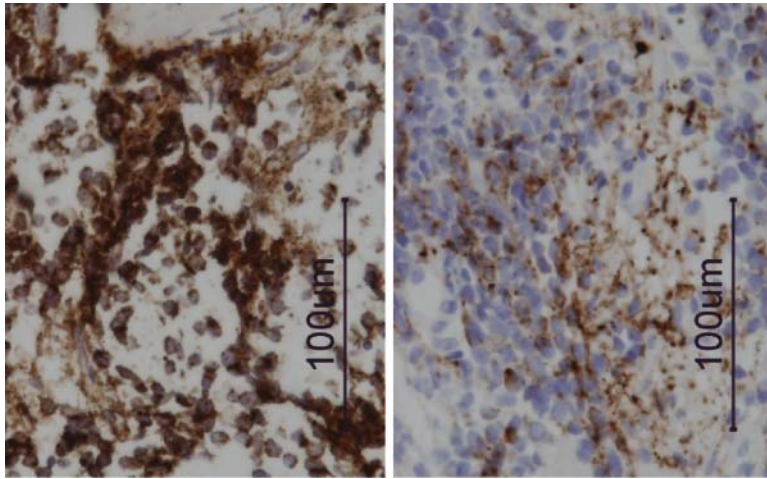


Fig. 22.14-3. Olfactory neuroblastoma. NB84 (*left*) and NF (*right*) immunohistochemistry.

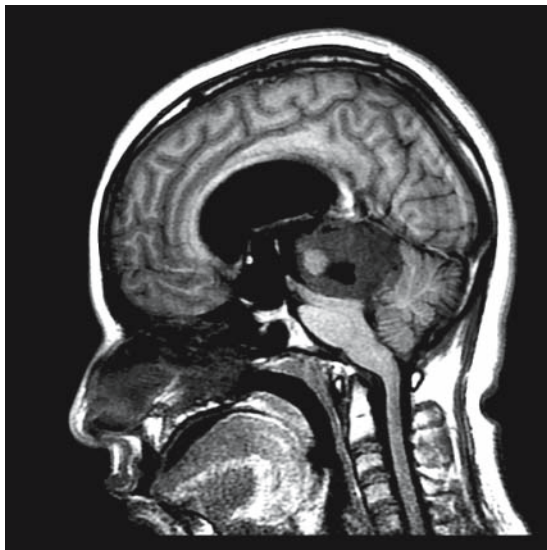


Fig. 22.14-4. Ganglioneuroblastoma. T1-weighted MRI with contrast shows a pineal-region tumor.

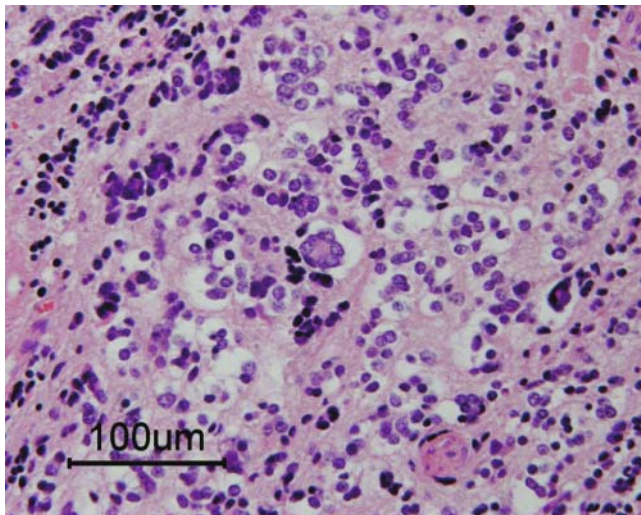


Fig. 22.14-5. Ganglioneuroblastoma. Histology shows both undifferentiated and ganglionic elements. H&E.

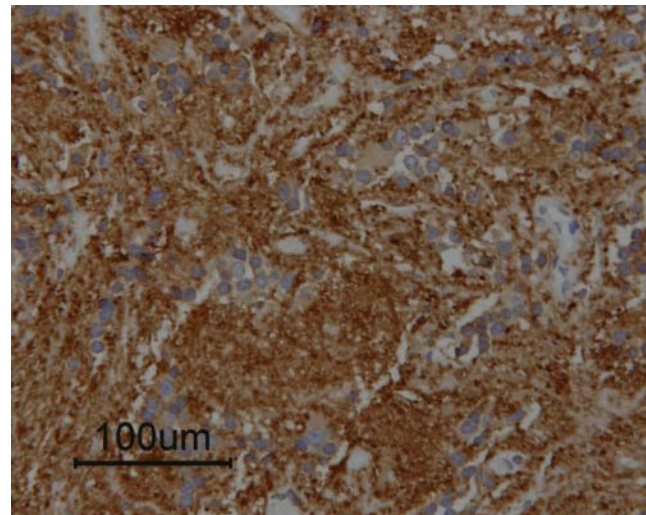


Fig. 22.14-6. Ganglioneuroblastoma. There is widespread synaptophysin immunoreactivity.

22.15 Pineal Parenchymal Tumors

The *pineoblastoma* (grade IV) is an embryonal tumor (grade IV) of children composed of sheets of small cells with round or irregular nuclei and little cytoplasm. It resembles other PNETs. There may be Homer-Wright or Flexner-Wintersteiner rosettes and fleurettes. Melanin, cartilage, and rhabdomyoblastic differentiation may be present. It can be admixed with pineocytoma. Cells react with synaptophysin, NSE, NF, class III β -tubulin, chromogranin A, and retinal S antigen. The tumors are large and invasive with frequent CSF dissemination. The tumor shares histological and immunological features of the developing pineal gland and retina. Patients with retinoblastomas occasionally have a pineal tumor resembling a pineoblastoma.

Pineocytoma (grade II) is a pineal parenchymal tumor of all ages composed of cells resembling mature pineo-

cytes (cells with club-shaped cytoplasmic expansions). Pineocytomas are localized to the pineal region and may expand to compress the aqueduct or grow into the third ventricle. The pineocyte has neuroendocrine and photosensory function, and the tumor cells mark with neuronal markers, serotonin, the retinal S antigen, and rhodopsin. EM shows electron-dense granules and clear vesicles, junctional complexes, synapses, and cilia.

Pineal parenchymal tumor of intermediate differentiation is a tumor that presents at all ages. It has a monomorphous appearance, nuclear atypia, and occasional mitosis. The clinical behavior is variable with rare metastases.

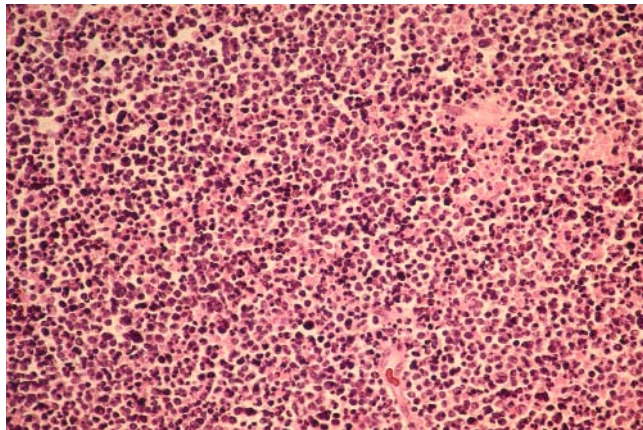


Fig. 22.15-1. Pineoblastoma. Microscopy shows sheets of undifferentiated cells. H&E.

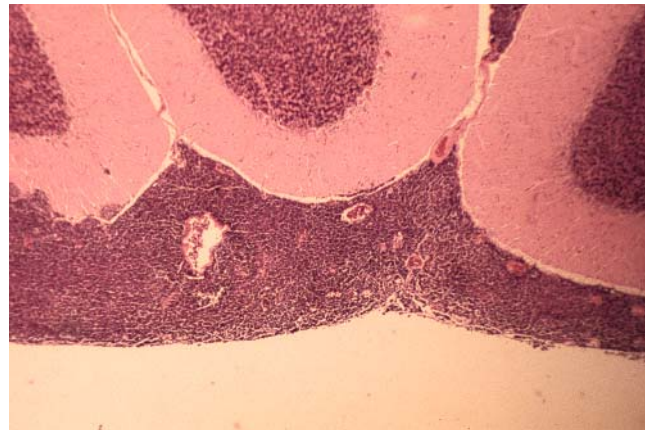


Fig. 22.15-2. Pineoblastoma. Microscopy shows cerebellar subarachnoid spread. H&E.

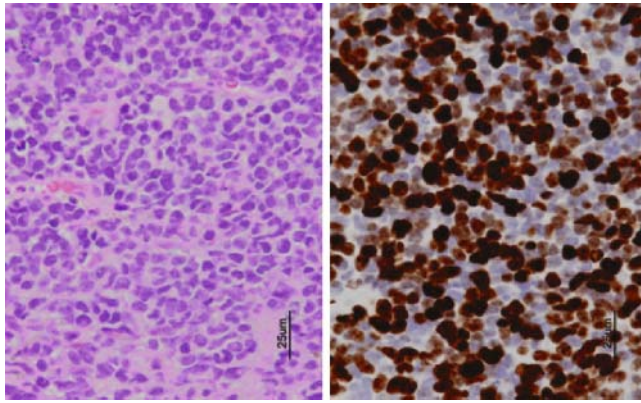


Fig. 22.15-3. Pineoblastoma. *Left.* H&E. *Right.* MIB-1 immunohistochemistry.

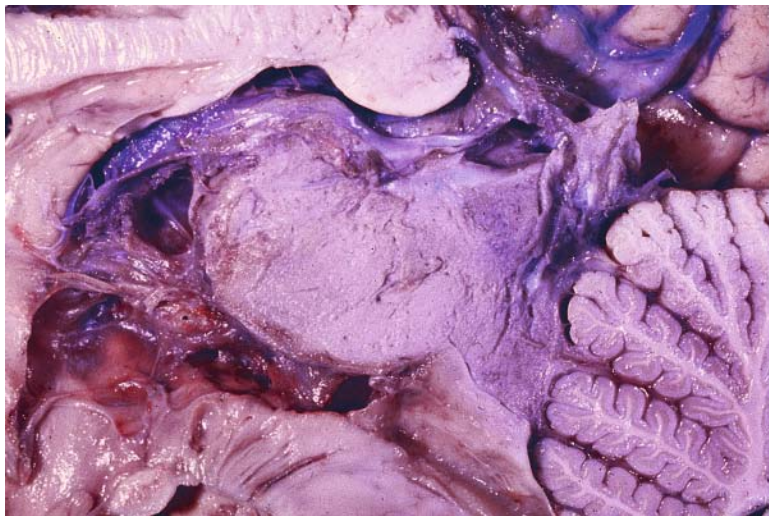


Fig. 22.15-4. Pineocytoma. Gross brain in a sagittal section showing a localized tumor in the pineal region.

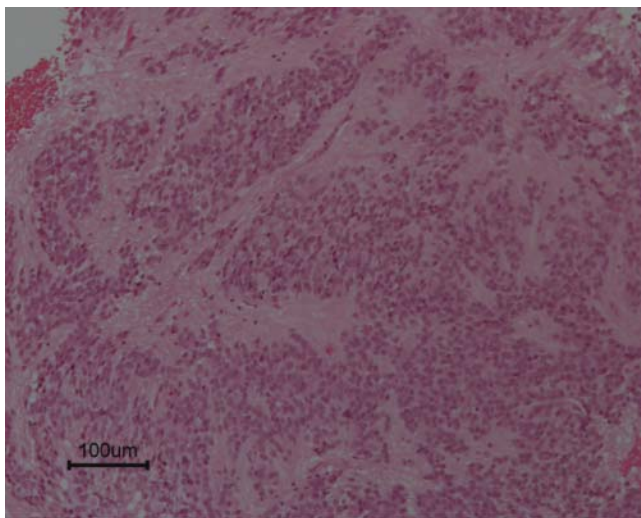


Fig. 22.15-5. Pineocytoma. Histology shows monomorphic round nuclei on a fine fibrillary background. H&E.

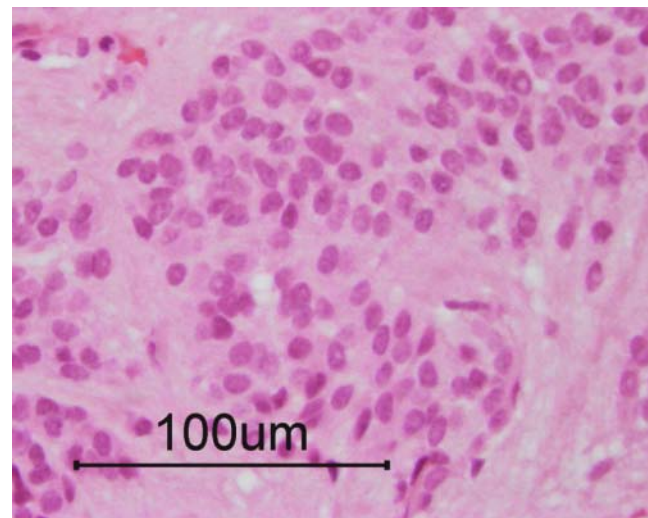


Fig. 22.15-6. Pineocytoma. Histology at higher magnification. H&E.

22.16 Meningeal Tumors

Meningeal tumors [17] are rare during childhood but do occur and are diagnostic challenges. A recent review is useful and comprehensive [18]. All histological types of *meningiomas* have been reported in children, and they may be encountered in unusual sites: within the ventricles, in the posterior fossa, or in spinal epidural regions. In infantile cases the tumors are usually unique. They may be very large, contain cysts, and arise from meningotheelial cells of the parenchyma in Virchow-Robins spaces. They may have an anaplastic histology and behave aggressively. There is an equal male and female distribution. Meningiomas are associated with NF2 and can occur following irradiation. Meningiomas may be grade I, grade II, or atypical. In atypical meningiomas there is a mitotic index of 4 or more per 10 high-power fields or three of the following histological features: sheeting architecture, macronuclei, small cells with a

high nuclear/cytoplasmic ratio, hypercellularity, necrosis. Grade III meningiomas have anaplastic/malignant carcinomatous, sarcomatous, or melanoma-like appearances.

There are rare primary *sarcomas* in the meninges of children. They include the hemangiopericytoma, fibrosarcoma/malignant fibrous histiocytoma, mesenchymal chondrosarcoma, rhabdomyosarcoma, and leiomyosarcoma. Some benign or low-grade tumors of the meninges are the chondroma, low-grade chondrosarcoma, hemangioma, lipoma, and solitary fibrous tumor.

Melanocytic meningeal tumors have been reported in children. They may arise from the meningeal melanocytes or as a component of neurocutaneous melanosis. There are both low-grade melanocytomas, and high-grade melanomas.

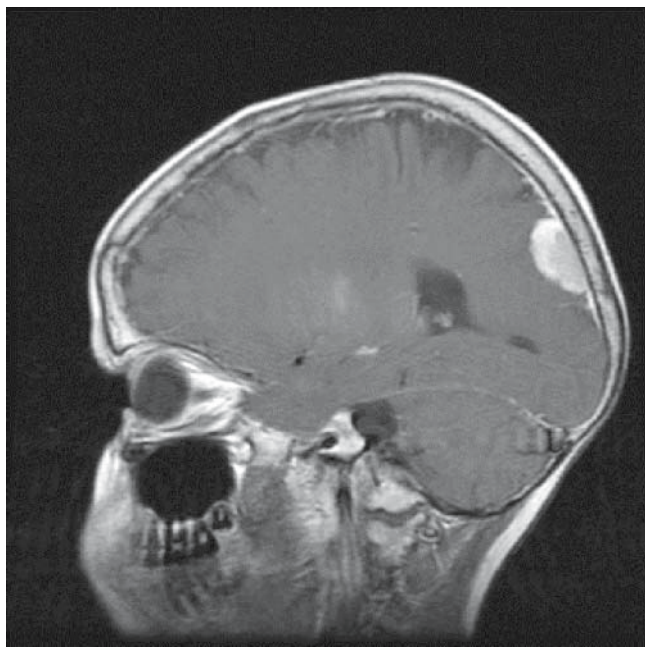


Fig. 22.16-1. Atypical meningioma in a 14-year-old girl as seen using T1-weighted MRI with contrast.

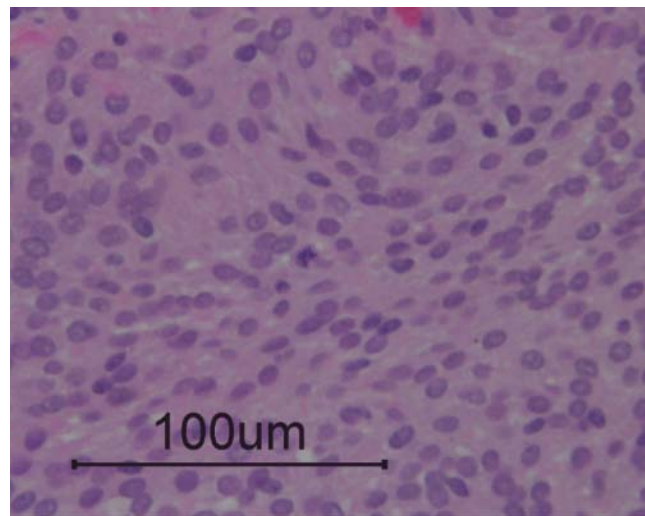


Fig. 22.16-2. Atypical meningioma. Histology shows atypical features. H&E.

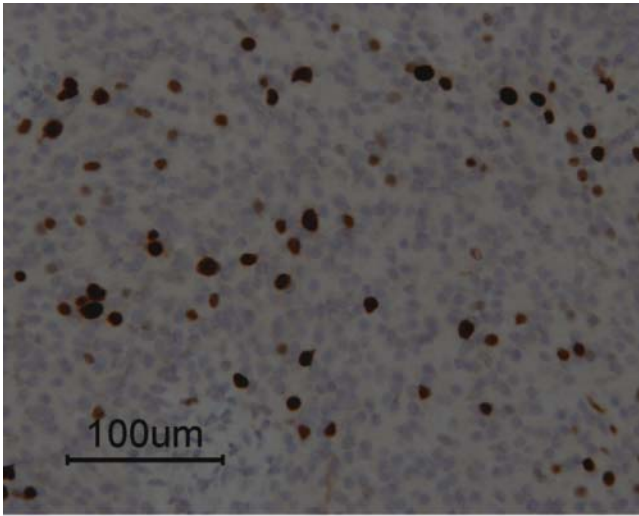


Fig. 22.16-3. Atypical meningioma. MIB-1 immunohistochemistry.

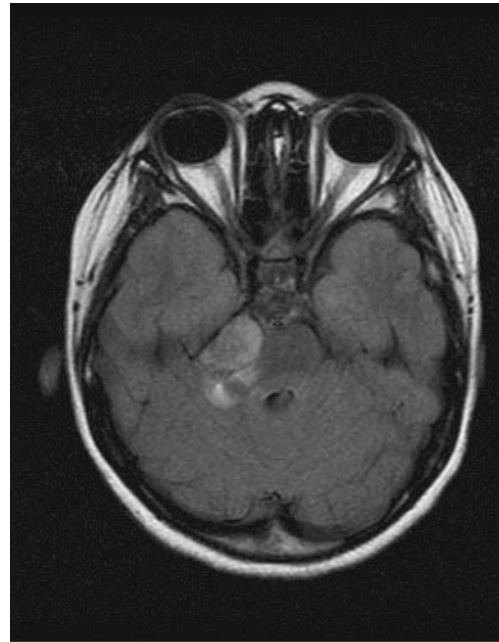


Fig. 22.16-4. Meningeal sarcoma. MRI shows a dural based lesion, in the region of the right cerebellar pontine angle, that is pressing on and distorting the brainstem.

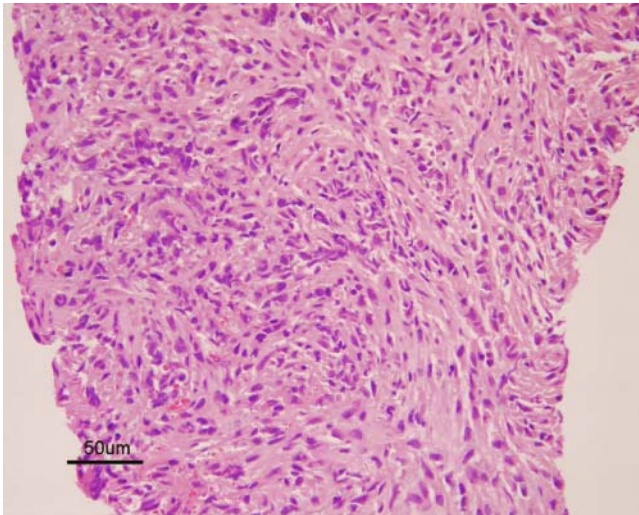


Fig. 22.16-5. Meningeal sarcoma. A biopsy of the tumor (22.16-4) shows it to be an undifferentiated sarcoma. H&E.

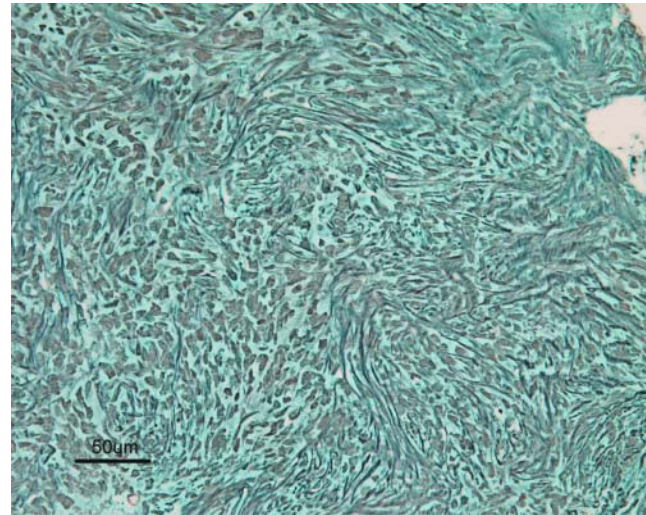


Fig. 22.16-6. Meningeal sarcoma, undifferentiated. Reticulin stain.

22.17 Tumors of the Sellar Region: Developmental Mass Lesions and Cysts

The *craniopharyngioma* is a benign grade I epithelial tumor derived from Rathke pouch epithelium. These lesions account for 5%–10% of childhood intracranial tumors. They are usually suprasellar, frequently with an intrasellar component. There are two histological types. The adamantinomatous form contains multistratified squamous epithelium with peripheral palisading of nuclei on a basement membrane. They contain nodules of compact keratin and calcifications. There may be cholesterol clefts, foamy cells, and chronic inflammation. The papillary craniopharyngioma is composed of disrupted sheets of squamous epithelium with a fibrovascular stroma, thus forming pseudopapillae [19].

Pituitary adenomas occasionally present during childhood. Skull-based lesions may expand to involve the

pituitary gland, optic nerve, or hypothalamus. The *chordoma* [20] can arise from notochordal tissue at either end of the vertebral column. Some chordomas arise from notochordal ectopias, the *ecchordosis*. The tumors are bulky and may invade the dura and subarachnoid space, causing compression of the base of the brain. Chordoma cells are large with dense nuclei and vesicular cytoplasm. They have a characteristic immunohistochemical profile: EMA-, S100-, and CK-reactive.

The lesions of *Langerhans histiocytosis* may occur in the sellar region (see Fig. 22.19). The hypothalamus is the usual site of the type of *hamartomas* to read like pituitary adenomas or Langerhans, benign masses that are composed of mature neurons and normal neuropil.

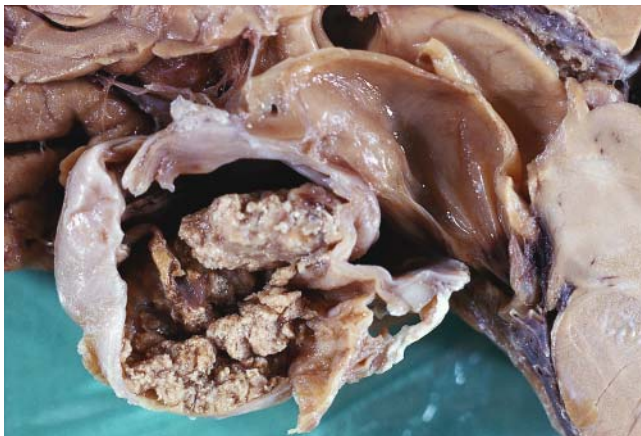


Fig. 22.17-1. Craniopharyngioma. Note the large cystic calcified lesion below the brain and above the sella.

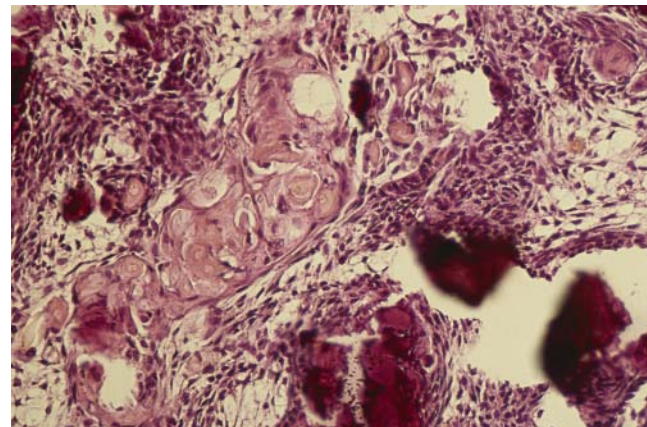


Fig. 22.17-2. Craniopharyngioma. Note the adamantinomatous stratified squamous epithelium with basal palisading and keratin nests. H&E.

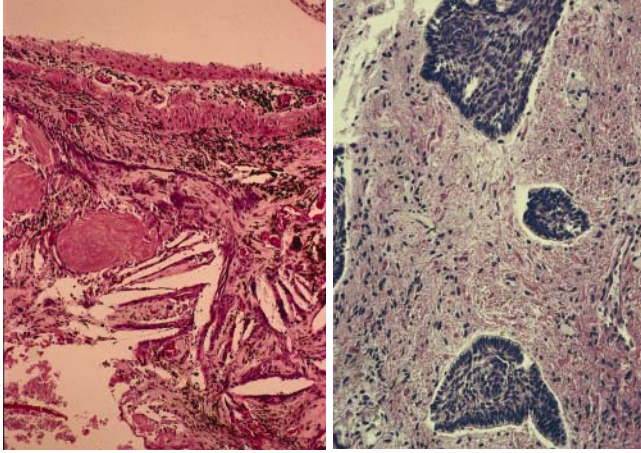


Fig. 22.17-3. Craniopharyngioma. There are keratin nests, cholesterol clefts, and inflammatory cells (*left*) and a craniopharyngioma, adamantinomatous type, with projection into the surrounding hypothalamus which shows innumerable Rosenthal fibers (*right*). H&E.



Fig. 22.17-4. Hypothalamic hamartoma at the base of the brain. Gross illustration.

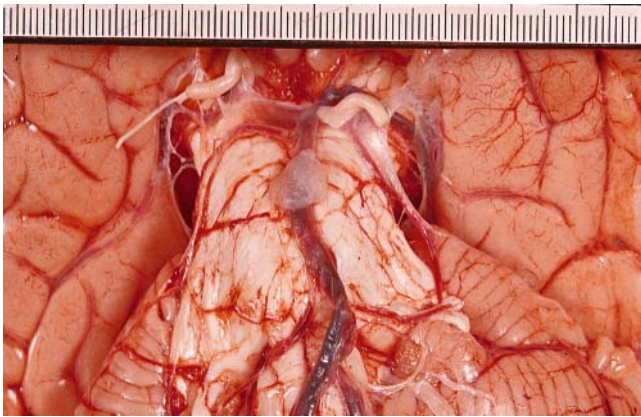


Fig. 22.17-5. Notochordal ecchordosis. The prepons lesion was found incidentally at autopsy.

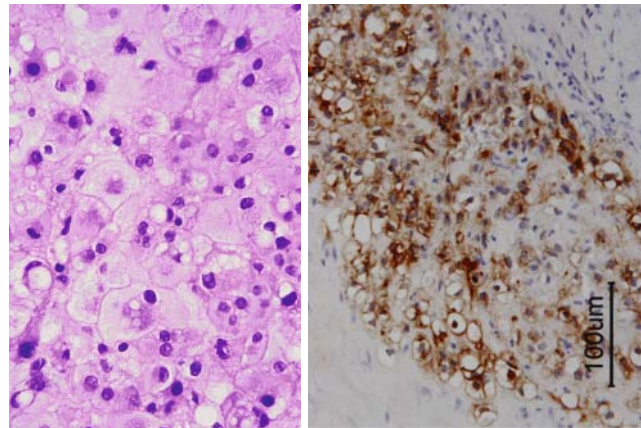


Fig. 22.17-6. Chordoma. Histology. *Left*. H&E. *Right*. EMA immunoreactivity.

22.18 Developmental Masses and Cysts

Epidermoid tumors may be found throughout the neuraxis. They are composed of the superficial layers of the skin [21].

Dermoid cysts are frequently associated with a dermal sinus and are found in the occipital region involving the cerebellum and fourth ventricle, the lumbar spinal region, and the anterior fontanelle. They contain all skin layers and appendages.

There are other cysts in the CNS [16] that are uncommon and are poorly classified. They may be composed of fibrous tissue with arachnoid or ependyma or neuroepithelial linings. Depending on their site of origin, these cysts may present with spinal cord compression, seizures, hydrocephalus, or hypothalamic dysfunction. They are found along the spine in an intra- or extradural

position. The benign *teratomatous cyst* is located posterior to the spinal cord. The *neuroenteric cyst* (which may contain respiratory and/or intestinal mucosa sometimes with muscle layers) is usually anterior to the spine and can involve the posterior mediastinum.

Spinal arachnoid cysts are commonly posterior to the mid-thoracic cord, and intracranial arachnoid cysts are usually in the temporal or frontal fossas and the paracollicular regions. *Epithelial or ependymal cysts* may be found along the sylvian fissure, in the paracollicular region, or in the third ventricle. Some cysts occur in the brain parenchyma.

Glial heterotopias are located in the subarachnoid space, particularly at the base of the brain, with or without other malformations of the brain.

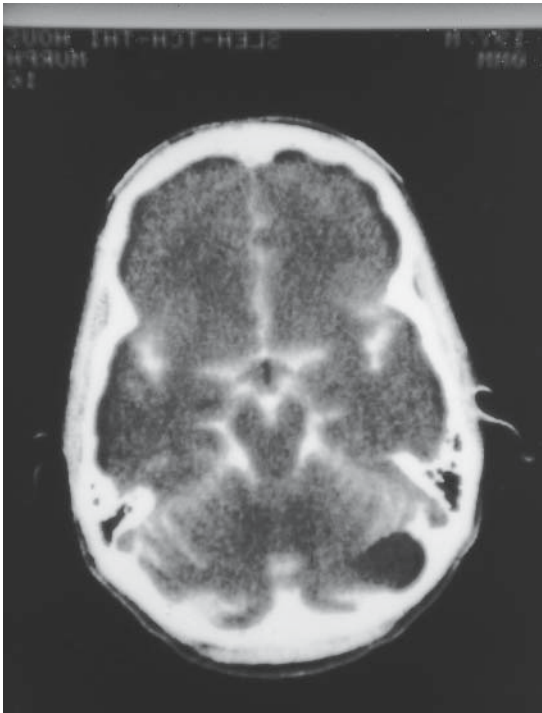


Fig. 22.18-1. Arachnoid cyst of the posterior fossa. CT scan.



Fig. 22.18-2. Glial ependymal cyst of the third ventricle. Gross specimen.

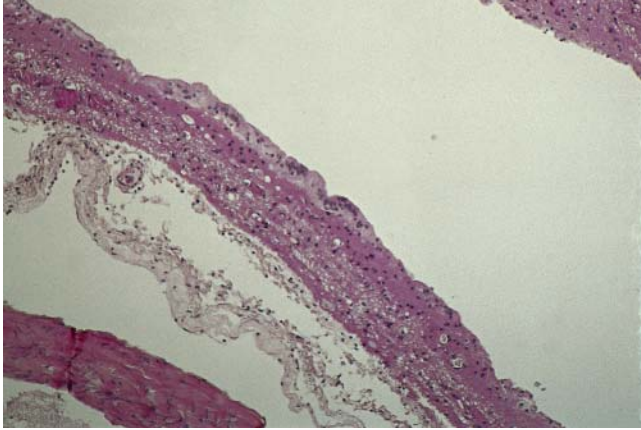


Fig. 22.18-3. Glial ependymal cyst of the third ventricle. Microscopy shows an ependyma-like lining over a glial wall. H&E.

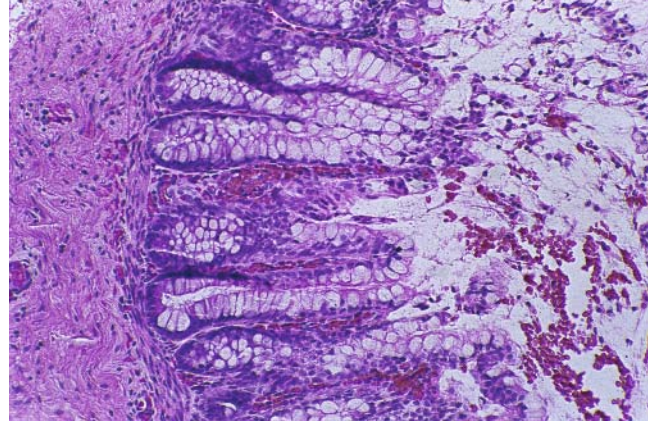


Fig. 22.18-4. Neuroenteric cyst of the posterior mediastinum. Microscopy shows intestinal epithelium in one region. H&E.

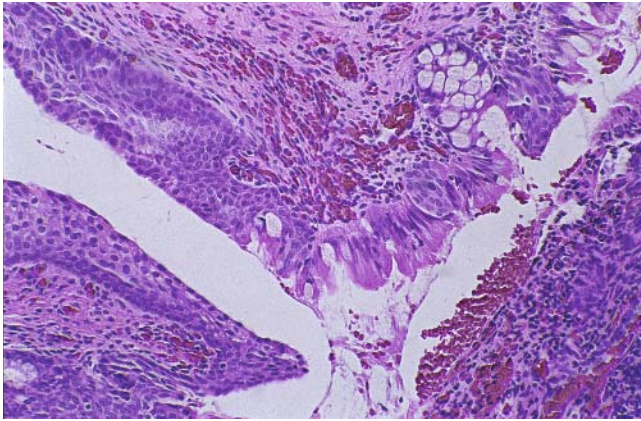


Fig. 22.18-5. Neuroenteric cyst of the posterior mediastinum. Note the mixture of esophageal and respiratory epithelium. H&E.

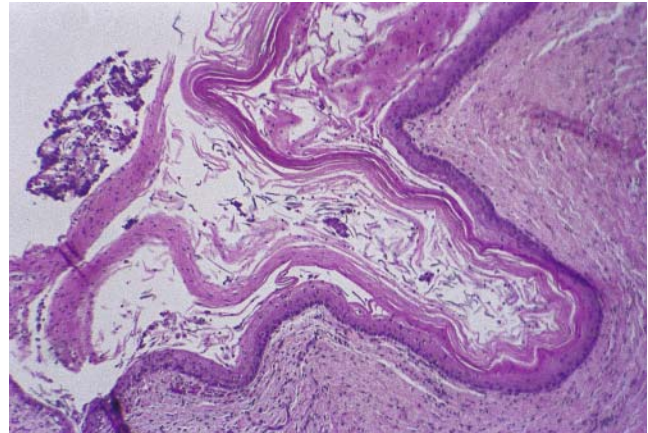


Fig. 22.18-6. Epidermoid cyst of the posterior fossa. Microscopy shows stratified squamous epithelium lining the cyst. H&E.

22.19 Tumors of the Hematopoietic System

Leukemia, *Hodgkin's lymphoma*, and *non-Hodgkin's lymphoma* together make up 40% of neoplasms in children under 15 years of age [22]. In some cases of acute lymphoblastic leukemia (*ALL*) the disease presents in the meninges, and in acute myeloblastic leukemia (*AML*) a mass may form on the dura. *Malignant lymphomas* of the CNS do occur rarely in children, particularly in children with an inherited immunodeficiency. The lymphoma may present in all regions of the CNS as single or multiple lesions. They are diffusely infiltrating in an angiocentric pattern. Most are B-cell lymphomas marking with CD20 and CD79a. All subtypes have been reported, with diffuse large cell or large cell immunoblastic lymphomas being the most common.

Histiocytic disorders are classified as dendritic cell disorders, such as *Langerhans cell histiocytosis* (LCH)

and *juvenile xanthogranuloma*, or as macrophage-related disorders, such as *lymphohistiocytosis* and *Rosai-Dorfman* disease. Malignant histiocytic disorders, such as monocytic leukemia and histiocytic sarcoma, may present during childhood.

Langerhans cell histiocytosis is classified as unifocal, multifocal, or disseminated. The commonest lesion is an osteolytic lesion of the skull or spine. The hypothalamus is frequently involved in the multifocal variant. The gross lesions may be yellow and discrete or infiltrating. The histology consists of Langerhans cell histiocytes expressing CD1a and langerin; and EM may reveal them to have Birbeck granules. Rosai-Dorfman disease in children usually affects lymph nodes.

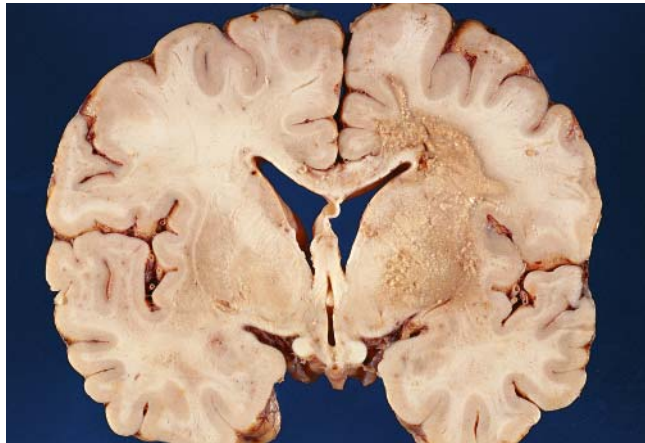


Fig. 22.19-1. Lymphoma of the CNS. Coronal section shows a large discolored area of softening extending from the cingulate gyrus through the centrum semiovale to the thalamus.

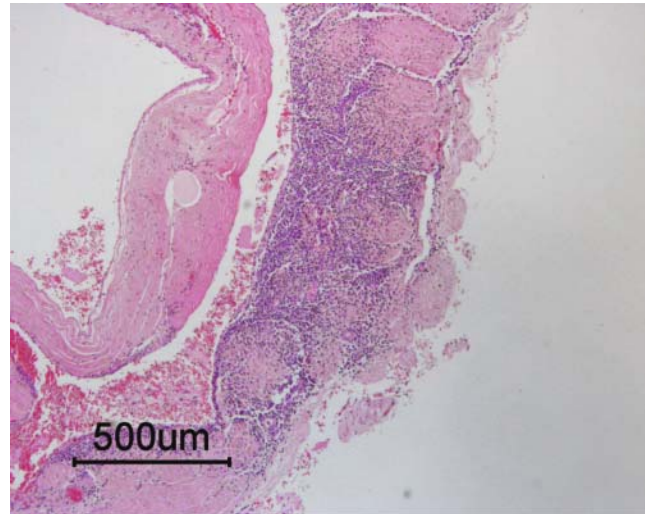


Fig. 22.19-2. Acute lymphocytic leukemia. Histology shows invasion of the dura, producing nodular masses on the inner surface. H&E.

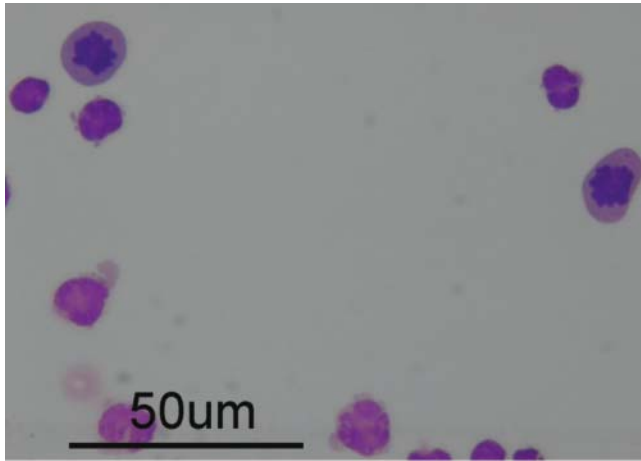


Fig. 22.19-3. Acute lymphocytic leukemia. CSF shows cytology that is positive for malignant cells. Wright stain.

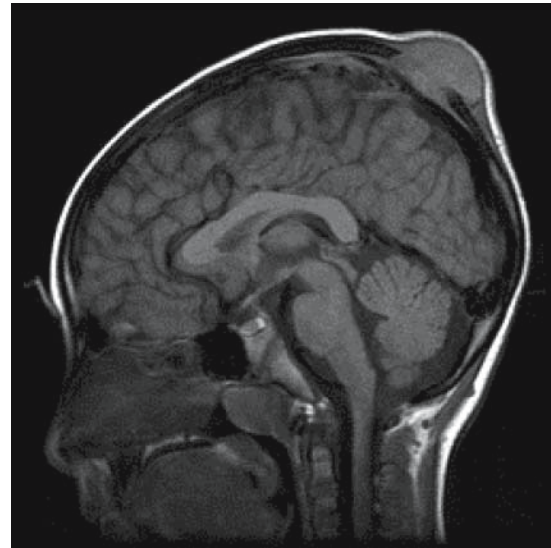


Fig. 22.19-4. Langerhans cell histiocytosis. MRI.

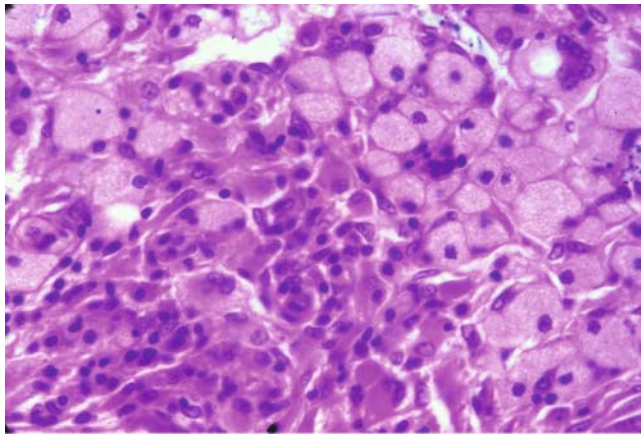


Fig. 22.19-5. Langerhans cell histiocytosis. Histology of a skull lesion exhibiting Langerhans cells and foamy macrophages. H&E.

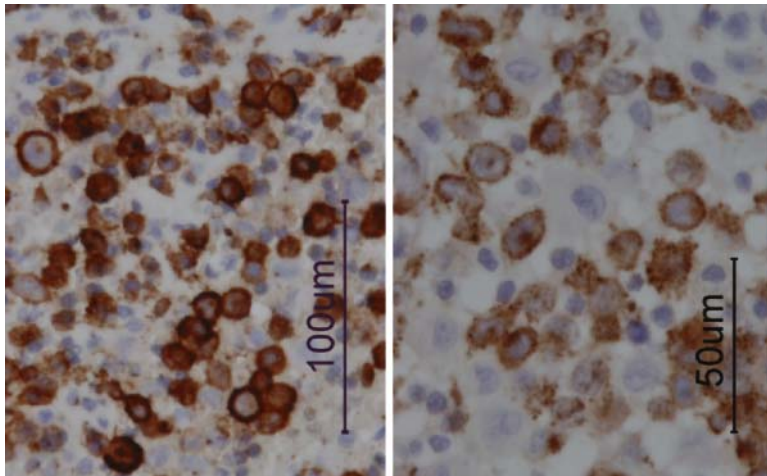


Fig. 22.19-6. Langerhans cell histiocytosis. Immunohistochemistry CD1a (*left*) and Langerin (*right*).

22.20 Germ Cell Tumors

Germ cell tumors [23] of the CNS occur mostly in children and teenagers. They are the same as the germ cell tumors of the gonads. Germinomas and teratomas occur as pure tumor types. Most of the others are a mixture of types. They are found along the midline, usually in the pineal or suprasellar regions, and may be associated with precocious puberty. They produce tissue-related proteins that are measurable in the blood and CSF. Placental alkaline phosphatase (PLAP) is associated with germinoma. β -Human chorionadotrophin (β -HCG) is observed in choriocarcinomas and in germinomas containing HCG-producing giant syncytiotrophoblastic cells. α -fetoprotein (AFP) is seen with yolk sac tumors. The gross appearance suggests the tumor type. The germinoma is solid with or without small cysts. The choriocarcinoma usually has hemorrhage and necrosis. The teratoma may contain teeth, hair, or bone.

The *germinoma* is composed of large, uniform cells with prominent nucleoli; and it characteristically reacts for PLAP and CD117. There is a variable infiltrate of

lymphocytes, and there may be syncytiotrophoblastic giant cells.

The *teratoma* contains elements from the three germ cell layers. The mature teratoma has well-differentiated adult tissues. The immature teratoma has incompletely differentiated components that resemble fetal tissue. The teratoma with malignant transformation contains malignant elements of a somatic cancer, such as rhabdomyosarcoma.

The *yolk sac tumor* is composed of primitive epithelial cells (from the yolk sac) in a loose myxoid matrix that resembles extraembryonic mesoblast. There are hyaline globules that are reactive for AFP.

Embryonal carcinoma is composed of large cells that grow in sheets, forming structures that resemble early embryonic tissues.

Choriocarcinoma differentiates along extraembryonic lines with cytotrophoblasts and syncytiotrophoblastic giant cells. The latter label with β -HCG and human placental lactogen (HPL).

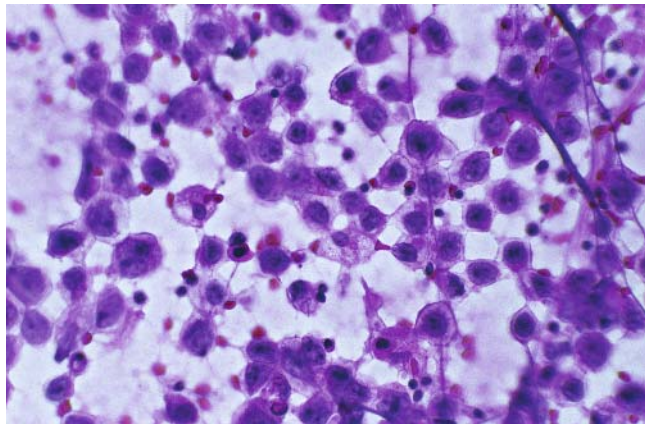


Fig. 22.20-1. Germinoma. Touch preparation shows large tumor cells and lymphocytes. H&E.

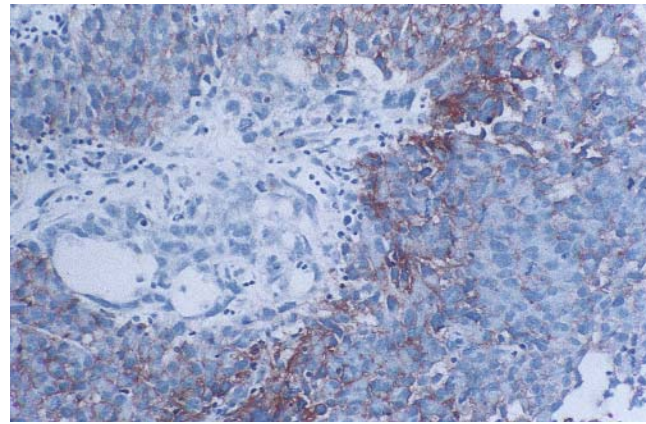


Fig. 22.20-2. Germinoma. Immunohistochemistry with some cells showing PLAP reactivity.

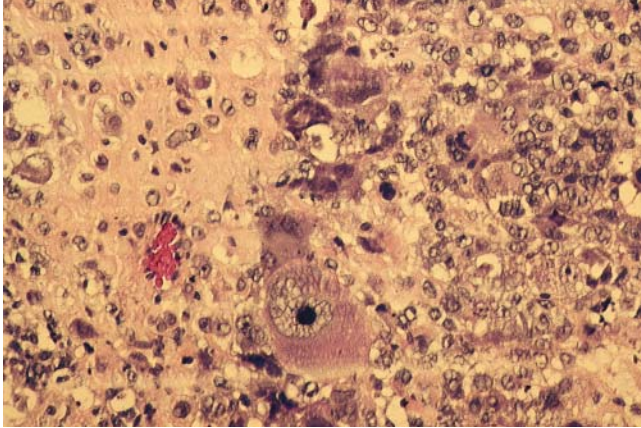


Fig. 22.20-3. Choriocarcinoma with large syncytiotrophoblastic cell. H&E.

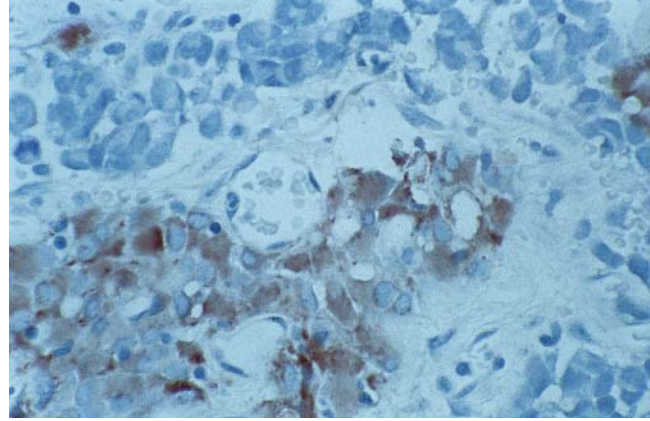


Fig. 22.20-4. Choriocarcinoma. Immunohistochemistry for β-HCG.

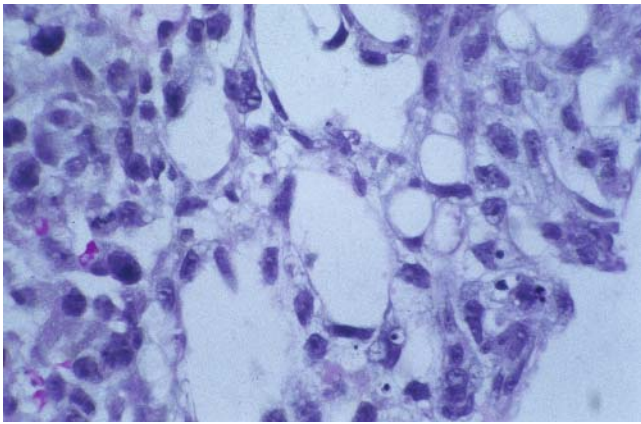


Fig. 22.20-5. Yolk sac tumor. Epithelial-like cells in a loose matrix. H&E.

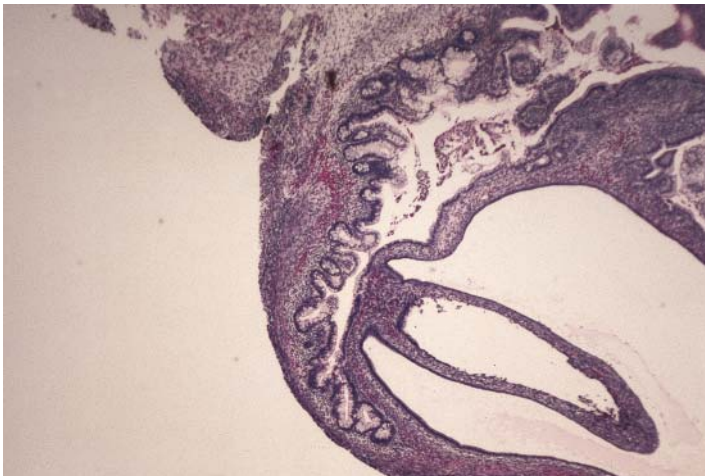


Fig. 22.20-6. Teratoma. Microscopy shows mature epithelial elements. H&E.

22.21.1 Tumors of Cranial and Peripheral Nerves: Schwannoma and Neurofibroma

Schwannoma (grade 1), a slow-growing tumor that may be found anywhere in the peripheral nervous system, is commonly seen in cranial nerve VIII [24]. It is composed of spindle-shaped Schwann cells with alternating dense (Antoni A) and loose (Antoni B) areas. Cells are S100-positive and show basal lamina by EM. Vessels are thick-walled and hyalinized. Most of these tumors are sporadic, but in neurofibromatosis type II (NF2) there are bilateral schwannomas of cranial nerve VIII. The NF2 gene is a tumor-suppressing gene that is mutated in 60% of schwannomas.

The *neurofibroma* (grade 1) is composed of a mixture of Schwann cells, perineurial cells, and endoneurial fibroblasts surrounded by collagen fibers and a myxoid

matrix [24]. They may remain in the perineurium of large nerves or infiltrate the surrounding tissues of small nerves. Plexiform neurofibromas are multiple nerves expanded by the tumor and collagen. The Schwann cells are S-100-positive, and the perineurial cells (S100-negative) react for EMA. EM reveals Schwann cells with a basement membrane and perineurial cells with a thick basement membrane, scattered junctional complexes, and pinocytotic vesicles and fibroblasts with abundant rough endoplasmic reticulum and having no basement membrane. They may be solitary and sporadic or multiple and associated with pigmented café au lait spots and freckling of the axilla in neurofibromatosis type I (NF1) (see Chapter 7, Section 7.2).

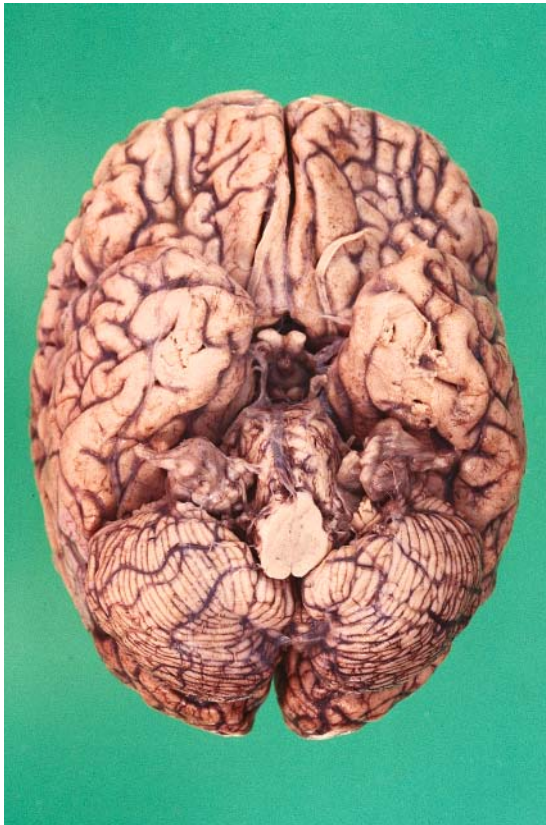


Fig. 22.21.1-1. Schwannoma. Neurofibromatosis type II with bilateral acoustic nerve schwannomas.

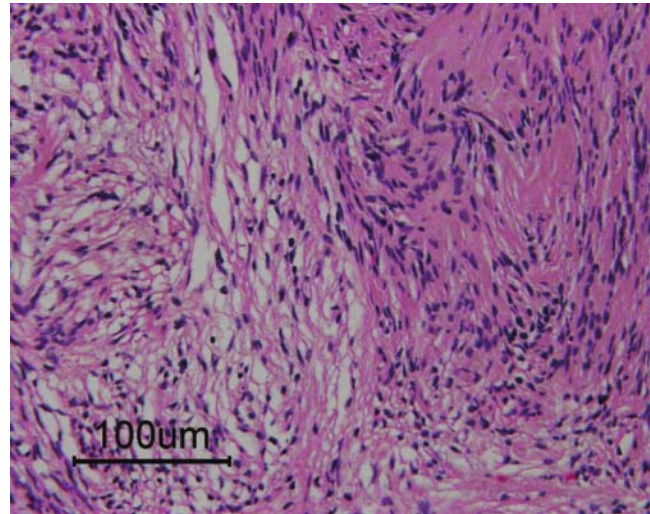


Fig. 22.21.1-2. Microscopy shows compact (Antoni A) and loose (Antoni B) regions. H&E.

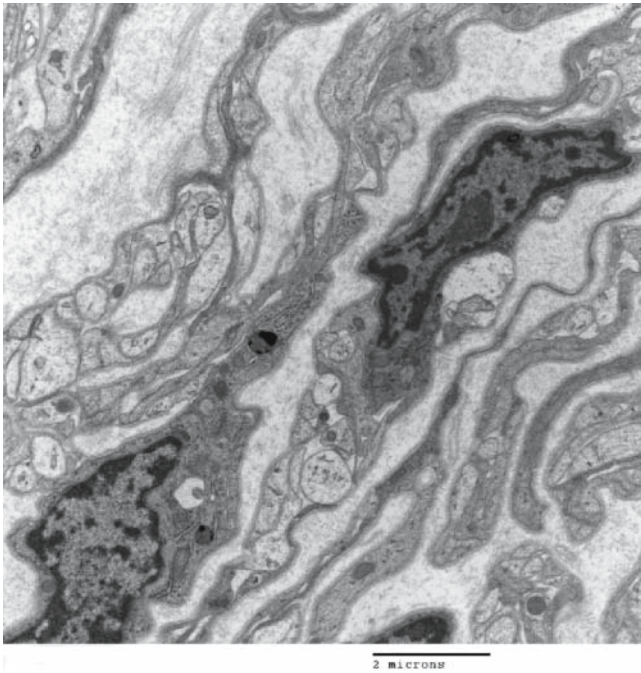


Fig. 22.21.1-3. EM shows cells processes surrounded by basement membrane.

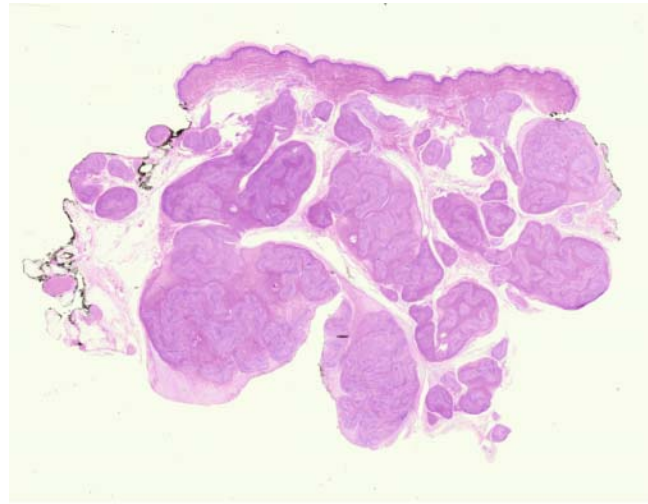


Fig. 22.21.1-4. Plexiform schwannoma. Whole mount view of a subcutaneous lesion from a digit.

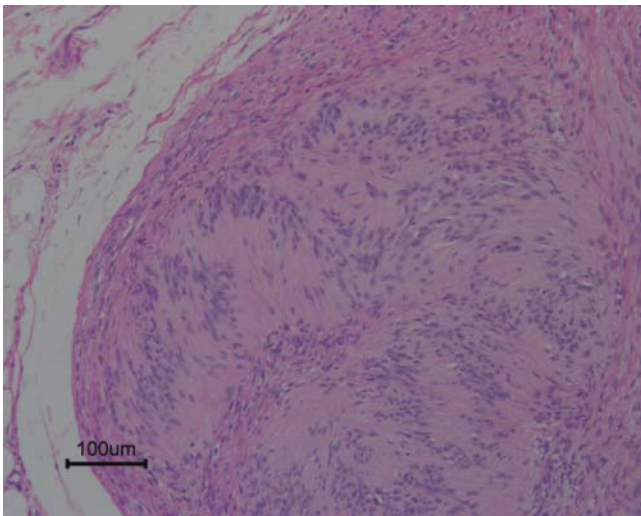


Fig. 22.21.1-5. Plexiform schwannoma: histology. H&E.

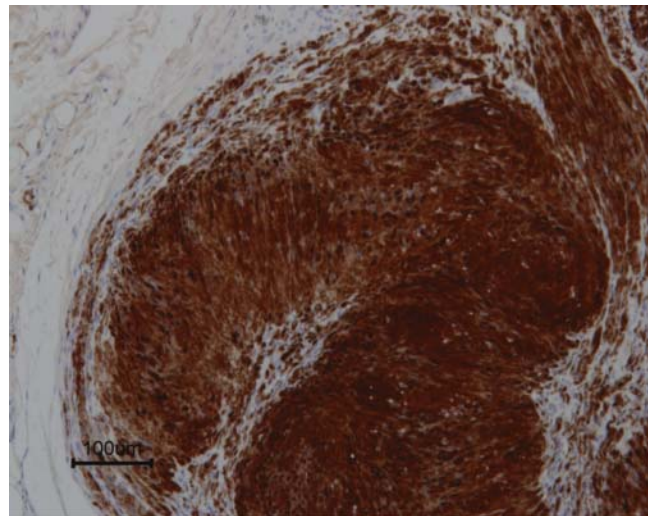


Fig. 22.21.1-6. Plexiform schwannoma. Immunohistochemistry for S100.

22.21.2 Tumors of Cranial and Peripheral Nerves: Perineurinoma and Malignant Peripheral Nerve Sheath Tumor

The *perineurioma* (grade 1) is a rare benign tumor composed of perineurial cells. It may be located in a nerve or in soft tissues. In the nerve it produces an onion skin appearance. Cells react with EMA but not with S100. The perineurioma exhibits monosomy of chromosome 22.

Malignant peripheral nerve sheath tumors (MPNSTs) (grades III or IV) are rare in children. They are malignant tumors arising from large nerves of the buttock,

thigh, brachial plexus, upper arm, and paraspinal region. They are composed of fascicles of hyperchromatic spindle cells and exhibit geographic necrosis and a high mitotic index. They grow in the perineurium but can break into adjacent soft tissues. The malignant triton tumor is a MPNST with rhabdomyosarcomatous differentiation. The MPNSTs react for both S-100 and p53. One-half of patients with this tumor have NF1.

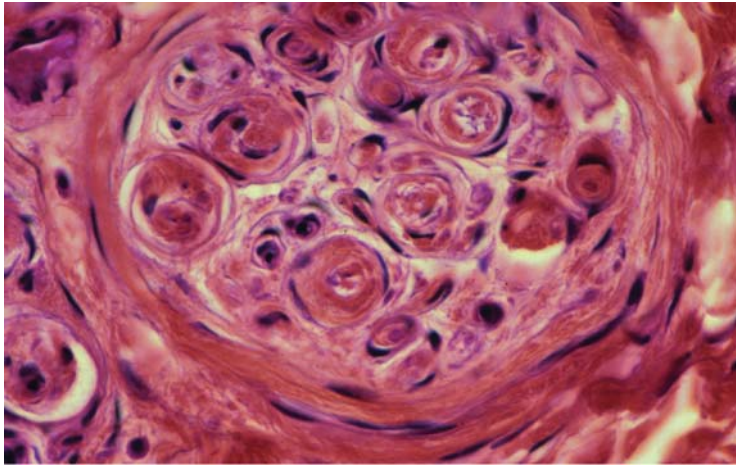


Fig. 22.21.2-1. Perineurinoma. Histology. HPS stain.

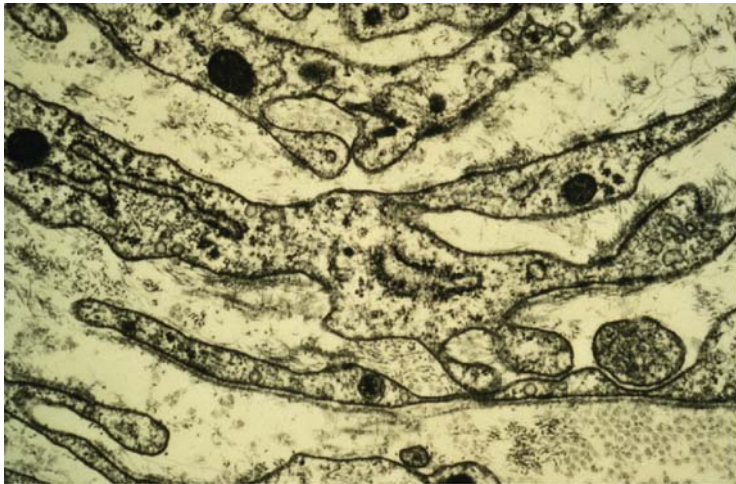


Fig. 22.21.2-2. Perineurinoma. EM shows delicate cell processes with variable numbers of pinocytotic vesicles, discontinuous basement membrane and scattered, intercellular junctional complexes.



Fig. 22.21.2-3. Plexiform neurofibroma. Gross view of a lesion from the chest wall.

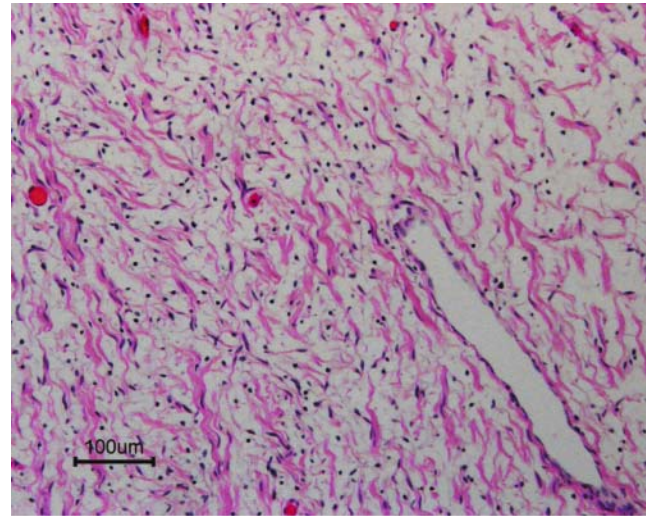


Fig. 22.21.2-4. Plexiform neurofibroma. Histology. H&E.

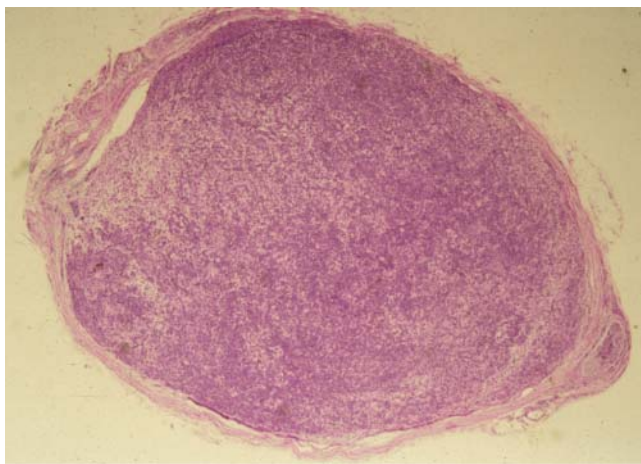


Fig. 22.21.2-5. Malignant peripheral nerve sheath tumor (MPNST). Whole mount of the malignant tumor.

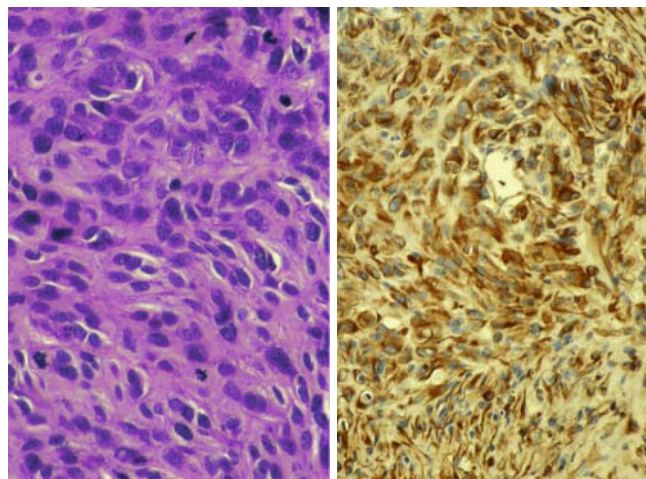


Fig. 22.21.2-6. MPNST. *Left.* H&E. *Right.* Immunohistochemistry for S100.

22.22 Familial Tumor Syndromes Involving the Nervous System

There are some tumors of the nervous system that have been identified in families who have a constellation of lesions and abnormal genes [25]. Some of these syndromes have been described elsewhere in this book. They are repeated here to emphasize these associations so genetic counseling can be considered in appropriate cases.

Neurofibromatosis 1. The gene is *NF1*. There are skin lesions with café au lait spots and axillary freckling. There may be hamartomas of the iris, bone lesions, pheochromocytomas, and leukemia. The nervous system tumors are neurofibromas, MPNST, optic nerve gliomas and astrocytomas. (see Sections 22.3 and 22.21)

Neurofibromatosis 2. The gene is *NF2*. There may be retinal hamartomas and lens opacities. The nervous system tumors are bilateral VII schwannomas, peripheral schwannomas, meningiomas, meningioangiomatosis, spinal ependymomas, astrocytomas, and glial hamartias (see Section 22.21).

Von Hippel-Lindau. The gene is *VHL*. There may be retinal hemangioblastomas, renal cell carcinomas, pheochromocytomas. The nervous system tumor is the hemangioblastoma.

Tuberous sclerosis. There are two genes, *TSC1* and *TSC2*. The skin lesions are angiofibromas and sub-

ungual fibromas. The somatic lesions include cardiac rhabdomyomas, polyps of small bowel, cysts of lungs and kidneys, and renal angiomyolipomas. The brain tumors are subependymal giant cell astrocytomas and cortical tubers (see Chapter 7, Section 7.1 and Section 22.1).

Li-Fraumeni syndrome. The gene is *TP53*. The somatic lesions are breast cancer, sarcoma, adrenocortical carcinoma, and leukemia. The brain tumors are PNET and astrocytomas.

Cowden syndrome. The gene is *PTEN*. The somatic lesions are colonic polyps and thyroid neoplasms. Brain findings include the dysplastic gangliocytoma (Lhermitte-Duclos) and megalencephaly.

Turcot syndrome. There are several genes involved. With an abnormality of *APC* there are colorectal polyps and medulloblastoma. With abnormalities of *hMLH1* and *hPSM2* there are café au lait spots and colorectal polyps. The brain tumor is glioblastoma multiforme.

Nevoid basal cell carcinoma syndrome (Gorlin). The gene is *PTCH*. The skin lesions are basal cell carcinomas and palmar and planter pits. The somatic lesions are cysts of the jaw, ovarian fibromas and skeletal abnormalities. The brain lesion is the medulloblastoma.

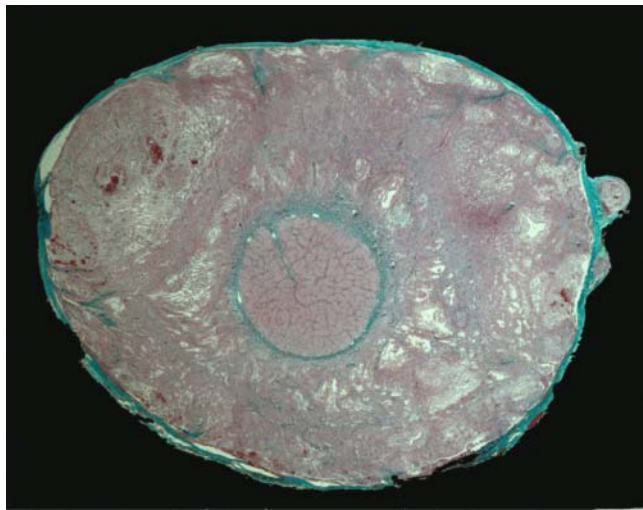


Fig. 22.22-1. Optic nerve glioma. Whole mount showing circumferential growth of the tumor in the subarachnoid space around the optic nerve. Trichrome.

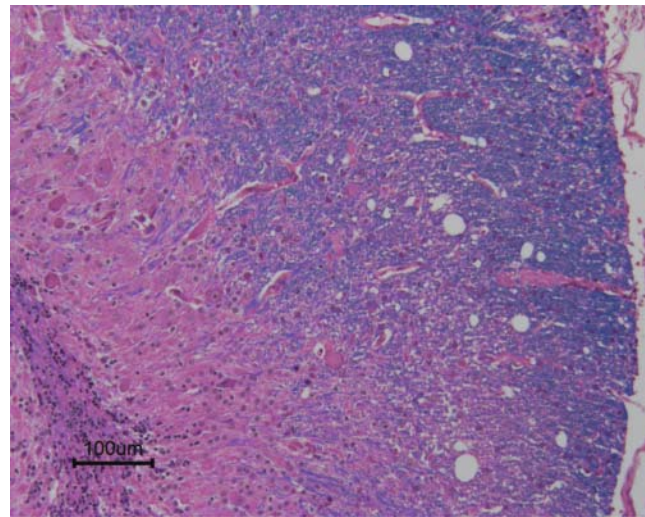


Fig. 22.22-2. Dysplastic gangliocytoma (Lhermitte-Duclos). Microscopy shows disorganization of the internal granular layer, which contains large ganglion cells, an absence of Purkinje cells, and enlargement of the molecular layer. H&E/LFB.

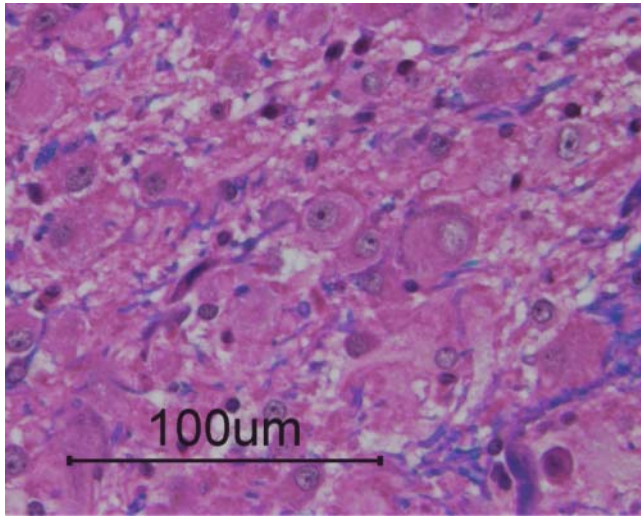


Fig. 22.22-3. Higher magnification of the case in 22.22-2. Dysplastic gangliocytoma (Lhermitte-Duclos).

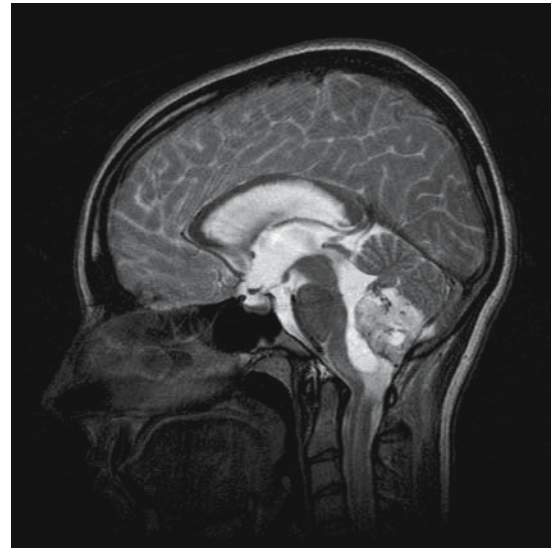


Fig. 22.22-4. Hemangioblastoma. T2-weighted fast spin echo MRI shows a large tumor in the inferior vermis.



Fig. 22.22-5. Hemangioblastoma. Gross specimen of the cerebellum shows a discrete mural nodule and adjacent cyst.

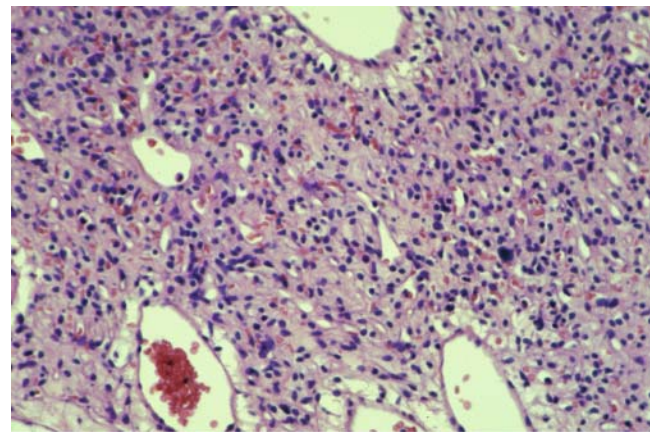


Fig. 22.22-6. Hemangioblastoma. Histology shows the stromal cells and vascularity associated with this tumor. H&E.

23 Motor Neuron Disease

23.1 Spinal Muscular Atrophy (Werdnig-Hoffmann Disease)

The most common childhood forms of spinal muscular atrophy (SMA) are early-onset severe type 1 SMA (*Werdnig-Hoffmann disease*), chronic intermediate type 2 SMA, and chronic mild type 3 SMA (*Kugelberg-Welander disease*). Werdnig-Hoffmann disease (WHD) is an autosomal recessive, early-infantile form of spinal and bulbar muscular atrophy, sparing only the extraocular muscles. In late-infantile forms of SMA, the onset is between 3 and 24 months of age. The juvenile form of SMA (Kugelberg-Welander syndrome) has its onset between 2 and 10 years, or adolescence.

Muscle biopsy from WHD shows group atrophy of many small, rounded muscle fibers, variable intermixture of normal-sized fibers in some fascicles, and the presence of hypertrophied fibers three to four times the normal size for the patient's age. Histochemically, the smallest caliber fibers are a mixture of type 1 and type 2 fibers.

Pathology

The spinal cord shows atrophy of the anterior spinal nerve roots. The primary pathological abnormality is progressive degeneration of the anterior horn cells of

the spinal cord, which exhibit various stages of degeneration, such as chromatolysis and neuronophagia. Sparing of the phrenic motoneurons and nucleus of Onuf in the anterior horn correlates with clinical symptoms in that diaphragmatic movement and sphincter functions are usually not affected. In the brain stem, the nucleus of cranial nerve XII is most commonly and severely affected. The same changes are usually seen in the motor nuclei of cranial nerves V, VI, VII, IX, X, and XI. The brain stem is relatively spared in Kugelberg-Welander syndrome. In unusual variants of WHD, there is prominent involvement of areas outside the lower motor neuron territory, including, in decreasing frequency, the dorsal root ganglion, posteroventral nuclei of the thalamus, and cerebellum [1].

Genetics

Spinal muscular atrophy is caused by a deficiency of the ubiquitous protein (survival of motor neuron, SMN) whose genes *SMN1* and *SMN2* are mainly on chromosome 5q11.3-13.3. At least three SMA-related genes have been identified: *SMN*, *NAIP*, and *p44*.

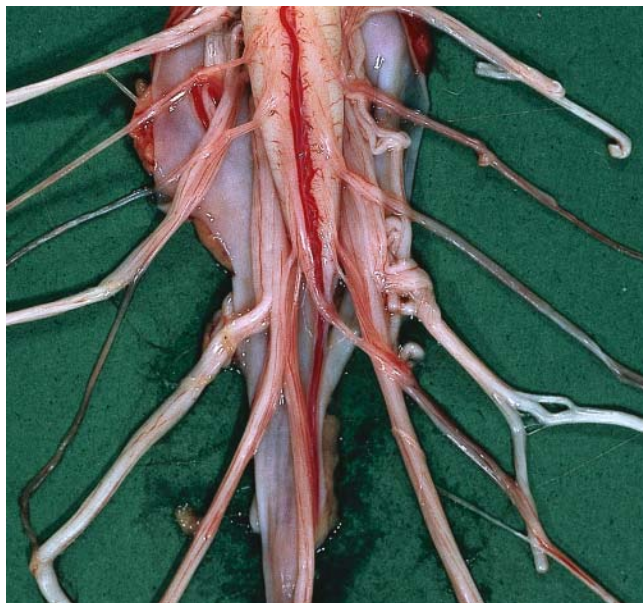


Fig. 23.1-1. Werdnig-Hoffmann disease. Macroscopically, the spinal cord exhibits marked atrophy of the anterior roots.



Fig. 23.1-2. The anterior roots of the spinal cord are markedly atrophic and lack myelination. KB stain.

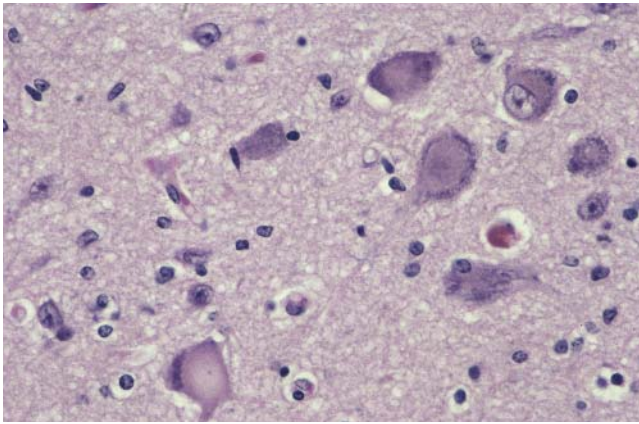


Fig. 23.1-3. Anterior horn cells show central chromatolysis.

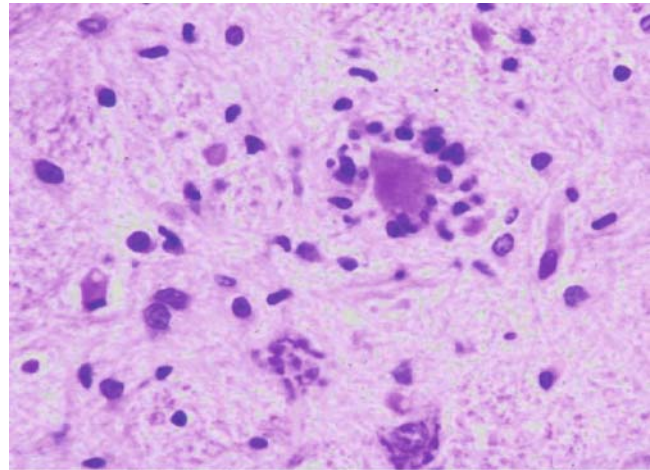


Fig. 23.1-4. Neuronophagia of anterior horn cells. H&E.

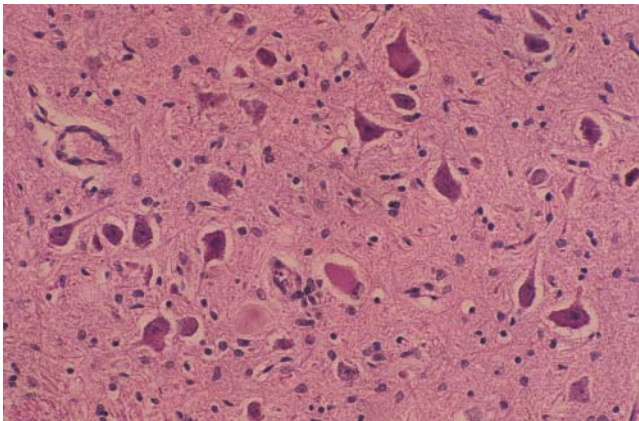


Fig. 23.1-5. Oculomotor nucleus shows central chromatolysis. H&E.

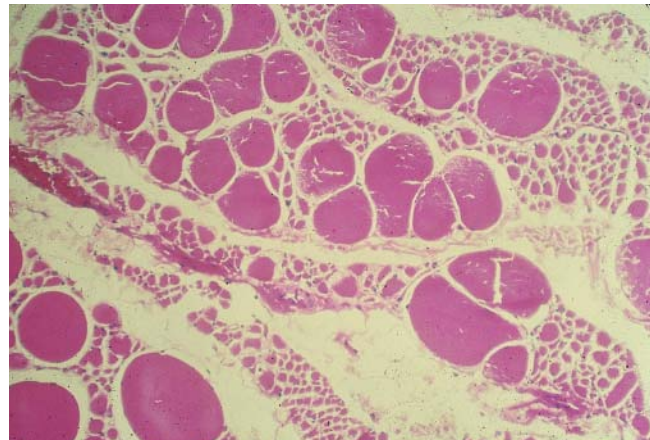


Fig. 23.1-6. Muscle shows group atrophy. H&E.

24 Peripheral Neuropathy

24.1 Peripheral Neuropathy Diseases

The primary diseases of the peripheral nervous system are clinically classified as sensorimotor neuropathies and motor or sensory neuropathies. They present with some of the following signs and symptoms: weakness, sensory loss, muscle atrophy, autonomic dysfunction. The disorders may present as symmetrical polyneuropathies (usually hereditary disorders) or as focal and multifocal neuropathies (usually diabetes, arteritis, trauma). In children and adolescents, the hereditary disorders are the commonest causes of peripheral nerve disease. In some cases the peripheral neuropathy is a part of a multisystem disorder, involving other parts of the nervous system and/or body, whereas with other disorders the peripheral nerve is the main site of the disease.

Pathology

The pathology may be related to segmental demyelination, sometimes with remyelination and onion bulb

formation (associated with decreased nerve conduction velocity) or to primary neuroaxonal degeneration (with loss of nerve fibers). Frequently there is a mixture of these pathologies. In patients with sensorimotor and motor polyneuropathies the differential diagnosis includes hereditary sensorimotor neuropathies, diseases of the anterior horn cells (spinal muscle atrophies), leukodystrophies (metachromatic leukodystrophy and Krabbe's disease), and Refsum's disease. For the disorders with predominant sensory and autonomic symptoms, the differential diagnosis includes the hereditary sensory and autonomic neuropathies, Fabry's disease, and Friedreich's ataxia [1].

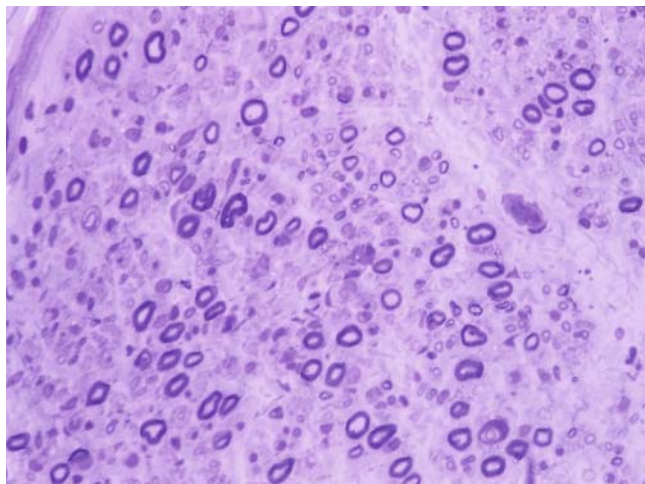


Fig. 24.1-1. Peripheral nerves. Electron microscopy (EM) of a normal nerve shows a good complement of large and small myelinated axons interspersed with groups of nonmyelinated axons.

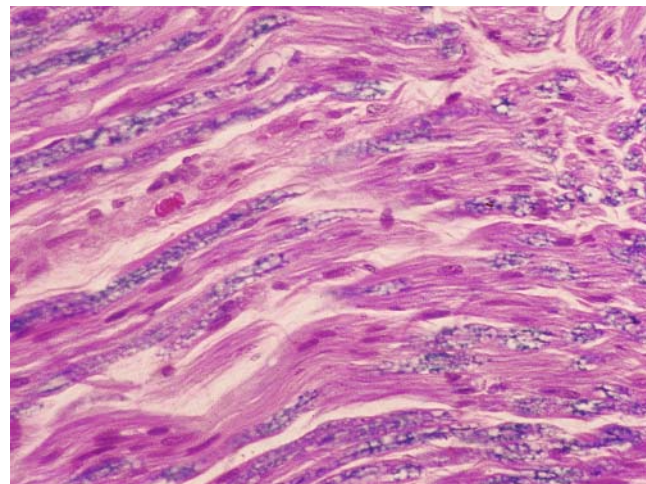


Fig. 24.1-2. Abnormal nerve biopsy. Paraffin preparation of a longitudinal section stained with LFB/H&E shows a severe loss of myelin.

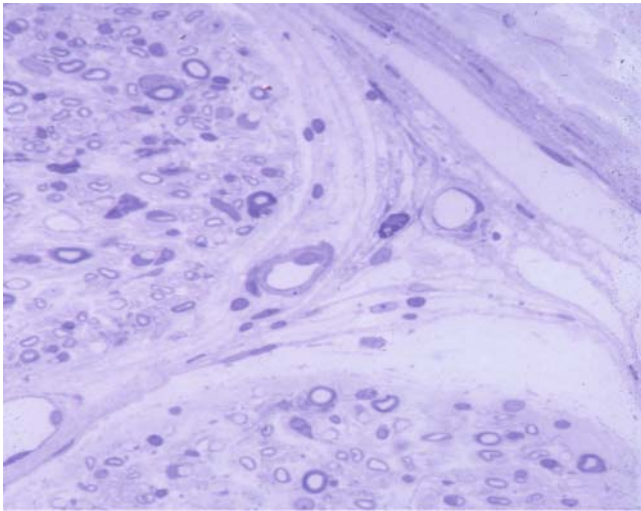


Fig. 24.1-3. Abnormal nerve biopsy. Thick section shows a reduction in the number of large myelinated axons.



Fig. 24.1-4. Teased fiber preparation shows several unmyelinated axons and the central axon with a short internode of hypomyelination suggesting remyelination.



Fig. 24.1-5. EM shows a normal axon with a Schwann cell nucleus situated above a second axon exhibiting remyelination. The axon is the same diameter as the normal one above but has reduced thickness of myelin.

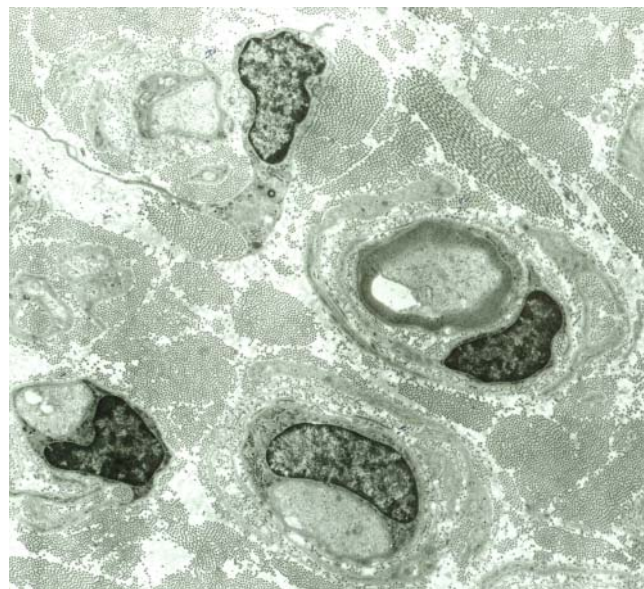


Fig. 24.1-6. EM shows remyelinating axons surrounded by Schwann cell cytoplasm, which forms "onion bulbs."

24.2 Hereditary Motor and Sensory Neuropathies (Charcot-Marie-Tooth Disease)

Charcot-Marie-Tooth disease (CMT) is the commonest Mendelian disorder of the peripheral nervous system, with a prevalence of 1:2500. It constitutes a group of clinically similar but genetically heterogeneous disorders that occur sporadically or with autosomal dominant, autosomal recessive, or X-linked inheritance. The pathology is either myelinopathy (previously named CMT1) or axonopathy (previously named CMT2). There are now four recognized disorders associated with demyelination: early-onset CMT, previously named Dejerine-Sottas syndrome (DSS); congenital disorder of myelin formation, or congenital hypomyelinating neuropathy (CHN); hereditary neuropathy with liability to pressure palsy (HNPP); and, the most common, CMT1. Genetic analyses of the various presentations of CMT have identified numerous genes that are associated with

demyelination: peripheral myelin protein 22 (*PMP22*), myelin protein zero (*MPZ*), early response gene 2 (*EGR2*), myotubularin-related protein 2 (*MTMR2*), connexin (*GJB1*).

CMT2 is an axonopathy. In the dominantly inherited form, several genes including *MPZ* and neurofilament light gene (*NF-L*) have been found to be abnormal. The X-linked dominant disorder of CMT2 has a mutation in the *GJB1* gene.

There are complex forms of CMT in which other disease symptoms are associated. One is CMT with tremor, also known as Roussy-Levy syndrome, which is associated with a mutation of the *MPZ* gene and duplication of *PMP22* as well as point mutations in *GJB1* [2].

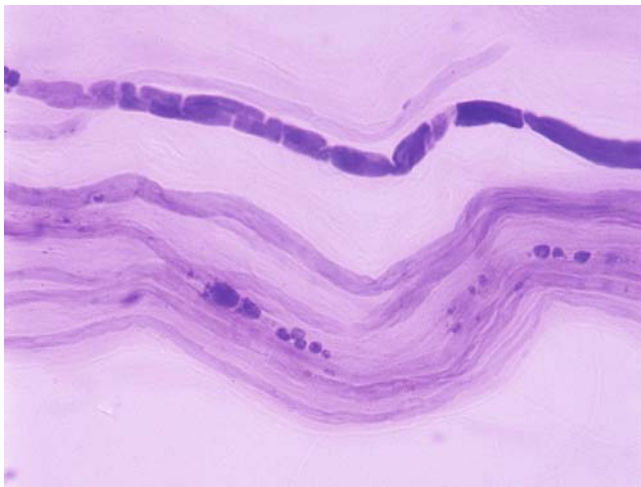


Fig. 24.2-1. Abnormal peripheral nerve, teased fiber preparation showing several axons without myelin and two axons showing Wallerian degeneration.

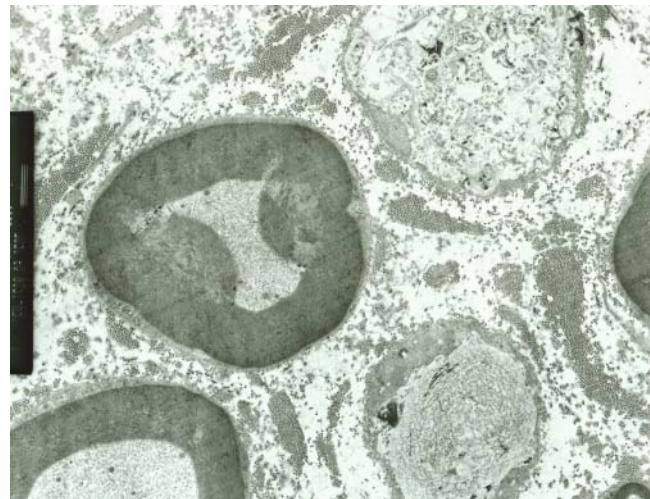


Fig. 24.2-2. Abnormal peripheral nerve, axonopathy. Electron microscopy (EM) shows two axons undergoing degeneration.

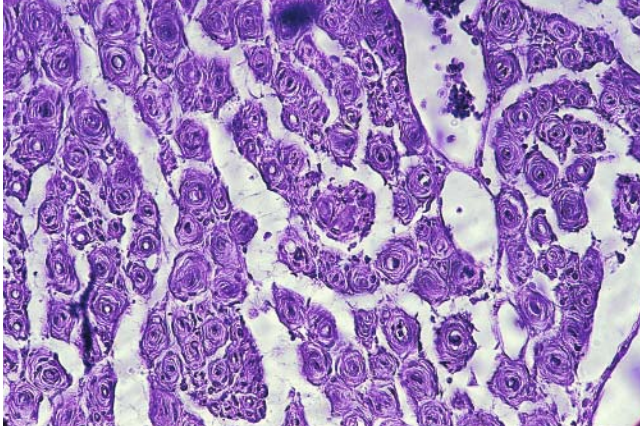


Fig. 24.2-3. Peripheral nerve in Dejerine-Sottas disease. There are increased number of Schwann cells in onion bulb fashion around axons (hypertrophic neuropathy).

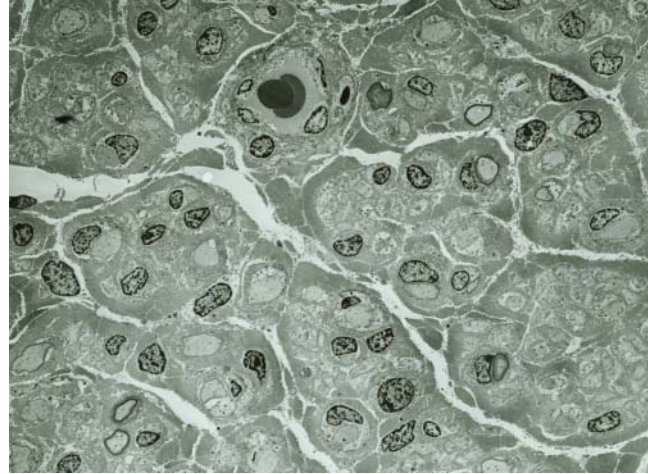


Fig. 24.2-4. Peripheral nerve in congenital hypomyelinating neuropathy. Note the presence of many axons without myelin.

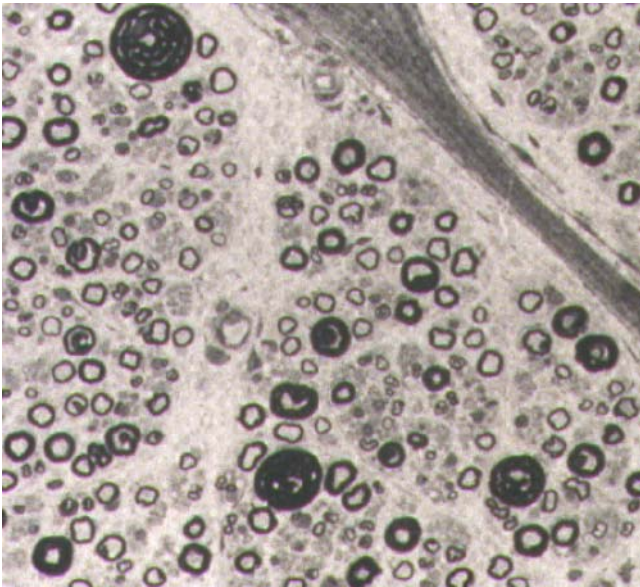


Fig. 24.2-5. Abnormal peripheral nerve in hereditary neuropathy with a liability to pressure palsy (HNPP). Note several enlarged nerves fibers which exhibit tonacula.

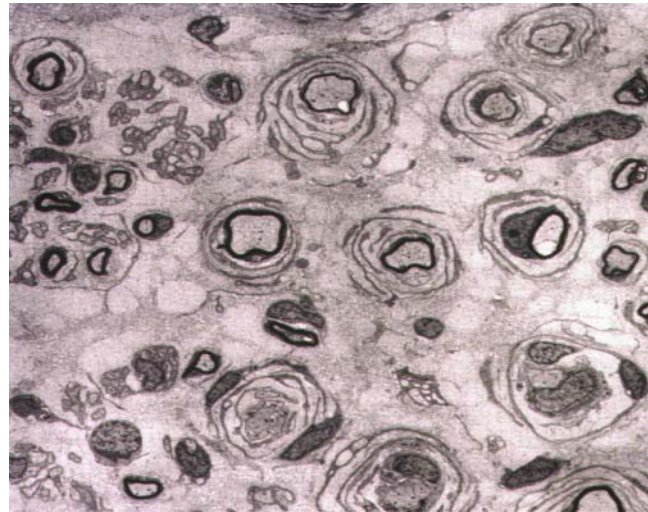


Fig. 24.2-6. Peripheral nerve in Dejerine-Sottas syndrome. Note the large number of "onion bulbs" producing the hypertrophic neuropathy.

24.3 Hereditary Sensory and Autonomic Neuropathies

Hereditary sensory and autonomic neuropathies (HSANs) II–V are autosomal recessive conditions that begin at birth and are nonprogressive.

- HSAN II has an absence of myelinated fibers and decreased numbers of unmyelinated fibers.
- HSAN III (Riley-Day syndrome) has a normal density of myelinated fibers, decreased number of unmyelinated fibers, and decreased neurons in the autonomic and spinal ganglia.

- HSAN IV has normal myelinated fibers, an absence of unmyelinated fibers, and an absence of small neurons in the spinal ganglia.
- HSAN V has a decrease of both small myelinated fibers and unmyelinated fibers.

It is apparent that the diagnosis of the inherited neuropathies is complex, requiring a careful examination, history, including family history, electrical studies, and DNA analysis. In some cases nerve biopsy provides useful information [2].

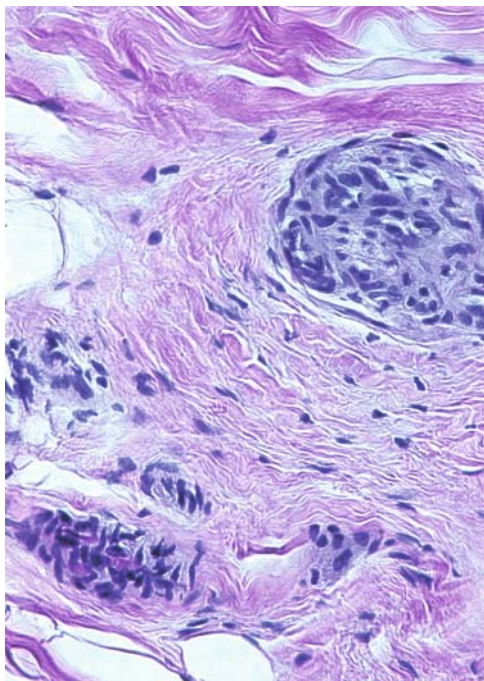


Fig. 24.3-1. Peripheral nerve biopsy in vasculitis. There are several small vessels with inflammatory cells in the walls. During this healing phase there is endothelial proliferation, with a reduction in the diameter of the lumen.

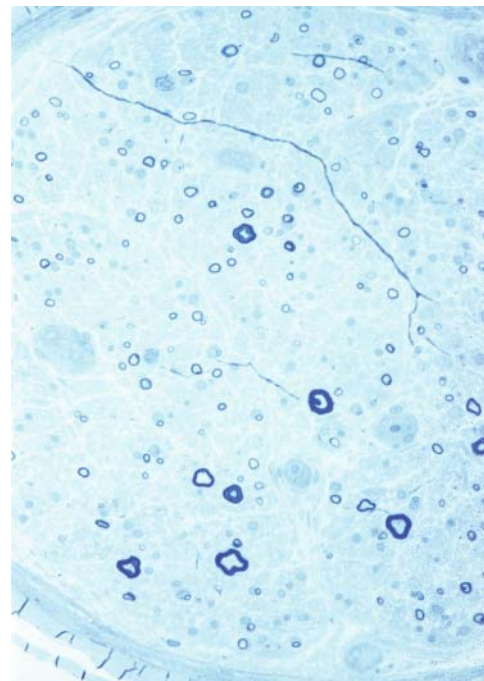


Fig. 24.3-2. Peripheral nerve biopsy in vasculitis. Thick section shows a marked reduction in the number of axons.

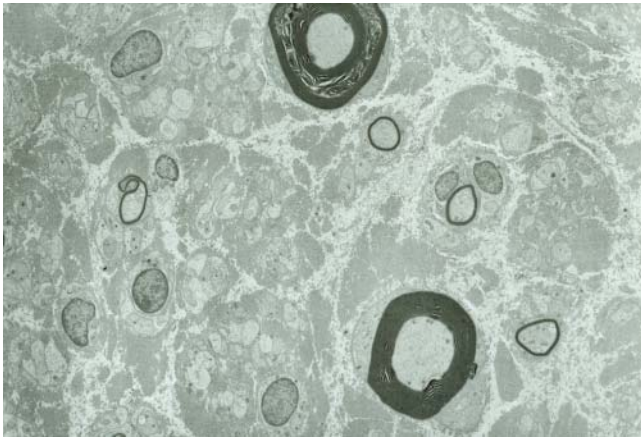


Fig. 24.3-3. Peripheral nerve biopsy in vasculitis. EM shows a marked reduction in the number of axons.

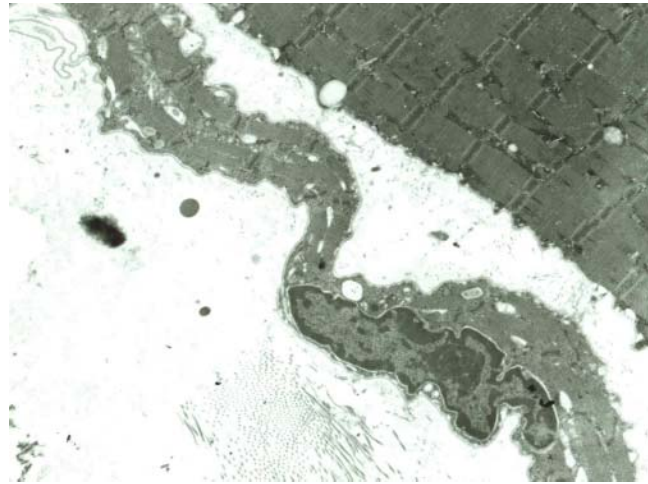


Fig. 24.3-4. Muscle biopsy. EM shows atrophy of one muscle fiber caused by denervation. Note the decreased diameter of the fiber and the redundant basement membrane.



Fig. 24.3-5. Arm of a child with median nerve injury.

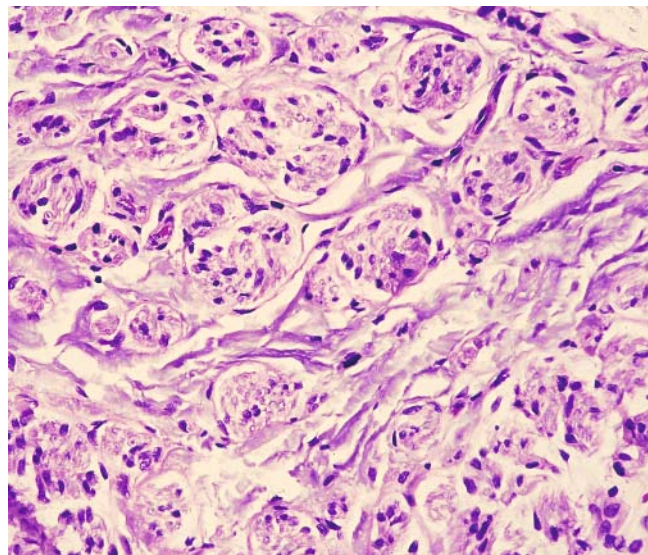


Fig. 24.3-6. Peripheral nerve biopsy following trauma shows a "traumatic neuroma." Small groups of axons are surrounded by collagenous scar tissue.

25 Muscle Disease

Table 25.1. Classification of childhood muscle disease

Muscular dystrophy
Duchenne/Becker muscular dystrophy (dystrophinopathy)
Facioscapulohumeral dystrophy (telomeric deletion disease)
Limb-girdle dystrophy (sarcoglycanopathy)
Emery-Dreifuss dystrophy (defective nuclear membrane proteins)
Congenital muscular dystrophies
Fukuyama congenital muscular dystrophy
Merosin deficiency (mutations in merosin $\alpha 7$ integrin)
Myotonic dystrophy (repeat expansion disorders)
Congenital myotonic dystrophy
Congenital myopathies
Nemaline (rod) myopathy
Centronuclear and myotubular myopathy
Central core disease
Congenital fiber type disproportion
Desminopathies
Metabolic myopathies
Glycogen storage disease
Lipid disorders
Mitochondrial myopathies
Inflammatory myopathies
Infective myositis
Dermatomyositis syndrome
Polymyositis
Disorders of muscle membranes (channelopathies)
Myotonia congenita
Periodic paralysis
Paramyotonia congenita
Diseases of neuromuscular junction
Congenital myasthenic syndromes
Myasthenia gravis
Neurogenic atrophies

25.1 Muscle Development

Skeletal muscle begins to develop in the mesodermic somites at 2–3 weeks' gestation. At 4–5 gestational weeks (GW), the myotomes develop as a syncytium of nuclei and cytoplasm. At 7–9 GW, the syncytium elongates, and cells fuse and form the primitive myotubes. These are multinucleated cells with nuclei situated centrally in a hollow tube of thin cytoplasm. This process continues, with the newest myotubes being the smallest. Actin and myosin filaments develop and form myofibrils in the myotubes. At 10 GW, the embryonic muscle is well formed into myotubes. The muscle fibers are larger, and striations are evident. At 12 GW, motor end

plates and muscle spindles are developing. At 13 GW, the myofibrils become thicker in the older fibers, and new smaller myotubes continue to develop. At 15 GW, two populations of muscle fibers are present: (1) large, more mature fibers with peripheral nuclei and filled-in cytoplasm and (2) smaller, more immature myotubes. After 16 GW, all of the muscle fibers continue to increase in size, and the myotubes gradually disappear. However, the pattern of large and small muscle fibers persists into the postnatal period and into the second year of life. The large fibers have been called Wohlfart B and the smaller fibers Wohlfart A [1].

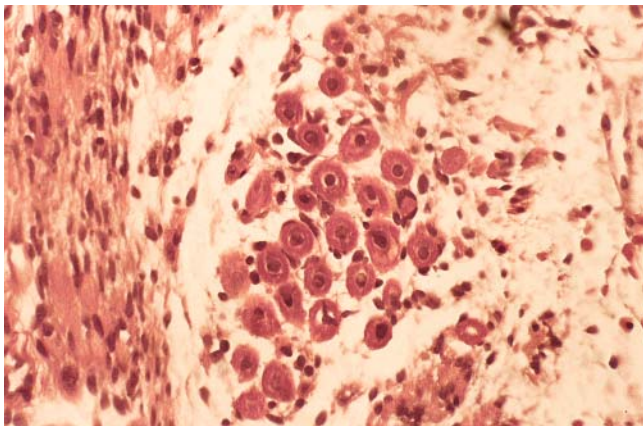


Fig. 25.1-1. Developing muscle. At 8 GW. Note myotubes with central nuclei. H&E.

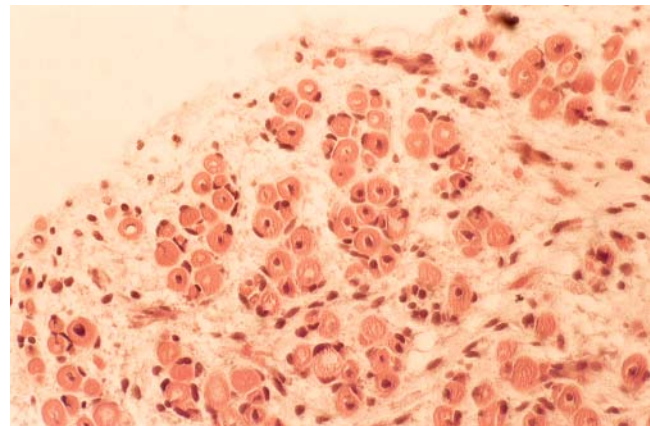


Fig. 25.1-2. At 11 GW. Some fibers have peripheral nuclei. H&E.

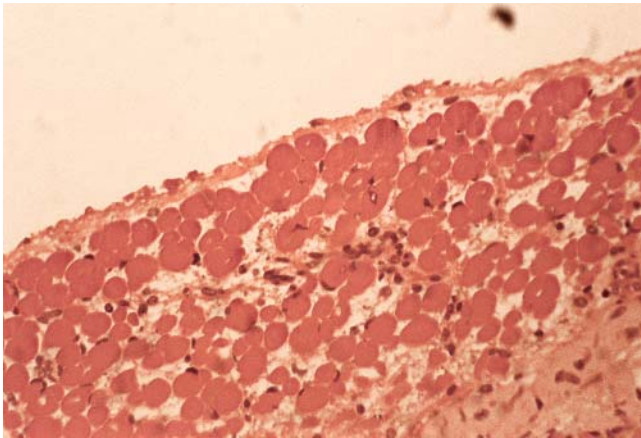


Fig. 25.1-3. At 15 GW. Note the Wohlfart B (large) and Wohlfart A (small) fibers. H&E.

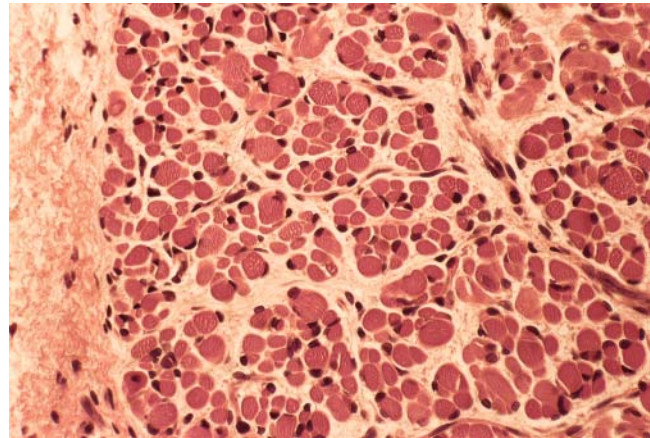


Fig. 25.1-4. At 20 GW. Note that most fibers have peripheral nuclei. H&E.

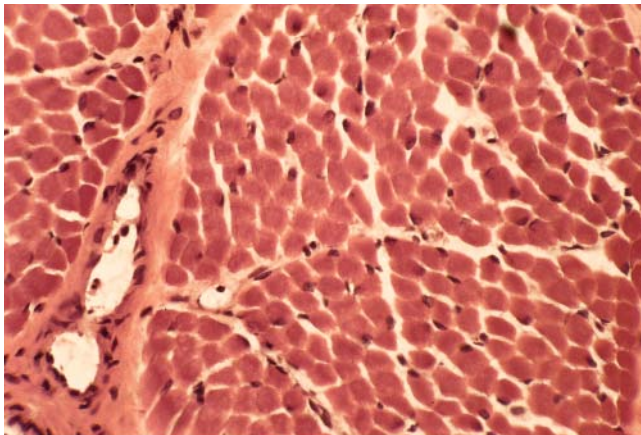


Fig. 25.1-5. At 40 GW. Fibers are generally uniform with isolated larger fibers. H&E.

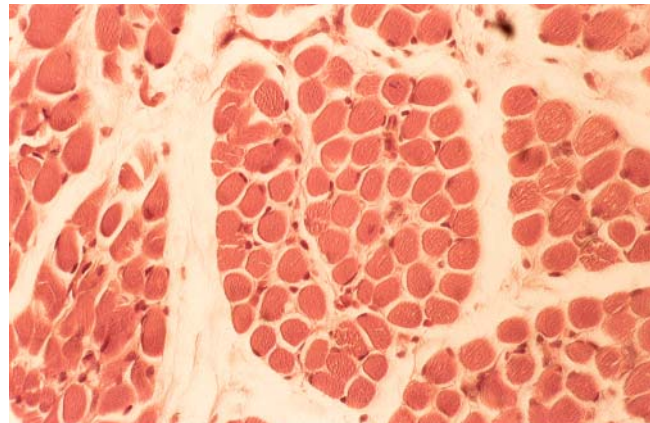


Fig. 25.1-6. At 4 months of age. H&E.

25.2 Classification of Muscle Disease: Normal Muscle Structure

Previous classification of muscle disease was based on the histological or histochemical appearance of the muscle. The types of muscle disorder, based on morphology, were the dystrophies and the congenital, inflammatory, and metabolic myopathies. In the *muscular dystrophies* the muscle fibers exhibit a loss of structural integrity; there is a variation in fiber size, a central location of nuclei, a breakdown of fibers, regeneration of fibers, and fibrosis. In the *congenital myopathies* the muscle fibers appear to be malformed. There may be central cores of irregularity, central nuclei, or abnormal structures of Z bands. In the *inflammatory myopathies* there is invasion and destruction of muscle by an inflammatory process. In the *metabolic myopathies* there are abnormalities in the staining characteristics of muscle mitochondria, lipid, or glycogen (Table 25.1).

In this molecular era of myopathology, gene defects have been shown to produce defects in muscle proteins that account for structural changes in the muscle cell or for its dysfunction, damage, or death. This identification of previously unknown muscle proteins has provided immunocytochemical tools for the identification of

structural deficiencies that are not otherwise apparent. This new approach to myology has allowed muscle diseases to be classified according to an etiology that may be genetic or related to abnormal immune regulation, or it may be related to an exogenous toxin or drug [2].

The muscle biopsy specimen is usually taken from a limb muscle. The extrinsic muscle fibers are round, uniform in size, with peripheral nuclei and no obvious interstitial collagen. The muscle fibers with their associated capillaries are arranged into fascicles separated by collagenous septa that contain nerves, larger vessels, and muscle spindles and terminate as tendons. Near the tendons where muscle fibers are generated, there is variation in fiber size and internal nuclei. The diameter of the limb muscle fibers is 15–20 μm at birth and increases by 2 μm per year until reaching adult size (50–60 μm). The intrinsic muscles of the muscle spindle are smaller and are intimately related to specialized nuclear bag or flower spray nerve endings. Biopsies in very young patients require expert surgeons and knowledge of the normal changes in developing muscle [1].

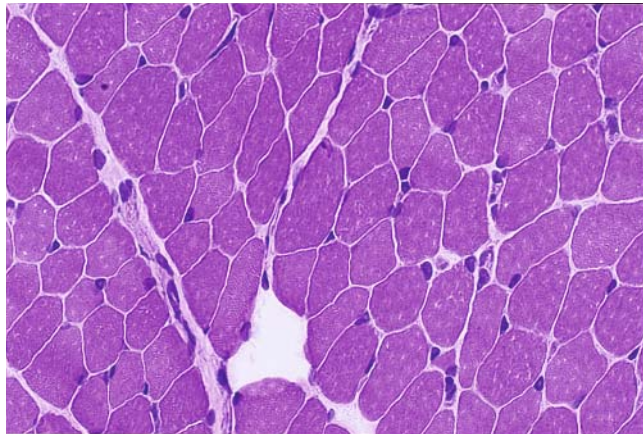


Fig. 25.2-1. Normal muscle. Uniform fiber size, peripheral nuclei, normal connective tissue and vessels, no inflammation. H&E.

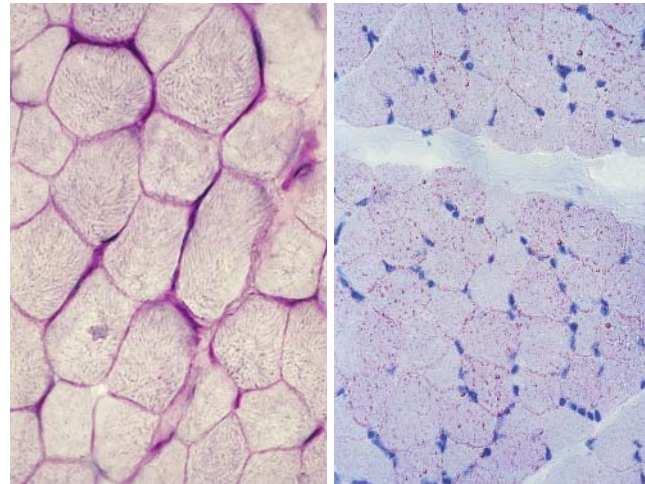


Fig. 25.2-2. *Left.* PAS. Note the even staining in all fibers. *Right.* Sudan black-B. Type I fibers have stronger staining.

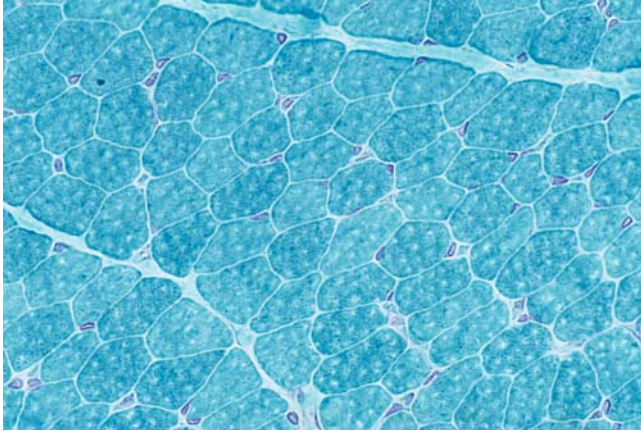


Fig. 25.2-3. Modified Gomori trichrome stain. Mitochondria are red, as are the nuclei.

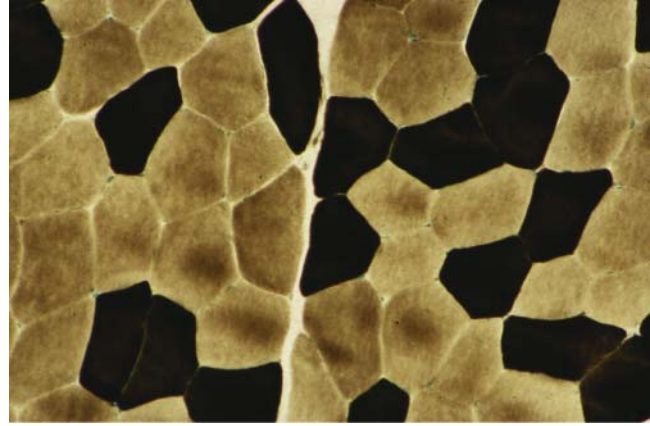


Fig. 25.2-4. ATPase reaction at pH 4. Type I and II fibers are arranged in a checkerboard distribution.

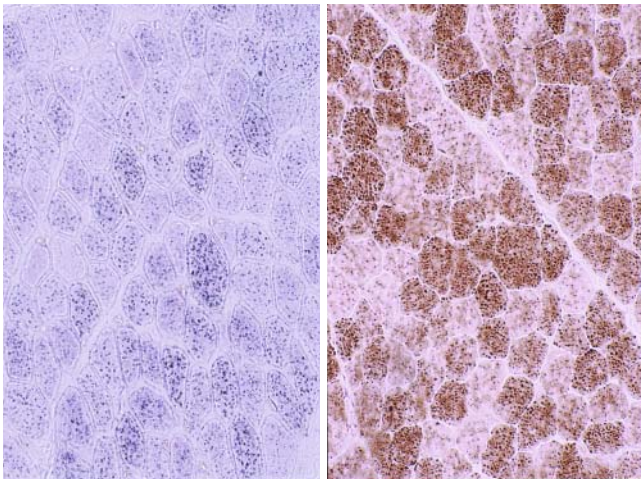


Fig. 25.2-5. *Left.* Succinate dehydrogenase (SDH). The intensity is higher for type I than for type II fibers. *Right.* NADH (NADH-tetrazolium reductase). The intensity is higher for type I than for type II fibers.

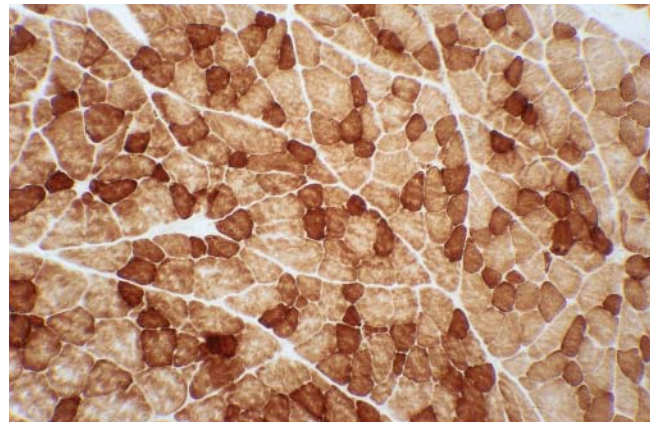


Fig. 25.2-6. Cytochrome c oxidase (COX). The intensity is higher for type I than for type II fibers. This reaction is negative in fibers with cytochrome c oxidase deficiency.

25.3 Progressive Muscular Dystrophy

Many of the previously recognized “muscular dystrophies” have been shown to have abnormalities on the surface of the muscle fiber, the sarcolemma, which is composed of the basal lamina and the plasma membrane. The basal lamina is part of the extracellular matrix, providing a mechanical connection between the muscle and the endomysial connective tissue. Some of its proteins—merosin, perlecan, integrin—may be altered in muscle disease: The plasma membrane is the boundary between the intracellular and extracellular compartments and is critically related to the endoplasmic reticulum of the fiber. The plasma membrane contains ion channels and receptors and is the source of the T tubules. Some of the plasmalemmal proteins that may be altered in disease include dystrophin, sarcoglycans, dysferlin, and caveolin [3,4].

Duchenne muscular dystrophy with dystrophin deficiency has the most severe dystrophic changes, with variation in fiber size, central nuclei, muscle fiber breakdown, fiber hypertrophy with characteristic eosinophilic staining of cytoplasm, basophilic changes in regenerating fibers, endomysial fibrosis, loss of muscle fibers with fatty replacement, and some inflammation.

Becker’s muscular dystrophy with minimal dystrophin deficiency produces less degeneration and fibrosis than Duchenne dystrophy. Regeneration is prominent.

α -*Sarcoglycan deficiency* produces dystrophic changes in the muscle that resemble those of the dystrophinopathies. The severity of the muscle fiber degeneration is related to the type of mutation in the gene [4].

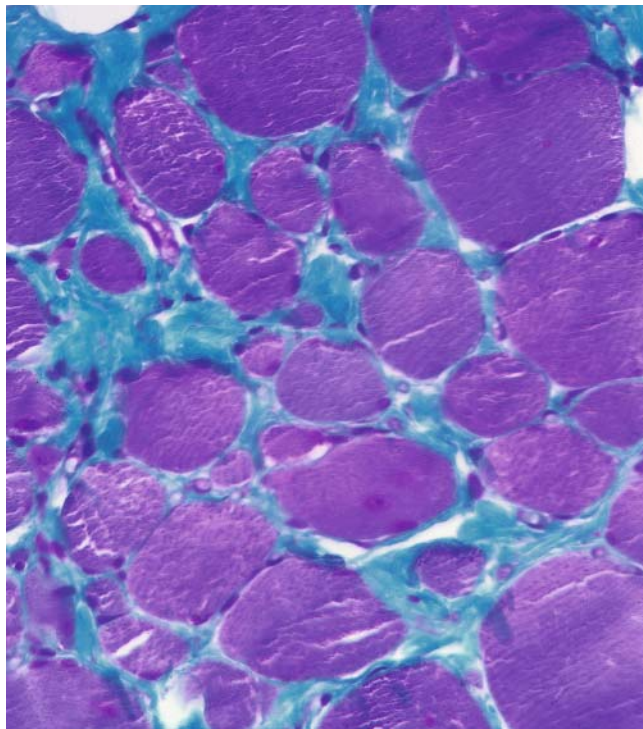


Fig. 25.3-1. Duchenne muscular dystrophy with variation in fiber size, internal nuclei, and endomysial fibrosis. Masson trichrome.

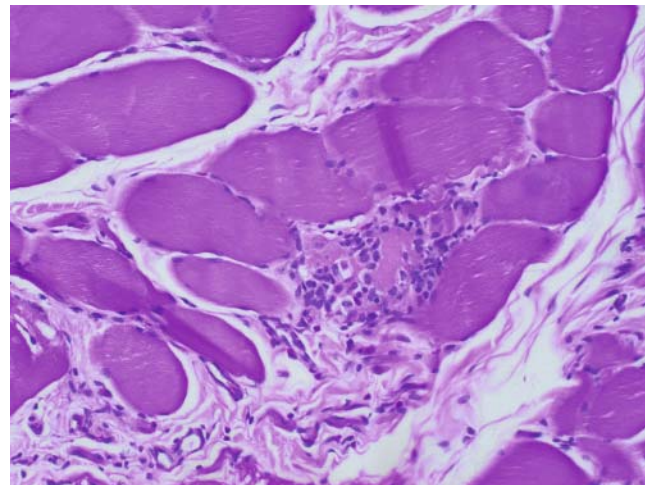


Fig. 25.3-2. Duchenne muscular dystrophy with fiber degeneration and cellular response by myoblasts and lymphocytes. H&E.

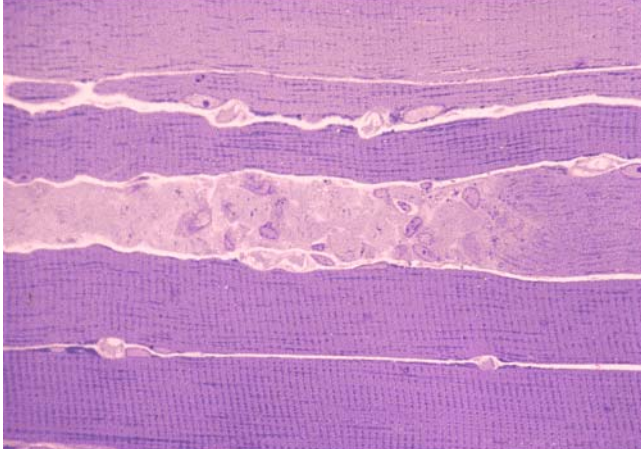


Fig. 25.3-3. Duchenne muscular dystrophy illustrating segmental breakdown of muscle fibers. H&E.

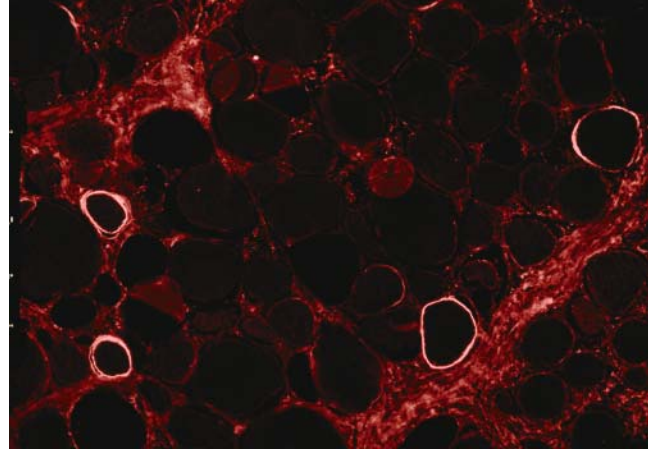


Fig. 25.3-4. Becker's muscular dystrophy with partial loss of dystrophin staining.

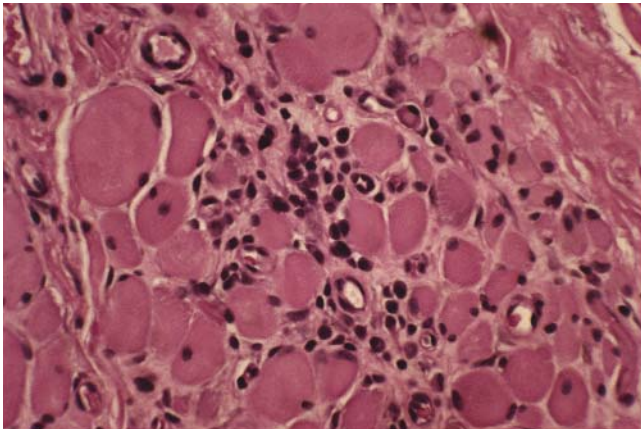


Fig. 25.3-5. α -Sarcoglycan deficiency showing variation fiber size, internal nuclei, fiber degeneration and regeneration, and slight endomysial fibrosis. H&E.

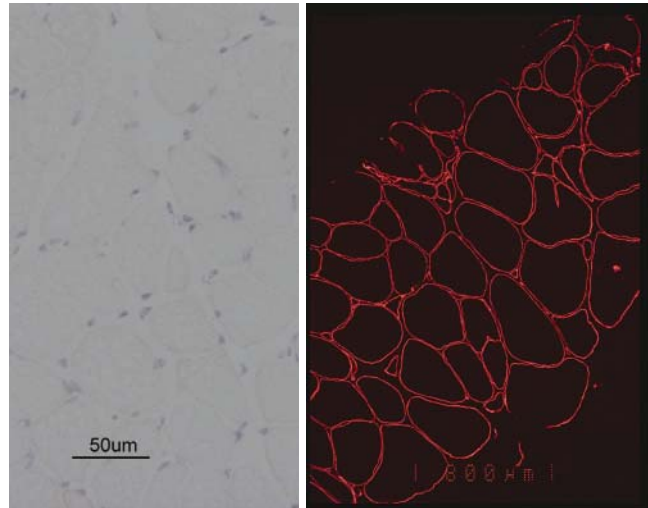


Fig. 25.3-6. Muscle immunohistochemistry reveals complete absence for adhalin, a dystrophin associated glycoprotein. This results from mutation in the sarcoglycan complex. (*left*). *Right*. Normal muscle with anti-adhalin antibody.

25.4 Congenital and Other Muscular Dystrophies (Merosin Deficiency, Fukuyama Congenital Muscular Dystrophy)

Fukuyama Congenital Muscular Dystrophy. See Chapter 2, Section 2.14.

Merosin deficiency (laminin $\alpha 2$) is a congenital dystrophy with absence of merosin in the basal lamina. There is an associated white matter abnormality. Complete absence of merosin leads to infant fatality [5].

Sarcoglycan deficiency causes dystrophic change in muscle. The sarcoglycans are four integral membrane proteins that are directly associated with the dystroglycans and indirectly with dystrophin.

Fascioscapular humeral dystrophy is an autosomal dominant dystrophy with deletion of 3.3-kb D4Z4 repeat units in the subtelomeric region of chromosome 4q. The weakness begins in the shoulders and spreads. There may be cardiac conduction blocks, deafness, scoliosis, and retinal vasculopathy [6].

Congenital myotonic dystrophy is a dominantly inherited disease of muscle, heart, brain, and lens. There are three forms of myotonic dystrophy: a congenital form, a classic form, and a minimal phenotype form [7].

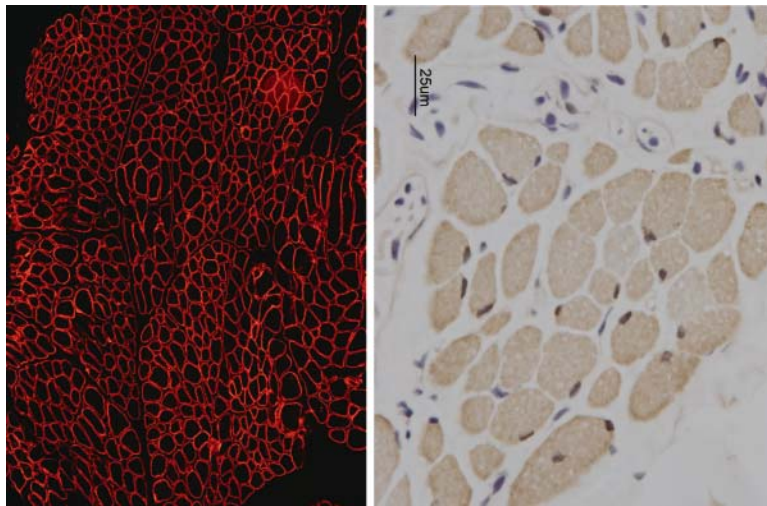


Fig. 25.4-1. Merosin immunohistochemistry in normal muscle (*left*) and merosin deficiency (*right*).

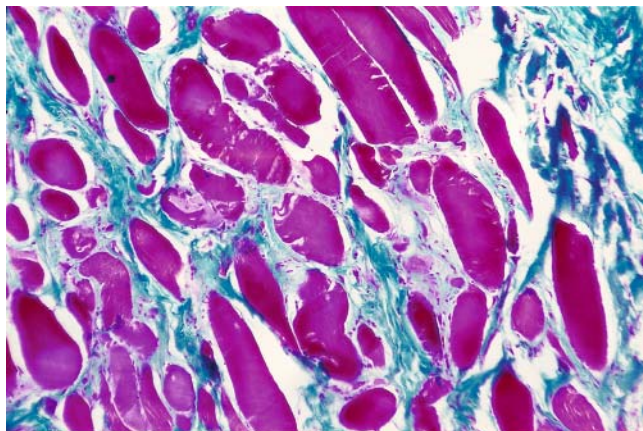


Fig. 25.4-2. Merosin deficiency: muscle shows interstitial fibrosis, Masson trichrome stain.

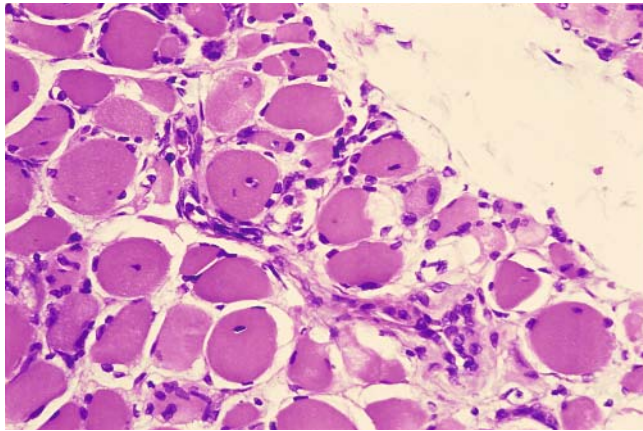


Fig. 25.4-3. Merosin deficiency (laminin $\alpha 2$) is a congenital muscular dystrophy with inflammation and white matter disease. H&E.

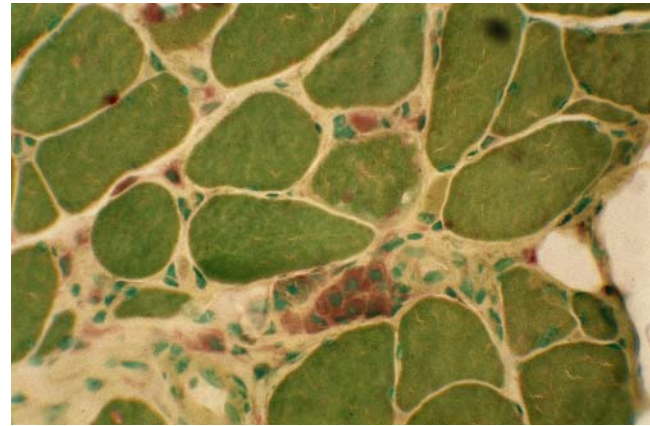


Fig. 25.4-4. Fascioscapular humeral dystrophy shows degeneration and regeneration of fibers, some inflammation, and some angular fibers. Masson trichrome.

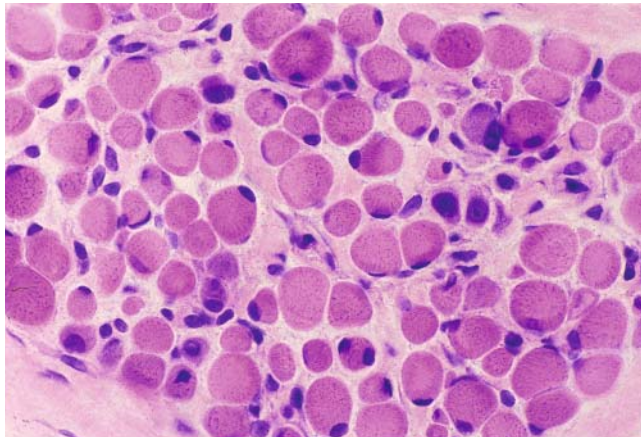


Fig. 25.4-5. Fukuyama congenital muscular dystrophy with mild variation in fiber size, degeneration, and regeneration in a neonate. H&E.

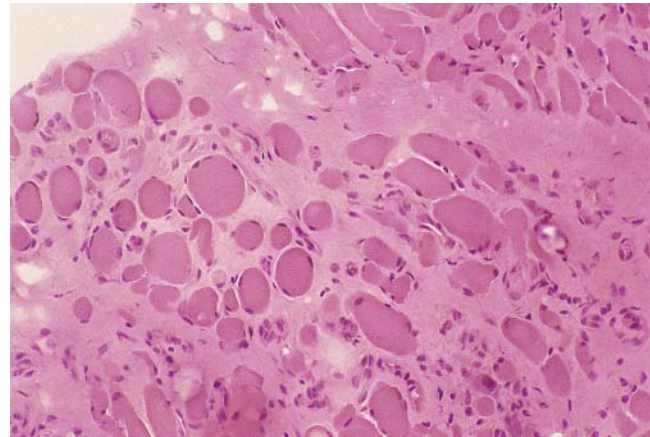


Fig. 25.4-6. Fukuyama congenital muscular dystrophy with severe variation in fiber size, degeneration, and fibrosis in a child. H&E.

25.5 Congenital Myotonic Dystrophy and Late-Onset Myotonic Dystrophy

Myotonic dystrophy is a multisystem syndrome involving brain, muscle, heart, and lens and includes myotonic dystrophy type 1 (DM1), type 2 (DM2), and type 3 (DM3). DM1 is caused by the expansion of a cytosine-thymidine-guanine (CTG) repeat in the DM protein kinase (*DMPK*) gene on chromosome 19; and DM2 is caused by expansion of a cytosine-cytosine-thymine-guanine (CCTG) repeat in the zinc finger protein 9 (*ZNF9*) gene on chromosome 3. DM3 is a multisystem disorder with myotonic dystrophy and frontotemporal dementia with linkage to chromosome 15q21-24.

In congenital myotonic dystrophy, distal muscles are more severely involved than proximal muscles. Muscle

biopsy shows round fibers, large central vesicular nuclei, a type 1 predominance, lack of type 2B fiber differentiation, and undifferentiated type 2C fibers, all indicative of delayed maturation. The neonate born to a mother with myotonic dystrophy usually shows marked hypotonia, intellectual delay, respiratory distress, hydrocephalus, and periventricular leukomalacia. Neuroimaging of congenital DM1 shows characteristic hyperintensity of white matter at the posterosuperior trigone and ventricular dilatation. Classic DM1 shows hyperintense lesions in the bilateral frontal and/or temporal region; and the muscle biopsy shows type 1 predominance, central nuclei, ringed fibers, and sarcoplasmic masses [7].

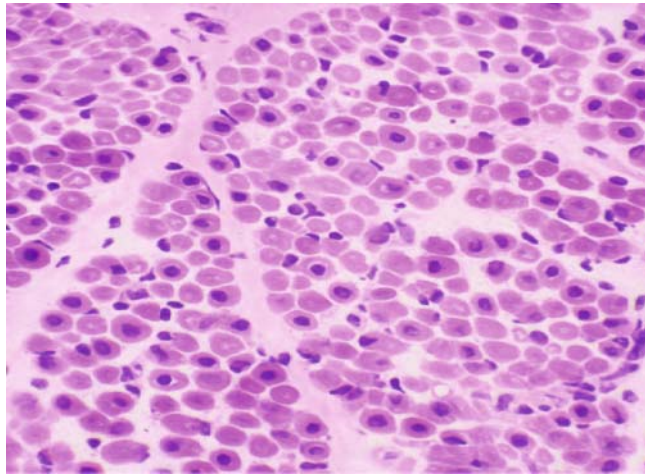


Fig. 25.5-1. Congenital myotonic dystrophy. Note the small, round fibers with central nuclei. H&E.

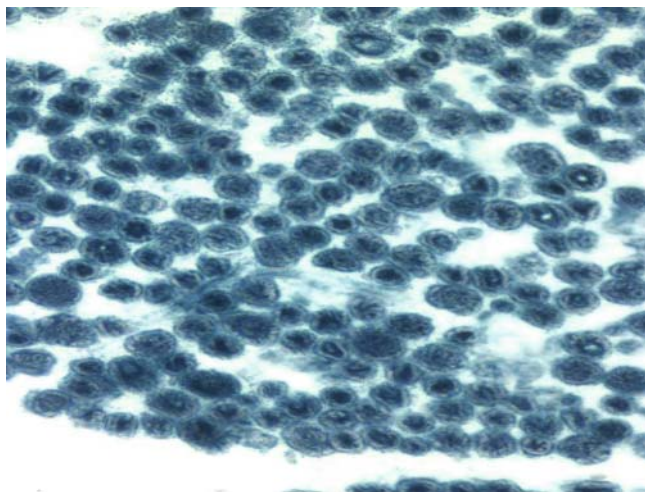


Fig. 25.5-2. Congenital myotonic dystrophy. NADH staining shows poor fiber type differentiation and central concentration of mitochondrial enzyme activity.

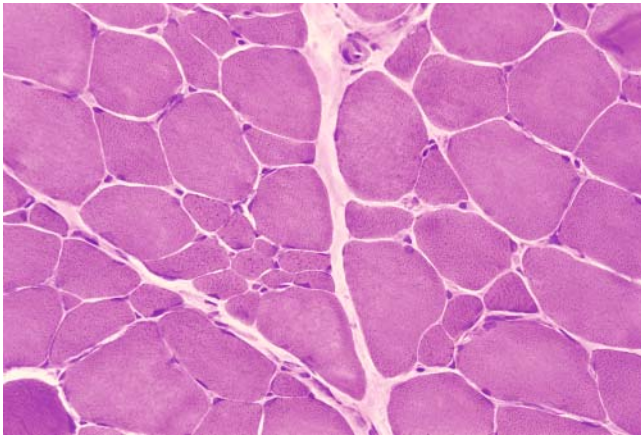


Fig. 25.5-3. DM1. Myotonic dystrophy fibers with variation in size and internal nuclei. H&E.

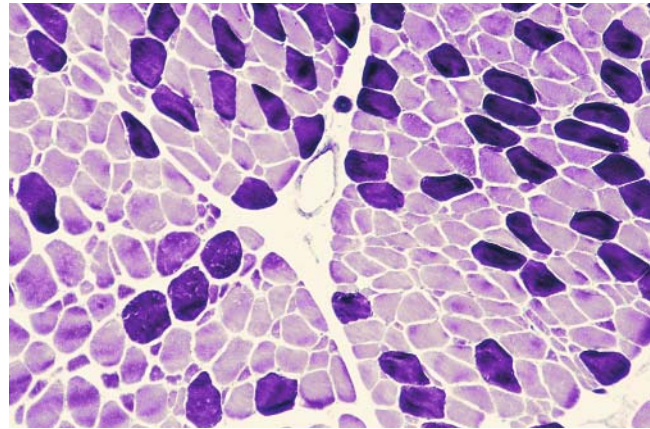


Fig. 25.5-4. DM1. ATPase pH 9.4 with type I predominance.

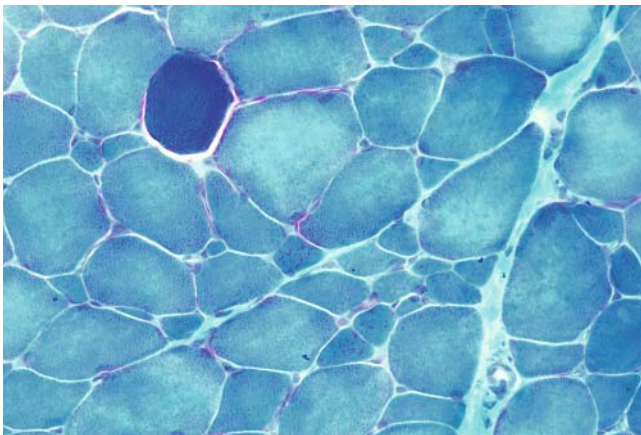


Fig. 25.5-5. DM1. Trichrome shows variation in fiber size and internal nuclei.

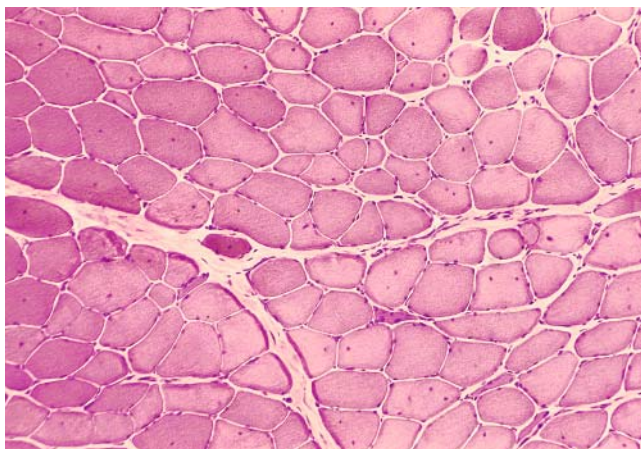


Fig. 25.5-6. Limb girdle dystrophy showing variation in size and internal nuclei. H&E.

25.6 Congenital Myopathies; Myopathies With Abnormal Structure

Congenital myopathies develop during muscle formation. Clinically, they are usually characterized by an early onset, a slow course, and hypotonia. Genetic defects are recognized in some disorders. Muscle pathology is characteristic.

Centronuclear myopathy has two forms: early childhood onset with ophthalmoplegia and bulbar signs and adult onset with limb-girdle involvement. No genetic defect has been identified. The childhood form is more severe (but not as severe as the X linked myotubular myopathy) [8].

X-linked myotubular myopathy is severe congenital myopathy with floppy muscles, decreased movement, respiratory and feeding distress, and joint contractures. There is a defect in the myotubularin gene [9].

Nemaline myopathy consists of a diverse group of disorders with nemaline bodies in the muscle. There is a severe neonatal form, a classic adult form, and a childhood autosomal dominant form. There are defects in various thin filament protein genes, such as α -actin, β -tropomyosin, and slow troponin T [10].

Central core myopathy usually manifests as nonprogressive limb weakness and hypotonia. It is associated with malignant hyperthermia and mutant ryanodine receptor proteins [11].

Congenital fiber type disproportion is usually a nonprogressive disorder with predominance and hypotrophy of type I fibers. The clinical course is variable, and no genetic defect is known [12].

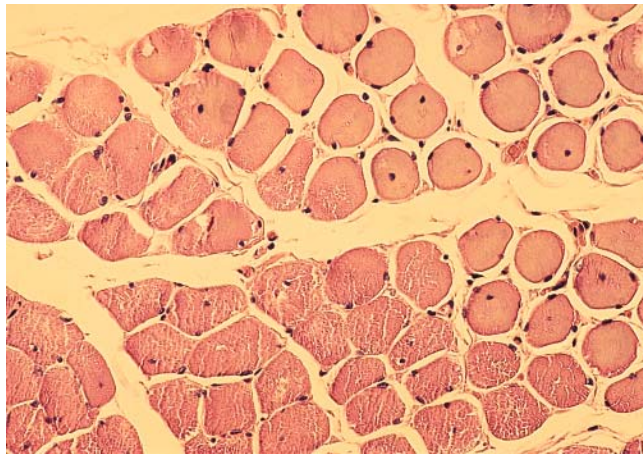


Fig. 25.6-1. Centronuclear myopathy with 25%–75% central nuclei. H&E.

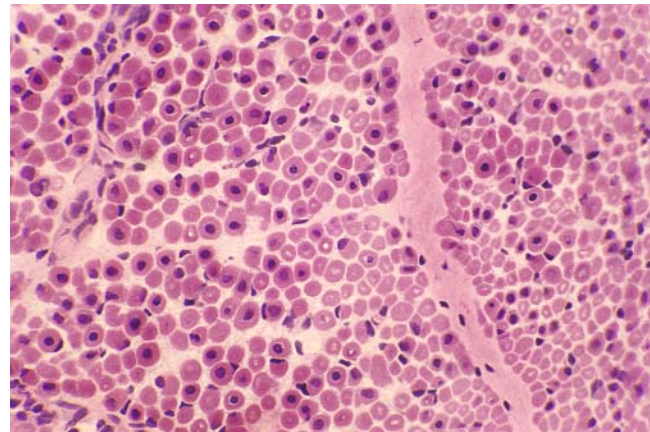


Fig. 25.6-2. Myotubular myopathy with small fibers and central nuclei. H&E.

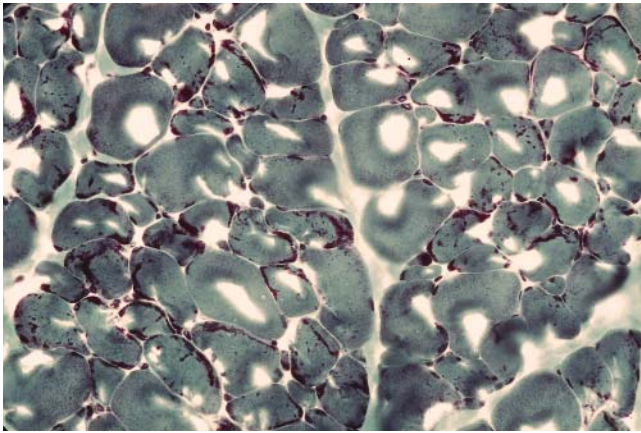


Fig. 25.6-3. Nemaline myopathy. Red rods are seen with Gomori stain.

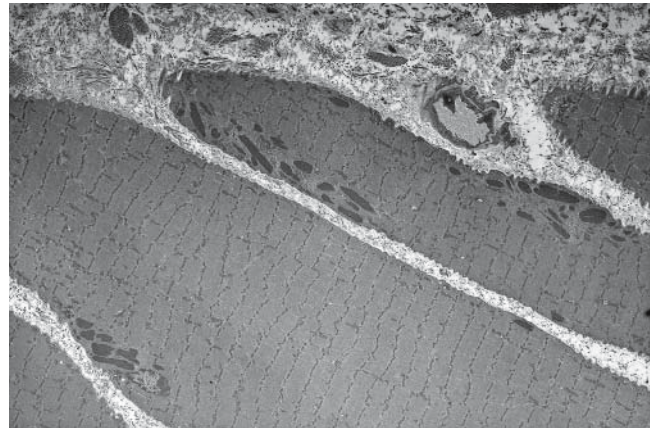


Fig. 25.6-4. Electron microscopy (EM) of nemaline rod myopathy with streaming of Z-band elements.

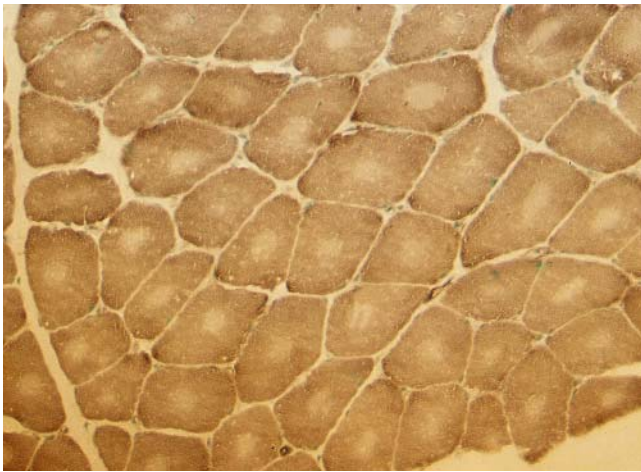


Fig. 25.6-5. Central core myopathy with nonstaining cores. NADH.

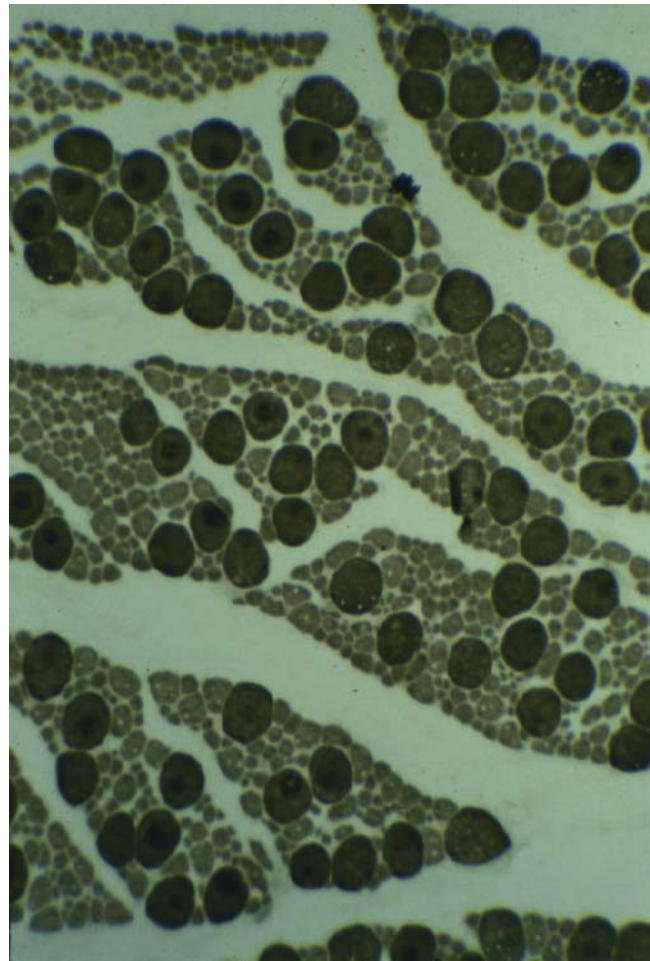


Fig. 25.6-6. Congenital fiber type disproportion with large type II fibers and hypoplastic type I fibers. ATPase pH 9.4.

25.7 Inflammatory Myopathies

Childhood dermatomyositis is a relatively common, serious disorder. It presents with an erythematous skin rash on the extensor surfaces of the joints and on the face as well as weakness and tenderness in limb-girdle muscles. There may be a generalized vasculitis that involves the gastrointestinal tract, causing mucosal ulceration and hemorrhage. In the muscle there is inflammatory cell infiltration (B cells and CD4 T cells) in perivascular spaces. The vessels develop endothelial swelling, sometimes producing vascular occlusion and muscle infarction. There is a reduction in the number of capillaries and a characteristic perifascicular atrophy of type I and type II fibers. Immune complexes containing

immunoglobulin G (IgG), IgM, and C3 are present in arterial walls; and there is deposition of membrane attack complex. The muscle fibers undergo segmental necrosis and are invaded by macrophages and T lymphocytes. There is regeneration of muscle fibers by the satellite cells. Endomysial fibrosis may be present.

Polymyositis may occur as an isolated muscle disease or in association with a collagen vascular disorder. The biopsy shows fiber atrophy, isolated fiber degeneration, and inflammatory cells.

Myositis can be caused by parasites, viruses, and immune disorders [13].

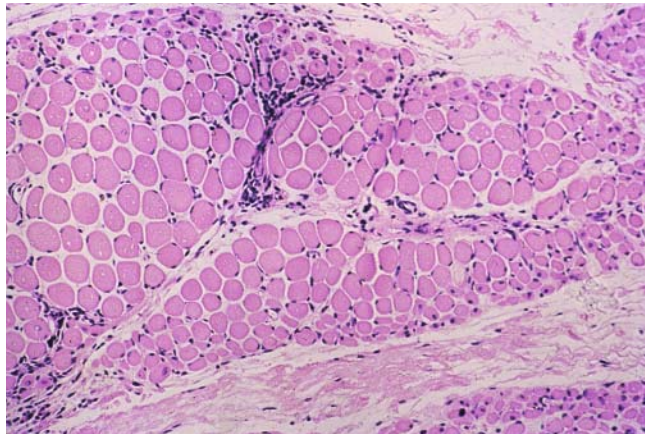


Fig. 25.7-1. Childhood dermatomyositis with perifascicular atrophy, perivascular and intrafascicular inflammation, fiber degeneration and regeneration, and slight fibrosis. H&E.

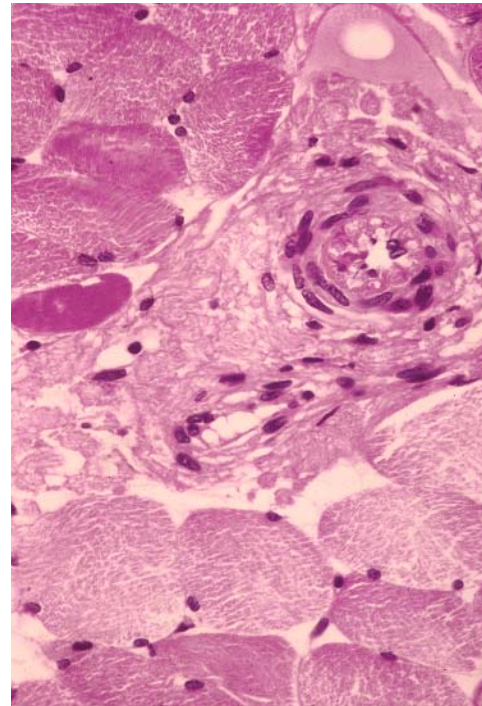


Fig. 25.7-2. Childhood dermatomyositis with vascular endothelial hyperplasia leading to occlusion and loss of intrafascicular capillaries. H&E. See also Fig. 25.6-6.

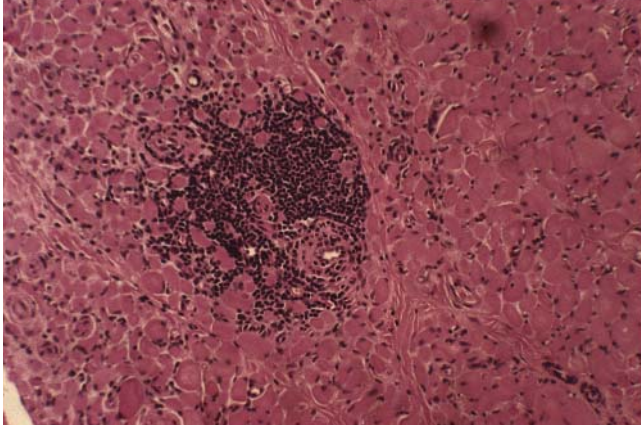


Fig. 25.7-3. Childhood dermatomyositis with perivascular and intrafascicular inflammatory cell infiltration. H&E.

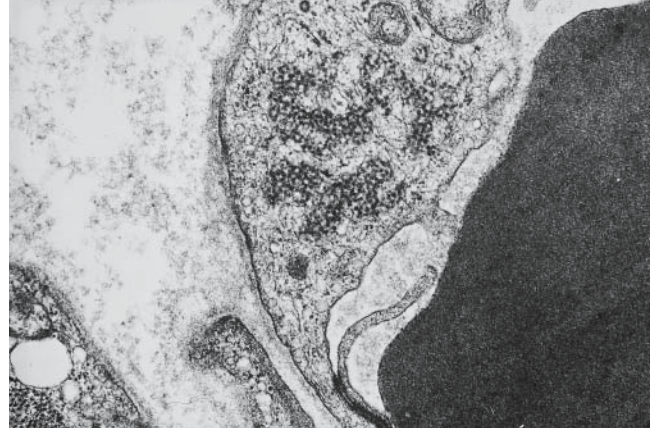


Fig. 25.7-4. Childhood dermatomyositis. EM of a capillary shows endothelial tubular arrays.

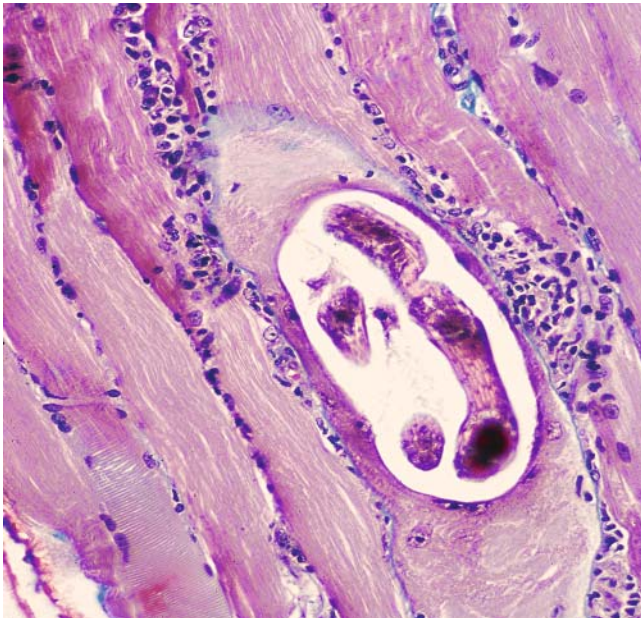


Fig. 25.7-5. Inflammatory myopathy caused by *Trichinella* infestation. H&E.

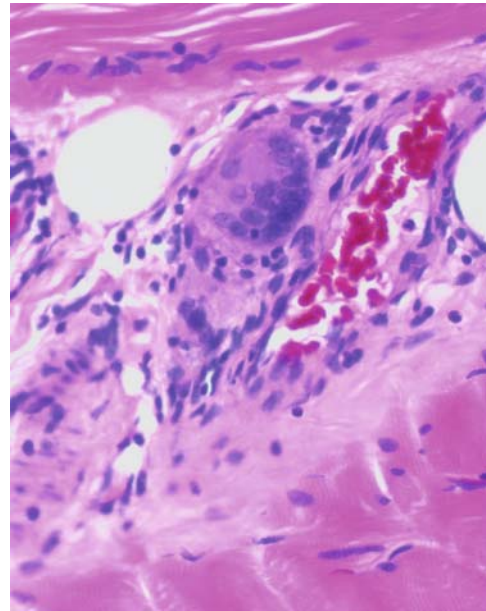


Fig. 25.7-6. Inflammatory muscle biopsy, showing granulomatous inflammation in a case of sarcoidosis. H&E.

25.8 Metabolic Myopathies

The muscle biopsies in these disorders is not usually pathognomonic of a specific disease but suggest metabolic pathways that can be further investigated biochemically or genetically. Glycogen storage and lipid storage (related sometimes to carnitine deficiency) in muscle is illustrated below.

Pompe's disease, or the infantile form of generalized glycogenesis (infantile type II glycogenesis), is an autosomal recessive lysosomal glycogen storage disease resulting in early onset of cardiomegaly, hypotonia, cerebral dysfunction, failure to thrive, and early death. Lysosomal glycogen storage affects practically all the tissues in the body and results from a deficiency of acid maltase. Screening the peripheral blood may demonstrate disease-specific lysosomal inclusions in lymphocytes. Both the central nervous system (CNS) and the peripheral nervous system (PNS) are involved (see

Chapter 10, Section 10.1). In the PNS neuronal glycogen storage is prominent in the dorsal root ganglia, autonomic ganglia, neurons of the myenteric plexus, and ganglia cells of the retina. EM demonstrates lysosomal glycogen in Schwann cells, mesenchymal cells, mural cells of the vasculature, and perineural cells. In the CNS, neuronal glycogen storage is most severe in anterior horn cells of the spinal cord and motor nuclei of the brain stem (cranial nerves III–XII).

Lipid myopathy occurs in the presence of primary carnitine deficiency and acyl-CoA dehydrogenase deficiencies including medium-chain acyl-CoA dehydrogenase (MCAD), long-chain acyl-CoA dehydrogenase deficiency (LCAD), short-chain L-3 hydroxyacyl-CoA dehydrogenase deficiency (SC HAD), and coenzyme Q10 deficiency. These may present during infancy or childhood [14].

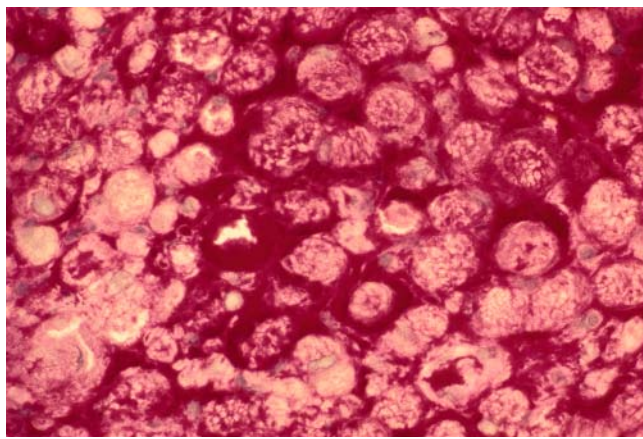


Fig. 25.8-1. Glycogen storage myopathy in Pompe's disease with a marked increase in muscle glycogen. PAS.

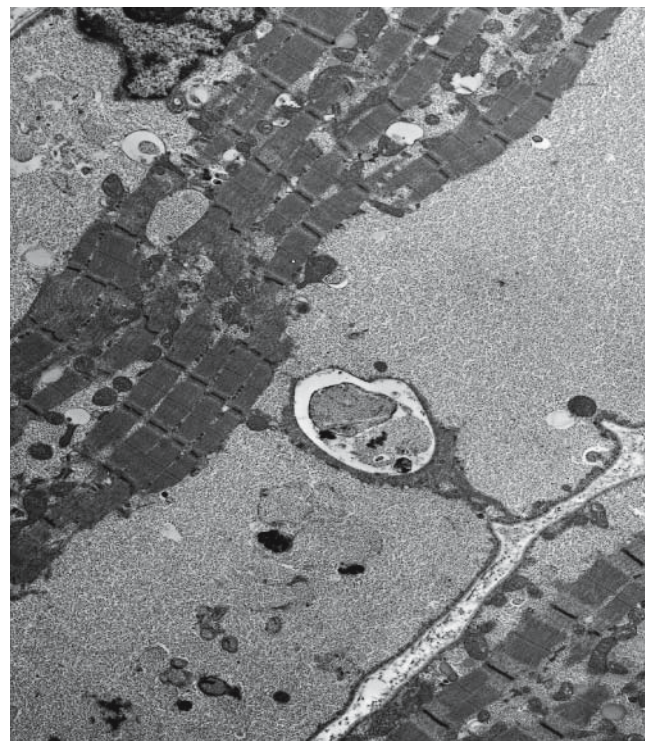


Fig. 25.8-2. Glycogen storage myopathy. EM reveals glycogen accumulation, both free and in lysosomes, and disruption of the muscle architecture.

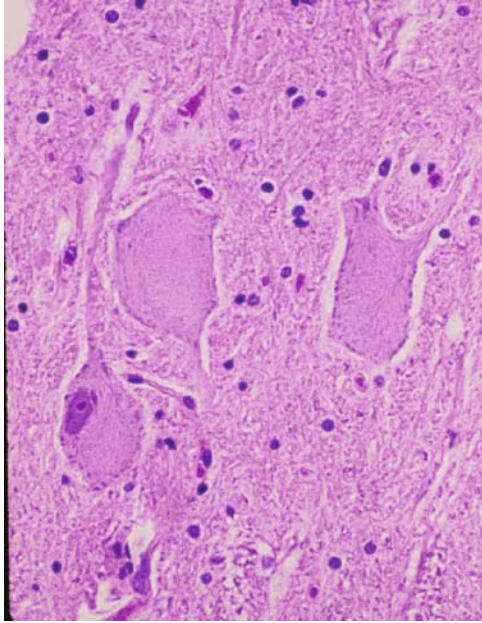


Fig. 25.8-3. Pompe's disease with ballooned neurons containing glycogen in the brain stem. H&E.

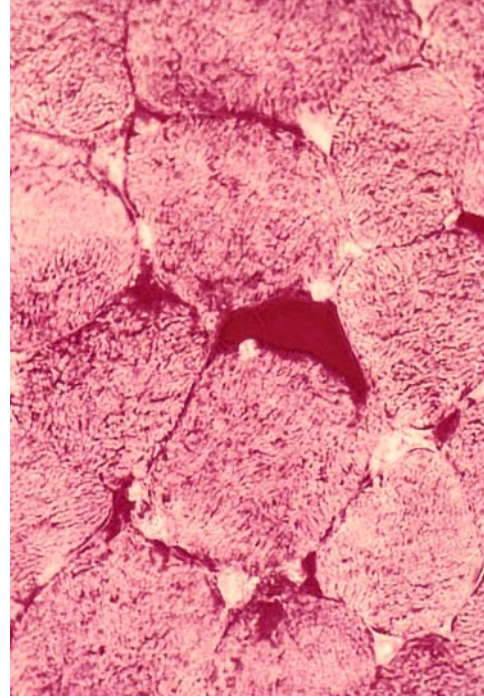


Fig. 25.8-4. Glycogen storage myopathy in McArdle's disease (myophosphorylase deficiency). PAS reaction shows increased glycogen in isolated fibers.

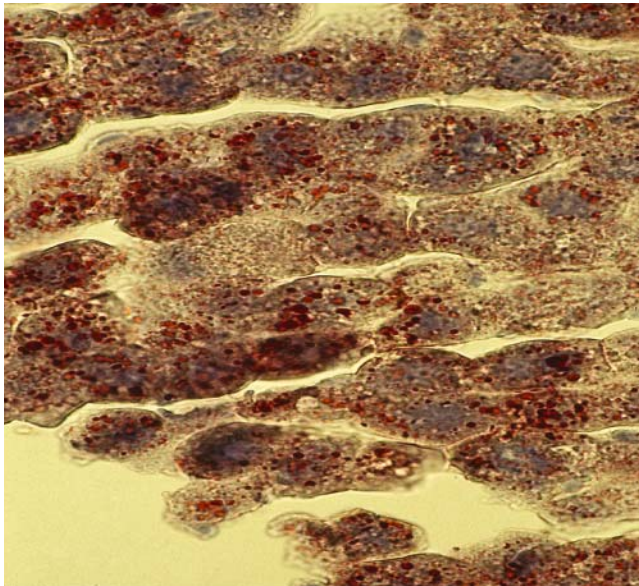


Fig. 25.8-5. Lipid storage in carnitine deficiency. Oil red O reaction shows increased neutral lipid.

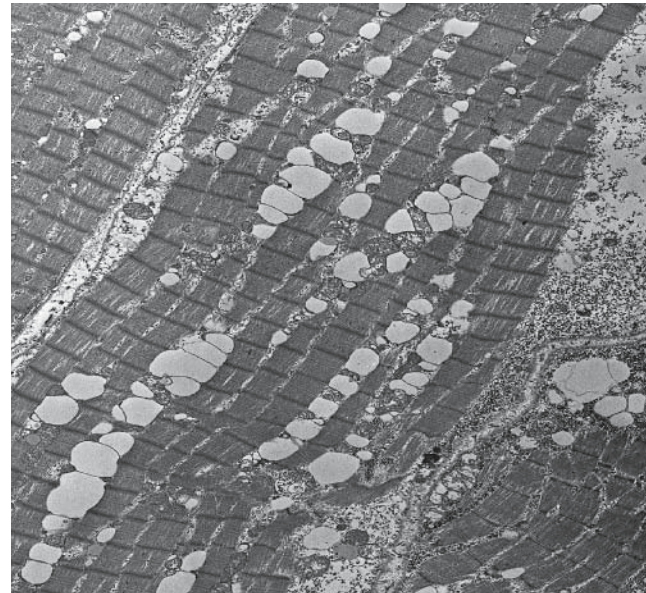


Fig. 25.8-6. Lipid storage in carnitine deficiency. Ultrastructural demonstration of increased myofiber lipid.

25.9 Mitochondrial Cytopathies

The muscle biopsy may reveal abnormalities in mitochondrial respiratory chain enzymes or in the structure of mitochondria that suggest the presence of nuclear or mitochondrial DNA mutations. Histochemistry may define a specific deficiency or demonstrate increased enzyme reactivity, reflecting a nonspecific mitochondrial response to deficits in muscle energy metabolism. Further studies of specific respiratory chain enzymes or mitochondrial DNA will further define the etiology. Some examples are the following.

- *MELAS* (mitochondrial encephalomyopathy with lactic acidosis and stroke-like episodes) may exhibit “ragged red fibers,” reflecting increased numbers and

size of muscle mitochondria. Most cases are related to an A3243G point mutation in the tRNA gene.

- *Cytochrome c oxidase (COX) deficiency* can be caused by several nuclear or mitochondrial genetic defects.
- *Kearns Sayre syndrome* is a multisystem disorder (cardiac conduction system, diabetes mellitus, ataxia, retinitis pigmentosa, and neurodegeneration) and is caused by large-scale mitochondrial DNA deletions. Chronic progressive external ophthalmoplegia may be a mild form of this disease.
- *Myoclonus epilepsy with ragged red fibers (MERRF)*, *neuropathy, ataxia, retinitis pigmentosa (NARP)*, and *Leber hereditary optic neuropathy (LHON)* are also expressed during childhood [14,15].

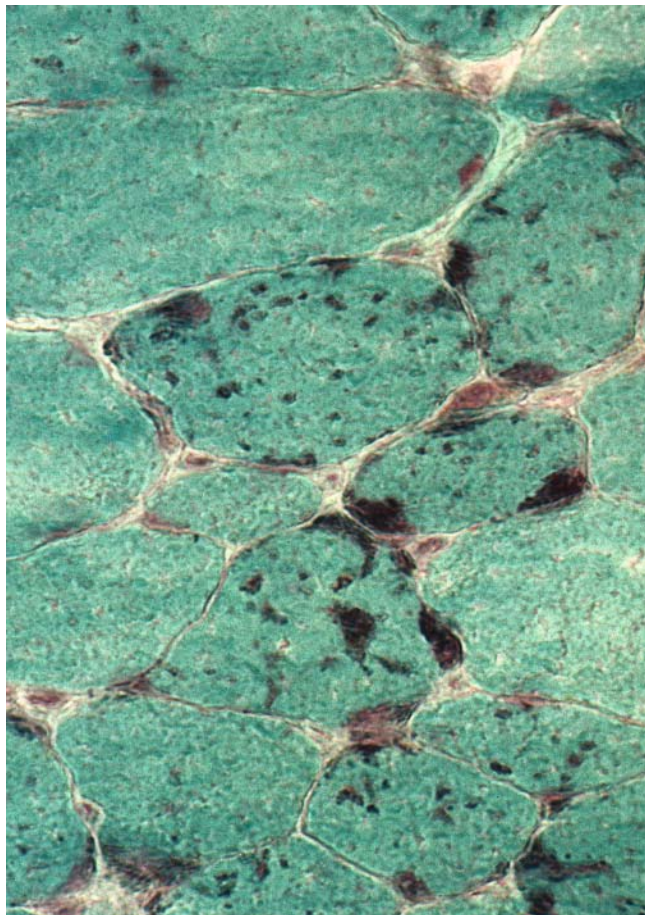


Fig. 25.9-1. Mitochondrial encephalomyopathy with lactic acidosis and stroke-like episodes (MELAS). Muscle in a case of MELAS. Gomori stain demonstrates ragged red fibers.

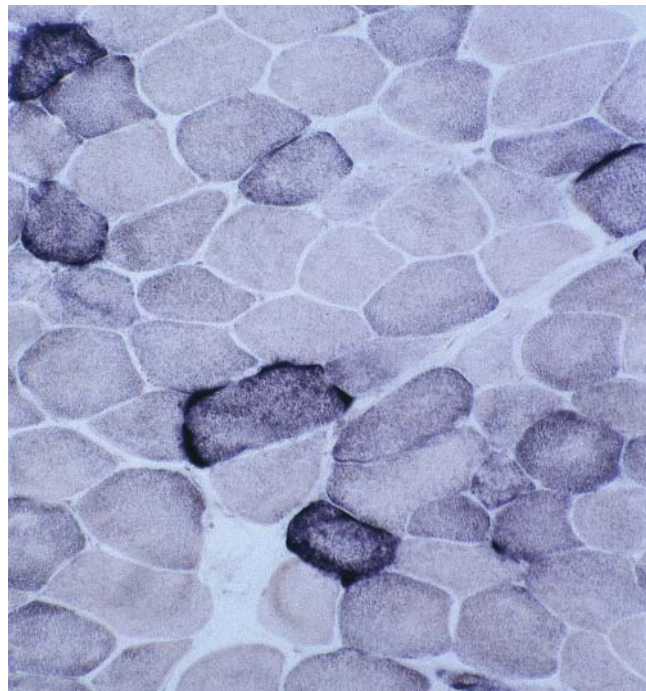


Fig. 25.9-2. Muscle in a case of MELAS. NADH shows increased oxidative enzyme reactions.

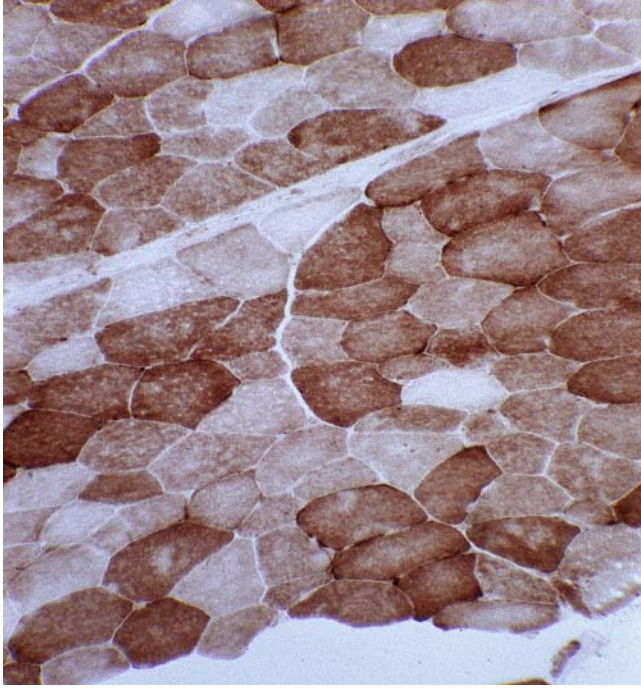


Fig. 25.9-3. Cytochrome c oxidase reaction in muscle exhibiting many negative fibers, suggesting a primary cytochrome c oxidase (COX) disorder. Negative parts of the COX reaction are segmental in long muscle fibers.

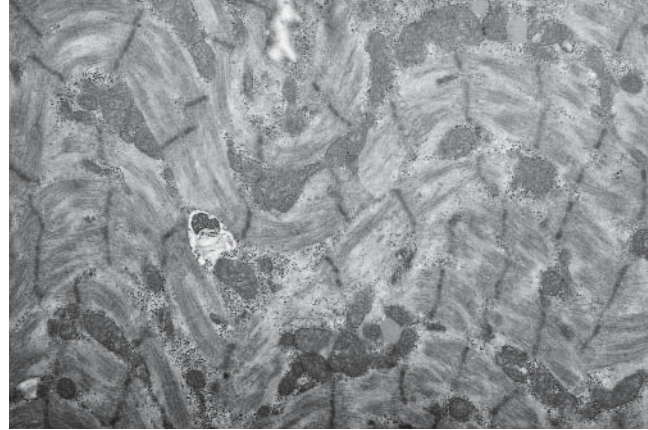


Fig. 25.9-4. Kearns-Sayre syndrome. EM demonstrates abnormally enlarged mitochondria with paracrystalline inclusions.

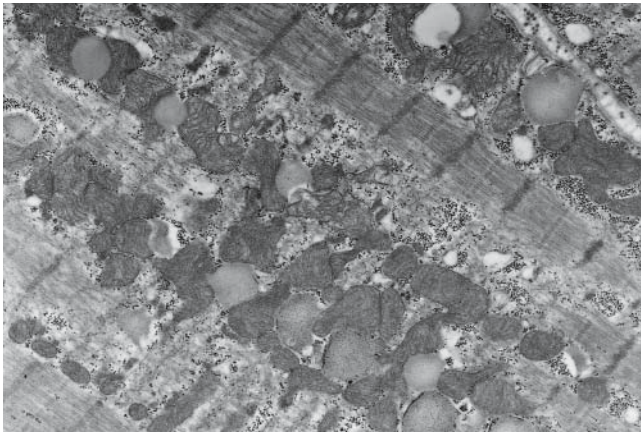


Fig. 25.9-5. Unclassified metabolic myopathy. EM indicates an increase in the number of mitochondria.

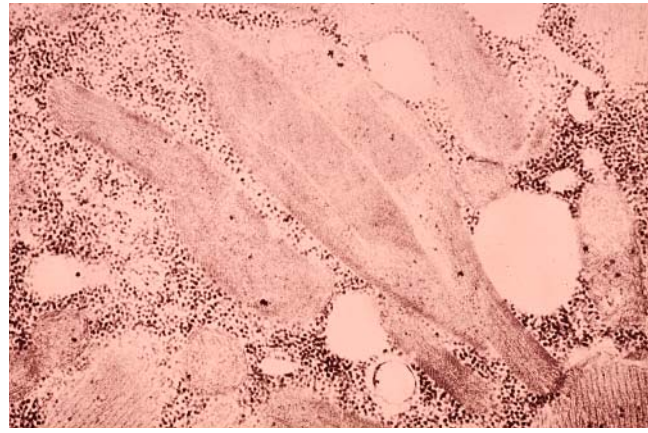


Fig. 25.9-6. Unclassified metabolic myopathy. EM reveals enlarged abnormal mitochondria.

25.10 Miscellaneous Muscle Pathology

There are morphological features of muscle biopsies that suggest certain pathogenic mechanisms. For example, *generalized type 1 atrophy* suggests a myopathic process.

Generalized type 2 atrophy may be seen in CNS disorders, with steroid effects, and with disuse [1].

Generalized muscle fiber hypoplasia can be seen in infants who have been paralyzed [16].

Generalized muscle fiber hyperplasia is seen in malignant hyperthermia and in myotonic dystrophy.

Poor differentiation of fiber types may be seen in Duchenne muscular dystrophy and in congenital sensory neuropathy [17].

Rhabdomyolysis, in which there is extensive breakdown or degeneration of muscle fibers associated with a regeneration of muscle fibers, can be seen in the presence of muscle exertion, ischemia, toxic infections, hyperthermia, muscle injury, electrolyte disturbances, drugs, toxins, and idiopathic rhabdomyolysis [1].

Deposition of immunoglobulins in vessels and muscles suggests an immune etiology for the muscle disease.

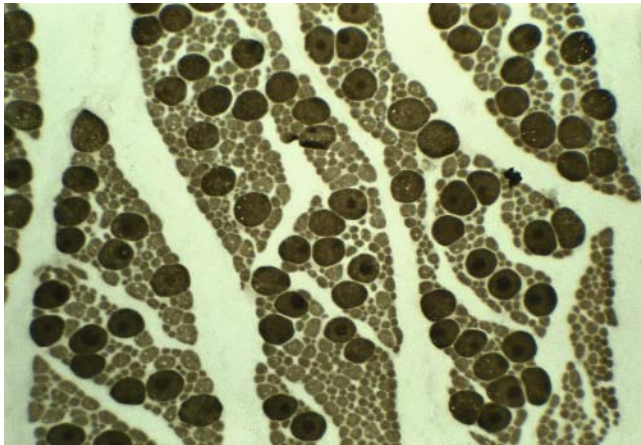


Fig. 25.10-1. Generalized type 1 atrophy and predominance. ATPase pH 9.4.

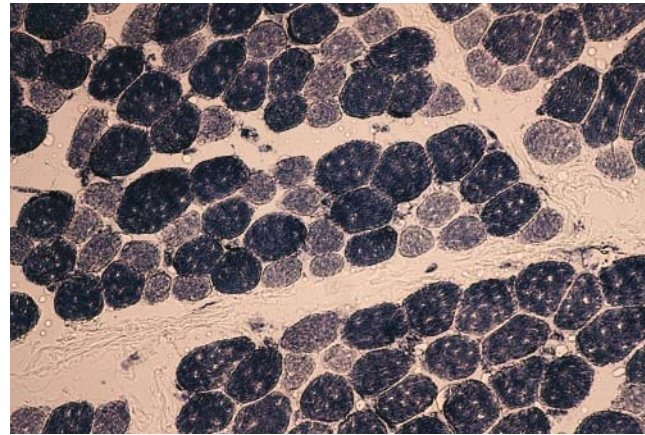


Fig. 25.10-2. Generalized type 2 atrophy. ATPase pH 4.3.

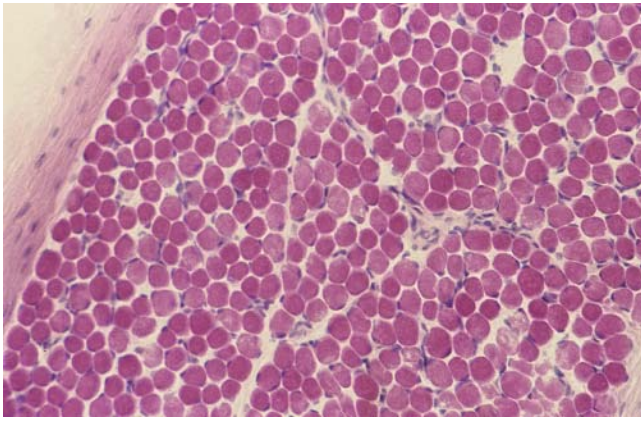


Fig. 25.10-3. Generalized fiber hypoplasia. H&E.

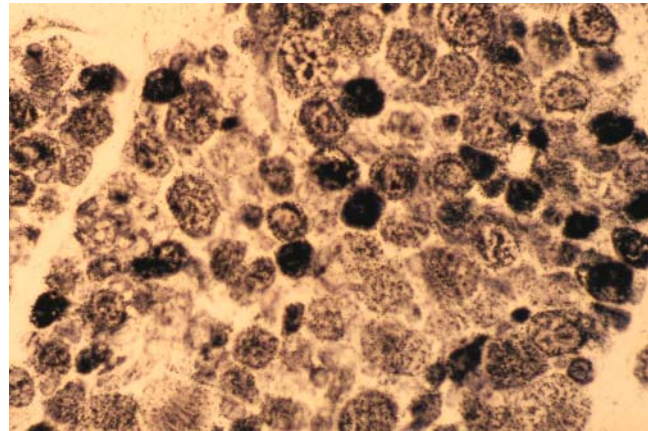


Fig. 25.10-4. Poor differentiation of fiber types. NADH reaction.

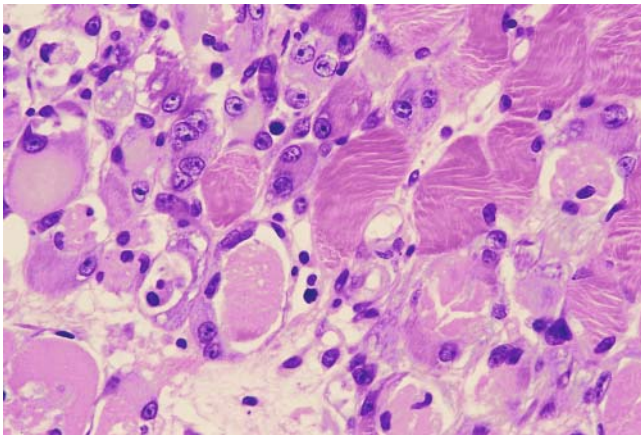


Fig. 25.10-5. Rhabdomyolysis with fiber degeneration and regeneration (basophilic fibers with large nuclei). H&E.

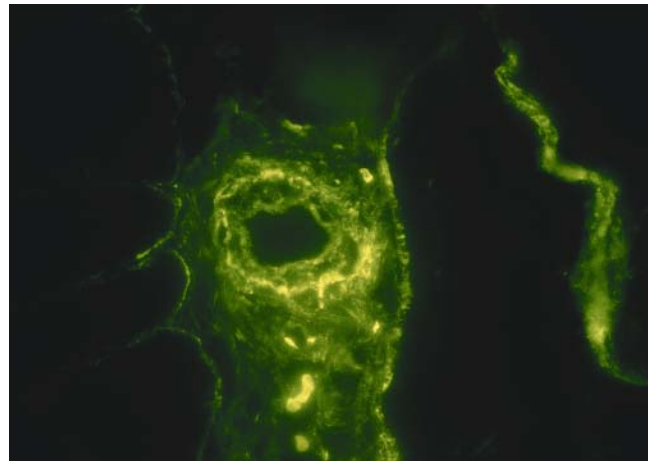


Fig. 25.10-6. Deposition of immunoglobulins and membrane attack complex in small arterioles and veins in a case of dermatomyositis.

25.11 Muscle in Neurogenic Disorders

The anterior horn cells of the spinal cord are motor neurons with axons that extend into the periphery, where they innervate muscle fibers. The axon and the muscle fibers it innervates constitute the functional motor unit of the neuromuscular system. During muscle development (at approximately 18 gestational weeks) each anterior horn cell determines the muscle fiber type of the muscle fibers in its motor unit. The mixture of types creates a normal checkerboard distribution of

fiber types. The ratio of the two main fiber types in infants and young children is approximately 50%. With neurogenic disorders the muscle fibers become atrophic, and surviving axons reinnervate the muscle, changing the fiber types and producing a “reinnervation pattern.” The effects of denervation are well illustrated in spinal muscular atrophy type 1, which is caused by a genetic defect at 5q13 [2].

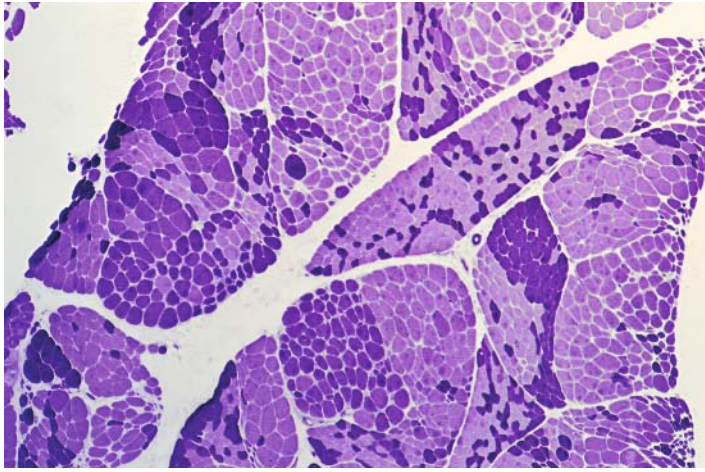


Fig. 25.11-1. Muscle biopsy showing a reinnervation pattern consisting of large groups of type I or II fibers and loss of the normal checkerboard pattern of fiber types. ATPase pH 9.4.

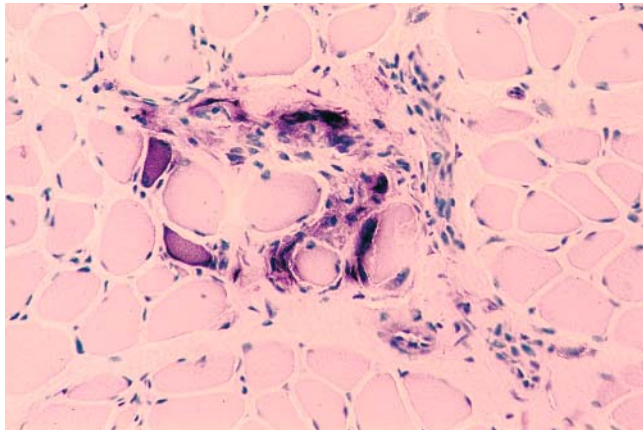


Fig. 25.11-2. Muscle with neurogenic atrophy. Small groups of small denervated fibers stained with neuron-specific enolase.

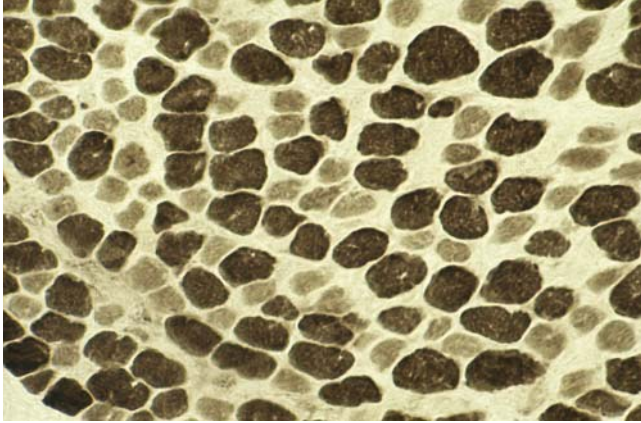


Fig. 25.11-3. The selective atrophy of type II fibers suggests neurogenic atrophy, disuse, or steroid therapy. ATPase pH 4.3.

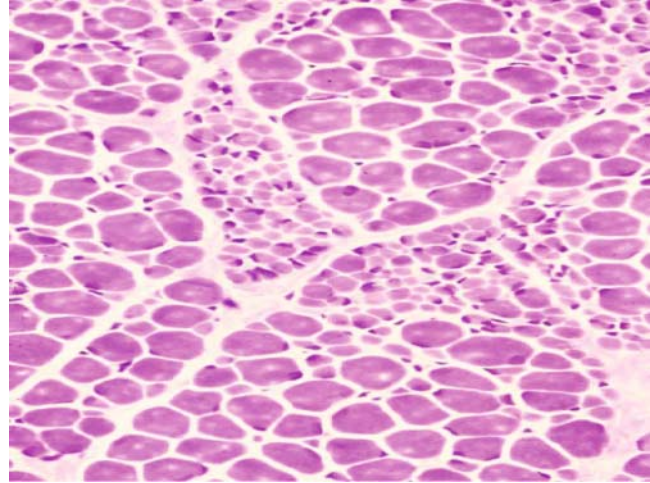


Fig. 25.11-4. SMA type I, exhibiting small fibers with occasional internal nuclei, reflecting abnormalities of early muscle development in a congenital denervating condition.

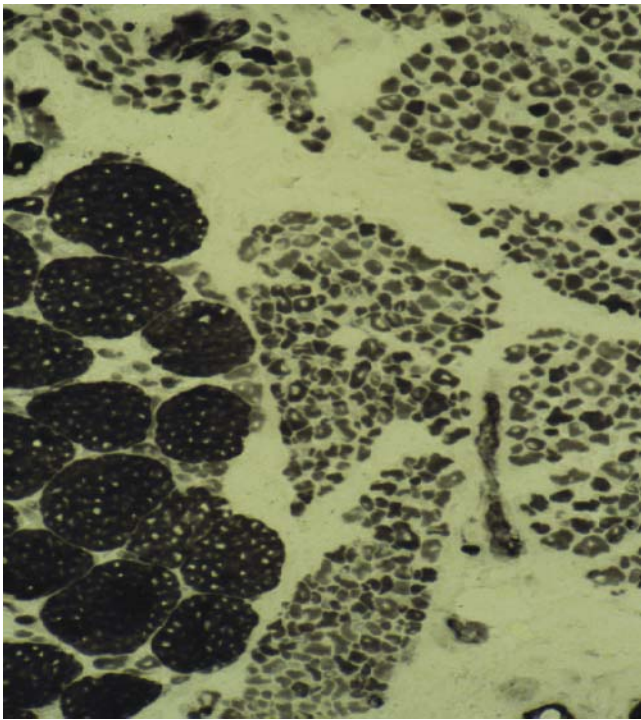


Fig. 25.11-5. SMA1. ATPase reaction at pH 4.3 shows rounded muscle fibers with atrophy of type I and II fibers and hypertrophy of surviving type I fibers.

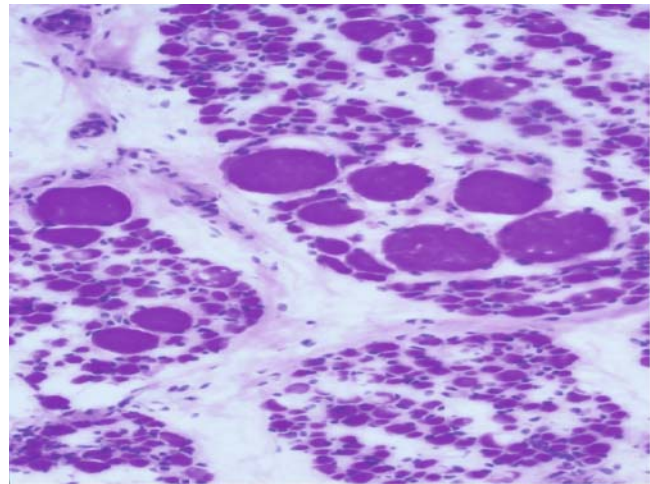


Fig. 25.11-6. SMA3, showing groups of small denervated muscle fibers and large remaining fibers.

26 Epilepsy

26.1 Ammon's Horn Sclerosis

Epilepsy is more common during childhood than in adulthood, suggesting that the developing brain is more prone to seizure activity than the mature brain. Epilepsy has been defined as an episodic disorder of the central nervous system (CNS) characterized by paroxysmal abnormal brain electrical activity and recurrent behavioral seizures [1]. The pathological substrates of epilepsy include malformations, metabolic errors, neoplasia, hypoxic-ischemic and traumatic lesions, and infection and are discussed elsewhere in this present volume. In this chapter the lesions that are observed during surgical resection for intractable epilepsy are illustrated.

Ammons horn sclerosis (AHS) is the commonest temporal lobe lesion responsible for intractable complex partial seizures [1]. In classic AHS, the dentate gyrus exhibits neuronal loss and frequently dispersion of the granular neurons. There is also loss of neurons in CA4,

CA3, and CA1. In a less common lesion, end folium sclerosis, there is loss of neurons only in CA4. In classic AHS, surviving granule neurons produce abnormal sprouting of their axons, causing reorganization of the circuitry, which creates an excitable epileptogenic focus. Figure 26.1-6 depicts the normal and AHS hippocampus. The granule neurons of the dentate gyrus (yellow) are kept from discharging by inhibitory interneurons (blue). In AHS there is loss of this inhibition. A continuous excitatory circuit is established by the sprouting of aberrant mossy fibers of the granule neurons, which excite both the pyramidal neurons of Ammon's horn and the granular neurons of the dentate. The cause of AHS is not known, but infantile febrile seizures (particularly complex febrile seizures) are a risk factor. In families with febrile seizures, mutations in sodium channel genes have been identified [2].

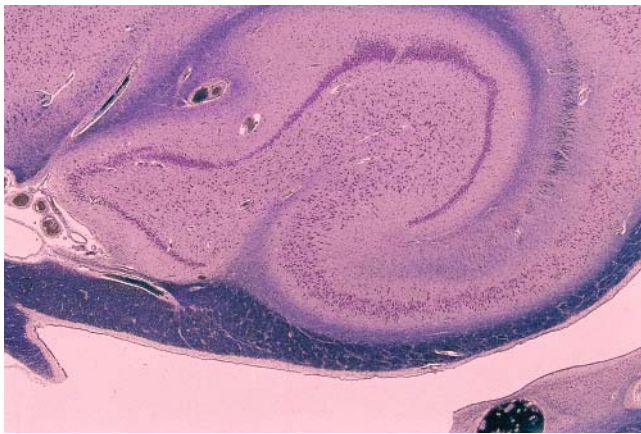


Fig. 26.1-1. Normal hippocampus, showing the dentate gyrus and the four sectors of Ammon's horn. Cresyl violet stain.

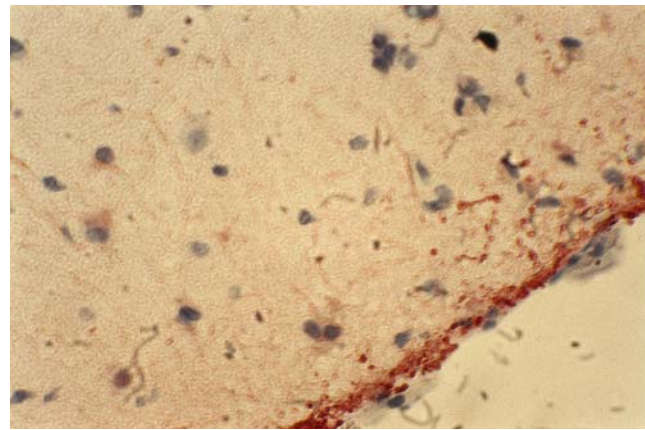


Fig. 26.1-2. Hippocampus resection for intractable epilepsy showing Chaslin's subpial gliosis. GFAP.

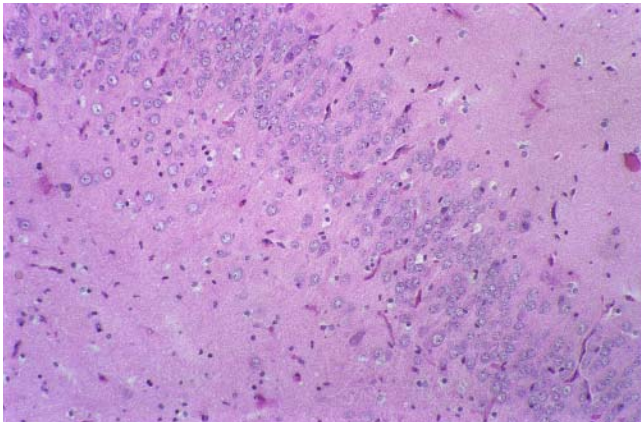


Fig. 26.1-3. Dentate gyrus in Ammon's horn sclerosis (AHS) showing dispersion of the granule neurons. H&E.

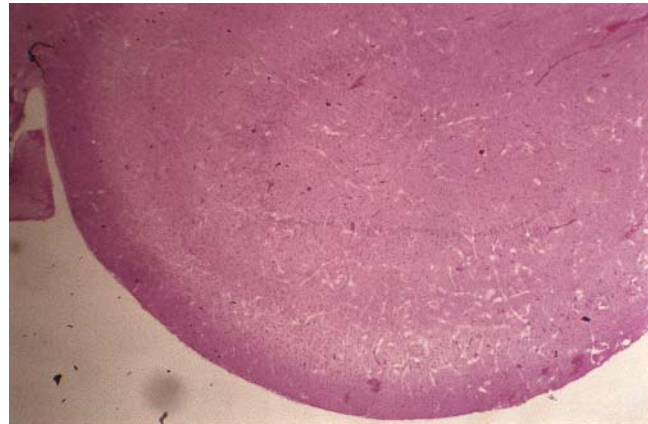


Fig. 26.1-4. CA1 in AHS showing almost complete loss of pyramidal neurons. H&E.



Fig. 26.1-5. AHS with accumulation of corpora amylacea. PAS.

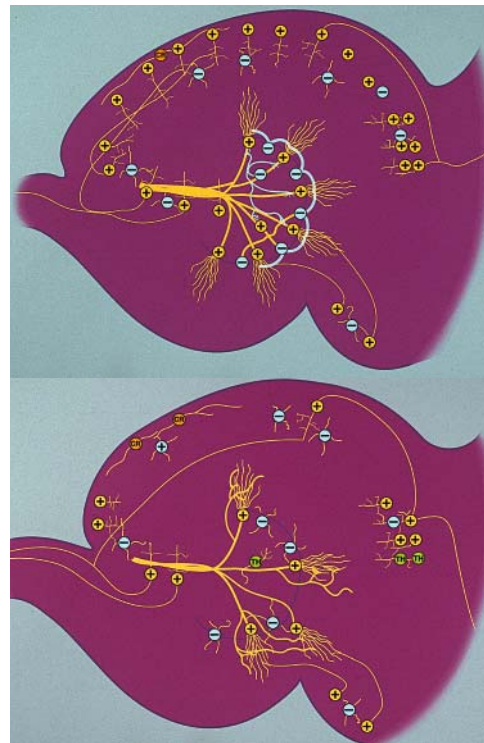


Fig. 26.1-6. Normal hippocampus (*top*) and AHS hippocampus (*bottom*).

26.2 Microdysgenesis

Abnormalities of the microarchitecture of the cortex and white matter observed in the brains of patients with generalized epilepsy are named *microdysgenesis* [3]. These abnormalities are not visible grossly or by current imaging techniques but are present to a variable degree in the resected brains from cases of intractable epilepsy associated with AHS, tumors, and malformations. Their significance in the pathogenesis of seizures is controversial because they have also been recorded in some normal subjects and in patients with other neurological disorders. [4,5]

Ectopic neurons are those neurons present in the white matter in greater than normal numbers [5].

Gray matter heterotopia are foci of displaced “gray matter” composed of neurons, glia, and neuropil char-

acteristic of the cortex. They are probably the result of a migration abnormality. They may be microscopic in size or large enough to be seen on imaging studies [3,4].

Hamartia are microscopic collections of small, round “oligodendroglia-like” cells. They may be in cortex or white matter and have some staining characteristics of immature neurons [3].

Perivascular glia nuclei refer to the presence of chains of bare glial nuclei in the white matter, around vessels, or in the white matter neuropil [4].

Neuronal clusters are present in the cortex of some epilepsy patients [4].

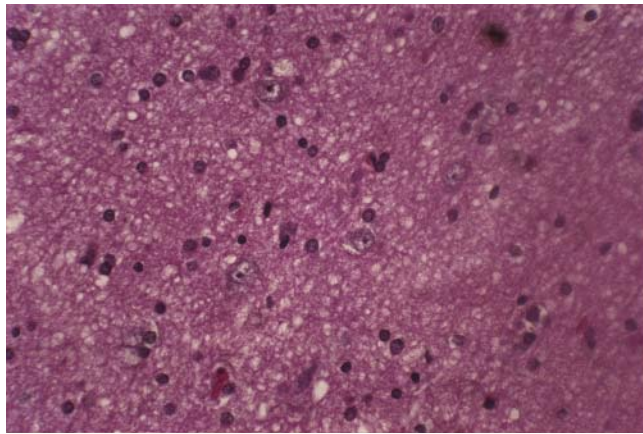


Fig. 26.2-1. Ectopic neurons in the white matter of a patient with intractable epilepsy. These neurons are more numerous than in normal white matter.

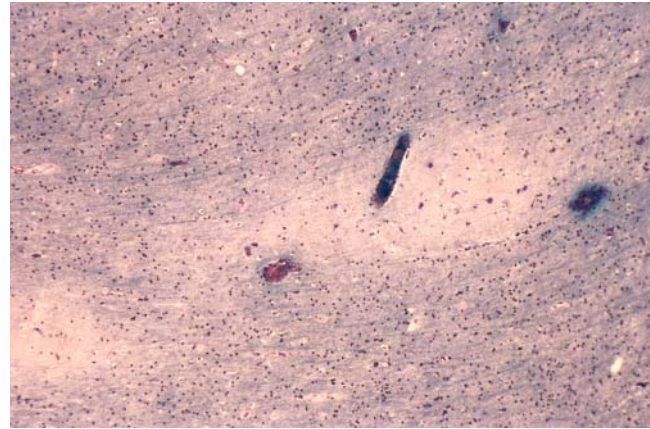


Fig. 26.2-2. Gray matter heterotopia in the temporal lobe. AHS was also present.

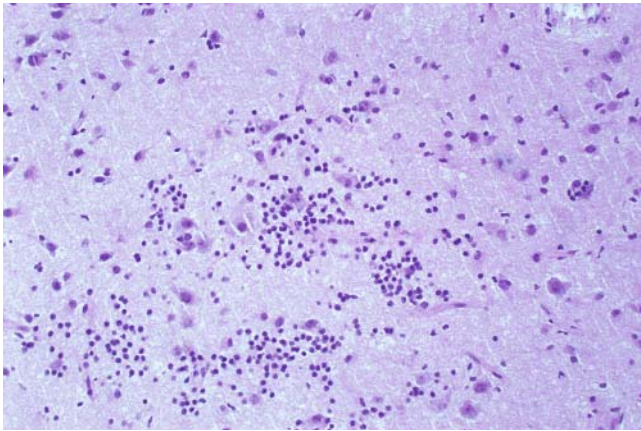


Fig. 26.2-3. "Hamartia": clusters of immature looking oligodendroglia-like cells.

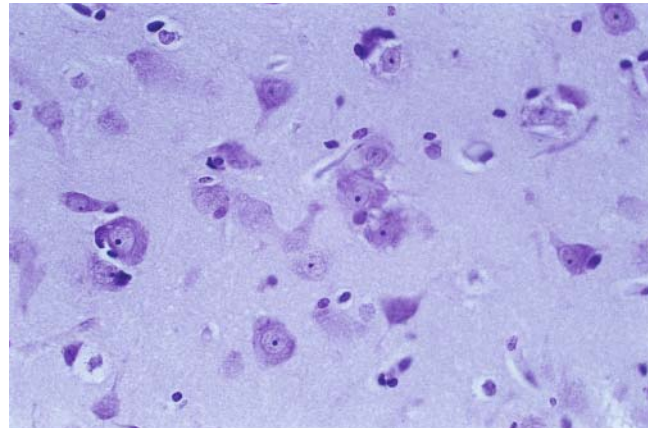


Fig. 26.2-4. Lateral temporal cortex exhibiting clusters of cortical neurons.

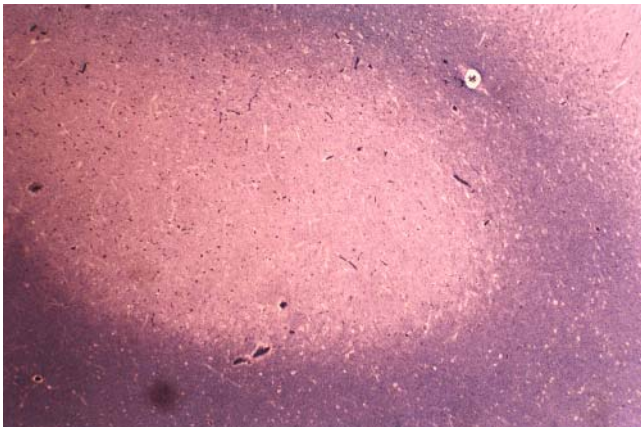


Fig. 26.2-5. Gray matter heterotopia in the temporal lobe.

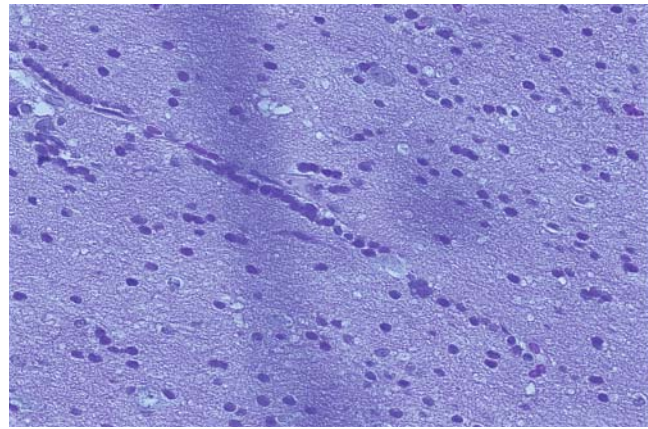


Fig. 26.2-6. White matter showing chains of perivascular glial nuclei.

26.3 Epilepsy with Inflammatory Lesions

Seizures may occur during the course of CNS infections; and in some cases epilepsy develops subsequently. Infections that are particularly prone to produce seizures are brain abscesses and parasitic and protozoan infections. Rasmussen's syndrome or encephalitis is an inflammatory condition of unknown etiology that presents as an intractable seizure disorder. It occurs in children 14 months to 14 years of age beginning as an abrupt onset of partial seizures that increase in severity and produce unilateral (usually) inflammatory brain lesions and neurological deficits. There is brain atrophy, and the meninges contain lymphocytes and macrophages. In the cortex

there are microglial nodules, a diffuse inflammatory cell infiltrate of lymphocytes and microglia, capillary proliferation, and perivascular inflammatory cell cuffing. The changes may involve part or all of the cortex and white matter. As the lesion advances there is gliosis and cell loss, with microcyst formation. Many infectious agents and autoimmune phenomena have been investigated, but as yet the responsible cause has not been identified. Treatment, which is challenging, includes surgical resection, high-dose steroids, immunoglobulins, plasmapheresis, and immunosuppression [6].

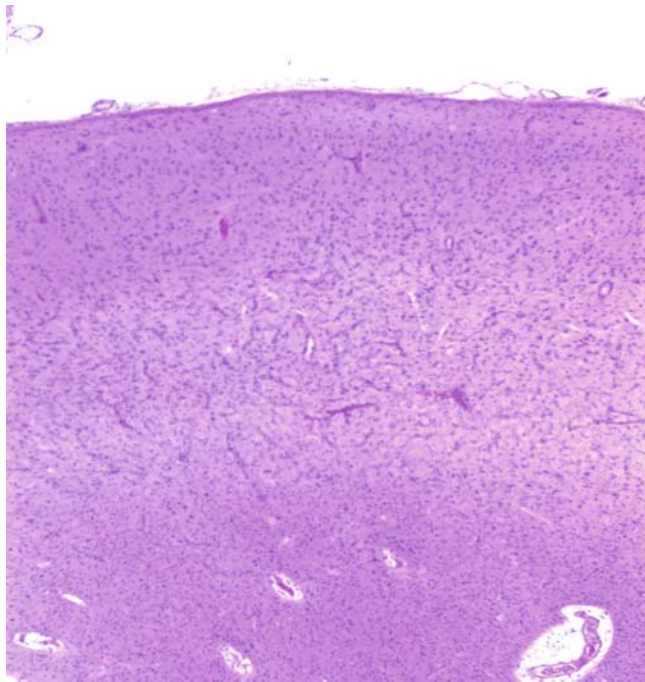


Fig. 26.3-1. Rasmussen's encephalitis. Microscopy (low power) shows diffuse loss of neurons. H&E.

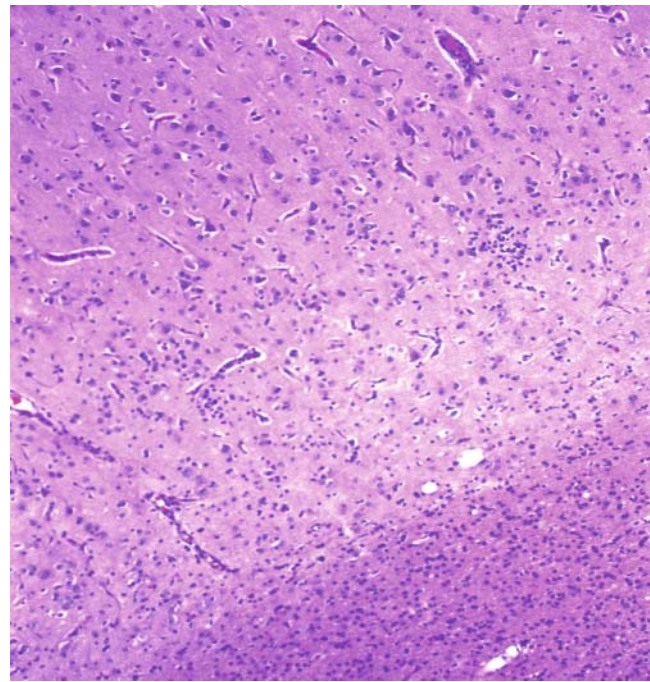


Fig. 26.3-2. Microscopy of the cortex shows focal inflammatory cells. H&E.

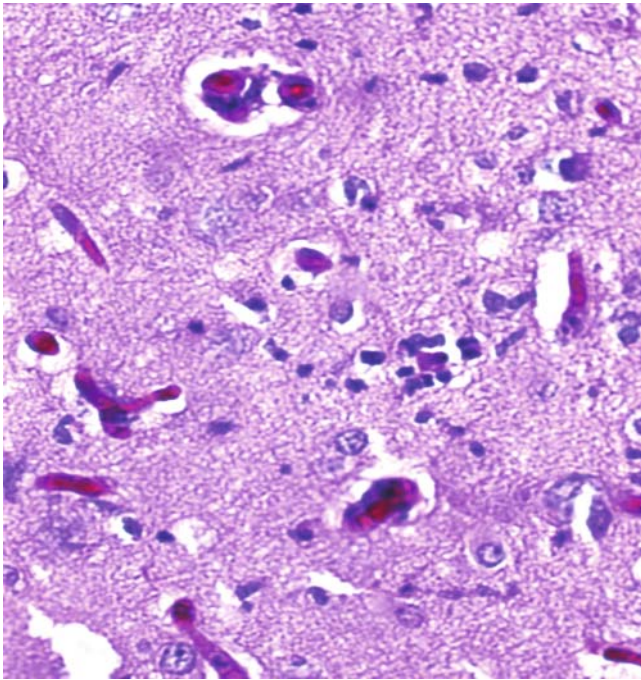


Fig. 26.3-3. Microscopy shows neuronophagia. H&E.

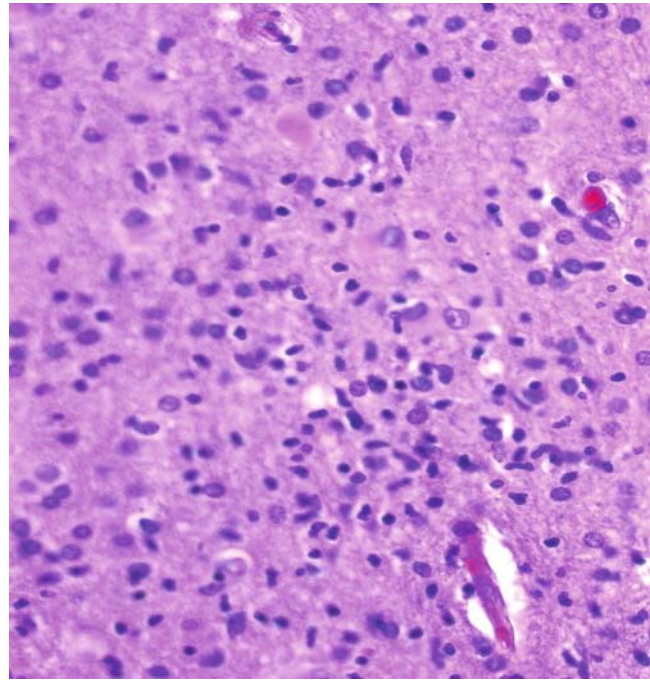


Fig. 26.3-4. Microscopy of white matter shows increased microglial cells. H&E.

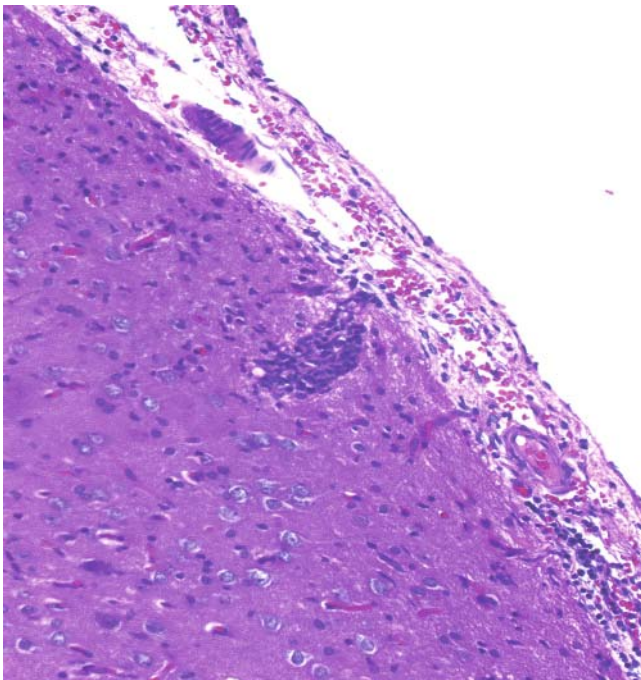


Fig. 26.3-5. Microscopy shows inflammation in the meninges and cuffing of vessels by lymphocytes. H&E.

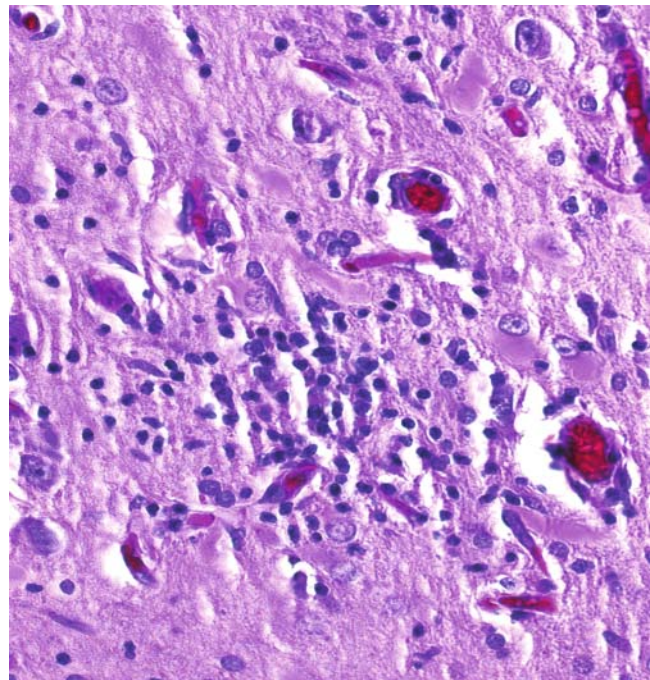


Fig. 26.3-6. Microscopy shows a microglial nodule. H&E.

26.4 Malformations and Epilepsy

Epilepsy is usually associated with severe brain malformations, including lissencephaly, focal cortical dysplasia, heterotopia [particularly periventricular nodular heterotopias and band heterotopias (double cortex)], and hemimegalencephaly. These disorders may be diagnosed by imaging studies, and genetic abnormalities have been identified in some (e.g., there is an abnormality of the *Lis -1* gene in Miller Dieker syndrome, which exhibits lissencephaly). The *fukutin* gene is abnormal in the cortical dysplasia associated with Fukuyama muscular dystrophy; *doublecortin* is abnormal in X-linked band heterotopia. Vascular malformations may also cause epilepsy [1,7].

Focal cortical dysplasia refers to a focal region of the cerebral cortex that shows loss of laminar organization, isolated abnormally large neurons, disorientation of neurons, and widening of the cortex with poor distinction between white matter and cortex (see Chapter 2, Section 2.13) [8].

Diffuse cortical dysplasia shows numerous regions of cortical dysplasia, sometimes interspersed with more normal cortex.

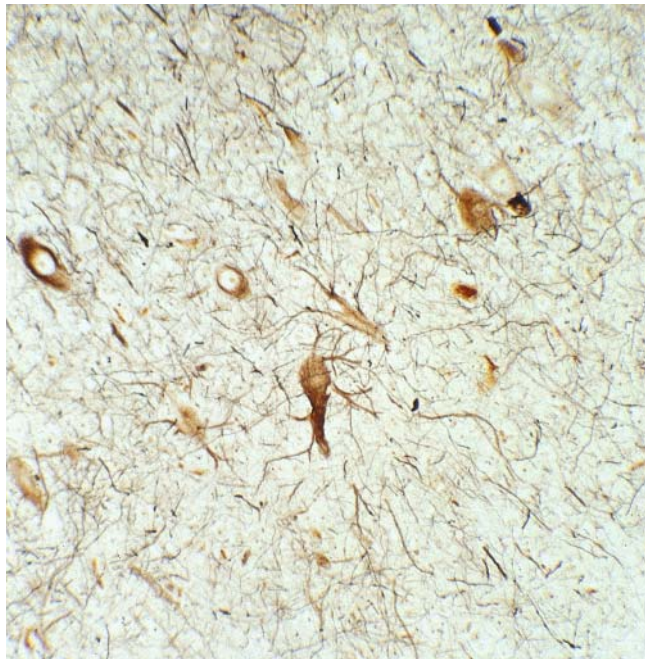


Fig. 26.4-1. Cortical dysplasia. Silver stain reveals abnormally large neurons.



Fig. 26.4-2. Hemimegalencephaly. The thick cortex is composed of polymicrogyria (see Chapter 2, Section 2.13).

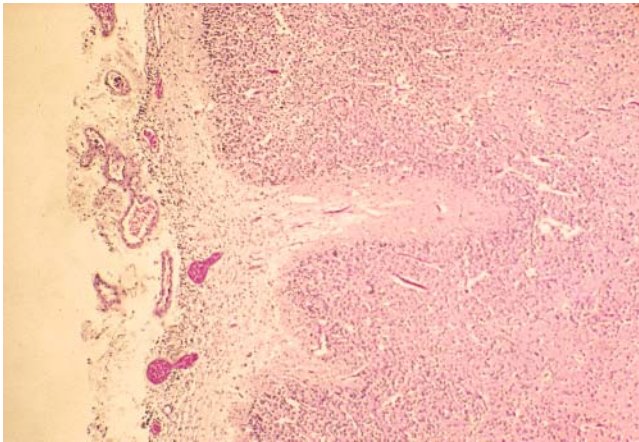


Fig. 26.4-3. Polymicrogyria. Note the poorly formed gyri and four-layer cortex. H&E.

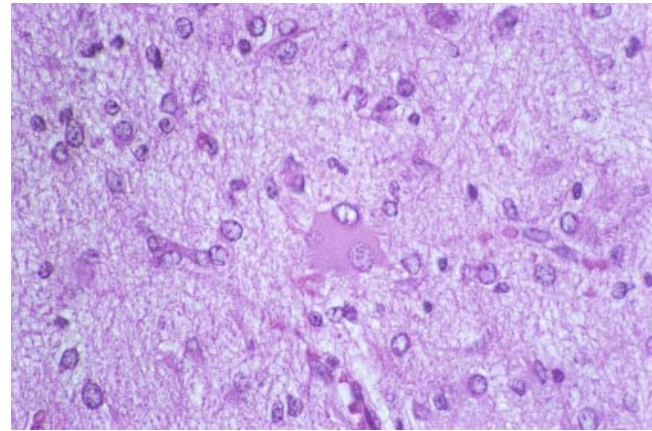


Fig. 26.4-4. Microscopy of cortical dysplasia containing balloon cells (see Chapter 2, Section 2.13). H&E.

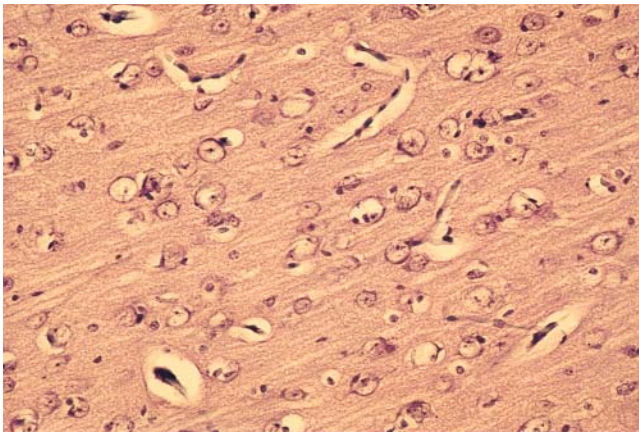


Fig. 26.4-5. Microscopy of cortical dysplasia. Note the vertical columns of large neurons. H&E.

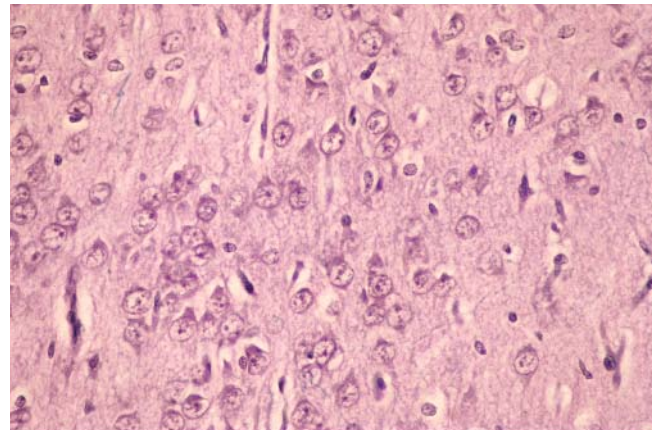


Fig. 26.4-6. Microscopy of cortical dysplasia. Note the clusters of large dysplastic neurons. H&E.

26.5 Tumors and Epilepsy

Low-grade tumors frequently present as a seizure disorder. The tumors are very slow growing, and surgical excision is usually curative regarding the tumor and the seizures. These tumors are described elsewhere in the Atlas and include the ganglioglioma, the dysembryoplastic neuroepithelial tumor (DNET), the desmoplastic infantile ganglioglioma, and the pleomorphic xanthoastrocytoma. Masses produced by infectious agents may mimic low-grade neoplasms [1].

Some tumors, such as the ganglioglioma and the DNET, are associated with foci of cortical dysplasia. This association raises questions about whether the tumor arose in the abnormal cortex or the seizure disorder caused by the neoplasm was responsible for the dystrophic changes in the nearby cortex [9].

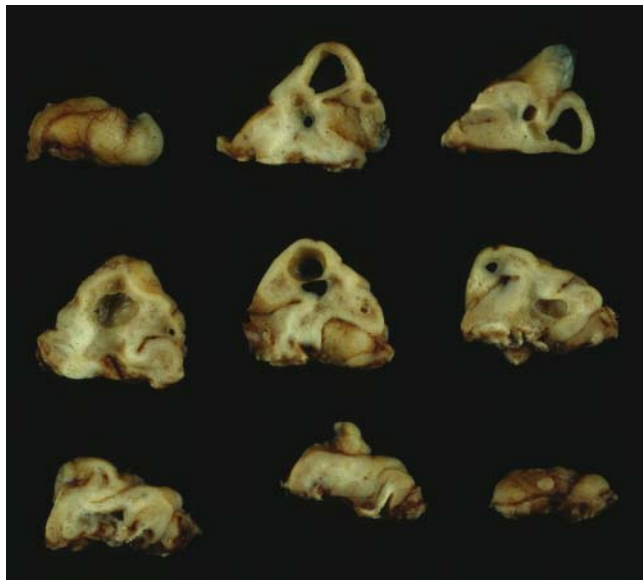


Fig. 26.5-1. Dysembryoplastic neuroepithelial tumor (DNET)-gross. This tumor resection demonstrates the superficial and cystic nature of some DNETs.

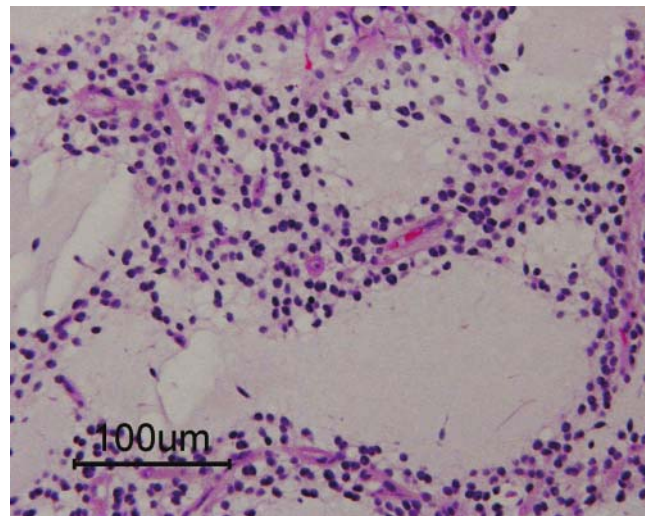


Fig. 26.5-2. DNET. Microcystic areas contain a myxoid material that typically stains with Alcian Blue. Centrally an isolated neuron is noted amongst the obligodendroglial-like cells which tend to drape delicate strands of tissue.

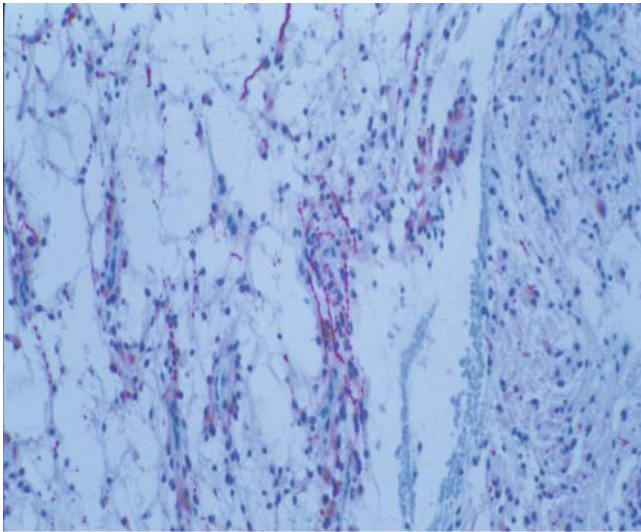


Fig. 26.5-3. DNET. The neuronal component is stained with anti-neurofilament.

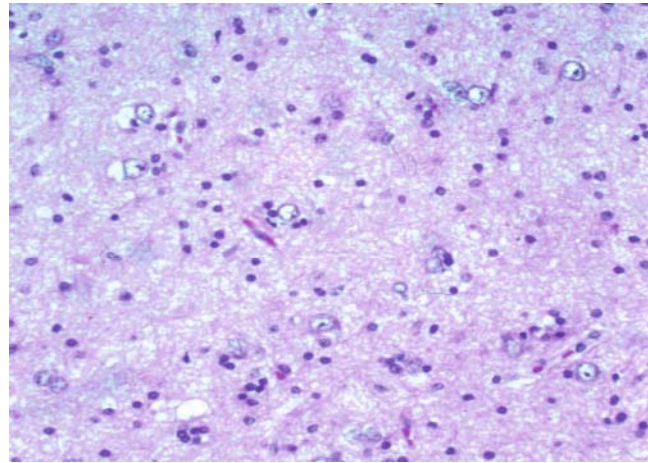


Fig. 26.5-4. Ganglioglioma composed of neurons and astrocytes with a delicate vasculature. H&E.

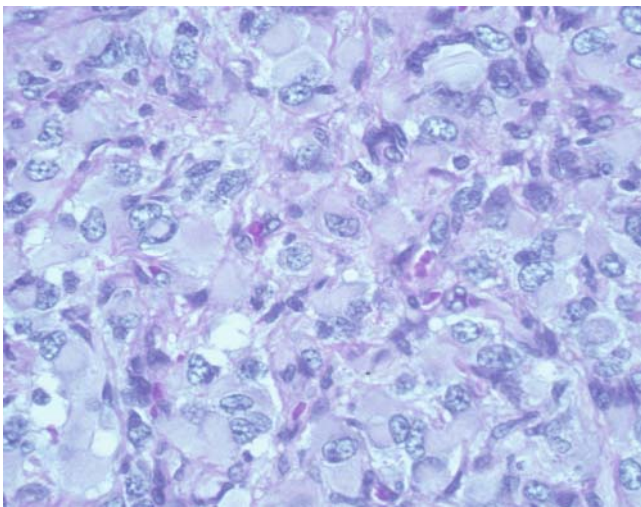


Fig. 26.5-5. Desmoplastic infantile ganglioglioma with a mixture of mature neurons and astrocytes. H&E.

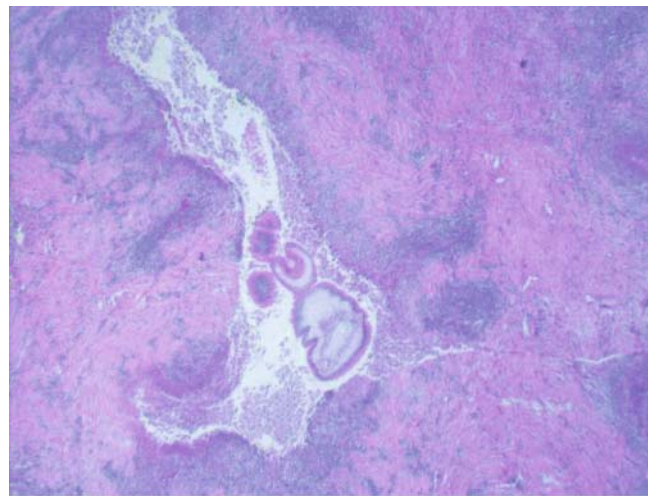


Fig. 26.5-6. Brain mass and inflammation caused by cysticercosis. H&E.

27 Accidents, Sudden Death

27.1 Trauma During Infancy

Head and brain injury after birth may be the result of accidental trauma or nonaccidental trauma. Impact injuries can be divided into those in which the head is struck by an object, as with a blow, or the head hits a surface, as with a fall. In the former circumstance, the head may be struck by a hand, fist, elbow, or foot or by a held or falling object. When the blow is by a “blunt” instrument, it usually leaves no identifying mark.

Analysis of bruises is an important aspect of the forensic examination. A primary principle, especially in infants and children, is that the degree of physical injury

to underlying tissues and organs may not correspond in severity to the surface bruising. Usually the underlying injuries are more extensive and severe than one would be led to expect on the basis of external injuries alone. Correlating external injuries with internal injuries at autopsy is vital. It requires diagrams, sketches, a verbal description, or photographs as well as a histological sample of many or all external injuries for evaluating the process of aging and for dating the lesions. No special permission need be obtained if the autopsy has been officially requested or ordered [1].

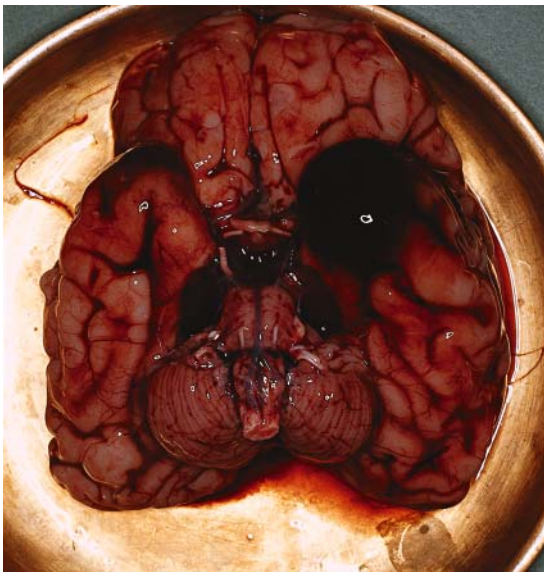


Fig. 27.1-1. Head trauma. Subarachnoid hemorrhages are found at the left temporal tip and brain stem in an infant.

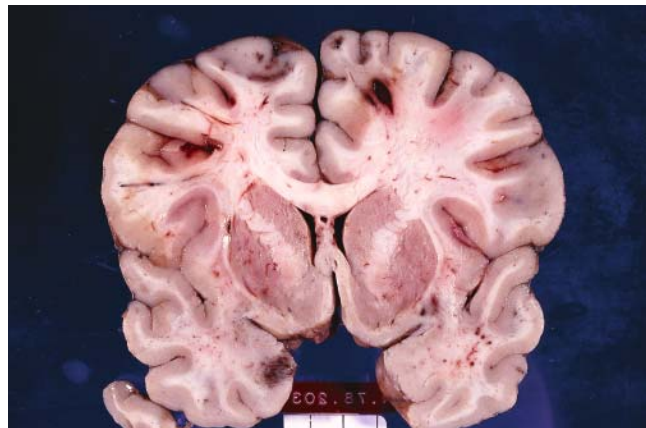


Fig. 27.1-2. Head trauma. Subarachnoid and cortical hemorrhages in the deep sulci of the frontal lobes.



Fig. 27.1-3. Head trauma. Pontine hemorrhage.

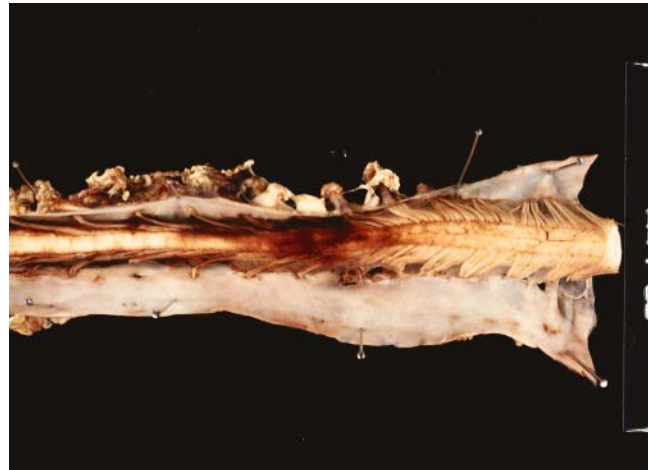


Fig. 27.1-4. Motor vehicle accident and cervical-to-thoracic spinal cord hemorrhage.

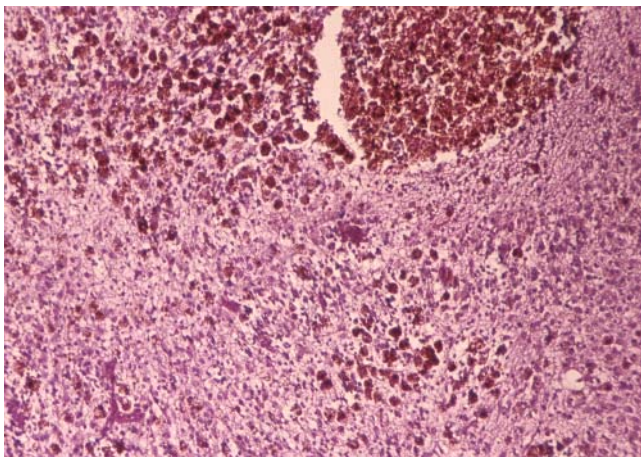


Fig. 27.1-5. Head injury. Remote hemorrhage with hemosiderin-laden macrophages.

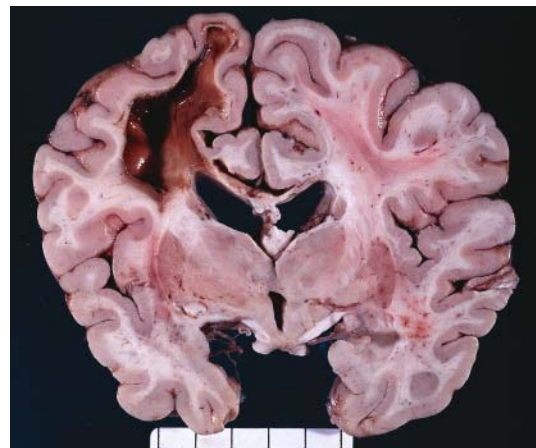


Fig. 27.1-6. Head injury. Cavity formation and hemosiderin deposition in remote lesions of a subcortical hemorrhage.

27.2 Sudden Infant Death Syndrome

Sudden infant death syndrome (SIDS) accounts for 26%–46% of all post neonatal deaths, and its cause is unknown. It is defined as “the sudden death of an infant under 1 year of age which remains unexplained after a thorough case investigation, examination of the death scene, and review of the clinical history.” Characteristics of SIDS are (1) victims are found apneic or dead in their cribs, when asleep, or in transition between sleep and waking; (2) there are no pathological or circumstantial findings at autopsy to adequately explain death; (3) victims are less than 1 year of age, usually 2–4 months; (4) the male/female ratio is 60:40; (5) there is a seasonal drop in cases between March and September; (6) the incidence of SIDS has decreased from 2/1000 to less than 0.5/1000 live births per year since the campaign of placing babies to sleep in the supine position in a no-smoking environment. The factors that may contribute to the risk of prone sleeping include rebreathing of

expired gases, hypoxia, asphyxia, upper airway obstruction, impaired arousal mechanisms, and compromised upper airway reflexes. These factors suggest that there is impaired brain stem activity. A triple-risk hypothesis for SIDS suggests that SIDS occurs when three factors are present: an underlying vulnerability in the infant’s homeostatic mechanisms; a critical developmental period for autonomic, respiratory, and arousal reflexes; and an exogenous stressor such as hypoxia, hypercapnea, reflex apnea in the prone position, or hyperthermia from overbundling [1,2].

In the brains of SIDS victims, there are subtle pathological changes, such as subcortical leukomalacia [3], brain stem gliosis [4], delayed development of dendritic spines and abnormalities of catecholaminergic and serotonergic neurons in respiratory centers [5–7]. These various lesions may be indicative of the infants’ underlying vulnerability in their brain stem homeostatic mechanisms.

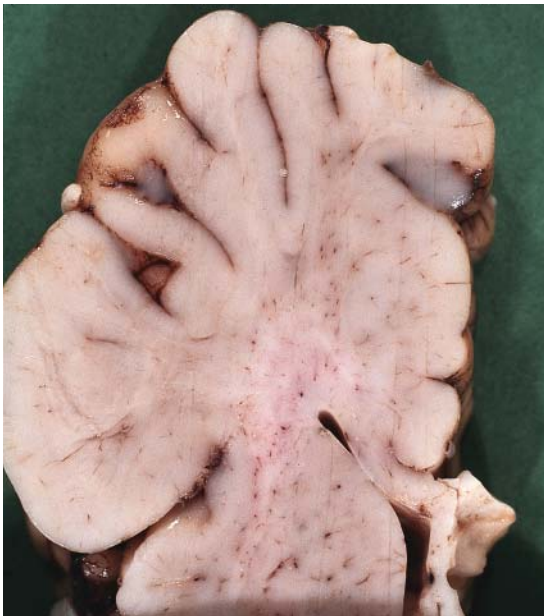


Fig. 27.2-1. Sudden infant death syndrome (SIDS). Section of cerebral hemisphere showing focal translucent area of subcortical leukomalacia underneath the cortex of the deep sulcus.

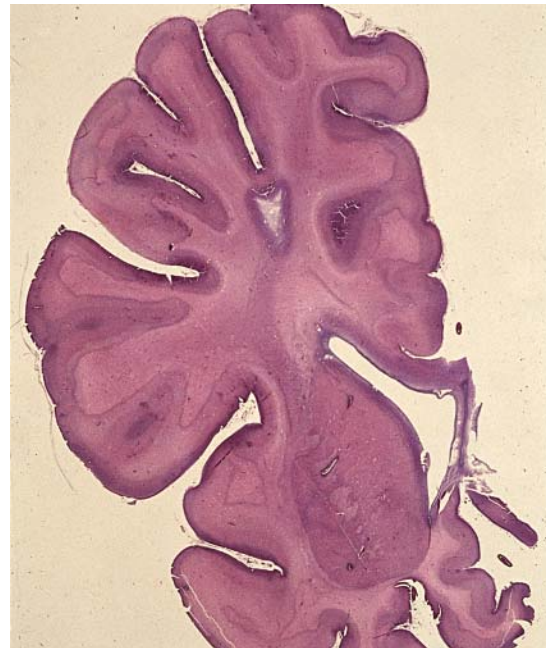


Fig. 27.2-2. Whole mount of cerebral hemisphere with subcortical leukomalacia. PTAH.

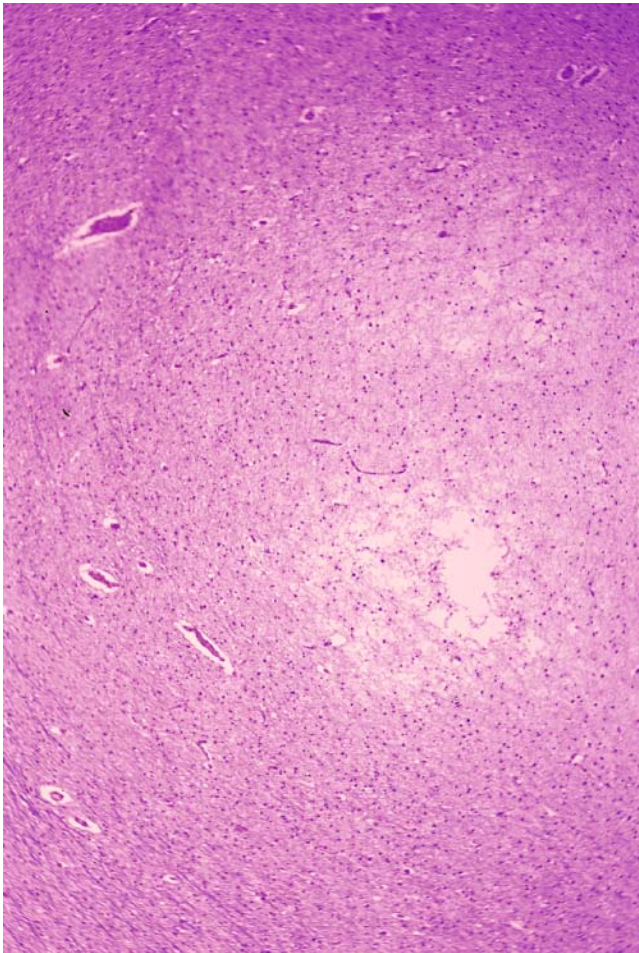


Fig. 27.2-3. Histology of subcortical leukomalacia shows rarefaction area with spongy changes.

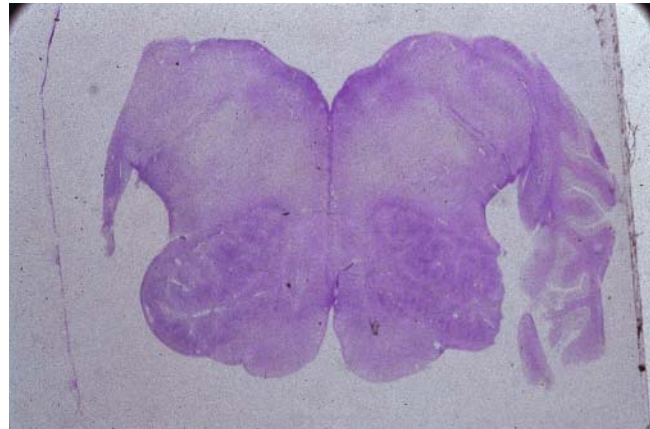


Fig. 27.2-4. Gliosis in the tegmentum of the medulla oblongata. Holzer stain.

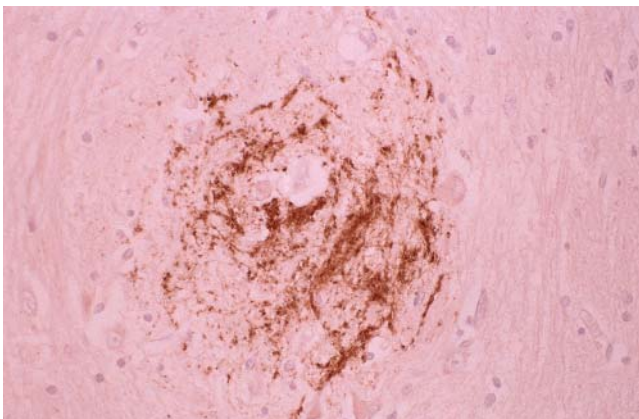


Fig. 27.2-5. Substance P immunoreactivity in the trigeminus nucleus.

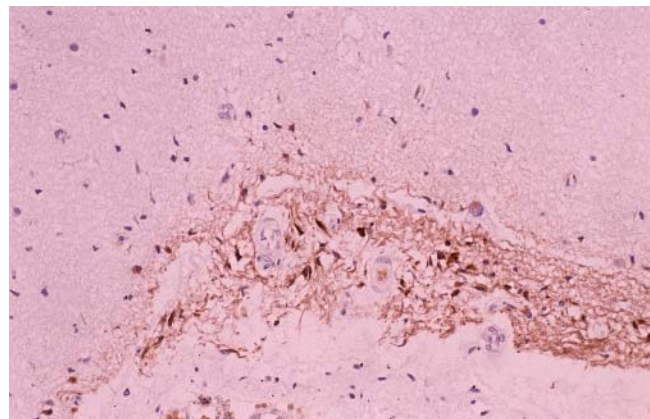


Fig. 27.2-6. Incidental leptomeningeal glioneuronal heterotopia in the base of a SIDS brain. GFAP.

27.3 Child Abuse

Whiplash or shaking injuries involving the brain are unique forms of willful trauma seen almost exclusively in infants. Shaking is particularly dangerous because the infant has insufficient strength to control the head owing to the disproportionate mass of the head and the lack of muscular development and coordination in the neck. The head “whips” back and forth in response to shaking, imposing accelerative and decelerative forces on the brain, meninges, and eyes. There is controversy as to whether an impact injury is also required when severe brain injury occurs. The injuries of child abuse include retinal hemorrhage, epidural and subdural hem-

orrhage, subarachnoid hemorrhage, cerebral contusion, white matter injury, and diffuse axonal injury [1]. A careful examination of the infant is mandatory. The external injuries appear less severe than the internal injuries.

Inflicted traumatic brain injury often results in subdural, subarachnoid, retinal, and optic nerve sheath hemorrhage. Recent hemorrhage sometimes is associated with hemosiderin-containing macrophages, suggesting repeated trauma. β -amyloid precursor protein immunostains may be helpful in illustrating the traumatic nature of the injuries [8].

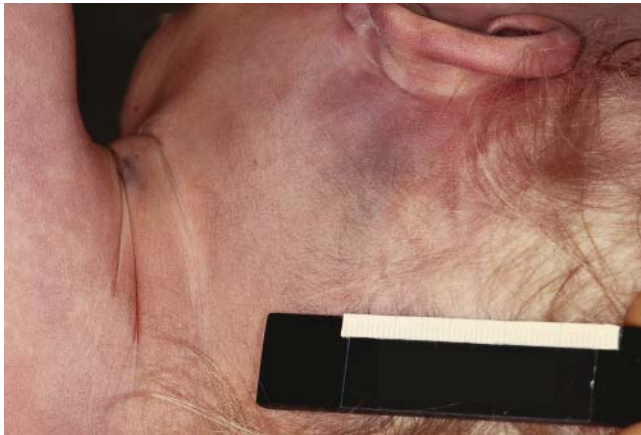


Fig. 27.3-1. Child abuse. Subcutaneous hemorrhage in the retroauricular region.

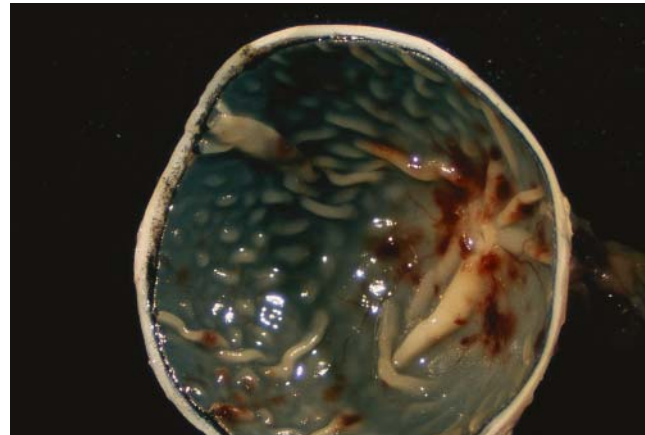


Fig. 27.3-2. Child abuse. Hemorrhage in the retina.



Fig. 27.3-3. Child abuse. Dura mater with chronic subdural hematoma showing fibrous thickening and recent hemorrhage.

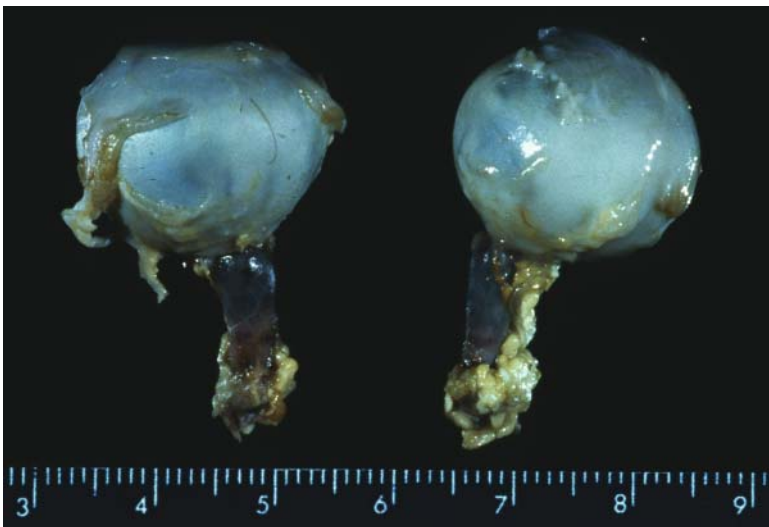


Fig. 27.3-4. Child abuse. Optic nerve sheath hemorrhage. There are hematomas in the retrobulbar optic nerve sheaths of bilateral eyes in a case of shaking baby syndrome.



Fig. 27.3-5. Head injury. Petechial hemorrhage in the corpus callosum and cortical infarction.

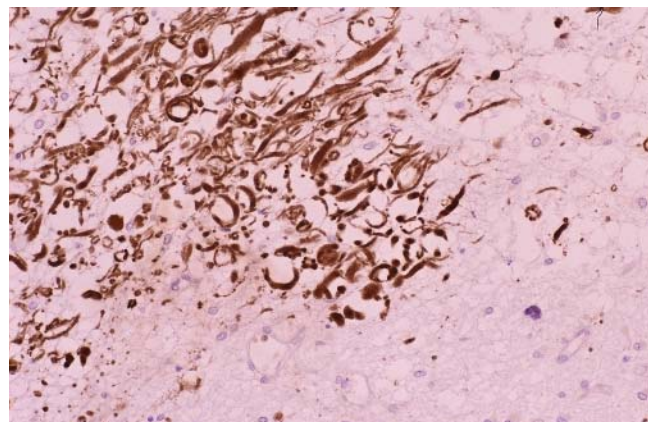


Fig. 27.3-6. Brain trauma. Axonal injury in the white matter expressing amyloid precursor protein immunoreactivity.

References

1 Normal Development

1. Pryse-Davies J, Beard RW (1973) A necropsy study of brain swelling in the newborn with special reference to cerebral herniation. *J Pathol* 109:51–73.
2. Gilles FH, Levinton A, Dooling EC (1983) The developing human brain. John Wright, Boston, pp 117–183.
3. Sanes DH, Reh TA, Harris WA (2000) Development of the nervous system. Academic, San Diego.
4. Bayer S, Altman J (1991) Neocortical development. Raven, New York.
5. Rakic P (1972) Mode of cell migration to the superficial layers of fetal monkey neocortex. *J Comp Neurol* 145:61–84.
6. Conte JE, Golden JA, Kipps J, Zurlinden E (2004) *Lis1* is necessary for normal non-radial migration of inhibitory neurons. *Am J Pathol* 16:775–784.
7. Deguchi K, Inoue K, Avila W, Lopez-Terrada D, Antalffy B, Quattrocchi CC, Sheldon M, Mikoshiba K, D’Arcangelo (2003) Reelin and Disabled-1 expression in developing and mature human cortical neurons. *J Neuropathol Exp Neurol* 62:676–684.
8. Brun A (1965) The subpial granular layer of the fetal cerebral cortex in man: its ontogeny and significance in congenital cortical malformations. *Acta Pathol Microbiol Scand Suppl* 179.
9. Ben-Arie N, Bellen HJ, Armstrong D, McCall A, Gordadze PR, Guo Q, Matzuk MM, Zoghbi HY (1997) *Math1* is essential for genesis of cerebellar granule neurons. *Nature* 390:169–172.
10. Friede RL (1989) Developmental neuropathology. Springer, New York, pp 1–21.
11. Purpura DP (1975) Normal and abnormal neuronal development in the cerebral cortex of human fetal and young infant. In: Buchwald NA, Brazier MAB (eds) Mental retardation. Academic, San Diego, pp 141–169.
12. Sanes DH, Reh TA, Harris WA (2000) Development of the nervous system. Academic, San Diego.
13. Takashima S, Chan F, Becker LE, Armstrong DL (1980) Morphology of the developing visual cortex of the human infant: a quantitative and qualitative Golgi study. *J Neuropathol Exp Neurol* 39:487–501.
14. Back SA, Luo NL, Borenstein NS, Levine JM, Volpe JJ, Kinney HC (2001) Late oligodendrocyte progenitors coincide with the developmental window of vulnerability

for human perinatal white matter injury. *J Neurosci* 21:1302–1312.

15. Hasegawa M, Houdou S, Mito T, Takashima S, Asanuma K, Ohno T (1992) Development of myelination in the human fetal and infant cerebrum: a myelin basic protein immunohistochemical study. *Brain Dev* 14:1–6.
16. Berry M, Butt AM, Wilkin G, Perry VH (2002) Structure and function of glia in the central nervous system. In: Graham DI, Lantos PL (eds) Greenfield’s neuropathology, 7th edn, Vol 1. Arnold, London, pp 75–123.
17. Hirayama A, Okoshi Y, Hachiya Y, Ozawa Y, Ito M, Kida Y, Imai Y, Kohsaka S, Takashima S (2001) Early immunohistochemical detection of axonal damage and glial activation in extremely immature brains with periventricular leukomalacia. *Clin Neuropathol* 20:87–91.
18. Takashima S, Becker LE (1983) Developmental changes of glial fibrillary acidic protein in cerebral white matter. *Arch Neurol* 40:14–18.
19. Takashima S, Tanaka K (1987) Development of cerebrovascular architecture and its relationship to periventricular leukomalacia in infancy. *Arch Neurol* 35:11–16.
20. Inage YW, Itoh M, Takashima S (2000) Correlation between cerebrovascular maturity and periventricular leukomalacia. *Pediatr Neurol* 22:204–208.

2 Malformations

1. Lemire RJ, Loeser JD, Leech RW, Alvord EC (1975) Normal and abnormal development of the human nervous system. Hagerstown, MD, Harper & Row, pp 54–69.
2. Harding B, Copp AJ (2002) Malformations. In: Graham DI, Lantos PL (eds) Greenfield’s neuropathology, 7th edn, Vol 1. Arnold, London, pp 375–392, 410–416, 429–432, 457–460.
3. Wald NJ, Law MR, Morris JK, Wals DS (2001) Quantifying the effects of folic acid. *Lancet* 358:2069–2073.
4. MRC Vitamin Study Research Group (1991) Prevention of neural tube defects: results of the Medical Research Council Vitamin Study. *Lancet* 338:131–137.
5. Copp AJ (1994) Genetic models of mammalian neural tube defects. In: Bock G, Marsh J (eds) Neural tube defects. Ciba Foundation Symposium 181. Wiley, Chichester, pp 118–134.

6. Greene NDE, Copp AJ (1997) Inositol prevents folate-resistant neural tube defects in the mouse. *Nat Med* 3:60–66.
7. Mitchell LE (2005) Epidemiology of neural tube defects. *Am J Med Genet* 135:88–94.
8. Nishimura H, Okamoto N (1972) Iniencephaly. In: Vinken PJ, Bruyn GW (eds) *Handbook of clinical neurology*, Vol 30. North-Holland, New York, pp 257–268.
9. Lemire RJ, Beckwith JB, Shepard TH (1972) Iniencephaly and anencephaly with spinal retroflexion: a comparative study of 8 human specimens. *Teratology* 6:27–36.
10. Lemire RJ, Loeser JD, Leech RW, Alvord EC (1975) Normal and abnormal development of the human nervous system. Harper & Row, Hagerstown, MD, pp 54–69.
11. Friede RL (1989) *Developmental neuropathology*. Springer-Verlag, Berlin, pp 248–262, 347–350.
12. Beuls E, Vanormelingen L, Van Aalst J, Vandersteen M, Adraenssens P, Cornips E, Vles H, Temel Y, Galen J (2003) The Arnold-Chiari type 2 malformation at midgestation. *Pediatr Neurosurg* 39:149–158.
13. Barkovich AJ, Kjo BO, Norman D, Edward MJ (1989). Revised classification of posterior fossa cysts and cyst-like malformations based on results of multiplanar MRI. *Am J Roentgenol* 153:289–300.
14. Hart MN, Malamud N, Ellis WG (1972) The Dandy-Walker syndrome: a clinicopathologic study based in 28 cases. *Neurology* 22:771–780.
15. Rayboud C (1982) Cystic malformations of the posterior fossa: abnormalities associated with the development of the roof of the fourth ventricle and adjacent meningeal structures. *J Neuroradiol* 9:103–133.
16. Cazor LA, Calleja MR, Verdu A, Felix V (2003) Dandy-Walker malformation in an infant with tetrasomy 9p. *Brain Dev* 25:220–223.
17. Metzke-Heidenmann S, Kuhling-von Kaisenberg H, Caliebe A, Janssen D, Jonat W, Grote W, von Kaisenberg CS (2004) Phenotypical variation in cousins with the identical partial trisomy 9 (pter-q22.2) and 7 (q35-qter) at 16 and 23 weeks gestation. *Am J Med Genet* 126:197–203.
18. Grinberg I, Northrupn H, Ardinger H, Prasad C, Dobyns WB, Millen KJ (2004) Heterozygous deletion of the linked genes ZIC1 and ZIC4 in Dandy Walker malformation. *Nat Genet* 36:1053–1055.
19. Ferland RJ, Eyaid W, Collura RV, Tully LD, Hill RS, Al-Nouri D, Al-Rumayyan A, Topcu M, Gascon G, Bodell A, Shugart YY, Ruvolo M, Walsh CA (2004) Abnormal cerebellar development and axonal decussation due to mutations in AHI1 in Joubert syndrome. *Nat Genet* 36:1008–1013.
20. Dixon-Salazar T, Silhavy JL, Marsh SE, Loue CM, Scott LC, Girura JA, Al-Gazali L, Al-Gzal AL, Tawari AA, Kayaserili H, Sztriha L, Gleeson JG (2004) Mutations in the AHI1 gene, encoding joubertin, cause Joubert syndrome with cortical polymicrogyria. *Am J Hum Genet* 75:979–987.
21. Lagier-Tourenne C, Boltshauser E, Breivik N, Gribaa M, Betard C, Barbot C, Koenig M (2004) Homozygosity mapping of a third Joubert syndrome locus to 6q23. *J Med Genet* 41:273–277.
22. Mizuguchi M, Maekawa S, Kamoshita S (1994) Distribution of leptomeningeal glioneuronal heterotopia in alobar holoprosencephaly. *Arch Neurol* 51:951–954.
23. Wallis DE, Roessler E, Hehr U, Nanni L, Richier-Costa A, Gillissen-Kaesbach G, Zackai EH, Rommens J, Muenke M (1999) Mutations in the homeodomain of the human SIX3 gene cause holoprosencephaly. *Nat Genet* 22:196–198.
24. Brown LY, Odent S, David V, Blayau M, Dubourg C, Apacik C, Delgado MA, Hall BD, Reynolds JF, Sommer A, Wiczorek D, Brown SA, Muenke M (2001) Holoprosencephaly due to mutations in ZIC2: alanine tract expansion mutations may be caused by parental somatic recombination. *Hum Mol Genet* 10:791–796.
25. Aguilla C, Dubourg C, Attia-Sobol J, Vigneron J, Blayau M, Pasquier L, Lazaro L, Odent S, David V (2002) Molecular screening of the TGIF gene in holoprosencephaly: identification of two novel mutations. *Hum Genet* 112:131–134.
26. Brown LY, Kottmann AH, Brown S (2003) Immunological localization of Zic2 expression in the developing mouse forebrain. *Gene Expr Patterns* 3:361–367.
25. Schell-Apacik C, Rivero M, Knepper JL, Roessler E, Muenke M, Ming JE (2003) SONIC HEDGEHOG mutations causing human holoprosencephaly impair neural patterning activity. *Hum Genet* 113:170–177.
27. Sarnat HB, Flores-Sarnat L (2001) Neuropathologic research strategies in holoprosencephaly. *Child Neurol* 16:918–931.
28. Loeser JD, Ellsworth CA, Alvord EC (1968) Agenesis of the corpus callosum. *Brain* 91:533–570.
29. Aicardi J (2005) Aicardi syndrome. *Brain Dev* 27:164–171.
30. Fox JW, Lamperti ED, Eksioglu YZ, Hong SE, Feng Y, Graham DA, Scheffer IE, Dobyns WB, Hirsch BA, Radtke RM, Berkovic SF, Huttenlocher PR, Walsh CA (1998) Mutations in filamin 1 prevent migration of cerebral cortical neurons in human periventricular heterotopia. *Neuron* 21:1315–1325.
31. Kakita A, Hayashi S, Moro F, Guerrini R, Ozawa T, Ono K, Kaneyama S, Walsh CA, Takahashi H (2002) Bilateral periventricular nodular heterotopia due to filamin 1 gene mutation: widespread glomerular microvascular anomaly and dysplastic cytoarchitecture in the cerebral cortex. *Acta Neuropathol (Berl)* 104:649–657.
32. Guerrini R, Filippi Y (2005) Neuronal migration abnormalities, genetics and epileptogenesis. *J Child Neurol* 20:287–299.
33. Gleeson JG, Allen KM, Fox JW, Lamperti ED, Berkovic S, Scheffer I, Cooper EC, Dobyns WB, Minneram SR, Ross ME, Walsh CA (1998) Doublecortin, a brain-specific gene mutated in human X-linked lissencephaly and double cortex syndrome, encodes a putative signaling protein. *Cell* 92:63–72.
34. Hattori M, Adachi H, Tsujimoto M, Arai H, Inoue K (1994) Miller-Dieker lissencephaly gene encodes a subunit

- of brain platelet-activating factor acetylhydrolase. *Nature* 370:216–218.
35. Reiner O, Carrozzo R, Shen Y, Wehnert M, Faustinella F, Dobyns WB, Caskey CT, Ledbetter DH (1993) Isolation of Miller-Dieker lissencephaly gene containing G protein beta-subunit-like repeats. *Nature* 364:717–721.
 36. Guerrini R, Filippi Y (2005) Neuronal migration abnormalities, genetics and epileptogenesis. *J Child Neurol* 20:287–299.
 37. Kato M, Das S, Petras K, Kitamura K, Morohashi K, Abuelo DN, Barr M, Bonneau D, Brady AF, Carpenter NJ, Cipero KL, Frisone F, Fukuda T, Guerrini R, Iida E, Itoh M, Lewanda AF, Nanba Y, Oka A, Proud VK, Saugier-Verber P, Schelley SL, Selicorni A, Shaner R, Silengo M, Stewart F, Sugiyama N, Toyama J, Toutain A, Vargaas AL, Yanazawa M, Zackai EH, Dobyns WB (2004) Mutations of ARX are associated with striking pleiotrophy and consistent genotype-phenotype correlation. *Hum Mutat* 23:147–159.
 38. Kato M, Dobyns WB (2005) X-linked lissencephaly with abnormal genitalia as a tangential migration disorder causing intractable epilepsy; proposal for a new term, “interneuronopathy.” *J Child Neurol* 20:392–397.
 39. Damska M, Wisniewski K, Sher JH (1983) Lissencephaly: two distinct clinico-pathologic types. *Brain Dev* 5:302–310.
 40. Kato M, Dobyns WB (2003) Lissencephaly and the molecular basis of neuronal migration. *Hum Mol Genet* 12: R89–R96.
 41. Mizuguchi M, Takashima S, Kakita A, Yamada M, Ikeda K (1995) Lissencephaly gene product: localization in the central nervous system and loss of immunohistochemistry in Miller-Dieker syndrome. *Am J Pathol* 147:1142–1151.
 42. Takashima S, Chan F, Becker LE, Kuruta H (1991) Aberrant neuronal development in hemimegalencephaly: immunohistochemical and Golgi studies. *Pediatr Neurol* 7:275–280.
 43. Yu J, Baybis M, Lee A, McKhann G, Chugani D, Kupsky WJ, Aronica E, Crino PR (2005) Targeted gene expression analysis in hemimegalencephaly: activation of beta-catenin signaling. *Brain Pathol* 15:179–186.
 44. Darras BT (1997) Neuromuscular disorders in the newborn. *Clin Perinatol* 24:827–844.
 45. Saito Y, Mizuguchi M, Oka A, Takashima S (2000) Fukutin protein is expressed in neurons of the normal developing human brain but is reduced in Fukuyama-type congenital muscular dystrophy brain. *Ann Neurol* 47:756–764.
 46. Toda TM, Segawa M, Nomura Y, Nonaka I, Masuda K, Ishihara T, Sakai M, Tomita I, Origuchi Y, Suzuki MI (1993) Localization of a gene for Fukuyama type congenital muscular dystrophy to chromosome 9q31–33. *Nat Genet* 5:283–286.
 47. Yamamoto T, Kato Y, Kawaguchi M, Shibata N, Kobayashi M (2004) Expression and localization of fukutin, POMGnT1, and POMT1 in the central nervous system: consideration for functions of fukutin. *Med Electron Microsc* 37:200–207.
 48. Takada K, Nakamura H, Takashima S (1988) Cortical dysplasia in Fukuyama congenital muscular dystrophy (FCMD): a Golgi and angioarchitectonic analysis. *Acta Neuropathol (Berl)* 76:170–178.
 49. Beltran-Valero de Bernabe D, Currier S, Steinbrecher A, Celli J, van Beuskom E, van der Zwaag B, Kayserili H, Merlini L, Chitayat D, Dobyns WB, Cormand B, Lehesjoki AE, Cruces J, Voit T, Walsh CA, van Bokhoven H, Brunner HG (2002) Mutations in O-mannosyltransferase gene POMT-1 gives rise to severe neuronal migration disorder Walker-Warburg syndrome. *Am J Hum Genet* 51:1032–1043.
 50. Michele DE, Barresi K, Kanagawa Manito F, Cohn RD, Satz JS, Dollar J, Nishino I, Kelley RI, Somer H, Straub V, Mathews K, Moore SA, Campbell KP (2002) Post translational disruption of dystroglycan–ligand interactions in congenital muscular dystrophies. *Nature* 418:376–377.
 51. Yoshida A, Kobayashi K, Many H, Taniguchi K, Kano H, Mizuno M, Inazu T, Mitsuhashi H, Takahashi S, Takeuchi M, Herrmann R, Straub V, Talim B, Voit T, Topaloglu H, Toda T, Endo T (2001) Muscular dystrophy and neuronal migration disorder caused by mutations in a glycosyltransferase, POMGnT1. *Dev Cell* 1:717–724.
 52. Yamamoto T, Kato Y, Kawaguchi M, Shibata N, Kobayashi M (2004) Expression and localization of fukutin, POMGnT1, and POMT1 in the central nervous system: consideration for functions of fukutin. *Med Electron Microsc* 37:200–207.
 53. Jansen A, Andermann E (2005) Genetics of the polymicrogyria syndromes. *J Med Genet* 42:369–378.
 54. Piao X, Basel-Vanagaite L, Straussberg R, Grant PE, Pugh EW, Doheny K, Doan B, Hong SE, Shugart YY, Walsh CA (2002) An autosomal recessive form of bilateral frontoparietal polymicrogyria maps to chromosome 16q12.2–21. *Am J Hum Genet* 70:1028–1033.
 55. Villard L, Nguyen K, Cardoso C, Martin CL, Weiss AM, Sifry-Platt M, Griix AW, Graham JM Jr, Winter RM, Leventer RJ, Dobyns WB (2002) A locus for bilateral perisylvian polymicrogyria maps to Xq28. *Am J Hum Genet* 70:1003–1008.
 56. Tsuru A, Mizuguchi M, Uemura K, Takashima S (1997) Abnormal expression of cell adhesion molecule L1 in migration disorders: a developmental immunohistochemical study. *Clin Neuropathol* 16:122–126.
 57. Chen CP, Chern SR, Chang TY, Lin CJ, Wang W, Tzen CY (2002) Second trimester diagnosis of a stop codon *FGFR3* mutation in a type 1 thanatophoric dysplasia fetus following abnormal ultrasound findings. *Prenatal Diagn* 22:736–737.
 58. Hevner RF (2005) The cerebral cortex malformation in thanatophoric dysplasia: neuropathology and pathogenesis. *Acta Neuropathol (Berl)* 110:208–221.
 59. Bickers DS, Adams RD (1949) Hereditary stenosis of aqueduct of Sylvius as a cause of congenital hydrocephalus. *Brain* 72:246–262.
 60. Fukumizu M, Becker LE, Takashima S (1994) Periaqueductal microdysplasia in children with congenital aqueductal stenosis. *Clin Neuropathol* 13:46–52.
 61. Fryns JP, Spaepen A, Cassiman JJ, van den Berghe H (1991) X-linked complicated spastic paraplegia, MASA

- syndrome and X-linked hydrocephalus owing to congenital stenosis of the aqueduct of Sylvius: variable expression of the same mutation at Xq28. *J Med Genet* 28:429.
62. Schrander-Stumpel C, Meyer H, Merckx D, Jones M, Israel I, Sommer A, Stevens C, Tinschert S, Wilson S, Willems P (1994) The spectrum of complicated spastic paraplegia, MASA syndrome and X-linked hydrocephalus: contribution of DNA linkage analysis in genetic counseling of individual families. *Genet Counsel* 5:1–10.
 63. Fowler M, Dow R, White TA, Greer CH (1972) Congenital hydrocephalus-hydranencephaly in five siblings with autopsy; a new disease. *Dev Med Child Neurol* 14: 173–188.
 64. Debus OM, Kosch A, Strater R, Rossi R, Nowak-Gottl U (2004) The factor V G1691A mutation is a factor for porencephaly: a case-control study. *Ann Neurol* 56:287–290.
 65. Manson J, Speed I, Abbott K, Crompton J (1988) Congenital blindness, porencephaly, and neonatal thrombocytopenia; a report of 4 cases. *J Child Neurol* 3:120–124.
 66. Brunelli S, Faiella A, Capra V, Nigro V, Simeone A, Cama A, Boncinelli E (1996) Germline mutations in the homeobox gene EMX2 in patients with severe schizencephaly. *Nat Genet* 12:94–96.
 67. Armstrong D (1995) Neonatal encephalopathies. In: Duckett S (ed) *Pediatric neuropathology*. Williams & Wilkins, Baltimore, pp 334–351.
 68. Mito T, Ando Y, Takeshita K, Takada K, Takashima S (1989) Ultrasonographical and morphological examination of subependymal cystic lesions in maturely born infants. *Neuropediatrics* 20:211–214.
 69. Lantos P, Louis D, Rosenblum MK, Kleihues P (2002) In: Graham DI, Lantos PL (eds) *Greenfield's neuropathology*, 7th edn. Arnold, London, pp 966–970.
 70. Muenk M, Schell U, Hehr A, Robin NH, Losken HW, Schinzel A, Pulleyn LJ, Rutlama P, Reardon W, Malcolm S (1994) A common mutation in the fibroblast growth factor receptor 1 gene in Pfeiffer syndrome. *Nat Genet* 8:268.
 71. Wilkie AOM, Slaney SF, Oldridge M, Poole MD, Pulleyn LJ, Rutland P (1995) Apert syndrome results from localized mutations of FGFR2 and is allelic with Crouzon syndrome. *Nat Genet* 9:165–172.
 72. Kytälä M, Tallila J, Salonen R, Kopra O, Kohlschmidt N, Paavola Sakkio P, Peltonen L, Kestila M (2006) MKS1, encoding a component of the flagellar apparatus basal body proteome, is mutated in Meckel syndrome. *Nat Genet* 38:155–157.
 73. Morgan NV, Gissen P, Sharif SM, Baumber L, Sutherland J, Kelly DA, Aminu K, Bennett CP, Woods CG, Mueller RF, Trembath RC, Maher ER, Johnson CA (2002) A novel locus for Meckel-Gruber syndrome, MKS3 maps to chromosome 8q24. *Hum Genet* 111:456–461.
 74. Roume J, Genin E, Cormiere-Daire V, Ma HW, Mehaye B, Attie T, Razavi-Encha F, Fallet-Bianco C, Buenerd A, Clerget-Darpoux F, Munnich A, Le Merrer M (1998) A gene for Meckel syndrome maps to chromosome 11q13. *Am J Hum Genet* 63:1095–1101.
 75. Smith UM, Consugar M, Tee LJ, McKee BM, Maina EN, Whelan S, Morgan NV, Goranson E, Gissen P, Lillquist S, Aligianis IA, Ward CJ, Pasha S, Punyashthiti R, Malik D, Harif S, Batman PA, Bennett CP, Woods CG, McKeown C, Bucourt M, Miller CA, Cox P, Algazali L, Tomcat RC, Torres VE, Attie-Bitah T, Kelly DA, Maher ER, Gattone VH 2nd, Harris PC, Johnson CA (2006) The transmembrane protein meckelin (MKS3) is mutated in Meckel-Gruber syndrome and the wpk rat. *Nat Genet* 38:191–196.
 76. Verzijl HT, Valk J, de Vries R, Padberg GW (2005) Radiologic evidence for absence of the facial nerve in Mobius syndrome. *Neurology* 64:849–855.
 77. Verzijl HT, van der Zwag B, Lammens M, Donkelaar HJ, Padberg GW (2005) The neuropathology of hereditary congenital facial palsy vs. Mobius syndrome. *Neurology* 64:649–653.
 78. Dixon-Salazar T, Silhavy JL, Marsh SE, Louie CM, Scott LC, Gururaj A, Al-Gazal L, Al-Tawari AA, Kayserili H, Sztriha L, Gleeson JG (2004) Mutations in the AHI1 gene, encoding joubertin, cause Joubert syndrome with cortical polymicrogyria. *Am J Hum Genet* 75:979–987.
 79. Ferland RJ, Eyaid W, Collaura RV, Tully LD, Hill RS, Al-Nouri D, Al-Rumayyan A, Topcu M, Gascon G, Bodell A, Shugart YY, Ruvolo M, Walsh CA (2004) Abnormal cerebellar development and axonal decussation due to mutations in AHI1 in Joubert syndrome. *Nat Genet* 36:1008–1013.
 80. Gardner WJ, Karnosh LJ, Angel L (1957) Syringomyelia: a result of embryonal atresia of foramen of Magendie. *Trans Am Neurol Assoc* 82:144–145.
 81. Albrecht S, Schneider MC, Belmont J, Armstrong DL (1993) Fatal infantile encephalopathy with olivopontocerebellar hypoplasia and micrencephaly. *Acta Neuropathol (Berl)* 85:394–399.
 82. Hashimoto K, Takeuchi Y, Kida Y, Hasegawa H, Kantake M, Sasaki A, Asanuma K, Isumi H, Takashima S (1998) Three siblings of fatal infantile encephalopathy with olivopontocerebellar hypoplasia and microcephaly. *Brain Dev* 20:169–174.
 83. Horslen SP, Clayton PT, Harding BN, Hall NA, Keir G, Winchester B (1991) Olivopontocerebellar atrophy with neonatal onset and disialotransferrin developmental deficiency syndrome. *Arch Dis Child* 66:1027–1032.
 84. Chou SM, Gilbert EF, Chum RWM, Loxava R, Tuffli GA, Sufit RL, Krassikot N (1990) Infantile olivopontocerebellar atrophy with spinal muscular atrophy (infantile OPCA+SMA). *Clin Neuropathol* 9:21–32.
 85. Patel MS, Becker LE, Toi A, Armstrong DL, Chitayat D (2006) Severe fetal onset form of olivopontocerebellar hypoplasia in three sibs: PCH type 5? *Am J Med Genet* 140:594–603.
 86. Rajab A, Mochida GH, Hill A, Ganesh V, Bodell A, Riaz A, Grant PE, Shugart YY, Walsh CA (2003) A novel form of pontocerebellar hypoplasia maps to chromosome 7q11–21. *Neurology* 60:1664–1667.

3 Chromosomal Abnormalities

1. Becker LE, Mito T, Takashima S, Onodera K, Friend WC (1993) Association of phenotypic abnormalities of Down syndrome with an imbalance of genes on chromosome 21. *APMIS Suppl* 40:57–70.
2. Takashima S, Becker LE (1985) Basal ganglia calcification in Down's syndrome. *J Neurol Neurosurg Psychiatry* 48:61–64.
3. Becker L, Mito T, Takashima S, Onodera K (1991) Growth and development of the brain in Down syndrome. *Prog Clin Biol Res* 373:133–152.
4. Takashima S, Becker LE, Armstrong DL, Chan F (1981) Abnormal neuronal development in the visual cortex of the human fetus and infant with Down's syndrome: a quantitative and qualitative Golgi study. *Brain Res* 225:1–21.
5. Hirayama A, Horikoshi Y, Maeda M, Ito M, Takashima S (2003) Characteristic developmental expression of amyloid beta 40, 42 and 43 in patients with Down syndrome. *Brain Dev* 25:180–185.
6. Motonaga K, Itoh M, Becker LE, Goto Y, Takashima S (2002) Elevated expression of beta-site amyloid precursor protein cleaving enzyme 2 in brains of patients with Down syndrome. *Neurosci Lett* 326:64–66.
7. Gullotta F, Rehder H, Gropp A (1981) Descriptive neuropathology of chromosomal disorders in man. *Hum Genet* 57:337–344.
8. Inagaki M, Ando Y, Mito T, Ieshima A, Ohtani K, Takashima S, Takeshita K (1987) Comparison of brain imaging and neuropathology in cases of trisomy 18 and 13. *Neuroradiology* 29:474–479.
9. Michaelson PS, Gilles FH (1972) Central nervous system abnormalities in trisomy E (17–18). *J Neurol Sci* 15: 193–208.
10. Maggio MC, Iachininoto R, Arena V, Liotta A (2003) Interstitial deletion of the long arm of chromosome 1(1q25–32): clinical and endocrine features with a long follow-up. *Minerva Pediatr* 55:55–61.
11. Lo LJ, Noordhoff MS, Huang CS, Chen KT, Chen YR (1993) Proximal deletion of the long arm of chromosome 1:[del(1)(q23–q25)]. *Cleft Palate Craniofac* 30: 586–589.
12. Titomanlio L, Romano A, Conti A, Genesio R, Salerno M, De Brasi D, Nitsch L, Del Giudice E (2004) Mild Wolf-Hirschhorn phenotype and partial GH deficiency in a patient with a 4p terminal deletion. *Am J Med Genet* 127:197–200.

4 Perinatal Brain Damage

1. Friede RL (1989) *Developmental neuropathology*. 2nd edn. Springer, Heidelberg, pp 28–43, 50–51, 61, 153.

2. Takashima S, Tanaka K (1978) Microangiography and vascular permeability of the subependymal matrix in the premature infants. *Can J Neurol Sci* 5:45–50.
3. Volpe JJ (2001) *Neurology of the newborn*, 4th edn. Saunders, Philadelphia, pp 304–307, 428–493, 699–701.
4. Fukumizu M, Takashima S, Becker LE (1995) Neonatal posthemorrhagic hydrocephalus: neuropathologic and immunohistochemical studies. *Pediatr Neurol* 13:230–234.
5. Takashima S (1982) Olivocerebellar lesions in infants born prematurely. *Brain Dev* 4:361–366.
6. Kinney HC, Armstrong DD (2002) In: Graham DI, Lantos P (eds) *Greenfield's neuropathology*, 7th edn, Vol 1. Arnold, London, pp 536–555.
7. Ansari MQ, Chincanchan CA, Armstrong DL (1990) Brain calcification in hypoxic-ischemic lesions: an autopsy review in children. *Pediatr Neurol* 6:94–101.
8. Banker QB, Larroche JC (1962) Periventricular leukomalacia of infancy: a form of neonatal anoxic encephalopathy. *Arch Neurol* 7:386–410.
9. Armstrong D, Norman M (1974) Periventricular leukomalacia in neonates; complications and sequelae. *Arch Dis Child* 49:367–375.
10. Hirayama A, Oka A, Ito M, Tanaka F, Okoshi Y, Takashima S (2003) Myelin transcription factor 1 (MyT1) immunoreactivity in infants with periventricular leukomalacia. *Dev Brain Res* 140:85–92.
11. Takashima S, Tanaka K (1978) Development cerebrovascular architecture and its relationship to periventricular leukomalacia. *Arch Neurol* 35:11–16.
12. Takashima S, Armstrong DL, Becker LE (1978) Subcortical leukomalacia. *Arch Neurol* 35:470–472.
13. Friede RL (1974) Pontosubicular lesions in perinatal anoxia. *Arch Pathol* 94:343–354.
14. Bruck Y, Bruck W, Kretzschmar HA, Lassmann H (1996) Evidence for neuronal apoptosis in pontosubicular neuron necrosis. *Neuropathol Appl Neurobiol* 22:23–29.
15. Isumi H, Uchida Y, Hayashi T, Furukawa S, Takashima S (2000) Neuron death and glial response in pontosubicular necrosis: the role of the growth inhibition factor. *Clin Neuropathol* 19:77–84.
16. Stadelman C, Mews I, Srinivasan A, Deckwerth TL, Lassmann H, Bruck W (2001) Expression of cell death-associated proteins in neuronal apoptosis associated with pontosubicular neuron necrosis. *Brain Pathol* 11:273–281.
17. Takashima S, Ichinohe A, Itoh M (2005) Pathogenesis and prevention of pontosubicular necrosis. *Neuroembryology* 3:42–46.
18. Torvik A, Skullerud K, Andersen SN, Hurum J, Maehlen J (1992) Affection of the hippocampal granule cells in pontosubicular neuron necrosis. *Acta Neuropathol (Berl)* 83:535–537.
19. Mito T, Kamei A, Takashima S, Becker LE (1993) Clinicopathological study of pontosubicular necrosis. *Neuropediatrics* 24:204–207.
20. Ozawa H, Fukuda T, Nishida A, Takashima S (1997) Cu, Zn-superoxide dismutase reaction in neonatal pontosubicular neuron necrosis. *Pediatr Neurol* 16:126–130.

21. Meng SZ, Itoh M, Obonai T, Takashima S (2000) Roles of glutamate transporter and receptors, poly (ADPribose) polymerase, and transforming growth factor- β 1 in pontosubicular neuron necrosis. *J Child Neurol* 15:362–369.
22. Gilles FH (1969) Hypotensive brain stem necrosis: selective symmetrical necrosis of tegmental neuronal aggregates following cardiac arrest. *Arch Pathol* 88:32–41.
23. Myers RE (1975) Four patterns of perinatal brain damage and their conditions of occurrence in primates. *Adv Neurol* 10:223.
24. Leech RW, Brumback RA (1988) Massive brain stem necrosis in the human neonate, presentation of three cases with review of the literature. *J Child Neurol* 3:258–262.
25. Roland EH, Hill A, Norman MG, Flodmark O, MacNab AJ (1988) Selective brain stem injury in an asphyxiated newborn. *Ann Neurol* 23:89–92.
26. Verzijl HT, Valk J, de Vries R, Padberg GW (2005) Radiologic evidence for absence of the facial nerve in Mobius syndrome. *Neurology* 64:849–855.
27. Verzijl HT, van der Zwag B, Lammens M, Donkelaar HJ, Padberg GW (2005) The neuropathology of hereditary congenital facial palsy vs. Mobius syndrome. *Neurology* 64:649–653.
28. Armstrong D, Sachis P, Bryan C, Becker L (1982) Pathological features of persistent infantile sleep apnea with reference to the pathology of sudden infant death syndrome. *Ann Neurol* 12:169–174.
29. Becker LE, Takashima S (1985) Chronic hypoventilation and development of brain stem necrosis. *Neuropediatrics* 16:189–123.
30. Tsuru A, Mizuguchi M, Takashima S (1995) Cystic leukomalacia in the cerebellar folia of premature infants. *Acta Neuropathol (Berl)* 90:400–402.
31. Ostrow JD, Pascolo L, Shapiro SM, Tiribelli C (2003) New concepts in bilirubin encephalopathy. *Eur J Clin Invest* 33:987–988.
5. Sahoo T, Johnson EW, Thomas JW, Kuehl PM, Jones TI, Dokken CG, Touchman JW, Gallione CJ, LeepLin SQ, Kosofsky B, Kurth JH, Louis DN, Mettler G, Morrison L, Gil-Nagel A, Rich SS, Zabramski JM, Bogus MS, Green ED, Marchuk DA (1999) Mutations in the gene encoding KRIT 1, a Krev-1/rap1a binding protein, cause cerebral cavernous malformations (CCM1). *Hum Mol Genet* 8:2325–2333.
6. Alberts MJ (1999) Subarachnoid hemorrhage and intracranial aneurysms. In: Albert MJ (ed) *Genetics of cerebrovascular disease*. Futura, New York, pp 237–259.
7. Hart RG, Kagan-Hallet K, Joerns SE (1987) Mechanisms of intracranial hemorrhage in infective endocarditis. *Stroke* 18:1048–1056.
8. Fukui M, Kono S, Sueishi K, Ikezaki K (2000) Moyamoya disease. *Neuropathology* 20(Suppl):S61–S64.
9. Ikeda H, Sasaki T, Yoshimoto T, Fukui M, Arinami T (1999) Mapping of a familial moyamoya disease gene to chromosome 3p24.2-p26. *Am J Hum Genet* 64:533–537.
10. Kalimo H, Kaste M, Haltia M (2001) Vascular diseases. In: Graham DI, Lantos PL (eds) *Greenfields' neuropathology*, 7th edn, Vol 1. Arnold, London, pp 281–342.
11. Barmada MA, Moossy J, Shuman RM (1979) Cerebral infarcts with arterial occlusion in neonate. *Ann Neurol* 6:495.
12. Eda I, Takashima S, Takeshita K (1983) Acute hemiplegia with lacunar infarct after varicella infection in childhood. *Brain Dev* 5:494–499.
14. Carvalho KS, Bodensteiner JB, Connolly PJ, Garg BP (2001) Cerebral venous thrombosis in children. *J Child Neurol* 16:574–580.
13. Friede RL (1989) *Developmental neuropathology*, 2nd edn. Springer, Heidelberg, pp 138–146.
15. Volpe JJ (2001) *Neurology of the newborn*, 4th edn. Saunders, Philadelphia, pp 315–323.

6 Increased Intracranial Pressure

1. Volpe JJ (2001) *Neurology of the newborn*, 4th edn. Saunders, Philadelphia, p 780.
2. Auer RN, Sutherland GR (2002) Hypoxia and related conditions. In: Graham DI, Lantos PL (eds) *Greenfields' neuropathology*, 7th edn, Vol I. Arnold, London, pp 233–264.

7 Neurocutaneous Syndromes

1. Maria BL, Deidrick KM, Roach ES, Gutmann DH (2004) Tuberous sclerosis complex. *J Child Neurol* 19:632–642.
2. Harding BN, Copp AJ (2001) Malformations. In: Graham DI, Lantos PL (eds) *Greenfields' neuropathology*, 7th edn, Vol 1. Arnold, London, pp 452–456.
3. Mizuguchi M, Takashima S (2001) Neuropathology of tuberous sclerosis. *Brain Dev* 23:508–515.

5 Vascular Diseases

1. Takashima S, Becker LE (1980) Neuropathology of cerebral arteriovenous malformations in children. *J Neurol Neurosurg Psychiatry* 43:380–385.
2. Vinters HV (2004) Pediatric vascular malformations. In: Golden JA, Harding BN (eds) *Pathology and genetics: developmental neuropathology*. ISN Neuropath Press, Basel, pp 116–124.
3. Labauge P, Enjolras O, Bonerandi JJ, Laberge S, Dandurand M, Joujoux JM, Tournier-Lasserre E (1999) An association between autosomal dominant cerebral cavernomas and a distinctive hyperkeratotic cutaneous vascular malformation. *Ann Neurol* 45:250–254.
4. Rigamonti D, Hadley MN, Drayer BP (1988) Cerebral cavernous malformations: incidence and familial occurrence. *N Engl J Med* 319:343–347.

4. Mizuguchi M, Kato M, Yamanouchi H, Ikeda K, Takashima S (1997) Loss of tuberlin from cerebral tissues with tuberous sclerosis and astrocytoma. *Ann Neurol* 42:270–272.
5. Lantos PL, Louis CN, Rosenblum MK, Kleihues (2001) In: Graham DI, Lantos P (eds) *Greenfields' neuropathology*, 7th edn, Vol 1. Arnold, London, pp 452–456.
6. Gutmann DH (2002) Neurofibromin in the brain. *J Child Neurol* 17:592–601.
7. Kato M, Mizuguchi M, Hattori S, Nakamura S, Takashima S (1998) Loss of neurofibromin in the leptomeningeal astroglial heterotopia of NF1. *Pediatr Neurol* 18:227–230.
8. Thomas-Sohl KA, Vaslow DF, Maria BL (2004) Sturge-Weber syndrome: a review. *Pediatr Neurol* 30:303–310.
9. Comi AM, Hunt P, Vawter MP, Pardo CA, Becker KG, Pevsner J (2003) Increased fibronectin expression in Sturge-Weber syndrome fibroblasts and brain tissue. *Pediatr Res* 53:762–769.
10. Chun HH, Gatti RA (2004) Ataxia telangiectasia, an evolving phenotype. *DNA Repair* 3:1187–1196.
11. Lowe JS, Leigh N (2001) In: Graham DI, Lantos PL (eds) *Greenfields' neuropathology*, 7th edn, Vol 2. Arnold, London, pp 364–365.
12. Oka A, Takashima S (1998) Expression of the ataxia-telangiectasia gene (ATM) product in human cerebellar neurons during development. *Neurosci Lett* 252:195–198.
8. Schuchman EH, Desnick RJ (1995) Niemann-Pick disease types A and B: acid sphingomyelinase deficiencies. In: Scriver CR, Beaudet AL, Sly WS, Valle RD (eds) *The metabolic and molecular basis of inherited disease*, 7th edn. McGraw-Hill, New York, pp 2601–2624.
9. Pentchev, P, Vanier MT, Suzuki K, Patterson MC (1995) Niemann-Pick disease type C: a cellular cholesterol lipodosis. In: Scriver CR, Beaudet AL, Sly WS, Valle RD (eds) *The metabolic and molecular basis of inherited disease*, 7th edn. McGraw-Hill, New York, pp 2625–2639.
10. Kurachi Y, Oka A, Itoh M, Mizuguchi M, Hayashi M, Takashima S (2001) Distribution and development of CLN2 protein, the late-infantile neuronal ceroid lipofuscinosis gene product. *Acta Neuropathol (Berl)* 102:20–26.
11. Mole SE (2004) The genetic spectrum of human neuronal ceroid-lipofuscinoses. *Brain Pathol* 14:70–76.
12. Zhang Z, Mandal AK, Mital A, Popescu N, Zimonjic D, Moser A, Moser H, Mukherjee AB (2000) Human acid ceramidase gene: novel mutations in Farber disease. *Mol Genet Metab* 70:30–39.

8 Lipidosis

1. Callahan JW (1999) Molecular basis of GM₁ gangliosidosis and Morquio disease, type B: structure-function studies of lysosomal β -galactosidase and nonlysosomal β -galactosidase-like protein. *Biochim Biophys Acta* 1455:89–103.
2. Suzuki K, Suzuki K (1996) The gangliosidoses. In: Moser (ed) *Neurodystrophies and neurolipidosis* (revised series 22). Elsevier, Amsterdam, pp 247–280.
3. Suzuki K, Suzuki K (2002) Lysosomal diseases. In: Graham DI, Lantos PL (eds) *Greenfields' neuropathology*, 7th edn, Vol 1. Arnold, London, pp 654–753.
4. Guazzi GC, D'Amore I, Van Hoof F, Fruschelli C, Alessandrini, Palmeri S, Federico A (1988) Type 3 (chronic) GM₁ gangliosidosis presenting as infant-choreo-athetotic dementia, without epilepsy, in three sisters. *Neurology* 38:1124–1127.
5. Gravel RA, Clarke JTR, Kaback D (1995) The GM₂ gangliosidosis. In: Scriver CR, Beaudet AL, Sly WS, Valle RD (eds) *The metabolic and molecular basis of inherited disease*, 7th edn. McGraw-Hill, New York, pp 2639–2679.
6. Balicki D, Beutler E (1995) Gaucher disease. *Medicine* 74:305–323.
7. Beutler E, Grabowski GA (1995) Gaucher disease. In: Scriver CR, Beaudet AL, Sly WS, Valle D (eds) *The metabolic and molecular basis of inherited disease*. McGraw-Hill, New York, pp 2641–2670.

9 Mucopolipidosis

1. Sohma O, Mizuguchi M, Takashima S, Satake A, Itoh K, Sakuraba H, Suzuki Y, Oyanagi K (1999) Expression of protective protein in human tissue. *Pediatr Neurol* 20:210–214.
2. Lyon G, Adams RD, Kolodny EH (1996) *Neurology of hereditary metabolic diseases in childhood*, 2nd edn. McGraw-Hill, New York, pp 132–135, 161–164.
3. Suzuki K, Suzuki K (2002) Lysosomal diseases. In: Graham DI, Lantos PL (eds) *Greenfields' neuropathology*, 7th edn, Vol 1. Arnold, London, pp 675–679, 683–693, 699–700, 708–709.
4. Seyrantep V, Poupetova H, Froissart R, Zabot MT, Maire I, Pshezhetsky AV (2003) Molecular pathology of *NEU1* gene in sialidosis. *Hum Mutat* 22:343–352.

10 Glycogen Storage Disease

1. Suzuki K, Suzuki K (2002) Lysosomal diseases. In: Graham DI, Lantos PL (eds) *Greenfields' neuropathology*, 7th edn, Vol 1. Arnold, London, pp 713–714.

11 Peroxisomal Disorders

1. Shimozawa N, Nagase T, Takemoto Y, Kondo N, Suzuki Y (2005) Molecular and neurologic findings of peroxisome biogenesis disorders. *J Child Neurol* 20:326–329.

2. Suzuki Y, Simozawa N, Imamura A, Fukuda S, Zhang Z, Orii T, Kondo N (2001) Clinical, biochemical and genetic aspects and neuronal migration in peroxisome biogenesis disorders. *J Inherit Metab Dis* 24:151–165.
3. Loes JD, Fatami A, Melhem ER, Gupte N, Bezman, L, Moser HW, Raymond GV (2003) Analysis of MRI patterns aids prediction of progression in X-linked adrenoleukodystrophy. *Neurology* 61:369–374.
4. Powers JM, DeVivo DC (2002) Peroxisomal and mitochondrial disorders. In: Graham DI, Lantos PL (eds) *Greenfields' neuropathology*, 7th edn, Vol 1. Arnold, London, pp 737–749.
5. Ohama E, Ohara S, Ikuta F, Ikuta F, Tanaka K, Nishizawa M, Miyatake T (1987) Mitochondrial angiopathy in cerebral blood vessels of mitochondrial encephalomyopathy. *Acta Neuropathol (Berl)* 74:226–233.
6. Chow CW, Thorburn DR (2000) Morphological correlates of mitochondrial dysfunction in children. *Hum Reprod* 15(Suppl 2):68–78.

12 Urea Cycle Disorders

1. Lyon G, Adams RD, Kolodny EH (1996) *Neurology of hereditary metabolic diseases of children*, 2nd edn. McGraw-Hill, New York, pp 12–14.
2. Kimura S, Hara M, Nezu A, Osaka H, Yamazaki S, Saitoh K (1994) Two cases of glutaric aciduria type 1: clinical and pathological findings. *J Neurol Sci* 123:38–44.
3. Gorden N (2006) Glutaric aciduria types 1 and 2. *Brain Dev* 28:136–140.
4. Harding BN, Surtees R (2002) Metabolic and neurodegenerative diseases of childhood. In: Graham DI, Lantos PL (eds) *Greenfields' neuropathology*, 7th edn, Vol 1. Arnold, London pp 507–509.

13 Amino Acid Metabolism Disorders

1. Harding BH, Surtees R (2002) Metabolic and neurodegenerative diseases of childhood. In: Graham DI, Lantos PL (eds) *Greenfields' neuropathology*, 7th edn, Vol 1. Arnold, London, pp 501–507.

14 Mitochondrial Cytopathy

1. Harper C, Butterworth R (2002) Nutritional and metabolic disorders. In: Graham DI, Lantos PL (eds) *Greenfields' neuropathology*, 7th edn, Vol 1. Arnold, London, pp 610–618.
2. Makino M, Horai S, Goto Y, Nonaka I (2000) Mitochondrial DNA mutations in Leigh syndrome and their phylogenetic implications. *J Hum Genet* 45:69–75.
3. Prasson RA, Whang N (2002) Mitochondrial myopathy, encephalopathy, lactic acidosis, and stroke-like episodes (MELAS) syndrome: an autopsy report. *Arch Pathol Lab Med* 122:978–981.
4. Powers JM, DeVivo DC (2002) Peroxisomal and mitochondrial disorders. In: Graham DI, Lantos PL (eds)

15 Other Heredodegenerative Diseases

1. Lowe JS, Leigh N (2002) Disorders of movement and system degenerations. In: Graham DI, Lantos PL (eds) *Greenfields' neuropathology*, 7th edn, Vol 1. Arnold, London, pp 361–370.
2. Delgado-Escueta AV, Serratosa JM, Liu-A, Weissbecker K, Medina MT, Gee M, Treiman LJ, Sparkes RS (1994) Progress in mapping human epilepsy genes. *Epilepsia* 25(Suppl 1):S29–S40.
3. Ganesh S, Agarwala KL, Ueda K, Akagi T, Shoda K, Usui T, Hashikawa T, Osada H, Delgado-Escueta AV, Yamakawa K (2000) Laforin, defective in the progressive myoclonus epilepsy of Lafora type, is a dual-specificity phosphatase associated with polyribosomes. *Hum Mol Genet* 9:2251–2261.
4. Honavar M, Meldrum BS (2001) Epilepsy. In: Graham DI, Lantos PL (eds) *Greenfields' neuropathology*, 7th edn, Vol 1. Arnold, London, pp 899–942.
5. Yokoi S, Austin J, Witmer F, Sakai M (1968) Studies in myoclonus epilepsy (Lafora body form). *Arch Neurol* 19:15–33.
6. Rett A (1977) Cerebral atrophy associated with hyperammonemia. In: Vinken PW, Bruyn GW (eds) *Handbook of clinical neurology*, Vol 29. North Holland, Amsterdam, pp 205–225.
7. Amir RE, Van den Veyver I, Wan M, Tran CQ, Franke U, Zoghbi HY (1999) Rett's syndrome is caused by a mutation in X-linked MECP2 encoding methyl-CpG-binding protein. *Nat Genet* 23:185–188.
8. Lasalle JM, Goldstine J, Balmer D, Greco CH (2001) Quantitative localization of heterogeneous methyl-CpG-binding protein: 2(MeCP2) expression phenotypes in normal and Rett syndrome brain by laser and scanning cytometry. *Hum Mol Genet* 10:1729–1740.
9. Kerr A, Engerström IW (2001) The clinical background to the Rett disorder. In: Kerr A, Engerström IW (eds) *Rett disorder and the developing brain*. Oxford University Press, Oxford pp 1–26.
10. Ronnet GV, Leopold D, Cai X, Hoffbuhr KC, Moses L, Hoffman EP, Naidu S (2003) Olfactory biopsies demonstrate a defect in neuronal development in Rett syndrome. *Ann Neurol* 54:206–218.
11. Esiri MM, Crow TJ (2002) Neuropathology of psychiatric disorders In: Graham DI, Lantos PL (eds) *Greenfields' neuropathology*, 7th edn, Vol 1. Arnold, London, pp 485–488, 780–784.

neuropathology, 7th edn, Vol 1. Arnold, London, pp 455–457.

12. Endo A, Motonaga K, Arahata K, Yamada T, Takashima S (2000) Developmental expression of myotonic dystrophy protein kinase in brain and its relevance to clinical phenotype. *Acta Neuropathol (Berl)* 100:513–520.
13. Kuo HC, Hsiao KM, Chen CJ, Hsieh YC, Huang CC (2005) Brain magnetic resonance image changes in a family with congenital and classic myotonic dystrophy. *Brain Dev* 27:291–296.

16 Basal Ganglia Diseases

1. Lyon G, Kolodny EM, Pastores GH (2006) Childhood and adolescent hereditary metabolic disorders. In *Neurology of hereditary metabolic diseases of children*, 3rd edn. McGraw-Hill, New York, pp 274–280.
2. Lyon G, Kolodny EM, Pastores GH (2006) Encephalopathy. In *Neurology of hereditary metabolic diseases of children*, 3rd edn. McGraw-Hill, New York, pp 118–122.
3. Lowe JS, Leigh N (2002) Disorders of movement and system degeneration. In: Graham DI, Lantos PL (eds) *Greenfields' neuropathology*, 7th edn, Vol 1. Arnold, London, pp 352–357, 455–457.

17 Neuroaxonal Degeneration

1. Wang AM, Schindler D, Desnick R (1990) Schindler disease: the molecular lesion in the alpha-N-acetylgalactosaminidase gene that causes an infantile neuroaxonal dystrophy. *J Clin Invest* 86:1752–1756.
2. Tanabe Y, Iai M, Ishii M, Tamai K, Maemoto T, Ooe K, Takashima S (1993) The use of magnetic resonance imaging in diagnosing infantile neuroaxonal dystrophy. *Neurology* 43:110–113.
3. Defendini R, Markesbery WR, Mastry AR, Duffy PE (1973) Hallervorden-Spatz disease and infantile neuroaxonal dystrophy: ultrastructural observations, anatomical pathology and nosology. *J Neurol Sci* 20:7.
4. Zarranz JJ, Gomez-Esteban JC, Atares B, Lezcano E, Forcadas M (2006) Tau-predominant-associated pathology in a sporadic late-onset Hallervorden-Spatz syndrome. *Mov Disord* 21:107–111.
5. Hayflick SJ, Westaway SK, Levinson B, Zhou B, Johnson MA, Ching KHL, Gitschier J (2003) Genetic, clinical, and radiographic delineation of Hallervorden-Spatz syndrome. *N Engl J Med* 348:33–40.

18 Leukodystrophy

1. Leegwater PA, Pronk JC, van der Knaap MS (2003) Leukoencephalopathy with vanishing white matter: from magnetic resonance imaging pattern to five genes. *J Child Neurol* 18:639–645.
2. Van der Knaap MS, Leegwater PA, Konst AA, Visser A, Naidu S, Oudejans CB, Schutgens RB, Pronk JC (2002) Mutations in each of the five subunits of translation initiation factor eIF2B can cause leukoencephalopathy with vanishing white matter. *Ann Neurol* 51:264–270.
3. Van der Knaap MS, Pronk JC, Scheper GC (2006) Vanishing white matter disease. *Lancet Neurol* 5:413–423.
4. Harding BH, Surtees R (2002) Metabolic and neurodegenerative diseases of childhood. In: Graham DI, Lantos PL (eds) *Greenfields' neuropathology*, 7th edn, Vol 1. Arnold, London, pp 494–501.
5. Suzuki K, Suzuki K (2002) Lysosomal diseases. In: Graham DI, Lantos PL (eds) *Greenfields' neuropathology*, 7th edn, Vol 1. Arnold, London, pp 675–682.
6. Eng LF, Lee YL, Kwan H, Brenner M, Messing A (1998) Astrocytes cultured from transgenic mice carrying the added human glial fibrillary acidic protein gene contain Rosenthal fibers. *J Neurosci Res* 53:353–360.
7. Neal JW, Cave EM, Singhrao SK, Cole G, Wallace SJ (1992) Alexander's disease in infancy and childhood: a report of two cases. *Acta Neuropathol (Berl)* 84:322–327.
8. Surendran S, Michals-Mataln K, Quast MJ, Tying SK, Wei J, Ezell EL, Matalon R (2003) Canavan disease: a monogenic trait with complex interaction. *Mol Genet Metab* 80:74–80.
9. Lyon G, Adams LG, Kolodny RD (eds) (1996) *Neurology of hereditary metabolic diseases of children*, 2nd edn. McGraw-Hill, New York, pp 71–72, 262–263.
10. Golomb MR, Walsh LE, Carvalho KS, Christensen CK, DeMyer WE (2004) Clinical findings in Pelizaeus-Merzbacher disease. *J Child Neurol* 19:328–331.
11. Hadson LD (2003) Pelizaeus-Merzbacher disease and spastic paraplegia type 2: two faces of myelin loss from mutations in the same gene. *J Child Neurol* 18:616–624.

19 Demyelination

1. Prineas JW, McDonald WI, Franklin RJM (2002) In: Graham DI, Lantos PL (eds) *Greenfield's neuropathology*, 7th edn, Vol 2. Arnold, London, pp 523–525.
2. Mizuguchi M, Abe J, Mikkaichi K, Noma S, Yoshida K, Yamanaka T, Kamoshita S (1995) Acute necrotizing encephalopathy of childhood: a new syndrome presenting with multifocal, symmetric brain lesions. *J Neurol Neurosurg Psychiatry* 58:555–561.

3. Mizuguchi M (1999) Acute necrotizing encephalopathy of childhood: a novel form of acute encephalopathy prevalent in Japan and Taiwan. *Brain Dev* 21:138–139.
4. Mizuguchi M, Hayashi M, Nakano I, Kuwashima M, Yoshida K, Nakai Y, Itoh M, Takashima S (2002) Concentric structure of thalamic lesions in acute necrotizing encephalopathy. *Neuroradiology* 44:489–493.
4. Volpe J. *Neurology of the newborn*, 4th edn. Saunders, Philadelphia, pp 858–889.
5. Graham D, Montine TJ (2002) Neurotoxicity. In: Graham DI, Lantos PL (eds) *Greenfield's neuropathology*, 7th edn. Vol 1. Arnold, London, pp 799–815.

20 Infection

1. Kinney HC, Armstrong DD (2002) Perinatal pathology. In: Graham DI, Lantos PL (eds) *Greenfield's neuropathology*, 7th edn. Arnold, London, pp 560–566.
2. Tran TD, Kubota M, Takeshita K, Yanagisawa M, Sakakibara Y (2001) Varicella-associated acute necrotizing encephalopathy with a good prognosis. *Brain Dev* 23:54–57.
3. Eda I, Takashima S, Takeshita K (1983) Acute hemiplegia with lacunar infarct after varicella infection in children. *Brain Dev* 5:494–499.
4. Takashima S, Becker LE (1979) Neuropathology of fatal varicella. *Arch Pathol Lab Med* 103:209–213.
5. Love S, Wiley CA (2002) Viral diseases. In: Graham DI, Lantos PL (eds) *Greenfield's neuropathology*, 7th edn, Vol 2. Arnold, London, pp 16–66.
6. Prineas JW, McDonald WI, Franklin RJM (2002) Demyelinating diseases. In: Graham DI, Lantos PL (eds) *Greenfield's neuropathology*, 7th edn, Vol 2. Arnold, London, pp 527–528.
7. Isumi H, Nunoue T, Nishida A, Takashima S (1999) Fetal brain infection with human parvovirus B19. *Pediatr Neurol* 21:661–663.
8. Gray F, Alonso JM (2002) Bacterial infections of the central nervous system. In: Graham DI, Lantos PL (eds) *Greenfield's neuropathology*, 7th edn, Vol 2. Arnold, London, pp 156–177.
9. Turner G, Scaravilli F (2002) Parasitic and fungal disease. In: Graham DI, Lantos PL (eds) *Greenfield's neuropathology*, 7th edn, Vol 2. Arnold, London, pp 107–141.

21 Intoxication

1. Eto K, Oyanagi, Itai Y, Tokunaga H, Takizawa Y, Suda I (1992) A fetal case of Minamata disease: an autopsy case report with special reference to the nervous system. *Mol Chem Pathol* 16:171–186.
2. Eto K, Yasutake A, Korogi Y, Akima M, Shimozeaki T, Tokunaga H, Kuwana T, Kaneko Y (2002) Methylmercury poisoning in common marmosets: MRI findings and peripheral nerve lesions. *Toxicol Pathol* 30:723–734.
3. Takeuchi T, Eto K (1999) The pathology of Minamata disease: a tragic story of water pollution. Kyushuu University Press, Fukuoka.

22 Tumors

1. Kleihues P, Cavenee WK (eds) (2000) *Tumours of the nervous system: pathology and genetics*. IARC Press, Lyon.
2. Cummings TJ, Klintworth GK (2006) Gliomas of the optic nerve and chiasm. In: McLendon RE, Rosenblum MK, Bigner DD (eds) *Russell and Rubinstein's pathology of tumors of the nervous system*, 7th edn, Hodder Arnold, London, pp 651–661.
3. McLendon RE, Provenzale JM, Friedman AH (2006) Astrocytoma of the brainstem. In: McLendon RE, Rosenblum MK, Bigner DD (eds) *Russell and Rubinstein's pathology of tumors of the nervous system*, 7th edn, Hodder Arnold, London, pp 89–96.
4. Kleihues P, Cavenee WK (eds) (2000) *Tumours of the nervous system: pathology and genetics*. IARC Press, Lyon, pp 52–54.
5. Kleihues P, Cavenee WK (eds) (2000) *Tumours of the nervous system: pathology and genetics*. IARC Press, Lyon, pp 227–230.
6. Kleihues P, Cavenee WK (eds) (2000) *Tumours of the nervous system: pathology and genetics*. IARC Press, Lyon, pp 72–81.
7. Wan M, Tihan T, Rojiani AM, Bodhireddy SR, Prayson RA, Iacuone JJ, Alles AJ, Donahue DJ, Hessler RB, Kim JH, Haas M, Rosenblum MK, Burger PC (2005) Monomorphous angiocentric glioma: a distinctive epileptogenic neoplasm with features of infiltrating astrocytoma and ependymoma. *J Neuropathol Exp Neurol* 64:875–881.
8. Roncaroli F, Consales A, Fioravanti A, Cenacchi G (2005) Supratentorial cortical ependymoma: report of three cases. *Neurosurgery* 57:E192.
9. Mork SJ, Lindegaard KF, Halvorsen TB, Lehmann EH, Solgaard T, Hatlevoli R, Harvei S, Ganz J (1985) Oligodendroglioma: incidence and biological behavior in a defined population. *J Neurosurg* 63:881–889.
10. Raghavan R, Balani J, Perry A, Maragrat L, Vono MB, Cai DX, Wyatt RE, Rushing EJ, Bowers DC, Hynan LS, White CL (2003) Pediatric oligodendrogliomas: a study of molecular alterations on 1p and 19q using fluorescence in situ hybridization. *J Neuropathol Exp Neurol* 62:530–537.
11. Kreiger PA, Okada Y, Simon S, Rorke LB, Louis DN, Golden JA (2005) Losses of chromosomes 1p and 19q are rare in pediatric oligodendrogliomas. *Acta Neuropathol (Berl)* 109:387–392.
12. Gessi M, Giangaspero F, Pietsch T (2003) Atypical teratoid/rhabdoid tumors and choroid plexus tumors: when genetics “surprise” pathology. *Brain Pathol* 13:409–414.

13. Kleihues P, Cavenee WK (eds) (2000) Tumours of the nervous system: pathology and genetics. IARC Press, Lyon, pp 87–94.
14. Kleihues P, Cavenee WK (eds) (2000) Tumours of the nervous system: pathology and genetics. IARC Press, Lyon, pp 95–112.
15. Kleihues P, Cavenee WK (eds) (2000) Tumours of the nervous system: pathology and genetics. IARC Press, Lyon, pp 123–145.
16. Eberhart CG, Burger PC (2003) Anaplasia and grading in medulloblastomas. *Brain Pathol* 13:376–385.
17. Kleihues P, Cavenee WK (eds) (2000) Tumours of the nervous system: pathology and genetics. IARC Press, Lyon, pp 175–196.
18. Perry A, Dehner LP (2003) Meningeal tumors of childhood and infancy: an update and literature review. *Brain Pathol* 13:386–408.
19. Kleihues P, Cavenee WK (eds) (2000) Tumours of the nervous system: pathology and genetics. IARC Press, Lyon, pp 243–248.
20. Rosenberg AE (2006) Chordoma and related lesions, chondrosarcoma and osteosarcoma of the cranium. In: McLendon RE, Rosenblum MK, Bigner DD (eds) Russell and Rubinstein's pathology of tumors of the nervous system, 7th edn, Hodder Arnold, London, pp 765–774.
21. Lemire R, Loeser JD, Leech RW, Alvord EC (eds) (1975) Normal and abnormal development of the human nervous system. Harper & Row, New York.
22. Kleihues P, Cavenee WK (eds) (2000) Tumours of the nervous system: pathology and genetics. IARC Press, Lyon, pp 197–206.
23. Kleihues P, Cavenee WK (eds) (2000) Tumours of the nervous system: pathology and genetics. IARC Press, Lyon, pp 207–214.
24. Kleihues P, Cavenee WK (eds) (2000) Tumours of the nervous system: pathology and genetics. IARC Press, Lyon, pp 163–174.
25. Kleihues P, Cavenee WK (eds) (2000) Tumours of the nervous system: pathology and genetics. IARC Press, Lyon, pp 216–242.
2. Boerkel CF, Lupski JR (2002) Hereditary motor and sensory neuropathies. In: Rimoin DL, Connor JM, Pyeritz RE (eds) Emery and Rimoin's principles and practice of medical genetics, 4th edn. Harcourt, New York, pp 3303–3320.

25 Muscle Disease

1. Adams RD (1975) Disease of muscle, a study of pathology, 3rd edn. Harper & Row, Hagerstown, MD, pp 2–53.
 2. Karpati G (2003) Structural and molecular basis of skeletal muscle disease. ISN Neuropath Press, Basel, pp 1–3.
 3. Dubowitz V (1985) Muscle biopsy a practical approach, 2nd edn. Bailliere Tindall, London.
 4. Anderson LVB (2003) Dystrophinopathies. In: Karpati G (ed) Structural and molecular basis of skeletal muscle disease. ISN Neuropath Press, Basel, pp 6–46.
 5. Hoffman EP, Pegoraro E (2003) Laminin $\alpha 2$ (merosin) gene mutations. In: Karpati G (ed) Structural and molecular basis of skeletal muscle disease. ISN Neuropath Press, Basel, pp 37–41.
 6. Padberg GW (2003) Large telomeric deletion disease: facioscapular humeral dystrophy. In: Karpati G (ed) Structural and molecular basis of skeletal muscle disease. ISN Neuropath Press, Basel, pp 119–122.
 7. Thornton C (2003) The myotonic dystrophies. In: Karpati G (ed) Structural and molecular basis of skeletal muscle disease. ISN Neuropath Press, Basel, pp 108–114.
 8. Carpenter S (2003) Abnormalities in nuclear positioning (centronuclear myopathies). In: Karpati G (ed) Structural and molecular basis of skeletal muscle disease. ISN Neuropath Press, Basel, pp 57–59.
 9. Mandel JL, Laporte J, Buj-Bello A, Sewry C, Wallgren-Pettersson C (2003) X-linked myotubular myopathy. In: Karpati G (ed) Structural and molecular basis of skeletal muscle disease. ISN Neuropath Press, Basel, pp 124–129.
 10. Goebel HH, Laing NG (2003) Nemaline myopathies. In: Karpati G (ed) Structural and molecular basis of skeletal muscle disease. ISN Neuropath Press, Basel, pp 74–76.
 11. MacLennan DH, Loke JCP (2003) Malignant hyperthermia and central core disease associated with defects in Ca^{2+} channels of the sarcotubular system. In: Karpati G (ed) Structural and molecular basis of skeletal muscle disease. ISN Neuropath Press, Basel, pp 99–102.
 12. Goebel HH (2003) Congenital fiber type disproportion. In: Karpati G (ed) Structural and molecular basis of skeletal muscle disease. ISN Neuropath Press, Basel, pp 130–131.
 13. Engel AG, Hohlfeld R, Banker BQ (1994) Inflammatory myopathies. In: Engel AG, Franzini-Armstrong C (eds) Myology, Vol 2. McGraw-Hill, New York, pp 1335–1418.
 14. Eller RO, Cumming WJK, Mahon M, Ellison DW (2002) Diseases of muscle. In: Graham DI, Lantos PL (eds)
- ## 23 Motor Neuron Disease
1. Weller RO, Cumming WJK, Mahan M, Ellison DW (2002) Diseases of muscle. In: Graham DI, Lantos PL (eds) Greenfield's neuropathology, 7th edn, Vol 2. Arnold, London, pp 708–711.
- ## 24 Peripheral Neuropathy
1. Lyon GM, Adams RDS, Kolodny EH (1996) Neurology of hereditary metabolic diseases of children. McGraw-Hill, New York, pp 310–321.

- Greenfield's neuropathology, 7th edn, Vol 2. Arnold, London, pp 677–756.
15. Shoubbridge EA, Molnar MJ (2003) Oxidative phosphorylation defects. In: Karpati G (ed) Structural and molecular basis of skeletal muscle disease. ISN Neuropath Press, Basel, pp 202–213.
 16. Rutledge ML, Hawkins EP, Langston C (1986) Skeletal muscle growth failure in premature newborns by chronic pancuronium treatment. *J Pediatr* 109:883–886.
 17. Szigeti K, Gulum MS, Armstrong A, Belmont JW, Miler G, Lupski J (2003) Disturbance of muscle fiber differentiation in congenital hypomyelinating neuropathy caused by a novel myelin protein zero mutation. *Ann Neurol* 54:389–402.
 7. Harding BN, Copp AJ (2002) Malformations. In: Graham DI, Lantos PL (eds) Greenfield's neuropathology, 7th edn, Vol 2. Arnold, London, pp 398–400.
 8. Thon M (2004) Epilepsy. Part 1. Cortical dysplasia. In: Golden JA, Harding BN (eds) Developmental neuropathology. ISN Neuropath Press, Basel, pp 61–66.
 9. Armstrong DD (2005) Epilepsy-induced microarchitectural changes in the brain. *Pediatr Dev Pathol* 8:607–614.

26 Epilepsy

1. Armstrong DD, Mizrahi EM (1998) Pathology of epilepsy in childhood. In: Scaravilli F (ed) Neuropathology of epilepsy. World Scientific, Singapore pp 169–338.
2. Ito M, Nagafuji H, Okazawa H, Yamakawa K, Sugawara T, Mazaki-Miyazaki E, Hirose S, Fukuma G, Mitsudome A, Wada K, Kaneki S (2002) Autosomal dominant epilepsy with febrile seizures plus missense mutations of the (Na⁺) channel $\alpha 1$ subunit gene, SCN1A. *Epilepsy Res* 48:15–26.
3. Meenke HJ, Janz D (1984) Neuropathological findings in primary generalized epilepsy: a study of eight cases. *Epilepsia* 25:8–21.
4. Thom M, Scaravilli F (1998) The neuropathology of epilepsy in adults. In: Scaravilli F (ed) Neuropathology of epilepsy. World Scientific, Singapore, pp 339–478.
5. Rojiani AM, Emery JA, Anderson KJ, Massey JK (1996) Distribution of heterotopic neurons in normal hemispheric white matter: a morphometric analysis. *J Neuropathol Exp Neurol* 55:178–183.
6. Honavar M (1998) Rasmussen's syndrome. In: Scaravilli F (ed) Neuropathology of epilepsy. World Scientific, Singapore, pp 479–499.

27 Accidents, Sudden Death

1. Kinney HC, Armstrong DD (2002) Perinatal neuropathology. In: Graham DI, Lantos PL (eds) Greenfield's neuropathology, 7th edn, Vol 1. Arnold, London, pp 563–586.
2. Filiano JJ, Kinney HC (1994) A perspective on neuropathologic findings in victims of the sudden infant death syndrome: the triple-risk model. *Biol Neonate* 66:194–197.
3. Takashima S, Armstrong D, Becker LE (1978) Cerebral white matter lesions in the sudden infant death syndrome. *Pediatrics* 62:155–159.
4. Takashima S, Armstrong D, Becker LE (1978) Cerebral hypoperfusion in the sudden infant death syndrome: brain stem gliosis and vasculature. *Ann Neurol* 4:257–261.
5. Narita N, Narita M, Takashima S, Nakayama M, Nagai T, Okado N (2001) Serotonin transporter gene variation is a risk factor for sudden infant death syndrome in the Japanese population. *Pediatrics* 107:690–692.
6. Ozawa Y, Okado N (2002) Alternation of serotonergic receptors in the brain stems of human patients with respiratory disorders. *Neuropediatrics* 33:142–149.
7. Paterson DS, Trachtenberg FL, Thompson EG, Belliveau RA, Beggs AH, Darnall R, Chadwick AE, Krous HF, Kinney HC (2006) Multiple serotonergic brainstem abnormalities in sudden infant death syndrome, *JAMA* 297:2124–2132.
8. Dolinak D, Reichard R (2006) An overview of inflicted head injury in infants and young children, with a review of beta-amyloid precursor protein immunohistochemistry. *Arch Pathol Lab Med* 130:712–717.

Subject Index

A

- α -actin 362
- α,β -crystallin 238, 297
- α -fetoprotein 136, 330
- α -fucosidase 156
- α -keto acid dehydrogenase 190
- α -L-iduronidase 162
- α -mannosidase 156
- α -N-acetylgalactosaminidase 156
- α -N-acetylglucosaminidase 162
- α -neuraminidase deficiency 164
- α -neuraminidase deficiency + galactosidase deficiency 156
- α -sarcoglycan deficiency 356, 357
- A3243G point mutation 368
- abscess 124, 272
- absence of olfactory bulbs 84
- absence of peroxisomes 174
- absent philtrum 286
- Acanthamoeba* 278
- Acanthamoeba* encephalitis 279
- acatalasemia (catalase deficiency) 171
- accidental trauma 388
- acetyl-CoA- α -glucosamide-N-acetyltransferase 162
- acetylglucosamine-4-sulfatase 162
- acid α -1,4-glucosidase 168
- acid β -galactosidase 140
- acid ceramidase 152
- acid lipase deficiency 152
- acid phosphatase 148
- acid sphingomyelinase gene 146
- acidic cresyl violet 235
- acquired toxoplasmosis 276
- acrocephalosyndactyly 62
- actin 352
- action myoclonus 164
- acute bacterial meningitis 272
- acute disseminated encephalomyelitis 248
- acute encephalitis 256
- acute hemorrhagic leukoencephalitis 264
- acute myeloblastic leukemia (AML) 328
- acute necrotizing encephalopathy (ANE) 250, 256
- acyl-CoA dehydrogenase deficiencies 366
- acyl-CoA oxidase 174
- acyl-CoA oxidase (AOX) deficiency 171
- adamaninomatous type 325
- ADEM 248
- adenovirus 248
- adhalin 357
- adrenal glands 152, 176, 177
- adrenal insufficiency 174, 176
- adrenal lesions 174
- adrenoleukodystrophy 171, 176
- adrenomyeloneuropathy 176
- adult CLN4 (Kufs' disease; adult batten disease)* 150
- agenesis of corpus callosum 286
- agenesis of the cerebellar vermis 66
- agenesis of the corpus callosum 50, 84
- agenesis of the corticospinal fiber system 50
- AHS 376–378
- alanine glyoxylate aminotransferase deficiency 171
- Alexander's disease 238
- alimentary tract 60
- alkyl-DHAP synthase deficiency 171
- Alpers-Huttenlocher syndrome 200
- Alpert's syndrome 116
- Alzheimer type II astrocytes 180, 184, 200, 218, 219, 240, 241
- Alzheimer-type dementia 78
- amebae 278, 279
- amebiasis 278
- amebic meningoencephalitis 278
- Ammon's horn 103
- Ammon's horn sclerosis 85, 103, 198, 376, 377
- amniotic bands 62, 63
- amygdala 212
- amyloid precursor protein (APP) 78, 96
- Anaplastic astrocytoma 291, 293
- Anaplastic ependymoma 291, 298, 299
- Anaplastic ganglioglioma 291
- Anaplastic oligoastrocytoma 291
- Anaplastic oligodendroglioma 291
- anencephaly 286
- aneurysm 114

- Angelman syndrome 210
 angiofibroma 336
 angioma 134
 anomalous dendritic arborization 136
 ansiform lobule 172
 anterior cerebral artery 57, 96
 anterior horn 156, 158, 159
 anterior horn cells 168, 266, 340, 341, 366, 372
 anterior horns of the spinal cord 108
 anterior spinal nerve roots 340
 anti-phospholipid antibodies 120
 antithrombin III 120
 Antoni A 332
 Antoni B 332
 APC 336
 Apert's syndrome 62
 aphasia 50
 apical dendritic branches 211
 apoptosis 94, 102, 262
 APP gene 78
 aqueduct 133
 aqueduct occlusion 238
 aqueduct stenosis 92
 aqueductal dilatation 93
 arachnoid cells 296
arachnoid cysts 60, 61, 326
 arboviral encephalitis 260
 arboviruses 254
 arcuate fibers (U fibers) 240
 arginase 180
 argininosuccinate lyase 180
 argininosuccinate synthetase (ASS) 180
 arginosuccinic aciduria 180
 arterial border zones 96, 126
 arterial vasculature 107
 arterIALIZATION 112, 113
 arteriovenous malformation (AVM) 112
 arteriovenous shunt 112
 arthropod-borne viruses 260
 arylsulfatase A 160, 234
 arylsulfatase A, B, and C 160
 ASPA 240
 aspartoacylase 240
 aspartylglucosaminidase 156
 aspartylglucosaminuria 156
 Asperger's syndrome 212
aspergillus 274
aspergillus infection 275
 astroblastoma 291, 302, 303
 astrocytic cell 292
 astrocytic foot processes 124
 astrocytic hyperplasia 142
 astrocytic tumors 291, 292
 astrocytomas 132, 292, 336
 ataxia telangiectasia 136, 137
 ataxia telangiectasia mutated gene (ATM) 136
 ATM reactivity 137
 ATPase reaction 355
 ATP-binding cassette-transporter gene 176
 atrophin-1 204
 atypical choroid plexus papilloma 300, 301
 atypical meningioma 322, 323
 atypical teratoid/rhabdoid tumor (AT/RT) 291, 310, 316
 Auerbach plexus neurons 151
 autism 212
 autofluorescent granular material 148
 autonomic ganglia 147, 152, 168, 366
 autonomic neuropathies 344
 autosomal recessive lysosomal glycogen storage disease 168
 AVM 112
 axillary freckling 336
 axonal damage 96
 axonal degeneration 236
 axonal injury 392, 393
 axonopathy 346
 axons 100, 142, 143, 172, 348
- B**
- β -amyloid precursor protein (β -APP) 392
 β -amyloid protein ($A\beta$) 78
 β -galactosidase 152, 162
 β -hexosaminidase 142
 β -human choriogonadotropin (β -HCG) 330
 β -mannosidase 156
 β -mannosidosis 156
 β -oxidation of fatty acids 171
 β -oxidation of VLCFAs 176
 β -tropomyosin 362
 BACE2 78
Balamuthia 278
 balloon cells 130, 131, 177, 383
 ballooned neurons 140, 143, 160, 367
 ballooning 140, 149, 156, 161
 ballooning of neuronal cytoplasm 140
 band heterotopia 382
 bare glial nuclei 378
 basal ganglia calcification 78, 243, 262
 basal ganglia necrosis 94, 95
 basilar artery 115
 basis pontis 71, 102
 basket brain 56, 57
 basophilic fibers with large nuclei 371
Batten-Spielmeyer-Vogt disease 150
 Becker's muscular dystrophy 356, 357
 Bergman glia 223, 287

Bergman glial proliferation 83, 106, 142
berry aneurysms 114, 115
 Betz cells 156
 Bielchowsky stain 79
 bifunctional protein 175
 bilateral striatal necrosis 95
 bilirubin encephalopathy 108
 biotinidase deficiency 196
 biopterin deficiency (PKU III) 190
 biphasic pattern 294
 Birbeck granules 328
 birth trauma 88, 89
 bleeding disorders 106
 blood brain barrier 124, 250
 Bodian stain 137, 285
 bone marrow 144, 163
 Bourneville's disease 130
 brachial plexus 88
 brain abscess 272, 273, 380
 brain calcification 276
 brain contusion 88
 brain cyst 280
 brain edema 125, 262
 brain injury 124, 388, 392
 brain purpura 256
 brain stem glioma 296, 297
 brain stem gliosis 390
 brain stem hemorrhage 88
 brain stem necrosis 94, 97, 104
 brain stem tegmentum 250
 brain tumors 292
 branched-chain amino acids 190
 brown pigmentation 218, 228
 bulbar paralysis 150
 bunyaviridae 260

C

CA1 103, 126, 376, 377
 cactus flower 242
 cadmium encephalopathy 288, 289
 cadmium intoxication 288
 café au lait spots 132, 332, 336
 CAG repeats 204, 222
 calcification in periventricular areas 255
 calcification in white matter 242
 calcium channel 288
 Canavan's disease 240
 Canavan–van Bogaert–Bertrand disease 240
Candida albicans 274
 Candidiasis 274
 capillary proliferation 196, 200
 capillary telangiectasia 112, 134
 capsule cells 206, 207

carbamoylphosphate synthetase (CPS) 180
 carbohydrate metabolism 208
 carbon monoxide 288
 carbon monoxide (CO) poisoning 94, 126
 carbon monoxide intoxication 288
 carbonic anhydrase isoenzyme II 310
 cardiac arrest encephalopathy 104
 cardiogenic embolism 118
 cardiomyopathy 206
 carnitine deficiency 366, 367
 catalase immunohistochemistry 173
 caudate nucleus 58, 213, 218, 286
 caveolin 356
 cavernous hemangioma 112
 cavity formation 104, 389
 CBS gene 188
 CCTG repeats 214
 CD117 330
 CD1a 328, 329
 cellular ependymoma 298
 central alveolar hypoventilation 104
 central chromatolysis 341
 central core disease 351
 central core myopathy 362, 363
 central cores 354
 central neurocytoma 291, 308
 central nuclei 354
 centromeric region 206
 centronuclear myopathy 351, 362
 centrum semiovale 279
 ceramidase deficiency 152
 ceramide 152
 cerebellar aplasia 68
 cerebellar ataxia 206
 cerebellar atrophy 136, 160, 164
 cerebellar cortical necrosis 94
 cerebellar cystic leukomalacia 94, 104, 106
 cerebellar efferent system 204
 cerebellar folia 140
 cerebellar granular cell layer hemorrhage 106
 cerebellar heterotopia 68
 cerebellar hypoplasia 62
 cerebellar infarction 106
 cerebellar liponeurocytoma 291
 cerebellar peduncle 68, 206
 cerebellar subarachnoid hemorrhage 92, 107
 cerebellar tonsillar herniation 125
 cerebellar vermis 71, 107
 cerebellar white matter necrosis 104
 cerebral abscess 272
 cerebral angiography 117
 cerebral asymmetry 212
 cerebral atrophy 150

- cerebral blood flow 90
- cerebral contusion 392
- cerebral cortical (laminar) necrosis 94
- cerebral cyst 281
- cerebral edema 124
- cerebral hypoperfusion 100
- cerebral hypoplasia 62
- cerebral infarction 94, 95, 274
- cerebral ischemia 96
- cerebral mantle 56
- cerebral mycosis 274
- cerebral neuroblastoma 314
- cerebral palsy 96–98, 103, 108
- cerebral perfusion pressure 96
- cerebral periventricular white matter 250
- cerebral swelling 88
- cerebral white matter 174
- cerebral white matter hemorrhage 89
- cerebrohepatorenal 172
- cerebrospinal fluid (CSF) 60, 68, 92, 172, 310
- cerebrovascular amyloidosis 78
- cerebrovascular autoregulation 96
- ceroid lipofuscinosis 148, 150, 151
- ceruloplasmin 218, 220
- cerebral infarction 119
- channelopathies 351
- Charcot-Marie-Tooth disease (CMT) 346
- Chaslin's subpial gliosis 376
- checkerboard pattern 372
- chemokines 262
- chickenpox 248
- child abuse 392, 393
- childhood ataxia with central hypomyelination syndrome 232
- childhood dermatomyositis 364, 365
- cholesterol clefts 325
- chondroma 322
- chondrosarcoma 322
- chordoma* 324, 325
- chorea 222
- choreoathetosis 108
- choreoathetotic-type cerebral palsy 95
- choriocarcinoma* 291, 330, 331
- chorioretinitis 276
- choroid glioma 291
- choroid plexus 58, 152, 159, 165
- choroid plexus carcinoma 291, 301, 300
- choroid plexus hyperplasia 50
- choroid plexus papilloma 291, 300, 301
- choroid plexus tumor 291, 300, 316
- choroidal macrophages 168
- chromatolysis 96, 266, 340
- chromosomal fragility 136
- chromosome 1q- 78
- chromosome 4p- 80
- chromosome 21 78
- chronic *Acanthamoeba* encephalitis 279
- chronic amebic encephalitis 279
- chronic diphenylhydantoin intoxication 287
- chronic progressive external ophthalmoplegia 368
- chronic subdural hematoma 393
- cingulate brain 124
- cingulate gyrus 56, 57, 97
- cingulate necrosis 94
- circle of Willis 116, 117, 220
- cisterna magna 60, 62
- CLAM 70
- clear cell ependymoma 298
- cleft lip or palate 80
- CLN2, CLN3, CLN4 type A, CLN4 type B, CLN5, CLN6, and CLN7 150
- closed lip 54
- cloverleaf skull 48
- clubfeet 158
- CMT 346
- CMT2 346
- CMV 255
- CNS candidiasis 274
- CO intoxication 56
- coagulative necrosis 96
- coarctation of the aorta 114
- cobalamine 188
- Cockayne's syndrome 242
- coenzyme Q10 deficiency 366
- cognitive impairment 140
- collagen vascular disorder 364
- collicular plate 64, 68
- colloid cyst 58, 59
- complete agenesis of the cerebellum 68
- complete duplication 68
- complex IV deficiency 200
- compression 162
- congenital aqueductal occlusion 50
- congenital cocaine syndrome 287
- congenital denervating condition 373
- congenital disorder of myelin formation 346
- congenital DM1 214
- congenital fiber type disproportion 351, 362, 363
- congenital heart disease 80, 95, 120
- congenital HIV infection 262
- congenital hydranencephalic-hydrocephalic syndrome 56
- congenital hydrocephalus 50, 51
- congenital hypomyelinating neuropathy (CHN) 346, 347
- congenital muscular dystrophy 351, 358, 359

congenital myasthenic syndromes 351
 congenital myopathies 351, 354, 362, 363
 congenital myotonic dystrophy 214, 358, 360, 361
 congenital porencephaly 52, 53
 congenital sensory neuropathy 370
 congenital toxoplasmosis 276, 277
 congenital varicella syndrome 256, 257
 congenital viral syndrome 254
 conjunctival telangiectasia 136
 connatal Cockayne's Syndrome 242
 connexin (*GJB1*) 346
 contiguous ABCD1 DXS1357E deletion syndrome (CADDs) 171
 contiguous gene syndrome 171
 contralateral inferior olivary nucleus 106
 contusion 124
 copper 218, 220
 copper-binding p-type ATPase 218
 copper transport deficiency 220
 cord ischemia 89
 corneal clouding 162, 164
 corneal opacities 158
 coronal, lambdoid, and sagittal 62
 coronaviruses 248
 corpora amylacea 377
 corpus callosum hypoplasia 50
 corpus callosum 84, 172, 213, 284, 286
 corpus Luysii 204
 cortical atrophy 127
 cortical calcification 95
 cortical dysplasia 55, 81, 82
 cortical hamartoma 130
 cortical hemorrhage necrosis 92
 cortical hemorrhage 388
 cortical hemorrhagic necrosis 92
 cortical infarction 393
 cortical laminar necrosis 94, 126
 cortical necrosis 95
 cortical tuber 131, 336
 corticospinal tract signs 206
 Cowden syndrome 336
 Cowdry's type A variety 268
 coxsackie virus 254
 cranial nerve deficits 104
 cranial nerve nuclear aplasia 64
 cranial nerve nuclei 104, 108, 156
 cranial nerve VIII 207
 craniofacial malformation 82
craniopharyngioma 291, 324, 325
 craniosynostosis 62
 Crouzon's syndrome 62
Cryptococcus meningitis 275
Cryptococcus abscess 275

Cryptococcus infection 275
Cryptococcus neoformans 274
 cryptogenic cerebral abscess 272
 crystalline curvilinear structures 199
 CTG 214
 cuneate fasciculus 206
 curved laminar profiles 141
 curvilinear osmophilic inclusions 150, 152
 cyanotic congenital heart disease 95, 100
 cyst 58, 96, 98, 101, 106, 172, 280, 292, 326
 cystathion β -synthase deficiency (CBS) 188
 cystic lesions 98, 99, 263
 cystic necrosis 251
 cysticercosis 280, 281
Cysticercus cellulosae 280
Cysticercus larvae 281
 cytochrome c oxidase (COX) 196, 355, 368, 369
cytochrome c oxidase (COX) deficiency 355, 368
 cytokeratins 300
 cytokines 262
 cytomegalovirus 248, 254
 cytoplasmic ceroid lipid 150
 cytoplasmic inclusions 146, 147, 176
 cytoplasmic vacuoles 168
 cytoplasmic vacuolization 156, 164
 cytosine-cytosine-thymine-guanine (CCTG) repeat 360
 cytosine-thymidine-guanine (CTG) repeat 360
cytotoxic edema 124
 cytotrophoblast 330

D

D4Z4 repeat 358
Dandy-Walker malformation (DWM) 66
Dandy-Walker variant (DWV) 66
 D-bifunctional protein (DBP) deficiency 171
 decerebrate rigidity 140
 deep cerebral veins 120
 deep medullary veins 90
 defective nuclear membrane proteins 351
 defective oxidation 176
 defective protective protein 156
 deformed skull 62
 dehydrofolate reductase 288
 dehydroxyacetone phosphate acyltransferase 172
 Dejerine-Sottas syndrome (DSS) 346, 347
 delayed myelination 152, 190
 delayed neuronal death 102
 dementia 222
 dementia with rigidity 150
 dendrite 78, 140, 143, 262
 dendritic aberrations 220
 dendritic branchings 221
 dendritic cell disorders 328

- dendritic degeneration 271
 - dendritic trees 107
 - denervation 349
 - denervation group atrophy 189
 - dense bundle of fibrils 208
 - dental defects 254
 - dentate gyrus 83, 85, 376, 377
 - dentate nucleus 48, 64, 85, 136
 - dentato-olivary dysplasia 64, 65
 - dentato-rubro-pallido-luysian atrophy 204
 - dentato-rubro-pallido-luysian atrophy (DRPLA) 204
 - dentritic spines 210
 - dermal sinus 326
 - dermatan sulfate 162
 - dermatomyositis 351
 - dermoid cyst* 326
 - Derry's disease* 140
 - desminopathies 351
 - desmoplastic cerebral astrocytoma 292
 - desmoplastic infantile astrocytoma 291, 306
 - desmoplastic infantile ganglioglioma 306, 384, 385
 - desmoplastic medulloblastoma 291, 312
 - desmoplastic stroma 306
 - developing microvasculature 100
 - developmental masses 326
 - diastase treatment 169
 - diastematomyelia 68, 69
 - diencephalon 57
 - diffuse astrocytoma 291
 - diffuse axonal injury 392
 - diffuse cortical dysplasia 382
 - diffuse glial tumor 302
 - diffuse gliosis 152, 265
 - diffuse white matter gliosis 245
 - diffusely infiltrating astrocytoma 292, 293
 - dihydropterin reductase deficiency (PKU II) 190
 - dihydroxyacetone phosphate (DHAP) acyltransferase deficiency 171
 - dimyelia* 68
 - diplegia 98
 - diplomyelia 69
 - disease-specific lysosomal inclusions 366
 - disialotransferrin developmental deficiency 70
 - dislocated hips 158
 - dissecting aneurysms* 114
 - disseminated intravascular coagulation (DIC) 118, 120
 - disseminated varicella zoster 256, 257
 - DM protein kinase (*DMPK*) gene 360
 - DM1 214, 360, 361
 - DM2 360
 - DNA fragmentation in situ 102
 - DNA helicase 242
 - DNA marker 222
 - DNA synthesis 242
 - DNET 298, 384, 385
 - dopamine 212
 - dorsal nucleus of Clarke 172
 - dorsal root ganglia 136, 165, 168, 207, 340, 366
 - dorsal spinocerebellar tract of Flechsig 206
 - double cortex 382
 - doublecortin* 382
 - Down syndrome 78
 - drug intoxication 286
 - drug-associated vasculitis 118
 - DS obligate region (DSOR) 78
 - DSCAM 78
 - Duchenne muscular dystrophy 356, 357, 370
 - dysarthria 140
 - dysembryoplastic neuroepithelial tumor (DNET) 291, 308, 384
 - dysferlin 356
 - dysmorphic features 156, 172
 - dysmyelination 190
 - dysostosis 160, 162
 - dysplasias of the skull 132
 - dysplastic changes 284
 - dysplastic gangliocytoma 291, 336, 337
 - dysplastic neurons 131
 - dystonic dyskinetic movement 182
 - dystroglycans 358
 - dystrophic change 356
 - dystrophin 356–358
 - dystrophinopathies 351, 356
- E**
- early response gene 2 (*EGR2*) 346
 - early-onset CMT 346
 - eastern equine 260
 - ecchordosis 324
 - echinococcosis* 280
 - Echinococcus* 280
 - echovirus 254
 - Ectopic neurons* 378
 - ectopic olivary segments 64
 - eIF2B 232
 - EIF2B5* 232
 - electrolyte imbalance 120, 370
 - electron transport flavoprotein 182
 - electron transport flavoprotein oxyreductase 182
 - electron-dense bodies 164
 - electron-lucent 148
 - elongated astrocyte 302
 - embolization 118
 - embryonal carcinoma* 291, 330
 - embryonal tumors 291, 310, 314, 320
 - embryonic hindbrain 66

Emery-Dreifuss dystrophy 351
 encephalitis 380
 encephalocele 62, 63
 encephalomyelitis 276
 encephalopathy 262
 encrustation of axon 98
 end folium sclerosis 376
 end zone areas of medullary arteries 98
 end-arteries 96
 endarteritis 281
 endomysial connective tissue 356
 endomysial fibrosis 356, 357, 364
 endoneurial fibroblast 332
 endoplasmic reticulum 356
 endothelial hypertrophy 194
 endothelial proliferation 348
 endothelial tubular arrays 365
 enkephalin 222
 enlarged mitochondria 220
 enteroviruses 254
 eosinophilic Cowdry's type A intranuclear inclusions 258
 eosinophilic granular bodies 112, 294, 304
 eosinophilic neuronal necrosis 108
 ependyma cyst 59
 ependymal canals 314
 ependymal differentiation 311
 ependymal rosettes 298, 310, 311
 ependymoblastoma 291, 310
 ependymoma 291, 298
 epidermoid cyst 327
epidermoid tumors 326
 epilepsy partialis continua 200
 epilepsy 103, 375, 376, 378, 380–385
epithelial or ependymal cysts 326
 epithelial tumor 324
 epithelial-like cells 331
 epithelioid cells 270, 271, 277
EPM2A gene 208
EPMA2B gene 208
 Epstein-Barr virus 248, 254
ErcG6 gene 242
 ether phospholipid biosynthesis 171
 exanthema subitum 250
 exchange blood transfusion 108
 excitatory amino acids 96
 excitatory circuit 376
 excitotoxic amino acids 184
 excitotoxicity 126
 exophthalmos 62
 external granular cell layers 106
 external granular layer 92
 extracalvarial hemorrhage 88
 extraembryonic mesoblast 330

extrapyramidal disease 150
 extrapyramidal signs 140, 144
 extravascular factors 90
 extravascular tissue pressure 90
 extraventricular central neurocytoma 308
 “eye of the tiger” 229

F

Fabry's disease 152, 153, 344
 facial diplegia 64, 104
 facial dysmorphic features 286
 facial dysmorphism 140
 facial dysmorphology 174
 facioscapulohumeral dystrophy 351
 factor VIII 120
 falx 124
 familial spastic paraplegia type 2 244
 Fanconi's anemia 116
 Farber body 152
 Farber's disease 153
 fascioscapular humeral dystrophy 351, 358, 359
 fastigiovestibular system 204
 fatty acid thioesters 148
 fetal alcohol syndrome 286
 fetal encephalitis 94
 fetal hypoxia 56, 94
 fetal Minamata disease 284, 285
 fetal trimethadione syndrome 286, 287
 fetal ultrasonography 94
FGFR gene 62
 fibrillary astrogliosis 199
 fibrillary pilocytic 130
 fibrinolysis 120
 fibrinolytic activity 90
 fibroblast growth factor receptor-3 (*FGFR3*) 48
 fibromuscular dysplasia 116, 118
 fibronectin 134
 fibrosarcoma 322
 fibrovascular stroma 324
 filament protein 362
 fingerprint inclusions 149, 150
 flaviviridae 260
 fleurettes 320
 Flexner rosettes 318
 Flexner-Wintersteiner rosettes 320
 floating neurons 309
 flower spray nerve endings 354
 foam cell infiltration 96, 101
 foam cells 97, 98, 146, 176
 foamy histiocytes 152, 165
 foamy macrophages 146
 focal cortical dysplasia 382

focal cortical hypoplasia 130
 focal hypoxic-ischemic injury 126, 127
 focal necrosis with spongy changes 251
 focal PVL 98
 focal subcortical leukomalacia 100
 folate metabolism 188
 folia 65, 148
 foramen magnum 124
 foramina of Luschka and Magendie 90
 forebrain 66, 156
 forehead 63
 forking 50, 51
 fossa hypoplasia 48
 four-layer cortex 383
 fourth ventricle 67, 90, 160
 four-layer pattern 255
 Fowler's disease 56
 fragmentation of the internal elastic lamina 220
 freckling of the axilla 332
 Friedreich's ataxia 206, 344
 frontal cortex 101
 frontonasal encephalocele 62
 frontoparietal hypoperfusion 194
 frontotemporal dementia 360
 fucosidosis 156
fukutin 382
 Fukuyama congenital muscular dystrophy 351, 358, 359
 fungal infections 274
 furious and paralytic rabies 266

G

GABA 222
 galactose-6-sulfatase 162
 galactosialidosis 156, 157
 galactosylceramide lipidosis 236
 gangliocytoma 291, 304
 ganglioglioma 304, 384, 385
 ganglion cells 147, 304, 318
 ganglioneuroblastoma 291, 314, 318, 319
 ganglioneuroma 318
 ganglioside storage in neurons (mucopolipidosis) 162
 Gaucher cell 144, 145
 Gaucher's disease 144
 generalized fiber hypoplasia 371
 generalized glycogenesis (infantile type II glycogenesis) 168
generalized muscle fiber hyperplasia 370
generalized type 1 atrophy 370
generalized type 2 atrophy 370
 germ cell tumors 291, 330
 germinal matrix 90, 284
 germinolysis 59

germinoma 291, 330
 germline mutations 54
 giant astrocytes 130, 264
 giant cell hepatitis 146
 gingival hypertrophy 158
GJB1 346
 glaucoma 134
 glial ependymal cyst 326, 327
 glial fibrillary acid protein 238
 glial hamartia 336
glial heterotopia 326
 glial intranuclear inclusions 204
 glial tumors 132
 glial-neuronal neoplasm 308
 glioblastoma 132, 291
 glioblastoma multiforme 292, 293
 gliopendymal cyst 58, 59
 gliomatosis cerebri 291, 302, 303
 glioneuronal heterotopia 48
 global ischemia 126
 globoid cell leukodystrophy 236
 globoid cells 236, 237
 globotriaosylceramide 152
 globus pallidus 108, 126, 141, 156, 205, 218, 228, 229, 288
 glomerular epithelium 158
 gluaryl-CoA dehydrogenase 182
 glucocerebrosidase 144
 glucocerebroside 144
 glucose phosphate polymers 208
 glutamate 126
 glutamate transporter (EAAT4)
 immunohistochemistry 107
 glutaric aciduria 182
glutaric aciduria type 1 182
glutaric aciduria type 2 182
 glutaric aciduria type 3 (glutaryl-CoA oxidase deficiency) 171
 glutaryl-CoA metabolism 171
 glycoasparagine 156
 glycogen 169
 glycogen storage 351, 366, 367
 glycogen storage disease 351
 glycogen storage myopathy 366, 367
 glycoproteins, glycolipids 156
 glycosaminoglycans 162
 glycosphingolipid storage 152, 153
 glyoxylate detoxification 171
 GM₁ gangliosidosis type 1 140
 GM₁ gangliosidosis type 2 140
 GM₁ gangliosidosis type 3 140
 GM₂ activator protein 142
 GM₂ gangliosidosis 142
GM₂ gangliosidosis type 0 142

GM₂ gangliosidosis type 2 142
GM₂ gangliosidosis type AB 142
GM₂ gangliosidosis type B₁ 142
GM₂ gangliosidosis: adult form 142
 Golgi impregnation 211
 Golgi study 263
 Gomori trichrome stain 355
 gracile fasciculus 206
 gracile nuclei 108
 gram-negative bacillary meningitis 272
 granular cell 83, 106, 149, 223, 284, 285, 287
 granular cell tumour 291
 granular neurons 142
 granular osmophilic deposits, or GRODs 148
 granule neurons 168, 376, 377
 granuloma of tuberculosis 271
 granulomatous amebic encephalitis 278
 granulomatous inflammation 365
gray matter heterotopia 378, 379
 Grocott methenamine silver stain 274
 group atrophy 340, 341
 growth retardation 82
 gyral pattern 52

H

Hallervorden-Spatz disease 228
Haltia-Santavuori Disease 148
 hamartia 378, 379
hamartoma 132, 292, 324, 325, 336
 HCG-producing giant syncytiotrophoblastic cells 330
 head injury 389, 393
 head trauma 388, 389
 hearing deficit 174
 hearing loss 254
 hemangioblastoma 336, 337
 hemangioma 134, 322
 hemangiopericytoma 322
 hemicords 68
 hemimegalencephaly 382
 hemiparesis 134
 hemiplegia 118
 hemispherectomy 134
 hemispheric defect 57
 hemispheric dysfunction 212
 hemolysis 108
 hemophilia 52
 hemorrhagic infarction 119, 120, 127
 hemorrhagic leukoencephalomyelitis 265
 hemorrhagic necrosis 250, 279
 hemosiderin 92, 93, 112
 hemosiderin deposition 389, 392
 hemosiderin-containing macrophage 185
 hemosiderin-laden macrophage 389

heparan sulfamidase 162
 heparan sulfate 162
 heparan sulfates 162
 hepatosplenomegaly 140, 144, 146, 152, 156, 158
 hereditary motor and sensory neuropathies 346
 hereditary neuropathy with liability to pressure palsy (HNPP) 346, 347
 hereditary sensorimotor neuropathies 344
 hereditary sensory and autonomic neuropathies 348
 herniation 124
 herpes simplex type 1 encephalitis 258
 herpes viruses 254
 herpes simplex 254, 258
 herpes simplex virus type 2 meningoencephalitis 258
 herringbone 234
 heterotopia 49, 54, 174, 378, 379, 382
 heterotopic gray matter 130
 heterotopic intraspinal cysts 60
 hexosaminidase β -subunit 142
 hexosaminidase A 142
 hexosaminidase B 142
 hexosaminidase S 142
 higher cortical function 160
 high-output cardiac failure 112
 hippocampal dysplasia 48, 81
 hippocampal necrosis 94, 102, 103
 hippocampal sclerosis 94
 hippocampus 79, 80, 85, 103, 126, 213, 376, 377
 Hirano bodies 242
 hirsutism 158
 histiocyte 152
 histiocytic disorder 328
hMLH1 336
Hodgkin's lymphoma 328
 holoprosencephaly 80
 Holzer stain 131, 133, 251
 homeobox gene *EMX2* 54
 Homer-Wright rosettes 314
 homocystinuria 118, 188
 homozygous males 152
 honeycomb patterns 234
hPSM2 336
 HSAN II 348
 HSAN III (Riley-Day syndrome) 348
 HSAN IV 348
 HSAN V 348
 HSANs 348
hSNF5/INI 316
hSNF5/INI-I 300
 human immunodeficiency virus (HIV) 118, 254
 human placental lactogen (HPL) 330
 Hunter's syndrome 162
 huntingtin 222
 Hurler's syndrome 158, 162, 163

Hurler-Scheie's syndrome 162
 Hurst's disease 264
 hyaluronan 162
 hyaluronidase 162
 hydranencephaly 56, 57
 hydrocephalus 50, 84, 106, 112, 160, 162, 214, 238, 270, 276, 360
 hydrocephalus ex vacuo 50
 hydrogen peroxide metabolism 171
 hydropic swelling 124
 hyperbilirubinemia 108
 hypermyelination 108
 hyperoxaluria type 1 171
 hyperoxemia 102
 hyperpnea 66
 hypersplenism 144
 hypertrophic cardiomyopathy 196
 hypertrophic neuropathy 347
 hyphal fungi 274
 hypocarbia 102
 hypoglycemia 102
 hypomyelination 85, 175, 182, 245, 345
 hypopigmented hair 220
 hypoplasia 64, 84
 hypoplasia of the cerebellar hemisphere 287
 hypoplasia of the cerebellum 68
 hypoplasia of the cerebral white matter 51, 85
 hypoplastic hypophysis 82
 hypotensive brain stem necrosis 104
 hypotrophy of type I fibers 362
 hypoventilation 104
 hypoxia 106, 108, 126, 390
 hypoxia-ischemia 52
 hypoxic brain injury 88
 hypoxic encephalopathy 126
 hypoxic-ischemic encephalopathy (HIE) 94, 100
 hypoxic-ischemic injury 90, 94, 100, 376

I

I cell disease 158
 iduronate 160
 immature teratoma 330
 immune disorders 364
 immunohistochemistry 96
 impact injuries 388
 impaired arousal mechanism 390
 inclusion bodies 256
 increased liability to malignancies 136
 increased microglial cells 381
 increased vascularity 197, 199
 induronate sulfatase 162
 infantile Minamata disease 284, 285
 infantile NCL1 148

infantile NCL1 (Infantile Batten Disease) 148
 infantile neuroaxonal dystrophy 226
 infantile olivopontocerebellar atrophy/hypoplasia 70
 infantile Refsum's disease (IRD) 171, 174
 infantile sialic storage disease 156
 infantile type II glycogenesis 366
 infarct 185, 188
 infarction 52, 106, 124, 289
 infection 52, 60, 106, 124, 376, 380
 infective myositis 351
 inferior olivary dysplasia
 inferior olivary nucleus 80, 104, 105, 156, 173, 207, 212
 inflammatory cytokines 96
 inflammatory myopathy 351, 354, 364, 365
 influenza 248, 250
 inhibitory interneurons 376
 integral membrane protein 358
 intellectual disabilities 103, 134
 interhemispheric fissure 60
 interior olivary nucleus 71
 intermediate filaments 292
 internal granular cell loss 92, 185
 internal nuclei 356
 intoxication 124, 287
 intracerebral arteries 114
 intracerebral calcifications 135
 intracerebral hemorrhage 184
 intracranial hemorrhage 88
 intracranial pressure 124
 intractable epilepsy 84, 376, 378
 intracytoplasmic inclusions 56
 intrafascicular inflammatory cell infiltration 365
 intraneuronal lamellar bodies 158
 intranuclear inclusion 269
 intrauterine growth retardation 84
intrauterine parvovirus B19 infection 266
 intraventricular hemorrhage 88, 93, 94, 104, 106
 intraventricular space 91
 iris hamartomas 132
 iron-positive pigments 229
 ischemia 102, 124
 ischemic necrosis 64, 95
 isoprenoid biosynthesis 171
 IVH 90–92

J

Jansky-Bielschowsky disease 150
 Japanese encephalitis 260
 Japanese encephalitis virus 260
 joint stiffness 162
 joubertin protein 66
 Joubert syndrome 66, 67

JS gene 66
 junctional complexes 299, 310
juvenile CLN3 (juvenile batten disease) 150
juvenile xanthogranuloma 328

K

karyorrhexis 102
 Kayser-Fleischer rings 218
Kearns sayre syndrome 368, 369
 keratan sulfate 162
 keratin nests 325
 kernicterus 108, 109
 Krabbe's disease 236, 344
KRIT 112
 Kugelberg-Welander syndrome 340

L

L1 CAM 51
 lactate/pyruvate ratio 220
 lacunar infarction 256
 Lafora bodies 208, 209
 Lafora Body Disease 208
 laforin 208
 laforin-interacting ubiquitin E3 ligase 208
 lamellar inclusions 164
 lamellar lipid profiles 172
 laminar necrosis 134, 142
 laminin $\alpha 2$ 358, 359
Langerhans cell histiocytosis (LCH) 328, 329
 langerin 328, 329
 Langhan's giant cells 271
 large cell medulloblastoma 291, 312
 large dysplastic neurons 383
 large myelinated axons 345
late infantile CLN2, CLN5, CLN6, CLN7 (late-infantile Batten disease) 150
 late-onset myotonic dystrophy 360, 361
 lateral cuneate nucleus 172
 lateral geniculate body 80, 81
 LCAD 366
 Leber hereditary optic neuropathy 368
 Leigh's syndrome 196
 leiomyosarcoma 322
 leptomenigeal angiomas 135
 leptomenigeal astroglial heterotopia 133
 leptomenigeal glioneuronal heterotopia 80, 215, 286, 287, 391
 leptomeningitis 120, 274
leukemia 120, 328, 336
 leukodystrophies 344
 leukoencephalopathy 182, 289
 Lhermitte-Duclos 336

LHOH 368
 Li-Fraumeni syndrome 336
 Limb-girdle dystrophy 351
 limbic regions 212
 limiting membrane 208
 lipid myopathy 366
 lipid storage 157, 366, 367
 lipofuscin 148, 164, 168, 242
lipogranulomatosis 152
 lipoma 322
Lis -1 382
 Lisch nodule 132
 lissencephaly 286, 382
 lissencephaly type 2 68
 liver cirrhosis 201, 218
 liver fibrosis 173
 liver steatosis 196
 lobar sclerosis 96, 97
 long-chain acyl-CoA dehydrogenase deficiency 366
 loss of granular cells 261
 loss of homozygosity (LOH) 292
 loss of myelin sheaths 99
 loss of oligodendroglia 264
 loss of Purkinje cells 181, 199, 223
 lumbar ganglion 161
 Luysian body 205
 lymphocytic choriomeningitis virus 254
 lymphocytic perivascular cuffing 174, 266
lymphohistiocytosis 328
 lymphomas and Haemopoietic Neoplasms 291
 lysosomal glycogen 168
 lysosomal glycogen storage 366
 lysosomal inclusions 168
 lysosomal membrane protein 150
 lysosomes 140, 162, 239

M

macrophages 100, 153
 macrophage proliferations 102, 266
 macular cherry red spot 156, 164
 malignant epithelial cells 317
 malignant fibrous histiocytoma 322
 malignant hyperthermia 362, 370
malignant lymphoma 328
malignant peripheral nerve sheath tumors (MPNSTs) 132, 291, 334, 335
 malin 208
 mammillary bodies 55, 194, 195
 MAP5 310
 maple syrup urine disease 190, 191
 Marfan's syndrome 116
 Maroteaux-Lamy 162

- MASA 50
 massive brain stem necrosis 104
 maternal HIV infection 262
 mature teratoma 330
 maxillary hypoplasia 286
 MCAD 366
 McArdle's disease 367
 measles 248, 268
 measles inclusion body encephalitis 268
 measles virus 254
 Meckel-Grüber syndrome 62, 63
 MeCP2 210, 211
 medial longitudinal fasciculus 70
 median nerve injury 349
 medium-chain acyl-CoA dehydrogenase 366
 medulla oblongata 65, 105, 152
 medulloblastoma 291, 310, 312, 313, 336
 medulloepithelioma 291, 310
 medullomyoblastoma 291, 314
 medusa head formation 220
 megalencephaly 48, 212, 336
 meganeurites 143
 melanin 314
 melanocytic meningeal tumor 322
 melanocytoma 322
 melanoma 322
 melanotic medulloblastoma 291, 314
 MELAS 198, 368
 membrane attack complex 364, 371
 membrane-bound round to ovoid inclusions 145
 membrane protein 150
 membranous bodies 140
 meningeal sarcoma 323
 meningeal tumor 322
 meningiogliomatosis 336
 meningioma 291, 322, 336
 meningocele 66
 meningoencephalitis 260, 278
 meningoencephalocele 66
 meningomyelocele 286
 Menkes syndrome 220
 mental deficiency 50
 mental retardation 50, 62, 66, 84, 118, 130, 134, 210
 mercury stain 285
 mercury 284
 merosin 357
 merosin deficiency 358, 359
MERRF 368
 mesenchymal chondrosarcoma 322
 mesodermic somites 352
 metabolic myopathy 351, 354, 369
 metachromatic inclusions 160
 metachromatic leukodystrophy 160, 234, 344
 metachromatic substance 161, 162, 235
 metastatic cerebral abscess 272
 methotrexate intoxication 288, 289
 methylmercury poisoning 284
 mevalonate kinase deficiency 171
 microangiography 101, 113
 microcephalus 84, 254
 microcephaly 62, 80, 84, 190, 242, 262, 286
 microcysts 97
 microdysgenesis 378, 379
 microencephaly 70
 microglia 142, 152
 microglial activation 96
 microglial aggregation 102
 microglial nodules 258, 259, 380, 381
 microgyria 84, 172
 microphthalmia 80
 microtubules 228
 microvesicular fatty change 200
 microvilli 299
 midbrain 57, 64, 68
 migration disorders 84, 130
 Miller-Dieker syndrome 382
 Minamata Disease 284
 minimal dystrophin deficiency 356
 mitochondria 354, 355, 368, 369
 mitochondrial DNA 196, 368
 mitochondrial DNA deletions 368
 mitochondrial DNA mutations 368
 mitochondrial encephalomyopathy with lactic acidosis
 and stroke-like episodes (MELAS) 198, 368
 mitochondrial encephalopathy 94
 mitochondrial membranes 108
 mitochondrial myopathies 351
 mitochondrial protein 206
 mitochondrial respiratory chain enzymes 368
 mitotic index 300, 322
 mixed germ cell tumour 291
 mixed gliomas 291
 mixed neuronal-glial tumors 304
 MKS1 62
 MKS2 62
 MKS3 62
 MLD 234
 Moebius syndrome 64, 104, 105
 molar tooth sign 67
 molar tooth sign on MRI 66
 monosaturated (C26:1) VLCFA 172
 monosomy 82
 Morquio A 162
 Morquio B 162
 mossy fiber 376
 motor deficit 98
 motor deterioration 176
 motor end plates 352

motor nuclei 168, 366
 motor or sensory neuropathies 344
 moyamoya disease 116, 117
 moyamoya vessels 116, 117
 MPNST 336
 MPS in the lysosomes of lymphocytes 162
 MPS storage 162
 MPZ 346
 mtDNA 196
 mtDNA depletion 200
 mtDNA polymerase deficiency 200
 mucopolipidosis type 1 164
 mucopolipidosis type 2 158
 mucopolysaccharide 160
 mucopolysaccharidosis 160, 162
 multicystic encephalomalacia 94, 95, 100
 multicystic leukomalacia 97, 99
 multilamellar bodies 147
 multinucleated cells 352
 multinucleated giant cells 270
 multiple endocrine deficiencies 82
 multiple sclerosis 248
 multiple sulfatase deficiency (MSD) 160, 161
 mumps virus 254
 mural cells 168
 muscle 169
 muscle development 352
 muscle fibers 354
 muscle infarction 364
 muscle injury 370
 muscle spindles 352, 354
 muscular dystrophy 351, 354
 mutant ryanodine receptor proteins 362
 mutations in the *N*-acetylglucosaminyl-1-phosphotransferase 158
 myasthenia gravis 351
 MYCN 318
Mycobacterium tuberculosis 270
mycotic aneurysms 114
 myelin degeneration 176
 myelin figures 164
 myelin protein zero (MPZ) 346
 myelin splitting 232
 myelination 8, 174, 284
 myelinopathy 346
 myeloneuropathy 176
 myenteric plexus neurons 168
 myenteric plexus 164
 myoblasts 356
 myoclonic epilepsy 204
 myoclonic seizures 164
myoclonus epilepsy with ragged red fibers 368
 myofibrils 352
 myopathology 354

myophosphorylase deficiency 367
 myosin filaments 352
myositis 351, 364
 myotonia congenita 351
 myotonic dystrophy 351, 358, 360, 361, 370
 myotubes 352
 myotubular myopathy 351, 362
 myotubularin gene 362
 myotubularin-related protein 2 (*MTMR2*) 346
 myxopapillary ependymoma 291, 298

N

N-acetylaspartate (NAA) 240
N-acetylgalactosaminidase deficiency 226
N-acetylglucosamine-1-phosphotransferase 158
N-acetylglucosamine-6-sulfate sulfatase 162
N-acetylglutamate synthetase (NAGS) 180
N-acetylneuraminic acid 165
N-acetylneuraminic acid, free sialic acid 156
 NADH-dehydrogenase 196
 NADH-tetrazolium reductase 355
Naegleria encephalitis 279
Naegleria fowleri 278
Naegleria fowleri infection 278
Naegleria meningitis 278
 NAIP 340
 Na-K distribution 124
 NARP 368
 necrotizing encephalitis 258
 Negri bodies 266
 nemaline myopathy 362, 363
 nemaline rod myopathy 351, 363
 neocerebellar aplasia 68
 neonatal adrenoleukodystrophy (NALD) 171, 174
 neonatal asphyxia 95
 neonatal hypoxia or ischemia 94
 neovascularization 96
 nestin 131, 310
 neural crest cells 318
 neuritic plaque 78
 neuroaxis 304
 neuroaxonal degeneration 344
 neuroaxonal dystrophy 146, 172
 neuroblastic tumor 291, 318
 neuroblastoma 291, 318
 neurocutaneous melanosis 322
 neurocutaneous syndrome 132
 neuroectodermal 58
 neuroectodermal tumor 318
 neuroenteric cysts 60, 61, 326, 327
 neuroepithelial cyst 58
 neuroepithelial tumors 302
 neuroepithelium 306

neurofibrillary tangles (NFTs) 78, 146, 228, 242
neurofibroma 291, 332
 neurofibromatosis 1 (NF1) 116, 132, 296, 332, 336
neurofibromatosis 2 332, 336
 neurofibromin 132
 neurofilament immunohistochemistry 227
 neurofilament light gene (*NF-L*) 346
 neurofilaments 228
 neurogenic atrophy 351, 372, 373
 neuroglial elements 307
 neurological regression 160
 neuronal and mixed neuronal-glial tumours 291
 neuronal ballooning 141
 neuronal ceroid lipofuscinosis (NCL) 148, 150
neuronal clusters 378
 neuronal degeneration 95, 106
 neuronal differentiation 311
 neuronal glycogen storage 168, 366
 neuronal heterotopias 53, 173
 neuronal karyorrhexis 102
 neuronal migration 54, 254
 neuronal migration defects 172, 174
 neuronal storage 144, 146, 156
 neuronal swelling 142
 neuronal tumor 308
 neuronophagia 95, 144, 266, 340, 341, 381
 neuropathy, ataxia, retinitis pigmentosa 368
 neurotransmitter 262
 neurotransmitter release 288
 neurovisceral storage 144
 nevoid basal cell carcinoma syndrome (Gorlin) 336
NF1 132, 334, 336
NF2 322, 336
 Niemann Pick type D 146
 Niemann-Pick cells 146
 Niemann-Pick disease 146
 Niemann-Pick foam cells 147
 Niemann-Pick type C (NPC) 146
 nodular cirrhosis 200
nonfetal infantile Minamata disease 284
non-Hodgkin's lymphoma 328
 norepinephrine deficiency 220
 normal-pressure or low-pressure hydrocephalus 50
Norman-landing disease 140
 northern epilepsy CLN8 (variant NCL) 150
 notochordal ectoderm 325
 notochordal ectopia 324
 Nova Scotia variant 146
NPC1 and *NPC2* 146
 nuclear atypia 242, 320
 nuclear bag 354
 nuclear inclusions 222
 nuclear pyknosis 96
 nucleus of Onuf 340

O

obligodendroglial-like cells 384
 obliterative arachnoiditis 106
 obstructive hydrocephalus 88, 276, 280, 295
 occipital skull defect 62
 ocular abnormalities 164, 174
 oculomotor nucleus 341
 Ohtahara syndrome 64
 olfactory neuroblastoma 291, 318, 319
 olfactory neuroepithelioma 291
 oligoastrocytoma 291
 oligodendrocyte 98, 152, 164, 264, 265, 288
 oligodendroglial tumours 291
 oligodendroglia-like cells 308, 309, 378, 379
 oligodendroglioma 291, 298
 oligomembranous bodies 147
 oligosaccharide 156, 165
 olivary dysplasia 64, 81
 olivary nuclei 48, 64
 olivocerebellar degeneration 92, 104, 105, 106
 olivocerebellar transneuronal degeneration 106
 olivopontocerebellar atrophy (OPCA) 64, 70
 olivopontocerebellar hypoplasia (OPCH) 70
 oncospores 280
 Ondine's curse 104, 105
 onion bulb 345, 347
 onion bulb formation 344
 Opalski cell 218
 optic atrophy 160
 optic nerve glioma 132, 296
 optic nerve sheath hemorrhage 393
 optic nerve tumor 310
 organomegaly 162, 164
 ornithine transcarbamylase (OTC) 180
 ornithine transcarbamylase deficiency 184
 orofacial malformations 64
 osmophilic globules 148
 OTC 184
 overproduction of CSF 50

P

p.I278T 188
p44 340
 pachygyria 48, 52, 94
 pallido-luysian tracts 204
 pallidonigral system 228
 palmitoyl-protein thioesterase 148
 pantothenate kinase (*PANK2*) 228
 pantothenate kinase-associated
 neurodegeneration 228
 papillary craniopharyngioma 324
 papillary ependymoma 298
 Papillary glioneuronal tumor 304, 305

- paracrystalline inclusion 369
- paraganglioma 318
- paraganglioma of the filum terminale 291
- parahypophyseal cyst 58
- parallel lamellar inclusions 157
- paramyotonia congenita 351
- parasagittal infarction 94, 96, 127
- parasagittal water shed infarction 96
- parasites 364
- “parking lot” inclusions 199
- pars reticularis 288
- partial agenesis of the corpus callosum 287
- partial deletion 82
- partial seizures 376, 380
- PDGFRA* 292
- Pelizaeus-Merzbacher Disease 244
- pepstatin-insensitive peptidase 150
- periadventitial macrophages 152
- perifascicular atrophy 364
- perinatal asphyxia 102
- perinatal hypoxia 94
- perinatal hypoxic-ischemic encephalopathy (HIE) 94
- perinatal ischemia 96
- perineurial cells 152, 168, 332, 334
- perineurioma* 291, 334
- periodic paralysis 351
- peripheral myelin protein 22 (*PMP22*) 346
- peripheral nerves 161, 162, 174
- peripheral nerve axonopathy 347
- peripheral nerve injuries 88
- peripheral nervous system (PNS) 168
- peripheral neuroblastic tumors 318
- peripheral neurofibromas 132
- peripheral neuropathy 160, 174, 234, 344
- peripheral nuclei 353
- perivascular cuffing 249, 259, 261, 380, 381
- perivascular hemosiderin-laden macrophages 195
- perivascular inflammatory cells 176, 380
- perivascular inflammatory round cell infiltration 176
- perivascular pseudorosette 298
- periventricular calcification 164, 254, 277
- periventricular germinal epithelium (matrix) 90
- periventricular giant cell astrocytoma 131
- periventricular hemorrhagic infarction (PVHI) 90
- periventricular high echo density 98
- periventricular leukomalacia 94, 96–98, 214, 360
- periventricular nodular heterotopias 382
- periventricular nodules 130
- periventricular white matter hemorrhage 91, 93
- periventricular/intraventricular hemorrhage (PVH/IVH) 90
- peroxisomal biogenesis 172
- peroxisomal membrane 172
- peroxisomal membrane protein (ALDP) 176
- peroxisome 172, 176
- peroxisome biogenesis disorders (PBDs) 171, 174
- persistent cavum pellucidum 212
- Pfeiffer’s syndromes 62
- phenylketonuria 190
- pheochromocytomas 336
- phosphatidyl ethanolamine plasmalogen 172
- phrenic motoneurons 340
- phytanoyl-CoA hydroxylase deficiency 171
- pigmentary degeneration 160
- pili torti 220, 221
- pilocytic astrocytomas 291, 292, 294, 295
- pilomyxoid astrocytoma 295
- pineal gland 320
- pineal parenchymal tumor of intermediate differentiation 320
- pineal parenchymal tumors 291, 320
- pineoblastoma 291, 320, 321
- pineocytomas 291, 320, 321
- pituitary adenomas* 324
- PKU-I, II, III 190
- placental barrier 276
- PLAP 330
- plaque fibromyeliniqne 95
- plasma cell infiltration 281
- plasma membrane 356
- plasmalemmal proteins 356
- plasmalogen synthesis 172
- platelet-activating factor 172
- plateletaggregating factor 120
- pleomorphic xanthoastrocytoma 291, 292, 296, 297, 384
- plexiform neurofibroma 132, 133, 333, 335
- PLP 244
- PML 264
- poliomyelitis 266, 267
- poliovirus 254
- polycystic kidney 114
- polyglucosan 208
- polyglutamine 222
- polygyria 62
- polymicrogyria 48, 49, 52, 54, 55, 63, 68, 80, 82, 94, 95, 172, 174, 254, 255, 287, 382, 383
- polymorphous cytoplasmic bodies 146
- polymyoclonus 164
- polymyositis 351, 364
- polyneuropathies 344
- polyps 336
- Pompe’s disease 168, 366, 367
- pontine hemorrhage 389
- pontine nuclei 103
- pontocerebellar hypoplasia 70, 71
- pontosubicular neuron necrosis (PSN) 94, 102
- poor differentiation of fiber types* 370, 371

porencephalic cyst 52, 53
 porencephaly 52, 53, 54, 94, 118, 276
 port-wine stain 134
 posterior cerebral arteries 96
 posterior colliculi of the tectum 104
 posterior columns 136, 172, 206, 207
 posterior fossa 88, 93, 106, 124
 posterior roots 206
 posteroventral nuclei of the thalamus 340
 posthemorrhage hydrocephalus (PHH) 92, 93
 posthemorrhage subependymal cyst 92
 postinfectious encephalitis 256
 postinfectious encephalomyelitis 264
 postinfectious vasculitis 118
 postinfectious/postvaccination perivenous
 encephalomyelitis 248
 postmortem microangiography 91, 96, 97, 98, 103, 121
 poststenotic aneurysms 116
 premyelinating metabolic activity 100
 prenatal infections 58, 96
 preoligodendrocyte 96
 primitive epithelial cells 330
 primitive myotubes 352
 primitive neuroepithelium 311
 primitive type IIC fibers 196
 principal olivary nucleus 65, 173
 progressive cerebellar ataxia 136
 progressive dementia 150
 progressive hemiplegia 176
 Progressive multifocal leukoencephalitis 264, 265
 progressive muscular dystrophy 356
 progressive myoclonic epilepsy 150
 progressive myoclonus epilepsy 208
 progressive neuronal degeneration in childhood with
 liver disease 200
 progressive paraparesis 176
 progressive quadriparesis 152
progressive rubella panencephalitis 268
 progressive spinocerebellar ataxia 206
 protective protein 156, 157, 159
 protein C 120
 protein C deficiency 118
 protein S 120
 proteolipid protein (PLP) 244, 245
 protozoan infections 380
 pseudo-form of NALD 174
 pseudo-Huntington 204
 pseudopalisade 293
 pseudopapillae 324
 pseudorosettes 298
 pseudostratified epithelium 310
PTCH 336
PTEN 336
 Purkinje cell heterotopias 172

Purulent meningitis 272
 putamen 108, 218, 250, 286
 PVL 96–99, 214, 215
 pyramidal cell layer 94, 103, 213
 pyramidal tract 51
 pyramid 175
 pyruvate carboxylase 196
 pyruvate dehydrogenase complex 196
 pyruvate dehydrogenase complex deficiency 196

Q

quadriplegia 160

R

rabies 248, 266, 267
 racemase deficiency 171
 ragged red fibers 368
 Rasmussen's syndrome 380
 Rathke pouch epithelium 324
 reactive astrogliosis 96, 100, 102
 rectilinear profiles 150
 red nucleus 109
 Refsum's disease 171, 344
 Reilly bodies 162
 reinnervation pattern 372
 remyelinating axons 345
 remyelination 344, 345
 renal cell carcinomas 336
 renal cysts 62, 172
 renal tubule 285
 renal tubulopathy 196
 respiratory arrest 126
 respiratory chain 198
 reticular formation 104
 reticulin stain 295
 reticulin-rich desmoplastic component 307
 retina 130, 147, 152, 160, 168, 172, 320
 retinal dysplasia 80
 retinal dystrophy 70
 retinal ganglia cells 168
 retinal hemorrhage 392
 retinal pigmentary degeneration 196
 retinal vasculopathy 358
 retrograde degeneration 92
 Rett brain 211
 Rett syndrome 210
 Rett variants 210
 Reye syndrome 256
 rhabdoid cells 316
 rhabdoid predisposition syndrome (*INI-1*) 300
 rhabdomyoblastic differentiation 320
rhabdomyolysis 370, 371

rhabdomyoma 336
 rhabdomyosarcoma 322, 330
 rhinovirus 248
 rhizomelic chondrodysplasia punctata (RCDP) 171
 rhombencephaloschisis 66
 rhombic lip 64
 rhomboencephalosynapsis 67
 rigidity 222
 “rod cells” 268
 roof nuclei of the cerebellum 108
Rosai-Dorfman disease 328
 Rosenthal fiber 238, 239, 294, 295
 rosette 83, 298
 Roussy-Levy syndrome 346
 rubella 248
 rubella virus 254

S

S-100 78, 300
 saccular aneurysm 114
 sagittal sinus 121
 sagittal sinus thrombosis 120, 121
 Salla disease 156
Sandhoff disease 142
 Sanfilippo A, B, C, D 162
 Sanfilippo's syndrome 163
 saposin-B 234
 sarcoglycans 356
sarcoglycan deficiency 358
 sarcoglycanopathy 351
 sarcoidosis 365
 sarcolemma 356
 sarcoma 316, 322
 satellite cell 136
 SC HAD 366
 scalp defect 84
 Schimke's immunosseous dysplasia 116
 Schindler's disease 156, 226
 schizencephaly 54, 55, 254
 scholastic performance 208
 Scholl analysis 79
 Schwann cells 152, 168, 332, 366
 Schwann cell nucleus 345
 schwannian stroma 318
schwannomas 291, 332, 336
 sea-blue histiocytes 146
 segmental demyelination 344
 SEH 91, 92
 Seitelberger's disease 226
 selective neuronal necrosis 126
 sensorimotor neuropathies 344
 sensory ganglion 143
 septic infarcts 274
 septum pellucidum 59, 84
 sequela of fetal hypoxia 94
 sequelae of cerebral necrosis 94
 sequelae of cortical laminar necrosis 95
 sequelae of IVH 92
 sequelae of kernicterus 109
 sequelae of periventricular leukomalacia 98
 serotonergic neurons 390
 serotonin 212
 shaking injuries 392
 shearing forces 89
 sheath hemorrhage 392, 393
 short-chain L-3 hydroxyacyl-CoA dehydrogenase deficiency 366
 sialic acid 156
 sialic acid disorders 156
 sialic storage disease 161
 sialidosis type 1 164
sialidosis type 1 (cherry red spot-myoclonus syndrome) 164
 sialidosis type 2 156, 164
sialidosis type 2 (dysmorphic group or lipomucopolysaccharidosis) 164
 Sialin (transporter protein) 156
 sialuria 156
 sialyl oligosaccharide, cathepsin A 156
 sickle cell anemia 116, 118, 120
 “simple form” of DNET 308
 single peroxisomal enzyme deficiencies 171
 sinus injury 88
 skeletal dysplasia 164
 skull defect 63
 skull sutures 124
 slender tubular structures of galactocerebroside 236
 slow troponin T 362
 Sly 162
 SMA 1, -3 373
 smallpox immunization 248
 SMN 340
SMN1 340
SMN2 340
 sodium channel genes 376
 solitary fibrous tumor 322
 somatic sprouts 220
 Sommer's sector 103, 198
 spastic diplegia 96
 spastic paraplegia 50, 98
 spastic quadriplegia 140
 spastic tetraplegia 150
 specific respiratory chain enzymes 368
 SPG2 244
 spherical membranous sacs 147
 spheroid 226, 228, 229
 sphingolipid activator proteins A and D 150

- sphingomyelinase activity 146
 - sphingomyelin-cholesterol lipidosis 146
 - spina bifida 68
 - spinal cord 56, 61, 68, 89, 94, 146, 152, 157, 159, 164, 168, 175, 176, 206
 - spinal cord hemorrhage 89, 389
 - spinal cord syringomyelia 69
 - spinal ependymoma 336
 - spinal ganglia 147, 158, 206
 - spinal muscular atrophy 340, 344
 - spinal muscular atrophy type 1 372
 - spines 60, 78
 - spiny projecting neurons 222
 - splenomegaly 144
 - spongy degeneration of the neuraxis 240
 - spongy white matter 232, 233
 - squints 160
 - St. Louis encephalitis virus 260
 - stacked lamellae 164
 - status marmoratus 83, 94, 95, 108, 109
 - status spongiosis 182, 190
 - steal 113, 134
 - stenosis 50, 92
 - stenosis of the aqueduct of Sylvius 50
 - stereotypic behavior 212
 - steroid sulfatase 160
 - striae terminalis 58
 - striatal necrosis 125, 182
 - striated inclusions 172, 177
 - strokes 116, 118
 - Sturge-Weber syndrome 134
 - subacute measles encephalitis* 268
 - subacute necrotizing encephalopathy 196
 - subacute sclerosing panencephalitis (SSPE) 268
 - subarachnoid hemorrhage (SAH) 89, 90, 92, 93, 104, 106, 116, 120, 388, 392
 - subcortical heterotopias 82
 - subcortical leukomalacia (SCL) 94, 100, 101, 390, 391
 - subcortical neuronal heterotopia 49
 - subcortical white matter 53, 99, 101, 241
 - subcortical white matter necrosis 94
 - subdural hematoma 88, 392, 393
 - subdural hemorrhage 88, 89, 392
 - subependymal cyst 58, 58, 59, 92, 172, 173
 - subependymal germinal layer 58
 - subependymal germinolysis 58
 - subependymal giant cell astrocytomas 130, 291, 292, 296, 297, 336
 - subependymal hemorrhage (SEH) 58, 90, 94
 - subependymal layer 59
 - subependymal matrix 90
 - subependymal nodules 130
 - subependymal regions 172
 - subependymomas* 291, 298
 - subgaleal hemorrhage 88
 - subiculum 102
 - subpial cells 306
 - subpial hemorrhage 88
 - substantia nigra 209, 288
 - subthalamus 108
 - subungual fibromas 336
 - subunit C of mitochondrial ATP synthetase 150
 - succinate dehydrogenase (SDH) 355
 - sudanophilic leukodystrophy 172, 174
 - sudanophilic storage 152
 - sudden death 210
 - sudden infant death syndrome 100, 390, 391
 - sulcus 96, 100, 101
 - sulfatides 160
 - sulfatide storage (metachromatic material) 234
 - superficial molecular layer 221
 - superior cerebellar peduncles 66, 67
 - superior colliculi 204
 - superior parietal gyri 97
 - superior sagittal sinus 120
 - superior temporal gyrus 78, 79
 - superoxide dismutase-1 78
 - supranuclear gaze palsy 146
 - supratentorial primitive neuroectodermal tumor (sPNET) 291, 310, 314
 - sural nerve biopsy 235
 - sustentacular cells 318
 - swollen axons 100
 - swollen dendrites 220
 - swollen myelin sheaths 124
 - synaptic damage 262
 - synaptic level 126
 - syncytiotrophoblastic giant cells 330
 - syndactyly of the hands and feet 62
 - syphingolipid activator proteins A and D 148
 - syringomyelia* and *syringobulbia* 68
- T**
- T tubules 356
 - Taenia solium* 280
 - taeniasis 280
 - tanycytic ependymoma 298
 - Tay-Sachs disease* 142
 - teased fiber preparation 345, 346
 - tegmental necrosis 104
 - tegmentum 64
 - tegmentum of the medulla oblongata 105
 - tegmentum of the pons 105, 109
 - telangiectasia 112
 - telangiectatic skin rash 164
 - telomeric deletion disease 351
 - temporal lobes 48, 49, 53

temporal lobe epilepsy 304
 teratogen 286
 teratogenous cyst 61
teratoma 291, 330, 331
teratomatous cyst 326
 thalamic fusion 51, 80
 thalamic hemorrhage 95
 thalamostriatal regions 117
 thalamus 58, 97, 108, 156, 250, 251
 thanatophoric dysplasia type 1 48
 thiamine deficiency 194
 third ventricle 58, 205
 thoracic cord 89
 thrombosis 118, 120
 thymus 137
 “tigroid” appearance 244
 tigroid fashion 242
 tigroid-state demyelination 243
 Togaviridae 260
 tonsillar herniation 124, 289
 torpedo formation 71, 285
 torpedo 137, 226, 242
 tortuous cerebral arteries 220
 toxic infections 370
Toxoplasma cyst 277
Toxoplasma encephalitis 276
Toxoplasma gondii 276
 Toxoplasmosis 276
 TP53 300, 336
 TP53 mutations 292
 trabecula 52
 trafficking 146
 translation factor eIF2B 232
 transport of enzyme cofactors 176
 transporter 124
 transthyretin 300, 301
 transverse sulcus 48
 trauma 56, 60, 68, 106, 114, 116
 trauma-related cerebral abscesses 272
 traumatic lesions 376
 traumatic neuroma 349
Trichinella infestation 365
Trichinella spiralis 280, 281
Trichinosis 280
 trichorrhesis nodosa 220, 221
 triglyceride 152
 trimethadione 286
 triple-risk hypothesis 390
 trisomy 13 (Patau syndrome) 80, 81
 trisomy 18 (Edwards syndrome) 80, 81
 trisomy 21 78
 trisomy 21 brain 211
 tRNA leucine gene 198
TSC1 (hamartin) 130, 336

TSC2 (tuberin) 130
 tuber 131
 tuberculosis 270
 tuberculous meningitis 270
 tuberous sclerosis 116, 130, 131, 296, 336
 tubular and fibrillary inclusions 144
 tubular epithelium 165
 tubular structures 237
 tuffstone 234
 Turcot syndrome 336
 twisted tubular structures 145
 type I or II fibers 354, 372
 type I predominance 361
 tyrosine phosphatase 208

U

U fibers 176, 232, 236
 ubiquitin 222, 238
 ubiquitous protein 340
 UDP-GlcNAc2-epimerase 156
 ulegyria 94, 96, 97
 ulegyria formation 96
 ultrasonography 97–99, 113, 173
 uncal 124
 unconjugated bilirubin 108
 unlayered polymicrogyria 94
 unmyelinated axons 168, 345
 urea cycle 180, 184
 urinary homocystine 188

V

V motor nucleus 157
 vacuolated cells 159
 vacuolated fibroblasts 158
 vacuolated lymphocytes 150
 vacuolization 96, 240, 241
 vanishing leukoencephalopathy 232
 varicella 254
 varicella infection 256
 vascular endothelial proliferation 304
 vascular immaturity 96
 vascular insufficiency 56
 vascular malformations 112, 382
 vascular occlusions 272, 364
 vascular proliferation 194
 vascular steal 112
 vasculature 168
 vasculitis 118, 348
 vasculopathy 56
 vasogenic edema 124, 250
Vein of Galen Aneurysm (VGA) 112
 venous angioma 112

venous drainage 90
 venous infarction 91
 venous thrombosis 120, 121
 ventral pons 102
 ventral spinocerebellar tract of Gowers 206
 ventricles 50, 51, 52, 63, 90, 142, 172
 ventricular septal defect 119
 ventricular system 50
 venules 90, 91
 vermis 66, 68, 136
 vermis hypoplasia 66
 vertebral fractures 89
 vertebral scalloping 132
 vertical columns of large neurons 383
 very long-chain fatty acids (VLCFAs) 176
 very low-birth-weight infants 90, 92, 93, 98, 104
 vimentin 300, 310
 Virchow-Robin space 144
 visceromegaly 146
 visual difficulties 164
 vitamin B₁ 194
 vitamin B₁₂ 188
von Hippel-Lindau disease 336
 von Recklinghausen's disease 132
 von Willebrand's factor 120
 vulnerability 96, 100, 126

W

Walker-Warburg syndrome 68
 Wallerian degeneration 346
 walnut brain 184
 watershed zones 96, 127
 weakness 140, 160
 weeping willow formations 220
 Werdnig-Hoffmann disease 70, 340, 372
 Wernicke's encephalopathy 194, 196
 West Nile virus 260

western equine viruses 260
 whiplash 392
 white matter degeneration 146
 white matter gliosis 70
 white matter injury 392
 white opaque lesions 97
 widespread subcortical leukomalacia 100
 willful trauma 392g
 Wilson's disease 218
 with cerebral palsy 95
 Wohlfart A 352, 353
 Wohlfart B 352, 353
 Wolf-Hirschhorn syndrome 84
 Wolman's disease 152, 153

X

Xlinked *ALD* gene 176
 X-linked adrenoleukodystrophy 174
 X-linked band heterotopia 382
 X-linked congenital hydrocephalus 50
 X-linked lysosomal disorder 152
X-linked myotubular myopathy 362

Y

yellow staining 108
 yold sac tumour 291, 330, 331

Z

Z bands 354
 zebra bodies 152, 160
 Zellweger spectrum 171
 Zellweger's syndrome (ZS) 64, 65, 171, 172, 174
 Ziel-Nielsen stain 275
 zinc finger protein 9 (*ZNF9*) 360
 zona fasciculata 176